

University of Southampton

Faculty of Environmental and Life Sciences

Ocean and Earth Science

Early Carboniferous Palynology and Tetrapod Evolution

by

Emma Jane Reeves

Thesis for the degree of Doctor of Philosophy

November 2019

Abstract

Faculty of Environmental and Life Sciences

Ocean and Earth Science

Thesis for the degree of Doctor of Philosophy

Early Carboniferous Palynology and Tetrapod Evolution

by Emma Jane Reeves

Following the End Devonian Mass Extinction, the development of complex plant communities facilitated the evolution of terrestrial vertebrate animals (tetrapods). However, a gap in the fossil record (Romer's Gap) prevented the identification of the key anatomical features that enabled the study of tetrapod terrestriality.

As part of the interdisciplinary TW:eed project, palynomorphs from the NWMF borehole and Burnmouth outcrop section revealed the pattern of plant recovery and the changing palaeoenvironment of the Tournaisian.

Assigning an accurate biozonation to the new palynomorph data enabled the tetrapods to be relatively dated and incorporated into a time resolved cladistic analysis. Initially, the palynomorph distribution did not produce a clear biozonation, but applying the zonal indicator taxa from the published schemes of Higgs *et al.* (1988) and Turnau (1978) produced four palynozones: VI, HD, PC and CI.

The VI zone comprised simple survival flora, then the HD zone signified the beginning of the recovery vegetation. The first dominant plant, the r-selected lycopsid *Oxroadia conferta*, thrived in unstable conditions. Its decline marked the step-wise dominance of three K-selected inception taxa: *Genomosperma kidstoni* (pteridosperm), a putative medullosan pteridosperm, then *Stauropteris burntislandica* (fern). Concurrently, there was a continuous presence of two pteridosperms: *Lyrasperma scotica* (small shrub) and *Stamnostoma huttonense* (tree-sized) and an intermittent progymnosperm *Protopitys scotica*. This recovery shows how the Ballagan environment became populated by a diversity of plants that formed a structured ecosystem.

As palaeosols provide a record of changes in the climate and landscape architecture, comparing CONISS dendrograms for the palaeosols from the NWMF borehole core and the palynomorphs revealed a correlation. This showed, for the first time, that fossil soils and palynomorphs can be related directly. Additionally, the fluctuating relative abundances of the miospore *Schopfites claviger* defined repeated drier and wetter climatic intervals.

In summary, palynological evidence from the NWMF borehole and Burnmouth of the Tournaisian Ballagan Formation has demonstrated how the vegetation recovered after the End Devonian Mass Extinction event. Both the plant distribution and the soil formation were driven by changes in the climate, which generated a succession of vegetation types.

LIST OF CONTENTS

Abstract.....	iii
List of Figures	xv
Introduction	xv
Materials and methods	xvii
The palynomorphs	xx
Tournaisian biozonation.....	xxiii
Plant recovery	xxiii
Conclusions	xxvi
Appendix 1	xxvii
Appendix 2.....	xxvii
Appendix 3.....	xxviii
Appendix 17.....	xxx
List of Tables.....	xxxi
Introduction	xxxi
Materials and methods	xxxi
The palynomorphs	xxxi
Tournaisian biozonation.....	xxxii
Plant recovery	xxxii
Declaration of Authorship.....	xxxiii
Acknowledgements.....	xxxv
Abbreviations	xxxvii
 1. INTRODUCTION	 1
1.1. What are mass extinctions?	3
1.2. Comparing mass extinction events.....	5
1.2.1. Late Ordovician	5
1.2.2. End Permian	6
1.2.3. End Triassic	7
1.2.4. End Cretaceous	7
1.3. The End Devonian Mass Extinction (EDME)/Hangenberg Event	7
1.3.1. The EDME was different to other mass extinctions	9
1.3.2. Possible drivers of the EDME.....	10

1.3.2.1. Glaciation.....	12
1.3.3. The effects of the EDME	14
1.3.3.1. The effects of the EDME on terrestrial biotas	15
1.3.4. The evolution of terrestrial vegetation	15
1.3.4.1. Ordovician.....	15
1.3.4.2. Silurian.....	16
1.3.4.3. Devonian.....	16
1.3.4.4. Devonian–Carboniferous boundary	17
1.3.4.5. Carboniferous	17
1.3.5. The effects of the EDME on vertebrates	18
1.3.5.1. The fishes	18
1.3.5.1.1. Agnatha.....	19
1.3.5.1.2. Gnathostomata.....	20
1.3.5.2. The tetrapods.....	22
1.4. Tetrapod evolution.....	22
1.4.1. Summary of the skeletal adaptations of the tetrapods to life on land	23
1.4.1.1. The skull and jaws	24
1.4.1.2. Hearing	24
1.4.1.3. The neck.....	24
1.4.1.4. The fore limbs	24
1.4.1.5. The hind limbs	28
1.4.1.6. Scales	29
1.4.2. Trackways	29
1.4.3. The sequence of developments	31
1.5. Why the tetrapods made the transition onto land	33
1.6. Romer’s Gap	35
1.7. Tetrapod localities in Scotland.....	38
1.7.1. Burnmouth.....	39
1.7.2. Willie’s Hole.....	39
1.7.3. Coldstream.....	39
1.7.4. Tantallon	39
1.7.5. Dumbarton	39
1.8. The TW:eed project.....	40
1.8.1. The palaeontological framework.....	41

1.8.2.	The stratigraphical framework	41
1.8.3.	The palynological framework.....	41
1.8.4.	The sedimentological framework.....	42
1.8.5.	The isotopic framework	43
2.	MATERIALS AND METHODS	45
2.1.	Carboniferous geology	46
2.1.1.	Tectonic setting during the Tournaisian and Viséan.....	47
2.1.2.	Tournaisian climate	49
2.1.3.	Palaeogeography of the Tournaisian.....	49
2.1.4.	Principal lithofacies.....	50
2.1.4.1.	Continental and peritidal facies	50
2.1.4.2.	Volcanic facies	51
2.1.5.	The Ballagan Formation	51
2.1.5.1.	The Midland Valley of Scotland.....	52
2.1.5.2.	Northern England.....	53
2.2.	The Norham West Mains Farm borehole.....	54
2.2.1.	Borehole objectives	55
2.2.2.	Siting the borehole	56
2.2.3.	West Mains Farm, Norham	60
2.2.4.	Drilling the borehole	62
2.2.5.	Borehole core	63
2.2.6.	Decommissioning	64
2.2.7.	Drilling issues	65
2.3.	The Burnmouth outcrop section.....	65
2.4.	Palynomorphs.....	67
2.5.	Palaeosols	69
2.6.	Core sampling	71
2.6.1.	Sampling procedure	71
2.6.2.	Sampling for thin sections	73
2.7.	Processing palynological samples.....	76
2.8.	Residue and slides storage	79
2.9.	Microscopy and photomicroscopy	79
2.9.1.	Light microscopy (LM)	80

2.9.2. Infrared (IR) microscopy	81
2.9.3. Scanning Electron Microscopy (SEM)	84
2.10. Data collection	85
2.11. Data analysis	86
2.11.1. Range charts	86
2.11.2. Relative abundances	86
2.11.3. Principal Component Analysis (PCA)	87
2.11.4. Constrained Incremental Sum of Squares (CONISS).....	87
2.12. Image manipulation	87
2.13. The England Finder	88
2.14. Fossil sampling	88
2.15. Megaspores	89
2.16. Coal sample.....	91
2.16.1. Further analysis	92
2.16.1.1. Elemental analysis	93
2.16.1.2. Ash content	93
2.17. Scolecodont analysis	93
 3. THE PALYNOMORPHS	 97
3.1. Miospores/microspores	99
<i>Acinosporites</i> cf. <i>acanthomammillatus</i>	100
<i>Anaplanisporites baccatus</i> (Hoffmeister <i>et al.</i>) Smith & Butterworth 1967..	101
<i>Anaplanisporites centrosus</i> Higgs <i>et al.</i> 1988.....	103
<i>Anaplanisporites</i> sp. A	104
<i>Anaplanisporites</i> sp. B	105
<i>Apiculatisporis</i> sp. A	106
<i>Apiculiretusispora fructicosa</i> Higgs 1975.....	108
<i>Apiculiretusispora multiseta</i> (Luber) Butterworth & Spinner 1967.....	109
<i>Apiculiretusispora nitida</i> Owens 1971.....	111
<i>Apiculiretusispora</i> sp. A Higgs <i>et al.</i> 1988	112
<i>Auroraspora asperella</i> (Kedo) Van der Zwan 1980	113
<i>Auroraspora macra</i> Sullivan 1968	114
<i>Auroraspora solisorta</i> Hoffmeister <i>et al.</i> 1955.....	115
<i>Baculatisporites fusticulus</i> Sullivan 1968	118

<i>Bascaudaspora submarginata</i> (Playford) Higgs <i>et al.</i> 1988.....	119
<i>Calamospora nigrata</i> (Naumova) Allen 1965.....	121
<i>Calamospora perrugosa</i> (Loose) Schopf <i>et al.</i> 1944	122
<i>Calamospora</i> spp.	123
<i>Cingulizonates bialatus</i> (Waltz) Smith & Butterworth 1967.....	124
<i>Cingulizonates</i> sp. A.....	125
<i>Claytonispora distincta</i> (Clayton) Playford & Melo 2012.....	128
<i>Colatisporites decorus</i> (Bharadwaj & Venkatachala) Williams <i>In: Neves et al.</i> 1973	131
<i>Colatisporites denticulatus</i> Neville <i>In: Neves et al.</i> 1973	133
<i>Colatisporites?</i> <i>papillatus</i> Ravn 1991	135
<i>Convolutispora caliginosa</i> Clayton & Keegan <i>In: Clayton et al.</i> 1982	136
<i>Convolutispora circumvallata</i> Clayton 1970.....	137
<i>Convolutispora florida</i> Hoffmeister <i>et al.</i> 1955.....	138
<i>Convolutispora harlandii</i> Playford 1962	139
<i>Convolutispora major</i> (Kedo) Turnau 1978.....	139
<i>Convolutispora mellita</i> Hoffmeister <i>et al.</i> 1955	140
<i>Crassispora aculeata</i> Neville 1968	141
<i>Crassispora trychera</i> Neves & Ioannides 1974	143
<i>Crassispora</i> cf. <i>trychera</i>	144
<i>Cristatisporites bellus</i> Bharadwaj & Venkatachala 1961	145
<i>Cristatisporites echinatus</i> Playford 1963	147
<i>Cristatisporites indignabundus</i> (Loose) Staplin & Jansonius 1964	148
<i>Cristatisporites matthewsii</i> Higgs <i>et al.</i> 1988	149
<i>Cristatisporites menendezii</i> (Menéndez & Azcuy) Playford 1978	150
<i>Curculomonoletes orbis</i> McLean & Neves 2003.....	152
<i>Cymbosporites cyathus</i> Allen 1965	153
<i>Cymbosporites magnificus</i> (McGregor) McGregor & Camfield 1982	154
<i>Densosporites variomarginatus</i> Playford 1963	156
<i>Dictyotriletes fimbriatus</i> (Winslow) Kaiser 1970.....	157
<i>Dictyotriletes fragmentimurus</i> Neville <i>In: Neves et al.</i> 1973.....	158
<i>Dictyotriletes pactilis</i> Sullivan & Marshall 1966.....	159
<i>Dictyotriletes trivialis</i> Naumova <i>In: Kedo</i> 1963	159
<i>Discernisporites irregularis</i> Neves 1958	161

<i>Discernisporites macromanifestus</i> (Hacquebard) Higgs <i>et al.</i> 1988	162
<i>Discernisporites micromanifestus</i> (Hacquebard) Sabry & Neves 1971	163
<i>Discernisporites sullivanii</i> Higgs & Clayton 1984	165
<i>Endoculeospora gradzinskii</i> Turnau 1975	166
<i>Geminospora lemurata</i> (Balme) Playford 1983.....	168
<i>Grandispora echinata</i> Hacquebard 1957	169
<i>Grandispora microdecora</i> Phillips & Clayton 1980	171
<i>Granulatisporites pustulatus</i> Hacquebard & Barss 1957	172
<i>Insculptospora incrustata</i> (Arkhangelskaya) Marshall 1985	173
<i>Knoxisporites literatus</i> (Waltz) Playford 1963	175
<i>Knoxisporites polymorphus</i> (Naumova) Braman & Hills 1992	177
<i>Knoxisporites pristinus</i> Sullivan 1968	178
<i>Knoxisporites triangularis</i> Higgs <i>et al.</i> 1988.....	179
<i>Lophozonotriletes tuberosus</i> Sullivan 1964	180
<i>Monilospora mutabilis</i> (Staplin) Clayton <i>In: Neves et al.</i> 1973.....	181
<i>Pilosisporites verutus</i> Sullivan & Marshall 1966	183
<i>Plicatispora scolecophora</i> (Neves & Ioannides) Higgs <i>et al.</i> 1988.....	184
<i>Prolycospora claytonii</i> Turnau 1978	185
<i>Punctatisporites irrasus</i> Hacquebard 1957	187
<i>Punctatisporites? limbatus</i> Hacquebard 1957	188
<i>Punctatisporites planus</i> Hacquebard 1957	189
<i>Punctatisporites solidus</i> Hacquebard 1957	190
<i>Pustulatisporites dolbii</i> Higgs <i>et al.</i> 1988	191
<i>Raistrickia corynoges</i> Sullivan 1968	192
<i>Raistrickia cf. ponderosa</i>	193
<i>Retusotriletes incohatus</i> Sullivan 1964.....	195
<i>Retusotriletes rotundus</i> (Streel) Streel 1967	196
<i>Rugospora lactucosa</i> Higgs <i>et al.</i> 1988	197
<i>Rugospora vieta</i> Higgs <i>et al.</i> 1988.....	198
<i>Schopfites claviger</i> (Sullivan) Higgs <i>et al.</i> 1988.....	199
<i>Schopfites claytonii</i> Mahdi & Butterworth 1994.....	200
<i>Schopfites delicatus</i> (Higgs) Higgs <i>et al.</i> 1988	201
<i>Spelaeotriletes crustatus</i> Higgs 1975	203
<i>Spelaeotriletes microspinosus</i> Neves & Ioannides 1974	204

<i>Spelaeotriletes resolutus</i> Higgs 1975	205
<i>Velamispores corporatus</i> (Neves & Owens) Ravn 1991	207
<i>Velamispores minutus</i> (Neves & Ioannides) Ravn 1991	208
<i>Velamispores polyptychus</i> (Neves & Ioannides) Ravn 1991	209
<i>Verrucosisporites baccatus</i> Staplin 1960.....	211
<i>Verrucosisporites congestus</i> Playford 1963	212
<i>Verrucosisporites depressus</i> Winslow 1962	213
<i>Verrucosisporites gibberosus</i> (Hacquebard) Higgs <i>et al.</i> 1988.....	213
<i>Verrucosisporites irregularis</i> Philips & Clayton 1980	214
<i>Verrucosisporites nitidus</i> Playford 1963	215
<i>Verrucosisporites scoticus</i> Sullivan 1968	218
 3.2. Megaspores.....	219
<i>Didymosporites scottii</i> Chaloner 1958	219
<i>Laevigatisporites cf. cheveriensis</i> (Bell) Glasspool & Scott 2005	221
<i>Lagenicula mixta</i> (Winslow) Wellman <i>et al.</i> 2009	222
<i>Setispora pannosa</i> (Alvin) Spinner 1982	223
<i>Setispora pseudoreticulata</i> (Butterworth & Spinner) Spinner 1982	224
<i>Setosisporites</i> sp. A.....	225
<i>Triangulatisporites membranatus</i> Butterworth & Spinner 1967	227
<i>Tuberculatisporites mamillarius</i> (Bartlett) Potonié & Kremp 1955	228
Spore Type D Spinner 1983	229
 3.3. Pollen	229
<i>Remysporites magnificus</i> (Horst) Butterworth & Williams 1958.....	230
 3.4. Acritarchs	231
<i>Acanthotriletes socraticus</i> Neves & Ioannides 1974.....	232
<i>Carbaneuletes cf. micromuratus</i>	233
 3.5. Euglenoids.....	234
<i>Chomotriletes multivittatus</i> Playford 1978	234
<i>Chomotriletes vedugensis</i> Naumova 1953	235

3.6. Scolecodonts	236
Plate 1	238
Plate 2.....	240
Plate 3.....	242
Plate 4.....	244
Plate 5.....	246
Plate 6.....	249
 4. TOURNAISIAN BIOZONATION	251
4.1. Challenges.....	251
4.1.1. The NWMF borehole did not encompass the entire Ballagan Fm	251
4.1.2. The new data did not fit published Tournaisian biozonation schemes....	252
4.2. Correlation to published biozonation schemes	254
4.2.1. The zonation scheme of Higgs <i>et al.</i> (1988).....	254
4.2.2. The zonation scheme of Turnau (1978)	257
4.3. The newly proposed biozonation scheme for the Tournaisian.....	262
 5. PLANT RECOVERY	265
5.1. Principal Component Analysis (PCA)	265
5.2. Relative abundances	266
5.3. Plant affinities	268
5.4. The dominant plants of the Ballagan environment.....	268
5.4.1. <i>Oxroadia conferta</i> Bateman 1992.....	268
5.4.2. <i>Genomosperma kidstoni</i> (Calder) Long 1960.....	269
5.4.3. Putative Medullosan pteridosperm	271
5.4.4. <i>Stauropteris burntislandica</i> Bertrand 1909	272
5.5. Other plants of the Ballagan environment	274
5.5.1. <i>Lyrasperma scotica</i> (Calder) Long 1960	274
5.5.2. <i>Stamnostoma huttonense</i> Long 1960.....	275
5.5.3. <i>Protopitys scotica</i> Walton 1957	276
5.6. Summary	277
5.7. Palaeoenvironment – Introduction	277
5.7.1. Constrained Incremental Sum of Squares (CONISS).....	278

5.8. <i>Schopfites claviger</i>	281
5.9. Palaeosols	282
5.9.1. Palaeosols and palynomorphs	283
5.10. Roots	285
5.11. Anastomosing river channels	286
5.11.1. The evolution of anastomosing river channels	288
5.12. Megaspores analysis	289
5.13. Coal analysis	291
5.13.1. Megaspore content.....	292
5.13.2. Further analyses	294
5.13.3. Conclusions.....	295
5.14. Scolecodonts	296
5.15. Summary	297
 6. CONCLUSIONS	 299
 Appendix 1: TW:eed project team staff profiles.....	 305
Appendix 2: Work Instruction: Sampling procedure	315
Appendix 3: Work Instruction: Processing palynological samples.....	319
Appendix 4: Work Instruction: Canon EOS 70D operating instructions.....	351
Appendix 5: Work Instruction: Olympus Stream (Basic) operating instructions ..	353
Appendix 6: Work Instruction: Infrared microscope set up	355
Appendix 7: Work Instruction: Using Tilia software to produce range charts	359
Appendix 8: Work Instruction: Using Tilia software to relative abundance charts	361
Appendix 9: Work Instruction: Using PAST software to perform a Principal Component Analysis (PCA).....	363
Appendix 10: Work Instruction: Using Tilia software to perform a Constrained Incremental Sum of Squares (CONISS) analysis	365
Appendix 11: Work Instruction: Using Photoshop software to manipulate microphotographs.....	369
Appendix 12: Work Instruction: Fossil sampling.....	371
Appendix 13: Work Instruction: Megaspore picking	373
Appendix 14: Work Instruction: Using the ultrasonic probe to remove AOM from palynology samples that contained scolecodonts.....	375

Appendix 15: Work Instruction: Using Tilia to plot scolecodonts data	377
Appendix 16: Work Instruction: Calculating Van Krevelen values.....	379
Appendix 17: International Chronostratigraphic Chart	381
Appendix 18: Suprageneric classification of the NWMF borehole palynomorphs	383
Appendix 19: List of additional identified palynomorphs not included in the 'Systematic description' section.....	391
Appendix 20: List of Accompanying Material	395
 List of references	 397

LIST OF FIGURES

INTRODUCTION

Figure 1. Total extinction rate (extinctions per million years) through time for families of marine invertebrates and vertebrates. The plot shows statistically significant mass extinctions in the late Ordovician (ASHG), Permian (GUAD-DZHULF), Triassic (NOR) and Cretaceous (MAEST). An extinction event in the late Devonian (GIV-FRAS-FAME) was considered to be noticeable but not statistically significant. Circled points are those where the departure from the main cluster is highly significant. Xs indicate those cases where inclusion of Lagerstätten substantially increases the calculated extinction rate (the point directly below the X is the rate calculated without the Lagerstätten data). The figure also shows a general decline in background extinction rate through time. The regression line is fit to the 67 points having extinction rates less than eight families per 10^6 years, and the dashed lines define the 95 percent confidence band for the regression. Abbreviations: TEM = Templetonian, ASHG = Ashgillian, SIEG = Siegenian, GIV = Givetian, FRAS = Frasnian, FAME = Famennian, MOSC = Moscovian, GUAD = Guadeloupian, DZHULF = Dzhulfian, NOR = Norian, TITH = Tithonian, MAEST = Maestrichtian. From Raup & Sepkoski (1982).

Figure 2. Stratigraphical correlation scheme for the Hangenberg Event, DCB and relative sea-level change. After Kaiser (2005).

Figure 3. Time-rock transect showing transgressions and regressions from Early Devonian to early Carboniferous time in the Rhenish Slate Mountains. From Johnson *et al.* (1985). Note that the Liegende Alaunschiefer (Lower Alum Shale) and Hangenberg Sandstone (highlighted) are also shown on Figure 2.

Figure 4. An overview of diamictite occurrences from Bolivia, Brazil and the Appalachian Basin and their stratigraphic position. After Lakin *et al.* (2016).

Figure 5. Phylogenetic tree of the major living and fossil jawless vertebrate groups. This tree suggests that prior to the appearance of the mineralised skeletal elements of ostracoderms, vertebrates had no mineralised tissues and could only be fossilised in exceptional circumstances as shown by fossils such as

those discovered by Shu *et al.* (1999; asterisks) in the Chengjiang Lagerstätte, China. BP = before present. After Petrou & Zappitidis (2016).

Figure 6. Gnathostome generic level diversity curves for the Givetian to Serpukhovian. From Sallan & Coates (2010).

Figure 7. Diversity patterns in marine fishes during the Phanerozoic. Vertical dashed lines represent the 'Big Five' extinctions of Raup & Sepkoski (1982): Ord. = end Ordovician, FF = Frasnian-Famennian, PTB = Permian-Triassic Boundary, TJB = Triassic-Jurassic Boundary and KTB = Cretaceous-Tertiary Boundary. The DCB has been added. The chart illustrates generic richness divided into traditional groupings (conodonts, ostracoderms, placoderms, acanthodians, chondrichthyans and osteichthyans). After Friedman & Sallan (2012).

Figure 8. Fore limbs and humeri of fossil tetrapodomorphs. The top row shows fore limbs or humeri in dorsal view. The bottom row shows humeri in ventral view, note the direction and orientation of the ventral ridge (vr) which changes from passing diagonally across the bone (*Eusthenopteron* through to *Tiktaalik*) to running more or less transversely across the bone (ANSP 21350 through to *Tulerpeton*). Abbreviations: dpc = deltopectoral crest, ectep = ectepicondyle, entep = entepicondyle, for = foramina, ra = radius, ul = ulna, vr = ventral ridge. Not to scale. From Clack (2009).

Figure 9. The skeletons of *Eusthenopteron* (top), *Panderichthys* (middle) and *Acanthostega* (bottom) shown in lateral aspect to demonstrate the fish to tetrapod morphological transition. From Coates *et al.* (2008).

Figure 10. Devonian tetrapod trackways. A. Two adjacent tracks from Genoa River. Arrow shows direction of travel. Scale bar = 50 mm. B. Hoy track. Scale bar = 10 mm. C. Glen Isla tracks. D. Tarbat Ness tracks. E. Short section of the Valentia Island tracks. F. Short section of one of the Kap Graah tracks. Scale bars for C to F = 100 mm. From Clack (1997).

Figure 11. Cladogram of the key tetrapodomorphs and limbed tetrapods with their major evolutionary advances to the right. From Clack (2009).

Figure 12. Geochronologic range data for terrestrial arthropod and vertebrate clades. Major arthropod clades: Myriapoda (yellow), Arachnida (red) and Hexapoda (purple) are divided into orders. Limbed vertebrates are in green and Romer's Gap in orange. Two separate colonisations onto land are

shown. Phase 1 involved the arthropods initially (Phase 1A) followed by the first tetrapods (Phase 1B). Phase 2 comprised new major originations and radiations of terrestrialised arthropods and limbed vertebrates. Penn = Pennsylvanian, E = Early, M = Mid, L = Late. After Ward *et al.* (2006).

Figure 13. The approximately 30 million year gap in the fossil record between the Tournaisian and the early part of the Viséan, later dubbed ‘Romer’s Gap’, that spanned the transition of aquatic tetrapodomorphs of the Devonian and the fully terrestrial tetrapods of the early Carboniferous. The hatched portions of the squares in the last two columns entitled ‘To 1900’ and ‘1955’ indicate the amount of data regarding tetrapods that was then available. From Romer (1956).

Figure 14. Map of southern Scotland and northern England showing the locations of the Tournaisian sites in Scotland. From Smithson *et al.* (2012).

MATERIALS AND METHODS

Figure 15. Palaeogeographic reconstruction showing the continental distribution during the early Carboniferous (Viséan) with Great Britain highlighted in red. From Scotese & McKerrow (1990).

Figure 16. Principal structural features of the British Isles, onshore and offshore, that exerted a significant influence on the deposition of Carboniferous strata. The depositional basins and highs shown are those that developed during the Tournaisian to Viséan. BH = Bowland High, CLH = Central Lancashire High, DH = Derbyshire High, EG = Edale Gulf, GB = Gramscatho Basin, HB = Humber Basin, LDH = Lake District High, MH = Manx High, NDB = North Devon Basin, MVS = Midland Valley of Scotland, SDB = South Devon Basin. The location of the NWMF borehole and Burnmouth outcrop section in the Tweed Basin are marked with a red square. After Waters *et al.* (2007).

Figure 17. The Kinnesswood, Ballagan and Clyde Sandstone formations comprising the Inverclyde Group. After McLean & Neves (2003) and Marshall *et al.* (2019).

Figure 18. Early Carboniferous stratigraphies for the Midland Valley of Scotland and the Northumberland and Solway basins. KCBV = Kelso, Cottonshope

and Birrenswark volcanic formations, W = Whita Sandstone Member. After Waters *et al.* (2011).

Figure 19. Outcrop and subcrop map of Tournaisian rocks in the Midland Valley of Scotland and the Tweed and Northumberland-Solway basins. These strata include the Ballagan Formation and part of the Lyne Formation in the latter basin. Major boreholes and the thickness of the formation are shown. The Burnmouth outcrop and Norham (NWMF) borehole localities are highlighted in yellow. From Millward *et al.* (2018).

Figure 20. Summary lithological logs and environmental interpretations for selected boreholes in the east of the Midland Valley of Scotland. Borehole locations are shown in Figure 19. From Millward *et al.* (2018).

Figure 21. Summary lithological logs and environmental interpretations for selected boreholes in the west and north of the Midland Valley of Scotland. Borehole locations are shown in Figure 19. The black curves within the stratigraphic columns represent the proportional thickness of grey, laminated siltstone/mudstone per 10 m interval through each succession. From Millward *et al.* (2018).

Figure 22. Aerial photograph of West Mains Farm. From [google.co.uk/maps](https://www.google.co.uk/maps).

Figure 23. Location map of the Ballagan Formation outcrops (green), Norham West Mains Farm borehole and Burnmouth outcrop sites. After Kearsley *et al.* (2016).

Figure 24. Photograph of the drilling rig in operation at West Mains Farm with some of the core in wooden transport boxes. Courtesy of Sarah Davies 2016.

Figure 25. Photograph of a small bay in the Burnmouth cliffs showing the almost vertical bedding. From tetrapods.org.

Figure 26. Sedimentary logs of sections from Burnmouth and the Norham (NWMF) borehole. After Kearsley *et al.* (2016).

Figure 27. Locations of the palynology samples that were processed from the Norham (NWMF) borehole core. Based on Kearsley *et al.* 2016.

Figure 28. Sedimentary log (left-hand side) and variation in the thickness and distribution of the four pedotypes (right-hand side) through the Norham (NWMF) borehole core. The length of each horizontal line represents the thickness of that palaeosol, and, so, also signifies their net accumulation (i.e.

the duration of soil formation processes minus later erosion). After Kearsey *et al.* (2016).

Figure 29. Photograph of a box of core from the NWMF borehole showing the box's starter depth in the top right-hand corner.

Figure 30. Photographs of the tools used to sample the NWMF borehole core.

Figure 31. Photograph of the bench vice used to split sediments of moderate hardness.

Figure 32. Photograph of the pneumatic jack used to split hard sediments.

Figure 33. A summarised flow diagram of the standard acid preparation techniques that were used to process the palynological samples from the NWMF borehole core.

Figure 34. Photograph of the Olympus BH-313 light microscope (number: 210685) with an Olympus SC30 3 Megapixel camera mounted on a trinocular head.

Figure 35. Photograph of the PC monitor with the Olympus Stream (Basic) photomicroscopy software loaded showing a live image of a *Plicatispora scolecophora* miospore at x100 on the Olympus BH-313 light microscope in Figure 34.

Figure 36. Photograph of the infrared microscopy setup.

Figure 37. Photograph of the analogue video digitizer to output digital images from analogue signal.

Figure 38. Photomicrographs of a fragment of *Setispora pseudoreticulata* using light on the left and infrared on the right (x100 oil immersion). The IR image highlights the characteristic reticulate pattern of this species. Scale bar = 200 μm .

Figure 39. Photograph of gold-coated specimens on SEM stubs ready to be examined in the scanning electron microscope at NOCS (on the left hand side) and a diagram of the contents of each stub (on the right hand side).

Figure 40. Photograph of the Carl Zeiss Leo 1450VP SEM with Oxford Instruments Energy Dispersive Spectrometer at the University of Southampton. From <https://cdn.southampton.ac.uk>.

Figure 41. Diagram of a section of an England Finder slide (left hand side) with a cartoon example of a spore with the co-ordinates: A17/4 on the right-hand side.

Figure 42. Photograph of the equipment used to hand pick megaspores from a wet residue.

Figure 43. Photograph of me (ER) intently hand-picking megaspores from a wet residue.

Figure 44. Photograph of the coal sample taken from the NWMF borehole core.

Figure 45. Photograph of the ultrasonic probe used to remove extraneous AOM from palynomorph samples that contained scolecodonts.

THE PALYNOMORPHS

Figure 46. (a) Verrucae with spinae and (b) coni of *Acinosporites* cf. *acanthomammillatus*.

Figure 47. (a) Pila and (b) to (d) spinae of *Anaplanisporites centrosus*.

Figure 48. (a) Spinae and (b) grana of *Anaplanisporites* sp. A.

Figure 49. Pila of *Anaplanisporites* sp. B.

Figure 50. (a) to (b) sharp-tipped and (c) to (d) blunt-tipped spinae of *Apiculiretusispora multiseta*.

Figure 51. Spinae of *Apiculiretusispora nitida*.

Figure 52. X-Y scatter plot of the diameters of the intexines and the exoexines for the three most commonly occurring species of *Auroraspora* identified from the NWMF borehole core with Standardised Major Axis applied and r^2 values given.

Figure 53. (a) to (c) spinae (d) inner body clava (e) and (f) outer body spinae (g) and (h) central and (i) outer clava of *Cingulizonates bialatus*.

Figure 54. Diagram to define the structures of *Cingulizonates* sp. A. The 'bizonate cingulum' comprises the cingulum and the zona.

Figure 55. (a) Clava (b) to (c) baculi (d) spinae and (e) coni of *Cingulizonates* sp. A.

Figure 56. Examples of the morphological differences between the apiculate elements of *Umbonatisporites variabilis* Hibbert & Lacey 1969 (A, B is an expansion of the element circled in A) and *Claytonispora distincta* (Clayton) Playford & Melo 2012 (C, D is an expansion of the element circled in C). After Playford & Melo (2012).

Figure 57. Tubercles of *Claytonispora distincta* from the NWMF borehole core. (a)

Elongate with a disc and surmounted by a spina (b) elongate with terminal constriction, disc and surmounted by a spina. Specimen sample number, slide and E. F. co-ordinates: (a) SSK37853, 129.0, 06.8, U29/0 (b) SSK37853, 117.9, 15.6, L17/4.

Figure 58. Pila of *Colatisporites papillatus*.

Figure 59. (a) and (b) spinae and (c) biform elements of *Crassispora aculeata*.

Figure 60. (a) Pila and (b) bacula of *Crassispora trychera*.

Figure 61. (a) Pila and (b) bacula of *Crassispora* cf. *trychera*.

Figure 62. Diagram to define the parts of *Cristatisporites* miospores.

Figure 63. Diagram to define the dimensions of *Cristatisporites bellus*.

Figure 64. (a) to (d) spinae (e) to (i) verrucae (j) clava (k) edge coni (l) central pila (m) to (q) various sculptural elements (r) spinae on some verrucae (s) spinae, (t) to (v) outer spinae (w) inner spinae and (x) centre spinae of *Cristatisporites bellus*.

Figure 65. (a) to (b) spinae and (c) pila of *Cristatisporites echinatus*.

Figure 66. (a) and (b) outer body spinae and (c) coni (d) and (e) central body bacula and (f) verrucae and (g) spinae of *Cristatisporites indignabundus*.

Figure 67. (a) to (b) simple spinae and (c) to (d) spinae surmounting coni of *Cristatisporites matthewsii*.

Figure 68. (a) to (b) verrucae (c) and (d) spinae surmounting verrucae and (e) to (g) spinae of *Cristatisporites menendezii*.

Figure 69. (a) Sharp-topped (b) round-topped and (c) flat-topped spinae and (d) clava of *Cymbosporites cyathus*.

Figure 70. (a) and (b) verrucae (c) and (d) spinae (e) clava and (f) to (h) other sculptural elements of *Cymbosporites magnificus*.

Figure 71. Shape of the tall muri of *Dictyotriletes pactilis*.

Figure 72. Ridge muri of *Discernisporites irregularis*.

Figure 73. (a) Grana base and (b) to (g) grana, pila and bacula of *Endoculeospora gradzinskii*.

Figure 74. (a) to (c) broad-based spinae (d) tapering and (e) recurved spinae of *Grandispora echinata*.

Figure 75. (a) to (c) spinae and (d) pila of *Grandispora microdecora*.

Figure 76. Diagram to explain the dimensions of the grana of *Granulatisporites pustulatus*.

Figure 77. (a) to (i) various sculptural elements and (j) to (m) broader-based sculptural elements of *Knoxisporites polymorphus* with coalesced bases resembling an irregular cingulum.

Figure 78. Verrucae of *Lophozonotriletes tuberosus*.

Figure 79. (a) Bacula (mostly) and (b) spinae (few) of *Pilosporites verutus*.

Figure 80. Various shaped verrucae of *Prolycospora claytonii*.

Figure 81. Various shaped verrucae of *Pustulatisporites dolbii*.

Figure 82. Various shaped spinae of *Raistrickia corynoges*.

Figure 83. Diagram to define the dimensions of the clava of *Raistrickia* cf. *ponderosa*.

Figure 84. Examples of the shapes of the clava of *Raistrickia* cf. *ponderosa*.

Figure 85. Grana of *Retusotriletes rotundus*.

Figure 86. Diagram to define the dimensions of the clava of *Schopfites claviger*.

Figure 87. (a) Pila and (b) clava of *Schopfites claytonii*.

Figure 88. Comparison of the morphology of (a) the clava of *Schopfites claviger* and (b) the pila of *Schopfites delicatus*.

Figure 89. Comparisons of the sizes of the pila of *Schopfites delicatus* and the clava of *S. claviger* (in μm).

Figure 90. Verrucae of *Verrucosisporites congestus*.

Figure 91. Various shaped verrucae of *Verrucosisporites gibberosus*.

Figure 92. Irregular verrucae of *Verrucosisporites irregularis*.

Figure 93. (a) and (b) verrucae of *Verrucosisporites nitidus*.

Figure 94. Verrucae of *Verrucosisporites scoticus*.

Figure 95. Diagram to define the dimensions of the spinae with expanded bases of *Acanthotriletes socraticus*.

Figure 96. (a) Most common (b) few (c) some and (d) sparse spinae (e) to (i) examples of the variability of the spinae and (j) to (n) spinae with expanded bases of *Acanthotriletes socraticus*.

TOURNAISIAN BIOZONATION

Figure 97. Two key spore taxa, *Anaplanisporites baccatus* (in blue) and *Prolycospora claytonii* (in red), were used to splice together the NWMF borehole and the Burnmouth outcrop to obtain a complete record of the Ballagan Formation (produced by John Marshall 2017).

Figure 98. Chart of the ranges of the 105 identified palynomorphs that represent >9 specimens/taxon from the NWMF borehole core (see Chapter 3).

Figure 99. The miospore biozones and their characteristic taxa of Higgs *et al.* (1988) with the Tournaisian biozones coloured. From Higgs *et al.* (1988).

Figure 100. Range chart (presence-absence) of the distribution of the diagnostic taxa used to define the palynozones of Higgs *et al.* (1988) that were present in the NWMF borehole core. The colour changes denote the start of each biozone.

Figure 101. The miospore biozones and their characteristic taxa of Turnau (1978) with the Carboniferous Tournaisian biozones coloured. After Turnau (1978).

Figure 102. Range chart (presence-absence) of the distribution of the spores used to define the palynozones of Turnau (1978) that were present in the NWMF borehole core. The colour changes denote the start of each biozone.

Figure 103. Chart to show the varying relative abundances of *A. baccatus* (= *Oxroadia conferta* plant) and *P. claytonii* (= *Genomosperma kidstoni* plant) and how their peaks never overlap indicating a mutually exclusive relationship (see Sections 5.4.1 and 5.4.2 for details of the plant affinities).

Figure 104. Comparing the biozones for the Burnmouth outcrop (left) and the NWMF borehole core (right) to encompass the entire 12 million years of the Tournaisian Ballagan Formation.

PLANT RECOVERY

Figure 105. The results of the PCA of palynomorphs from the NWMF borehole core identified 8 outgroup taxa which are labelled.

Figure 106. The fluctuating relative abundances (by percentage of sample) of 12 significant palynomorph taxa from the NWMF borehole core used to illustrate

the plant recovery in the Ballagan environment. Eight taxa represent the PCA outgroup (in green and blue) and four taxa with recognised botanical affinities (in red). Greater peaks indicate higher abundance and the depth is stratigraphically constrained.

Figure 107. A. Microphotogrammetry of a *Genomosperma kidstoni* nucellus (central part of ovule) x4, slide FSC1116 K5 housed in the Albert Long Collection at the Hunterian Museum, Glasgow with the pollen chamber circled in red. B. Close up of the pollen chamber of A with spore C of Figure 108 circled in red.

Figure 108. Photomicrograph of *Prolycospora claytonii* spores inside an ovule of *Genomosperma kidstoni* housed in the Albert Long Collection at the Hunterian Museum, Glasgow. The x inside A highlights the infragranular sculpture of the proximal face. The arrow in D indicates the outline of the verrucae on the distal face. A and B slide FSC1100, C and D slide FSC1116 K5. Scale bars = 10 μ m.

Figure 109. A to D photomicrographs of *Curriculomonoletes orbis* from the NWMF borehole core and E to F *Monoletes* (=Schopfipollenites) pollen grains to compare their morphological similarities. A to D slide details and England Finder co-ordinates given: A and B = 421.68 m depth (picked megaspores slide), 123.7, 09.3, S23/2 and 106.8, 19.8, F5/4 respectively. C and D = 475.82 m depth (megaspores strew slide), 118.7, 23.2, C18/0 and 110.7, 22.0, E10/0 respectively. Scale bars = 50 μ m. E Proximal surface of *Monoletes* pollen grain showing median deflection of suturae. F Distal surface of *Monoletes* pollen. Scale bars = 100 μ m. From Taylor *et al.* (2009 p. 592, figures 14.153 and 14.154 respectively).


Figure 110. A summary diagram of the plant recovery interpreted from relative palynomorph abundance of the Tournaisian Ballagan environment. The DCB is shown at the base with the VI-HD biozones boundary above. On the left-hand axis are the Burnmouth outcrop heights (red) and NWMF borehole depths (black). The spindle plots (centre) show the relative abundances of the dominant plants (wider shape = higher abundance). A summary description of the changing dominant plants is listed on the right-hand side.

- Figure 111. Photomicrograph of part of the ovule of *Lyrasperma scotica* (slide FSC1411 Albert Long Collection, Glasgow) containing multiple specimens of *Colatisporites denticulatus* highlighted in red. Magnification x4.
- Figure 112. Photomicrograph of part of an ovule of *Stamnostoma huttonense* (slide FSC1148 Albert Long Collection, Glasgow) containing multiple specimens of *Colatisporites decorus* highlighted in red circles. Magnification x10.
- Figure 113. Three grains of *Remysporites magnificus* from the *Protopitys scotica* type slide FSC1372 at the Hunterian Museum, Glasgow. A. Laevigate *Punctatisporites*-type inner body. B. Laevigate *Punctatisporites*-type inner body (left-hand side) with laevigate to finely sculptured exine partially surrounding the inner body (right-hand side). C. Complete specimen of *R. magnificus* with the laevigate inner body (centre) inside the laevigate to finely sculptured exoexine.
- Figure 114. Simple non-depth constrained chart of the total number of spore taxa per NWMF borehole core sample with possible groupings indicated by the red brackets.
- Figure 115. Chart of the fluctuating relative abundances of 12 significant spore taxa by depth (m) used to illustrate the plant recovery in the Ballagan environment. A CONISS dendrogram (on the right-hand side) identifies distinctive natural assemblages of spores.
- Figure 116. Figure 115 with horizontal lines added to signify that the spore clusters produced by the CONISS analysis could be further grouped.
- Figure 117. Extract from Figure 116 showing the fluctuating relative abundance of *Schopfites claviger* from the NWMF borehole core. The grouped clusters produced a good match with greater relative abundance indicating drier conditions (shaded in yellow).
- Figure 118. The occurrences (by depth) and thicknesses (horizontal length) of the palaeosols from the NWMF borehole core (left-hand side; after Kearsley *et al.* 2016) with CONISS dendrogram (right-hand side) to show the clusters of distinctive natural assemblages.
- Figure 119. A comparison of the CONISS dendrograms for the palaeosols and the palynomorphs from the NWMF borehole.

- Figure 120. Photograph of a large *in situ* axis of *Stigmaria ficoides* from the Burnmouth outcrop section, British National Grid reference: NT 95797 60944. Note the spiral rootlet bases highlighted inside the red rectangle.
- Figure 121. Fluvial sandstones (outlined in black) at Burnmouth. Scale bar = 100 m. Courtesy of Sarah Davies 2016.
- Figure 122. Summary diagram of the plant recovery of the Tournaisian Ballagan environment (Figure 110) with the location of the fluvial sandstone bodies at the Burnmouth outcrop that are interpreted as anastomosing river channels highlighted in blue.
- Figure 123. The distribution and relative abundances of the megaspores from the NWMF borehole core with a CONISS dendrogram. The two megaspore phases and the megaspore-free interlude are annotated.
- Figure 124. Figure 123 with the drier climatic phases from the *Schopfites claviger* miospore data shaded in yellow (see Section 5.8). The location of a thin coal horizon representing *in situ* peat is also shown (see Section 5.13).
- Figure 125. Log of a coal horizon at 256.10 m depth in the NWMF borehole core. From Kearsey *et al.* (2016).
- Figure 126. Megaspores isolated from the coal seam of the NWMF borehole core. 1. *Setispora pannosa*. Scale bar = 50 μm . 2. A mass of *Anaplanisporites baccatus* (the microspore of *S. pannosa*). 3. *Didymosporites scottii* tetrad. Scale bars = 20 μm .
- Figure 127. A PCA of the megaspores from the coal horizon of the NWMF borehole core revealed two outgroup taxa (*Setispora pannosa* and *Didymosporites scottii*).
- Figure 128. Van Krevelen diagram with the H/C and O/C atomic ratios of the coal sample from the NWMF borehole core (256.10 m) marked as a red circle. After Flores (2014).
- Figure 129. The distribution and numbers of scolecodonts identified in palynological samples from the NWMF borehole core.

CONCLUSIONS

- Figure 130. Summary of the floral recovery of the Tournaisian Ballagan environment. The DCB is shown at the base. The VI-HD biozones boundary

is shown above. On left-hand side are the Burnmouth outcrop heights (red) and the NWMF borehole depths (black) shown in metres. The spindle diagrams represent the relative abundances (wider shape = higher abundance) of the dominant plants. On the left-hand side are the inceptions of *O. conferta*, a putative medullosan pteridosperm, *S. burntislandica* and *G. kidstoni* (the key to the plant icons is at the top of the diagram), the heights of the Lepidodendroid roots () , tetrapods and anastomosing river channels (A) found at outcrop and the depth of the coal horizon from the NWMF borehole core. The blue squares denote the borehole samples that contained scolecodonts. The spore diversity curve is shown beneath the sandstone body. The two phases of the megaspores' distribution are shown on the right-hand side. A summary description of the changing dominant plants is listed to the far right. The drier climatic intervals are shaded yellow.

APPENDIX 1

Figure 131. Organisational diagram to show the relationships between the core TW:eed team members and the project frameworks.

APPENDIX 2

Work Instruction: Sampling procedure

Figure 132. Photograph of the field notebook being completed during sampling with the BGS reference number (e.g. SSK38186), the measurement of the base of the sample from the base of the core box, the depth that measurement represented in the borehole, any further information e.g. TS only = sample taken for thin section only.

Figure 133. A bag containing a sedimentary sample taken from the core where: P indicated it was a palynological sample, SSK39199 was the BGS borehole sample number, 826 was the BGS database number (i.e. the NWMF borehole was number 826), 74.99 was the depth of the sample in metres.

APPENDIX 3

Work Instruction: Processing palynological samples

Figure 134. Me wearing basic laboratory attire.

Figure 135. Photograph of the 'Palynology Processing Book' that was completed before processing palynological rock samples (top) and the details that were entered (bottom).

Figure 136. Hammer (Draper 1 lb on left-hand side) and metal block (right-hand side) used to crush rock samples to pea-sized chips before processing.

Figure 137. Ohaus balance used to weigh rock samples before processing.

Figure 138. Numbered bags of crushed rock samples (at the bottom) to be placed into the correspondingly numbered containers (at the top) before processing.

Figure 139. Adding the numbered rock sample to the correspondingly numbered container before processing.

Figure 140. Containers with rock samples to be processed.

Figure 141. Photograph of numbered containers with rock samples in the fume cupboard prior to processing.

Figure 142. Photograph of numbered containers with rock samples in the fume cupboard during processing using hydrochloric acid.

Figure 143. Photograph of the emergency shower and eye wash station in the Palynology Processing Laboratories at NOCS for use in case of extensive exposure of naked skin or the eyes to hydrofluoric acid.

Figure 144. Photograph of the Calgonate® emergency first aid kit that contains a 2.5% topical calcium gluconate gel to treat HF burns.

Figure 145. Photograph of me gripping a section of the water hose to increase the pressure to rinse the HF acid from the rock sample.

Figure 146. Photograph of numbered containers with rock samples in the fume cupboard during processing using hydrofluoric acid.

Figure 147. Me carefully pouring off the HF acidified water, taking care not to disturb the residue.

Figure 148. Photograph of the 3 sizes of sieves (with their diameter in cm) used to concentrate the residue from palynomorph processing before storage in vials.

Figure 149. Photograph of the large sieve after it has been taken apart.

- Figure 150. Photograph of the elasticated grey stand used to house the medium sieve to enable it to drain while setting the next sample to boil.
- Figure 151. Photograph of the laboratory water pump attached to the water tap inside a fume cupboard.
- Figure 152. Boiling residue in hydrochloric acid to remove fluorides formed during processing with hydrofluoric acid.
- Figure 153. Photographs of the dishwasher used to clean containers, lids and beakers used in palynological processing – door closed (left hand side) and door open (right hand side).
- Figure 154. Photograph of the Brother QL-570 label printer used to label vials and slides containing palynological specimens.
- Figure 155. Photograph of the PC in the Palynology Processing Laboratories with P-touch Editor software showing a blank vial label on the screen.
- Figure 156. Photograph of the clamp and pipette used to transfer palynological residues into vials.
- Figure 157. Photograph of processed palynological samples from the NWMF borehole core that have been transferred to labelled vials.
- Figure 158. Photograph of a squeeze bottle containing deionised water with a narrow nozzle attachment.
- Figure 159. Screen shot of part of the NWF_Paly sampling_MASTER.xls database that included details of which samples had been processed for palynomorphs, a very basic list of what each sample contained e.g. wood, spores, minerals (samples that had been top-sieved for megaspores were additionally annotated with '150 =' and then the contents e.g. wood, spores) and diary-style entries of which processing steps each batch had received.
- Figure 160. Photograph of vials containing NWMF borehole core samples, grouped into processing batches of 15. The lids are marked with the batch number and the relative quantity of palynomorphs contained within (None/Few/Lots). Vials that contain megaspores are annotated with 'MEGA' and were also top-sieved.
- Figure 161. Photograph of a metal vial rack with palynological samples in vials.
- Figure 162. Photograph of a slide tray with numbered segments to place coverslips containing palynological samples during drying before being made into permanent slides.

Figure 163. Photograph of a slide containing palynomorphs from the NWMF borehole core.

APPENDIX 17

Figure 164. International Chronostratigraphic Chart (2018) indicating the Ages, Epochs, Periods, Eras and Eons of all geological time. From stratigraphy.org.

LIST OF TABLES

INTRODUCTION

Table 1. Magnitudes of mass extinctions (by percentage at the family level) for different subsets, indicated as the percent decreases in diversity based on unequivocal stratigraphic and habitat data. From Benton (1995).

Table 2. Devonian biotic crisis events. From Kaiser (2005).

Table 3. Locations and ages of Devonian tetrapod trackways (see Figure 10).

MATERIALS AND METHODS

Table 4. A summary of the lithological characteristics and depositional environments for the three formations of the Inverclyde Group. From Waters *et al.* (2007).

Table 5. Summary of the thickness of the Ballagan Formation with the units above and below in selected BGS boreholes (shown on Figure 19). CYD = Clyde Sandstone Formation, PDB = Pathhead Formation, LLGS = Lower Limestone Formation, GHV = Garleton Hills Volcanic Formation, GUL = Gullane Formation, KNW = Kinnesswood Formation. After Millward *et al.* (2018).

Table 6. Borehole location and registration data. SOBI = Single Online Borehole Index (at the BGS). From Millward *et al.* (2013).

THE PALYNOMORPHS

Table 7. The number of palynomorphs that were extracted from the NWMF borehole core, broken down by genera, species and specimens. The scolecodonts were classified in terms of 'morphotypes'.

Table 8. Breakdown of the palynological counts and the number of taxa for 3 categories: 10 or more specimens per taxon, less than 10 specimens per taxon and the total number of specimens per taxon. The top 10 specimens per taxon is included as a comparison.

TOURNAISIAN BIOZONATION

Table 9. The top 10 most abundant spores that were extracted from the NWMF borehole core. Total number of all spores: 39,389. Total number of top 10 spores: 23,522 (= 59.7% of all spores).

Table 10. The spores used to define the two subzones of the Tournaisian CI biozone of Turnau (1978) and their varying abundances.

PLANT RECOVERY

Table 11. Results of the elemental analysis of two samples of the same coal from the NWMF borehole core.


Table 12. Recalculated elemental analysis results from Table 11.

DECLARATION OF AUTHORSHIP

I, Emma Jane Reeves declare that this thesis 'Early Carboniferous Palynology and Tetrapod Evolution' and the work presented in it are my own and has been generated by me as the result of my own original research.

I confirm that:

1. This work was done wholly or mainly while in candidature for a research degree at this University;
2. Where any part of this thesis has previously been submitted for a degree or any other qualification at this University or any other institution, this has been clearly stated;
3. Where I have consulted the published work of others, this is always clearly attributed;
4. Where I have quoted from the work of others, the source is always given. With the exception of such quotations, this thesis is entirely my own work;
5. I have acknowledged all main sources of help;
6. Where the thesis is based on work done by myself jointly with others, I have made clear exactly what was done by others and what I have contributed myself;
7. Either none of this work has been published before submission, or parts of this work have been published as:
 - Clack *et al.*, 2016, Phylogenetic and environmental context of a Tournaisian tetrapod fauna, *Nature Ecology & Evolution*, 1, 1-11.
 - Bennett *et al.*, 2017, Ichnofauna record cryptic marine incursions onto a coastal floodplain at a key Lower Mississippian tetrapod site. *Palaeogeography, Palaeoclimatology, Palaeoecology*, 468, 287-300.
 - Marshall *et al.*, 2019, Reinterpreting the age of the uppermost 'Old Red Sandstone' and Early Carboniferous in Scotland. *Earth and Environmental Science Transactions of the Royal Society of Edinburgh*, 1-14.

Signed:.....

Date: 4/11/19...

ACKNOWLEDGEMENTS

This study was funded by NERC Consortium Grant 'The Mid-Palaeozoic biotic crisis: setting the trajectory of tetrapod evolution', led by Professor Jennifer Clack (University Museum of Zoology, Cambridge) and involved the Universities of Cambridge (NE/J022713/1), Leicester (NE/J020729/1), Southampton (NE/J021091/1), the British Geological Survey (NE/J021067/1) and the National Museum of Scotland.

I am highly grateful to my supervisors Professor John Marshall and Dr. Ian Harding and to my Panel Chair Dr. Jessica Whiteside from NOCS, University of Southampton.

Professor Marshall provided invaluable supervision and guidance throughout the research. I especially appreciate:

- The opportunities to attend national and international conferences to present research findings and to network;
- The loan of the many references to facilitate palynomorph identification;
- The loan of the Canon Eos field camera;
- The loan of the office, microscope, computer and software to photograph and measure palynomorphs;
- Arranging the isotopic analysis of the coal sample;
- Producing Figure 97;
- Performing the extensive literature research on Albert Long's material to facilitate the association between *Genomosperma kidstoni* and *Prolycospora claytonii* and for organising the visit to the Hunterian Museum, Glasgow to view the type specimens.

Dr. Ian Harding's time and effort are appreciated for reviewing this thesis and for providing the many constructive ideas that significantly improved the manuscript.

Dr. Jessica Whiteside gave many useful suggestions during the panel chairing of the advisory meetings.

I am also most appreciative of the assistance that was provided to me by the following people during the course of my studies:

Mr. Shir Akbari (NOCS, University of Southampton) for training me to process rock samples for palynomorph analysis and for help with processing the coal sample.

Dr. Dave Carpenter (NOCS, University of Southampton) for providing the vitrinite reflectance information on the coal sample.

Dr. Richard Pearce (NOCS, University of Southampton) for his assistance with the scanning electron microscopy.

Professor Sarah Davies (University of Leicester) for providing information on the anastomosing river channels at Burnmouth.

Dr. Carys Bennett (University of Leicester) for producing the log of the NWMF borehole core.

Dr. Tim Kearsey (BGS) for providing information on the NWMF palaeosols.

Dr. Neil Clark (Hunterian Museum, Glasgow) for access to the Albert Long Collection.

Marcos Echeverria for posting his excellent Tutorial Tilia 2.0.4 Coniss on YouTube.

Mary Smith (NOCS, University of Southampton) for resolving the many administrative challenges that were encountered during my study.

ABBREVIATIONS

AOM = amorphous organic matter
BGS = British Geological Survey
CCD = Charged Coupled Device
CONISS = Constrained Incremental Sum of Squares
CR = core run
DCB = Devonian-Carboniferous boundary
E. F. = England Finder
EDME = End Devonian Mass Extinction
Fm = Formation
ICBN = International Code of Botanical Nomenclature
ICS = International Commission on Stratigraphy
IR = Infrared
IS(M) = BGS borehole identification reference number
LM = light microscopy
Lmst. = limestone
LPIA = Late Palaeozoic Ice Age
LWD = large woody debris
NERC = Natural Environment Research Council
NIGL = NERC Isotope Geosciences Laboratories
NOCS = National Oceanography Centre, Southampton
NWMF = Norham West Mains Farm
PAST = Paleontological Statistics
PCA = Principal Component Analysis
PPE = Personal Protective Equipment
Sdst. = sandstone
SEM = Scanning Electron Microscopy
SOES = School of Ocean and Earth Science
TS = thin section
TW:eed = Tetrapod World: early evolution and diversification
VP = variable pressure

CHAPTER 1

INTRODUCTION

The main focus of this research project has been to investigate the recovery of the early Carboniferous vegetation after the End Devonian Mass Extinction (EDME; 359 Ma) – a period associated with the evolution of terrestrial vertebrate animals.

To provide a context for this thesis, the introductory chapter begins with a definition of what is meant by the term ‘mass extinction’, how such events differ from background extinctions and a discussion of the different patterns of extinction shown between marine and terrestrial biotas. Summary descriptions of four mass extinction events are provided, against which the EDME can be shown to be of a quite different character, as the EDME represented the culmination of an extended, multi-phased series of crises, rather than being driven by a single catastrophic event.

Owing to its exceptional complexity, the EDME is described in more detail, including a discussion of previous work that has determined the duration of the extinction. Drivers of the EDME are addressed, before the effects of the extinction on the marine and terrestrial biotas are considered. This section of the text will provide a background to the research presented here.

The effects of the EDME on the terrestrial biota are prefaced by an explanation that emphasises the fundamental importance of the evolution of different plant groups in the early Palaeozoic. Starting with the development of embryophytes in the Ordovician, early plant evolution will be tracked through the appearance of the small tracheophytes with trilete spores and rudimentary root systems that arose during the Silurian, through to the development of Devonian lignophytes with their substantial roots that bound sediments and formed soils, and, as these plants grew taller, how they developed arborescence and gave rise to the first forests. This evolutionary progression increased biomass and facilitated niche expansion into previously uncolonised land areas, with seed plants eventually populating dry and disturbed areas. Against this backdrop of increased Devonian floral

complexity, the effects of the EDME on terrestrial biotas are discussed, as will the subsequent recovery of the Tournaisian flora, setting the stage for the Carboniferous and beyond.

Having examined the terrestrial floral record, the effects of the EDME on vertebrates then follows, considering how the large-scale global turnover of taxa affected all marine and non-marine communities. It is shown how the major restructuring of marine vertebrates culminated in Carboniferous ecosystems that were distinctly different to those of the Devonian.

The turnover of the fishes is examined in more detail, as their major taxonomic restructuring reduced Devonian fish diversity to just three groups, which still dominate modern vertebrate biodiversity. These animals included the tetrapodomorphs and tetrapods, which evolved a range of morphologies following the EDME to exploit the newly evolving terrestrial habitats. The fossil evidence for the acquisition of novel vertebrate anatomies to enable life on land is discussed, as are the driving forces for this momentous achievement.

Of crucial importance to the current research is the widely perceived ‘gap’ in the fossil evidence for the transition of fully aquatic tetrapods to those occupying fully terrestrial habitats. Known as ‘Romer’s Gap’, the span of geological time between 359 and 329 Ma (Tournaisian – Viséan) was believed to contain the transitional forms of fossil tetrapods and had obscured understanding of how the vertebrate water-to-land transition occurred. Following the reclassification of previously unidentified Devonian museum specimens as tetrapods, a resurgence of interest in tetrapod origins led to the active search for new tetrapod-bearing sites. After new tetrapod fossils were collected from younger early Carboniferous sites in Scotland, the interdisciplinary, four-year Natural Environment Research Council (NERC)-funded *Tetrapod World: early evolution and diversification* (TW:eed) project was convened. The work presented here forms one component of this much larger project.

The TW:eed project’s aims were to investigate the palaeontology, sedimentology, stratigraphy, stable isotopes and palynology of newly discovered tetrapod fossil-

bearing sites across Romer's Gap in the northeast of England and southern Scotland. This information would provide a stratigraphically well-constrained and more complete picture of the vertebrate transition onto land. The final part of this chapter explains the background to the research conducted for this thesis, the use of palynomorphs to provide a robust stratigraphic framework for the wider project and to investigate the recovery of the plant life following the EDME. The data presented here come mostly from a borehole that was drilled specifically for the TW:eed project. The findings of this thesis are discussed further in chapters 3, 4 and 5.

1.1. What are mass extinctions?

Mass extinction events record when extinction rates significantly exceeded origination rates, such that more than 75% of living species disappeared within a geologically short time span, which was typically less than 2 million years (Barnosky *et al.* 2011). These events generally resulted from catastrophic events or environmental perturbations that occurred so quickly that organisms were unable to adapt and so perished (Raup 1994, Jablonski 2005, McElwain & Punyasena 2007).

Many extinction events have happened throughout the Phanerozoic Eon but they are only considered to be 'mass' extinction events when the rate at which taxa are lost significantly exceeds background extinction rates (Raup & Sepkoski 1982). To calculate these rates, Raup & Sepkoski (1982) analysed data for families of marine vertebrates, invertebrates and protozoans. They divided the number of families that became extinct during each of the 76 post-Tommotian (early Lower Cambrian) stages by the estimated duration of the stage. Background extinction was considered to be represented by data points that clustered tightly at extinction rates of less than 8.0 extinctions per million years (Figure 1). The data points signifying mass extinction events were considerably greater than the background rates. Four events stood out as mass extinctions – the late Ordovician, end-Permian, end-Triassic and end-Cretaceous with the late Devonian (Frasnian-Famennian) extinctions being considered initially as 'noticeable but not statistically significant'.

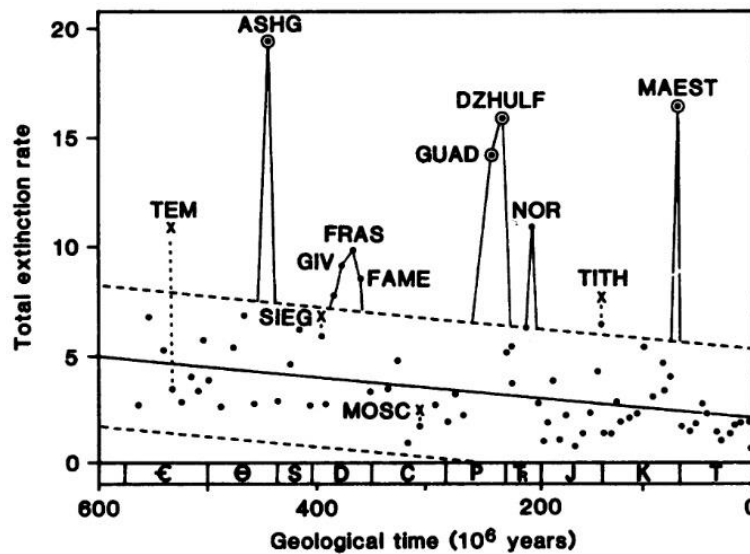


Figure 1. Total extinction rate (extinctions per million years) through time for families of marine invertebrates and vertebrates. The plot shows statistically significant mass extinctions in the late Ordovician (ASHG), Permian (GUAD-DZHULF), Triassic (NOR) and Cretaceous (MAEST). An extinction event in the late Devonian (GIV-FRAS-FAME) was considered to be noticeable but not statistically significant. Circled points are those where the departure from the main cluster was highly significant. Xs indicate those cases where inclusion of Lagerstätten substantially increased the calculated extinction rate (the point directly below the X is the rate calculated without the Lagerstätten data). The figure also shows a general decline in background extinction rate through time. The regression line is fit to the 67 points having extinction rates less than eight families per 10^6 years, and the dashed lines define the 95 percent confidence band for the regression. Abbreviations: TEM = Templetonian, ASHG = Ashgillian, SIEG = Siegenian, GIV = Givetian, FRAS = Frasnian, FAME = Famennian, MOSC = Moscovian, GUAD = Guadeloupian, DZHULF = Dzhulfian, NOR = Norian, TITH = Tithonian, MAEST = Maestrichtian. From Raup & Sepkoski (1982).

Mass extinctions are considered to be complex events that involve interactions spanning multiple processes and their related risk factors (Finnegan *et al.* 2012). Although Raup & Sepkoski (1982) used only data from marine fossils, it was

assumed that mass extinctions affected terrestrial and aquatic biotas in a similar manner and occurred on a global scale (Cascales-Miñana & Cleal 2013).

Whether directly or indirectly, these events would have caused ecological disruption to vegetation, however, the plant fossil record shows a different pattern of major extinctions compared to that of marine organisms (Wing 2004, McElwain & Punyasena 2007, Cascales-Miñana & Cleal 2013; Table 1). Only two major extinctions can be recognised in plant families, during the Carboniferous-Permian transition and at the End-Permian, with only the latter coinciding with a major extinction in the marine realm (Cascales-Miñana & Cleal 2013).

Event	All	Terrestrial	Marine
Late Ordovician	22.5	Uncertain	24.3
End-Permian	31.0	37.2	28.1
End-Triassic	15.2	10.6	12.7
End-Cretaceous	11.5	6.3	14.7

Table 1. Magnitudes of mass extinctions (by percentage at the family level) for different subsets, indicated as the percent decreases in diversity based on unequivocal stratigraphic and habitat data. From Benton (1995).

1.2. Comparing mass extinction events

To highlight how much more complex the EDME was compared to the other mass extinctions, brief summaries of four of the mass extinction events follows, with the EDME being discussed in more detail afterwards.

1.2.1. Late Ordovician (Finnegan *et al.* 2012):

The Late Ordovician Event occurred in two phases – one at the start of the Hirnantian stage (445 Ma) and the second in the middle of the stage (circa 444.5 to 444 Ma; Branchley *et al.* 2001) and lasted for 3.3 to 1.8 million years (Barnosky *et al.* 2011). Climate change has been attributed as the cause of the Late Ordovician Event as the primary pulse of extinction coincided closely with the rapid

growth of the south polar ice sheets on Gondwana. This expansion of the continental ice sheets was accompanied by substantial cooling of the tropical oceans, a major perturbation of the global carbon cycle and a drop in the eustatic sea level, which drained the vast cratonic seaways of the late Ordovician. The reduced sea level contracted the area for shallow marine habitats and caused their taxonomic restructuring. The climatic cooling forced tropical taxa to experience water temperatures beyond the limits of their adaptive range. Therefore, any taxa that could not adapt quickly to these changes became extinct.

Globally, the second extinction pulse largely affected a minor group of cold-adapted taxa that flourished and expanded their ranges during the peak glaciation. Most of these taxa were either relicts from the previous Katian stage, invaders from other low latitude areas or endemics that had evolved after the first extinction.

1.2.2. End Permian (Cao *et al.* 2009, Reichow *et al.* 2009):

The End Permian Event, around 252 Ma, lasted for 2.8 million to 160 thousand years (Barnosky *et al.* 2011) and represents the largest extinction of marine fauna in the Phanerozoic. It corresponded with a protracted and widespread oceanic anoxic event. The marine plankton community was dominated by bacteria and experienced perturbations in the environmental conditions and profound changes to their ecology. Moreover, the presence of anoxygenic green sulphur bacterial biomarkers (Chlorobiaceae) identify times when euxinic conditions extended into the photic zone.

The climatic changes at the end of the Permian period coincide with the formation of the Siberian Traps Large Igneous Province. The inundation of the continents and the sea floor by vast volumes of magma during short periods of time produces Large Igneous Provinces (LIPs). The Siberian Traps, most visible at outcrops on the Siberian craton, represent the largest continental flood basalt province, covering an area of ca. 2.5 million km² and reaching a total thickness of ca. 3.5 km. The volcanic eruptions and the degassing of magma have been associated with changes to the global climate and are considered as a cause of mass extinctions, including the End Permian Event.

1.2.3. End Triassic (Hesselbo *et al.* 2002):

The mass extinction at the end of the Triassic period, 200 Ma, which lasted for 8.3 million to 600 thousand years (Barnosky *et al.* 2011), occurred around the same time as one of the largest volcanic eruptive events known. Changes in the terrestrial and marine plant and animal life happened synchronously, which strongly suggests a causal link between the loss of taxa and the first eruptive phases of the Central Atlantic Magmatic Province (CAMP) lavas.

1.2.4. End Cretaceous (Schulte *et al.* 2010):

Against the backdrop of the Deccan Traps flood basalt volcanism in India, the end-Cretaceous event, at 66 Ma, lasted for at most 2.5 million years (Barnosky *et al.* 2011). It coincided with a large asteroid impact at Chicxulub on what is today the Yucatan Peninsula in Mexico. A single ejecta-rich deposit, which is linked compositionally and temporally to the Chicxulub impact, marks this geological boundary worldwide. The contemporaneous extinctions and the environmental perturbations that have been modelled from such an impact indicate that the Chicxulub impact triggered this mass extinction.

1.3. The End Devonian Mass Extinction (EDME)/Hangenberg Event

During the search for an international stratotype to define the Devonian-Carboniferous Boundary (DCB), high resolution stratigraphic work has been carried out at many localities all over the world (Becker 1996). This has produced a vast repository of data about the precise ranges and co-occurrences of various fossil groups, regional and local facies developments and sea-level fluctuations across this boundary period (Becker 1996). Furthermore, examination of extinction, survival and radiation patterns enabled the recognition of an extinction event (Becker 1996).

In Europe, the EDME is known as the “Hangenberg Event” as it was associated stratigraphically with the deposition of the Hangenberg Black Shale just below the DCB (Walliser 1984). The Hangenberg Event commences at the base of the

poorly defined Middle *praesulcata* conodont zone (top of the Wocklum Limestone) and includes all beds up to the middle part of the *sulcata* conodont zone (at the base of the Hangenberg Limestone/*Gattendorfia* ammonoid genozone; Kaiser 2005; Figure 2).

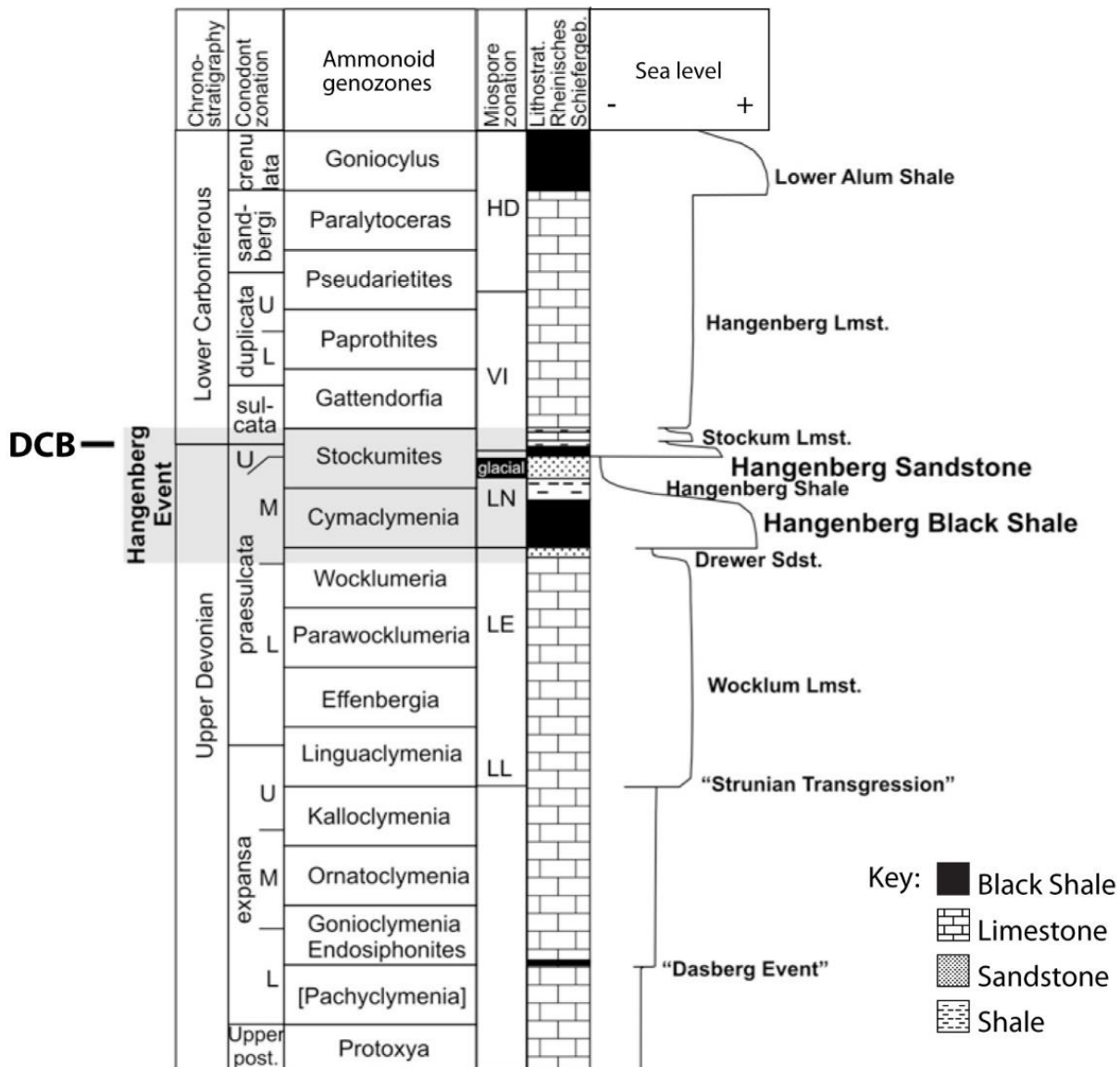


Figure 2. Stratigraphical correlation scheme for the Hangenberg Event, DCB and relative sea-level change. After Kaiser (2005).

The DCB itself, is defined by the first occurrence of the conodont *Siphonodella sulcata* within the *Stockumites* ammonoid genozone and near the base of the miospore zone VI (Figure 2) and represents the final in a series of Devonian biotic crises (Paproth & Streel 1984, Becker 1993, Higgs *et al.* 1992; Table 2). The

stratotype section is at La Serre, Montagne Noire in southern France (Paproth *et al.* 1991).

1.3.1. The EDME was different to other mass extinctions

The noticeable decline in biodiversity at the end of the Devonian has been the subject of numerous studies. However, unlike other mass extinction events, the EDME did not represent a single catastrophe but rather a multi-phased, prolonged series of crises that was preceded by a cycle of events throughout the Devonian Period (Table 2), which culminated in the EDME/Hangenberg Event (Kaiser *et al.* 2015).

Epoch	Age	Extinction event
Upper Devonian	Famennian	Hangenberg
		Dasberg
		Annulata
		Enkeberg
		Condroz
	Frasnian	Upper Kellwasser
		Lower Kellwasser
		Rhinestreet
		Middlesex
Middle Devonian	Givetian	Frasne
		Taghanic
	Eifelian	Kačák
		Choteč
Lower Devonian	Emsian	Daleje
		Zlíčov

Table 2. Devonian biotic crisis events. From Kaiser (2005).

Named after the Hangenberg Black Shale of middle and southern Europe, the Hangenberg Event represents a brief disruption of ammonoid-bearing limestones by black shales, just below the DCB (Becker 1992). Hangenberg facies deposits have been found globally in different palaeogeographical settings and affected many fossil groups in all ecosystems at different times (Sallan & Coates 2010, Kaiser *et al.* 2015). However, there is a prominent temporal difference between the main extinction events affecting the marine and the terrestrial biomes (Prestianni *et al.* 2016).

Based on radiometric dating of ash layers in Poland, the main black shale interval lasted from less than 50 up to 190 thousand years (Myrow *et al.* 2014, Kaiser *et al.* 2015). This timeframe substantiates a very sudden extinction and alludes to the entire Hangenberg Event representing only between 100 thousand years and several hundred thousand years (Sandberg & Ziegler 1996, Trapp *et al.* 2004, De Vleeschouwer *et al.* 2013).

1.3.2. Possible drivers of the EDME

Although the causes for the EDME have been much-discussed, the matter is still not resolved. Suggestions include:

- Iridium anomalies found globally at the DCB pointing to an impact-extinction model. But non-chondritic ratios of iridium to other important elements (Au, Co, Fe, Ni, Cr, Al) and a lack of physical evidence such as shocked quartz and microtektites do not corroborate this hypothesis (Wang *et al.* 1993).
- Climatic cooling – deteriorating from the late Devonian greenhouse conditions of high atmospheric and oceanic carbon dioxide concentrations (Caputo & Crowell 1985, Berner 1991).
- Marine disturbances, such as changing oceanic circulation patterns attributed to global tectonics, rapid sea-level fluctuations and ocean anoxia (Copper 1986, Johnson *et al.* 1985, House 1985, Becker 1993, 1996).

Perhaps the most likely explanations are centred on eustacy. Johnson *et al.* (1985) hypothesised that sea-level fluctuations during the Devonian Period were of a sufficient scale to affect sedimentation simultaneously across disconnected

geographical regions that had varying rates and patterns of subsidence and uplift. Using conodonts, which provide a global high resolution zonation for the entire Devonian, the relative timing of transgressive-regressive (T-R) cycles was calculated from sedimentary sequences of contrasting lithotypes that indicated significant eustacy (Figure 3). To denote deepening events (sea-level rise/transgression), they used the bases of black shales, inceptions of reef growth, drownings of platforms, subtidal shales over platform carbonate rocks and sedimentary rocks above unconformities. These contrasting lithotypes were taken to imply diverse climates and tectonic regimes. To gauge geographical distance, five regions were selected in the United States, Canada, New York State, Germany and Belgium. Johnson *et al.* (1985) found that the well-dated transgressive events coincided in the disparate sites, which, therefore, agreed with their sea-level fluctuation hypothesis.

Additionally, eustacy was regarded as the cause of the extinction event at the Frasnian-Famennian boundary, where important groups of brachiopods, colonial corals and stromatoporids died out in the late Frasnian (Johnson *et al.* 1985). Cessations in reef-growth matched intervals of black-shale deposition recorded in the Kellwasser Limestone and as the products of anoxic bottom water conditions, black shales also represent times of reduced living space in basinal areas (Eder & Franke 1982, Johnson *et al.* 1985).

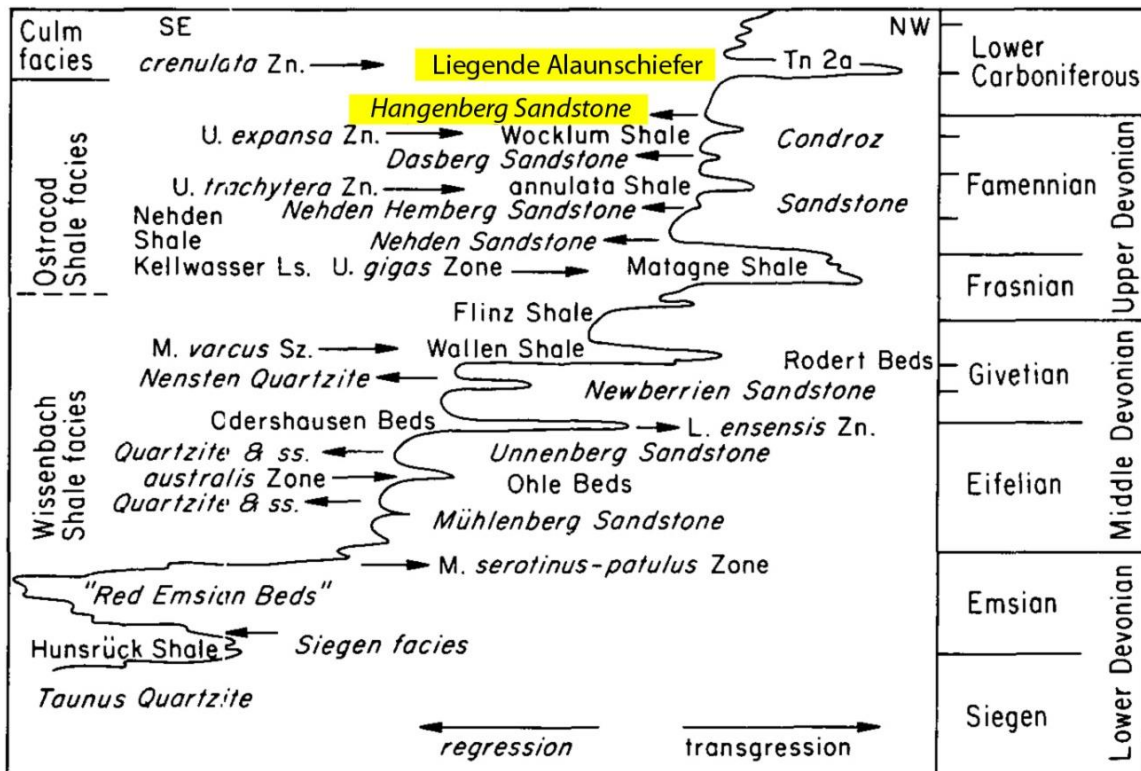


Figure 3. Time-rock transect showing transgressions and regressions from Early Devonian to early Carboniferous time in the Rhenish Slate Mountains. From Johnson *et al.* (1985). Note that the Liegende Alaunschiefer (Lower Alum Shale) and Hangenberg Sandstone (highlighted) are also shown on Figure 2.

If, however, changes in sea-level were the causes for the EDME, the obvious next stage would be to find out the cause of the eustasy.

1.3.2.1. Glaciation

During the latest Devonian to early Carboniferous, the Late Palaeozoic Ice Age (LPIA) began, with three minor glaciations in the latest Famennian, mid Tournaisian and Viséan (Caputo *et al.* 2008). Glaciation reached its maximum extent during the late Carboniferous, when continental-scale ice sheets covered large parts of Gondwana and ended in the late Permian (Veevers & Powell 1987, Powell & Veevers 1987, Fielding *et al.* 2008).

Eustatic fluctuations, stable isotopic excursions and global oceanic anoxic events associated with mass extinctions approximately coincide with these glaciations

(Caplan & Bustin 1999, Kaiser *et al.* 2015, Sallan & Coates 2010, Streel 1986).

Figure 4 demonstrates the evidence for glaciation at the DCB in South America and North America.

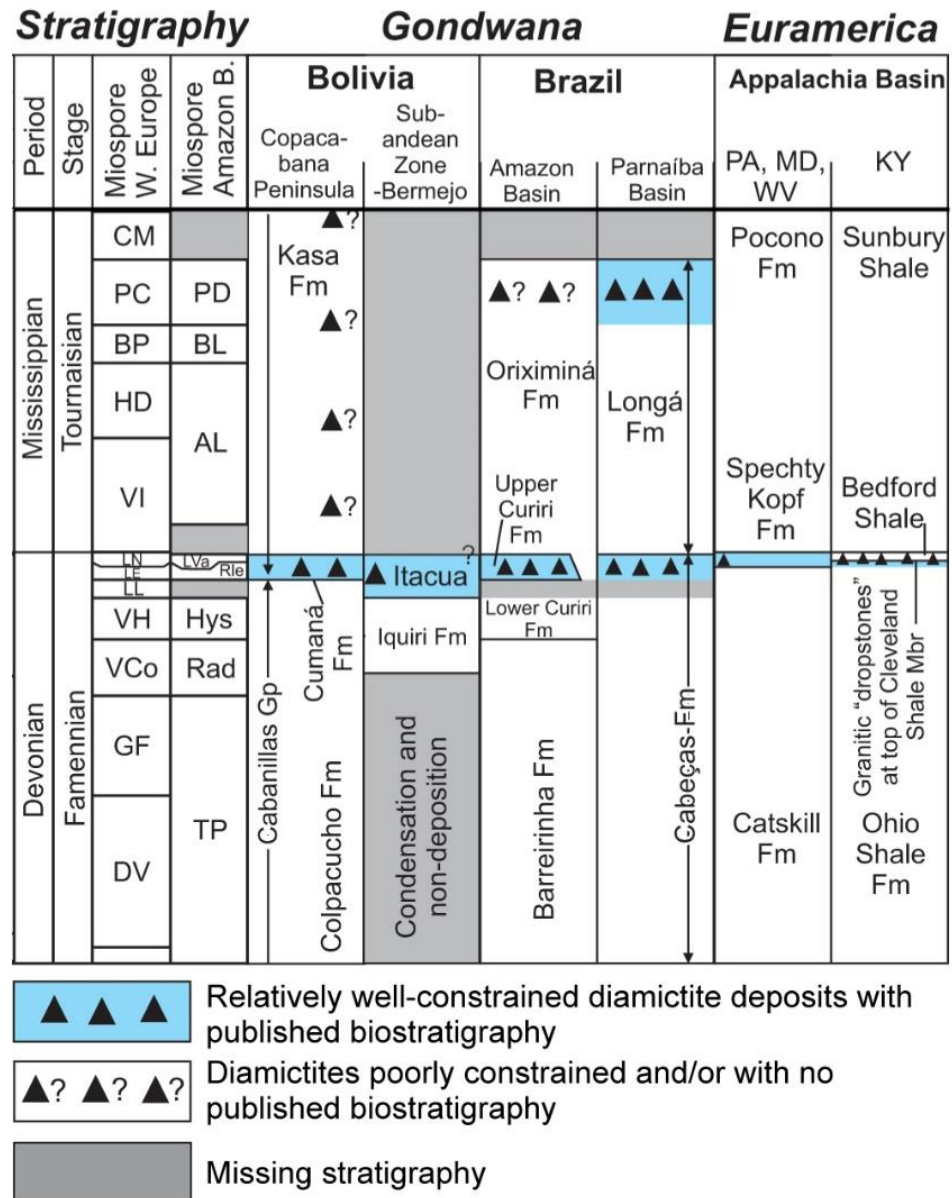


Figure 4. An overview of diamicite occurrences from Bolivia, Brazil and the Appalachian Basin and their stratigraphic position. After Lakin *et al.* (2016).

In northern Brazil, evidence for glacial and periglacial conditions, during the late Devonian, includes faceted and striated pebbles, striated rock pavements (which

indicate direct contact with a continental ice sheet), varved sediments and the widespread distribution of diamictites (Caputo 1985, Caputo & Crowell 1985).

Evidence for the late Devonian and early Carboniferous glaciations is also found on the African continent in Niger, Egypt, Sudan and the Central African Republic as diamictite deposits and striated pavements (Caputo *et al.* 2008, Isaacson *et al.* 2008).

Although evidence for glaciers may be inferred in field sections, calculations of the timings, ice volumes (ice sheet, ice cap, alpine glacier sizes) and number of ice centres present during the glacial episodes of the LPIA are more challenging to define (Fielding *et al.* 2008). Large changes in sea level require large changes in ice volume, but this relationship is difficult to resolve owing to the incomplete character of the glacial record (Fielding *et al.* 2008).

Repeated sea-level fluctuations explain many Famennian and Tournaisian events and marine palaeo-temperature models indicate that oceans were generally warmer during the Famennian than the Tournaisian (Brand 1993). Rather than being a single, drawn-out interval of icehouse conditions, the LPIA was a succession of shorter, discrete intervals, each lasting up to a few million years, separated by intervals of more temperate climatic conditions of similar durations (Fielding *et al.* 2008).

1.3.3. The effects of the EDME

Although the timing of extinctions varied between the fossil groups, shallow- and deep-marine, non-marine and terrestrial ecosystems were all severely affected by the EDME (Simakov 1993, Sallan & Coates 2010, Streel 2000). In line with the background aims of the TW:eed project and to provide a context to the work of this thesis to investigate the recovery of the vegetation after the EDME, summaries of the effects of the EDME on terrestrial and vertebrate biotas follows.

1.3.3.1. The effects of the EDME on terrestrial biotas

Increased extinction rates coupled with elevated origination rates imply high taxonomic turnover during the late Devonian (Silvestro *et al.* 2015). However, the effects of the EDME on terrestrial ecosystems happened during the Hangenberg Event, 12 million years after the main extinction phase of marine taxa during the Kellwasser Event (Kaiser *et al.* 2015). Evidence from land plants and miospores indicate that they were more severely affected by the Hangenberg Event than during the Frasnian-Famennian Event (Fairon-Demaret 1986, 1996, Jarvis 1990, Algeo & Scheckler 1998, Decombeix *et al.* 2011, Streel *et al.* 2000, Kaiser *et al.* 2015).

Late Devonian spore-bearing plants experienced high extinction rates, including the disappearance of several early lineages, such as the zosterophylls (Silvestro *et al.* 2015, Cascales-Miñana & Meyer-Berthaud 2014). This interval was also characterised by the diversification of arborescent lycopsids, early seed ferns and lignophytes (Wang *et al.* 2005, Galtier & Meyer-Berthaud 2006, Meyer-Berthaud *et al.* 2010, Decombeix *et al.* 2011).

1.3.4. The evolution of terrestrial vegetation

To clarify the fundamental importance of the Devonian Period in the evolution of terrestrial plant life, a synopsis of the phases of plant development follows:

1.3.4.1. Ordovician

Discoveries of cryptospores from a number of localities across the globe indicate that embryophyte plants first colonised terrestrial habitats at the start of the Darriwilian (Mid Ordovician; Wellman & Gray 2000, Edwards & Wellman 2001, Steemans *et al.* 2009). However, these forms were restricted to moist lowland habitats and their short anchoring structures would not have interacted significantly with the substrate (Algeo & Scheckler 1998).

1.3.4.2. Silurian

The global development of more advanced tracheophytes in the late Llandovery (early Silurian) is signified by major palynological changes, such as the diversification of trilete spores (Steemans 2000, Wellman & Gray 2000, Gensel 2008). Characterised by increasingly diverse, small-sized sporophyte plants, these new forms most likely possessed rudimentary structures to secure themselves to their substrates (Raven & Edwards 2001). The first evidence for charcoal comes from the Pridoli (late Silurian) in England, which demonstrates that plants were sufficiently abundant to sustain wildfires (Glasspool *et al.* 2004, Davies & Gibling 2010).

1.3.4.3. Devonian

Numerous innovations in the evolution of terrestrial vegetation occurred during the Devonian Period, including the earliest evidence for the rooting systems of tracheophytes in the Pragian Stage (Davies & Gibling 2010, Algeo & Scheckler 1998, Gensel *et al.* 2001). These branching root systems grew vertically or sub-vertically into terrestrial substrates for significant depths, providing a means of water supply and for stabilising tree-like plants (Gensel *et al.* 2001, Hiller *et al.* 2008, Hao *et al.* 2010).

The development of arborescence in all major groups of extant vascular plants (i.e. lycopsids, ferns, sphenopsids and lignophytes) denoted the appearance of advanced terrestrial vegetation systems by the Eifelian (Mid Devonian), whilst the worldwide colonisation of lowlands by the archaeopteridalean progymnosperms, established the earliest forests in the Givetian (Mid Devonian; Decombeix *et al.* 2011, Stein *et al.* 2007, Meyer-Berthaud & Decombeix 2009, Beck & Wight 1988). Archaeopterids tolerated a wide variety of soil conditions but prevailed in well-drained sites (Decombeix *et al.* 2011). They occurred in both distal and proximal floodplain environments and formed the first true upper canopy layer (Algeo & Scheckler 1998, Decombeix *et al.* 2011, Berry & Fairon-Demaret 2001). Moreover, the accumulation of significant biomass on terrestrial substrates increased the

area available for plant colonisation and soil formation, supporting widespread niche expansion (Stein *et al.* 2007, Robinson & Berner 1991).

By the Late Devonian, arborescent vegetation dominated terrestrial and marginal marine settings from tropical to boreal palaeolatitudes (Algeo & Scheckler 1998). However, the establishment of small, bushy, seed-producing lignophytes also enabled the colonisation of dry or disturbed environments (Decombeix *et al.* 2011).

1.3.4.4. Devonian–Carboniferous boundary

Archaeopteridalean progymnosperms became extinct near the DCB, but, in addition to the simple spore-producing plants, a major seed-plant radiation followed (Streel *et al.* 2000, DiMichele & Bateman 1996). As the majority of the seed plants belonged to non-arborescent pteridosperm orders such as the Calamopityales, Lyginopteridales and Buteoxylales, the early transitional phase has been interpreted as an open vegetation composed of shrubby, r-selected species (Decombeix *et al.* 2011, DiMichele & Hook 1992).

1.3.4.5. Carboniferous

Early Carboniferous seed plants radiated, encompassing a series of r- to K-selected species, from small shrubs to large trees, in habitats ranging from wet stream margins to dry soils in disturbed environments (DiMichele & Bateman 1996). Plant assemblages were often dominated by a single taxon, and fusinisation (charcoal preservation) was common, indicating that ferns exploited areas where habitat disruption favoured rapidly reproducing, coloniser plants that could spread rapidly to new sites (Scott *et al.* 1984, Scott & Galtier 1985, Bateman & Scott 1990).

During the late Tournaisian and Serpukhovian, there was a substantial increase in the number of arborescent lignophyte taxa, such as the progymnosperm *Protopitys* (Walton 1969, Decombeix *et al.* 2011). Most grew in well-drained areas, often with volcanic activity, which implies that they were adapted to dry and/or

disturbed conditions more successfully than other plant groups (Decombeix *et al.* 2011).

1.3.5. The effects of the EDME on vertebrates

The extinction events of the Devonian Period had as profound an effect on vertebrate faunas as they did the restructuring of marine non-vertebrates and of terrestrial plant life. The vertebrates referred to here comprise fishes and tetrapods with the latter forming the main focus. A discussion of fishes is included as they were the ancestors of the tetrapods and because they too suffered greatly during the EDME.

Sallan & Coates (2010) found that the changes in marine invertebrate biotas through the Frasnian-Famennian extinction event had little effect on the vertebrates. By comparison, the vertebrate ecosystems of the later Devonian were distinctly different from those of the early Carboniferous (Sallan & Coates 2010). Therefore, the EDME represented a time of significant change and large scale turnover of vertebrate taxa, with mass extinction and the subsequent refilling of niche space (Sallan & Coates 2010, Jablonski 2005). Sallan & Coates (2010) concluded that the EDME was comparable to the ‘big five’ mass extinctions (see Section 1.1), with respect to the vertebrates, and that this extinction event affected global communities of all ecosystems, whether non-marine or marine.

1.3.5.1. The fishes

Fishes are primitively aquatic backboned animals, exhibit a vast range of morphological characteristics and comprise more than half of all living vertebrate species (Friedman & Sallan 2012, Nelson 2006). Fishes have a fossil record that extends back to the early Cambrian and are divided into two major clades: the Agnatha and the Gnathostoma (Shu *et al.* 2003).

1.3.5.1.1. Agnatha

This minor group of fishes are the most primitive and lack jaws and fins (Petrou & Zapitis 2016). They formed 3 groups (Figure 5):

1. **Ostracoderms** (meaning 'shell-skinned') appeared in the Ordovician, were covered in bony plates and became extinct during the late Devonian (Benton 2015).
2. **Myxiniiformes** are the hagfish and there are 76 extant species (Petrou & Zapitis 2016).
3. **Petromyzontiformes** are the lampreys, with 38 extant species (Petrou & Zapitis 2016).

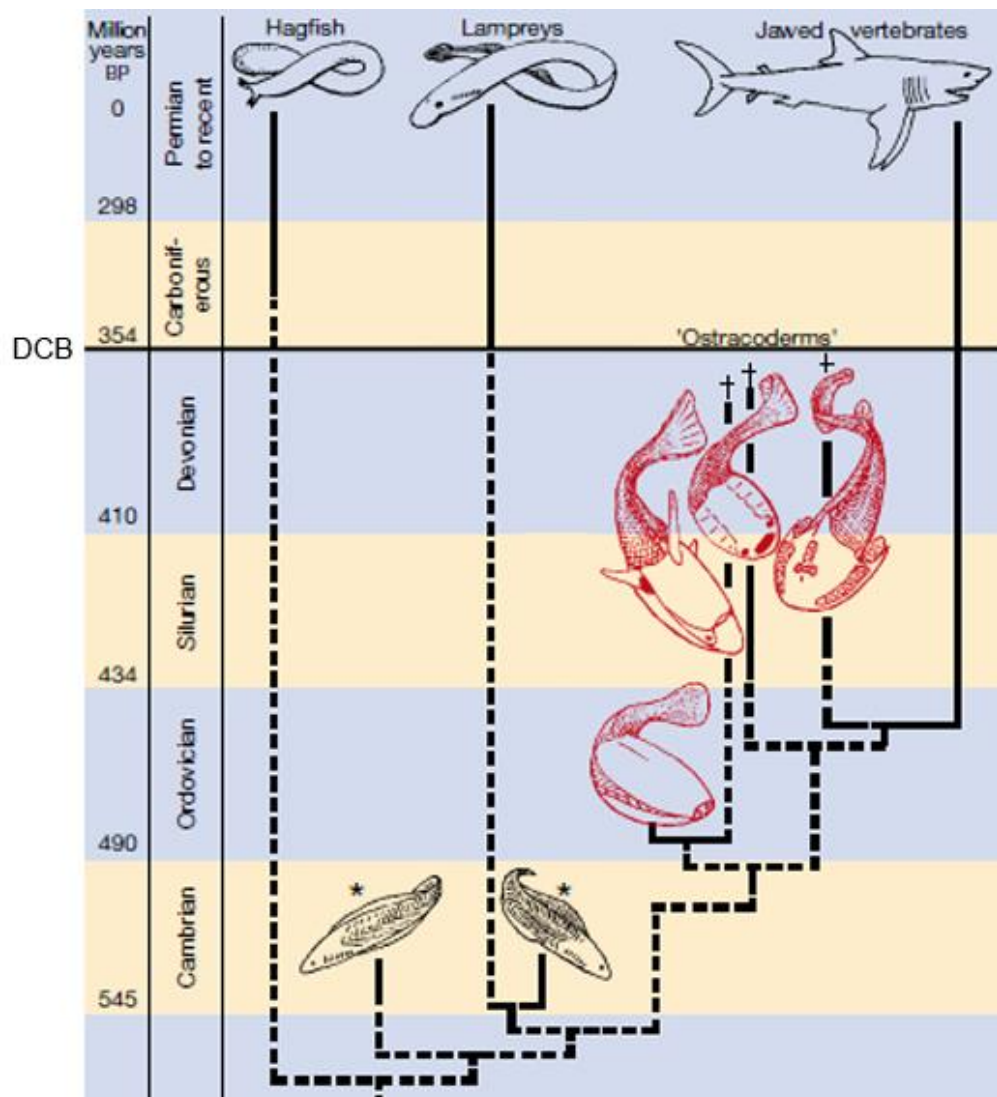


Figure 5. Phylogenetic tree of the major living and fossil jawless vertebrate groups. This tree suggests that prior to the appearance of the mineralised skeletal elements of ostracoderms, vertebrates had no mineralised tissues and could only be fossilised in exceptional circumstances as shown by fossils such as those discovered by Shu *et al.* (1999; asterisks) in the Chengjiang Lagerstätte, China. BP = before present. After Petrou & Zaptis (2016).

The agnathans reached their peak of diversity by the end of the Silurian but declined during the Devonian (Petrou & Zaptis 2016).

1.3.5.1.2. Gnathostomata

By far the largest group of living vertebrates are the gnathostomata (jawed vertebrates). Throughout the Devonian, a series of diversification events occurred among the vertebrate groups, including the appearance of the Osteichthyes (bony fishes such as the ray-finned Actinopterygii and lobe-finned Sarcopterygii), Chondrichthyes (cartilaginous fishes: Elasmobranchii and Holocephalii), Placodermi and Acanthodii (Janvier 1996, Benton 1993, Brazeau 2009, Sepkoski 2002).

Across the EDME, the gnathostome biota underwent major restructuring, with losses calculated as 50% of orders, 32% of genera and >96% of species (Benton 1993, Sepkoski 2002, Sallan & Coates 2010, Sallan & Galimberti 2015). Among the vertebrate groups that were affected by the EDME, many major taxa, such as the placoderms, acanthodians and several sarcopterygian groups became extinct or were seriously reduced in abundance (Sallan & Coates 2010; figures 6 and 7). The casualties had populated different habitats and exhibited divergent ecomorphologies (Sallan & Coates 2010, Anderson *et al.* 2011). Whether occupying marine or non-marine environments, the faunas of the Devonian and of the Carboniferous were mutually distinct (Friedman & Sallan 2012). For example, all of the sarcopterygian and acanthodian groups were restricted to either the Devonian or the Carboniferous Period (Sallan & Coates 2010). The few Devonian survivors, represented by a low number of relict genera, persisted only as far as the late Palaeozoic (Sallan & Coates 2010).

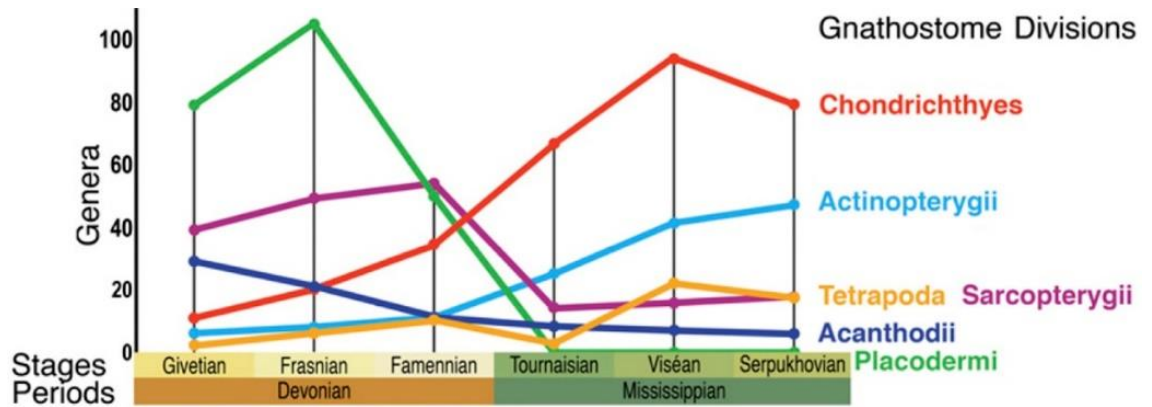


Figure 6. Gnathostome generic level diversity curves for the Givetian to Serpukhovian. From Sallan & Coates (2010).

On the other hand, actinopterygians, chondrichthyans and early tetrapods increased in diversity and abundance (Sallan & Coates 2010; figures 6 and 7). By migrating into areas formerly dominated by placoderms, they increased their range of ecological niches and continue to dominate modern vertebrate biodiversity (Clement *et al.* 2004, Benton 1993, Sepkoski 2002, Nelson 2006, Friedman & Sallan 2012).

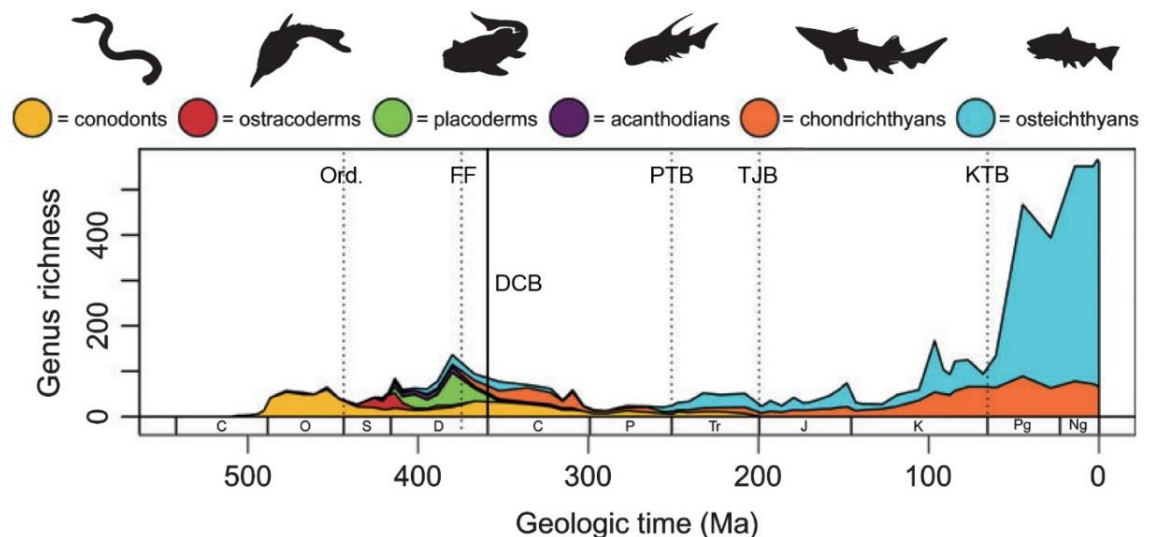


Figure 7. Diversity patterns in marine fishes during the Phanerozoic. Vertical dashed lines represent the 'Big Five' extinctions of Raup & Sepkoski (1982): Ord. = end Ordovician, FF = Frasnian-Famennian, PTB = Permian-Triassic Boundary, TJB = Triassic-Jurassic Boundary, KTB = Cretaceous-Tertiary Boundary.

TJB = Triassic-Jurassic Boundary and KTB = Cretaceous-Tertiary Boundary. The DCB has been added. The chart illustrates generic richness divided into traditional groupings (conodonts, ostracoderms, placoderms, acanthodians, chondrichthyans and osteichthyans). After Friedman & Sallan (2012).

During the Tournaisian, actinopterygians and chondrichthyans experienced a phase of morphological diversification in terms of jaw mechanics and dentitions (particularly durophagy) and novel body forms (mainly benthic types; Sallan & Coates 2010, Sallan *et al.* 2011, Sallan & Friedman 2012). This suggests the refilling of all of the ecological niches that were left vacant by the loss of the incumbent Devonian taxa i.e. the placoderms, ostracoderms and a large number of the sarcopterygians, especially the cosmine-covered lungfishes (Friedman & Sallan 2012, Janvier 2003). Simultaneously, shifts in habitats were recorded in three previously marine groups. The Dipnoi (lungfishes), Gyracanthida (acanthodians) and Elasmobranchii (sharks) moved into lacustrine and riverine environments, whereas two previously continental tetrapodomorph sarcopterygian clades (Rhizodontida and Megalichthyidae) moved into marine areas (Friedman & Sallan 2012).

1.3.5.2. The tetrapods

The most important event for future vertebrate evolution was the morphological transition of wholly aquatic fish to become terrestrial tetrapods, beginning in the late Devonian (Coates *et al.* 2008). Following the EDME restructuring, the tetrapods developed a range of sizes and morphologies to equip them to exploit the newly evolving habitats on land (Clack 2006). The anatomical evidence for how this was achieved, with examples from the fossil record will be discussed next.

1.4. Tetrapod evolution

The origin of the tetrapods is currently fixed to a 5 million year time span between the mid Givetian and the mid Frasnian (Clack 2006). Fossil evidence from the many tetrapod-like fish and early tetrapods from the Devonian records the earliest

phases of limbed vertebrate evolution (Smithson *et al.* 2012). Using these fossils, it has been possible to document the developmental stages that were necessary to adapt fully to terrestrial conditions, and the order in which those characters arose can also be investigated (Clack 2009).

Robustly supported phylogenetic analysis groups certain fossil sarcopterygian (lobe-finned) fish and the early tetrapods together as the Tetrapodomorpha (Clack 2009). Unlike modern forms, these animals were fully or partially aquatic and retained the more archaic fish-like bony fin webs on the tail, had paddle-like limbs and were polydactylous (Clack 2009).

Although the appearance of limbs with digits would most commonly be considered to characterise the origin of tetrapods, many other equally profound changes to the head region can also be demonstrated in the fossil record, such as those associated with air-breathing, feeding and the sensory systems (Clack 2009). Major components of the tetrapod bauplan originated through a succession of intermediate forms that evolved new characters both in mosaic form and in parallel among the sarcopterygians on the tetrapod lineage, which allowed them to exploit diverse Devonian habitats (Daeschler *et al.* 2006).

The transition from aquatic to terrestrial life seems to have taken place in estuarine or riverine environments, during a time of increasing vegetation cover on the land and water margins (Clack 2009). By the mid-Carboniferous, tetrapods had become terrestrialised, with pentadactylous limbs, and had diversified into a wide range of recognisably modern morphologies and ecologies (Smithson *et al.* 2012).

1.4.1. Summary of the skeletal adaptations of the tetrapods to life on land

The evolution of tetrapods from sarcopterygian fish involved numerous structural and functional innovations, including new means of locomotion, breathing and hearing (Daeschler *et al.* 2006). The fossils of the fishes and tetrapods across this transitional period reveal how these innovations originated (Daeschler *et al.* 2006).

1.4.1.1. The skull and jaws

Inside the skull, the braincase (neurocranium), that had previously been separated into anterior and posterior parts, joined together and the proportions changed to produce a longer anterior area (Coates *et al.* 2008). The size of the auditory capsules increased relative to the posterior area of the neurocranium and the notochord retracted from a channel beneath the rear of the neurocranium (Coates *et al.* 2008). The snout elongated and became more robust and the eyes enlarged and moved towards the top of the head (Clack 2009). These changes transformed the overall skull morphology to facilitate new sensory adaptations to life on land (Coates *et al.* 2008). At the same time, the lower jaw became fortified and modifications to the proportions, number and positions of the teeth reflected adaptations to new diets and feeding mechanisms (Clack 2006, 2009).

1.4.1.2. Hearing

As tetrapods transitioned to live on land, gill breathing declined in importance (Clack 2002a). Changes to the ear, occiput and the skull roof included a reduction in the hyomandibula bone that controlled gill breathing, and the gill skeleton or viscerocranium was reduced (Clack 2002a, 2009, Coates *et al.* 2008). As the palate became attached securely to the braincase, the hyoid arch was transformed: the lower part (ceratohyal) remained large, but the upper hyomandibula part reduced and was re-oriented as a primitive stapes (Coates *et al.* 2008). No longer associated with jaw suspension, the hyomandibula/stapes undertook a role in sound conduction (Clack 2002, 2007). By increasing the size of the external opening of the spiracular pouch in the front gill chamber and filling it with air, the middle ear cavity in modern tetrapods was formed (Clack 2009).

1.4.1.3. The neck

Modifications in the cranial architecture were also associated with new modes of locomotion and breathing (Shubin *et al.* 2006). The loss of the opercular, subopercular and the extrascapular series bones disconnected the skull from the pectoral girdle and formed a neck joint (Daeschler *et al.* 2006, Clack 2009). This

enabled the head to have an independent range of movement and freed the pectoral girdle, which enabled the tetrapods to raise their heads out of the water to improve air-breathing efficiency (Daeschler *et al.* 2006, Clack 2009). At the back of the skull, an extensive area for cervical muscle insertion developed to augment the mobility of the head (Shubin *et al.* 2006). Later, in the amniote stem lineage, heads reduced in size and deepened, a feature associated with the evolution of costal ventilation (Janis & Keller 2001).

1.4.1.4. The fore limbs

The key events in the evolution of the fore limb concern the loss of the fin rays, the remodelling of the humerus and the acquisition of digits (Coates *et al.* 2008).

Fins had ossified and segmented fin rays and the endoskeleton was encased within a scale-covered muscular lobe (Coates *et al.* 2008). A strong and flexible appendage that was capable of moving across the substrate is inferred from the presence of a robust scapulocoracoid and reduced lepidotrichia of the pectoral fin (Shubin *et al.* 2006).

As the humerus is the most robust element of the pectoral appendage, this is usually well preserved and provides evidence for fore limb development through time (Clack 2009; Figure 8). There is a clear trend of the humerus becoming relatively larger over time, with the lengthening of the proximal shaft and for the head (that articulates with the shoulder) to flatten and develop a more elongate rather than bulbous articular surface (Clack 2009). The longer proximal shaft increases the area for the attachment of the muscles that stabilise the shoulder joint (Clack 2009).

Other indicators of the development of muscles for land locomotion are seen on the dorsal and ventral surfaces of the humerus. On the dorsal surface, a posterior, rectangular blade (entepicondyle) bore the muscles to the ulna and a dorsal, vertically oriented ridge (ectepicondyle) bore the muscles to the radius (Clack 2009). In tetrapodomorph fish, the entepicondyle is smaller and more triangular

and the ectepicondyle is an ill-defined ridge, which suggests a minimal musculature for the lower front limbs (Clack 2009).

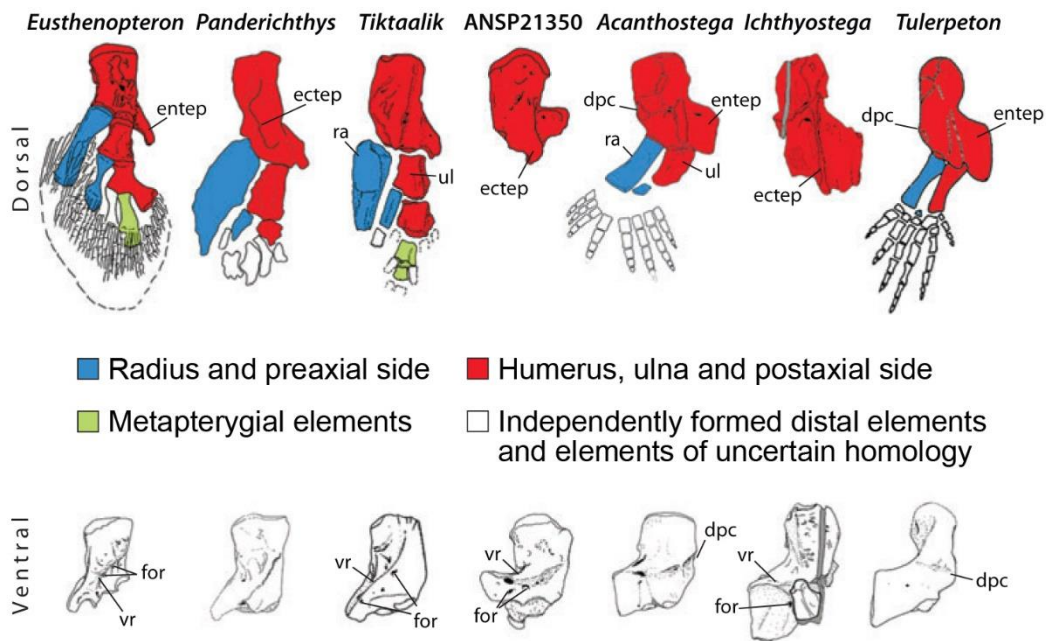


Figure 8. Fore limbs and humeri of fossil tetrapodomorphs. The top row shows fore limbs or humeri in dorsal view. The bottom row shows humeri in ventral view, note the direction and orientation of the ventral ridge (vr) which changes from passing diagonally across the bone (*Eusthenopteron* through to *Tiktaalik*) to running more or less transversely across the bone (ANSP 21350 through to *Tulerpeton*). Abbreviations: dpc = deltopectoral crest, ectep = ectepicondyle, entep = entepicondyle, for = foramina, ra = radius, ul = ulna, vr = ventral ridge. Not to scale. From Clack (2009).

On the ventral surface of the humerus, a 'ventral ridge' runs diagonally from near the head to end at or near the sloping edge of the ventral surface of the entepicondyle (Clack 2009). The ventral ridge was where the muscles from the shoulder to the forearm, and those from the forearm to the rest of the appendage, met each other (Clack 2009). From ANSP 21350 (an isolated humerus specimen) onward, the ventral ridge runs more or less across the bone at right angles to the length of the shaft (Clack 2009; Figure 8). Its reorientation may correlate with the realignment of the appendage from a more posterior to a more lateral position

(Clack 2009). In later tetrapods, this feature disappears more or less completely until only the more anterior part remains as a process that probably bore the deltoid and pectoralis shoulder muscles of more terrestrial tetrapods (Clack 2009). The distal parts of the humerus, where the muscles that operate the radius and ulna attach, enlarged and became more elaborate (Clack 2009).

Several foramina located in the ventral ridge carried blood vessels to the more distal parts of the appendage (Clack 2009). The foramina diminished and eventually disappeared, suggesting that the blood vessels relocated from bony tunnels to run through soft tissue instead, increasing their blood volume as the musculature for terrestrial locomotion developed (Lebedev & Coates 1995, Shubin *et al.* 2004).

There were further modifications to the articular facets that bore the radius and ulna; rather than being entirely distal as in the fin, the facets moved to a more ventral position (Clack 2009). This indicates the start of an elbow-bend and bringing the radius and ulna to a downwardly sloping angle, although, initially, the hand would still have been positioned laterally and not forwards as in later tetrapods (Clack 2009).

Digits can be regarded as a subgroup of radials with distinguishing characteristics (Coates *et al.* 2008). Functionally they unite the distal ends of the radius and ulna and are aligned to form a series across the distal end of the appendage rather than exhibiting a branched pattern as seen in fishes (Coates *et al.* 2008). Digits are known only in appendages where fin rays and scales are absent i.e. in tetrapods (Coates *et al.* 2008; Figure 9).

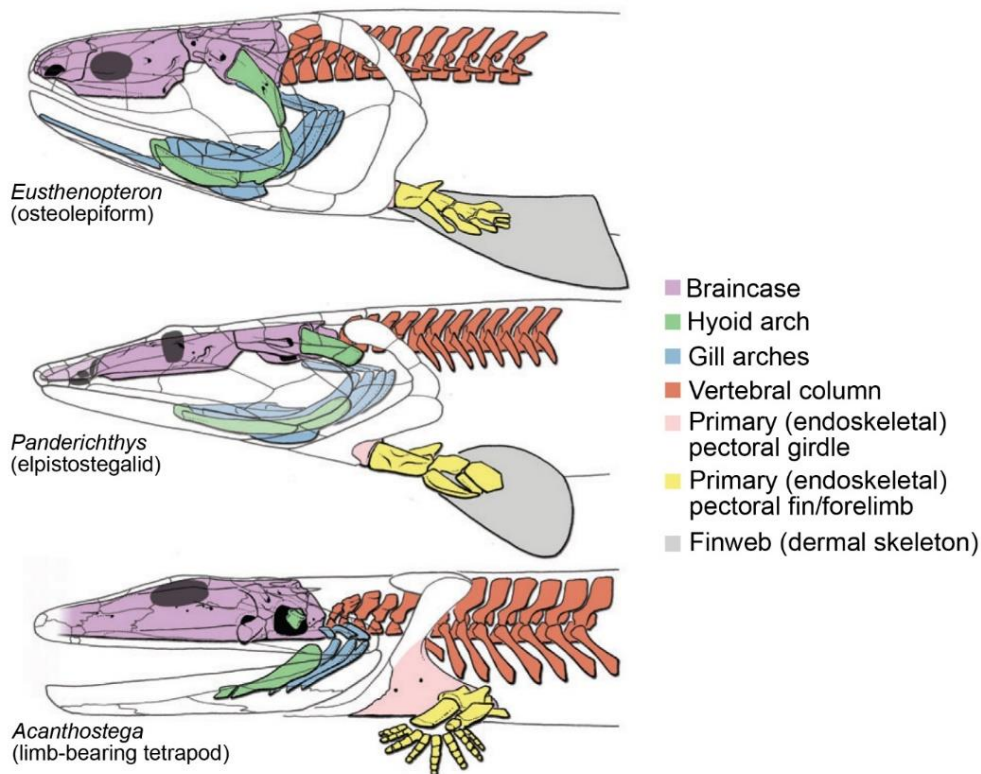


Figure 9. The skeletons of *Eusthenopteron* (top), *Panderichthys* (middle) and *Acanthostega* (bottom) shown in lateral aspect to demonstrate the fish to tetrapod morphological transition. From Coates *et al.* (2008).

1.4.1.5. The hind limbs

Fossils that illustrate the fin to limb transition reveal great morphological differences between the pelves and hind limbs of the finned tetrapodomorphs to those of the limbed tetrapods (Shubin *et al.* 2014). The entire hind limb is significantly smaller than the fore limb in finned tetrapodomorphs and could not have provided extensive body support or propulsion (Shubin *et al.* 2014). Conversely, the pectoral fins were enlarged and the pelvic girdles were robust (Shubin *et al.* 2014).

In fish, the pelvis is not connected to the vertebral column, which has morphologically undifferentiated vertebrae, but for tetrapods to be able to walk requires a connection between the axial skeleton and the ground, so the pelvis and vertebral column must be linked (Clack 2009). To achieve this, the pelvis

enlarged, as shown in the basal tetrapods *Acanthostega* and *Ichthyostega* and the lungfish, which have fused bony pelvic girdles (Boisvert *et al.* 2013, Coates 1996, Jarvik 1996). The pelvis also attached directly to the vertebral column by sacral ribs and the hip socket (acetabulum) and surrounding support structures re-oriented to face laterally (as the scapulocoracoid) to enable a walking gait (Coates *et al.* 2008).

The notochordal vertebral column developed expanded centra and upright neural spines and ribs that enlarged, acquired broad ends and extended laterally to accommodate the increased musculature (Coates *et al.* 2008). The trunk ribs also expanded and the vertebrae developed interarticulating processes to strengthen the vertebral column to carry the weight of the body (Daeschler *et al.* 2006, Clack 2009).

The fin-to-limb transition, therefore, involved the separate developments of the pectoral and pelvic girdles (Coates *et al.* 2002).

1.4.1.6. Scales

Regarding the external surface of the animals, the scales covering the body and fins of fish reduced considerably in limbed tetrapods (Coates *et al.* 2008). Early tetrapod taxa had ossified scales present only as gastral plates on the ventral surface of the trunk but these were lost later (Coates *et al.* 2008).

1.4.2. Trackways

In addition to skeletal evidence for terrestrialisation, trackways provide ichnological evidence of terrestrial locomotion. The first Devonian trackways to be described are from the Famennian Combyingbar Formation of the Genoa River Beds in New South Wales, Australia (Warren & Wakefield 1972, Young 1993; Figure 10).

This location preserves two trackways, the first of which has sets of overlapping manus and pes imprints arranged in the characteristic tetrapod pattern of alternations of left and right sides (Clack 1997). Several prints show at least five

digits, and the animal that made them did not leave drag marks from the abdomen or tail (Clack 1997; Figure 10 A left). The second trackway is different, running parallel to the first, it shows alternations of a small manus and larger pes and has a sinuous central drag mark from the abdomen or tail (Clack 1997; Figure 10 A right).

Devonian trackways are known from several localities (Table 3). However, although trackways are indicative of the terrestrial locomotion of animals, many have been preserved from subaqueous environments (McAllister 1989). Indeed, the laterally-placed digit impressions of the first of the Genoa River Beds trackways indicate that the animal's manus and pes were aligned perpendicular to the body, which characterises a more paddle-like stroke rather than being the power stroke in walking (Clack 1997). Therefore, Devonian age trackways cannot be assumed to have been made by tetrapods that had become wholly terrestrialised (Clack 1997).

County	Location	Age
Australia	Glen Isla, Grampians (Warren <i>et al.</i> 1986)	Early or Mid-Devonian (Clack 1997)
Scotland	Tarbat Ness (Rogers 1990)	Devonian
Scotland	Hoy Sandstone, Orkney (Sarjeant 1974)	Late Devonian (Wilson <i>et al.</i> 1935)
Ireland	Valentia Island (Stössel 1995)	Eifelian to Famennian
Greenland	Kap Graah (Friend <i>et al.</i> 1976)	Frasnian

Table 3. Locations and ages of Devonian tetrapod trackways (see Figure 10).

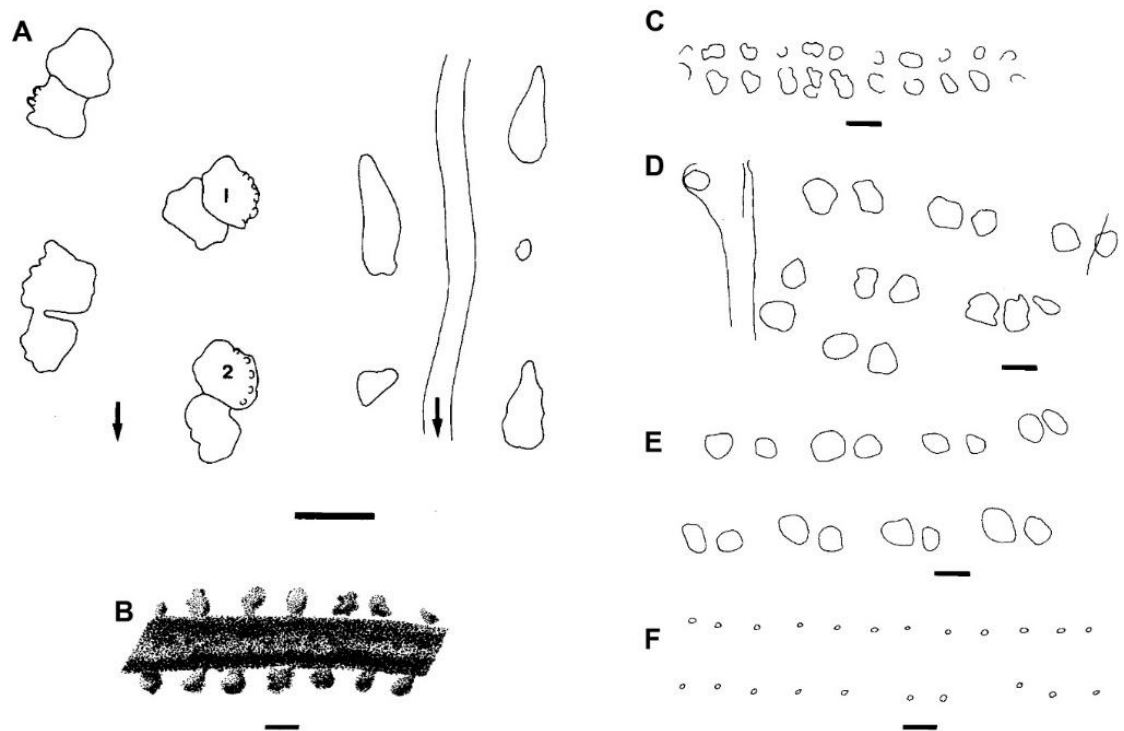


Figure 10. Devonian tetrapod trackways. A. Two adjacent tracks from Genoa River. Arrow shows direction of travel. Scale bar = 50 mm. B. Hoy track. Scale bar = 10 mm. C. Glen Isla tracks. D. Tarbat Ness tracks. E. Short section of the Valentia Island tracks. F. Short section of one of the Kap Graah tracks. Scale bars for C to F = 100 mm. From Clack (1997).

1.4.3. The sequence of developments

Newly discovered fossils of tetrapods and their antecedents continually improve consensus phylogenies, which provide a platform for debating the sequences of character acquisition (Clack 2009). For example, the re-evaluation of *Acanthostega* changed the theory behind the evolution of limbs and terrestrialisation (Clack 2006, 2009).

Initial hypotheses that fish emerged onto land first and subsequently evolved limbs from fins have now been revised (Clack 2006, 2009). When Coates (1996) demonstrated that the fish-like characters of *Acanthostega* tended to be concentrated in the posterior parts of the animal, this suggested that the initial stages of the fish-tetrapod transition only concerned the head and anterior parts of

the trunk (Clack 2009). Moreover, as *Acanthostega* had digits as well as fully functional internal gills, this showed that the development of the tetrapod limb preceded changes in the respiratory system (Clack 2009). Therefore, limbs with digits must have evolved while the animals still primarily lived and moved in water, and adaptations to terrestrial locomotion came later (Clack 2006).

The current view of the evolutionary development of tetrapodomorphs towards terrestrialisation is that it seems to have begun with improving the air-breathing capabilities of animals that were still aquatic, with the adaptations for terrestrial locomotion being later developments and pentadactyly among the last to be completed (Clack 2009). Figure 11 provides a summary of the skeletal adaptations towards terrestrialisation discussed above and the sequence in which these changes took place.

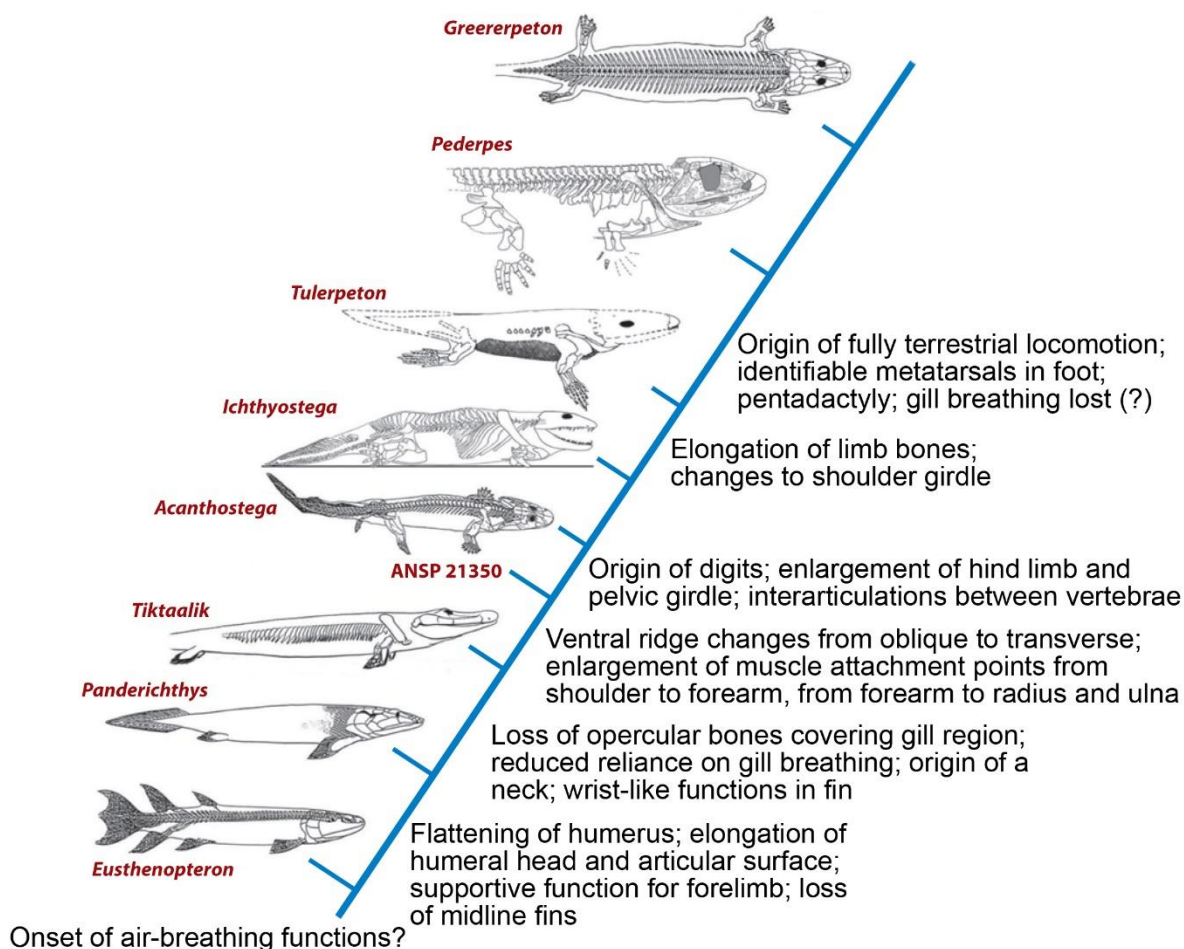


Figure 11. Cladogram of the key tetrapodomorphs and limbed tetrapods with their major evolutionary advances to the right. From Clack (2009).

Having established how early tetrapods evolved to live on land, the next question to answer is *why* did tetrapods move onto the land?

1.5. Why the tetrapods made the transition onto land

The expansion of the aquatic and terrestrial habitats of plants from the late Silurian through to the mid Devonian represented a late phase in a vast sequence of continental invasions (Labandeira 2005). A significant rise in atmospheric oxygen levels to >20% occurred during the Silurian to early Devonian and enabled arthropods to become terrestrialised (Ward *et al.* 2006).

Three major clades of arthropod herbivores and their consumers (myriapods, arachnids and hexapods) colonised terrestrial habitats (Ward *et al.* 2006).

Figure 12 shows two separate colonisation phases onto land. Phase 1 from 425 to 360 Ma initially involved the three previously mentioned arthropod clades during Phase 1A (425 to 385 Ma), followed by the first aquatic to semi-terrestrial limbed vertebrates during Phase 1B (385 to 360 Ma). Phase 2, from 345 Ma to the early Permian, which followed Romer's Gap, shows major originations and radiations of both the newly terrestrialised arthropods and the tetrapods.

That vertebrate terrestrialisation closely followed arthropod terrestrialisation cannot be coincidental. Invertebrates form a major food source for extant aquatic animals and so the expansion of the invertebrates' habitats onto land would have been a strong driver for the tetrapods to follow suit. Once the transition onto land had been made, tetrapods continued to evolve in tandem with new forms of plant life to exploit the newly emerging habitats and food webs, including those that developed after the EDME.

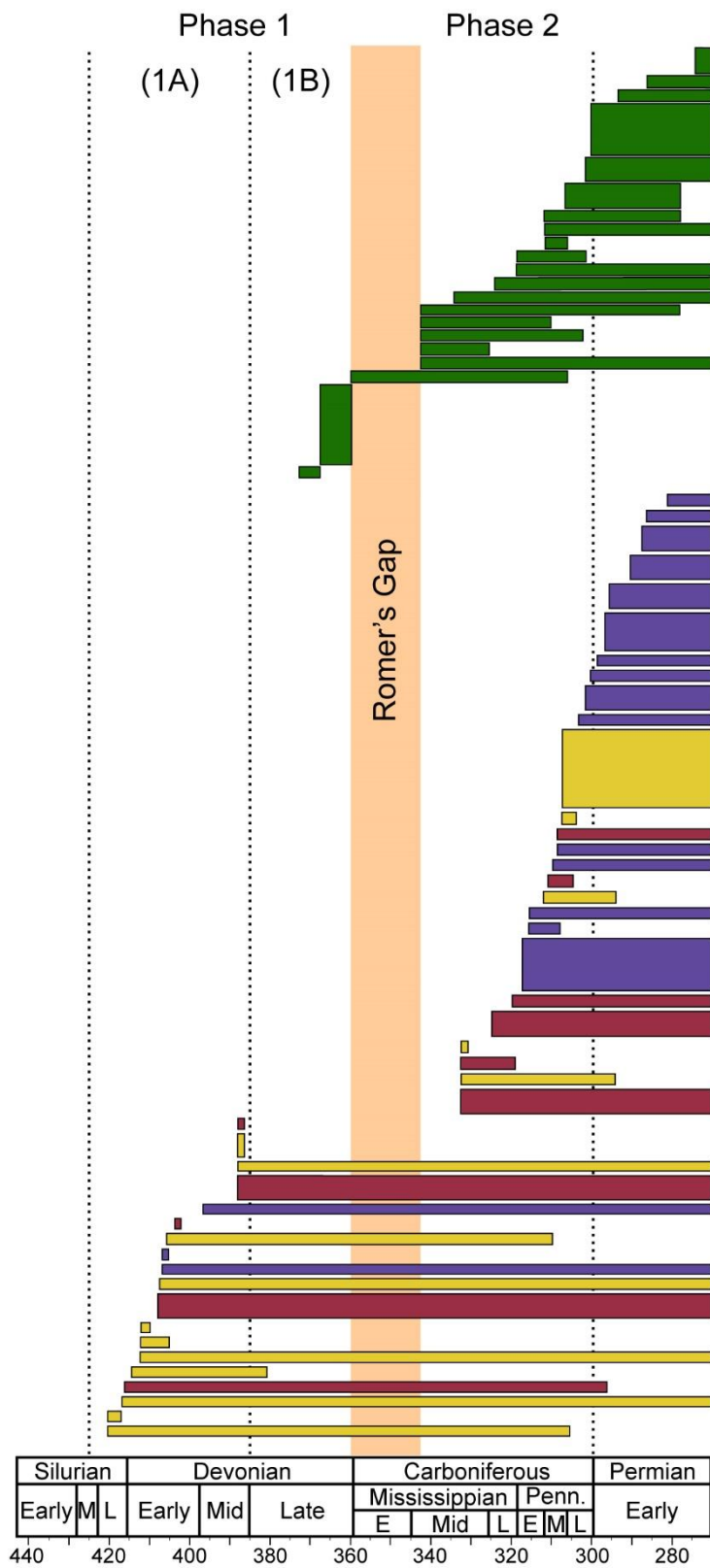


Figure 12. Geochronologic range data for terrestrial arthropod and vertebrate clades. Major arthropod clades: Myriapoda (yellow), Arachnida (red) and Hexapoda (purple) are divided into orders. Limbed vertebrates are in green and

Romer's Gap in orange. Two separate colonisations onto land are shown. Phase 1 involved the arthropods initially (Phase 1A) followed by the first tetrapods (Phase 1B). Phase 2 comprised new major originations and radiations of terrestrialised arthropods and limbed vertebrates. Penn = Pennsylvanian, E = Early, M = Mid, L = Late. After Ward *et al.* (2006).

1.6. Romer's Gap

When discussing why tetrapods evolved towards terrestrialisation, the phrase 'Romer's Gap' was used. This is a crucially important concept as it underpins the work behind this thesis and the TW:eed project for which it forms a part.

In 1956, Dr. Alfred Sherwood Romer, an American palaeontologist who specialised in the evolutionary history of vertebrate animals using comparative anatomy, published a paper entitled 'The early evolution of land vertebrates'. In this, he identified a complete lack of data that covered the many important steps in the evolutionary progression of vertebrates emerging from water on to land. He highlighted the 'very inadequate' nature of the fossil record during this transitional period and produced a diagram to visualise this (Figure 13).

It is apparent from Romer's figure that no fossil data were available at that time from the early Carboniferous (Mississippian), which coincides with the fish-tetrapod transition. The missing fossil evidence masked our understanding of evolutionary developments that facilitated this phase and, hence, became known as 'Romer's Gap'.

To clarify this situation, the transitional fossils that evidenced the various complex stages in evolution that facilitated this extreme skeletal, physiological, ecological and behavioural overhaul of vertebrate life needed to be found. These would then elucidate the mechanisms, directions and timings of each change that were linked to contemporary changes in the environment, climate, vegetation and invertebrate life.

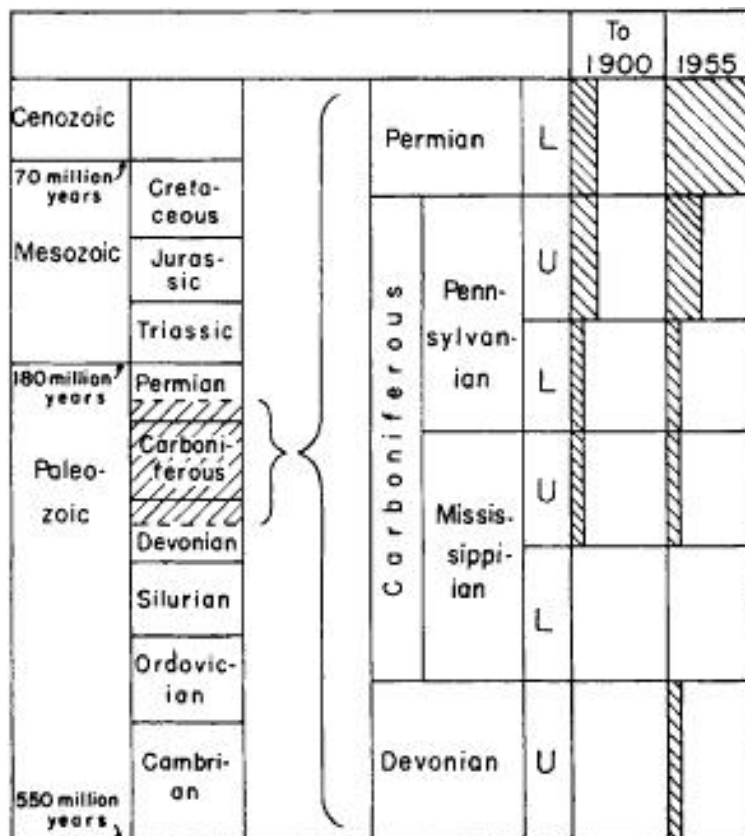


Figure 13. The approximately 30 million year gap in the fossil record between the Tournaisian and the early part of the Viséan, later dubbed 'Romer's Gap', that spanned the transition of aquatic tetrapodomorphs of the Devonian and the fully terrestrial tetrapods of the early Carboniferous. The hatched portions of the squares in the last two columns entitled 'To 1900' and '1955' indicate the amount of data regarding tetrapods that was then available. From Romer (1956).

At the time Romer was writing, the gap represented a period of about 30 million years covering all of the Tournaisian and most of the Viséan stages (Smithson *et al.* 2012). Gradually, with the discovery of more mid to late Viséan (Asbian/Brigantian) age tetrapod fossils, the length of the gap was reduced to about 15 million years (Smithson *et al.* 2012).

However, although the 'gap' was closing, the fossils representing the transitional morphologies between the aquatic tetrapodomorphs of the Devonian and the fully terrestrial tetrapods of the Tournaisian and early part of the Viséan were missing. The gap in the fossil record that still remained, therefore, concealed the order, time

and frequency of the acquired characters that related to the many fundamental evolutionary changes in the skeleton associated with breathing, feeding, locomotion and hearing as tetrapods became terrestrial. Only a robust phylogeny would resolve this question with data from new fossils to complete the picture (Clack 2006).

Various reasons accounting for 'Romer's Gap' have been suggested. As it occurred immediately following a mass extinction event (EDME), the gap in the fossil record was thought to represent a 'post-extinction trough' i.e. a decline in the abundance and diversity of the tetrapods that lasted for millions of years (Sahney & Benton 2008, Erwin 1998). An alternative explanation was that it represented an interval of low atmospheric oxygen, which hindered the animals' ability to breathe on land (Ward *et al.* 2006). However, the presence of a diverse tetrapod fauna located at Blue Beach in Canada during this interval suggested that the main cause for the lack of early Tournaisian fossils was simply due to collection failure rather than being indicative of biological or physical phenomena (Anderson *et al.* 2015).

Over the years since Romer's paper (1956), many new discoveries of 'transitional' fossils have reduced the gap. But many fundamental questions, as to how and when the profound anatomical, physiological and ecological changes took place, remained largely unanswered.

A more determined search for these answers began when a specimen found in 1971, which had been misidentified as a rhizodont fish, was prepared and revealed the mostly complete skeleton of the first late Tournaisian tetrapod from western Scotland (Clack 2002). Known as *Pederpes*, this specimen not only extended the known geographical range for early tetrapods in the earliest Carboniferous, that had previously only been found as isolated bones from Canada, but it suggested a new source of finds in the Ballagan Formation of the UK (Clack 2002).

The resultant upsurge of interest in tetrapod origins, and the re-classification of previously unidentified fragments in museum collections as Devonian tetrapods,

led to active searches for new tetrapod-bearing localities (Clack 2006). Some of these that are of relevance to the present work are described briefly below.

1.7. Tetrapod localities in Scotland

In 2012, Smithson *et al.* reported the discovery of a suite of tetrapod fossils from one previously known and 4 new Tournaisian localities in southern Scotland (Figure 14; Smithson & Wood 2009a, 2009b, Waters *et al.* 2007).

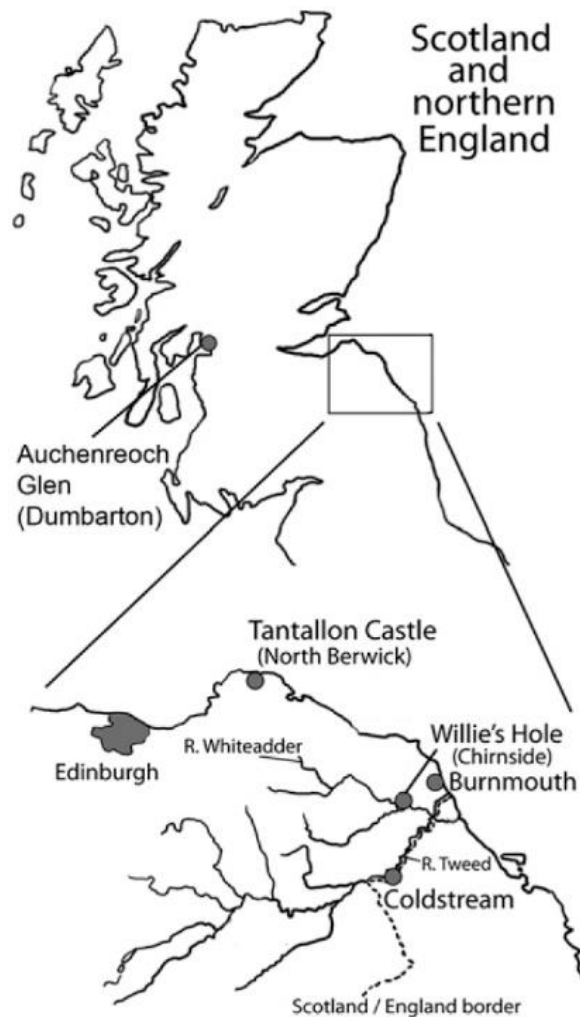


Figure 14. Map of southern Scotland and northern England showing the locations of the Tournaisian sites in Scotland. From Smithson *et al.* (2012).

1.7.1. Burnmouth (Tweed Basin, Borders Region)

A coastal section at Burnmouth north of Berwick on Tweed has yielded isolated and partially associated tetrapod, lungfish and arthropod material (Smithson *et al.* 2012). The finds include some unusually small individuals and the tetrapods are unlike other early Carboniferous forms such as *Pederpes*, *Crassigyrinus*, *Greererpeton* or *Proterogyrinus* (Clack 2002, Clack & Finney 2005, Smithson & Panchen 1990, Godfrey 1989, Holmes 1980). The Burnmouth site also confirms the early presence of large vertebrates with later Carboniferous rather than Devonian affinities (Smithson *et al.* 2012).

1.7.2. Willie's Hole (Tweed Basin, Borders Region)

The banks and bed of the gently dipping Ballagan Formation strata of the Whiteadder River near Chirnside have produced a wealth of tetrapods, rhizodonts, lungfish and actinopterygians from three separate beds (Smithson *et al.* 2012).

1.7.3. Coldstream (Tweed Basin, Borders Region)

The fossils recently discovered from the banks of the Tweed River near Coldstream include tetrapod skull bones and vertebrae and elements from lungfish and rhizodonts (Smithson *et al.* 2012).

1.7.4. Tantallon (Midland Valley Basin, East Lothian Region)

Close to the fossil plant localities of Castleton Bay and Oxroad Bay, sediments near Tantallon Castle on the south shore of the Firth of Forth have yielded isolated vertebrate bones and teeth, including the large partial lower jaw of a tetrapod (Smithson *et al.* 2012, Chen & Ahlberg 2009).

1.7.5. Dumbarton (Western Scotland)

Dumbarton is the location from where the most complete articulated skeleton of *Pederpes finneyae* was discovered (Clack 2002, Clack & Finney 2005).

Phylogenetically, it is considered to be basal to all post-Carboniferous tetrapods apart from *Crassigyrinus* and appears to have had hind limbs that were adapted for walking on land (Coates *et al.* 2008, Clack 1998, Ruta & Clack 2006).

1.8. The TW:eed project

The new tetrapod fossil sites of Tournaisian age have begun to provide a more complete picture of the events during the fish to tetrapod transition that occurred through the shortening Romer's Gap period. The new fossils strongly suggest that the apparent gap in the fossil record was indeed purely an artefact of the lack of successful collecting from suitable sediments and localities, rather than reflecting actual evolutionary events (Smithson *et al.* 2012).

As a consequence of the success of finding these new Tournaisian tetrapod-bearing sites, the four-year *Tetrapod World: early evolution and diversification* (TW:eed) project was instigated and funded by the NERC Consortium Grant: "The Mid-Palaeozoic biotic crisis: setting the trajectory of tetrapod evolution".

This was a programme of scientific research investigating the fossils and environments of the Tournaisian stage of the early Carboniferous Epoch. The project's main aim was to study newly discovered fossils that were filling Romer's Gap. Supplemental to this, were studies of the contemporaneous plants and animals and the environment in which they lived.

An interdisciplinary team was assembled to investigate the palaeontology, sedimentology, stratigraphy, palynology and stable isotopes, to determine how the tetrapods became terrestrialised and how the other animals, plants and their environment changed alongside the tetrapods. The TW:eed team was a consortium of three universities, the British Geological Survey and the National Museum of Scotland and the project was divided into five frameworks. For details of the members of the TW:eed Project team, please refer to Appendix 1.

1.8.1. The palaeontological framework

The TW:eed project was led by Professor Jennifer Clack of the University of Cambridge. She and her team, Dr. Timothy Smithson and Keturah Smithson were responsible for the palaeontological framework.

This team aimed to visit a number of field sites repeatedly, to collect more tetrapod specimens to find new transitional fossils to fill in Romer's Gap.

1.8.2. The stratigraphical framework

Led by the British Geological Survey, and headed by Dr. David Millward with Dr. Timothy Kearsy, this team was responsible for the stratigraphic part of the project. This was based on drilling a 500 m deep borehole through the Ballagan Formation (which incorporates the Romer's Gap interval) to form the spatial and temporal standard against which to log the evolutionary advances of the tetrapods and establish the timeframe in which the recovery from the EDME occurred.

A comprehensive set of stratigraphic methods was employed to examine the borehole sediments: palynology and ostracod biostratigraphy, lithostratigraphy, sequence stratigraphy, wireline correlations and chemo-stratigraphy. The aims were to understand how the sedimentary and climate systems changed through time and to correlate this information with new tetrapod-bearing localities in the Scottish Borders and Northumberland area. This information would both place the sites into their correct chronological order, to date the evolutionary relationships between the different organisms, and create robust models to understand the ecosystems across a broad area.

1.8.3. The palynological framework

The palynological framework was headed by Professor John Marshall of the University of Southampton with palynological analysis of the borehole by the current author (ER) and with charcoal analysis by (now Dr.) Dave Carpenter.

It was hoped that by obtaining a complete, cored succession from the borehole, it would be possible to generate a quantitative palynological zonation, with which to date the isolated tetrapod localities and to place the tetrapods they contained into chronological order. The palynological data, coupled with the other stratigraphic data from the borehole, would also provide information for reconstructing climatic conditions.

As one previous explanation for Romer's Gap was that low atmospheric oxygen levels during the early Carboniferous drove tetrapods and arthropods back into aquatic environments, the project aimed to test this idea by using the abundance of fossil charcoal.

1.8.4. The sedimentological framework

Professor Sarah Davies of the University of Leicester was responsible for delivering the sedimentological framework of the project, with the involvement of Dr. Carys Bennett and Janet Sherwin.

A detailed sedimentary analysis of the borehole core, coupled with the study of a 450 m thick section at Burnmouth, would investigate the conditions in which the tetrapods lived and how the depositional environments in south-eastern Scotland contributed to the preferential preservation of early tetrapods.

Many of the key tetrapod finds were from fine-grained layers within the Ballagan Formation. This was believed to have represented an extensive low relief, muddy, vegetated floodplain that was traversed by numerous river systems, surrounding mountainous areas now represented by the Cheviot and the Southern Uplands hills.

The borehole core sediments were to be compared to those of the Burnmouth succession and together this framework was designed to provide a template to pinpoint known and new fossil discoveries and to correlate the isolated sections exposed on riverbanks. This would ensure that the different datasets from each of the frameworks were amalgamated to provide a full interpretation of the

depositional environment, which provided a comprehensive foundation for reconstructing the terrestrial ecosystems.

1.8.5. The isotopic framework

Professor Melanie Leng of the NERC Isotope Geosciences Laboratory (NIGL) was responsible for the isotopic framework part of the project.

In conjunction with the Palynological and Stratigraphical frameworks, stable carbon isotope stratigraphy ($\delta^{13}\text{C}$) would be used to enhance the correlation between the different sites.

The total organic carbon content (TOC), the specific carbon and the bulk carbon isotope signature of sedimentary rocks would be used to investigate the marine or terrestrial origin of the plant matter they contained. This would provide a palaeoenvironmental context to the tetrapod fossils.

Data from oxygen ($\delta^{18}\text{O}$) and carbon ($\delta^{13}\text{C}$) stable isotopes obtained from well-preserved shelly fossils, such as ostracods, would interpret the palaeoenvironment of the water, both in terms of its salinity and temperature. Locally, this would indicate whether the environment in which the tetrapods lived was freshwater, brackish or marine. Globally, this would provide geochemical evidence for the timing of the Devonian-Carboniferous ice age and when its glacial phases occurred.

CHAPTER 2

To investigate the plant recovery following the EDM, this doctoral research project examined palynomorph-containing material from borehole core.

The geological context for the broader TW:eed project, of which the work of this thesis forms a part, is given. This discusses the tectonic setting, climate and palaeogeography of the Tournaisian and the principal lithofacies of the Midland Valley of Scotland and Northern England to explain the environment of the study area in which the plants and animals were living.

Following this, the scientific rationale for the Norham West Mains Farm (NWMF) borehole is discussed, which further details its objectives, its siting requirements and why West Mains Farm in Norham was selected, as well as the drilling operation and the core recovery. These were the materials that were used in this thesis.

However, owing to drilling issues relating to the base of the tetrapod-bearing Ballagan Formation not being reached, additional information comes from an outcrop section at Burnmouth in the Tweed Basin. Further to the palynological data, palaeosols are discussed as they also represent vegetated land surfaces and add more to the story of the plant recovery.

Finally, the techniques used to analyse the data that are discussed in chapters 3, 4 and 5 of this thesis are given in the 'Methods' section, with some detailed work instructions also listed in the appendices.

MATERIALS

2.1. Carboniferous geology

The Carboniferous strata of the UK encompass a range of facies and depositional environments, which partly represents the northward drift of the UK across the equator during this time (Figure 15; Waters *et al.* 2007, Scotese & McKerrow 1990). At the beginning and the end of the Carboniferous, the climate was at least seasonally arid, which led to the widespread development of red continental alluvial clastic-dominated facies during the Tournaisian and late Pennsylvanian (Waters *et al.* 2007). The intervening climate was tropical (Waters *et al.* 2007).

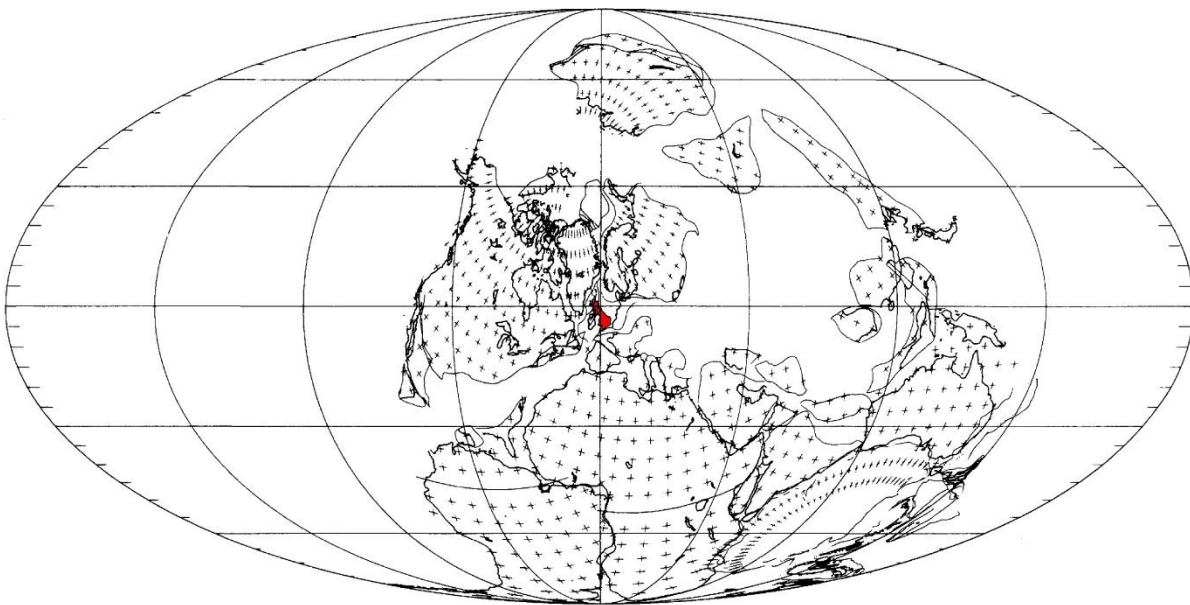


Figure 15. Palaeogeographic reconstruction showing the continental distribution during the early Carboniferous (Viséan) with Great Britain highlighted in red. From Scotese & McKerrow (1990).

Tectonic processes also influenced lithofacies development (Waters *et al.* 2007).

2.1.1. Tectonic setting during the Tournaisian and Viséan

During the late Devonian to early Carboniferous, a phase of north-south rifting started to affect all of central and northern Britain, producing numerous basins in a series of subsiding graben and half-graben structures, separated by platforms associated with horsts and tilt-blocks (Leeder 1982, 1988). From north to south these Carboniferous blocks and basins include the Midland Valley of Scotland, the Northumberland Trough, Alston Block, Stainmore Trough, Askrigg Block and Craven Basin (Figure 16; Waters *et al.* 2007). The block and basin margins were due to the reactivation of pre-existing basement lineaments but following the cessation of most of the rifting processes in the Viséan, a phase of regional subsidence saw the infilling of the resultant basins (Waters *et al.* 2007).

Also, during the late Devonian, the reactivation of pre-existing east-north-east-trending Caledonian structures initiated the east-north-east-trending graben of the Midland Valley of Scotland (Waters *et al.* 2007). The graben was positioned between the eroded remains of the Caledonian Mountains north of the Highland Boundary Fault to the north-west and by the Southern Uplands to the south-east (Waters *et al.* 2007).

As depocentres within the graben subsided at different rates over time, their location and trend also changed (Brown & Monro 1989). Associated with minor phases of compression, particularly during the mid-Carboniferous, marked thickness variations resulted from synsedimentary movement on north-east- and east-trending faults in a strike-slip regime (Read 1988, Waters *et al.* 2007).

The Northumberland Trough, including the Tweed and Solway Firth basins, was separated from the Midland Valley of Scotland by the Southern Uplands (Waters *et al.* 2007). It was constrained by the North Solway Fault to the north and by the Stublick-Ninety Fathom Fault to the south, both of which were active during deposition (Chadwick *et al.* 1995).

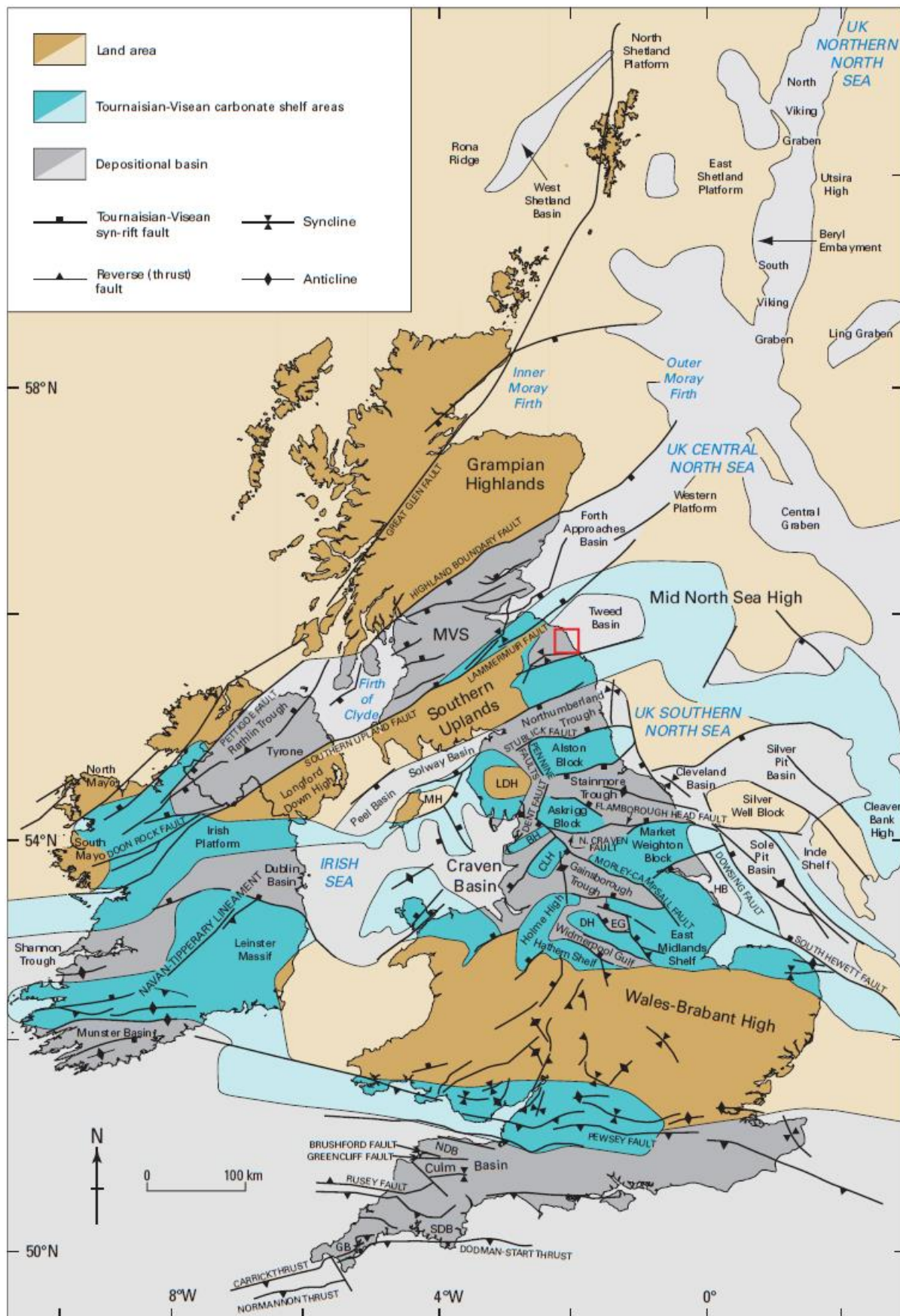


Figure 16. Principal structural features of the British Isles, onshore and offshore, that exerted a significant influence on the deposition of Carboniferous strata. The depositional basins and highs shown are those that developed during the

Tournaisian to Viséan. BH = Bowland High, CLH = Central Lancashire High, DH = Derbyshire High, EG = Edale Gulf, GB = Gramscatho Basin, HB = Humber Basin, LDH = Lake District High, MH = Manx High, NDB = North Devon Basin, MVS = Midland Valley of Scotland, SDB = South Devon Basin. The locations of the NWMF borehole and Burnmouth outcrop section in the Tweed Basin are marked with a red square. After Waters *et al.* (2007).

2.1.2. Tournaisian climate

During the Tournaisian, Scotland and Northern England were situated 4 degrees south of the equator, within a region of tropical climatic conditions (Scotese & McKerrow 1990, Peel *et al.* 2007). Tournaisian tree rings from the Scottish Borders and Viséan palaeosols from South Wales suggest a monsoonal climate, with thin evaporites and calcretes from the Tweed Basin, halite in the Northumberland Trough and palaeosols in Southern England supporting periodic aridity (Falcon-Lang 1999, Wright *et al.* 1991, Scott 1986, Andrews & Nabi 1998, Leeder 1974, Wright 1990, Bennett *et al.* 2016).

2.1.3. Palaeogeography of the Tournaisian

In the Midland Valley of Scotland, fluvial inflow from the south-west that was established during the late Devonian continued into the early Carboniferous (Read & Johnson 1967). The basin fill, chiefly composed of fluvial siliciclastic sediments, was transported along the axis of the graben (Browne *et al.* 1999). Significant contributions came from the Scottish Highlands to the north, and the input from the Southern Uplands to the south was minimal (Browne *et al.* 1999, Waters *et al.* 2007). These strata, deposited in a semi-arid climate, are characterised by calcareous and dolomitic pedogenic horizons (cornstones) that formed on stable alluvial plains (Waters *et al.* 2007). During the mid-Tournaisian, a mudstone-dominated succession, characterised by ferroan dolostone beds (cementstones) and evaporites (predominantly gypsum), was deposited on alluvial plains and marginal marine flats (sabkhas) that underwent periodic desiccation and fluctuating salinities (Waters *et al.* 2007).

2.1.4. Principal lithofacies

Nine major lithofacies have been identified for the Carboniferous of Great Britain. The two most relevant to this research project are detailed below (based on Waters *et al.* 2007):

2.1.4.1. Continental and peritidal facies

Deposited from late Devonian to Viséan times, continental and peritidal facies are widespread across northern Britain from the Midland Valley of Scotland to central England. The continental fluvial clastic subfacies commonly forms the earliest basin infill and extends onto horst and tilt-block highs. The peritidal marine and evaporite subfacies are generally limited to troughs associated with grabens and half-grabens in more marginal regions, for example the Midland Valley of Scotland and the Northumberland and Stainmore troughs. These occur as two commonly interdigitating facies:

A. Continental fluvial clastic ('cornstone') facies

Lithologies comprise purple-red conglomerates, sandstones and red mudstones, with characteristic nodules and thin beds of concretionary carbonate (calcrete = cornstones) deposited in environments ranging from alluvial fans, fluvial channels and floodplain overbanks, in semi-arid climatic conditions.

B. Peritidal marine and evaporites ('cementstone') facies

Lithologies of this facies include grey mudstones, siltstones and sandstones, characterised by the presence of nodules and beds of ferroan dolostone ('cementstone') and evaporites (mainly gypsum and anhydrite). These lithologies were deposited in environments that included alluvial plains and marginal marine flats subject to periodic desiccation and fluctuating salinities, directly influenced by the semi-arid climate.

2.1.4.2. Volcanic facies

Volcanics are distributed commonly throughout the Carboniferous succession of the Midland Valley of Scotland, with significant but less extensive developments of Tournaisian and Viséan age in the Solway Firth and along the England-Scotland border. They include basaltic lavas, bedded tuffs and volcanoclastic sedimentary rocks, with subordinate interbedded sedimentary rocks. They were erupted in subaerial to submarine environments from major Carboniferous eruptive centres in localities around Edinburgh and East and West Lothian that were active at various times.

2.1.5. The Ballagan Formation

The tetrapods under investigation by the TW:eed project were found in the generally poorly exposed Tournaisian Ballagan Formation of the Inverclyde Group (Figure 17). This unit crops out in the Midland Valley of Scotland and the Northumberland Trough in England (Browne *et al.* 1999, Marshall *et al.* 2019).

Period	Stage	Group	Formation	Member
Carboniferous Mississippian	Viséan	Inverclyde	Clyde Sandstone	
	Tournaisian		Ballagan	Newburgh
				Dron
				Mains of Errol
Devonian			Kinnesswood	

Figure 17. The Kinnesswood, Ballagan and Clyde Sandstone formations comprising the Inverclyde Group. After McLean & Neves (2003) and Marshall *et al.* (2019).

2.1.5.1. The Midland Valley of Scotland

There are four main sedimentary groups found in the Midland Valley of Scotland. In order of age these are the Inverclyde Group (partly Devonian), the Strathclyde, Clackmannan and Scottish Coal Measures groups (Browne *et al.* 1999). The Inverclyde Group is the only one of these groups discussed here as it encompasses the Ballagan Formation, which is the subject of this work.

The Inverclyde Group of continental and peritidal facies, comprises, in ascending order, the Kinnesswood, Ballagan and Clyde Sandstone Formations (Paterson & Hall 1986; Figure 17; Table 4). The approximately 1500 m thick Inverclyde Group is typically recognised by the presence of cornstones (Waters *et al.* 2007).

Formation	Lithological characteristics	Depositional environment
Clyde Sandstone	White, fine- to coarse-grained sandstone, commonly pebbly, with beds of red-brown or grey mudstone and nodules or beds of pedogenic limestone.	Fluvial environments ranging from braided stream to floodplain with pedogenetically altered over-bank deposits.
Ballagan	Grey silty mudstone containing nodules and thin beds of dolostone and limestone ('cementstone').	Peritidal environment associated with intermittent emergence.
Kinnesswood	Purple-red, yellow, white and grey-purple, fine- to coarse-grained, mostly cross-bedded, sandstone with characteristic pedogenic carbonate nodules and horizons ('cornstones').	Fluvial environments ranging from braided stream to floodplain with pedogenetically altered over-bank deposits.

Table 4. A summary of the lithological characteristics and depositional environments for the three formations of the Inverclyde Group. From Waters *et al.* (2007).

2.1.5.2. Northern England

The Tournaisian and early Viséan succession of the Northumberland Trough is distinct from the rest of the province (Waters *et al.* 2007). The earliest Carboniferous strata along the southern margin of the Southern Uplands, of continental and peritidal facies, are very similar to the Inverclyde Group of the Midland Valley of Scotland, with the group and some formation names having been used to describe the stratigraphic units in the northern part of the Northumberland Trough (Waters *et al.* 2007). Here, the Inverclyde Group is overlain by the Border Group of early Viséan age (Waters *et al.* 2007).

The thickness of the Inverclyde Group reaches 640 m in the Solway Firth area and 900 m in the Tweed Valley, Northumberland and its base is typically unconformable on Silurian strata (Waters *et al.* 2007).

The Devonian Kinnesswood Formation, composed of red sandstone, siltstones and conglomerates, crops out intermittently along the northern margin of the Northumberland Trough (Waters *et al.* 2007). It was formed by calcrete-rich alluvial fans and deposited in a series of small, linked basins that developed during the early stages of crustal extension (Chadwick *et al.* 1995).

The Ballagan Formation, of Tournaisian age, comprises interbedded sandstone, mudstone, limestone and anhydrite (Armstrong & Purnell 1987, Waters *et al.* 2007). It crops out in the north-east of the Northumberland Trough and in the Solway Firth area, but in the central part of the Northumberland Trough, it changes laterally into the Lyne Formation of the Border Group (Figure 18; Waters *et al.* 2007). The deposition of the Ballagan Formation was dominated by the influx of alluvial fans, fluvial and fluviodeltaic sediments from the Southern Uplands that were intercalated with lacustrine and arid coastal plain deposits (Deegan 1973, Leeder 1974, 1992).

The Kinnesswood and Ballagan formations are separated locally by the Birrenswark and Kelso Volcanic formations in the Solway Basin and Berwick area, respectively (Lumsden *et al.* 1967, Greig 1988, Waters *et al.* 2007). The Birrenswark and Kelso Volcanic formations, of mid-Tournaisian age, are

composed of alkaline olivine-basalts, subordinate tuffs and other sedimentary strata and developed during the main initial phase of extensional faulting associated with the development of the Northumberland Trough (Armstrong & Purnell 1987, Waters *et al.* 2007). There is no equivalent of the Clyde Sandstone Formation of the Midland Valley of Scotland in northern England (Waters *et al.* 2007).

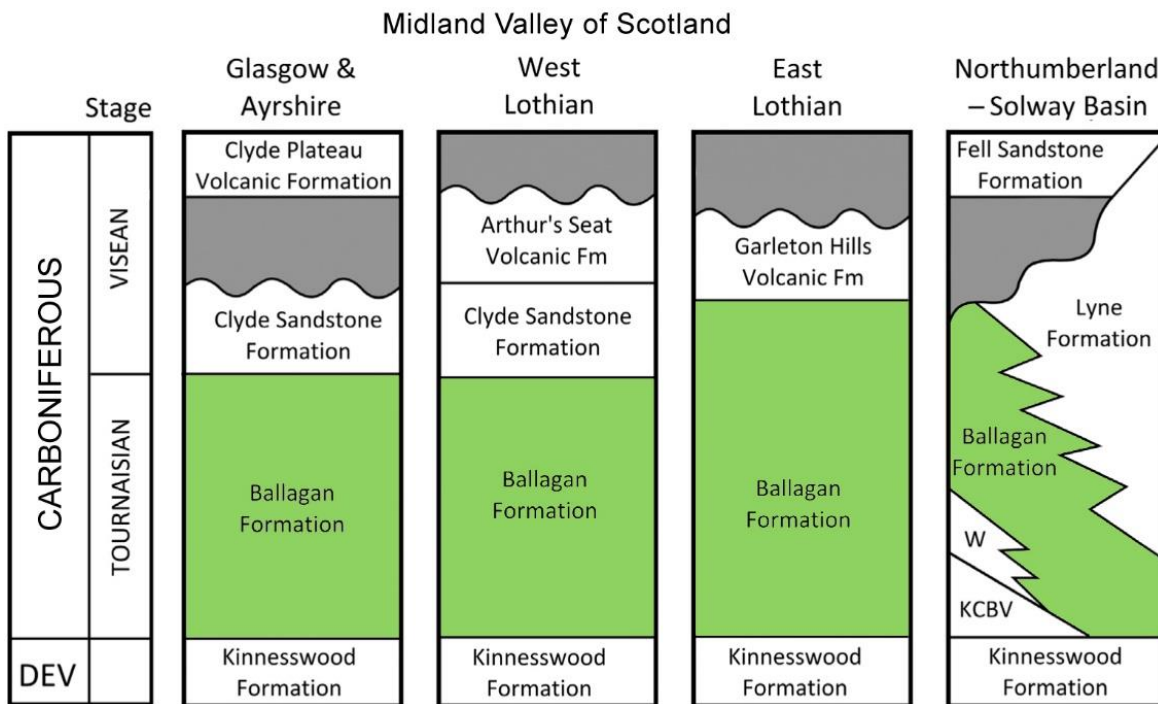


Figure 18. Early Carboniferous stratigraphies for the Midland Valley of Scotland and the Northumberland and Solway basins. KCBV = Kelso, Cottonshope and Birrenswark volcanic formations, W = Whita Sandstone Member. After Waters *et al.* (2011).

2.2. The Norham West Mains Farm borehole

As part of the TW:eed project, the Norham West Mains Farm (NWMF) borehole was commissioned to produce a high resolution, continuous record of the Ballagan Formation sediments that contained the early terrestrially-capable tetrapods of Romer's Gap age. Importantly, this was the first time that the Ballagan Formation has been cored specifically for an integrated palaeontological and palaeoclimatic project. The objectives and siting of the borehole and the core recovery are

discussed below, based, except where stated, on the more detailed 'Norham Operations Report' produced by Millward *et al.* 2013.

2.2.1. Borehole objectives

Procuring cores from a borehole was one of the primary objectives of the TW:eed project, as it would provide the spatial and temporal framework on which to underpin the research. Specifically, it would facilitate the establishment of the evolutionary sequence of the tetrapods' anatomical novelties and provide a timeframe for the biotic and environmental recovery following the EDME.

Detailed lithological, sedimentological, lithostratigraphical, biostratigraphical, palynological, petrological and isotope analyses of the core samples would enable a greater understanding of how the sedimentary and climate systems changed through time. By integrating these new data with studies of the tetrapod-bearing localities across the Midland Valley of Scotland, the project was designed to provide robust models to understand these late Devonian-early Carboniferous ecosystems.

Borehole core was preferred to outcrop data owing to its better preservation. Core often retains features that are easily lost through erosion e.g. evaporites and features that can be obscured in the field e.g. palaeosols. Additionally, inspecting core is completed under controlled conditions inside a building with all facilities immediately available. Working at outcrop is weather-, daylight- and sometimes tide-dependent, so takes longer and may require multiple visits. Continuous borehole core, therefore, provides a quicker and more accurate means of analysing and sampling sediments than at outcrop.

The main aim of the borehole drilling programme was to core through the entire Ballagan Formation and into the underlying Kinnesswood Formation. The specifications for the borehole were that it should be nearly vertical, to retain sedimentary structures *in situ*, and drilled to a maximum depth below ground level of approximately 500 m to accommodate the maximum length of the budgeted drill-string.

The specifications for the cores were that they should encompass a full sequence through Lower Carboniferous sedimentary rocks from rockhead to total depth (TD) and should be of 100 mm in diameter.

2.2.2. Siting the borehole

A resurvey of the Coldstream district, the area of the Tweed Valley south of the Whiteadder River at 1:10,000 scale provided outcrop locations of the Ballagan Formation, as well as valuable structural data. Although the Ballagan Formation had been verified from British Geological Survey (BGS) stratigraphical boreholes at Spilmersford, East Linton and Burnieknowes, none of these had reached the base of the formation and all were located in the East Lothian 'basin', away from the main tetrapod-bearing sites. None of the boreholes in the BGS archive within the Berwick-Chirnside-Coldstream Ballagan Formation outcrop area substantiated the full thickness of the unit, but the Hutton Castle Barns Borehole documented its base. Additionally, the drill site was located approximately 6 km north of Norham, in an area that did not exhibit significant structural deformation of the rocks (figures 19 to 21, Table 5).

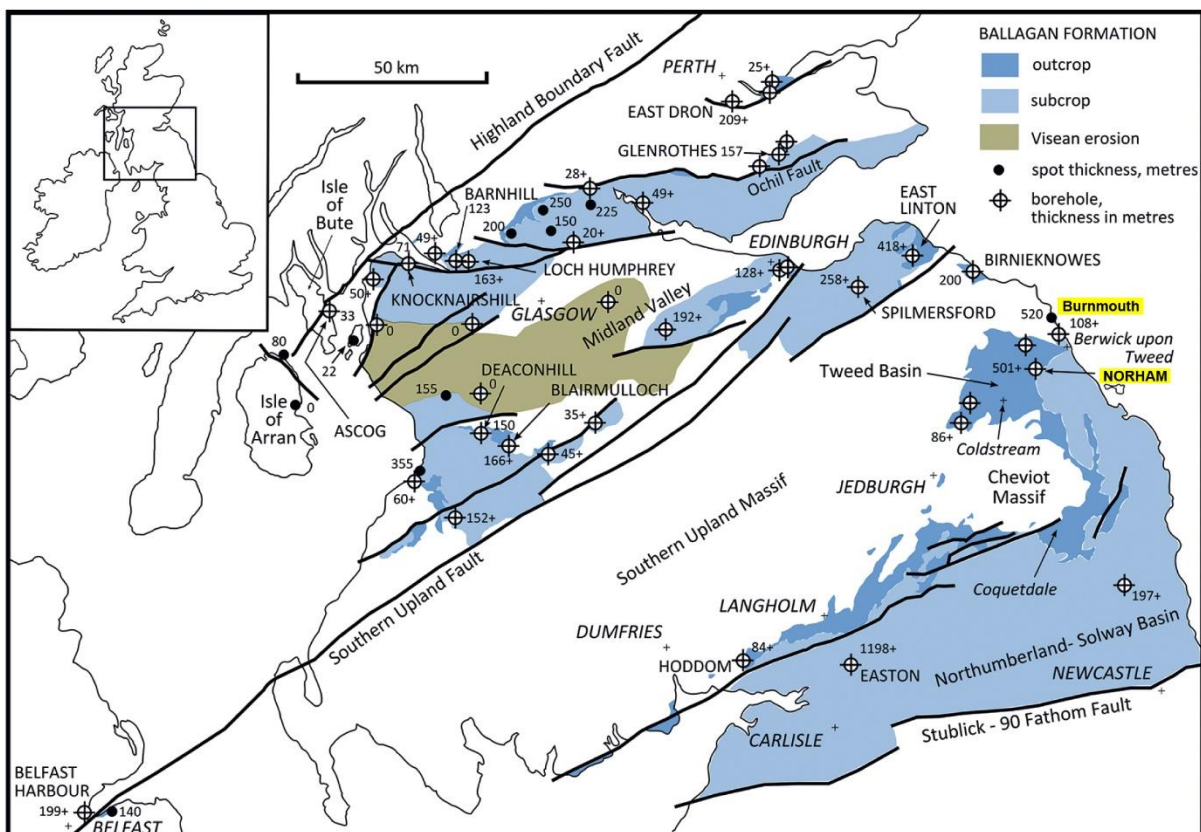


Figure 19. Outcrop and subcrop map of Tournaisian rocks in the Midland Valley of Scotland and the Tweed and Northumberland-Solway basins. These strata include the Ballagan Formation and part of the Lyne Formation in the latter basin. Major boreholes and the thickness of the formation are shown. The Burnmouth outcrop and Norham (NWMF) borehole localities are highlighted in yellow. From Millward *et al.* (2018).

Borehole name	BGS Registered No.	Ballagan Formation thickness (m)	Unit above	Unit below
Ascog	NS06SE 8	33.09	CYD	KNW
Knocknairshill	NS37SW 10	70.87	CYD	KNW
Barnhill	NS47NW 2	123.08	CYD	KNW
Loch Humphrey	NS47NE 1	162.95	CYD	Not reached
East Dron	NO11NW 24	209.54	Not seen	KNW
Glenrothes	NO20SE 385	157.43	PDB	KNW
Deaconhill	NS43SE 81	150.03	LLGS	KNW
Blairmulloch	NS52NE 21	166.58	CYD	Not reached
Spilmersford	NT46NE 73	258.24	GHV	Fault
East Linton	NT57NE 2	418.17	GHV	Not reached
Birnieknowes	NT77SE 9	200.21	GUL	KNW
Norham	NT94NW 20	490.50	Not seen	Not reached

Table 5. Summary of the thickness of the Ballagan Formation with the units above and below in selected BGS boreholes (shown on Figure 19). CYD = Clyde Sandstone Formation, PDB = Pathhead Formation, LLGS = Lower Limestone Formation, GHV = Garleton Hills Volcanic Formation, GUL = Gullane Formation, KNW = Kinnesswood Formation. After Millward *et al.* (2018).

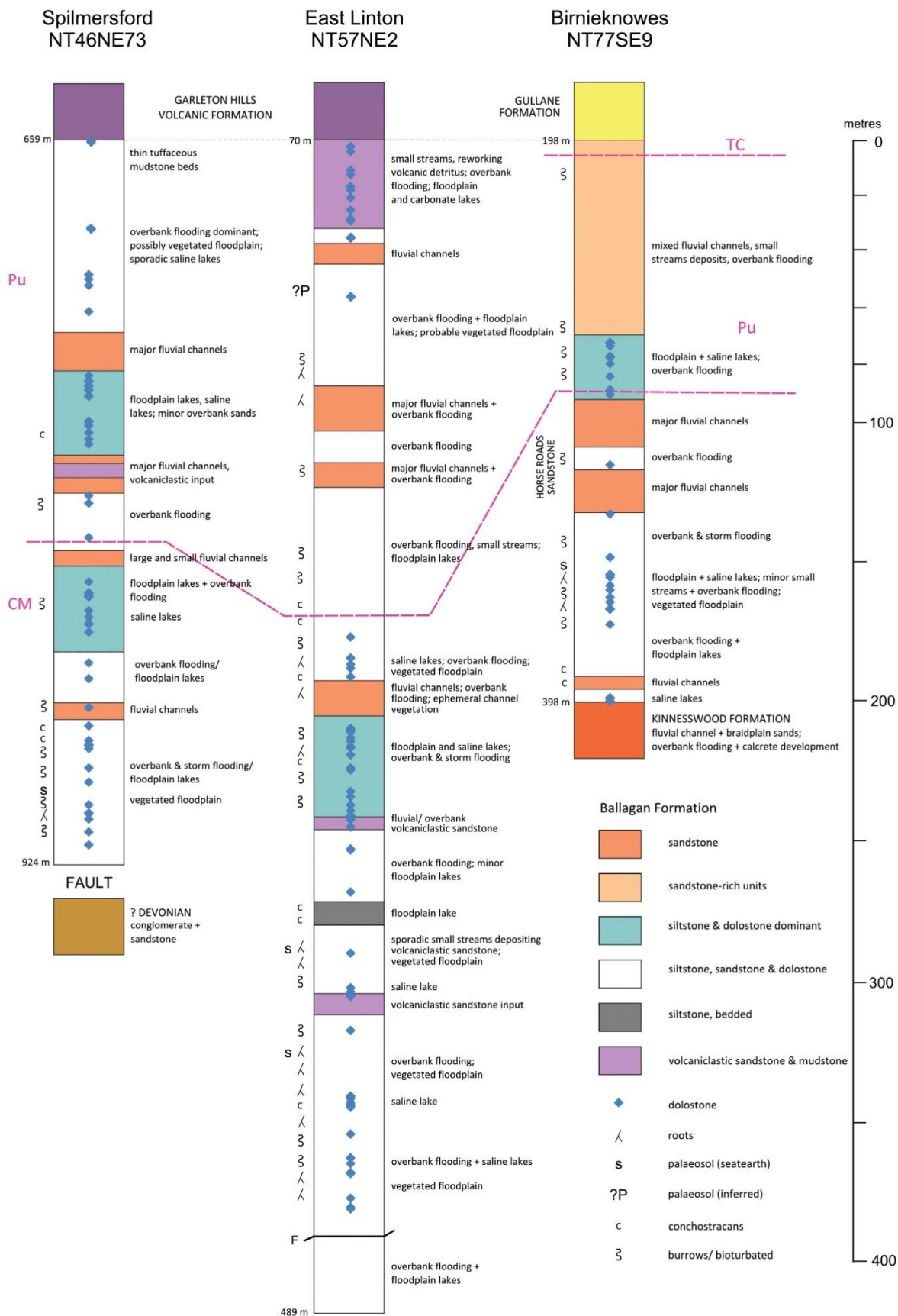


Figure 20. Summary lithological logs and environmental interpretations for selected boreholes in the east of the Midland Valley of Scotland. Borehole locations are shown in Figure 19. From Millward *et al.* (2018).

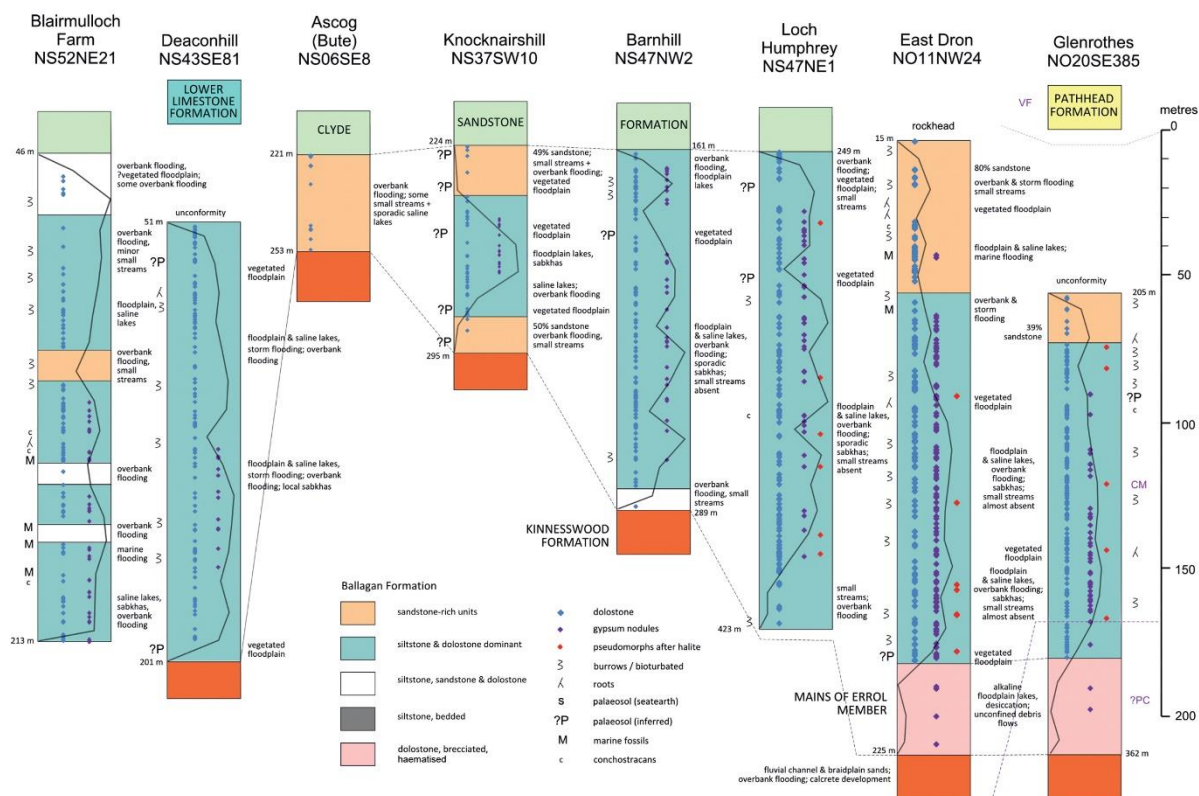


Figure 21. Summary lithological logs and environmental interpretations for selected boreholes in the west and north of the Midland Valley of Scotland. Borehole locations are shown in Figure 19. The black curves within the stratigraphic columns represent the proportional thickness of grey, laminated siltstone/mudstone per 10 m interval through each succession. From Millward *et al.* (2018).

To permit the greatest thickness of the Ballagan Formation to be cored and for its base to be determined, the siting of the borehole was crucial. To this end, BGS staff made several field visits to the Chirnside-Whiteadder-Coldstream area. The base was considered to be more important than the top of the formation as the latter is well exposed at the Burnmouth outcrop section, and recovery of the base of the formation would permit study of the recovery phase immediately after the EDME. However, the budget and drilling rig capacity had a set limit equivalent to a 500 m depth.

Owing to the great lateral extent of the Ballagan Formation in the Chirnside-Whiteadder-Coldstream area, to ensure its predicted thickness encompassed the

500 m constraint, a location was preferred beneath the base of the Fell Sandstone Formation (Figure 18; Chadian to early Asbian; Waters *et al.* 2007). The wide plateau area south of the River Tweed between Norham and Horncliffe was considered to be the most suitable, as it is underlain by a sandstone unit that is below the base of the Fell Sandstone Formation and it did not appear to have significant fault displacement. Residential areas were rejected to minimise disturbance but the remaining area comprised prime agricultural land, which was already in use and, therefore, unavailable.

2.2.3. West Mains Farm, Norham

The Norham West Mains Farm (NWMF) location was considered to be ideal, with access from the main road and the presence of an unused concrete platform (figures 22 and 23). The site measured 25 x 30 m, which was adequate for the contractors, and there was a water supply which was essential for the drilling fluids. The only constraint was the four occupied cottages located within 100 m of the site, which meant that working hours were restricted to daytime only.



Figure 22. Aerial photograph of West Mains Farm. From google.co.uk/maps.

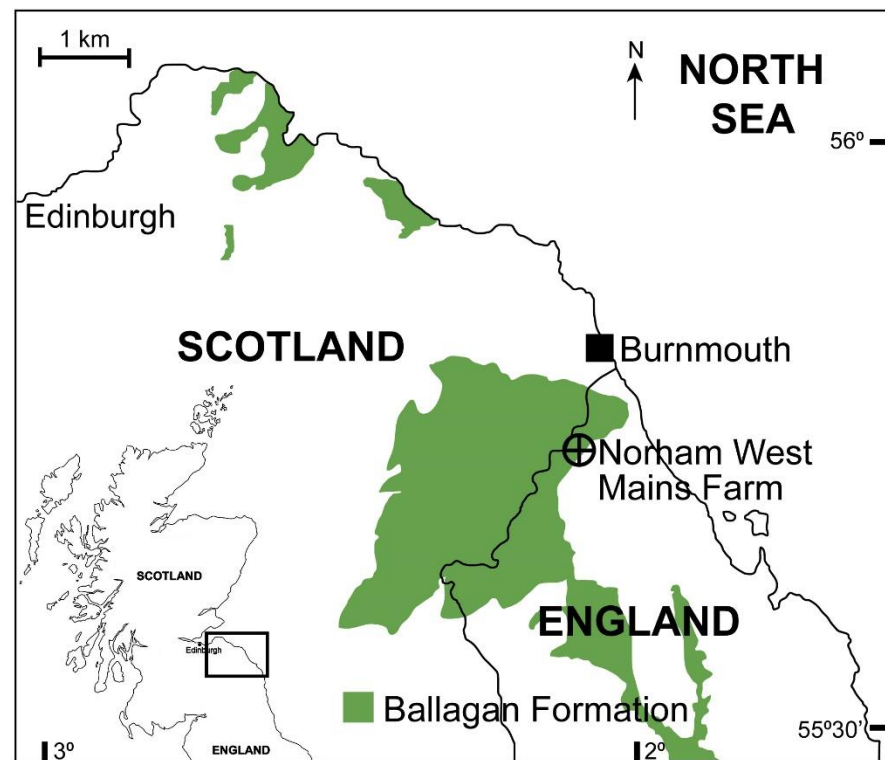


Figure 23. Location map of the Ballagan Formation outcrops (green), Norham West Mains Farm borehole and Burnmouth outcrop sites. After Kearsey *et al.* (2016).

No planning permission was required from Northumberland County Council, as drilling a scientific borehole is not classed as ‘development’ under the Town and Country Planning Act. As no groundwater would be sought or extracted, a licence or permit was not required from the Environment Agency. However, the appropriate health and safety documents were generated.

The protection of the natural environment was integral to the TW:eed project and was monitored throughout the operation. Precautions were taken to protect the groundwater against contamination. All waste materials (i.e. drilling fluids, spoil and slurry from the borehole) were disposed of according to legal obligations and no environmental incidents were recorded. In addition to restricting the drilling operation to day shifts only, noise levels at the nearby cottages were monitored and found to be beneath levels that required action.

Borehole name	Norham West Mains Farm
Location	West Mains Farm, Norham, near Berwick upon Tweed, Northumberland TD15 2JY
100 km grid square	NT 94 NW
Grid reference	391600 648130
Surface level	51.0 m above Ordnance Datum
Total depth	501.33 m
SOBI Registration No.	NT 94 NW 20
Date drilling commenced	6 th April 2013
Date drilling completed	25 th May 2013
Drilling company	Drilcorp Ltd, Kinley Hill Farm, Hawthorn, Seaham, Co. Durham SR7 8SW
Wireline geophysical logging company	European Geophysical Services Ltd, 22 The Stables, Sansaw Business Park, Hadnall, Shrewsbury SY4 4AS

Table 6. Borehole location and registration data. SOBI = Single Online Borehole Index (at the BGS). From Millward *et al.* (2013).

2.2.4. Drilling the borehole

A Beretta T151S track-mounted top drive drilling rig (Figure 24) was used with an Atlas Copco Geobor-S wireline triple-barrel coring system. A biodegradable polymer-based mud-flush was circulated using a positive displacement mud pump through settling tanks and mud-cleaning facility. The upper part of the borehole was reamed (216 mm rock roller) and cased (9.625" diameter grouted casing) with a gas diverter fitted to control any gas released during the drilling of the lower part of the borehole.

On 27th March 2013, prior to excavating the drilling chamber, a ground penetrating radar survey of the site was performed to confirm the absence of services. Drilling commenced on 6th April until TD was reached on 25th May.



Figure 24. Photograph of the drilling rig in operation at West Mains Farm with some of the core in wooden transport boxes. Courtesy of Sarah Davies 2016.

2.2.5. Borehole core

The three main concerns of drilling the NWMF borehole were:

- that it contained a significant proportion of mudrock (that could swell and disintegrate)
- maintaining a vertical shaft

- stabilising the borehole wall.

To address these points, an oversized drill bit at 151 mm diameter (the usual being 147 mm) was used, which provided added clearance between the casing and the borehole wall and reduced the number of blockages caused by accumulated drilling cuttings. Also, a polycrystalline diamond compact (PDC) bit was changed to a Carbonado bit as it did not perform adequately in the hard cementstones. This minimised the surface damaged to the recovered core.

In total, 490 m of continuous core was obtained from the NWMF borehole. Overall, the quality of the cores was high, with little evidence of drilling-induced damage. Generally, the core recovery approached 100%, although a few instances of core loss or poor recovery were associated with faults and their damage zones. Also, acoustic image logs revealed that the borehole was maintained within 1.5° of vertical.

To retrieve the core, the 3 m long plastic liners extracted from the core barrel were split into 1.5 m lengths. Plastic end caps were fitted and the cores were placed into wooden boxes for protection during transport.

The core was taken to the National Geological Repository at the BGS, Keyworth, where it was accessioned as part of the National Boreholes Core Collection. The core liners were slabbed (split lengthways) and one half was photographed and kept as a reference section and the other half was logged and sampled for analysis. All materials from the borehole will be archived in the BGS collections.

2.2.6. Decommissioning

The NWMF borehole site was decommissioned following the Environment Agency's 'Good practice for decommissioning redundant boreholes and wells' document (2012; available from www.environment-agency.gov.uk). The borehole was backfilled with pea gravel to a depth of 117 m and cement grouted to the base of the drilling chamber, which was then filled with concrete. Finally, the site was handed back to the owner on 7th June 2013.

2.2.7. Drilling issues

Although the geological succession obtained from the NWMF borehole core was entirely within the Ballagan, unfortunately, the main objective of reaching the base of the formation was not attained as it was thicker than anticipated for the length of the budgeted drill string (Millward *et al.* 2013). Therefore, to complete the study, the base of the nearby outcrop locality at Burnmouth was integrated with the borehole data.

2.3. The Burnmouth outcrop section

At the coastal locality of Burnmouth in the Tweed Basin (British National Grid reference: NT 95797 60944; Figure 23), is a 520 m thick section of almost vertical strata of wave-cut platform and cliff, passing up sequence from the west to the east (Figure 25; Smithson *et al.* 2012, Kearsley *et al.* 2016, Millward *et al.* 2018). The sediments record a conformable (although condensed) record through the 12 million years of the Tournaisian, with the Kinnesswood Formation marking the base and the Viséan Fell Sandstone Formation at the top (Smithson *et al.* 2012, Kearsley *et al.* 2016).



Figure 25. Photograph of a small bay in the Burnmouth cliffs showing the almost vertical bedding. From tetrapods.org.

In addition to providing the information that was missing from the base of the Ballagan Formation in the NWMF borehole, the Burnmouth section was logged and sampled (Figure 26). Whereas borehole core preserves the fidelity of more friable rocks such as shales, sandy siltstones and palaeosols, the field site enables broader relationships, such as the lateral extent of strata, to be assessed (Bennett *et al.* 2016).

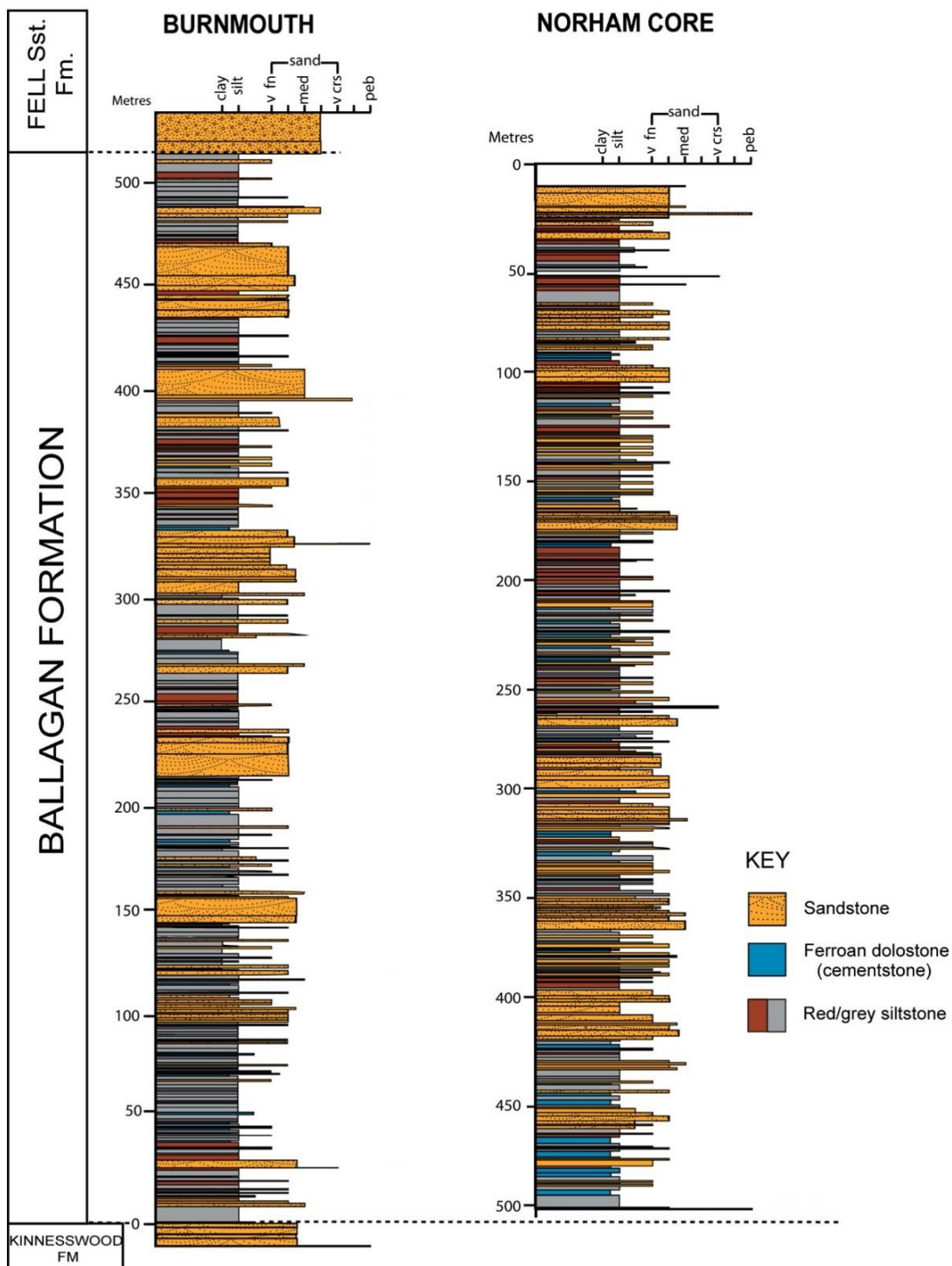


Figure 26. Sedimentary logs of sections from Burnmouth and the Norham (NWMF) borehole. After Kearsey *et al.* (2016).

2.4. Palynomorphs

A total of 570 samples were taken from the NWMF borehole core for palynological analysis (see Section 2.6 for an overview of the core sampling techniques used). Of these, 348 samples were processed to provide an interval resolution of one sample approximately every 3 m (see Section 2.7 for an overview of the palynology processing techniques used). Palynomorphs were present in samples from 501.18 m to near the base of the overlying sandstone (at 39.11 m; Figure 27). The analyses of the palynomorphs are discussed in chapters 3, 4 and 5.

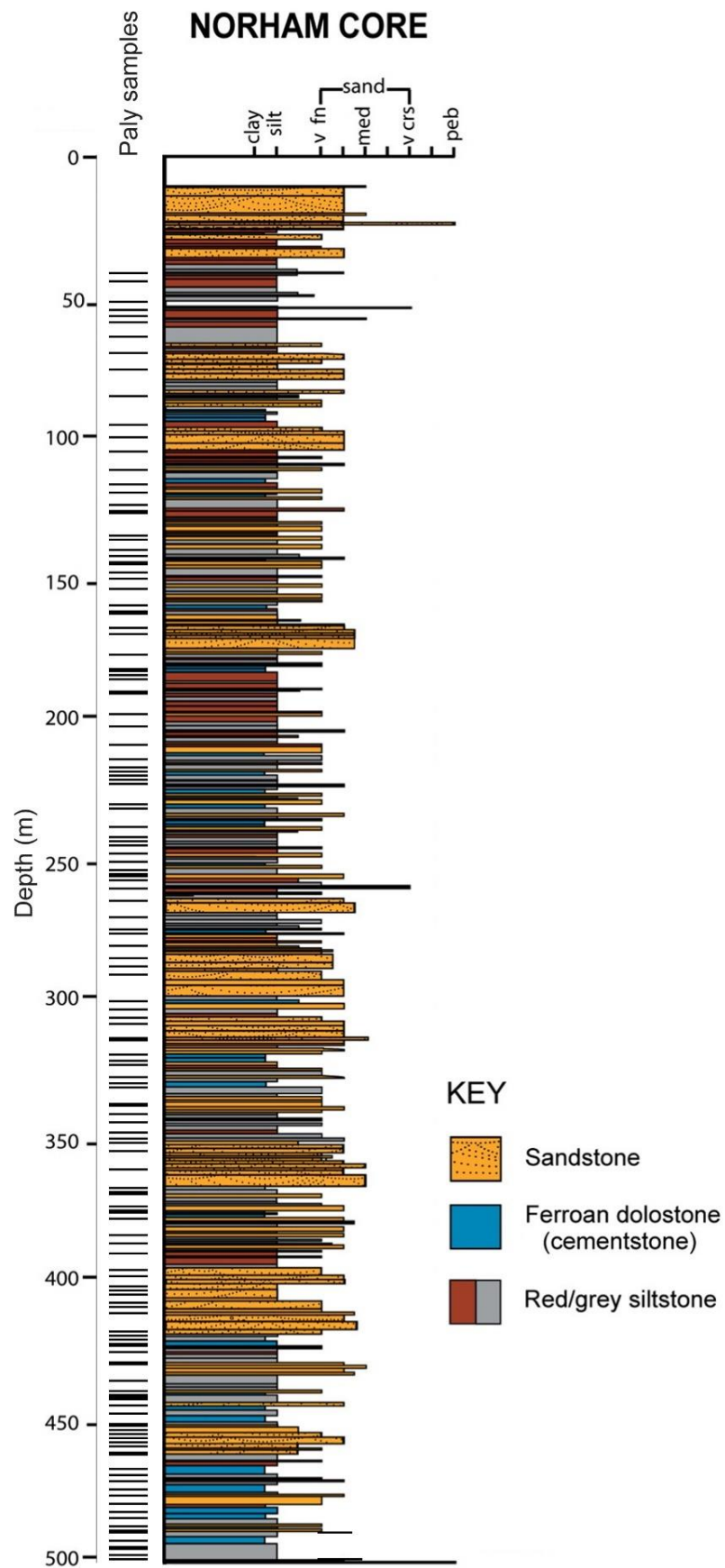


Figure 27. Locations of the palynology samples that were processed from the Norham (NWMF) borehole core. Based on Kearsley *et al.* (2016).

2.5. Palaeosols

Palaeosols are incorporated with the palynomorph analysis because they indicate stabilised land surfaces. Additionally, fossils of terrestrial ground-dwelling arthropods, such as myriapods and scorpions, have also been found at Burnmouth and at Willie's Hole, which may have provided a potential food source for the tetrapods (Clack *et al.* 2016).

During the logging of the NWMF borehole core, 216 palaeosols of 4 pedotypes were described and interpreted by Tim Kearsley of the BGS (Figure 28; Kearsley *et al.* 2016). Note that the palaeosols in the NWMF borehole core were not sampled for palynomorphs as the altered nature of the sediment (i.e. reduced or oxidised), did not meet the sampling criteria (see Section 2.6.).

Although the remaining sediments from the NWMF borehole core contain vast amounts of important palaeoenvironmental information, they are not included in this thesis as they were not used in conjunction with the borehole palynological work. Refer to Bennett *et al.* (2016) for a detailed sedimentary analysis of the fossil-containing sandy siltstones of the NWMF borehole and the Burnmouth outcrop, and Bennett *et al.* (2017) for a study of the ichnofossils of the NWMF borehole and the Burnmouth outcrop, which contributed to understanding the complex mosaic of environments that were present when the terrestrial tetrapods first appeared.

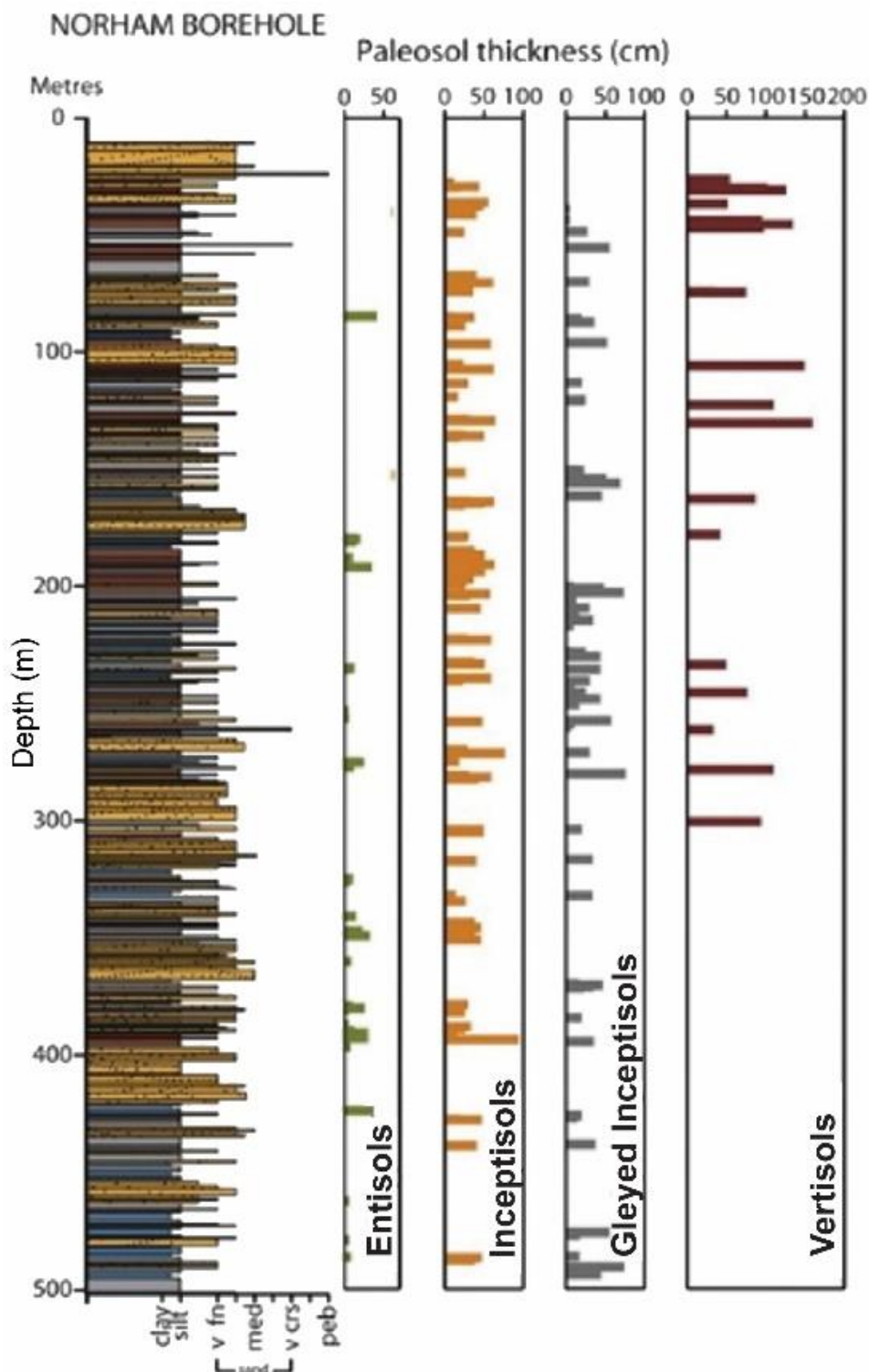


Figure 28. Sedimentary log (left-hand side) and variation in the thickness and distribution of the four pedotypes (right-hand side) through the Norham (NWMF) borehole core. The length of each horizontal line represents the thickness of that palaeosol, and, so, also signifies their net accumulation (i.e. the duration of soil formation processes minus later erosion). After Kearsey *et al.* (2016).

METHODS

This section describes how the palynology data were collected from the NWMF borehole. This entailed sampling the core, processing the samples to produce palynological residues, investigating the residues using various forms of microscopy, using photography and image manipulation to assist with the identification of the palynomorphs, collating the data from the specimens and, finally, analysing those data. Further detailed work instructions of some of the processes discussed in this section are also listed in Appendices 2 to 15.

2.6. Core sampling

Logging and sampling of the entire core took place at the BGS in Keyworth, Nottinghamshire from 23rd September to 18th October 2013. Dr. Carys Bennett (University of Leicester) logged the sediments at a scale of 1 m = 8 cm with Dr. Tim Kearsey (BGS) focussing on the palaeosols. Dr. Andrea Snelling (NIGL) took samples for isotope analysis and I collected samples for palynological analysis.

For the palynological analyses, samples of approximately 15 g were collected from dark coloured, fine-grained sediments that showed no obvious signs of reduction or oxidation. These characteristics had been identified as the most likely to yield plant spores, based on previously collected and processed outcrop samples. To assist with sampling the appropriate material, samples that had already been processed and which were known to contain spores and those that were typically barren were glued to boards for comparison purposes to demonstrate the required sediment characteristics.

2.6.1. Sampling procedure

Refer to Appendix 2 for a work instruction that details the steps that were taken to sample the NWMF borehole core for palynological specimens.

Firstly, the box and core run numbers were added to the BGS 'Record of samples taken during inspection' worksheet, then the box's starter depth was annotated in the field notebook (Figure 29).

Note: The depths were measured from the base of the box towards the top, regardless of where the inner plastic core sleeve began, because the sleeves were often at different positions along the box and were occasionally missing. This approach ensured that all depth measurements were taken in a standardised manner, so that any errors could be accounted for easily. Exceptions were when there was core loss marked on the box at an interval other than at the start – in that case the written depth was taken as the marker.



Figure 29. Photograph of a box of core from the NWMF borehole showing the box's starter depth in the top right-hand corner.

The box of core was inspected visually for suitable samples and the centre of each sample horizon was measured. The paperwork was then completed with the unique IS(M) number, the sample's depth measurement and thin section information.

One copy of a 'Borehole Subsample' label was adhered to the 'Record of samples taken during inspection' worksheet, one was adhered to a white card, which was

placed where the sample had been removed and the final copy was adhered to the palynology sample bag which was also annotated with a 'P'. Additional sample bags were annotated with the IS(M) number, the sample depth, with 'TS' for the thin sections and with 'I' for isotopes.

Palynological samples were taken wherever the lithology matched the sampling criteria (see Section 2.6) and for isotopes, samples of approximately 15 g were taken with every palynological sample, where there were significant changes in the lithology and where requested.

Sample contamination was avoided by brushing extraneous sediment from the work surface and an Excel spreadsheet of each sample was maintained.

2.6.2. Sampling for thin sections

- Sections of sediment were removed with the aid of a broad bladed paint scraper.
- Particularly friable sediment was removed in pieces using a leaf and square trowel.
- Additionally, a broad bladed chisel was used where a greater percussive force of the hammer was required.
- Three sizes of hammers were used: 380 g, 550 g and 624 g (Figure 30).
- Safety glasses were worn at all times.
- Unconsolidated samples were wrapped in tin foil with the top and way up marked in indelible ink.



Figure 30. Photographs of the tools used to sample the NWMF borehole core.

1. Soft sediments

- Samples that parted easily under pressure were split by tapping along sedimentary planes, preferably just above the sample horizon to release the required layer below.
- Where sediments disaggregated in layers, it was preferable to hammer/chisel the layers separately, whilst always maintaining the correct way up.

2. Sediments of moderate hardness

- Sediments that were too hard to split using a hammer or hammer-chisel combination were split using the bench vice whilst wearing heavy duty gloves (Figure 31).
- The rock sample was placed between the cutting blades with one hand and the vice handle was turned clockwise to grip the sample.
- The vice handle was then turned clockwise with both hands to increase the pressure on the rock sample until it cleaved.

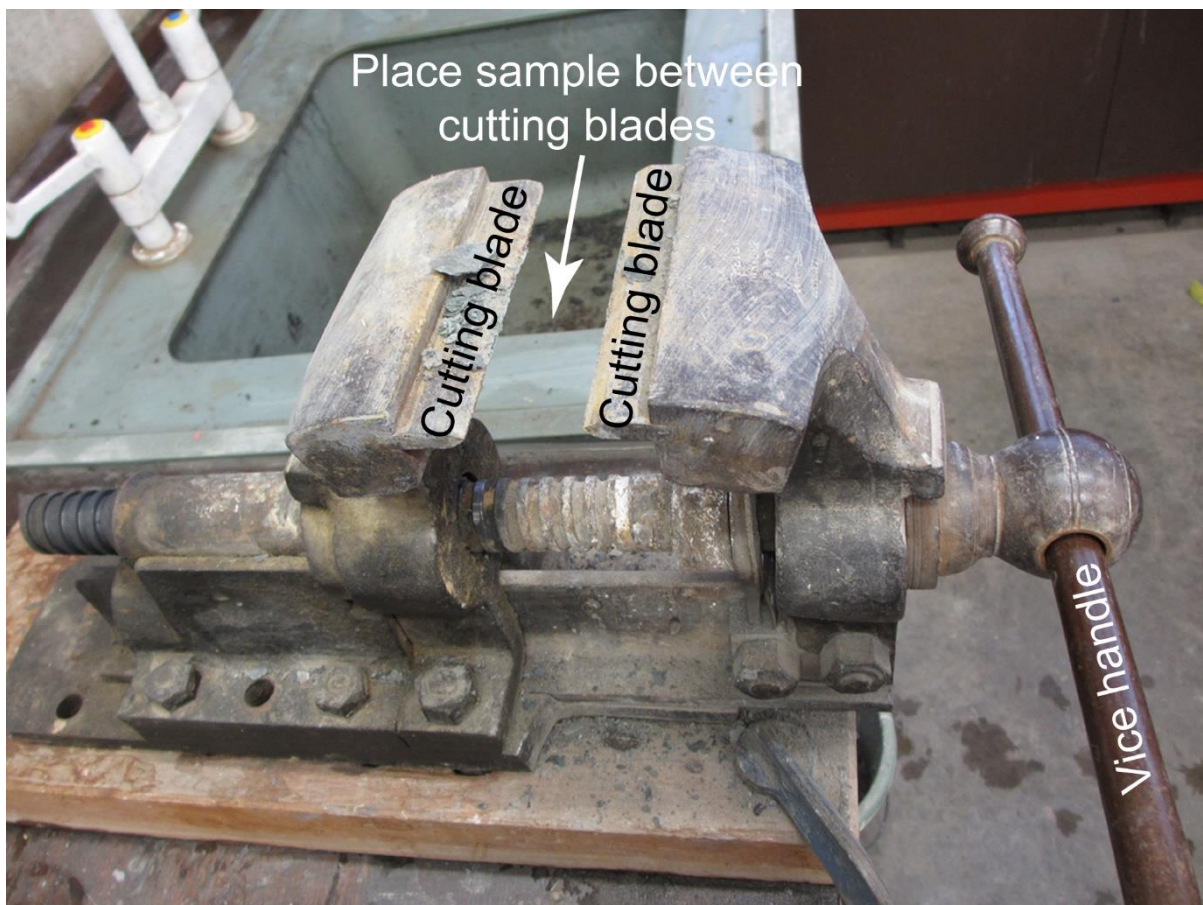


Figure 31. Photograph of the bench vice used to split sediments of moderate hardness.

3. Hard sediments

- These required the use of a pneumatic jack, which could deliver up to 8 tons of force (Figure 32).
- The sample was placed between the cutting blades and the top screw bar was turned clockwise until the blades gripped the sample.
- A metal bar was inserted into the crank sleeve and pumped to increase the pressure until the sample broke.
- The metal bar was removed from the crank sleeve, inserted onto the release nut and turned anticlockwise to release the pressure.
- The sample could then be removed from the base of the jack.



Figure 32. Photograph of the pneumatic jack used to split hard sediments.

2.7. Processing palynological samples

All palynological samples were processed in the Palynology Processing Laboratories of the School of Ocean and Earth Science of the University of Southampton in the National Oceanography Centre, Southampton.

In total, 361 samples were processed, which represented an interval resolution of approximately 3 m. Standard acid preparation techniques were employed and none of the samples required oxidation. All residues were stored in labelled vials.

A summarised flow diagram of the techniques that were used follows (Figure 33; refer to Appendix 3 for further details).

Preparation

5 g of 15 samples were crushed and added to 15 numbered containers and the Paly Processing logbook was completed

Wearing basic laboratory attire

Stage 1: HCl
(to remove fluorides)

Day 1

15 sample containers were placed into a fume cupboard and 1 cm depth of HCl was added to each

Wearing basic laboratory attire and HCl PPE

Day 2

Reacted HCl was poured off and the containers were filled with water

2 hours elapsed

The water was poured off and replaced with fresh water

After 2 hours the pH was tested

Yes

Neutral?

No

Stage 2: HF
(to remove silicates)

Day 1

The pH neutral water was poured off and 2 cm depth of HF was added

Wearing basic laboratory attire and HF PPE

Day 2

The containers were shaken to encourage further acid reaction

Day 3

The containers were filled with water

2 hours elapsed

The water was poured off and replaced with fresh water

After 2 hours the pH was tested

Yes

Neutral?

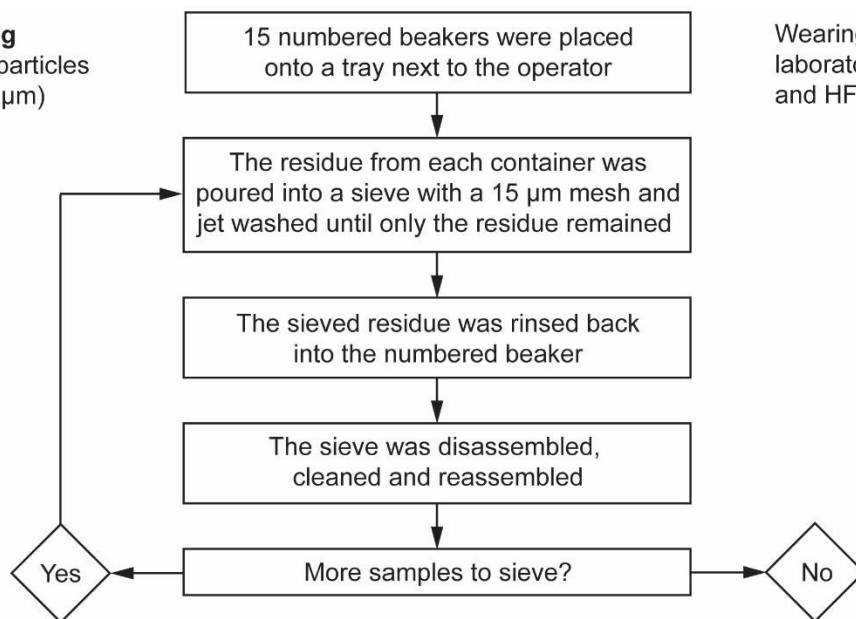
No

Go to 'Stage 3: Sieving' on the following page...

Stage 3: Sieving

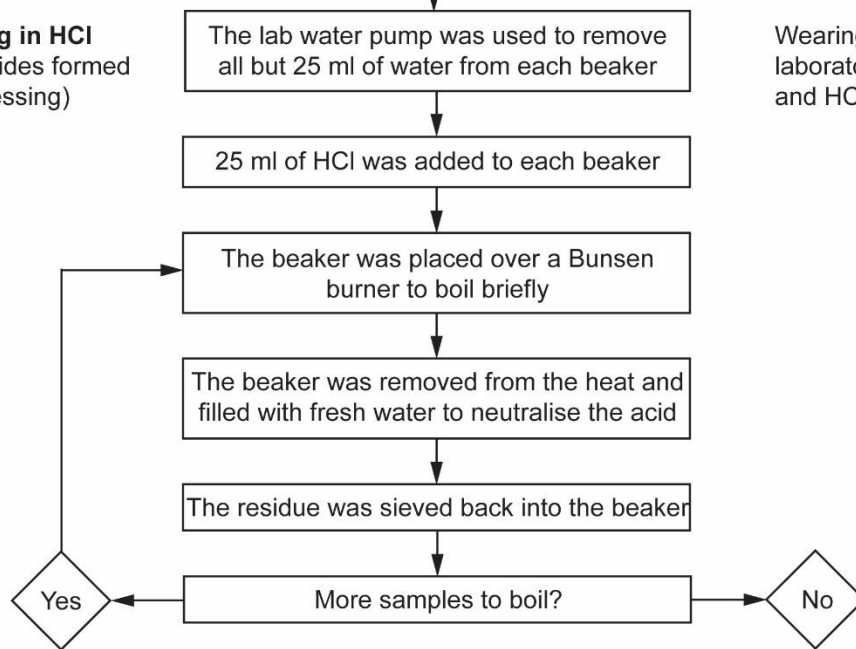
(to removed all particles smaller than 15 μm)

Wearing basic laboratory attire and HF PPE

**Stage 4: Boiling in HCl**

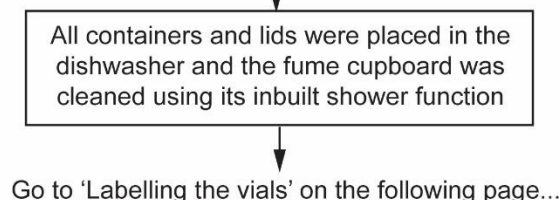
(to remove fluorides formed during HF processing)

Wearing basic laboratory attire and HCl PPE

**Cleaning**

(to prevent contamination of other samples)

Wearing basic laboratory attire



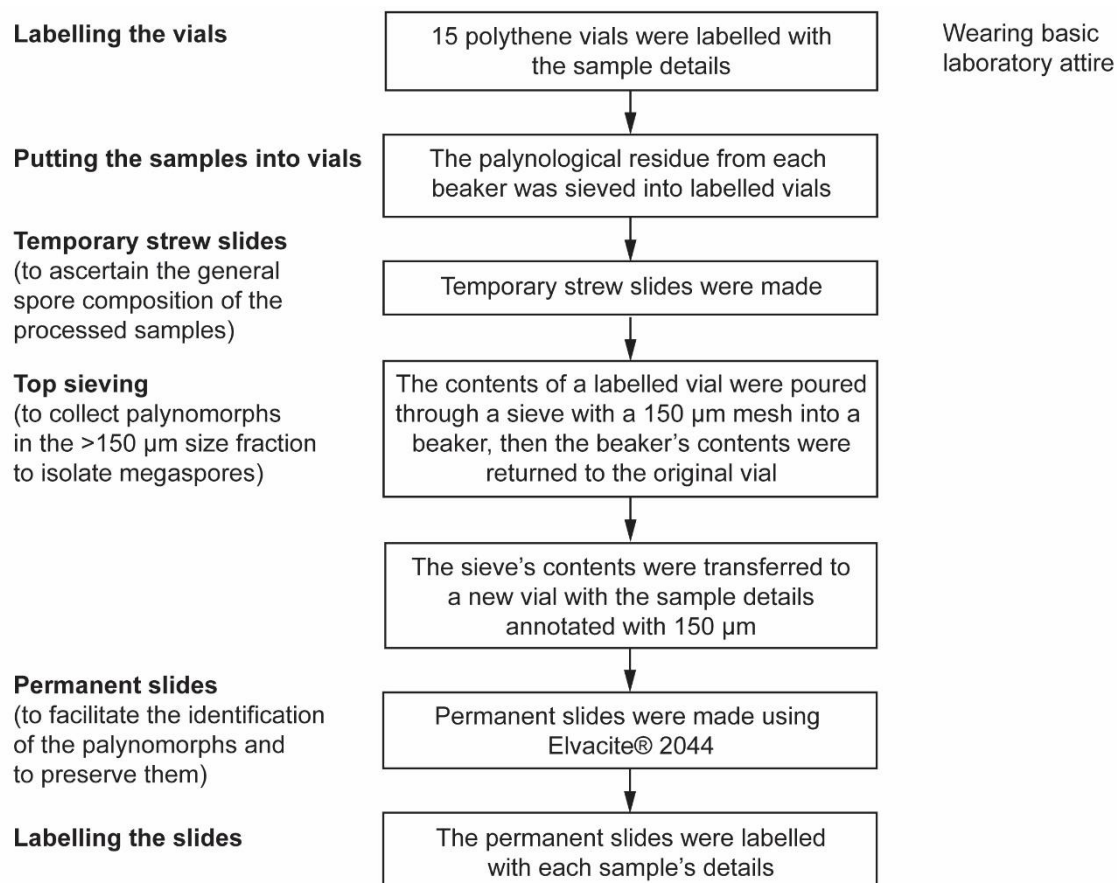


Figure 33. A summarised flow diagram of the standard acid preparation techniques that were used to process the palynological samples from the NWMF borehole core.

2.8. Residue and slides storage

All unprocessed residue in sample bags, processed residue in small, labelled, polythene specimen vials with tight-fitting screw tops and all palynological slides will be catalogued and housed in the BGS collection in Keyworth.

2.9. Microscopy and photomicroscopy

To photograph and aid the identification of the palynomorphs, a mixture of light, infrared and scanning electron microscopy was employed.

2.9.1. Light microscopy (LM)

A light microscope was used for the majority of the palynomorph identification and analysis. An Olympus BH-2 microscope (number: 205255) was used at x4, x10, x20 and x40 magnification in air and x100 magnification in oil using Olympus immersion oil. A Canon EOS 70D DSLR camera was used to produce photomicrographs (saved as JPEG files) to record and identify the palynology specimens (refer to Appendix 4 for detailed instructions).

For high quality, publishable light photomicrographs, Olympus Stream (Basic) software was used with an Olympus BH-313 light microscope number: 210685, with an Olympus SC30 3 Megapixel camera mounted on a trinocular head (figures 34 and 35; refer to Appendix 5 for detailed instructions).



Figure 34. Photograph of the Olympus BH-313 light microscope (number: 210685) with an Olympus SC30 3 Megapixel camera mounted on a trinocular head.



Figure 35. Photograph of the PC monitor with the Olympus Stream (Basic) photomicroscopy software loaded showing a live image of a *Plicatispora scolecophora* miospore at x100 on the Olympus BH-313 light microscope in Figure 34.

The Olympus Stream software was also used to measure palynomorphs and their features much more quickly and accurately than by doing so manually (refer to Appendix 5).

2.9.2. Infrared (IR) microscopy

After standard palynological processing, several megaspores that had been recovered from the core samples were too opaque to be identified using transmitted light microscopy. Although oxidation would have rendered the spores translucent, other palynomorphs in the residue may have been destroyed, thereby biasing the results of the spore counts.

Scanning electron microscopy shows only surface features, but as a degree of transparency could be achieved using infrared, an infrared microscope from a

previous study was used. A limitation, however, was that the image output was to analogue video, whereas digital stills were required for constructing photomicrographic plates of the megaspores. Therefore, an analogue video digitizer device was purchased at minimal cost and attached to the output cable. This enabled infrared images to be captured and stored digitally. Using infrared revealed enough morphological detail to enable identification of the megaspores.

The equipment used was an Olympus BH-2 IR microscope converted from transmitted light to the near-infrared by removing the coatings to suppress the transmission of infrared light (Marshall 1995). This microscope had been fitted with a trinocular head into which was mounted a monochrome CCD video camera module with its infrared short pass barrier filter removed and a 100 W quartz halogen bulb to supply the required level of infrared illumination, with infrared long pass filters manually placed into the field aperture filter holder (Figure 36; Marshall 1995).

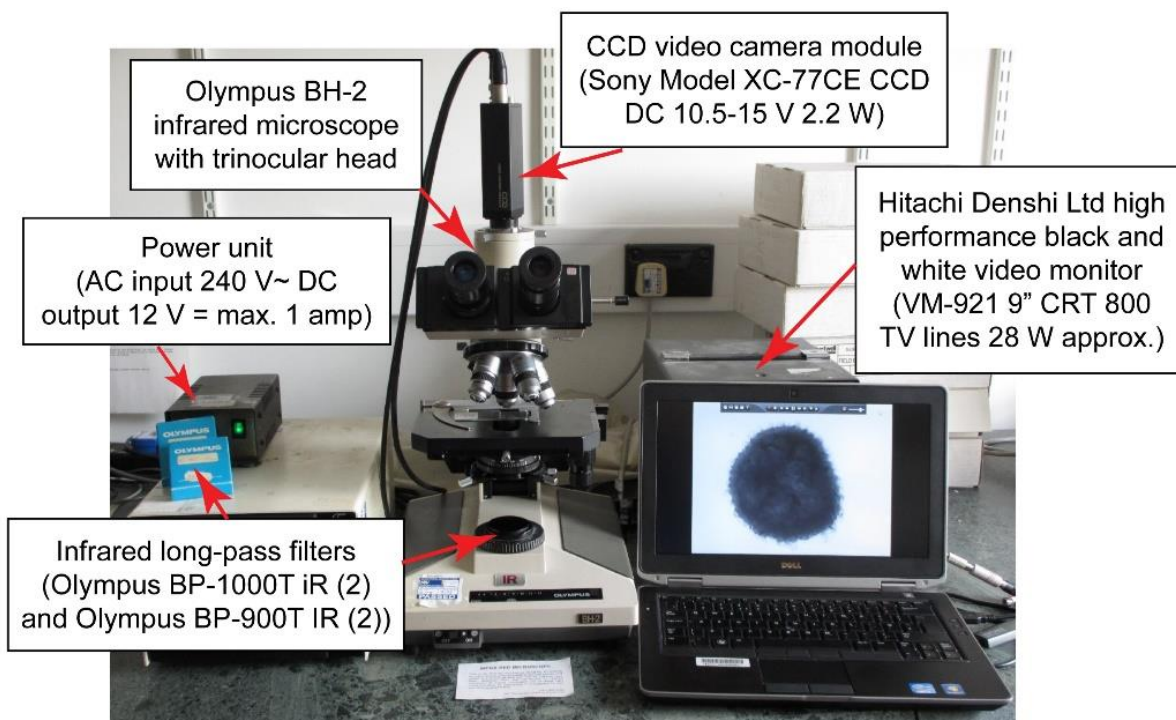


Figure 36. Photograph of the infrared microscopy setup.

Originally, the analogue video images were viewed on a Hitachi Denshi video monitor, but this was bypassed by attaching it to a Hauppauge WinTV-USB-Live 2

device via an S-video cable connector and USB. The images were then viewed with more clear definition on a Dell laptop running Windows 7 Enterprise (Figure 37; refer to Appendix 6 for details).



Figure 37. Photograph of the analogue video digitizer to output digital images from analogue signal.

The focal depth and aperture size were adjusted manually and Olympus immersion oil was used at x100 magnification. The maximum illumination was used for the x100 lens, but it had to be reduced at lower magnifications.

The trinocular head of the microscope was swivelled around to reposition the camera for the optimum shot. As with the light microscope photography, micrographs of the specimens were taken at successive focal depths. The images were then manipulated using Adobe Photoshop to form stacked ('3D') images (see Section 2.12).

An example of how IR microscopy was used to enhance palynomorph identification can be demonstrated by the megaspore *Setispora pseudoreticulata*. Spinner's (1982) later description of this taxon states that: "localised thickenings of the exine and the sculptural elements adpressed against the exine may simulate a reticulate pattern". However, although this reticulation is suggested in light

microscopy, it is more clearly defined in infrared light, thus enabling confirmation of the identification (Figure 38).

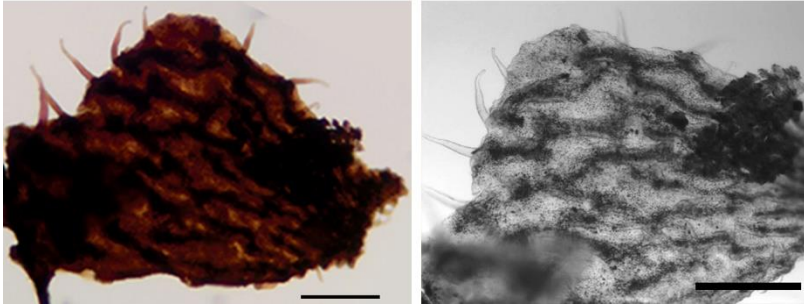


Figure 38. Photomicrographs of a fragment of *Setispora pseudoreticulata* using light on the left and infrared on the right (x100 oil immersion). The IR image highlights the characteristic reticulate pattern of this species. Scale bar = 200 μm .

2.9.3. Scanning Electron Microscopy (SEM)

Scanning Electron Microscopy was used to facilitate the identification of the surface morphological features of megaspores that were too opaque or too small to be determined using light microscopy.

Individual megaspores were picked using a Daler Rowney No. 3 paintbrush and carefully placed onto SEM stubs, adhered with a sticky carbon film. They were then sputter coated with gold to produce an electrically conductive surface (Figure 39).



Figure 39. Photograph of gold-coated specimens on SEM stubs ready to be examined in the scanning electron microscope at NOCS (on the left hand side) and a diagram of the contents of each stub (on the right hand side).

A Carl Zeiss LEO 1450 VP scanning electron microscope with Zeiss Smart software V05.01.08 18 Apr 06 was used in the SEM Laboratory of the School of Ocean and Earth Science, University of Southampton (Figure 40).



Figure 40. Photograph of the Carl Zeiss Leo 1450VP SEM with Oxford Instruments Energy Dispersive Spectrometer at the University of Southampton. From <https://cdn.southampton.ac.uk>.

All greyscale scanning electron photomicrographs were taken using the SEM camera and saved in TIFF format.

2.10. Data collection

The palynomorphs that had been extracted from the NWMF borehole core were identified using photographs and descriptions from many published reference sources (refer to the References section).

Quantitative counts of 200 identified palynomorphs, representing the bulk of the specimens, were logged manually onto a logging sheet for each sample. Additional 'out of count' palynomorphs, representing rarer elements, were also recorded for range information. These data were then added to Excel spreadsheets.

2.11. Data analysis

Having collated identified palynomorphs and recording semi-quantitative relative abundance data, the data were analysed using the methods described below.

2.11.1. Range charts

The purpose of producing range charts was to use diagnostic palynomorph taxa to identify biozones to be used as a relative dating tool. This would permit the use of the new borehole-defined biozones as the standard against which to date the tetrapod sites and the tetrapod fossils.

Tilia (v 2.0.41; www.tiliait.com) was used to produce range charts (see Sections 4.2 and 4.3; refer to Appendix 7 for details).

Note: The range charts were produced as Tilia diagrams which most software cannot open. To resolve this, the resulting files were saved as Enhanced Windows Metafile (emf) format, which could be opened using Adobe Illustrator for editing.

2.11.2. Relative abundances

A plot of relative abundance data was constructed using Tilia to show how the quantities of palynomorph taxa changed through time (refer to Appendix 8 for details). These data were used to interpret the plant recovery following the EDME and to demonstrate changes in the local climate (see Sections 5.2 and 5.8 respectively).

2.11.3. Principal Component Analysis (PCA)

PAST (PAleontological STatistics v 3.19), a free comprehensive statistics package, designed specifically for palaeontological studies (Hammer *et al.* 2001), was used to perform a Principal Component Analysis (PCA; refer to Appendix 9 for details).

This was used to identify outgroup spore taxa which represented plants that were statistically different from all of the others and may, therefore, have represented the dominant plants that were responding to changes in the Ballagan environment following the EDME (see Section 5.1).

2.11.4. Constrained Incremental Sum of Squares (CONISS)

Having identified the outgroup taxa using Principal Component Analysis (see Section 5.1), a CONISS analysis was then performed in Tilia to divide the spores into distinctive natural assemblages (see Section 5.7.1; refer to Appendix 10 for details).

The assemblages could be further grouped and the spores' fluctuating abundances were then used to track environmental changes through the studied section. The type of analysis conducted was stratigraphically constrained and run with square root transformation using the Cavalli-Sforza & Edwards (1967) chord distance. CONISS dendrograms clustered the data, which were further highlighted using the 'Zones' function in Tilia.

2.12. Image manipulation

As each spore represents a compressed three-dimensional biological object, the focal depth required adjustment to ensure that all parts of each specimen were recorded in focus. To do this, each individual part was photographed following refocussing, which resulted in a series of images to be composited later.

The saved images were manipulated using the commercially available software Adobe Photoshop CS6 (64 bit) (part of the Adobe Design and Web Premium CS6

suite). To produce one composite image incorporating the varying focal depths, the 'autoblend layers' function was applied. This stacks each 2D image as a layer on top of each other and interpolates differences in the image's quality to produce a single '3D' image (refer to Appendix 11 for details).

To reduce the file size, the files were saved in JPEG format, conserving the image quality in case further photographic manipulation was required later.

2.13. The England Finder

Figured specimens are located on individual slides by their England Finder co-ordinates (Figure 41).

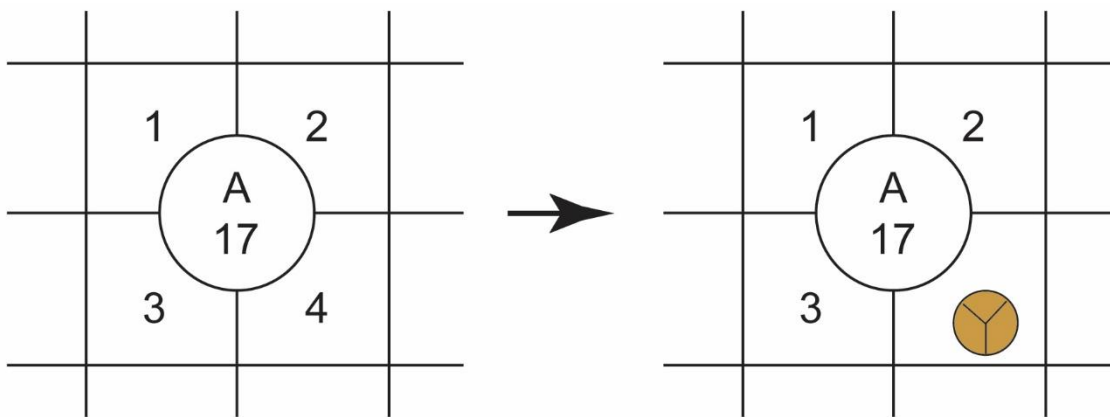


Figure 41. Diagram of a section of an England Finder slide (left hand side) with a cartoon example of a spore with the co-ordinates: A17/4 on the right-hand side.

2.14. Fossil sampling

Micropalaeontological sampling was conducted at the BGS in Edinburgh from 2nd to 13th December 2013, by a team from the BGS (Dr. Dave Millward and Dr. Mike Browne) and the Universities of Cambridge (Ket Smithson) and Southampton (Dave Carpenter and I). The purpose of this sampling was to collect environmentally sensitive microfossils, e.g. plant fragments of leaves, stems and roots, charcoal and megaspores and invertebrates, including ostracods, other bivalves and eurypterid cuticle and very rare shrimps, orthocones and scolecondonts (Bennett *et al.* 2016). Samples/specimens were recorded by depth/

depth range and any significant sedimentary features associated with the sampled horizon were also recorded. This data was entered into a separate log with a BGS 'SSK' number (refer to Appendix 12 for details).

2.15. Megaspores

Owing to their physical size, megaspores have low transport potential compared with miospores, which allows the inference of the vegetation of the local environment rather than the entire basin catchment (Wellman *et al.* 2009).

Although megaspores are known from several localities across the Southern Scotland-Northumberland area (e.g. Barnard 1959, Alvin 1965, Scott *et al.* 1984), this is the first time that megaspores have been studied from a continuous succession through the entire Ballagan Formation.

Megaspores were picked by hand from a wet palynological residue using a low power Wild Heerbrugg M3C stereoscopic binocular microscope with power supply unit 463 6V A.C. 20W (Figure 42; refer to Appendix 13 for details).

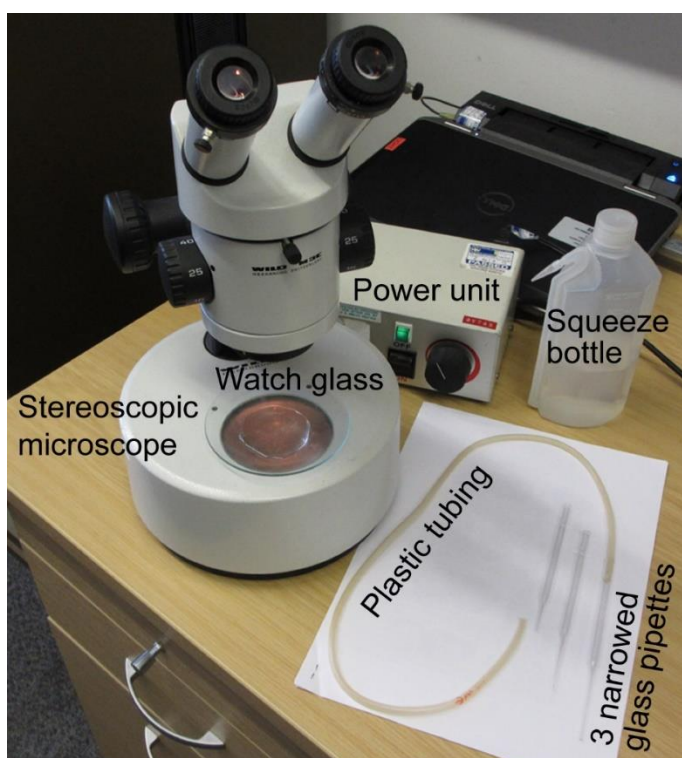


Figure 42. Photograph of the equipment used to hand pick megaspores from a wet residue.

Specimens were extracted from residues poured into a watch glass using a narrowed pipette with a piece of plastic tubing fitted inside, the other end of the tubing being placed into the operator's mouth (Figure 43).



Figure 43. Photograph of me (ER) intently hand-picking megaspores from a wet residue.

Using the capillary action of the pipette combined with a gentle chewing action of the operator's teeth on the tubing, megaspores and pieces of megaspore were isolated for picking.

The megaspores were identified and all data were recorded on a spreadsheet.

2.16. Coal sample

When sampling the core for microfossils (see Section 2.14.), a thin (2 cm) coal seam was discovered at 256.10 m depth (Figure 44). The spore content of the coal was investigated to determine the plant composition of the coal and its physiochemical properties were analysed to determine its rank.



Figure 44. Photograph of the coal sample taken from the NWMF borehole core.

Work carried out by Smith & Butterworth (1967) has shown that the exines of different spore types can be affected differentially during processing. The oxidising reagents and type of alkali used can, therefore, influence the quantitative character of an assemblage, with over-maceration leading to the over-representation of the more resistant spores (Smith & Butterworth 1967). Fuming nitric acid was, therefore, the preferred oxidising agent for this sample as the method is simple and the duration is comparatively short, being achievable within a 24-hour period (Smith & Butterworth 1967).

The methodologies of Spinner (1965) and Smith & Butterworth (1967) were employed to extract the megaspores from the coal sample.

The coal sample was decanted into a 0.5 mm sieve over an agate mortar (smaller fractions fell through the mesh and were set aside). A balance (Ohaus) was tared with an empty freshly cleaned and dried 50 ml PYREX® beaker. Coal pieces of

approximately 5 mm in diameter were picked and placed into the beaker using tweezers to a total mass of 1 g.

In a fume cupboard, 1 cm depth of fuming nitric acid was added to the coal pieces using a large dropping pipette. The beaker was covered with a small watch glass to act as a lid and the sample was left to macerate overnight.

The following day, the nitric acid mixture was poured into a polythene jug of water, which fumed violently. The residue was sieved through a 15 μm mesh and rinsed into labelled vials.

Microscopic investigation by temporary strew slide indicated that a high amount of organic matter remained. This extraneous material was removed by reducing the water volume to approximately 150 ml by re-sieving through a 15 μm mesh and adding 7.5 g (= 5%) of Potassium Hydroxide (KOH) in tablet form. After approximately 15 minutes, the residue was sieved at 15 μm with pressured water to neutralise the pH.

Another microscopic investigation by temporary strew slide indicated that, although the vitrinite had broken down, a high amount of minerals remained. This could make the identification and counting of isolated spores challenging if too great (Smith & Butterworth 1967) and so the silicates were removed using hydrofluoric acid.

The following day, the vials and their contents (the coal residue and HF) were placed into a large jug of water to dilute the acid, sieved through a 15 μm mesh and the residue was added to fresh vials.

Megaspores from the coal sample were hand-picked from a wet residue (see Section 2.15) and permanently mounted onto microscope slides for further investigation (refer to Appendix 3).

2.16.1. Further analysis

In addition to extracting the megaspores, a crushed sample was sent away for

elemental analysis (by John Marshall), the ash content was measured (by Shir Akbari at the School of Ocean and Earth Science) to assess its inert components and the vitrinite reflectance was measured to evaluate the coal's thermal maturity (by Dave Carpenter at the School of Ocean and Earth Science). The results of these physiochemical properties were used to determine the rank of the coal, which is the extent to which the organic matter has progressed through the coalification process (Groppo 2017).

2.16.1.1. Elemental analysis

The largest pieces of the coal sample, retained on the 0.5 mm sieve (see Section 2.16), were crushed in an agate pestle and mortar to a fine powder. Some of the powder was transferred from the mortar to a clean 12 mm diameter glass tube to a depth of 8 mm using a stainless-steel scoop. The sample was then sent to OEA Laboratories Limited, Callington, Cornwall for elemental analysis.

2.16.1.2. Ash content

One gram of the powdered coal was transferred to a ceramic crucible and placed into a furnace at 430°C for 6 hours. The furnace door was opened briefly every hour to replenish the oxygen.

The crucible was removed from the furnace and the contents were dried in a desiccator and the resultant ash content was weighed.

2.17. Scolecodont analysis

A total of 80 scolecodont specimens were found in 23 of the NWMF borehole core's palynological samples (see Section 5.14).

Scolecodonts are the dispersed fossilised compound jaw apparatuses of polychaete annelid worms (Benton & Harper 2009). The majority of Palaeozoic scolecodonts belonged to the order Eunicida, which was a diverse and abundant group that inhabited different marine environments (Szaniawski 1996).

The jaw elements exhibit varied morphologies (see Section 3.6 and Plate 6), in life comprising of one pair of ventral mandibles, which were anchored by the jaw muscles, and several pairs of dorsal maxillae, which were used for biting and grasping prey or for burrowing in the substrate (Szaniawski 1996). As the soft-bodied animals are rarely preserved, scolecodonts constitute the fossil record of polychaetes as far back as the late Cambrian (Williams *et al.* 1999).

Scolecodonts are composed of chitin, which is highly resistant to chemical decomposition, and they are, therefore, often found associated with graptolites, chitinozoans, acritarchs and spores (Szaniawski, 1996). The only additional palynological processing required to study scolecodonts in organic residues is the removal of Amorphous Organic Matter (AOM). AOM is the standard name given to all particulate organic fragments in palynological preparations that appear structureless using light microscopy (Pacton *et al.* 2011). Although the presence of AOM did not affect the scolecodonts in the NWMF borehole samples, it could have hidden them from view and was removed using a tunable ultrasonic probe.

Twelve scolecodont-containing palynological samples with a high quantity of AOM were processed using a tunable ultrasonic probe made by Jencons (Scientific) Limited (Figure 45; refer to Appendix 14 for details).

The ultrasonic probe was rinsed with deionised water and activated inside a clean polythene tube for 2 pulses of 10 seconds to ensure that it was clean. A scolecodont-containing sample was transferred to the polythene tube and the probe inserted into the tube. The probe was activated for 10 seconds, then the tube was removed and the contents were decanted into the medium sieve to capture the residue. This was rinsed into a smaller sieve to return the residue to the sample's original vial. The probe, polythene tube and both sieves were washed thoroughly between the samples to prevent contamination.



Figure 45. Photograph of the ultrasonic probe used to remove extraneous AOM from palynomorph samples that contained scolecodonts.

The distribution and abundances of the scolecodonts that had been found in the NWMF borehole samples were plotted using Tilia (see Section 5.14, Figure 129; refer to Appendix 15 for details).

CHAPTER 3

THE PALYNOMORPHS

Of the 348 samples processed from the NWMF core, 295 were palynomorph-productive, which gave a recovery rate of 85%. In total, 40,558 identified palynomorphs and 80 scolecodonts were extracted, which are broken down by the number of genera, species (where applicable) and specimens in Table 7.

Category	Genera	Species	Specimens
Miospores and microspores	66	288	39,315
Megaspores	8	9	926
Pollen	1	1	85
Acritarchs	2	2	209
Euglenoids	1	2	23
Scolecodonts	-	-	80

Table 7. The number of palynomorphs that were extracted from the NWMF borehole core, broken down by genera, species and specimens. The scolecodonts were classified in terms of 'morphotypes'.

These data form the basis for the palynological analysis of the biozonation and plant recovery discussions that follow in chapters 4 and 5, respectively.

Systematic descriptions have been completed for the most abundant miospores/microspores (which have been grouped together for convenience), and all megaspores, pollen, acritarchs and euglenoids. These represent 50 genera and 103 species, including 4 as *cf.* (comparison records; Bengtson 1988) and 5 identified only to generic level (see 'Systematic descriptions' and Plates 1 to 5).

Most other palynomorphs in low abundance, i.e. with counts of fewer than 10, were not described as these (16% by count of numbers) were considered to be of

low importance (Table 8; refer to Appendix 19 for a list of these additional palynomorphs).

Number of spores	Count of spores	As % of total
>9 specimens/taxon	33,074	84
<10 specimens/taxon	6,315	16
Total	39,389	100
Top 10 specimens/taxa	23,522	60
Number of taxa	Count of taxa	As % of total
>9 specimens/taxon	105	36
<10 specimens/taxon	185	64
Total	290	100
Top 10 specimens/taxon	10	3

Table 8. Breakdown of the palynological counts and the number of taxa for 3 categories: 10 or more specimens per taxon, less than 10 specimens per taxon and the total number of specimens per taxon. The top 10 specimens per taxon is included as a comparison.

The systematic information is presented using a standard layout and terminology based on Smith & Butterworth (1967). The taxa are first described at the generic level, with the 'Type species' named, a synonymy list and then the generic description with further comments, comparisons and remarks as necessary. This information explains why the species was assigned to that genus.

This is followed by the description for each species belonging to each genus. The plate and figure references are given to provide a visual representation of the palynomorph. This is followed by the synonymy list, the description of the species, the range of dimensions and the number of specimens that had been measured and the distribution range within the NWMF borehole, which also gives a relative chronology. Where appropriate, remarks and comparisons with other taxa have been provided, in addition to diagrams to illustrate specific aspects of the taxon

e.g. defining the dimensions of the sculptural elements as given in the species description or demonstrating the varying shapes of the sculptural elements. Where the parent plant affinity is known this information has also been noted. The author references are listed alphabetically in the References section. Refer to Appendix 18 for the suprageneric classification of the described NWMF borehole palynomorphs.

An attempt to identify the scolecodonts from the core proved problematic as there is scarce literature on scolecodonts of Tournaisian age. Therefore, they have been assigned to 6 broad morphotypes (see Section 4.2.5 and Plate 6).

SYSTEMATIC DESCRIPTIONS

3.1. MIOSPORES/MICROSPORES

Genus ***ACINOSPORITES*** Richardson 1965

Type species: *Acinosporites acanthomammillatus* Richardson 1965

1965 *Acinosporites* Richardson, p. 577.

1969 *Biornatisporites* Lele & Streel.

Generic description: Spores radial, trilete; amb subcircular to subtriangular; sculpture of convoluted and anastomosing ridges bearing verrucae with spinae, spinae or coni.

Comparison: *Convolutispora* has convoluted and anastomosing ridges only.

Acinosporites* cf. *acanthomammillatus

Plate 1 Figure a

Description: Miospores, radial, trilete; amb subcircular to convexly triangular; exine with round-topped verrucae, height: 1 to 1.5 μm (6 verrucae), base width: 2 to 5 μm (6 bases), that are joined at the bases to produce convolute and anastomosing ridges, surmounted by a slender straight or slightly recurved spina, height: 1 μm (5 spinae), occasionally interspersed with coni, height: 1 to 2 μm (13 coni); sutures hidden.

Dimensions: Length: 33 (44) 49 μm , width: 30 (38) 47 μm (7 specimens).

NWMF borehole distribution: 201.95 to 73.95 m depths.

Remarks: The size range for *Acinosporites acanthomammillatus* is quoted as: 85 to 141 μm (Richardson 1965), which is significantly greater than the NWMF borehole spores, but otherwise the description is very similar.

Comparison: The genus *Acinosporites* bears a sculpture of various types topping convoluted ridges, whereas *Convolutispora* only has the convolute and anastomosing ridges (Richardson 1965).

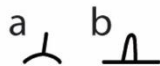


Figure 46. (a) Verrucae with spinae and (b) coni of *Acinosporites* cf. *acanthomammillatus*.

Genus **ANAPLANISPORITES** Jansonius 1962

Type species: *Anaplanisporites telephorus* (Klaus) Jansonius 1962

1962 *Anaplanisporites* Jansonius.

Generic description: Microspores radial, trilete; amb circular to subcircular; exine relatively thin with regularly distributed verrucae, grana or low coni, usually not more than 2 µm in height, on the distal surface, the proximal surface is laevigate.

Anaplanisporites baccatus (Hoffmeister *et al.*) Smith & Butterworth 1967

Plate 1 Figure b

- 1955 *Punctatisporites ? baccatus* Hoffmeister *et al.*, p. 392, Pl. 36, Fig. 2.
- 1958 *Apiculatisporis baccatus* (Hoffmeister *et al.*) Butterworth & Williams, p. 363, Pl. 1, Fig. 25.
- 1960 *Apiculatisporis baccatus* (Hoffmeister *et al.*) Butterworth & Williams; Staplin, Pl. 2, Figs. 9, 13.
- 1966 *Apiculatisporis baccatus* (Hoffmeister *et al.*) Butterworth & Williams; Sullivan & Marshall, Pl. 1, Figs. 18-19.
- 1967 *Anaplanisporites baccatus* (Hoffmeister *et al.*) Smith & Butterworth, pp. 166-167, Pl. 7, Figs. 1-5.
- 1970 *Anaplanisporites baccatus* (Hoffmeister *et al.*) Smith & Butterworth; Clayton, Pl. 1, Figs. 1-2.
- 1972 *Anapiculatisporites baccatus* (Hoffmeister *et al.*) Smith & Butterworth; Bertelsen, pp. 33-34, Pl. 5, Fig. 7, Pl. 6, Figs. 1-4.
- 1973 *Anapiculatisporites baccatus* (Hoffmeister *et al.*) Smith & Butterworth; Neves *et al.*, Pl. 3, Fig. 4.
- 1974 *Anaplanisporites delicatus* Neves & Ioannides, p. 76, Pl. 5, Figs. 2-4.
- 1977 *Anaplanisporites delicatus* Neves & Ioannides; Owens *et al.*, Pl. 1, Fig. 9.
- 1977 *Anaplanisporites delicatus* Neves & Ioannides; Clayton *et al.*, p. 39, Pl. 9, Fig. 19.
- 1978 *Anaplanisporites cf. delicatus* Neves & Ioannides; Turnau, Pl. 1, Figs. 14, 16.
- 1984 *Anaplanisporites baccatus* (Hoffmeister *et al.*) Smith & Butterworth; Scot *et al.*, p. 313, Fig. 2 c.
- 1985 *Anaplanisporites baccatus* (Hoffmeister *et al.*) Smith & Butterworth; Clayton, Pl. 2, Fig. a.

- 1986 *Anapiculatisporites baccatus* (Hoffmeister *et al.*) Ravn, p. 85, Pl. 23, Figs. 2-3.
- 1988 *Anaplanisporites baccatus* (Hoffmeister *et al.*) Smith & Butterworth; Higgs *et al.*, p. 53, Pl. 3, Fig. 1.
- 1988 *Anaplanisporites baccatus* (Hoffmeister *et al.*) Smith & Butterworth; McNestry, Pl. 3, Fig. 6.
- 1990 Unnamed, *in situ* microspores of *Oxroadia* sp. nov. Bateman & Rothwell, p. 146, Fig. 9 (d).
- 1990 *Anapiculatisporites baccatus* (Hoffmeister *et al.*) Smith & Butterworth; Clayton & Turnau, p. 51. Pl. 1, Fig. 1.
- 1991 *Anapiculatisporites baccatus* (Hoffmeister *et al.*) Ravn; Ravn, Pl. 2, Figs. 6-7.
- 1992 Unnamed, *in situ* microspores of *Oxroadia conferta* Bateman, Pl. 1, Figs. 2, 5, Pl. 6, Figs. 60, 61, 64, 67.
- 1994 *Anapiculatisporites baccatus* (Hoffmeister *et al.*) Smith & Butterworth; Avchimovitch & Turner, Pl. 1, Fig. 7.
- 1994 *Anaplanisporites baccatus* (Hoffmeister *et al.*) Smith & Butterworth; Mahdi & Butterworth, p. 163, Fig. 6, number 6.
- 2005 *Anaplanisporites baccatus* (Hoffmeister *et al.*) Smith & Butterworth; Turnau *et al.*, p. 96, Fig. 3 c.
- 2007 *Anaplanisporites baccatus* (Hoffmeister *et al.*) Smith & Butterworth; Higgs & Forsythe, p. 189, Pl. 1, Fig. T.
- 2010 ?*Anaplanisporites baccatus* (Hoffmeister *et al.*) Smith & Butterworth; Stevens *et al.*, *in situ* microspores from a *Flemingites arcuatus* cone, p. 802, Fig. 10 D, Figs. 11 A-D.
- 2017 *Anaplanisporites baccatus* (Hoffmeister *et al.*) Smith & Butterworth; Lopes & Mangerud, p. 31, Pl. 1, Fig. 6.
- 2019 *Anapiculatisporites baccatus* [= *Anaplanisporites baccatus*]; Marshall *et al.*, p. 271, Fig. 6, number 11.

Description: Microspores radial, trilete; amb circular to convexly triangular; exine thin with densely distributed, discrete, coni, height: 0.5 (1) 1.5 μm (50 coni); suturae simple, terminating in curvaturae.

Dimensions: Length: 16 (24) 33 μm , width: 13 (19) 27 μm (50 specimens).

NWMF borehole distribution: 501.18 to 42.46 m depths.

Remarks: The specimens are frequently found in masses and account for most of the tetrads (73%). The accompanying megaspore *Setispora pannosa* (Alvin) Spinner 1984 is present in NWMF borehole samples.

Affinity: *Oxroadia conferta* Bateman 1992. The affinity was identified from *in situ* spores that had been macerated from an intact cone borne by *O. conferta* from Oxroad Bay, Scotland (Bateman 1992, p. 42).

Anaplanisporites centrosus Higgs *et al.* 1988

Plate 1 Figure c

1988 *Anaplanisporites centrosus* Higgs *et al.*, p. 54, Pl. 3, Figs. 2-4.

Description: Miospores, radial, trilete; amb subcircular to convexly triangular; exine thin, distal face with discrete, densely distributed pila (rare), height: 1 μm , and broad-based spinae (common) with flattened, rounded or pointed, occasionally recurved tips, height 1 to 2 μm (26 spinae), base width: 1 (1.5) 3 μm (25 bases), proximal face exhibits more dispersed sculpture; suturae straight; compression folds common.

Dimensions: Length: 20 (42) 63 μm , width: 17 (34) 55 μm (12 specimens).

NWMF borehole distribution: 412.29 to 168.59 m depths.

Comparison: *A. centrosus* is distinguished from *A. baccatus* by its larger size and lack of curvaturae.

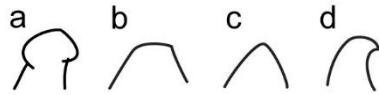


Figure 47. (a) Pila and (b) to (d) spinae of *Anaplanisporites centrosus*.

***Anaplanisporites* sp. A**

Plate 1 Figure d

Description: Miospores, radial, trilete; amb convexly triangular to subcircular; exine thin, proximal face laevigate, distal face laevigate with discrete, evenly spaced, tapering, pointed spinae and parallel sided, flat-topped grana, height: 0.5 to 1 μm ; suturae straight with narrow laesurae; contact areas laevigate; compression folds.

Dimensions: Length: 22 (25) 32 μm , width: 12 (21) 27 μm (18 specimens).

NWMF borehole distribution: 408.98 m to 90.33 m depths.

Remarks: These spores often occur as tetrads.

Comparisons: These spores resemble *A. baccatus* but have a sculpture of spinae and grana instead of coni.

They are not identified as *A. denticulatus* Sullivan 1964, which have coni with rounded or pointed tops of height: 0.5 to 1 μm , base width: 1 μm instead of grana, and the spore diameter is too large at 42 to 58 μm .

They are also not identified as *A. globulus* (Butterworth & Williams) Smith & Butterworth 1967, which have sculptural elements of a more varied morphology (coni, verrucae and 'globular protuberances') that are larger (up to 2.5 μm in height).



Figure 48. (a) Spinae and (b) grana of *Anaplanisporites* sp. A.

***Anaplanisporites* sp. B**

Plate 1 Figure e

Description: Miospores, radial, trilete; amb subcircular to convexly triangular; exine thin with regularly spaced, tapering-sided pila, height: approximately 1 μm , with an apical thickening; suturae simple; compression folds.

Dimensions: Length: 29 (32) 38 μm , width: 19 (27) 33 μm (24 specimens).

NWMF borehole distribution: 335.20 to 216.66 m depths.

Remarks: The fine sculpture of the pila is distinctive for this species.

Comparisons: These spores are not identified as *A. globulus* or *A. denticulatus* for the same reasons given for *Anaplanisporites* sp. A (see above).



Figure 49. Pila of *Anaplanisporites* sp. B.

Genus ***APICULATISPORIS*** (Ibrahim) Oschurkova 2003

Type species: *Apiculatisporis aculeatus* (Ibrahim) Potonié & Kremp 1956

1933 *Apiculatisporites* Ibrahim, p. 23.

1950 *Planisporites* Knox, p. 314.

1954 *Apiculatisporites* (Ibrahim) Potonié & Kremp, p. 130.

1954 *Planisporites* (Knox) Potonié & Kremp, p. 129.

1958 *Apiculatasporites* Potonié, p. 82.

2003 *Apiculatisporis* (Ibrahim) Oshurkova.

Generic description: Miospores, radial, trilete; amb subcircular; exine with regularly spaced coni of height: > 1.5 μm .

Discussion: According to the rules of the ICBN, the genus *Apiculatisporites* (Ibrahim) Potonié & Kremp 1954 was declared invalid and Oshurkova (2003) emended it to *Apiculatisporis* (Ibrahim) Oshurkova 2003. The genus was ascribed the diagnostic features: “radial trilete miospores with rounded amb; sculptured exine in the form of coni”. However, *Apiculatasporites* (Ibrahim) Smith & Butterworth 1967 has a similar diagnosis and was distinguished by the size of its sculptural elements being less than those of *Apiculatisporis*, but no dimensions were specified. In an earlier emendation, Visscher (1966) added that only specimens with sculptural elements of height: 0.5 to 1 μm belong to *Apiculatasporites*. McGregor & Camfield (1982) proposed that *Apiculatasporites* and *Apiculatisporis* are both genera of “subcircular, trilete spores bearing sculpture of rather regularly spaced coni”. They distinguished the two genera based on the height of most of the sculptural elements per specimen being 0.5-1.5 μm in *Apiculatasporites* and $> 1.5 \mu\text{m}$ in *Apiculatisporis*.

***Apiculatisporis* sp. A**

Plate 1 Figure f

Description: Miospores, radial, trilete; amb convexly triangular to subcircular; exine thin, minutely granulose with discrete, patchy, tapering sided, sharp- or blunt-topped spinae, height: 1 to 2 μm (28 spinae), base width: 1 (2) 3 μm (25 bases); suturae straight, simple; taper point folds common.

Dimensions: Length: 20 (42) 63 μm , width: 17 (34) 55 μm (12 specimens).

NWMF borehole distribution: 475.82 to 88.83 m depths.

Comparisons: These spores are not identified as those listed below, for the reasons outlined:

- *A. aculeatus* (Ibrahim) Potonié & Kemp 1955 has sculptural elements that are too densely distributed.
- *A. breviapiculatus* Danzé *et al.* 1964 is a megaspore of diameter 1325 to 2000 μm .
- *A. brevispiculus* (Schopf) Danzé *et al.* 1964 is a megaspore of diameter 1500 μm .
- *A. elegans* McGregor 1960 has smaller sculptural elements, height: up to 1.5 μm and is too large with a diameter of 67 to 85 μm .
- *A. globulus* Butterworth & Williams 1958 has sculptural elements of more varied morphology: coni, spinae and verrucae, height: up to 3 μm , diameter: 1 to 3 μm .
- *A. macrurus* (Luber) Potonié & Kemp 1955 has sculptural elements that are too large.
- *A. maculosus* (Knox) Potonié & Kemp 1955 has sculptural elements that are too robust and they are Namurian in age.
- *A. microconus* Richardson 1965 has coni and bacula height: < 1 μm , darkened contact areas and is too large with a diameter of 100 to 164 μm .
- *A. microechinatus* Owens 1971 has discrete sculptural elements of more varied morphology: coni, spinae and occasionally squat bacula and pila height: up to 1.5 μm and base width: 0.5 μm and is too large with a diameter of 68 to 89 μm .
- *A. morborus* Balme & Hassell 1962 has irregular sculptural elements of varied morphology: predominantly spinae with bacula and spinae, height: 1 to 7 μm , base width: 1 to 4 μm , raised labra, width: 2 μm and is too large with a diameter of 65 to 86 μm .
- *A. parviapiculatus* Danzé *et al.* 1964 is a megaspore of diameter 425 to 637 μm .
- *A. parvispinosus* Leschik 1956 has spines that are too small, height: 0.5 μm .
- *A. pineatus* Hoffmeister *et al.* 1955 has sculptural elements that are too large, height: 3 to 8 μm , and of a different morphology: spatulate with rounded to palmate tops and spinae.
- *A. porosus* Williams *In: Neves et al.* 1973 has sculptural elements of more varied morphology: verrucae, coni and bacula, mostly with round tops, few flat-topped and some showing basal fusion.

- *A. raistricki* Dybová & Jachowicz 1957 has longer processes height: up to 4 µm and basal diameter: 2 µm, raised suturae and is too small with a diameter of 28 to 31 µm.
- *A. subspinus* Danzé *et al.* 1964 is a megaspore of diameter 1625 to 1750 µm.
- *A. variocorneus* Sullivan 1964 has sculptural elements that are variable in size, shape and density: coni and spinae height: 0.5 to 1 µm, spinae height: 5.5 µm, and is too large with a diameter of 40 to 78 µm.
- *A. variornatus* Di Pasquo *et al.* 2003 has sculptural elements that are too robust.

Genus **APICULIRETUSISPORA** (Streel) Streel 1967

Type species: *Apiculiretusispora brandtii* Streel 1964

1964 *Apiculiretusispora* Streel, pp. 239-242.

1967 *Apiculiretusispora* (Streel) Streel, p. 32.

Generic description: Miospores, radial, trilete; amb circular to subtriangular; exine proximal face laevigate or minutely granulose, distal face with a highly variable sculpture of grana, coni and/or spinae or other biform elements, height: 1 µm; suturae often terminating in curvaturae.

Apiculiretusispora fructicosa Higgs 1975

Plate 1 Figure g

1962 *Retusotriletes verrucosus* Caro-Moniez, Pl. 1, Figs. 1-2.

1970 *Apiculiretusispora* sp. A Dolby & Neves, p. 636, Pl. 1, Fig. 5.

1974 *Apiculiretusispora verrucosa* (Caro-Moniez) Streel *In*: Becker *et al.*, p. 24.

1975 *Apiculiretusispora fructicosa* Higgs, p. 395, Pl. 1, Figs. 23-25.

1988 *Apiculiretusispora fructicosa* Higgs; Higgs *et al.*, p. 54, Pl. 3, Figs. 7, 12.

1994 *Apiculiretusispora fructicosa* Higgs; Mahdi & Butterworth, p. 163, Fig. 6, number 27.

Description: Miospores, radial, trilete; amb subcircular; exine thin with discrete, sparsely to densely distributed coni, pila and short bacula with rounded or flattened tops, height <1 µm; suturae distinct, straight, simple or with narrow labra, terminating in curvaturae; contact areas laevigate.

Dimensions: Length: 35 (51) 79 µm, width: 26 (38) 55 µm (50 specimens).

NWMF borehole distribution: 501.18 to 49.88 m depths.

Remarks: Conforms closely to the description by Higgs (1975), although the NWMF borehole spores are smaller than those recorded by Higgs (1975; 55 (73.5) 90 µm), which were oxidised and so may have expanded in size during processing.

Apiculiretusispora multiseta (Luber) Butterworth & Spinner 1967

Plate 1 Figure h

- 1938 *Azonotriletes multisetus* Luber *In*: Luber & Waltz, p. 23, Pl. 5, Fig. 61.
- 1955 *Filicitriletes multisetus* (Luber) Luber, pp. 55-56, Pl. 3, Fig. 52.
- 1955 *Acanthotriletes multisetosus* (Luber) Potonié & Kremp, p. 84.
- 1957 *Acanthotriletes multisetus* (Luber) Kedo, p. 1167.
- 1962 *Acanthotriletes multisetus* (Luber) Potonié & Kremp; Playford, Pl. 80, Figs. 14-15.
- 1963 *Acanthotriletes multisetus* (Luber) Kedo, p. 43, Pl. 2, Figs. 2, 51, 52.
- 1966 *Azonotriletes multisetus* (Luber) Kedo, p. 56, Pl. 1, Figs. 36-38.
- 1967 *Apiculiretusispora multiseta* (Luber) Butterworth & Spinner, pp. 5-6, Pl. 2, Figs. 13, 18.
- 1972 *Apiculiretusispora multiseta* (Luber) Butterworth & Spinner; Bertelsen, Pl. 8, Figs. 5, 7.
- 1973 *Colatisporites denticulatus* Neville *In*: Neves *et al.*, pp. 41-42, Pl. 2, Figs. 14-16.

- 1977 *Apiculiretusispora multiseta* (Luber) Butterworth & Spinner; Clayton *et al.*, p. 37, Pl. 8, Fig. 7, p. 41, Pl. 10, Fig. 21.
- non 1978 *Apiculiretusispora multiseta* (Luber) Butterworth & Spinner *In*: Turnau, p. 6, Pl. 1, Figs. 22-23.
- 1979 *Apiculiretusispora multiseta* (Luber) Butterworth & Spinner *In*: Turnau, Pl. 1, Figs 7-8.
- 1990 *Colatisporites denticulatus* Neville *In*: Clayton & Turnau, p. 51, Pl. 1, Figs. 2-3.
- non 1994 *Colatisporites multisetus* (Luber) Avchimovitch & Turnau, pp. 257-258, Pl. 1, Figs. 8-10.
- 1995 *Apiculiretusispora multiseta* (Luber) Butterworth & Spinner; Clayton, p. 119, Pl. 1, Fig. 6.
- 2000 *Apiculiretusispora multiseta* (Luber) Butterworth & Spinner; Melo & Loboziak, p. 149, Pl. 1, Fig. 1.
- 2005 *Apiculiretusispora multiseta* (Luber) Butterworth & Spinner; Dueñas & Césari, p. 143, Figs. 2 K, O.
- 2005 *Colatisporites multisetus* (Luber) Avchimovitch & Turnau; Turnau *et al.*, p. 96, Fig. 3 f.
- 2012 *Apiculiretusispora multiseta* (Luber) Butterworth & Spinner; Playford & Melo, Pl. 2, Figs. 12, 14.
- 2015 *Apiculiretusispora multiseta* Butterworth & Spinner 1967; Ariana-Sab *et al.*, Pl. 4, Fig. 9.

Description: Miospores, radial, trilete, camerate; amb convexly triangular to subcircular; intexine thin, laevigate, conformable with the amb; exoexine thin with discrete, densely distributed, tapering, mostly sharp- but occasionally blunt-tipped, upright or recurved spinae, height: < 1 to 1 µm; suturae straight with narrow labra, terminating in curvaturae; taper point folds common.

Dimensions: Length: 30 (39) 48 µm, width: 30 (34) 46 µm (8 specimens).

NWMF borehole distribution: 453.28 to 280.77 m depths.

Remarks: Conforms closely to the description by Butterworth & Spinner (1967), although the NWMF borehole spores are smaller than those recorded by Butterworth & Spinner (1967; length: 43 (54) 70 μm , width: 35 (46) 62 μm), which were oxidised and so may have expanded in size during processing.



Figure 50. (a) to (b) sharp-tipped and (c) to (d) blunt-tipped spinae of *Apiculiretusispora multiseta*.

***Apiculiretusispora nitida* Owens 1971**

Plate 1 Figure i

1971 *Apiculiretusispora nitida* Owens, p. 17, Pl. 3, Figs. 9-11.

2002 *Apiculiretusispora nitida* (McGregor) Owens; Higgs *et al.*, p. 146, Pl. 1, Fig. 7.

Description: Miospores, radial, trilete; amb subcircular; exine laevigate with discrete, scattered, parallel-sided, round-topped spinae and rare tapering, pointed spinae, height: < 1 μm ; suturae distinct, straight with broad labra, width: 2 μm , terminating in curvaturae; contact areas laevigate.

Dimensions: Length: 22 (27) 39 μm , width: 17 (23) 38 μm (6 specimens).

NWMF borehole distribution: 237.83 to 110.11 m depths.

Remarks: Conforms closely to the description by Owens (1971), although the NWMF borehole spores are smaller than those recorded by Owens (1971; 36 (44.6) 66 μm), which were oxidised and so may have expanded in size during processing. Owens (1971) also stated that these spores commonly occur in “sporangial masses” and those found in the NWMF borehole mostly occur as

tetrads. *A. nitida* was recorded in samples of Frasnian (Upper Devonian) age and has not been recorded in Tournaisian previously.



Figure 51. Spinae of *Apiculiretusispora nitida*.

***Apiculiretusispora* sp. A** Higgs *et al.* 1988

Plate 1 Figure j

1988 *Apiculiretusispora* sp. A Higgs *et al.*, Pl. 3, Fig. 9.

Description: Miospores, radial, trilete; amb subcircular; exine thin, minutely granulose with discrete, scattered pila, height: 0.5 to 1.5 μm ; suturae straight with narrow labra, width: 1.5 μm , terminating in curvaturae; contact areas laevigate; compression folds common.

Dimensions: Length: 35 (45) 61 μm , width: 31 (38) 56 μm (8 specimens).

NWMF borehole distribution: 284.75 to 42.46 m depths.

Remarks: The age range for this species has been stated as Devonian LE to LN biozones (Higgs *et al.* 1988) and it has not been recorded previously from the Tournaisian.

Genus ***AURORASPORA*** Hoffmeister *et al.* 1955

Type species: *Auroraspora solisorta* Hoffmeister *et al.* 1955

1955 *Auroraspora* Hoffmeister *et al.*, p. 381.

1960 *Auroraspora* Hoffmeister *et al.*; Richardson, p. 49.

Generic description: Miospores, radial, trilete, camerate; amb subcircular to convexly triangular; intexine laevigate, minutely granulose or weakly reticulate, conformable with the amb; exoexine thin, laevigate, minutely granulose or irregularly infrapunctate; suturae with labra; radial compression folds common.

Comparisons: Whereas *Auroraspora* is laevigate, minutely granulose or irregularly infrapunctate, the genus *Endoculeospora* (Staplin) Turnau 1975 has scattered to densely distributed grana, pili and/or bacula mostly on the distal face.

Also, the genus *Colatisporites* Williams *In: Neves et al.* 1973 has small elements that include spinae, coni and bacula, predominantly on the distal face but may extend slightly on to the proximal face and may have curvaturae.

Auroraspora asperella (Kedo) Van der Zwan 1980

Plate 1 Figure k

- 1974 *Archaeozonotriletes asperellus* Kedo *In: Golubtsov & Manjkin*, p. 55, Pl. 13, Fig. 12.
- 1980 *Auroraspora asperella* (Kedo) Van der Zwan, pp. 137-139, Pl. 2, Figs. 1-12, Pl. 3, Figs. 1-2.
- 1988 *Auroraspora asperella* (Kedo) Van der Zwan; Higgs *et al.*, pp. 68-69, Pl. 9, Figs. 11-12.
- 1988 *Auroraspora asperella* (Kedo) Van der Zwan; Avchimovitch *et al.*, Pl. 4, Fig. 15.
- 1992 *Auroraspora asperella* (Kedo) Van der Zwan; Avchimovitch, Pl. 5, Fig. 9.
- 1996 *Auroraspora asperella* (Kedo) Van der Zwan; Higgs, Pl. 6, Fig. 9.
- 2015 *Auroraspora asperella* (Kedo) Van der Zwan; Ariana-Sab *et al.*, Pl. 1, Fig. 6.

Description: Miospores, radial, trilete, camerate; amb circular to convexly triangular; intexine laevigate to minutely granulose, distinct, conformable with the amb; exoexine laevigate, minutely granulose or with variable sculpture of sparsely

to densely distributed small grana; ratio of intexine: exoexine $\frac{4}{5}$; suturae distinct, straight to slightly sinuous, bordered by labra which are often very prominent.

Dimensions: Total length: 32 (41) 55 µm, width: 29 (36) 51 µm, inner body length: 26 (33) 41 µm, width: 22 (29) 36 (45 specimens).

NWMF borehole distribution: 501.18 to 39.11 m depths.

Auroraspora macra Sullivan 1968

Plate 1 Figure I

- 1968 *Auroraspora macra* Sullivan, pp. 124-125, Pl. 27, Figs. 6-10.
- 1970 *Auroraspora macra* Sullivan; Clayton, p. 580, Pl. 1, Fig. 3.
- 1971 *Auroraspora macra* Sullivan; Johnson & Marshall, Pl. 23, Fig. 5.
- 1971 *Auroraspora macra* Sullivan; Playford, pp. 49-50, Pl. 17, Figs. 1-6.
- 1972 *Auroraspora macra* Sullivan; Bertelsen, Pl. 1, Figs. 5-6.
- 1973 *Auroraspora macra* Sullivan; Neves *et al.*, Pl. 3, Fig. 13.
- 1974 *Auroraspora macra* Sullivan; Neves & Ioannides, Pl. 8, Fig. 4.
- 1975 *Auroraspora macra* Sullivan; Higgs, Pl. 4, Fig. 11.
- 1977 *Auroraspora macra* Sullivan; Clayton *et al.*, p. 23, Pl. 1, Fig. 6, p. 29, Pl. 4, Fig. 3, p. 33, Pl. 6, Fig. 14, p. 35, Pl. 7, Figs. 18-19, p. 37, Pl. 8, Fig. 22.
- 1977 *Auroraspora macra* Sullivan; Keegan, p. 555, Pl. 4, Fig. 6.
- 1977 *Auroraspora macra* Sullivan; Owens *et al.*, Pl. 2, Fig. 11.
- 1978 *Auroraspora macra* Sullivan; Playford, p. 139, Pl. 10, Fig. 2.
- 1978 *Auroraspora macra* Sullivan; Turnau, Pl. 4, Figs. 7-8.
- 1979 *Auroraspora macra* Sullivan; Welsh, Pl. 1, Fig. 8.
- 1980 *Auroraspora macra* Sullivan; Phillips & Clayton, Fig. 9 R.
- 1980 *Auroraspora macra* Sullivan; Van der Zwan, p. 134, Pl. 1, Figs. 2, 4, 6.
- 1984 *Auroraspora macra* Sullivan; Scott *et al.*, p. 313, Fig 2 W.
- 1985 *Auroraspora macra* Sullivan; Clayton, p. 23, Fig. 2 p.
- 1987 *Auroraspora macra* Sullivan; Utting, Pl. 5, Fig. 12.
- 1988 *Auroraspora macra* Sullivan; Higgs *et al.*, p. 69, Pl. 9, Figs, 17-19.

- 1988 *Auroraspora macra* Sullivan; Turner & Spinner, Pl. 3, Fig. 7.
 1990 *Auroraspora macra* Sullivan; Playford, Pl. 4, Figs. 1-2.
 1994 *Auroraspora macra* Sullivan; Mahdi & Butterworth, p. 162, Fig. 5, number 8.
 1997 *Auroraspora macra* Sullivan; Carson & Clayton, Pl. 2, Fig. 17.
 2002 *Auroraspora macra* Sullivan; Stephenson *et al.*, p. 106, Fig. 10, number 23.
 2005 *Auroraspora macra* Sullivan; Dueñas & Césari, p. 148, Fig. 3 H.
 2005 *Auroraspora macra* Sullivan; Turnau *et al.*, p. 96, Fig. 3 k.
 2008 *Auroraspora macra* Sullivan; Pérez Loinaze, p. 432, Fig. 3, numbers 9, 11.
 2012 *Auroraspora macra* Sullivan; Melo & Playford, p. 117, Pl. 9, Figs. 3-4.
 2015 *Auroraspora macra* Sullivan; Ariana-Sab *et al.*, Pl. 2, Fig. 9.
 2016 *Auroraspora macra* Sullivan; Lopes *et al.*, p. 65, Pl. 1, Fig. 29.

Description: Miospores, radial, trilete, camerate; amb circular to convexly triangular; intexine thin, laevigate to minutely granulose, distinct, conformable with the amb; exoexine thin, laevigate to minutely granulose; ratio of intexine: exoexine $\frac{4}{5}$; suturae simple.

Dimensions: Total length: 40 (58) 96 μm , inner body length: 33 (46) 66 μm (50 specimens).

NWMF borehole distribution: 501.18 to 39.11 m depths.

Remarks: *A. macra* (mean length 58 μm) is larger than *A. asperella* (mean length 43 μm) with less prominent labra and finer sculpture.

Auroraspora solisorta Hoffmeister *et al.* 1955

Plate 1 Figure m

- 1948 Type 44K Knox.
 1955 *Auroraspora solisortus* Hoffmeister *et al.*, p. 381, Pl. 37, Fig. 3.
 1958 *Auroraspora solisortus* Hoffmeister *et al.*; Butterworth & Williams, p. 388, Pl. 4, Fig. 11.

- 1971 *Auroraspora solisortus* Hoffmeister *et al.*; Playford, p. 50, Pl. 17, Figs. 18-19.
- 1972 *Auroraspora* cf. *solisortus* Hoffmeister *et al.*; Bertelsen p. 57, Pl. 23, Figs 7-8.
- 1974 *Auroraspora solisorta* Hoffmeister *et al.*; Becker *et al.*, Pl. 21, Fig. 1.
- 1977 *Auroraspora solisorta* Hoffmeister *et al.*; Clayton *et al.*, p. 23, Pl. 1, Fig. 5, p. 25, Pl. 2, Fig. 4, p. 39, Pl. 9, Fig. 24.
- 1978 *Auroraspora* cf. *solisortus* Hoffmeister *et al.*; Turnau, pp. 10-11, Pl. 4, Figs. 17-18.
- 1984 *Auroraspora solisorta* Hoffmeister *et al.*; Higgs & Clayton, p. 25, Pl. 2, Fig. 16.
- 1988 *Auroraspora solisortus* Hoffmeister *et al.*; Higgs *et al.*, p. 69, Pl. 10, Figs. 1-2.
- 1987 *Auroraspora solisortus* Hoffmeister *et al.*; Utting, Pl. 5, Fig. 13.
- 1989 *Auroraspora solisortus* Hoffmeister *et al.*; Brindley & Spinner, p. 220, Fig. 5, number 11.
- 1991 *Auroraspora solisorta* Hoffmeister *et al.*; Ravn, Pl. 26, Fig. 1.
- 1993 *Auroraspora solisortus* Hoffmeister *et al.*; Turner & Spinner, Pl. 2, Fig. 6.
- 1995 *Auroraspora solisorta* Hoffmeister *et al.*; Clayton, p. 120, Pl. 2, Fig. 2.
- 2005 *Auroraspora solisorta* Hoffmeister *et al.*; Dueñas & Césari, p. 148, Fig. 3 R.
- 2012 *Auroraspora solisorta* Hoffmeister *et al.*; Melo & Playford, pp. 117-118, Pl. 9, Figs. 5-8.
- 2015 *Auroraspora solisortus* Hoffmeister *et al.*; Ariana-Sab *et al.*, Pl. 2, Fig. 12.
- 2016 *Auroraspora solisorta* Hoffmeister *et al.*, Lopes *et al.*, p. 67, Pl. 2, Fig. 7.

Description: Miospores, radial, trilete, camerate; amb convexly triangular; intexine distinct, subcircular, laevigate, offset from amb with wall thickness: 1 to 1.5 μm ; exoexine thin, minutely granulose; ratio of intexine: exoexine $\frac{1}{2}$ to $\frac{4}{5}$; suturae simple; radial folds common.

Dimensions: Total length: 41 (64) 89 μm (16 specimens), width: 31 (51) 73 μm (15 specimens), inner body length: 22 (41) 75 μm , width: 15 (31) 50 μm (16 specimens).

NWMF borehole distribution: 462.32 to 42.46 m depths.

Remarks: Conforms closely to the description by Hoffmeister *et al.* (1955) although their size range of 61 to 78 μm may now be extended to 41 to 89 μm .

Discussion: The question of whether continuous morphological variation could hamper the classification of early Carboniferous spores has been raised (e.g. Van der Zwan 1980). To test whether the species of *Auroraspora* identified from the NWMF borehole core exhibit continuous variation or represent distinct species, the diameters of the intexines and the exoexines for the three most commonly occurring species of *Auroraspora* were plotted (Figure 52).

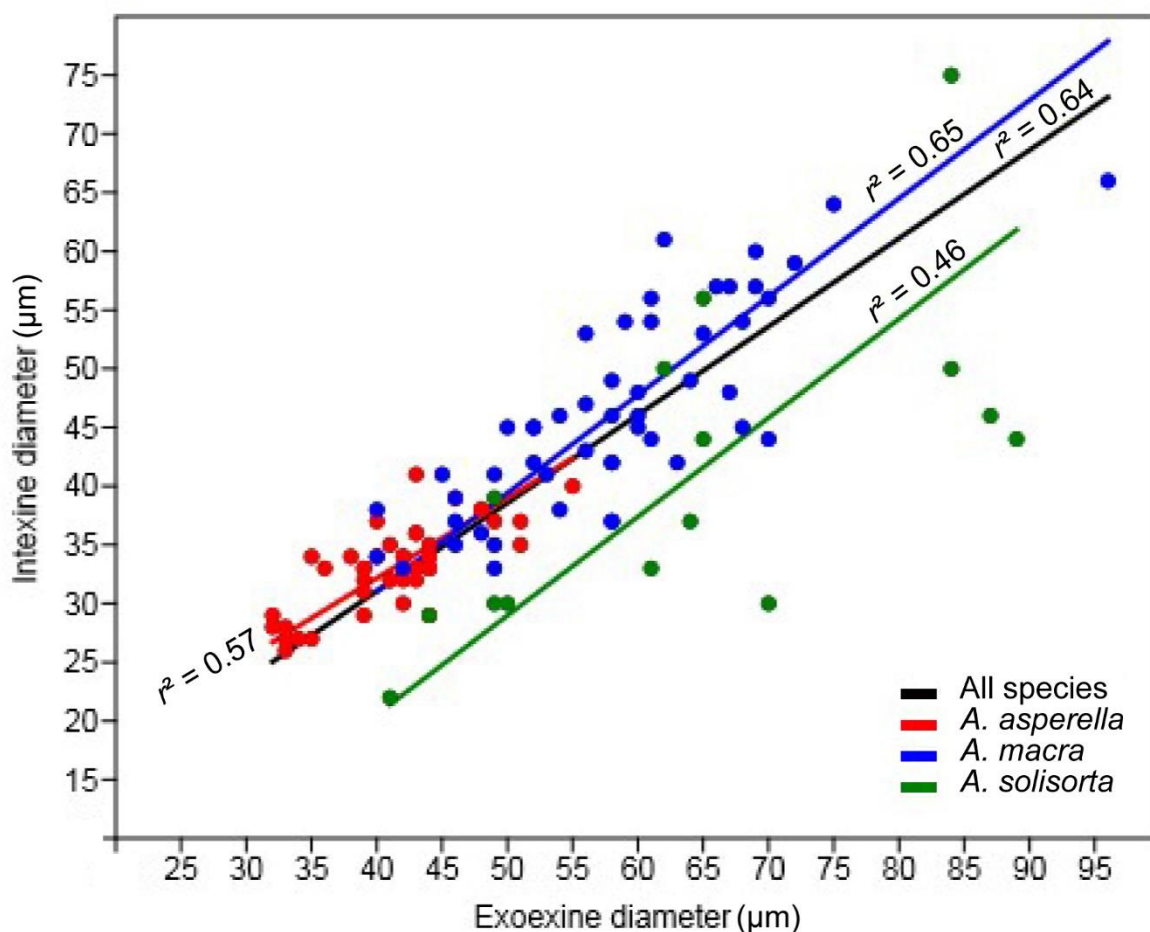


Figure 52. X-Y scatter plot of the diameters of the intexines and the exoexines for the three most commonly occurring species of *Auroraspora* identified from the NWMF borehole core with Standardised Major Axis applied and r^2 values given.

This showed that *A. solisorta* mostly fell outside of the scatter for *A. asperella* and *A. macra*, indicating that it forms a distinct taxon. However, the scatter for *A. asperella* and *A. macra* overlap, which could suggest continuous variation within a single taxon. But *A. asperella* clusters towards the lower intexine-exoexine diameter scale and overlaps with the smaller *A. macra* diameters. This suggests that they are separate form species with some of the *A. macra* population simply being composed of smaller spores.

Genus **BACULATISPORITES** Thomson & Pflug 1953

Type species: *Baculatisporites primarius* (Wolff) Thomson & Pflug 1953

1953 *Baculatisporites* Thomson & Pflug, p. 56, Pl. 2, Fig. 51.

Generic description: Miospores, radial, trilete; amb subcircular; exine with numerous, widely distributed, cylindrical bacula, usually with a truncated end, height: 3 µm.

Baculatisporites fusticulus Sullivan 1968

Plate 1 Figure n

- 1968 *Baculatisporites fusticulus* Sullivan, pp. 117, 119, Pl. 25, Figs. 1-2.
- 1970 *Baculatisporites fusticulus* Sullivan; Clayton, Pl. 1, Fig. 4, p. 33, Pl. 6, Fig. 8.
- 1972 *Baculatisporites fusticulus* Sullivan; Bertelsen, Pl. 3, Figs. 3-4.
- 1973 *Baculatisporites fusticulus* Sullivan; Neves *et al.*, Pl. 3, Fig. 5.
- 1975 *Baculatisporites fusticulus* Sullivan; Higgs, Pl. 1, Fig. 22.
- 1977 *Baculatisporites fusticulus* Sullivan; Keegan, p. 549, Pl. 1, Fig. 10.
- 1977 *Baculatisporites fusticulus* Sullivan; Owens *et al.*, Pl. 1, Fig. 6.
- 1978 *Baculatisporites fusticulus* Sullivan; Turnau, Pl. 1, Fig. 7.
- 1980 *Baculatisporites fusticulus* Sullivan; Phillips & Clayton, Fig. 8 J.
- 1988 *Baculatisporites fusticulus* Sullivan; Higgs *et al.*, p. 54, Pl. 3, Fig. 14.
- 1988 *Baculatisporites fusticulus* Sullivan; Turner & Spinner, Pl. 3, Fig. 10.

2005 *Baculatisporites fusticulus* Sullivan; Turnau *et al.*, p. 96, Fig 3 a.

2016 *Baculatisporites fusticulus* Sullivan; Lopes *et al.*, p. 67, Pl. 2, Fig. 5.

Description: Miospores, radial, trilete; amb circular to oval but usually irregular due to the presence of folds; exine thin with evenly distributed bacula and pila of uniform size, height: 1 μm ; suturae often obscured by folding; secondary folds common.

Dimensions: Length: 58 (73) 97 μm , width: 38 (52) 70 μm (30 specimens).

NWMF borehole distribution: 500.98 m to 39.11 m depths.

Genus **BASCAUDASPORA** Owens 1983

Type species: *Bascaudaspora canipa* Owens 1983

1983 *Bascaudaspora* Owens, pp. 45-46.

Generic description: Miospores, radial, trilete; amb rounded triangular to subcircular; uniform cingulum; exine has a variable reticulate sculpture with muri enclosing either large, irregular shaped lumen, or lumina of more or less regular shape and constant size, muri normally restricted to the distal face, fusing equatorially onto the distal surface of the cingulum but may spread onto the more equatorial portions of the proximal surface, particularly in the contact areas.

Bascaudaspora submarginata (Playford) Higgs *et al.* 1988

Plate 1 Figure o

1963 *Dictyotriletes submarginatus* Playford, p. 29-30, Pl. 8, Figs. 9-13.

1969 *Dictyotriletes submarginatus* Playford; Hibbert & Lacey, Pl. 80, Figs. 3, 6, 11, 12.

1969 *Dictyotriletes submarginatus* Playford; Varma, Pl. 2, Fig. 9.

- 1973 *Dictyotriletes submarginatus* Playford; Neves *et al.*, Pl. 4, Fig. 8.
- 1977 *Dictyotriletes submarginatus* Playford; Clayton *et al.*, p. 29, Pl. 4, Fig. 23, p. 31, Pl. 5, Fig. 16.
- 1977 *Dictyotriletes submarginatus* Playford; Keegan, p. 551, Pl. 2, Fig. 12.
- 1978 *Dictyotriletes submarginatus* Playford; Mortimer *et al.*, Pl. 29, Fig. 5.
- 1978 *Dictyotriletes submarginatus* Playford; Turnau, Pl. 2, Figs. 13-14.
- 1980 *Dictyotriletes submarginatus* Playford; Van der Zwan, p. 223, Pl. 27, Figs. 2-3, Pl. 28, Figs. 1-5, Pl. 29, Fig. 4.
- 1980 *Dictyotriletes* sp. A; Van der Zwan, p. 224, Pl. 29, Figs. 1-3.
- 1980 *Dictyotriletes submarginatus* Playford; Phillips & Clayton, p. 126, Figs. 9 A-C.
- 1987 *Cristatisporites submarginatus* (Playford) Utting, p. 32, Pl. 3, Fig. 9.
- 1988 *Bascaudaspora submarginata* (Playford) Higgs *et al.*; Avchimovitch *et al.*, p. 171.
- 1988 *Bascaudaspora submarginata* (Playford) Higgs *et al.*, p. 65, Pl. 7, Figs. 19-20.
- 1991 *Bascaudaspora submarginata* (Playford) Higgs *et al.*; Ravn, Pl. 12, Figs. 14-17.
- 1992 *Dictyotriletes submarginatus* Playford; Avchimovitch, Pl. 10, Fig. 6.
- 1996 *Bascaudaspora submarginata* (Playford) Higgs *et al.*; Higgs, Pl. 7, Figs. 1-8.
- 2000 *Bascaudaspora submarginata* (Playford) Higgs *et al.*; Melo & Loboziak, p. 149-151, Pl. 2, Fig. 1.
- 2005 *Bascaudaspora submarginata* (Playford) Higgs *et al.*; Dueñas & Césari, p. 146, Fig. 3 G.
- 2007 *Bascaudaspora submarginata* (Playford) Higgs *et al.*; Higgs & Forsythe, p. 189, Pl. 1, Fig. H.
- 2008 *Bascaudaspora submarginata* (Playford) Higgs *et al.*; Pérez Loinaze pp. 424-425, Fig. 1, numbers 10-12.
- 2012 *Bascaudaspora submarginata* (Playford) Higgs *et al.*; Melo & Playford, p. 99, Pl. 1, Fig. 5.

Description: Miospores, radial, trilete; amb subcircular to convexly triangular; exine thin: 0.5 to 2 μ m, laevigate with reticulate pattern of rounded, sinuous, irregularly

branching, occasionally anastomosing or terminating muri, height: 0.5 (2) 3.5 μm (13 muri); suturae often hidden by sculpture; frequent compression folds.

Dimensions: Length: 37 (50) 79 μm , width: 31 (47) 70 μm (12 specimens).

NWMF borehole distribution: 485.93 m to 158.77 m depths.

Comparisons: *Knoxisporites* has a cingulum that is distinguished by the development of variable, radial and/or concentric bands of thickening on the distal surface. *Dictyotriletes* lacks a cingulum.

Genus **CALAMOSPORA** Schopf *et al.* 1944

Type species: *Calamospora hartungiana* Schopf *In*: Schopf *et al.* 1944

1944 *Calamospora* Schopf *et al.*, pp. 49-51.

Generic description: Miospores, radial, trilete; amb circular to semi-circular; size highly variable from about 40 μm to several hundred μm ; exine thin, laevigate, minutely granulose or slightly rugose; contact areas sometimes exhibit a different surface texture to the rest of the exine; sutures distinct, sometimes with labra; arcuate ridges may be present as slight rounded thickenings; characteristic sharp taper-point folds.

Calamospora nigrata (Naumova) Allen 1965

Plate 1 Figure p

1953 *Leiotriletes nigratus* Naumova, p. 23, Pl. 1, Fig. 9.

1958 *Leiotriletes nigratus* Ishchenko, p. 35, Pl. 1, Fig. 5 *non* Naumova 1953.

1965 *Calamospora nigrata* (Naumova) Allen, p. 693.

1967 *Calamospora cf. nigrata* (Ishchenko); Butterworth & Spinner, p. 3, Pl. 1, Fig. S.

2012 *Calamospora nigrata* (Naumova) Allen; Playford & Melo, pp. 12-13, Pl. 1, Figs. 1-2.

Description: Miospores, radial, trilete; amb circular to oval; exine thin; laevigate to minutely granulose; suturae simple, short; darkened contact areas; taper point folds common.

Dimensions: Length: 42 (69) 105 μm (21 specimens), width: 33 (56) 88 μm (17 specimens).

NWMF borehole distribution: 501.18 to 93.38 m depths.

Remarks: The darkened contact areas distinguish this species (Higgs *et al.* 1988).

Calamospora perrugosa (Loose) Schopf *et al.* 1944

Plate 1 Figure q

1934 *Laevigati-sporites perrugosus* Loose, p. 145, Pl. 7, Fig. 13.

1943 *Triletes (Laevigati) perrugosus* (Loose) Horst, p. 83.

1944 *Calamospora perrugosus* (Loose) Schopf *et al.*, p. 52.

1955 *Calamospora perrugosa* (Loose) Potonié & Kremp, Pl. 12, Fig. 135.

1955 *Calamospora perrugosa* (Loose) Schopf *et al.*; Horst, p. 157.

1967 *Calamospora perrugosa* (Loose) Schopf *et al.*; Smith & Butterworth, p. 137, Pl. 3, Fig. 9.

1988 *Calamospora perrugosa* (Loose) Schopf *et al.*; Higgs *et al.*, p. 50, Pl. 1, Fig. 1.

Description: Miospores, radial, trilete; amb subcircular but usually irregular due to the presence of folds; exine thin, laevigate to minutely granulose; sutures simple; taper point folds common.

Dimensions: Length: 100 (171) 250 μm , width: 51 (123) 225 μm (11 specimens).

NWMF borehole distribution: 490.79 to 166.82 m depths.

Remarks: The large size distinguishes this species.

***Calamospora* spp.**

Other species of *Calamospora* were present in the NWMF borehole samples, but the genus was not speciated further as the remaining specimens, not described above, did not exhibit enough distinguishing features to identify them. This suggests that the genus has been over-speciated and that other *Calamospora* species could be lumped together.

NWMF borehole distribution: 500.98 to 42.46 m depths.

Genus **CINGULIZONATES** (Dybová & Jachowicz) Butterworth *et al.* In: Staplin & Jansonius 1964

Type species: *Cingulizonates bialatus* (Waltz) Smith & Butterworth 1967

1957 *Cingulizonates* Dybová & Jachowicz, p. 170-171.

1964 *Cingulizonates* Butterworth *et al.* In: Staplin & Jansonius, p. 105.

Generic description: Miospores, radial, trilete, camerate; amb convexly triangular to subcircular; intexine thin, laevigate and rarely seen; exoexine characterised by a sharply differentiated cingulum, where the cingulum is distinctly raised, sometimes internally vacuolate and tapers into a relatively thin zona towards the equator; proximal face laevigate to minutely granulose, distal face of the cingulum is usually granulose or verrucose and the zona is sometimes sculptured; suturae distinct.

Cingulizonates bialatus (Waltz) Smith & Butterworth 1967

Plate 1 Figures r and s

- 1938 *Zonotriletes bialatus* Waltz In: Luber & Waltz, p. 22, Pl. 4, Fig. 51.
- 1941 *Zonotriletes bialatus* var. *undulatus* Waltz In: Luber & Waltz, p. 28, Pl. 5, Figs. 71 a-b.
- 1941 *Zonotriletes bialatus* var. *costatus* Waltz In: Luber & Waltz, p. 29, Pl. 5, Fig. 72.
- 1952 *Hymenozonotriletes* aff. *bialatus* (Waltz) Ishchenko, p. 51, Pl. 13, Fig. 124.
- 1956 *Densosporites bialatus* (Waltz) Potonié & Kremp, p. 114.
- 1956 *Hymenozonotriletes bialatus* var. *undulatus* (Waltz) Ishchenko, pp. 63-64, Pl. 12, Figs. 135-137.
- 1957 *Cingulizonates tuberosus* Dybová & Jachowicz, p. 171, Pl. 53, Figs. 1-4.
- 1957 *Trematozonotriletes bialatus* (Waltz) Naumova; Byvscheva, p. 1010.
- 1958 *Densosporites striatus* (Knox) Butterworth & Williams, p. 380, Pl. 3, Fig. 36.
- 1963 *Densosporites bialatus* (Waltz) Potonié & Kremp; Playford, Pl. 88, Figs. 4-7.
- 1967 *Cingulizonates bialatus* (Waltz) Smith & Butterworth, pp. 260-261, Pl. 21, Figs. 3-4.
- 1969 *Cingulizonates* sp. n° 3282 of Lanzoni & Magloire, Pl. 3, Figs. 1-2.
- 1973 *Cingulizonates bialatus* (Waltz) Smith & Butterworth; Neves *et al.*, Pl. 4, Fig. 14.
- 1977 *Cingulizonates bialatus* (Waltz) Smith & Butterworth; Clayton *et al.*, p. 43, Pl. 11, Fig. 28, p. 45, Pl. 12, Fig. 4.
- 1989 *Cingulizonates bialatus* (Waltz) Smith & Butterworth; Brindley & Spinner, p. 222, Fig. 6, number 2.
- 1991 *Cingulizonates bialatus* (Waltz) Smith & Butterworth; Ravn, Pl. 23, Fig. 19.
- 2000 *Cingulizonates bialatus* (Waltz) Smith & Butterworth; Melo & Loboziak, p. 151, Pl. 2, Fig. 12.
- 2012 *Cingulizonates bialatus* (Waltz) Smith & Butterworth; Melo & Playford, p. 104, Pl. 2, Fig. 2.
- 2015 *Cingulizonates bialatus* (Waltz) Smith & Butterworth; Ariana-Sab *et al.*, Pl. 2, Fig. 2, Pl. 4, Figs. 3, 10.

2016 *Cingulizonates bialatus* (Waltz) Smith & Butterworth; Lopes *et al.*, p. 65, Pl. 1, Fig. 9.

2017 *Cingulizonates bialatus* (Waltz) Smith & Butterworth; Lopes & Mangerud, p. 31. Pl. 1, Figs. 13, 18.

Description: Miospores, radial, trilete, camerate; amb convexly triangular to subcircular; intexine obscured; exoexine thin, forming a bizonate cingulum; centre minutely granulose with occasional verrucae, the cingulum is laevigate with a ring of elongate vacuoles innermost, with sparsely distributed wide-based clava, height: 1 (6) 11.5 μm (10 clava) and spinae with blunt or sharp tips, height: 0.5 (1) 2.5 μm (15 spinae), rarely crossing to the edge of the zona; zona thin, conformable to the cingulum's outline, laevigate with occasional short, round topped coni, ring of oval to elongate vacuoles along outer edge of zona; suturae straight with narrow labra.

Dimensions: Total length: 45 (67) 107 μm , width: 37 (50) 98 μm , inner body length: 33 (50) 68 μm , width: 26 (38) 53 μm , centre length: 22 (31) 41 μm , width: 10 (22) 31 μm (22 specimens).

NWMF borehole distribution: 485.93 m to 213.38 m depths.



Figure 53. (a) to (c) spinae (d) inner body clava (e) and (f) outer body spinae (g) and (h) central and (i) outer clava of *Cingulizonates bialatus*.

***Cingulizonates* sp. A**

Plate 1 Figure t

Description: Miospores, radial, trilete, camerate; amb triangular to subcircular; intexine obscured; exoexine thin, forming a bizonate cingulum; centre minutely granulose; cingulum wider at the apices, laevigate with a ring of subcircular to

elongate vacuoles innermost; zona thin, conformable to the cingulum's outline with apices further widened, laevigate with occasional short projections of clava, baculi, spinae, coni and pila, height: 1 to 2 μm ; suturae sinuous, simple.



Figure 54. Diagram to define the structures of *Cingulizonates* sp. A. The 'bizonate cingulum' comprises the cingulum and the zona.

Dimensions: Total length: 44 (58) 74 μm , width: 37 (49) 63 μm , inner body length: 36 (45) 56 μm , width: 30 (39) 49 μm , centre length: 23 (31) 42 μm , width: 11 (24) 36 μm (18 specimens).

NWMF borehole distribution: 472.81 m to 54.56 m depths.

Comparisons: These spores are not identified as below for the reasons outlined:

- *C. capistratus* (Hoffmeister *et al.*) Staplin & Jansonius 1964 has a laevigate centre, the cingulum is narrower than the zona, the inner part of the zona has elongated vacuoles separated by narrow walls and the outer part of the zona is weakly striated with small coni.
- *C. flamulus* Ravn 1991 has irregular, sometimes bifurcating ribs from the cingulum to the margin, which is conspicuously serrated and their diameters are too small at 42 to 54 μm .
- *C. landesii* (Staplin) Staplin & Jansonius 1964 has scattered minute vacuoles (rather than a ring of vacuoles), the zona is apiculate (rather than laevigate), is variable in size and sharply pointed.
- *C. loricatus* (Loose) Butterworth *et al.* 1964 does not have sculptural elements projecting from the margin and their diameters are too small at 33 (36) 42 μm .



Figure 55. (a) Clava (b) to (c) baculi (d) spinae and (e) coni of *Cingulizonates* sp. A.

Genus **CLAYTONISPORA** Playford & Melo 2012

Type species: *Claytonispora variabilis* (Hibbert & Lacey) Playford & Melo 2012

- 1969 *Umbonatisporites* Hibbert & Lacey, p. 423.
- 1970 *Umbonatisporites* (Hibbert & Lacey) Clayton, p. 591.
- 1972 *Umbonatisporites* (Hibbert & Lacey) Clayton; Playford, pp. 304-305.
- 1976 *Dibolisporites* (Richardson) Playford, p. 14.
- 1978 *Umbonatisporites* (Hibbert & Lacey) Clayton; Turnau, p. 7.
- 1996 *Umbonatisporites* (Hibbert & Lacey) Higgs, pp. 281, 283.
- 2012 *Claytonispora* Playford & Melo, pp. 31-33.

Generic description: Miospores, radial, trilete; amb circular to convexly subtriangular; exine has densely to sparsely distributed, elongate, slender spina-like or baculum-like projections, with circular or subcircular bases, with or without undulations and commonly expanding distally to form a rounded or pointed termination, typically a collar- or bowl-like lateral expansion, that is commonly surmounted by a diminutive spina or conus; suturae simple, straight; contact areas laevigate to minutely granulose.

Discussion: Playford & Melo (2012) erected the genus *Claytonispora* to differentiate it from *Umbonatisporites* on the basis of morphological differences of their respective sculptural elements.

Umbonatisporites is defined as having compound, heteromorphic, apiculate elements that commonly broaden distally from a narrow base and have one to three verrucate terminations that are each surmounted by a spina (Figure 56 A and B).

Claytonispora, however, has elongate projections that taper from the base, with or without alternating lateral constrictions and expansions, commonly with a distal bowl-like lateral expansion that is usually surmounted by a spina or conus (Figure 56 C and D).

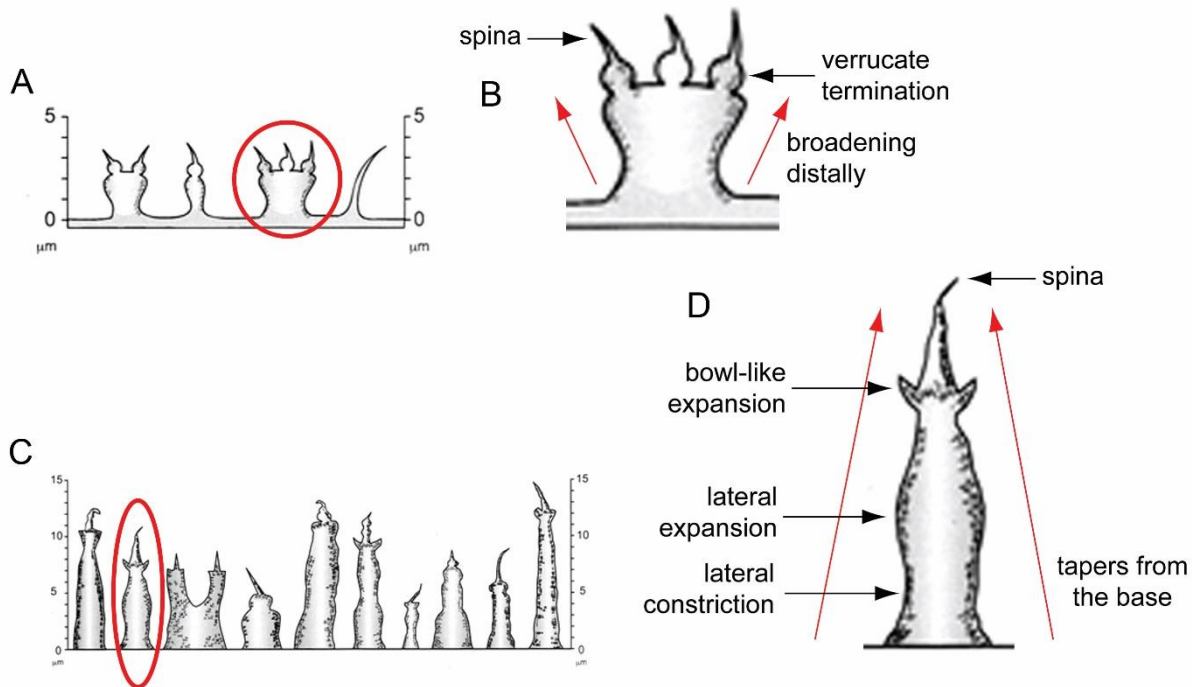


Figure 56. Examples of the morphological differences between the apiculate elements of *Umbonatisporites variabilis* Hibbert & Lacey 1969 (A, B is an expansion of the element circled in A) and *Claytonispora distincta* (Clayton) Playford & Melo 2012 (C, D is an expansion of the element circled in C). After Playford & Melo (2012).

Claytonispora distincta (Clayton) Playford & Melo 2012

Plate 1 Figure u

1960 *Apiculatisporites* sp. Balme, p. 28, Pl. 4, Figs. 10-11.

1970 *Umbonatisporites distinctus* Clayton, pp. 591-592, Pl. 4, Figs. 4-6.

- 1971 *Acanthotriletes turriculaeformis* Kemp & Playford *In*: Playford, p. 20, Pl. 6, Figs. 7-15.
- 1972 *Umbonatisporites distinctus* Clayton; Bertelsen, Pl. 8, Fig. 1.
- 1973 *Umbonatisporites distinctus* Clayton; Neves *et al.*, Pl. 3, Fig. 8.
- 1975 *Umbonatisporites distinctus* Clayton; Higgs, Pl. 2, Fig. 5.
- 1976 *Dibolisporites distinctus* (Clayton) Playford, p. 16, Pl. 2, Figs. 9-12.
- 1977 *Dibolisporites distinctus* (Clayton) Playford; Clayton *et al.*, p. 31, Pl. 5, Fig. 9, p. 25, Pl. 7, Fig. 6.
- 1978 *Dibolisporites distinctus* (Clayton) Playford; Playford, pp. 119-120, Pl. 5, Fig. 18.
- 1978 *Umbonatisporites distinctus* Clayton; Turnau, Pl. 1, Figs. 20, 24.
- 1979 *Dibolisporites distinctus* (Clayton) Playford; Welsh, Pl. 1, Fig. 4.
- 1984 *Umbonatisporites distinctus* Clayton; Higgs & Clayton, p. 23, Pl. 1, Fig. 7.
- 1984 *Umbonatisporites distinctus* Clayton; Scot *et al.*, p. 313, Fig 2 i.
- 1985 *Umbonatisporites distinctus* Clayton; Clayton, p. 23, Figs. 2 f, g.
- 1988 *Umbonatisporites distinctus* Clayton; Higgs *et al.*, p. 62, Pl. 5, Figs. 16-18.
- 1988 *Umbonatisporites distinctus* Clayton; McNestry, Pl. 2, Fig. 1.
- 1988 *Dibolisporites distinctus* (Clayton) Playford; Turner & Spinner, Pl. 2, Fig. 3.
- 1990 *Dibolisporites distinctus* (Clayton) Playford; Playford, Pl. 2, Figs. 13-15.
- 1991 *Dibolisporites distinctus* (Clayton) Playford; Ravn, pp. 48-49, Pl. 3, Figs. 18-19.
- 1992 *Umbonatisporites distinctus* Clayton; Avchimovitch, Pl. 11, Fig. 12.
- 1992 *Umbonatisporites distinctus* Clayton; Higgs *et al.*, Pl. 1, Fig. 10.
- 1996 *Umbonatisporites distinctus* Clayton; Higgs, Pl. 2, Figs. 2-9.
- 1997 *Umbonatisporites distinctus* Clayton; Carson & Clayton, Pl. 1, Fig. 5.
- 2007 *Umbonatisporites distinctus* Clayton; Higgs & Forsythe, p. 189, Pl. 1, Fig. K.
- 2012 *Claytonispora distincta* (Clayton) Playford & Melo, p. 33, Pl. 6, Fig. 17, Pl. 7, Figs. 1-2, Text-figs. 4 D-E.
- 2015 *Umbonatisporites distinctus* Sullivan 1968 [sic]; Ariana-Sab *et al.*, Pl. 3, Fig. 8.
- 2019 *Claytonispora distincta* (Clayton) Playford & Melo; Marshall *et al.*, p. 271, Fig. 6, number 5.

Description: Miospores, radial, trilete; amb subcircular; exine thin: 1 to 1.5 μm , laevigate with evenly spaced compound spinae, total length: 3 (7) 13 μm (60 spines), consisting of an elongate tubercle, width: 1 μm , occasionally with a basal constriction and usually with a terminal constriction, above which sits a disc, surmounted by a single spina, the spinae are usually longer at the equator (by 1 or 2 μm); suturae straight, simple; taper point folds common.

Dimensions: Length: 42 (62) 77 μm (15 specimens), width: 33 (39) 49 (5 specimens).

NWMF borehole distribution: 501.18 to 158.77 m depths.

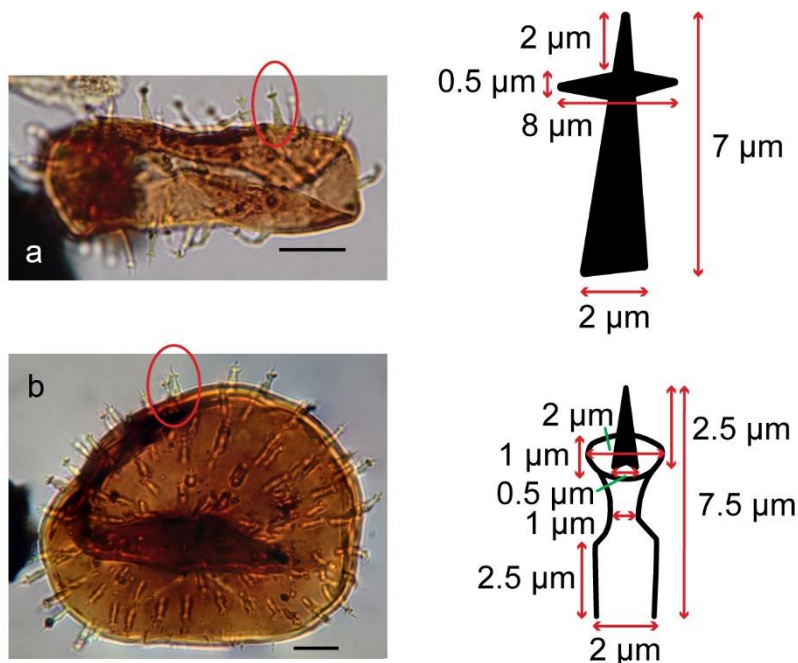


Figure 57. Tubercles of *Claytonispora distincta* from the NWMF borehole core.

(a) Elongate with a disc and surmounted by a spina (b) elongate with terminal constriction, disc and surmounted by a spina. Specimen sample number, slide and England Finder co-ordinates: (a) SSK37853, 129.0, 06.8, U29/0 (b) SSK37853, 117.9, 15.6, L17/4.

Genus **COLATISPORITES** Williams *In*: Neves *et al.* 1973

Type species: *Colatisporites decorus* (Bharadwaj & Venkatachala) Williams *In*: Neves *et al.* 1973

1973 Williams *In*: Neves *et al.*, pp. 40-41.

Generic description: Miospores, radial, trilete, camerate; amb circular, subcircular or oval; intexine thin, laevigate, conformable with the amb; exoexine infrapunctate, either unsculptured or with small elements that include spinae, coni and bacula, predominantly on the distal face but may extend slightly on to the proximal face; suturae straight or wavy, simple or with low, thin labra, and may terminate in curvaturae; contact areas laevigate; occasional compression folds.

Comparisons: Whereas *Colatisporites* has spinae, coni and bacula, variously labrate suturae and occasional compression folds, the genus *Auroraspora* Hoffmeister *et al.* 1955 is laevigate, minutely granulose or irregularly infrapunctate has suturae with labra and commonly radial compression folds.

Also, the genus *Endoculeospora* (Staplin) Turnau 1975 has scattered to densely distributed grana, pili and/or bacula mostly on the distal face.

Colatisporites decorus (Bharadwaj & Venkatachala) Williams *In*: Neves *et al.* 1973

Plate 1 Figure v

1961 *Tholisporites decorus* Bharadwaj & Venkatachala, p. 39, Pl. 10, Figs. 142-146.

1972 *Tholisporites decorus* Bharadwaj & Venkatachala; Bertelsen, Pl. 21, Figs. 4, 6.

1973 *Colatisporites decorus* (Bharadwaj & Venkatachala) Williams *In*: Neves *et al.*, p. 41, Pl. 2, Figs. 11-13, Pl. 4, Fig. 19.

- 1974 *Colatisporites decorus* (Bharadwaj & Venkatachala) Williams *In*: Neves *et al.*; Neves & Ioannides, Pl. 7, Figs. 10-11.
- 1977 *Colatisporites decorus* (Bharadwaj & Venkatachala) Williams *In*: Neves *et al.*; Clayton *et al.*, p. 37, Pl. 8, Fig. 21, p. 39, Pl. 9, Fig. 18.
- 1980 *Colatisporites decorus* (Bharadwaj & Venkatachala) Williams *In*: Neves *et al.*; Van der Zwan, pp. 141-143, Pl. 3, Figs. 3-5, Pl. 4, Figs. 1-5.
- 1986 *Colatisporites decorus* (Bharadwaj & Venkatachala) Williams *In*: Neves *et al.*; Ravn, pp. 120-121, Pl. 36, Fig. 5.
- 1987 *Colatisporites decorus* (Bharadwaj & Venkatachala) Williams *In*: Neves *et al.*; Utting, Pl. 5, Fig. 14.
- 1988 *Colatisporites decorus* (Bharadwaj & Venkatachala) Williams *In*: Neves *et al.*; Higgs *et al.*, p. 81, Pl. 17, Fig. 4.
- 1989 *Colatisporites decorus* (Bharadwaj & Venkatachala) Williams *In*: Neves *et al.*; Brindley & Spinner, p. 220, Fig. 5, number 10.
- 1991 *Colatisporites decorus* (Bharadwaj & Venkatachala) Williams *In*: Neves *et al.*; Ravn, Pl. 28, Fig. 20.
- 1994 *Colatisporites decorus* (Bharadwaj & Venkatachala) Williams *In*: Neves *et al.*; Mahdi & Butterworth, p. 162, Fig. 5, numbers 19-20.
- 2000 *Colatisporites decorus* (Bharadwaj & Venkatachala) Williams *In*: Neves *et al.*; Melo & Loboziak, p. 151, Pl. 1, Fig. 3
- 2005 *Colatisporites decorus* (Bharadwaj & Venkatachala) Williams *In*: Neves *et al.*; Dueñas & Césari, p. 148, Fig. 3 Q.
- 2008 *Colatisporites decorus* (Bharadwaj & Venkatachala) Williams *In*: Neves *et al.*; Pérez Loinaze pp. 433-434, Fig. 3, numbers 6-7.
- 2010 *Colatisporites decorus* (Bharadwaj & Venkatachala) Williams *In*: Neves *et al.*; Owens *et al.*, p. 35, Pl. 2, Fig. 13.
- 2012 *Colatisporites decorus* (Bharadwaj & Venkatachala) Williams *In*: Neves *et al.*; Melo & Playford, pp. 118-119, Pl. 9, Figs. 9-10.
- 2016 *Colatisporites decorus* (Bharadwaj & Venkatachala) Williams *In*: Neves *et al.*; Lopes *et al.*, p. 67, Pl. 2, Fig. 13.

Description: Miospores, radial, trilete, camerate; amb circular to oval; intexine thin, laevigate, conformable with the amb; exoexine thin with small, uniformly and

densely distributed grana; suturae distinct, simple or with thin labra, straight or sinuous.

Dimensions: Total length: 34 (50) 70 μm , width: 23 (40) 52, inner body length: 29 (45) 62 μm , width: 20 (35) 50 (50 specimens).

NWMF borehole distribution: 501.18 m to 42.46 m depths.

Affinity: *Stamnostoma huttonense* Long 1960c. Retallack & Dilcher (1988 p. 1013) reported *in situ* spores from *S. huttonense* ovules that had been figured by Long (1960c) in Plate 2 Figs. 35 and 26 of slide FSC 1148.

Colatisporites denticulatus Neville *In: Neves et al.* 1973

Plate 1 Figure w

- 1970 *Tholisporites* cf. *decorus* Bharadwaj & Venkatachala; *sensu* Clayton, pp. 590-591, Pl. 4, Figs. 2-3.
- 1973 *Colatisporites denticulatus* Neville *In: Neves et al.*, pp. 41-42, Pl. 2, Figs. 14-16, Pl. 3, Figs. 19-20.
- 1974 *Colatisporites denticulatus* Neville *In: Neves et al.*; Neves & Ioannides, Pl. 7, Fig. 9.
- 1978 *Apiculiretusispora multiseta* (Luber) Butterworth & Spinner; Turnau, p. 6, Pl. 1, Figs. 22-23.
- 1988 *Colatisporites denticulatus* Neville *In: Neves et al.*; Higgs *et al.*, p. 82, Pl. 17, Fig. 1.
- 1990 *Colatisporites denticulatus* Neville *In: Neves et al.*; Clayton & Turnau, p. 51. Pl. 1, Figs. 2-3.
- 1991 *Colatisporites denticulatus* Neville *In: Neves et al.*; Ravn, Pl. 28, Figs, 21-22.
- 1994 *Colatisporites denticulatus* Neville *In: Neves et al.*; Mahdi & Butterworth, p. 162, Fig. 5, numbers 17-18.

- 2012 *Colatisporites denticulatus* Neville *In*: Neves *et al.*; Melo & Playford, Pl. 9, Figs. 11-12.
- 2016 *Colatisporites denticulatus* Neville *In*: Neves *et al.*; Lopes *et al.*, p. 67, Pl. 2, Fig. 33.

Description: Miospores, radial, trilete, camerate; amb circular to oval; intexine thin, laevigate, conformable with the amb, may possess taper point folds; exoexine thin, sculptured with densely, uniformly distributed spinae, coni, baculi and grana, height: < 1 µm; suturae simple, straight.

Dimensions: Total length: 30 (42) 49 µm, width: 23 (34) 43 µm, inner body length: 24 (37) 48 µm, width: 18 (30) 39 µm (50 specimens).

NWMF borehole distribution: 501.18 m to 39.11 m depths.

Remarks: Conforms closely to the description by Neves *In*: Neves *et al.* (1973), although the NWMF borehole spores are smaller than those recorded by Neves *In*: Neves *et al.* (1973; 43 (59) 72 µm), which were oxidised and so may have been expanded in size during processing.

Comparison: *C. denticulatus* differs from *C. decorus* by its presence of a dense sculpture of spinae, coni and baculi.

Affinity: *Lyrasperma scotica* (Calder) Long 1960b. Retallack & Dilcher (1988 p. 1017) reported *in situ* spores from *L. scotica* ovules that had been figured by Long (1960b) in Plate 1 Fig. 4 of slide FSC 1405 and Fig. 7 of slide FSC 1406 and Plate 2 Fig. 28 of slide FSC 1405, Fig. 29 of slide FSC 1411 and Fig. 30 of slide FSC 1418.

Colatisporites? papillatus Ravn 1991

Plate 1 Figure x

1991 *Colatisporites? papillatus* Ravn, pp. 29-30, Pl. 28, Figs. 10-13, 17.

1994 *Colatisporites? papillatus* Ravn; Mahdi & Butterworth, p. 162, Fig. 5, numbers 21-22.

Description: Miospores, radial, trilete, camerate; amb subcircular; intexine distinct, conformable with the amb; exoexine minutely granulose with sparsely to densely distributed pila, height: 1.5 (3) 4 μm (50 pila); suturae straight.

Dimensions: Total length: 32 (36) 42 μm , width: 26 (31) 38 μm , inner body length: 26 (31) 38 μm , width: 22 (27) 33 μm (8 specimens).

NWMF borehole distribution: 501.18 to 242.96 m depths.

Remarks: Conforms closely to the description by Ravn (1991), although the NWMF borehole spores are smaller than those recorded by Ravn (1991; 53 to 65 μm), which were oxidised and so may have been expanded in size during processing.

Ravn (1991) questionably assigned this species to *Colatisporites* because “the papillate sculpture and variability of cameration are features considered different from those observed in other species of *Colatisporites*”. He considered that “the papillate sculpture resembles that seen on *Schopfites claviger*” but acknowledged that *S. claviger* is not camerate.



Figure 58. Pila of *Colatisporites papillatus*.

Genus **CONVOLUTISPORA** Hoffmeister *et al.* 1955

Type species: *Convolutispora florida* Hoffmeister *et al.* 1955

1955 *Convolutispora* Hoffmeister *et al.*, p. 384.

Generic description: Miospores, radial, trilete; amb circular to subcircular; size 40 to 150 µm in diameter; sculptured with densely distributed, overlapping anastomosing, vermiculate ridges, often giving a convoluted or coarsely reticulate appearance; suturae simple but may have labra that are often obscured by the ridges.

Convolutispora caliginosa Clayton & Keegan *In: Clayton et al.* 1982

Plate 2 Figure a

- 1967 *Convolutispora* sp. Neves & Dolby, Pl. 2, Fig. 7.
- 1977 *Convolutispora* sp. Clayton *et al.*, Pl. 5, Figs, 17-18.
- 1977 *Convolutispora* sp. A Keegan, p. 548, Pl. 2, Figs. 6-9.
- 1982 *Convolutispora caliginosa* Clayton & Keegan *In: Clayton et al.*, p. 516, Pl. 1, Figs. 5, 6, 8, 9.
- 1988 *Convolutispora caliginosa* Clayton & Keegan *In: Clayton et al.; Higgs et al.*, p. 63, Pl. 6, Figs. 9-11.
- 1992 *Convolutispora caliginosa* Clayton & Keegan *In: Clayton et al.; Higgs et al.*, Pl. 1, Fig. 7.
- 1996 *Convolutispora caliginosa* Clayton & Keegan *In: Clayton et al.; Higgs*, p. 4, Figs. 6-7.
- 2012 *Convolutispora caliginosa* Clayton & Keegan *In: Clayton et al.; Playford & Melo*, p. 41, Pl. 10, Figs. 3-4.
- 2016 *Convolutispora caliginosa* Clayton & Keegan *In: Clayton et al.; Lopes et al.*, p. 67, Pl. 2, Fig. 22.

Description: Miospores, radial, trilete; amb circular to convexly triangular; exine with a densely distributed, short, rounded to flat-topped muri, height: 2 (5) 8 μm (42 muri), with convoluted, anastomosing lumina; suturae obscured by the sculpture.

Dimensions: Length: 53 (69) 86 μm , width: 45 (58) 72 μm (15 specimens).

NWMF borehole distribution: 491.43 m to 83.10 m depths.

Comparison: *Convolutispora mellita* differs from *C. caliginosa* by having coarser sculpture.

***Convolutispora circumvallata* Clayton 1970**

Plate 2 Figure b

- 1970 *Convolutispora circumvallata* Clayton, p. 582, Pl. 1, Figs. 5-7.
- 1972 *Convolutispora circumvallata* Clayton; Bertelsen, Pl. 14, Figs. 5-6.
- 1973 *Convolutispora circumvallata* Clayton; Neves *et al.*, Pl. 3, Fig. 10.
- 1977 *Convolutispora circumvallata* Clayton; Clayton *et al.*, p. 35, Pl. 7, Fig. 8.
- 1980 *Convolutispora circumvallata* Clayton; Phillips & Clayton, Fig. 9 E.
- 1984 *Convolutispora circumvallata* Clayton; Scot *et al.*, p. 313, Fig. 2 m.
- 1985 *Convolutispora circumvallata* Clayton; Clayton, p. 23, Fig. 2 i.
- 1988 *Convolutispora circumvallata* Clayton; Higgs *et al.*, p. 63, Pl. 6, Fig. 12.
- 1997 *Convolutispora circumvallata* Clayton; Carson & Clayton, Pl. 2, Fig. 9.

Description: Miospores, radial, trilete; amb circular to oval; exine thick: 3 to 4 μm , laevigate with rounded, anastomosing ridges, height: 3 (9) 20 μm (104 muri), some of which may be fused, forming a partial reticulum, the ridges are characteristically variable in width along their length, and often have expanded tops, width: 9 (12) 15 μm (7 tops), columella width: 5 (6) 8 μm (7 columellae), round in cross section, particularly where the ridges join, the channels between the ridges are equal to, or greater in width than the width of the ridges; suturae distinct, straight, simple or

accompanied by labra; the ridges are much shorter on the contact faces of some specimens.

Dimensions: Length: 54 (85) 114 μm , width: 47 (71) 91 μm (20 specimens).

NWMF borehole distribution: 491.43 m to 56.84 m depths.

Convolutispora florida Hoffmeister *et al.* 1955

Plate 2 Figure c

1948 Type 42K Knox.

1955 *Convolutispora florida* Hoffmeister *et al.*, p. 384, Pl. 38, Figs. 5-6.

1958 *Convolutispora florida* Hoffmeister *et al.*; Butterworth & Williams, p. 371, Pl. 2, Figs. 24-25.

1965 *Convolutisporites floridus* (Hoffmeister *et al.*) Laveine, p. 132.

1971 *Convolutispora florida* Hoffmeister *et al.*; Playford, pp. 24-25, Pl. 6, Fig. 3.

1986 *Convolutispora florida* Hoffmeister *et al.*; Ravn, p. 58, Pl. 9, Figs. 1-6.

1991 *Convolutispora florida* Hoffmeister *et al.*; Ravn, Pl. 8, Fig. 6.

2007 *Convolutispora florida* Hoffmeister *et al.*; Higgs & Forsythe, p. 191, Pl. 2, Fig. D.

Description: Miospores, radial, trilete; amb subcircular; exine thin, densely distributed, coarse, vermiculate ridges with flattened or rounded tops, height: 2 (4) 6 μm (67 muri); suturae straight, low labra.

Dimensions: Length: 30 (44) 66 μm , width: 27 (38) 54 μm (36 specimens).

NWMF borehole distribution: 497.13 m to 54.56 m depths.

Remarks: The coarse, broad ridges together with its small size distinguish this species (Hoffmeister *et al.* 1955).

Convolutispora harlandii Playford 1962

Plate 2 Figure d

- 1962 *Convolutispora harlandii* Playford, pp. 593-594, Pl. 81, Figs. 6-9, Text-figs. 5 h, j.
- 1971 *Convolutispora harlandii* Playford; Playford, p. 25, Pl. 8, Figs. 1-3.
- 1974 *Archaeozonotriletes harlandii* (Playford) Kedo, pp. 60-61, Pl. 14, Figs. 3-4.
- 1975 *Convolutispora harlandii* Playford; Turnau, p. 512. Pl. 3, Fig. 1.
- 1985 *Convolutispora harlandii* Playford; Playford & Satterthwait, pp. 135-136, Pl. 2, Figs. 4-5.
- 1991 *Convolutispora harlandii* Playford; Ravn, p. 32, Pl. 8, Figs. 9-10.
- 1992 *Convolutispora harlandii* Playford; Avchimovitch, Pl. 3, Fig. 4.

Description: Miospores, radial, trilete; amb subcircular; exine with irregular, anastomosing ridges, height: 1 (7) 15 μm (60 muri) formed of a mixture of rugulae and verrucae; suturae simple.

Dimensions: Length: 56 (83) 114 μm , width: 36 (70) 99 μm (19 specimens).

NWMF borehole distribution: 457.29 m to 97.88 m depths.

Convolutispora major (Kedo) Turnau 1978

Plate 2 Figure e

- 1963 *Dictyotriletes major* Kedo, p. 55, Pl. 4, Fig. 97.
- 1978 *Convolutispora major* (Kedo) Turnau, p. 8, Pl. 2, Figs. 18-19.
- 1988 *Convolutispora major* (Kedo) Turnau; Avchimovitch *et al.*, Pl. 2, Fig. 18.
- 1988 *Convolutispora major* (Kedo) Turnau; Higgs *et al.*, p. 63, Pl. 6, Fig. 13.
- 1992 *Convolutispora major* (Kedo) Turnau; Avchimovitch, Pl. 7, Fig. 9, Pl. 9, Fig. 7.
- 1992 *Convolutispora major* (Kedo) Turnau; Higgs *et al.*, Pl. 1, Fig. 1.

- 1996 *Convolutispora major* (Kedo) Turnau; Higgs, Pl. 3, Figs. 10-11.
 1997 *Convolutispora major* (Kedo) Turnau; Carson & Clayton, Pl. 1, Fig. 6.
 2012 *Convolutispora major* (Kedo) Turnau; Playford & Melo, Pl. 10, Fig. 10.

Description: Miospores, radial, trilete; amb circular to oval; exine with densely distributed irregular, rounded muri, height: 3 (7) 23 μm (65 muri), convoluted, anastomosing ridges, forming an imperfect reticulum, irregular lumina; suturae distinct to obscure, straight, bordered by labra.

Dimensions: Length: 60 (86) 116 μm (40 specimens), width: 39 (73) 101 μm (15 specimens).

NWMF borehole distribution: 501.18 m to 56.84 m depths.

Comparisons: *C. major* and *C. circumvallata* are both large species of *Convolutispora*. The presence of the expanded tops of the ridges distinguish *C. circumvallata* from *C. major*.

Convolutispora mellita Hoffmeister *et al.* 1955

Plate 2 Figure f

- 1955 *Convolutispora mellita* Hoffmeister *et al.*, p. 384, Pl. 38, Fig. 10.
 1978 *Convolutispora mellita* Hoffmeister *et al.*; Turnau, Pl. 2, Figs. 2-3.
 1986 *Convolutispora mellita* Hoffmeister *et al.*; Ravn, p. 49, Pl. 9, Figs. 16-18.
 1987 *Convolutispora mellita* Hoffmeister *et al.*; Utting, Pl. 2, Fig. 8.
 1988 *Convolutispora mellita* Hoffmeister *et al.*; Avchimovitch *et al.*, Pl. 2, Fig. 13.
 1992 *Convolutispora mellita* Hoffmeister *et al.*; Avchimovitch, Pl. 3, Fig. 14, Pl. 9, Fig. 12.
 2008 *Convolutispora mellita* Hoffmeister *et al.*; Feng *et al.*, p. 498, Figs. 11-12.

Description: Miospores, radial, trilete; amb circular to oval; exine with densely distributed irregular, rounded muri, height: 3 to 8 μm , with convoluted, broad, anastomosing, irregular lumina; suturae straight, simple.

Dimensions: Length: 44 (63) 80 μm , width: 42 (68) 88 μm (20 specimens).

NWMF borehole distribution: 501.11 m to 122.16 m depths.

Remarks: *C. mellita* is characterised by its densely packed muri.

Genus **CRASSISPORA** (Bharadwaj) Sullivan 1964

Type species: *Crassispora kosankei* (Potonié & Kremp) Smith & Butterworth 1967

1957 *Crassispora* Bharadwaj, p. 125.

1964 *Crassispora* (Bharadwaj) Sullivan, pp. 375-376.

1967 *Crassispora* (Bharadwaj) Sullivan 1964; Smith & Butterworth pp. 233-234.

Generic description: Miospores, radial, trilete, camerate; amb circular to oval or roundly triangular; intexine thin, conformable with the amb; exoexine minutely granulose with coni and occasional spinae; equatorial thickening common; suturae indistinct; apical papillae visible in contact areas, particularly in over-macerated specimens; occasional compression folds.

Remark: Smith & Butterworth (1967) considered Sullivan's (1964) generic description to constitute an emendation of Bharadwaj's (1957) diagnosis.

Crassispora aculeata Neville 1968

Plate 2 Figure g

1968 *Crassispora aculeata* Neville, pp. 443-446, Pl. 2, Figs. 5-6.

1973 *Crassispora aculeata* Neville; Neves *et al.*, Pl. 4, Fig. 17.

- 1974 *Crassispora aculeata* Neville; Neves & Ioannides, Pl. 7, Fig. 5.
 1977 *Crassispora aculeata* Neville; Clayton *et al.*, p. 39, Pl. 9, Fig. 14, p. 43, Pl. 11, Figs. 26-27.
 1989 *Crassispora aculeata* Neville; Brindley & Spinner, p. 220, Fig. 5, number 22.
 1991 *Crassispora aculeata* Neville; Ravn, Pl. 20, Figs. 1-2.
 1993 *Crassispora aculeata* Neville; Turner & Owens, p. 194, Fig. 3, number 16.

Description: Miospores, radial, trilete, camerate; amb subcircular; intexine thin, laevigate; exoexine thin: 1 to 2 μm , minutely granulose with discrete, sparsely to densely distributed, evenly spaced, tapering, sharp-tipped spinae, height: 1 (4) 10 μm (82 spinae), occasionally biform with sharp-tipped, recurved or tapering spinae topping grana, base height: 2 μm , base width: 2 μm ; suturae straight to sinuous with narrow labra terminating in curvaturae; taper point folds.

Dimensions: Length: 48 (66) 119 μm , width: 35 (57) 117 μm (10 specimens).

NWMF borehole distribution: 496.62 to 56.84 m depths.

Remarks: Conforms closely to the description by Neville (1968), although Neville's size range may now be extended from 56 to 96 μm to 48 to 119 μm .

Remarks: The age range for this species has been stated as Upper Viséan (Neville 1968) and Viséan to early Serpukhovian (Clayton *et al.* 1977) and it has not been recorded previously from the Tournaisian.



Figure 59. (a) and (b) spinae and (c) biform elements of *Crassispora aculeata*.

***Crassispora trychera* Neves & Ioannides 1974**

Plate 2 Figure h

- 1973 *Crassispora trychera* Neves & Ioannides; Neves *et al.*, Pl. 3, Fig. 18.
- 1974 *Crassispora trychera* Neves & Ioannides, p. 78, Pl. 7, Figs. 6-8.
- 1977 *Crassispora trychera* Neves & Ioannides; Clayton *et al.*, p. 35, Pl. 7, Fig. 5, p. 36, Pl. 8, Fig. 2.
- 1977 *Crassispora trychera* Neves & Ioannides; Owens *et al.*, Pl. 2, Fig. 3.
- 1978 *Crassispora trychera* Neves & Ioannides; Turnau, Pl. 4, Figs. 9, 13.
- 1979 *Crassispora trychera* Neves & Ioannides; Welsh, Pl. 1, Fig. 11.
- 1980 *Crassispora trychera* Neves & Ioannides; Phillips & Clayton, Fig. 8 Q.
- 1983 *Crassispora trychera* Neves & Ioannides; Welsh & Owens, Pl. 1, Fig. 6.
- 1985 *Crassispora trychera* Neves & Ioannides; Clayton, p. 23, Fig. 2 j.
- 1987 *Crassispora trychera* Neves & Ioannides; Utting, Pl. 3, Figs. 6-8.
- 1988 *Crassispora trychera* Neves & Ioannides; Higgs *et al.*, p. 55, Pl. 3, Fig. 24.
- 1988 *Crassispora trychera* Neves & Ioannides; McNestry, Pl. 2, Fig. 9.
- 1994 *Crassispora trychera* Neves & Ioannides; Avchimovitch & Turnau, Pl. 1, Fig. 6.
- 2005 *Crassispora trychera* Neves & Ioannides; Turnau *et al.*, p. 96, Fig. 3 d.
- 2008 *Crassispora trychera* Neves & Ioannides; Pérez Loinaze, pp. 422-424, Fig. 1, numbers 6, 9.
- 2012 *Crassispora trychera* Neves & Ioannides; Melo & Playford, p. 103, Pl. 2, Fig. 1.

Description: Miospores, radial, trilete, camerate; amb circular to oval; intexine thin, laevigate, conformable with the amb; exoexine distally sculptured with coni, pila and bacula, interspersed with grana, height 0.5 μm (common) to 1 μm (rare), sculpture densely or sparsely distributed, sometimes with laevigate areas; suturae distinct, straight or sinuous, terminating in curvaturae.

Dimensions: Total length: 41 (64) 90 μm , width: 32 (47) 66 μm , inner body length: 31 (50) 70 μm , width: 25 (39) 51 μm (50 specimens).

NWMF borehole distribution: 501.18 m to 42.46 m depths.

Remarks: Conforms closely to the description by Neves & Ioannides (1974), although the size of the NWMF borehole spores extends the range recorded by Neves & Ioannides (1974; 48 (58) 67 μm) to 41 to 90 μm .

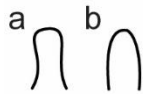


Figure 60. (a) Pila and (b) bacula of *Crassispora trychera*.

Crassispora cf. trychera

Plate 2 Figure i

Description: As for *Crassispora trychera* but with more robust sculpture, height: 0.5 (1) 3 μm (17 elements).

Dimensions: Total length: 42 (56) 69 μm (31 specimens), width: 30 (45) 59 μm (12 specimens), inner body length: 34 (50) 66 μm (28 specimens), width: 25 (39) 56 μm (11 specimens).

NWMF borehole distribution: 500.98 m to 49.88 m depths.

Comparison: This spore may be discounted as *C. maculosa* (Knox) Sullivan 1964 which differs in being larger in size (diameter: 76 to 120 μm).

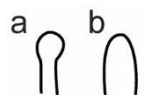


Figure 61. (a) Pila and (b) bacula of *Crassispora cf. trychera*.

Genus **CRISTATISPORITES** (Potonié & Kremp) Butterworth *et al.* 1964

Type species: *Cristatisporites indignabundus* (Loose) Staplin & Jansonius 1964

1954 *Cristatisporites* Potonié & Kremp, p. 142.

1964 *Asperispora* Staplin & Jansonius, p. 107.

1964 *Cristatisporites* (Potonié & Kremp) Butterworth *et al.* In: Staplin & Jansonius, p. 108.

1965 *Samarisporites* Richardson, p. 581.

Generic description: Miospores, radial, trilete, camerate; amb subcircular to subtriangular; margin irregular with small scattered processes or strongly incised if the distal sculpture continues to the equator; intexine laevigate, often indistinct; the central area of the proximal exoexine is minutely sculptured, usually surrounded by a ring of spinae, pili, grana or small pits, the zona beyond the ring is laevigate or minutely granulose; the distal face bears prominent, often mammillate, verrucae, the inner part may be vacuolate; suturae often indistinct.

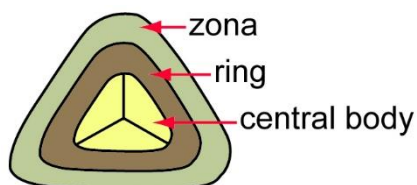


Figure 62. Diagram to define the parts of *Cristatisporites* miospores.

Cristatisporites bellus Bharadwaj & Venkatachala 1961

Plate 2 Figure j

1961 *Cristatisporites bellus* Bharadwaj & Venkatachala, p. 34, Pl. 6, Figs. 109-110.

1970 *Cristatisporites bellus* Bharadwaj & Venkatachala; Clayton, Pl. 2, Fig. 1.

1973 *Cristatisporites bellus* Bharadwaj & Venkatachala; Neves *et al.*, Pl. 3, Fig. 17.

1985 *Cristatisporites bellus* Bharadwaj & Venkatachala; Clayton, p. 23, Fig. 2 I.

1994 *Cristatisporites bellus* Bharadwaj & Venkatachala; Mahdi & Butterworth, p. 165, Fig. 8, number 13.

Description: Miospores, radial, trilete, camerate; amb oval to convexly triangular in general outline with coni along the edge, height: 1.5 to 2 μm , grana and occasional pila, height: 1.5 (3) 4.5 μm (6 pila); central body surrounded by a zona with low, broad based, sharp-tipped coni, a mixture of pointed and round-topped spinae, height: 0.5 (4) 18 μm (43 spinae), base width: 0.5 (1) 2 μm (8 bases), and clava, height: 3.5 (8) 16 μm (24 clava); verrucae form a ring around the edge of the central body and are scattered across the central body and zona, height 1 (6) 14 μm (100 verrucae), base width: 5.5 (6) 7 μm (6 bases), some verrucae have spinae, base width: 5 (6) 7 μm (2 bases), base height: 1.5 to 2 μm (6 bases), top spina height: 0.5 to 1 μm (10 spinae); suturae simple.

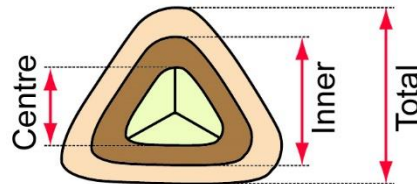


Figure 63. Diagram to define the dimensions of *Cristatisporites bellus*.

Dimensions: Total length: 48 (88) 122 μm (36 specimens), width: 41 (74) 111 μm (35 specimens), inner body length: 33 (62) 100 μm , width: 31 (51) 94 μm (29 specimens), centre length: 24 (43) 60 μm , width: 19 (32) 57 μm (15 specimens).

NWMF borehole distribution: 486.25 m to 54.56 m depths.

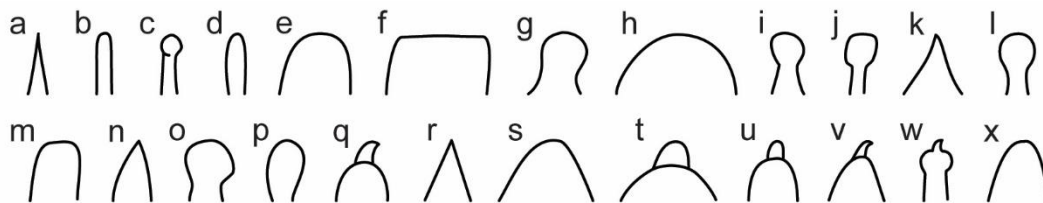


Figure 64. (a) to (d) spinae (e) to (i) verrucae (j) clava (k) edge coni (l) central pila (m) to (q) various sculptural elements (r) spinae on some verrucae (s) spinae (t) to (v) outer spinae (w) inner spinae and (x) centre spinae of *Cristatisporites bellus*.

Cristatisporites echinatus Playford 1963

Plate 2 Figure k

- 1963 *Cristatisporites echinatus* Playford, pp. 637-638, Pl. 91, Figs. 1-4.
 1972 *Cristatisporites echinatus* Playford; Bertelsen, Pl. 9, Figs. 5, 8.
 1974 *Cristatisporites echinatus* Playford; Becker *et al.*, Pl. 18, Fig. 1.
 1977 *Cristatisporites echinatus* Playford; Clayton *et al.*, p. 27, Pl. 3, Fig. 10.
 2000 *Cristatisporites echinatus* Playford; Melo & Loboziak, p. 154, Pl. 1, Fig. 12.

Description: Miospores, radial, trilete, camerate; amb convexly triangular; intexine laevigate, conformable with the amb; exoexine thick, proximal surface laevigate, distal surface minutely granulose with evenly distributed, parallel-sided or tapering, sharp- to blunt-tipped spinae and minute pila, height: 0.5 (1) 4 μm (18 elements); suturae straight to slightly sinuous, with broad labra.

Dimensions: Total length: 63 (79) 91 μm , width: 54 (66) 73 μm , inner body length: 47 (60) 66 μm , width: 43 (48) 54 μm (8 specimens).

NWMF borehole distribution: 340.71 m depth only.

Remarks: The zona is variably corroded.

Comparison: *Spelaeotrilites crustatus* Higgs 1975 appears like *C. echinatus* but has a thinner exoexine with shorter spinae, the suturae terminate in curvaturae and the spores are generally smaller.

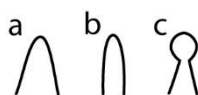


Figure 65. (a) to (b) spinae and (c) pila of *Cristatisporites echinatus*.

Cristatisporites indignabundus (Loose) Staplin & Jansonius 1964

Plate 2 Figure I

- 1932 *Sporonites indignabundus* Loose *In: Potonié et al.*, p. 451, Pl. 19, Fig. 51.
- 1933 *Zonales-sporites indignabundus* (Loose) Ibrahim, p. 32.
- 1934 *Apiculatisporites indignabundus* (Loose) Loose, p. 153.
- 1944 *Densosporites indignabundus* (Loose); Schopf *et al.*, p. 40.
- 1954 *Cristatisporites indignabundus* (Loose) Potonié & Kremp, p. 142, Pl. 20, Fig. 8.
- 1955 *Cristatisporites indignabundus* (Loose) Potonié & Kremp, Pl. 16, Fig. 294.
- 1964 *Cristatisporites indignabundus* (Loose) Staplin & Jansonius, pp. 108-109, Pl. 19, Figs. 7-9, 12, 14, 20, Text-fig. 2 c.
- 1965 *Densosporites indignabundus* (Loose) Laveine, p. 133.
- 1967 *Cristatisporites indignabundus* (Loose) Staplin & Jansonius; Smith & Butterworth, pp. 254-255, Pl. 20, Figs. 22-23.
- 1977 *Cristatisporites indignabundus* (Loose) Staplin & Jansonius; Clayton *et al.*, p. 53, Pl. 16, Fig. 10, p. 59, Pl. 19, Fig. 12.
- 1986 *Cristatisporites indignabundus* (Loose) Staplin & Jansonius; Ravn, p. 75, Figs. 12-16.
- 1990 *Cristatisporites indignabundus* (Loose) Staplin & Jansonius; Turner & Spinner, p. 93, Fig. 8, number 3.
- 1991 *Cristatisporites indignabundus* (Loose) Staplin & Jansonius; Ravn, Pl. 20, Figs. 12-13.

Description: Miospores, radial, trilete, camerate; amb subcircular to convexly triangular in general outline with broad based coni, height: 0.5 to 2 µm and spinae, height: 1 to 3.5 µm, along the edge; central body surrounded by sculptured zona with densely distributed, round topped bacula, height: 2.5 to 9.5 µm and verrucae, height: 0.5 to 1.5 µm, that appear to form rows conformable with the amb; where not obscured by sculpture, suturae straight, labra increase in height towards central proximal surface and terminate at the 'row' of bacula.

Dimensions: Total length: 70 (100) 130 μm , width: 48 (83) 114 μm (13 specimens), inner body length: 33 (67) 96 μm , width: 24 (57) 93 μm (9 specimens).

NWMF borehole distribution: 497.13 m to 54.56 m depths.

Remarks: The age range for this species has been stated as Westphalian B (Staplin & Jansonius 1964, Smith & Butterworth 1967) Namurian to Westphalian B (Ravn 1991) and it has not been recorded previously from the Tournaisian.

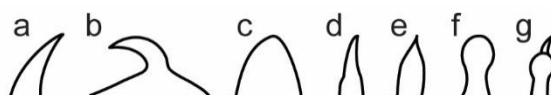


Figure 66. (a) and (b) outer body spinae and (c) coni (d) and (e) central body bacula and (f) verrucae and (g) spinae of *Cristatisporites indignabundus*.

Cristatisporites matthewsii Higgs *et al.* 1988

Plate 2 Figure m

- 1970 *Archaeozonotriletes* cf. *acutus* Kedo; Dolby & Neves, p. 638, Pl. 2, Figs. 3-6.
- 1978 *Archaeozonotriletes* aff. *acutus* Kedo; Sleeman *et al.* p. 178, Table 1.
- 1980 *Asperispora acuta* Kedo; Van der Zwan pp. 226-228, Pl. 13, Figs. 1-5.
- 1988 *Cristatisporites matthewsii* Higgs *et al.*, p. 78, Pl. 15, Figs. 5, 6, 8, 9.
- 1996 *Cristatisporites matthewsii* Higgs *et al.*; Higgs, Pl. 7, Fig. 11.
- 2008 *Cristatisporites matthewsii* Higgs *et al.*; Pérez Loinaze, pp. 425-426, Fig. 1, numbers 13-14, Fig. 2, number 9.

Description: Miospores, radial, trilete, camerate; amb subcircular to convexly triangular; intexine thin, laevigate; exoexine thin: 1 to 2 μm ; proximal face laevigate to minutely granulose, distal face with densely distributed spinae, height 0.5 (2) 4 μm (58 spinae), which often top coni; suturae straight to sinuous, often with narrow labra, terminate in curvaturae; taper point folds common.

Dimensions: Total length: 38 (54) 81 μm , width: 23 (43) 71 μm (15 specimens), inner body length: 27 (39) 50 μm (11 specimens), width: 16 (31) 43 μm (10 specimens).

NWMF borehole distribution: 478.12 m to 42.46 m depths.

Remarks: Conforms closely to the description by Higgs *et al.* (1988), but the NWMF borehole spores indicate that the size range quoted by Higgs *et al.* (1988; 35 (44) 65 μm) may now be extended to 81 μm .

Comparison: *C. menendezii* has a thicker exoexine and is sculptured with densely distributed, broad-based verrucae that are frequently topped with a single sharp-tipped spina, and broad-based, sharp- or round-tipped spinae.



Figure 67. (a) to (b) simple spinae and (c) to (d) spinae surmounting coni of *Cristatisporites matthewsii*.

Cristatisporites menendezii (Menéndez & Azcuy) Playford 1978

Plate 2 Figure n

- 1972 *Ancistrospora verrucosa* Menéndez & Azcuy, pp. 162-163, Pl. 1, Figs. 1-6, Pl. 3, Figs. 3-5; Text-fig 1, 2 a.
- 1978 *Cristatisporites menendezii* (Menendez & Azcuy) Playford, pp. 137-138, Pl. 10, Figs. 3-6.
- 1988 *Cristatisporites menendezii* (Menéndez & Azcuy) Playford; Higgs *et al.*, p. 78, Pl. 15, Figs. 12, 15.
- 1988 *Cymbosporites menendezii* (Menéndez & Azcuy) Higgs; Avchimovitch *et al.*, p. 171, Pl. 5, Figs. 1, 2.
- 1994 *Cristatisporites menendezii* (Menéndez & Azcuy) Playford; Mahdi & Butterworth, p. 165, Fig. 8, number 7.

2008 *Cristatisporites menendezii* (Menéndez & Azcuy) Playford; Pérez Loinaze, p. 426, Fig. 1, number 15, Fig. 2, numbers 1-2.

2015 *Cristatisporites menendezii* (Menéndez & Azcuy) Playford; Balarino *et al.*, Pl. 2, Fig. 3.

Description: Miospores, radial, trilete, camerate; amb subcircular to convexly triangular; intexine laevigate, conformable with the amb; exoexine thick, 5 to 8 μm ; proximal face laevigate to minutely granulose, distal face with broad-based verrucae, height: 2 (6) 11 μm (28 verrucae), base width: 2.5 (4) 5 μm (6 bases), closely spaced, often coalescent and frequently topped with a single sharp-tipped spina, height: 0.5 to 1 μm (6 spinae) and fewer broad-based, sharp- or round-tipped spinae, height: 0.5 (1) 3 μm (94 spinae); suturae straight, simple or with narrow labra; taper point folds common.

Dimensions: Total length: 41 (60) 87 μm , width: 35 (51) 67 μm (25 specimens), inner body length: 29 (45) 59 μm , width: 18 (36) 50 μm (23 specimens).

NWMF borehole distribution: 493.86 m to 54.56 m depths.



Figure 68. (a) to (b) verrucae (c) and (d) spinae surmounting verrucae and (e) to (g) spinae of *Cristatisporites menendezii*.

Genus **CURRICULOMONOLETES** McLean & Neves 2003

Type species: *Curriculomonoletes orbis* McLean & Neves 2003

2003 *Curriculomonoletes* McLean & Neves, pp. 155-159.

Generic description: Miospores, monolete, bilateral, camerate; amb circular to subcircular; intexine attached to the exoexine proximally; proximal face of exoexine laevigate, distal face with fairly regularly arranged thickenings – one

sited at the distal pole and surrounded by several others in a discontinuous, subcircular ring, additional thickenings may be present outside of this ring; distal exoexine commonly has a subequatorial ring of major folds, radial and/or concentric minor folds may develop in association with the distal thickenings; suturae straight with labra, terminating in curvaturae that develop into an equatorial thickening.

Curriculomonoletes orbis McLean & Neves 2003

Plate 2 Figure o

2003 *Curriculomonoletes orbis* McLean & Neves, pp. 159-161, Pl. 1, Figs. 1-8, Pl. 2, Figs. 1-8.

Description: Miospores, monolete, bilateral, camerate; amb circular to subcircular; intexine thin, laevigate to minutely granulose; exoexine of variable thickness, proximal face laevigate, distal face exhibits a single or double row of concentrically and regularly spaced low verrucae to pilate discrete elements, height: 6 (7) 9 μm (4 elements), lengths: 9 (20) 31 μm (13 grana); suturae distinct with labra, terminating in curvaturae.

Dimensions: Length: 155 (234) 360 μm (80 specimens), width: 120 (189) 290 μm (76 specimens).

NWMF borehole distribution: 501.18 to 161.57 m depths.

Remarks: Conforms closely to the description by McLean & Neves (2003) but the NWMF borehole spores expand the size ranges: length 96 (144.2) 182 μm , width 88 (122.9) 160 μm (McLean & Neves 2003).

Stratigraphic distribution: The type horizon for *C. orbis* in the Dron Member of the Ballagan Formation (McLean & Neves 2003). However, the specimens range

through most of the NWMF borehole, which shows it is not restricted to this member.

Genus **CYMBOSPORITES** Allen 1965

Type species. *Cymbosporites magnificus* (McGregor) McGregor & Camfield 1982

1965 *Cymbosporites* Allen, pp. 725-727, Pl. 101, Figs. 8-11.

Generic description: Miospores, radial, trilete, patinate; amb circular, subcircular to roundly triangular; proximal exine thin, distal and equatorial exine evenly thickened or with its greatest thickness in the distal polar region; patina variably sculptured with coni, spinae and grana; suturae with labra.

Comparison: *Tholisporites* Butterworth & Williams 1958 has its greatest thickness equatorially and is laevigate or with minute sculptural elements.

Cymbosporites cyathus Allen 1965

Plate 2 Figure p

1965 *Cymbosporites cyathus* Allen, pp. 725-727, Pl. 101, Figs. 8-11.

Description: Miospores, radial, trilete, patinate; amb subcircular to convexly triangular; proximal centre minutely granulose, distal patina has a variously shaped sculpture of sharp-, round- and flat-topped spinae and clava of height: 1.5 (3) 4 μm (9 elements); suturae straight, often with thin labra.

Dimensions: Total length: 50 (63) 80 μm , width: 45 (57) 72 μm , inner body length: 31 (43) 72 μm , width: 25 (39) 69 μm (10 specimens).

NWMF borehole distribution: 462.32 m to 49.88 m depths.

Remarks: The age range for this species has been stated as Givetian (Allen 1965) and it has not been recorded previously from the Tournaisian.

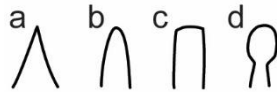


Figure 69. (a) Sharp-topped (b) round-topped and (c) flat-topped spinae and (d) clava of *Cymbosporites cyathus*.

***Cymbosporites magnificus* (McGregor) McGregor & Camfield 1982**

Plate 2 Figure q

- 1960 *Lycospora magnifica* McGregor, p. 35, Pl. 13, Figs. 2-4.
- 1960 *Lycospora magnifica* forma *endoformis* McGregor, p. 36, Pl. 12, Figs. 9-10.
- 1965 *Cymbosporites cyathus* Allen, p. 725, Pl. 101, Figs. 8-11.
- 1971 *Verruciretusispora magnifica* (McGregor) Owens var. *magnifica* (McGregor) Owens, p. 22, Pl. 5, Figs. 1-6.
- 1971 *Verruciretusispora magnifica* var. *endoformis* (McGregor) Owens, p. 24, Pl. 5, Fig. 7.
- 1982 *Cymbosporites magnificus* (McGregor) McGregor & Camfield, p. 32, Pl. 6, Figs. 4-5, Text-fig. 42.
- 1984 *Cymbosporites magnificus* (McGregor) McGregor & Camfield; Higgs & Clayton, p. 23, Pl. 1, Fig. 12.
- 1988 *Cymbosporites magnificus* (McGregor) McGregor & Camfield; Avchimovitch *et al.*, Pl. 5, Fig. 4.
- 1988 *Cymbosporites magnificus* (McGregor) McGregor & Camfield; Higgs *et al.*, p. 68, Pl. 9, Figs. 3-4.
- 2015 *Cymbosporites magnificus* (McGregor) McGregor & Camfield; Berry & Marshall, pp. 1044-1045, Figs. 4 A, 5.

Description: Miospores, radial, trilete, patinate; amb subcircular to convexly subtriangular; proximal exine thin, distal patina sculptured with discrete and closely spaced verrucae, height: 1 (2) 3.5 μm (10 verrucae), and broad based conical topped

with small, curved spinae, height: 0.5 to 1.5 μm , combined height: 1.5 (2) 3.5 μm (10 elements), which may coalesce to form short chains; suturae straight with narrow, elevated labra developing into an apical prominence and terminating in elevated curvaturae.

Dimensions: Total length: 42 (66) 89 μm , width: 34 (55) 87 μm (20 specimens); inner body length: 34 (49) 63 μm , width: 20 (37) 61 μm (18 specimens).

NWMF borehole distribution: 486.25 m to 54.56 m depths.

Remarks: Conforms closely to the description by McGregor & Camfield (1982), although the NWMF borehole spores are smaller than those recorded by McGregor & Camfield (1982; 66 (82) 107 μm), which were oxidised and so may have expanded in size during processing.

Berry & Marshall (2015) found *C. magnificus* in association with an *in situ* early Frasnian (late Devonian) lycopsid forest in Svalbard. The parent plant affinity has yet to be determined.



Figure 70. (a) and (b) verrucae (c) and (d) spinae (e) clava and (f) to (h) other sculptural elements of *Cymbosporites magnificus*.

Genus **DENSOSPORITES** (Berry) Butterworth *et al.* 1964

Type species: *Densosporites covensis* Berry 1937

1937 *Densosporites* Berry, p. 157.

1954 *Densosporites* (Berry) Potonié & Kremp, p. 160, Pl. 13, Fig. 57.

1964 *Densosporites* (Berry) Butterworth *et al.* In: Staplin & Jansonius, pp. 101-102.

Generic description: Miospores, radial, trilete, camerate; amb convexly triangular to subcircular; intexine thin, laevigate or minutely granulose; exoexine proximal face is evenly domed or with a zona slightly raised above the central proximal area, generally laevigate or with minor sculptural elements, except for scalloping of the zona in some species, central area minutely granulose but the zona has grana, spina or other small sculptural elements; the central distal face usually has grana and is differentiated from the zona, which is laevigate, has grana, spina, verruca etc., internal vacuoles are rare or absent; suturae indistinct, labra weak to strong and sometimes connected to the zona; apical papillae sometimes present.

Densosporites variomarginatus Playford 1963

Plate 2 Figure r

1963 *Densosporites variomarginatus* Playford, pp. 629-630, Pl. 89, Figs. 9-13.

1991 *Densosporites variomarginatus* Playford; Ravn, Pl. 21, Figs. 21-22.

1995 *Densosporites variomarginatus* Playford; Clayton, p. 121, Pl. 3, Fig. 3.

Description: Miospores, radial, trilete; amb irregularly subtriangular; exine of variable thickness, laevigate, central body may contain a network of irregular, shallow rugulae, a ring of oval vacuoles may surround the inner body, cingulum has undulations with thickenings and layering of variously shaped lobes, height: 3 (5) 8.5 μm (4 elements); suturae simple, straight.

Dimensions: Total length: 40 (52) 66 μm , width: 29 (43) 60 μm , inner body length: 28 (34) 50 μm , width: 20 (28) 47 μm (12 specimens).

NWMF borehole distribution: 430.37 to 54.56 m depths.

Remarks: Conforms closely to the description by Playford (1963), although the NWMF borehole spores are smaller than those recorded by Playford (1963; 44 to 102 μm), which were oxidised and so may have expanded in size during processing.

Comparisons: *Knoxisporites polymorphus* (Naumova) Braman & Hills 1992 is smaller in diameter (14 to 37 μm) with a thick distal patina and processes up to 15 μm in height that project from the proximal face.

Monilospora mutabilis (Staplin) Clayton *In*: Neves *et al.* 1973 is larger in diameter (49 to 85 μm) with irregular lobes to 5 μm in height that break the cingulum into uneven sections.

Genus ***DICTYOTRILETES*** (Naumova) Smith & Butterworth 1967

Type species: *Dictyotriletes bireticulatus* (Ibrahim) Potonié & Kremp 1954

1939 *Dictyotriletes* Naumova.

1954 *Dictyotriletes* (Naumova) Potonié & Kremp, p. 144.

1967 *Dictyotriletes* (Naumova) Smith & Butterworth, p. 194.

Generic description: Miospores, radial, trilete; exine with a well- or poorly-defined reticulum, which may project at the amb or be low and barely apparent, the lumina are regular or highly variable in shape, generally greater than 6 μm in diameter; the reticulum may be confined to distal surface.

Dictyotriletes fimbriatus (Winslow) Kaiser 1970

Plate 2 Figure s

1962 *Reticulatisporites? fimbriatus* Winslow, pp. 58-59, Pl. 14, Figs. 1-3, Pl. 22, Fig. 21.

1970 *Dictyotriletes fimbriatus* (Winslow) Kaiser, p. 95, Pl. 19, Figs. 4-6.

1988 *Dictyotriletes fimbriatus* (Winslow) Kaiser; Higgs *et al.*, p. 64, Pl. 7, Fig. 8.

Description: Miospores, radial, trilete; amb subcircular; exine thick: 1.5 to 5 μm , minutely granulose with a reticulum of sinuous muri, height: 2 (8) 25 μm (52 muri), enclosing irregularly shaped lumina; suturae straight, simple.

Dimensions: Length: 50 (88) 115 μm , width: 33 (67) 97 μm (11 specimens).

NWMF borehole distribution: 501.11 to 171.06 m depths.

Dictyotriletes fragmentimurus Neville *In: Neves et al. 1973*

Plate 2 Figure t

1973 *Dictyotriletes fragmentimurus* Neville *In: Neves et al.*, pp. 33-34, Pl. 1, Figs. 12-13.

1989 *Dictyotriletes fragmentimurus* Neville *In: Neves et al.*; Brindley & Spinner, p. 222, Fig. 6, number 5.

1994 *Dictyotriletes fragmentimurus* Neville *In: Neves et al.*; Mahdi & Butterworth, p. 164, Fig. 7, number 9.

Description: Miospores, radial, trilete; amb subcircular to convexly triangular; exine thin, 0.5 to 2 μm , laevigate with reticulum of irregular and broken muri with rounded apices, height: 0.5 (2) 5.5 μm (16 muri); suturae simple.

Dimensions: Length: 28 (42) 62 μm , width: 25 (36) 51 μm (14 specimens).

NWMF borehole distribution: 496.62 m to 143.88 m depths.

Remarks: This species is distinguished by its characteristic irregular reticulum with broken muri (Neville *In: Neves et al. 1973*).

***Dictyotriletes pactilis* Sullivan & Marshall 1966**

Plate 2 Figure u

- 1966 *Dictyotriletes pactilis* Sullivan & Marshall, pp. 270-271, Pl. 2, Figs. 3-4.
 1968 *Dictyotriletes pactilis* Sullivan & Marshall; Neville, Pl. 1, Fig. 7.
 1969 *Dictyotriletes pactilis* Sullivan & Marshall; Hibbert & Lacey, Pl. 79, Fig. 10.
 1988 *Dictyotriletes pactilis* Sullivan & Marshall; Turner & Spinner, Pl. 4, Fig. 10.
 1989 *Dictyotriletes pactilis* Sullivan & Marshall; Brindley & Spinner, p. 222, Fig. 6, number 7.

Description: Miospores, radial, trilete; amb subcircular; exine thin: 1 µm, laevigate with a reticulum of irregularly shaped lumina, muri height: 4 (5) 8 µm (30 muri), with broad bases: 2 to 3 µm and sharp or blunted apices; suturae simple; compression folds common.

Dimensions: Length: 33 (59) 98 µm; width: 22 (47) 87 µm (14 specimens).

NWMF borehole distribution: 478.12 m to 102.94 m depths.

Remarks: The age range for this species has been stated as Viséan (Love 1960, Sullivan & Marshall 1966) and it has not been recorded previously from the Tournaisian.



Figure 71. Shape of the tall muri of *Dictyotriletes pactilis*.

***Dictyotriletes trivialis* Naumova In: Kedo 1963**

Plate 2 Figure v

- 1963 *Dictyotriletes trivialis* Naumova In: Kedo, p. 52, Pl. 4, Figs. 87-88.
 1975 *Dictyotriletes trivialis* Naumova In: Kedo; Higgs, Pl. 3, Fig. 16.

- 1977 *Dictyotriletes trivialis* Naumova *In*: Kedo; Clayton *et al.*, p. 33, Pl. 6, Fig. 10.
- 1984 *Dictyotriletes trivialis* Naumova *In*: Kedo; Higgs & Clayton, p. 23, Pl. 1, Fig. 11.
- 1988 *Dictyotriletes trivialis* Naumova *In*: Kedo; McNestry, Pl. 1, Fig. 12.
- 1992 *Dictyotriletes trivialis* Naumova *In*: Kedo; Avchimovitch, Pl. 10, Fig. 8, Pl. 11, Fig. 13.
- 1992 *Dictyotriletes* cf. *D. trivialis* Naumova *In*: Kedo 1963; Braman & Hills, p. 26; Pl. 10, Figs. 4-5.
- 2012 *Dictyotriletes trivialis* Kedo; Playford & Melo, pp. 48-49, Pl. 12, Figs. 1-3.
- 2016 *Dictyotriletes trivialis* Naumova *In*: Kedo; Lopes *et al.*, p. 67, Pl. 2, Fig. 17.

Description: Miospores, radial, trilete; amb subcircular; exine thin, laevigate with reticulum of irregular lumina, muri height: 1 (3) 5 μm (45 muri) with rounded apices; suturae simple.

Dimensions: Length: 30 (51) 78 μm , width: 15 (40) 60 μm (16 specimens).

NWMF borehole distribution: 483.53 m to 54.56 m depths.

Genus **DISCERNISPORITES** (Neves) Neves & Owens 1966

Type species: *Discernisporites irregularis* Neves 1958

- 1958 *Discernisporites* Neves, p. 4.
- 1966 *Discernisporites* (Neves) Neves & Owens, pp. 357-358.

Generic description: Miospores, radial, trilete, camerate; amb convexly triangular; intexine laevigate or minutely granulose, often subcircular; exoexine laevigate or minutely granulose, sculpture may be present on the contact faces; suturae usually accompanied by long folds, labra thin often featuring intense flexures near the proximal pole.

***Discernisporites irregularis* Neves 1958**

Plate 2 Figure w

- 1958 *Discernisporites irregularis* Neves, p. 4, Pl. 3, Figs. 5-6.
 1987 *Spelaeotriletes tuberosus* Utting, p. 35, Pl. 4, Figs. 13-16.
 1991 *Discernisporites irregularis* Neves; Ravn, Pl. 26, Figs. 3-4.
 1993 *Discernisporites irregularis* Neves; Turner & Spinner, Pl. 3, Fig. 7.
 2003 *Discernisporites irregularis* Neves; Lindström, p. 340, Figs. 6 H, I.

Description: Miospores, radial, trilete, camerate; amb convexly triangular; intexine laevigate, conformable with the amb; exoexine thin, 1 μm , laevigate to minutely granulose, sinuous, irregularly distributed ridges, concentrated towards the pole, muri height: 0.5 (1) 2 μm (10 muri), with rounded apices, on some specimens the ridges fold back on themselves to give a bisected, thickened appearance, a conspicuous line conformable with the amb often present; suturae distinct, sinuous and thickened; taper point folds common.

Dimensions: Total length: 55 (78) 140 μm , width: 36 (62) 91 μm , inner body length: 41 (59) 90 μm , width 24 (49) 78 μm (16 specimens).

NWMF borehole distribution: 501.11 m to 49.88 m depths.

Remarks: Conforms closely to the description by Neves (1958) but the NWMF borehole specimens indicate that the size range quoted by Neves (1958; 50 to 100 μm) may now be extended up to 140 μm .



Figure 72. Ridge muri of *Discernisporites irregularis*.

Discernisporites macromanifestus (Hacquebard) Higgs *et al.* 1988

Plate 2 Figure x

- 1925 Type A Lang, p. 255, Pl. 1, Figs. 1-2.
- 1944 *Triletes velatus* Eisenack p. 108 (non Pl. 1, Figs. 1-3).
- 1957 *Endosporites macromanifestus* Hacquebard, p. 317, Pl. 3, Figs. 14-15.
- 1960 *Auroraspora macromanifestus* (Hacquebard) Richardson, p. 50, Pl. 14, Figs. 1-2, Text-fig. 6 A.
- 1963 *Endosporites macromanifestus* Hacquebard; Playford, Pl. 11, Fig. 1.
- 1965 *Auroraspora macromanifestus* (Hacquebard) Richardson; Allen, p. 730.
- 1971 *Auroraspora macromanifestus* (Hacquebard) Richardson; Owens, p. 55, Pl. 14, Figs. 5-6.
- 1975 *Auroraspora macromanifestus* (Hacquebard) Richardson; Turnau, Pl. 5, Fig. 4.
- 1987 *Discernisporites macromanifestus* (Hacquebard) Utting, p. 36, Pl. 5, Fig. 4.
- 1988 *Discernisporites macromanifestus* (Hacquebard) Higgs *et al.*, p. 76, Pl. 14, Fig. 8.
- 1991 *Discernisporites macromanifestus* (Hacquebard) Utting; Ravn, Pl. 26, Fig. 13.

Description: Miospores, radial, trilete, camerate; amb convexly triangular; intexine laevigate, conformable with the amb; exoexine thin, laevigate; suturae straight, simple; compression folds common.

Dimensions: Total length: 81 (116) 265 µm, width: 60 (98) 210 µm, inner body length: 67 (108) 240 µm, width: 55 (85) 180 µm (18 specimens).

NWMF borehole distribution: 462.32 m to 143.88 m depths.

Comparison: Hacquebard (1957) described *D. micromanifestus* (diameter: 58 to 100 µm) as being identical with *D. macromanifestus* (diameter: 122 to 173 µm) but smaller.

Discernisporites micromanifestus (Hacquebard) Sabry & Neves 1971

Plate 2 Figure y

- 1956 *Hymenozonotriletes* aff. *variabilis* Naumova; Ishchenko, p. 62, Pl. 11, Figs. 129-130.
- 1957 *Endosporites micromanifestus* Hacquebard, p. 317, Pl. 3, Fig. 16.
- 1958 *Discernisporites concentricus* Neves, p. 5, Pl. 3, Fig. 7.
- 1960 *Auroraspora micromanifestus* (Hacquebard) Richardson, p. 51 (not figured).
- 1961 *Endosporites micromanifestus* Hacquebard; Hughes & Playford, Pl. 4, Fig. 8.
- 1963 *Endosporites micromanifestus* Hacquebard; Playford, Pl. 11, Fig. 2.
- 1963 *Endosporites micromanifestus* Hacquebard; Playford, Pl. 93, Figs. 17-18.
- 1965 *Auroraspora micromanifestus* (Hacquebard) Richardson; Richardson, p. 586, Pl. 93, Fig. 1.
- 1966 *Endosporites micromanifestus* Hacquebard; Sullivan & Marshall, Pl. 3, Fig. 18.
- 1969 *Endosporites micromanifestus* Hacquebard; Varma, Pl. 3, Fig. 8.
- 1971 *Endosporites micromanifestus* Hacquebard; Playford, p. 52, Pl. 17, Fig. 17.
- 1971 *Discernisporites micromanifestus* (Hacquebard) Sabry & Neves, p. 1445, Pl. 3, Fig. 11.
- 1975 *Auroraspora micromanifestus* (Hacquebard) Richardson; Turnau, Pl. 5, Fig. 18.
- 1975 *Discernisporites micromanifestus* (Hacquebard) Sabry & Neves; Higgs, Pl. 5, Fig. 13.
- 1977 *Discernisporites micromanifestus* (Hacquebard) Sabry & Neves; Clayton *et al.*, p. 29, Pl. 4, Fig. 2, p. 37, Pl. 8, Fig. 24, p. 43, Pl. 11, Fig. 30.
- 1977 *Discernisporites micromanifestus* (Hacquebard) Neves & Belt; Clayton *et al.*, p. 41, Pl. 10, Fig. 31.
- 1978 *Discernisporites micromanifestus* (Hacquebard) Sabry & Neves; Turnau, Pl. 5, Fig. 4 (non 1, 2).
- 1978 *Endosporites micromanifestus* Hacquebard; Playford, p. 140, Pl. 11, Figs. 3-4.

- 1982 *Auroraspora micromanifestus* (Hacquebard) Richardson; McGregor & Camfield, p. 21, Pl. 3, Fig. 16.
- 1987 *Discernisporites micromanifestus* (Hacquebard) Sabry & Neves; Utting, Pl. 5, Figs. 5-6.
- 1988 *Discernisporites micromanifestus* (Hacquebard) Sabry & Neves; Higgs *et al.*, p. 76, Pl. 14, Fig. 9.
- 1988 *Discernisporites micromanifestus* (Hacquebard) Sabry & Neves; Turner & Spinner, Pl. 3, Fig. 2.
- 1990 *Endosporites micromanifestus* Hacquebard; Playford, Pl. 4, Figs. 6-7.
- 1991 *Discernisporites micromanifestus* (Hacquebard) Sabry & Neves; Ravn, Pl. 26, Figs. 9-10.
- 1993 *Endosporites micromanifestus* Hacquebard; Playford & McGregor, Pl. 16, Fig. 3.
- 1993 *Discernisporites micromanifestus* (Hacquebard) Sabry & Neves; Turner & Spinner, Pl. 3, Fig. 2.
- 2005 *Discernisporites micromanifestus* (Hacquebard) Sabry & Neves; Dueñas & Césari, p. 148, Fig. 2 J.
- 2012 *Endosporites micromanifestus* Hacquebard; Melo & Playford, p. 120, Pl. 9, Fig. 16.
- 2016 *Discernisporites micromanifestus* (Hacquebard) Sabry & Neves; Lopes *et al.*, p. 67, Pl. 2, Fig. 20.

Description: Miospores, radial, trilete, camerate; amb convexly triangular; intexine laevigate, conformable with the amb; exoexine thin: 1 µm, minutely granulose, rarely tripapillate; suturae distinct, sinuous, with labra.

Dimensions: Total length: 26 (54) 98 µm, width: 24 (48) 91 µm, inner body length 20 (43) 73 µm, width: 20 (37) 65 µm (17 specimens).

NWMF borehole distribution: 496.62 m to 56.84 m depths.

***Discernisporites sullivanii* Higgs & Clayton 1984**

Plate 2 Figure z

- 1964 *Discernisporites* sp. Sullivan, p. 1255, Figs. 5, 9.
 1970 *Discernisporites* sp. Utting & Neves, Pl. 27, Fig. 3.
 1978 *Discernisporites* sp. Keegan & Penney, Pl. 1, Fig. 6.
 1978 *Discernisporites micromanifestus* (Hacquebard) Sabry & Neves *In*: Turnau, Pl. 5, Figs. 1-2, non Fig. 4.
 1980 *Discernisporites* sp. A. Clayton *et al.*, Pl. 3, Fig. M.
 1984 *Discernisporites sullivanii* Higgs & Clayton, pp. 18-19, Pl. 2, Figs. 14-15.
 1988 *Discernisporites sullivanii* Higgs & Clayton; Higgs *et al.*, Pl. 14, Fig. 5.
 1988 *Discernisporites sullivanii* Higgs & Clayton; McNestry, Pl. 2, Fig. 7.
 1991 *Discernisporites sullivanii* Higgs & Clayton; Ravn, Pl. 26, Figs. 5-8.

Description: Miospores, radial, trilete, camerate; amb subcircular to convexly triangular; intexine laevigate, conformable with the amb; exoexine thin, minutely granulose with discrete, evenly distributed, verrucae, often mammillate, and blunt-topped spinae, height: 0.5 to 2 μm , width: 1.5 to 3 μm ; suturae distinct, straight to sinuous, bordered with narrow labra; occasional taper point compression folds.

Dimensions: Total length: 59 (80) 104 μm , width: 40 (67) 89 μm , inner body length: 45 (59) 76 μm , width: 38 (51) 69 μm (25 specimens).

NWMF borehole distribution: 490.75 to 49.88 m depths.

Remarks: Conforms closely to the description by Higgs & Clayton (1984) but the NWMF borehole spores do not have apical papillae.

Genus **ENDOCULEOSPORA** (Staplin) Turnau 1975

Type species: *Endoculeospora rarigranulata* Staplin 1960

1960 *Endoculeospora* Staplin, p. 34.

1975 *Endoculeospora* (Staplin) Turnau, p. 518.

Generic description: Miospores, radial, trilete, camerate; amb circular to subcircular; intexine laevigate; exoexine minutely granulose with irregularly to densely distributed grana, pili and/or bacula, mostly on the distal face; suturae indistinct.

Comparisons: Whereas *Endoculeospora* has irregularly to densely distributed grana, pili and/or bacula and indistinct suturae, the genus *Auroraspora* Hoffmeister *et al.* 1955 is laevigate, minutely granulose or irregularly infrapunctate has suturae with labra and commonly radial compression folds.

Also, the genus *Colatisporites* Williams *In: Neves et al.* 1973 is laevigate or has small elements that include spinae, coni and bacula, predominantly on the distal face but may extend slightly on to the proximal face and may have curvaturae.

Endoculeospora gradzinskii Turnau 1975

Plate 2 Figure aa

1975 *Endoculeospora gradzinskii* Turnau, p. 518, Pl. 7, Figs. 1-3.

1978 *Endoculeospora gradzinskii* Turnau; Turnau, Pl. 4, Fig. 16.

1980 *Endoculeospora gradzinskii* Turnau; Van der Zwan, Pl. 5, Figs. 1-5, Plate 6, Figs. 1-4.

1984 *Endoculeospora gradzinskii* Turnau; Higgs & Clayton, p. 25, Pl. 2, Fig. 13.

1988 *Endoculeospora gradzinskii* Turnau; Avchimovitch *et al.*, Pl. 4, Fig. 6.

1988 *Endoculeospora gradzinskii* Turnau; Higgs *et al.*, pp. 70-71, Pl. 11, Fig. 4.

1992 *Endoculeospora gradzinskii* Turnau; Avchimovitch, Pl. 2, Fig. 5.

1999 *Endoculeospora gradzinskii* Turnau; Maziane *et al.*, p. 20, Pl. 1, Fig. 9.

2013 *Endoculeospora gradzinskii* Turnau; Higgs *et al.*, p. 94, Pl. 3, Figs. L-M.

Description: Miospores, radial, trilete, camerate; amb subcircular to convexly triangular; intexine laevigate, conformable with the amb; exoexine thin: 0.5 to 1.5 μm , laevigate to minutely granulose with scattered grana, base height: 0.5 to 1 μm , pila and bacula, height: 0.5 to 2 μm ; suturae straight often with thin labra; compression folds common.

Dimensions: Total length: 29 (45) 68 μm , width: 27 (41) 68 μm (13 specimens), inner body length: 17 (34) 53 μm , width: 19 (33) 51 μm (11 specimens).

NWMF borehole distribution: 462.32 m to 64.31 m depths.



Figure 73. (a) Grana base and (b) to (g) grana, pila and bacula of *Endoculeospora gradzinskii*.

Genus **GEMINOSPORA** (Balme) Owens 1971

Type species: *Geminospora lemurata* (Balme) Playford 1983

1962 *Geminospora* Balme, p. 4.

1971 *Geminospora* (Balme) Owens, p. 59.

Generic description: Miospores, radial, trilete, camerate; amb circular to rounded triangular; intexine thin; exoexine differentially thickened (thickest over the distal surface), laevigate, punctate or sculptured with a variety of elements including grana, coni, verrucae and spinae, normally reduced or absent on the contact areas; suturae distinct, straight, commonly accompanied by thickened and/or elevated labra.

***Geminospora lemurata* (Balme) Playford 1983**

Plate 3 Figure a

- 1962 *Geminospora lemurata* Balme, p. 5, Pl. 1, Figs. 5-10.
- 1965 *Geminospora tuberculata* (non Kedo) Allen, p. 696, Pl. 94, Figs. 10-11.
- 1966 *Geminospora micrograna* de Jersey, pp. 17-18, Pl. 10, Figs. 4-6.
- 1966 ?*Archaeozonotriletes plicatus* Naumova *In*: McGregor & Owens, Pl. 23, Fig. 17.
- 1966 ?*Geminospora* sp. McGregor & Owens, Pl. 23, Fig. 19.
- 1967 *Geminospora maculata* Taugourdeau-Lantz, p. 49, Pl. 2, Fig. 11.
- 1981 *Geminospora lemurata* Balme; Higgs & Russell, p. 31, Pl. 2, Figs. 17-20.
- 1982 *Geminospora micromanifesta* (Naumova) McGregor & Camfield var. *minor* Naumova; McGregor & Camfield, p. 40, Pl. 8, Figs. 14-15, 19-22, Text-fig. 57.
- 1982 *Geminospora svalbardiae* (Vigran) Allen; Marshall & Allen, p. 301, Pl. 33, Fig. 12.
- 1982 *Geminospora tuberculata* (Kedo) Allen; Marshall & Allen, p. 301, Pl. 33, Fig. 11.
- 1983 *Geminospora lemurata* (Balme) Playford, Figs. 1 A-O, Figs. 2 A-N, Figs. 3 A-C, Figs. 4 A-C, Fig. 5, Figs. 6 A-G, Figs. 7 A-B, Figs. 8 A-D, Figs. 9 A-B.
- 1996 *Geminospora lemurata* (Balme) Playford; Marshall, pp. 169-171, Pl. 2, Figs. 1, 6, 8.

Description: Miospores, radial, trilete, camerate; amb convexly triangular; intexine thin, laevigate, conformable with the amb; exoexine laevigate with discrete, evenly spaced, densely distributed conic and tapering, sharp-tipped spinae, height: 0.5 µm; suturae straight to sinuous with narrow labra.

Dimensions: Total length: 33 (39) 53 µm, width: 24 (30) 34 µm, inner body length: 23 (32) 45 µm, width: 19 (23) 28 µm (10 specimens).

NWMF borehole distribution: 501.18 to 403.07 m depths.

Remarks: The age range for this species has been stated as Givetian to Frasnian (Allen 1965, Higgs & Russell 1981, McGregor & Camfield 1982) and it has not been recorded previously from the Tournaisian.

Genus **GRANDISPORA** (Hoffmeister *et al.*) McGregor 1973

Type species: *Grandispora spinosa* Hoffmeister *et al.* 1955

- 1955 *Grandispora* Hoffmeister *et al.*, p. 388.
- 1957 *Spinozonotriletes* Hacquebard, p. 315.
- 1960 *Cosmosporites* (pars.) Richardson, p. 62.
- 1962 *Calyptosporites* (pars.) Richardson, p. 192 [nom. nov. pro *Cosmosporites* Richardson].
- 1966 *Grandispora* (Hoffmeister *et al.*) Neves & Owens.
- 1971 *Grandispora* (Hoffmeister *et al.*) Neves & Owens; Playford, pp. 45-47.
- 1973 *Grandispora* (Hoffmeister *et al.*) McGregor, pp. 58-59.
- 2000 *Grandispora* (Hoffmeister *et al.*) McGregor; Higgs *et al.*, pp. 209-213.

Generic description: Miospores, radial, trilete, camerate; amb circular, subcircular to rounded triangular; intexine thin, laevigate or minutely granulose; exoexine thin, laevigate or minutely granulose with scattered verrucae, spinae, coni and biform elements on the distal face, equator and equatorial parts of the proximal face; suturae simple, usually distinct; characteristic compression folds.

Grandispora echinata Hacquebard 1957

Plate 3 Figure b

- 1957 *Grandispora echinata* Hacquebard, p. 317, Pl. 3, Fig. 17.
- 1963 *Grandispora echinata* Hacquebard; Playford, Pl. 5, Fig. 2.
- 1966 *Grandispora echinata* Hacquebard; Neves & Owens, Pl. 3, Fig. 6.
- 1966 *Grandispora echinata* Hacquebard; Sullivan & Marshall, Pl. 4, Figs. 1-3.

- 1968 *Grandispora echinata* Hacquebard; Neville, Pl. 2, Fig. 8.
- 1968 *Grandispora echinata* Hacquebard; Sullivan, pp. 126-127, Pl. 27, Figs. 11-13.
- 1969 *Grandispora echinata* Hacquebard; Varma, Pl. 2, Fig. 18.
- 1972 *Grandispora echinata* Hacquebard; Bertelsen, Pl. 22, Figs. 1-2.
- 1975 *Grandispora echinata* Hacquebard; Higgs, Pl. 4, Fig. 13.
- 1977 *Grandispora echinata* Hacquebard; Clayton *et al.*, p. 27, Pl. 3, Fig. 14, p. 33, Pl. 6, Fig. 17, p. 35, Figs. 21-22.
- 1978 *Grandispora echinata* Hacquebard; Turnau, Pl. 5, Fig. 5.
- 1984 *Grandispora echinata* Hacquebard; Byvsheva *et al.*, Pl. 2, Fig. 14.
- 1984 *Grandispora echinata* Hacquebard; Higgs & Clayton, p. 25, Pl. 2, Fig. 4.
- 1988 *Grandispora echinata* Hacquebard; Avchimovitch *et al.*, Pl. 4, Fig. 18.
- 1988 *Grandispora echinata* Hacquebard; Higgs *et al.*, p. 71, Pl. 11, Figs. 7, 9.
- 1988 *Grandispora echinata* Hacquebard; McNestry, Pl. 3, Fig. 3.
- 1988 *Grandispora echinata* Hacquebard; Turner & Spinner, Pl. 2, Fig. 6.
- 1989 *Grandispora echinata* Hacquebard; Brindley & Spinner, p. 222, Fig. 6, number 16.
- 1992 *Grandispora echinata* Hacquebard; Avchimovitch, Pl. 3, Fig. 7, Pl. 5, Fig. 6, Pl. 9, Fig. 5.
- 1993 *Grandispora echinata* Hacquebard; Playford & McGregor, Pl. 16, Figs. 4-7.
- 1993 *Grandispora echinata* Hacquebard; Turner & Owens, p. 149, Fig. 3, number 11.
- 1994 *Grandispora echinata* Hacquebard; Mahdi & Butterworth, p. 165, Fig. 8, number 5.
- 1996 *Grandispora echinata* Hacquebard; Higgs, Pl. 6, Fig. 7.
- 1999 *Grandispora echinata* Hacquebard; Maziane *et al.*, p. 20, Pl. 1, Fig. 8.
- 2000 *Grandispora echinata* Hacquebard; Higgs *et al.*, p. 217, Pl. 2, Figs. 4-9.
- 2002 *Grandispora echinata* Hacquebard; Stephenson *et al.*, p. 108, Fig. 11, number 1.
- 2010 *Grandispora echinata* Hacquebard; Owens *et al.*, p. 37, Pl. 3, Fig. 6.
- 2013 *Grandispora echinata* Hacquebard; Higgs *et al.*, p. 94, Pl. 3, Fig. G.

Description: Miospores, radial, trilete, camerate; amb subcircular to convexly triangular; intexine thin, laevigate; exoexine thin: 1 to 2 μm , proximal face laevigate, distal face laevigate with discrete, regularly distributed, broad-based spinae, base width: 1 (2) 4.5 μm (35 bases), parallel-sided, tapering or recurved, spinae with pointed apices, height: 1 (2) 5 μm (114 spinae); suturae straight with low labra.

Dimensions: Length: 30 (51) 81 μm , width: 30 (49) 71 (14 specimens).

NWMF borehole distribution: 501.11 m to 54.56 m depths.



Figure 74. (a) to (c) broad-based spinae (d) tapering and (e) recurved spinae of *Grandispora echinata*.

Grandispora microdecora Phillips & Clayton 1980

Plate 3 Figure c

1980 *Grandispora microdecora* Phillips & Clayton, p. 128, Figs. 9 H-K.

1988 *Grandispora microdecora* Phillips & Clayton; Higgs *et al.*, p. 71, Pl. 11, Fig. 6.

Description: Miospores, radial, trilete, camerate; amb convexly triangular; intexine thin, laevigate, more circular in shape than the amb and does not match the apices of the amb; exoexine thin, laevigate with densely distributed, round-tipped, tapering or parallel-sided spinae and pila, height: 0.5 (1) 2.5 μm (17 spinae); suturae slightly sinuous with narrow labra.

Dimensions: Total length: 73 (86) 108 μm , width: 57 (71) 87 μm , inner body length: 41 (57) 67 μm , width: 31 (47) 60 μm (9 specimens).

NWMF borehole distribution: 497.13 to 56.84 m depths.

Remarks: Phillips & Clayton (1980) distinguish *G. microdecora* from other species by its size, relatively large intexine and dense, low sculpture.

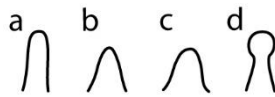


Figure 75. (a) to (c) spinae and (d) pila of *Grandispora microdecora*.

Genus **GRANULATISPORITES** (Ibrahim) Schopf *et al.* 1944

Type species: *Granulatisporites granulatus* Ibrahim 1933

1933 *Granulatisporites* Ibrahim, p. 22, Pl. 6, Fig. 51.

1944 *Granulatisporites* (Ibrahim) Schopf *et al.*, p. 32.

1954 *Granulatisporites* (Ibrahim) Potonié & Kremp, p. 126.

Generic description: Miospores, radial, trilete; amb triangular; exine with densely distributed grana of approximately the same size with circular bases and flat or rounded tops.

Granulatisporites pustulatus Hacquebard & Barss 1957

Plate 3 Figure d

1957 *Granulatisporites pustulatus* Hacquebard & Barss, p. 15, Pl. 2, Fig. 10.

Description: Miospores, radial, trilete; amb convexly triangular to subcircular; exine thin: 1 µm, laevigate with discrete, regularly spaced grana, height: 0.5 to 1 µm, base width: 1 to 2 µm; suturae distinct, straight, occasionally with labra that increase in height towards a central apex; compression folds common.



Figure 76. Diagram to explain the dimensions of the grana of *Granulatisporites pustulatus*.

Dimensions: Length: 22 (34) 40 μm , width: 22 (30) 39 μm (12 specimens).

NWMF borehole distribution: 488.86 to 97.88 m depths.

Genus ***INSCULPTOSPORA*** Marshall 1985

Type species: *Insculptospora confossa* (Richardson) Marshall 1985

1985 *Insculptospora* Marshall, pp. 456-458.

Generic description: Miospores, radial, trilete, camerate; intexine conformable with the amb with sparse to densely distributed coni and/or grana, that are discrete or fused into groups to form a reticulum; exoexine thick, laevigate or minutely granulose.

Insculptospora incrustata (Arkhangelskaya) Marshall 1985

Plate 3 Figure e

1963 *Archaeozonotriletes incrustatus* Arkhangelskaya, p. 21, Pl. 5, Figs. 1, 2, Pl. 6, Figs. 1-2.

1972 *Archaeozonotriletes incrustatus* Arkhangelskaya; Mortimer & Chaloner, p. 39.

1981 *Archaeozonotriletes incrustatus* Arkhangelskaya; Allen & Marshall, p. 266.

1985 *Insculptospora incrustata* (Arkhangelskaya) Marshall, p. 466, Pl. 2, Figs. 10, 12.

2002 *Insculptospora incrustata* (Arkhangelskaya) Marshall; Marshall & Fletcher, p. 202, Pl. 1, Fig. 2.

Description: Miospores, radial, trilete, camerate; amb subcircular; intexine laevigate, conformable with the amb; exoexine minutely granulose; suturae simple; taper point folds common.

Dimensions: Length: 101 (163) 270 μm , width: 82 (138) 295 μm (7 specimens).

NWMF borehole distribution: 472.81 to 408.98 m depths.

Remarks: Conforms closely to the description by Marshall (1985) but the NWMF borehole spores are smaller. Marshall (1985) quotes a single specimen of 320 μm but notes that Arkhangelskaya (1963) quoted 200 specimens ranging in size from 210 to 360 μm . Both sets of specimens were oxidised and so may have expanded in size during processing.

Comparisons: The major difference between *I. confossa* (Richardson) Marshall 1985 and *I. incrustata* is in the equatorial dimension of the exoexine which in the latter is greater than 200 μm (Marshall 1985).

Genus ***KNOXISPORITES*** (Potonié & Kremp) Neves & Playford 1961

Type species: *Knoxisporites hageni* Potonié & Kremp 1954

1954 *Knoxisporites* Potonié & Kremp, p. 147.

1961 *Knoxisporites* (Potonié & Kremp) Neves & Playford, p. 264-266.

Generic description: Miospores radial, trilete; equatorial extension of the exoexine in the form of a cingulum of uniform width, the distal face is characterised by a variable pattern of radial and/or concentric bands of thickening, the equatorial outline of the cingulum is conformable to that of the spore body, departing from it locally where the fusion of the radial elements and the equatorial cingulum produce nodes of thickening; small thickened lobes may project from the cingulum to the proximal face. Although the equatorial cingulum is a constant feature, the disposition of the distal thickenings varies considerably between species

Knoxisporites literatus (Waltz) Playford 1963

Plate 3 Figure f

- 1938 *Zonotriletes literatus* Waltz In: Luber & Waltz, p. 18, Pl. A, Fig. 11. (non Pl. 2, Fig. 21).
- 1941 *Stenozonotriletes literatus* (Waltz) Naumova Pl. 1, Fig. 5.
- 1956 *Euryzonotriletes literatus* (Waltz) Ishchenko, pp. 52-53, Pl. 9, Fig. 108.
- 1956 *Anulatisporites literatus* (Waltz) Potonié & Kremp, p. 111.
- 1957 *Cincturasporites literatus* (Waltz) Hacquebard & Barss, pp. 23-24, Pl. 3, Figs. 2-5.
- 1958 *Euryzonotriletes literatus* (Waltz) Ishchenko, Pl. 6, Fig. 76.
- 1961 *Labiadensites literatus* (Waltz) Bharadwaj & Venkatachala, p. 38, Pl. 8, Figs. 128-130.
- 1963 *Knoxisporites literatus* (Waltz) Playford, p. 634, Pl. 90, Figs. 7-8.
- 1963 *Archaeozonotriletes literatus* (Waltz) Kedo, pp. 75-76, Pl. 8, Figs. 188-190.
- 1963 *Archaeozonotriletes literatus* (Waltz) Naumova var. *triangularis* Kedo, Pl. 8, Figs. 191-193.
- 1966 *Knoxisporites literatus* (Waltz) Luber In: Pokrovskaya, Vol. 1, pp. 183-184, Vol. 3, Pl. 41, Fig. 2, Pl. 45, Fig. 10.
- 1969 *Knoxisporites literatus* (Waltz) Playford; Hibbert & Lacey, Pl. 81, Fig. 7.
- 1971 *Knoxisporites literatus* (Waltz) Playford; Playford, pp. 34-35.
- 1972 *Knoxisporites literatus* (Waltz) Playford; Bertelsen, Pl. 16, Fig. 2.
- 1975 *Knoxisporites literatus* (Waltz) Playford; Higgs, Pl. 3, Fig. 12.
- 1975 *Knoxisporites literatus* (Waltz) Playford; Turnau, p. 512, Pl. 4, Fig. 5.
- 1977 *Knoxisporites literatus* (Waltz) Playford; Clayton *et al.*, p. 31, Pl. 5, Figs. 14-15, p. 37, Pl. 8, Fig. 19.
- 1978 *Knoxisporites literatus* (Waltz) Playford; Playford, p. 134, Pl. 9, Figs. 11-12.
- 1983 *Knoxisporites literatus* (Waltz) Playford; Welsh & Owens, Pl. 1, Fig. 10.
- 1984 *Knoxisporites literatus* (Waltz) Playford; Scot *et al.*, p. 313, Fig. 2 u.
- 1985 *Knoxisporites literatus* (Waltz) Playford; Clayton, p. 23, Fig. 2 K.
- 1987 *Knoxisporites literatus* (Waltz) Playford; Utting, Pl. 2, Fig. 23.

- 1988 *Knoxisporites literatus* (Waltz) Playford; Avchimovitch *et al.*, p. 172, Pl. 3, Figs. 2-3.
- 1988 *Knoxisporites literatus* (Waltz) Playford; Higgs *et al.*, p. 66, Pl. 8, Figs. 1, 2, 5.
- 1988 *Knoxisporites literatus* (Waltz) Playford; McNestry, Pl. 1, Fig. 14.
- 1988 *Knoxisporites literatus* (Waltz) Playford; Turner & Spinner, Pl. 4, Fig. 3.
- 1989 *Knoxisporites literatus* (Waltz) Playford; Brindley & Spinner, p. 224, Fig. 7, number 2.
- 1990 *Knoxisporites literatus* (Waltz) Playford; Playford, Pl. 3, Figs. 8-9.
- 1991 *Knoxisporites literatus* (Waltz) Playford; Ravn, Pl. 14, Figs. 7-8.
- 1992 *Knoxisporites literatus* (Waltz) Playford; Avchimovitch, Pl. 3, Fig. 3, Pl. 4, Fig. 7, Pl. 5, Fig. 8, Pl. 9, Fig. 11.
- 1994 *Knoxisporites literatus* (Waltz) Playford; Mahdi & Butterworth, p. 164, Fig. 7, number 18.
- 1996 *Knoxisporites literatus* (Waltz) Playford; Higgs, Pl. 5, Fig. 9.
- 1999 *Knoxisporites literatus* (Waltz) Playford; Maziane *et al.*, p. 20, Pl. 1, Figs. 4-5.
- 2007 *Knoxisporites literatus* (Waltz) Playford; Higgs & Forsythe, p. 189, Pl. 1, Fig. B.
- 2012 *Knoxisporites literatus* (Waltz) Playford; Melo & Playford, p. 100, Pl. 1, Fig. 6.
- 2015 *Knoxisporites literatus* (Waltz) Playford; Ariana-Sab *et al.*, Pl. 2, Fig. 8, Pl. 3, Fig. 3.

Description: Miospores, radial, trilete; amb subcircular; exine laevigate with a subcircular to polygonal thickening with at least three extensions connecting it to the cingulum, muri height: 3 (7) 12 μm (34 muri); suturae straight, often with labra.

Dimensions: Total length: 48 (69) 83 μm ; width: 39 (61) 82 μm (9 specimens).

NWMF borehole distribution: 501.11 m to 54.56 m depths.

Remarks: Conforms closely to the description by Playford (1963) but the NWMF borehole spores are smaller than the sizes quoted by Playford (1963; 56 (76) 102 μm), but those specimens were oxidised and so may have expanded in size during processing.

Knoxisporites polymorphus (Naumova) Braman & Hills 1992

Plate 3 Figure g

1953 *Archaeozonotriletes polymorphus* Naumova, p. 78, Pl. 11, Figs. 19-21.

1992 *Knoxisporites polymorphus* Braman & Hills. p. 28, Pl. 11, Figs. 10-11.

Description: Miospores, radial, trilete; amb subcircular to convexly triangular; exine thin: 1 μm ; laevigate central body surrounded by thick distal patina resembling an irregular cingulum, with proximal processes or broad-based, blunt- to sharp-topped coni, which may have convex or tapering sides, clubs or flat-topped coni with apical spinae, height 2.5 (7) 15 μm (99 elements), base width 2 (6) 16 μm (45 elements); sutures simple.

Dimensions: Length: 14 (29) 37 μm , width: 8 (23) 30 μm (14 specimens).

NWMF borehole distribution: 472.81 to 54.56 m depths.

Remarks: Conforms to the description by Naumova (1953), although the NWMF borehole spores are smaller than those recorded by Naumova (1953; 35 to 55 μm) and by Braman & Hills (1992; 38.4 (60.3) 92.4 μm), both samples of which were oxidised and so may have expanded in size during processing.

Remarks: The age range for this species has been stated as Upper Devonian (Naumova 1953) and it has not been recorded previously from the Tournaisian.

Comparisons: *Densosporites variomarginatus* Playford 1963 may exhibit a network of irregular, shallow rugulae in the central body which is surrounded by a ring of vacuoles, and a cingulum with variously shaped lobes to 8.5 μm in height.

Monilospora mutabilis (Staplin) Clayton *In*: Neves *et al.* 1973 is large in diameter (49 to 85 μm) with irregular lobes to 5 μm in height that break the cingulum into uneven sections.



Figure 77. (a) to (i) various sculptural elements and (j) to (m) broader-based sculptural elements of *Knoxisporites polymorphus* with coalesced bases resembling an irregular cingulum.

***Knoxisporites pristinus* Sullivan 1968**

Plate 3 Figure h

- 1968 *Knoxisporites pristinus* Sullivan, pp. 123-124, Pl. 27, Figs. 1-5.
- 1969 *Knoxisporites pristinus* Sullivan; Hibbert & Lacey, Pl. 81, Figs. 5, 6, 9.
- 1972 *Knoxisporites pristinus* Sullivan; Bertelsen, Pl. 18, Figs. 3-6.
- 1975 *Knoxisporites pristinus* Sullivan; Turnau, p. 513, Pl. 4, Fig. 7.
- 1977 *Knoxisporites pristinus* Sullivan; Clayton *et al.*, p. 35, Pl. 7, Fig. 16.
- 1977 *Knoxisporites pristinus* Sullivan; Owens *et al.*, Pl. 2, Fig. 6.
- 1978 *Knoxisporites pristinus* Sullivan; Turnau, Pl. 3, Fig. 14.
- 1988 *Knoxisporites pristinus* Sullivan; Turner & Spinner, Pl. 2, Fig. 2.
- 1992 *Knoxisporites pristinus* Sullivan; Avchimovitch, Pl. 11, Fig. 8.
- 1994 *Knoxisporites pristinus* Sullivan; Mahdi & Butterworth, p. 164, Fig. 7, number 15.

Description: Miospores, radial, trilete; amb subcircular to irregular; exine thin, minutely granulose with variably shaped, irregularly distributed muri, height: 1 (3) 6 μm (53 muri); suturae straight, simple or with narrow labra.

Dimensions: Total length: 44 (54) 67 μm , width: 38 (43) 56 μm , inner body length: 36 (48) 59 μm , width: 30 (38) 48 μm (10 specimens).

NWMF borehole distribution: 445.51 to 77.99 m depths.

Remarks: Conforms closely to the description by Sullivan (1968) but the NWMF borehole spores are smaller than the sizes quoted by Sullivan (1968; 62 (85) 103 μm), but those specimens were oxidised and so may have expanded in size during processing. Sullivan (1968) distinguished this species by its ill-defined thickenings and lack of good proximo-distal orientation.

Knoxisporites triangularis Higgs *et al.* 1988

Plate 3 Figure i

- 1938 *Zonotriletes literatus* Waltz *In*: Luber & Waltz, Pl. 2, Fig. 21.
- 1941 *Stenozonotriletes literatus* (Waltz) Naumova, Pl. 1, Fig. 5.
- 1958 *Euryzonotriletes literatus* (Waltz) Ishchenko Pl. 6, Fig. 76.
- 1963 *Archaeozonotriletes literatus* (Waltz) Naumova var. *triangularis* Kedo, Pl. 8, Figs. 191-193.
- 1964 *Knoxisporites hederatus* (Ishchenko) Playford; Sullivan pp. 1253-1254, Pl. 2, Figs. 1-2.
- 1970 *Knoxisporites literatus* (Waltz) Playford var. *triangularis* (Kedo) Clayton, p. 584, Pl. 2, Fig. 5.
- 1971 *Knoxisporites literatus* (Waltz) Playford var. *triangularis* Kedo; Johnson & Marshall, Pl. 23, Fig. 10.
- 1973 *Knoxisporites literatus* (Waltz) Playford var. *triangularis* (Kedo) Clayton; Neves *et al.*, Pl. 3, Fig. 11.
- 1975 *Knoxisporites literatus* (Waltz) Playford var. *triangularis* (Kedo) Clayton; Higgs, Pl. 3, Fig. 13.
- 1976 *Knoxisporites literatus* (Waltz) Playford; Playford, Pl. 5, Fig. 6.
- 1977 *Knoxisporites literatus* (Waltz) Playford var. *triangularis* (Kedo) Clayton; Clayton *et al.*, p. 35, Pl. 7, Fig. 20.

- 1988 *Knoxisporites triangularis* Higgs *et al.*, p. 66, Pl. 8, Figs. 3, 6.
 1991 *Knoxisporites triangularis* (Kedo) Higgs *et al.*; Ravn, Pl. 14, Figs. 3-4.
 1994 *Knoxisporites triangularis* Higgs *et al.*; Mahdi & Butterworth, p. 164, Fig. 7, number 15.
 1996 *Knoxisporites triangularis* Higgs *et al.*; Higgs, Pl. 5, Fig. 10.

Description: Miospores, radial, trilete; amb subcircular to irregular; exine thin, laevigate to minutely granulose with three straight muri, height: 2 (8) 16 μm (25 muri) joined to form a distinctive triangle with the apices connected to the cingulum; suturae straight with broad labra.

Dimensions: Total length: 70 (85) 107 μm , width: 47 (67) 88 μm , inner body length: 57 (67) 76 μm , width: 36 (51) 74 μm (6 specimens).

NWMF borehole distribution: 496.62 to 171.06 m depths.

Genus ***LOPHOZONOTRILETES*** (Naumova) Van der Zwan 1980

Type species: *Lophozonotriletes lebedianensis* Naumova 1953

- 1953 *Lophozonotriletes* Naumova, p. 74.
 1958 *Lophozonotriletes* (Naumova) Potonié, pp. 27-28.
 1980 *Lophozonotriletes* (Naumova) Van der Zwan.

Generic description: Miospores, radial, trilete; exine thick, with verrucae, coni or spinae that are less densely distributed on the contact faces; narrow cingulum.

Lophozonotriletes tuberosus Sullivan 1964

Plate 3 Figure j

- 1964 *Lophozonotriletes tuberosus* Sullivan, p. 1254, Pl. 2, Fig. 6-7.
 1975 *Lophozonotriletes* cf. *tuberosus* Sullivan; Higgs, p. 398, Pl. 3, Fig. 15.

1988 *Lophozonotriletes tuberosus* Sullivan; Higgs *et al.*, p. 67, Pl. 8, Fig. 15.

1988 *Lophozonotriletes tuberosus* Sullivan; McNestry, Pl. 1, Fig. 10.

Description: Miospores, radial, trilete; amb convexly triangular to irregular; exine thin: 1.5 μm , laevigate with verrucae, height: 0.5 (2) 7 μm (112 elements), rarely discrete, mostly forming arcuate, sinuous and branching rugulae of varying thickness, base width: 2 (4) 7 μm (16 bases); suturae indistinct, straight, simple.

Dimensions: Length: 29 (49) 75 μm , width: 24 (38) 67 μm (22 specimens).

NWMF borehole distribution: 493.86 to 197.43 m depths.

Remarks: The NWMF borehole specimens usually appear to be broken at one end.



Figure 78. Verrucae of *Lophozonotriletes tuberosus*.

Genus **MONILOSPORA** (Hacquebard & Barss) Staplin 1960

Type species: *Monilospora moniliformis* Hacquebard & Barss 1957

1957 *Monilospora* Hacquebard & Barss, p. 38.

1960 *Monilospora* (Hacquebard & Barss) Staplin, p. 28.

Generic description: Miospores, radial, trilete; amb circular to convexly triangular; equatorial flange with a marginal thickening.

Monilospora mutabilis (Staplin) Clayton *In*: Neves *et al.* 1973

Plate 3 Figure k

1960 *Monilospora mutabilis* Staplin, p. 28, Pl. 6, Figs. 1-7, 9.

1968 *Monilospora mutabilis* Staplin 1960; Neville pp. 441-442, Pl. 1, Fig. 11.

1973 *Monilospora mutabilis* (Staplin) Clayton *In*: Neves *et al.*, p. 37, Pl. 2, Figs. 1-4.

1977 *Monilospora mutabilis* (Playford) Clayton; Clayton *et al.*, p. 41, Pl. 10, Fig. 18.

Description: Miospores, radial, trilete; amb broadly triangular to subcircular; exine: 2.5 to 4.5 μm , laevigate with irregular lobes, height: 1 to 5 μm , breaking the cingulum into uneven sections; suturae distinct, straight, often with low labra.

Dimensions: Total length: 49 (67) 85 μm , width: 37 (57) 78 μm ; inner body length: 28 (43) 53 μm , width: 21 (33) 46 μm (12 specimens).

NWMF borehole distribution: 459.19 to 54.56 m depths.

Comparisons: *Densosporites variomarginatus* Playford 1963 may exhibit a network of irregular, shallow rugulae in the central body which is surrounded by a ring of vacuoles, and a cingulum with variously shaped lobes to 8.5 μm in height.

Knoxisporites polymorphus (Naumova) Braman & Hills 1992 is small in diameter (14 to 37 μm) with a thick distal patina and processes up to 15 μm in height that project from the proximal face.

Genus ***PILOSPORITES*** (Delcourt & Sprumont) Döring 1965

Type species: *Pilosporites trichopapillosus* (Thiergart) Delcourt & Sprumont 1955

1955 *Pilosporites* Delcourt & Sprumont.

1965 *Pilosporites* (Delcourt & Sprumont) Döring.

Generic description: Miospores, radial, trilete; amb triangular with rounded apices and concave sides; exine with densely distributed, tapering, round-tipped spinae that measure longer than twice the diameter.

Pilosisorites verutus Sullivan & Marshall 1966

Plate 3 Figure I

1966 *Pilosisorites verutus* Sullivan & Marshall, pp. 267-268, Pl. 1, Figs. 10-11.

1977 *Pilosisorites venustus* Sullivan & Marshall; Clayton *et al.*, p. 43, Pl. 11, Fig. 13.

Description: Miospores, radial, trilete; amb triangular with rounded apices and slightly convex to deeply concave sides; exine thin: $\leq 1 \mu\text{m}$, laevigate with unevenly spaced, long bacula and spinae, height: 0.5 (3) 6.5 μm (58 elements), that are more concentrated towards the apices; suturae straight, simple; darkened contact areas common.

Dimensions: Length: 23 (38) 49 μm , width: 18 (37) 53 μm (8 specimens).

NWMF borehole distribution: 423.59 to 54.56 m depths.

Remarks: Conforms closely to the description by Sullivan & Marshall (1966), but their size range (40 (46) 50 μm) can now be extended from 23 μm .

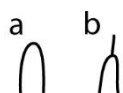


Figure 79. (a) Bacula (mostly) and (b) spinae (few) of *Pilosisorites verutus*.

Genus ***PLICATISPORA*** Higgs *et al.* 1988

Type species: *Plicatispora scolecophora* (Neves & Ioannides) Higgs *et al.* 1988

1962 *Pulvinispora* Balme & Hassell, pp. 10-11.

1988 *Plicatispora* Higgs *et al.*, p. 51.

Generic description: Miospores, radial, trilete; amb subcircular, rounded triangular or triangular with convex or straight sides; exine laevigate to irregularly granulate, proximal surface laevigate, distal surface with folds, wrinkles, rugulae and fine muri and may possess subordinate grana and coni of regular or irregular distribution and density; suturae straight, simple or with labra, terminating in curvaturae that are invaginated and often thickened in the radial positions.

Plicatispora scolecophora (Neves & Ioannides) Higgs *et al.* 1988

Plate 3 Figure m

- 1973 *Pulvinispora scolecophora* Neves & Ioannides; Neves *et al.*, Pl. 3, Fig. 2.
- 1974 *Pulvinispora scolecophora* Neves & Ioannides, p. 74, Pl. 1, Figs. 9-10.
- 1975 *Pulvinispora scolecophora* Neves & Ioannides; Higgs, Pl. 1, Figs. 11-12.
- 1977 *Pulvinispora scolecophora* Neves & Ioannides; Clayton *et al.*, p. 37, Pl. 8, Fig. 20.
- 1977 *Pulvinispora scolecophora* Neves & Ioannides; Keegan, p. 549, Pl. 1, Fig. 2.
- 1977 *Pulvinispora scolecophora* Neves & Ioannides; Owens *et al.*, Pl. 1, Fig. 11.
- 1979 *Pulvinispora scolecophora* Neves & Ioannides; Welsh, Pl. 1, Fig. 1.
- 1979 *Diaphanospora scolecophora* Van der Zwan, Pl. 20, Fig. 2.
- 1984 *Pulvinispora scolecophora* Neves & Ioannides; Higgs & Clayton, p. 23, Pl. 1, Fig. 3.
- 1988 *Pulvinispora scolecophora* Neves & Ioannides; Turner & Spinner, Pl. 3, Fig. 12.
- 1988 *Plicatispora scolecophora* (Neves & Ioannides) Higgs *et al.*, p. 51, Pl. 1, Figs. 10, 14.
- 1991 *Plicatispora scolecophora* (Neves & Ioannides) Higgs *et al.*; Ravn, Pl. 27, Figs. 12-13.
- 1996 *Plicatispora scolecophora* (Neves & Ioannides) Higgs *et al.*; Higgs, Pl. 1, Fig. 11.
- 1997 *Plicatispora scolecophora* (Neves & Ioannides) Higgs *et al.*; Carson & Clayton, Pl. 1, Fig. 3.

2002 *Plicatispora scolecophora* (Neves & Ioannides) Higgs *et al.*; Stephenson *et al.*, p. 106, Fig. 10, number 10.

2019 *Plicatispora scolecophora* (Neves & Ioannides) Higgs *et al.*; Marshall *et al.*, p. 271, Fig. 6, number 1.

Description: Miospores, radial, trilete; amb subcircular to convexly triangular; exine thin, laevigate; suturae straight with narrow labra, terminating in curvaturae, often with thickened extremities; sinuous, branching folds common.

Dimensions: Length: 28 (39) 57 μm , width: 27 (37) 53 μm (33 specimens).

NWMF borehole distribution: 501.18 to 39.11 m depths.

Genus **PROLYCOSPORA** Turnau 1978

Type species: *Prolycospora claytonii* Turnau 1978

1978 *Prolycospora* Turnau, pp. 9-10.

Generic description: Miospores, radial, trilete; amb rounded triangular or subcircular; size: 20 to 55 μm in diameter; narrow, uniformly thick (non-tapering) cingulum; exine with grana, rugulae, coni, pila, bacula and verrucae; sculpture on contact faces usually finer than that of the distal face; apical papillae may be present.

Prolycospora claytonii Turnau 1978

Plate 3 Figures n to t

1963 *Lophotriletes minutissimus* Naumova; Kedo, p. 49, Pl. 3, Figs. 76-77.

1966 *Lophotriletes minutissimus* Naumova; Kedo, p. 49, Pl. 2, Figs. 41-43.

1978 *Prolycospora claytonii* Turnau, p. 10, Pl. 4, Figs. 3 a-b, 6.

1991 *Prolycospora claytonii* Turnau; Ravn, p. 78, Pl. 19, Figs. 12-15.

- 1994 *Prolycospora claytonii* Turnau; Mahdi & Butterworth, p. 162, Fig. 5, numbers 5-6.
- 1994 *Prolycospora claytonii* Turnau; Avchimovitch & Turnau, p. 258-259, Pl. 1, Figs. 11-12.
- 2005 *Prolycospora claytonii* Turnau; Turnau *et al.*, p. 96, Figs. 3 m, n.
- 2019 *Prolycospora claytonii* Turnau; Marshall *et al.*, p. 271, Fig. 6, numbers 7, 8.

Description: Miospores, radial, trilete; amb subcircular; exine thin, proximal face laevigate or infragranulate, distal face with discrete, closely and evenly spaced verrucae, height: 0.5 (1) 2.5 μm (30 verrucae), rarely flat-topped, mostly with rounded tops, rarely on short, parallel-sided columellae, base width: 1.5 (2.5) 4 μm (30 verrucae), base outlines polygonal to irregular; suturae straight, often with narrow labra.

Dimensions: Length: 23 (28) 33 μm , width: 15 (21) 26 μm (50 specimens).

NWMF borehole distribution: 376.05 to 49.88 m depths.

Remarks: The NWMF borehole specimens are frequently found in pairs and occasionally in tetrads.



Figure 80. Variously shaped verrucae of *Prolycospora claytonii*.

Affinity: *Genomosperma kidstoni* (Calder) Long 1960a. This affinity was established during an inspection of *G. kidstoni* ovules that contained several *in situ* spores of *Prolycospora claytonii* at the Albert Long Collection at the Hunterian Museum, Glasgow in 2018. For details, refer to Section 5.4.2.

Genus **PUNCTATISPORITES** (Ibrahim) Potonié & Kremp 1954

Type species: *Punctatisporites punctatus* (Ibrahim) Ibrahim 1933

- 1933 *Punctatisporites* Ibrahim, p. 21.

- 1954 *Punctatisporites* (Ibrahim) Potonié & Kremp, p. 120.
 1958 *Todisporites* Couper, p. 134.
 1967 *Todisporites* (Couper) Hiltmann, p. 153.

Generic description: Miospores, radial, trilete; amb circular, subcircular or convexly triangular; exine laevigate or minutely granulose.

Discussion: The monosaccate pollen *Remysporites magnificus* (Horst) Butterworth & Williams 1958 consists of a laevigate intexine and thin exoexine. Smith (1962) noted that, in addition to complete grains, detached exoexines had been found following maceration and remarked that had the intexines been found as *spora dispersae* that they would be classified into a separate genus. Following a review of the type specimen of *Protopitys scotica* Walton 1957 in Glasgow (as studied by Smith (1962); see Section 5.5.3), three grains of *R. magnificus* were found in series that clearly show how the intexine separates from the exoexine layer to leave a 'spore' that resembles *Punctatisporites* (see Figure 113).

***Punctatisporites irrasus* Hacquebard 1957**

Plate 3 Figure u

- 1957 *Punctatisporites irrasus* Hacquebard, p. 308, Pl. 1, Figs. 7, 8.
 1963 *Punctatisporites irrasus* Hacquebard; Playford, Pl. 1, Fig. 5.
 1964 *Punctatisporites irrasus* Hacquebard; Sullivan, Pl. 1, Figs. 2-4.
 1967 *Punctatisporites irrasus* Hacquebard; Neves & Dolby, Pl. 1, Figs. 1, 2.
 1969 *Punctatisporites irrasus* Hacquebard; Hibbert & Lacey, Pl. 78, Fig. 1.
 1970 *Punctatisporites* cf. *irrasus* Dolby & Neves, p. 635, Pl. 1, Fig. 1.
 1974 *Punctatisporites irrasus* Hacquebard; Neves & Ioannides, Pl. 1, Fig. 1.
 1975 *Punctatisporites irrasus* Hacquebard; Higgs, Pl. 1, Fig. 2.
 1977 *Punctatisporites irrasus* Hacquebard; Clayton *et al.*, p. 33, Pl. 6, Fig. 5.
 1977 *Punctatisporites irrasus* Hacquebard; Owens *et al.*, Pl. 1, Fig. 1.
 1981 *Punctatisporites irrasus* Hacquebard; Higgs & Russell, p. 24, Pl. 1, Fig. 1.
 1986 *Punctatisporites irrasus* Hacquebard; Ravn, p. 26, Pl. 1, Figs. 15, 16.

- 1987 *Punctatisporites irrasus* Hacquebard; Utting, Pl. 1, Fig. 5.
 1988 *Punctatisporites irrasus* Hacquebard; Avchimovitch *et al.*, Pl. 1, Fig. 1.
 1988 *Punctatisporites irrasus* Hacquebard; Higgs *et al.*, p. 51, Pl. 1, Fig. 17.
 1991 *Punctatisporites irrasus* Hacquebard; Ravn, Pl. 1, Fig. 16.
 1993 *Punctatisporites irrasus* Hacquebard; Playford & McGregor, Pl. 8, Figs. 7, 8.
 2005 *Punctatisporites irrasus* Hacquebard; Dueñas & Césari, p. 142. Fig. 2 A.

Description: Miospores, radial, trilete; amb circular to subcircular; exine thin, laevigate; suturae straight with narrow labra.

Dimensions: Length: 26 (36) 48 μm , width: 26 (36) 47 μm (30 specimens).

NWMF borehole distribution: 501.18 to 49.88 m depths.

Remarks: Conforms closely to the description by Hacquebard (1957) but the quoted size (67-83 μm) is significantly greater than those of the NWMF borehole specimens.

***Punctatisporites? limbatus* Hacquebard 1957**

Plate 3 Figure v

- 1957 *Punctatisporites? limbatus* Hacquebard, p. 308, Pl. 1, Figs. 9-11.
 1963 *Punctatisporites limbatus* Hacquebard; Playford, Pl. 1, Figs. 7-8.

Description: Miospores, radial, trilete; amb subcircular; exine thick: 1 (3) 8 μm (27 specimens found); laevigate to infragranulate; suturae straight with narrow labra; compression folds common.

Dimensions: Length: 76 (129) 355 μm (26 specimens), width: 63 (113) 260 μm (24 specimens).

NWMF borehole distribution: 496.62 to 247.34 m depths.

Remarks: Conforms closely to the description by Hacquebard (1957), but the size range quoted (111-206 μm) may now be extended as above. Note that Hacquebard (1957) regarded the thickening at the equator as a 'limbus', a double-layered feature representing the proximal and distal walls being in contact. Hacquebard (1957) provisionally included this species in *Punctatisporites* owing to its structure but acknowledged that a limbus had not been reported before.

***Punctatisporites planus* Hacquebard 1957**

Plate 3 Figure w

- 1957 *Punctatisporites planus* Hacquebard, p. 308, Pl. 1, Fig. 12.
- 1963 *Punctatisporites planus* Hacquebard; Playford, Pl. 1, Figs. 9, 10.
- 1975 *Punctatisporites planus* Hacquebard; Higgs, Pl. 1, Fig. 2.
- 1984 *Punctatisporites planus* Hacquebard; Higgs & Clayton, p. 23, Pl. 1, Fig. 1.
- 1987 *Punctatisporites planus* Hacquebard; Utting, Pl. 1, Fig. 6.
- 1988 *Punctatisporites planus* Hacquebard; Higgs *et al.*, p. 51, Pl. 1, Fig. 18.
- 1993 *Punctatisporites planus* Hacquebard; Playford & McGregor, Pl. 8, Fig. 9.
- 2008 *Punctatisporites planus* Hacquebard; Heal & Clayton, p. 35, Pl. 1, Fig. 2.

Description: Miospores, radial, trilete; amb circular to subcircular; exine thin, laevigate; sutures straight, simple.

Dimensions: Length: 36 (43) 57 μm , width: 26 (38) 52 μm (30 specimens).

NWMF borehole distribution: 501.18 to 42.46 m depths.

Comparisons: *P. planus* and *P. irrasus* appear similar, but *P. irrasus* has raised labra.

Punctatisporites solidus Hacquebard 1957

Plate 3 Figure x

1957 *Punctatisporites solidus* Hacquebard, p. 308, Pl. 1, Fig. 13.

1963 *Punctatisporites solidus* Hacquebard; Playford, Pl. 1, Fig. 12.

1975 *Punctatisporites solidus* Hacquebard; Turnau, Pl. 1, Fig. 3.

1988 *Punctatisporites solidus* Hacquebard; Avchimovitch *et al.*, Pl. 1, Fig. 2.

1993 *Punctatisporites solidus* Hacquebard; Playford & McGregor, Pl. 8, Figs. 10, 11.

Description: Miospores, radial, trilete; amb circular to subcircular; exine thick: 2 (3) 5 μm (30 specimens), laevigate; suturae very distinct, prominent labra.

Dimensions: Length: 35 (41) 67 μm , width: 25 (37) 55 μm (30 specimens).

NWMF borehole distribution: 501.18 m to 49.88 m depths.

Remarks: The thickened exine distinguishes this species.

Genus ***PUSTULATISPORITES*** Potonié & Kremp 1954

Type species: *Pustulatisporites pustulatus* Potonié & Kremp 1954

1954 *Pustulatisporites* Potonié & Kremp p. 134.

Generic description: Miospores, radial, trilete; exine with widely distributed grana, verrucae or coni, the bases of which may occasionally touch.

***Pustulatisporites dolbii* Higgs et al. 1988**

Plate 4 Figure a

- 1970 *Pustulatisporites* cf. *gibberosus* (Hacquebard) Playford; Combaz & Streel, p. 230, Pl. 3, Fig. 2.
- 1975 *Pustulatisporites* sp. A Higgs, Pl. 2, Fig. 4.
- 1988 *Pustulatisporites dolbii* Higgs et al., p. 56, Pl. 4, Figs. 6, 9, 10.
- 1988 *Pustulatisporites dolbii* Higgs et al.; Avchimovitch et al., Pl. 1, Fig. 14.
- 1988 *Pustulatisporites dolbii* Higgs et al.; Turner & Spinner, Pl. 3, Fig. 4.
- 1993 *Pustulatisporites dolbii* Higgs et al.; Playford & McGregor, Pl. 10, Figs. 4-10.
- 2002 *Pustulatisporites dolbii* Higgs et al.; Higgs et al., p. 150, Pl. 2, Fig. 12.

Description: Miospores, radial, trilete; amb circular to subcircular; exine thin: 1 to 2 μm , laevigate with broader-based verrucae, height: 0.5 (3) 5 μm (75 verrucae), base width: 2 (5) 8.5 μm (45 verrucae), evenly spaced to densely distributed, discrete or occasionally attached at the bases, tapering, occasionally constricted, with round or flat tops; suturae straight, simple or with narrow labra; rare compression folds.

Dimensions: Length: 38 (57) 66 μm , width: 31 (48) 62 μm (10 specimens).

NWMF borehole distribution: 486.25 m to 102.94 m depths.

Comparisons: *Verrucosisporites gibberosus* (Hacquebard) Higgs et al. 1988 appears like *P. dolbii*, but the verrucae are taller, the bases may be wider, they are more evenly spaced, always discrete and the tops are rounded.



Figure 81. Various shaped verrucae of *Pustulatisporites dolbii*.

Genus **RAISTRICKIA** (Schopf *et al.*) Potonié & Kremp 1954

Type species: *Raistrickia grovensis* Schopf *In*: Schopf *et al.* 1944

1944 *Raistrickia* Schopf *et al.*, p. 55.

1954 *Raistrickia* (Schopf *et al.*) Potonié & Kremp, p. 133.

Generic description: Miospores, radial, trilete; exine with bacula and, occasionally, coni; the bacula are cylindrical, may be slightly wider at the base, the ends are flattened or rounded, often broken and so appear irregular, or have more than one papilla, the diameter of bacula is variable.

Raistrickia corynoges Sullivan 1968

Plate 4 Figure b

1963 *Acanthotriletes macrurus* (*non* Luber & Waltz 1938) Kedo, p. 44, Pl. 3, Fig. 57.

1964 *Raistrickia* sp. A. Sullivan, p. 1252, Pl. 1, Fig. 8.

1968 *Raistrickia corynoges* Sullivan, pp. 119-120, Pl. 25, Figs. 6-8.

1970 *Raistrickia corynoges* Sullivan; Clayton, Pl. 3, Fig. 1.

1971 *Raistrickia corynoges* Sullivan; Johnson & Marshall, Pl. 23, Fig. 7.

1972 *Raistrickia corynoges* Sullivan; Bertelsen, Pl. 9, Figs. 1, 4.

1973 *Raistrickia corynoges* Sullivan; Neves *et al.*, Pl. 3, Fig. 6.

1975 *Raistrickia corynoges* Sullivan; Higgs, Pl. 2, Fig. 12.

1977 *Raistrickia corynoges* Sullivan; Clayton *et al.*, p. 30, Pl. 5, Fig. 4, p. 35, Pl. 7, Fig. 7.

1977 *Raistrickia corynoges* Sullivan; Owens *et al.*, Pl. 1, Fig. 17.

1978 *Raistrickia corynoges* Sullivan; Turnau, Pl. 2, Fig. 7.

1983 *Raistrickia corynoges* Sullivan; Welsh & Owens, Pl. 1, Fig. 4.

1984 *Raistrickia corynoges* Sullivan; Higgs & Clayton, p. 23, Pl. 1, Figs. 20-21.

1984 *Raistrickia corynoges* Sullivan; Scot *et al.*, p. 313, Fig. 2 d.

1988 *Raistrickia corynoges* Sullivan; Avchimovitch *et al.*, Pl. 1, Fig. 15.

- 1988 *Raistrickia corynoges* Sullivan; Higgs *et al.*, p. 58, Pl. 4, Fig. 11.
 1988 *Raistrickia corynoges* Sullivan; Turner & Spinner, Pl. 4, Figs. 7-8.
 1992 *Raistrickia corynoges* Sullivan; Avchimovitch, Pl. 5, Fig. 10.
 1994 *Raistrickia corynoges* Sullivan; Mahdi & Butterworth, p. 164, Fig. 7, number 20.
 1996 *Raistrickia corynoges* Sullivan; Higgs, Pl. 3, Fig. 1.
 2002 *Raistrickia corynoges* Sullivan; Stephenson *et al.*, p. 108, Fig. 11, number 4.

Description: Miospores, radial, trilete; amb circular to convexly triangular; exine thin, laevigate with discrete, evenly- to often densely-spaced spinae, length: 2 (11) 23 μm (121 spinae), base width: 0.5 (3) 7 μm (100 spinae), with parallel or tapering sides, tops rounded, pointed, truncated or irregular; suturae obscured by sculpture.

Dimensions: Length: 28 (59) 94 μm , width: 22 (50) 78 μm (14 specimens).

NWMF borehole distribution: 501.11 to 201.95 m depths.

Remarks: Conforms closely to the description by Sullivan (1968), although the NWMF borehole spores may extend the size range quoted by Sullivan (1968) from 50 (64) 75 μm to 28 (59) 94 μm .



Figure 82. Various shaped spinae of *Raistrickia corynoges*.

Raistrickia cf. ponderosa

Plate 4 Figure c

Description: Miospores, radial, trilete; amb subcircular to convexly triangular; exine thick: 2 to 6 μm , laevigate with discrete, clava, total height: 7.5 (17) 37 μm (82 clava), with parallel sided columellae, height: 1.5 (7) 18 μm (67 clava), width: 3

(10) 20 μm (78 clava) and expanded, rounded capita, height: 4 (11) 19 μm (67 clava), width: 5 (17) 30 μm (78 clava); suturae straight with labra: 1 μm wide.

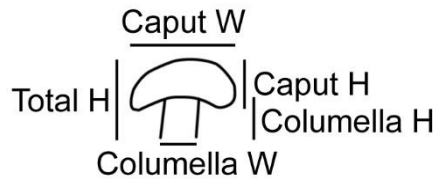


Figure 83. Diagram to define the dimensions of the clava of *Raistrickia cf. ponderosa*.

Dimensions: Length: 70 (92) 119 μm , width: 51 (70) 90 μm (29 specimens).

NWMF borehole distribution: 497.13 to 49.88 m depths.

Remarks: These spores appear similar to Playford's (1963) description of *Raistrickia ponderosa*. They have a similar size range of 69 (90) 115 μm compared to above, a thick exine and a sculpture of discrete pila with circular bases and rounded capita. However, although the lengths of the processes: 3.5–11 μm and their basal diameters: 2.5–7 μm overlap those of the NWMF borehole spores, the dimensions of the NWMF borehole spores' sculptural elements are much greater. *R. ponderosa* also have bacula, verrucae and coni, which the NWMF borehole spores do not.



Figure 84. Examples of the shapes of the clava of *Raistrickia cf. ponderosa*.

Genus **RETUSOTRILETES** (Naumova) Richardson 1965

Type species: *Retusotriletes simplex* Naumova 1953

1953 *Retusotriletes* Naumova.

1964 *Retusotriletes* (Naumova) StreeI, pp. 238-239.

1965 *Retusotriletes* (Naumova) Richardson, pp. 563-564.

Generic description: Miospores, radial, trilete; amb subcircular to subtriangular; exine laevigate; suturae terminate in distinct curvaturae.

***Retusotriletes incohatus* Sullivan 1964**

Plate 4 Figure d

- 1964 *Retusotriletes incohatus* Sullivan, pp. 1251-1252, Pl. 1, Figs. 5-7.
- 1967 *Retusotriletes incohatus* Sullivan; Butterworth & Spinner, p. 3, Pl. 2, Figs. 12, 13.
- 1967 *Retusotriletes incohatus* Sullivan; Neves & Dolby, Pl. 1, Fig. 3.
- 1970 *Retusotriletes incohatus* Sullivan 1964; Dolby & Neves, pp. 635-636, Pl. 1, Fig. 4.
- 1973 *Retusotriletes incohatus* Sullivan; Neves *et al.*, Pl. 3, Fig. 1.
- 1974 *Retusotriletes incohatus* Sullivan; Neves & Ioannides, Pl. 5, Fig. 8.
- 1974 *Aneurospora incohata* (Sullivan) Streeel *In: Becker et al.*, p. 24.
- 1975 *Retusotriletes incohatus* Sullivan; Higgs, Pl. 1, Figs. 7, 10.
- 1975 *Retusotriletes incohatus* Sullivan; Turnau, Pl. 1, Fig. 1.
- 1977 *Retusotriletes incohatus* Sullivan; Clayton *et al.*, p. 23, Pl. 1, Fig. 2, p. 27, Pl. 3, Fig. 1, p. 29, Pl. 4, Fig. 1, p. 30, Pl. 5, Fig. 3, p. 33, Pl. 6, Fig. 3.
- 1977 *Retusotriletes incohatus* Sullivan; Keegan, p. 549, Pl. 1, Fig. 3.
- 1977 *Retusotriletes incohatus* Sullivan; Owens *et al.*, Pl. 1, Fig. 5.
- 1978 *Retusotriletes incohatus* Sullivan; Mortimer *et al.*, Pl. 29, Figs. 1, 2.
- 1978 *Retusotriletes incohatus* Sullivan; Turnau, Pl. 1, Fig. 4.
- 1980 *Retusotriletes incohatus* Sullivan; Phillips & Clayton, Fig. 8 A.
- 1983 *Retusotriletes incohatus* Sullivan; Welsh & Owens, Pl. 1, Fig. 7.
- 1984 *Retusotriletes incohatus* Sullivan; Higgs & Clayton, p. 23, Pl. 1, Fig. 2.
- 1987 *Retusotriletes incohatus* Sullivan; Utting, Pl. 1, Fig. 7.
- 1988 *Retusotriletes incohatus* Sullivan; Avchimovitch *et al.*, Pl. 1, Figs. 5, 6.
- 1988 *Retusotriletes incohatus* Sullivan; Higgs *et al.*, p. 52, Pl. 1, Fig. 20.
- 1988 *Retusotriletes incohatus* Sullivan; Turner & Spinner, Pl. 4, Fig. 9.
- 1992 *Retusotriletes incohatus* Sullivan; Avchimovitch, Pl. 8, Fig. 17, Pl. 9, Fig. 14.

- 1995 *Retusotriletes incohatus* Sullivan; Clayton, p. 119, Pl. 1, Fig. 4.
 2005 *Retusotriletes incohatus* Sullivan; Dueñas & Césari, p. 142, Fig. 2 Q.
 2007 *Retusotriletes incohatus* Sullivan; Higgs & Forsythe, p. 189, p. 11, Fig. E.
 2008 *Retusotriletes incohatus* Sullivan; Heal & Clayton, p. 35, Pl. 1, Fig. 1.
 2012 *Retusotriletes incohatus* Sullivan; Playford & Melo, pp. 15-16, Pl. 2, Figs. 7, 8.

Description: Miospores, radial, trilete; amb subcircular; exine thin, laevigate to minutely granulose; suturae straight with thin labra and curvaturae.

Dimensions: Length: 33 (44) 66 μm , width: 26 (37) 48 μm (30 specimens).

NWMF borehole distribution: 501.18 m to 39.11 m depths.

***Retusotriletes rotundus* (Streel) Streel 1967**

Plate 4 Figure e

- 1964 *Phyllothecotriletes rotundus* Streel, p. 236, Pl. 1, Fig. 1.
 1967 *Retusotriletes rotundus* (Streel) Streel, p. 25, Pl. 1, Fig. 11, Pl. 2, Figs. 16, 17.

Description: Miospores, radial, trilete; amb subcircular to convexly triangular; exine thin: 1 to 2 μm , laevigate with discrete, sparsely distributed, grana, height: 0.5 to 1 μm , base width: 1 to 2 μm ; suturae straight, simple, terminating in curvaturae; occasional taper point folds.

Dimensions: Length: 52 (66) 97 μm , width: 33 (48) 53 μm (30 specimens).

NWMF borehole distribution: 501.18 m to 42.46 m depths.

Remarks: Conforms closely to the description by Streel (1964), although the NWMF borehole spore sizes may now extend the original range (36 to 64 μm) up to 97 μm .



Figure 85. Grana of *Retusotriletes rotundus*.

Genus **RUGOSPORA** (Neves & Owens) Turnau 1978

Type species: *Rugospora corporata* Neves & Owens 1966

1966 *Rugospora* Neves & Owens, pp. 350-352.

1978 *Rugospora* (Neves & Owens) Turnau, p. 11.

Generic description: Miospores, radial, trilete, camerate; amb subcircular to oval; intexine thin, laevigate, often indistinct; exoexine laevigate or microverrucate, with a series of plications that present an irregular, corrugated appearance; suturae often hidden, with narrow labra.

Comparison: The genus *Velamispories* Bharadwaj & Venkatachala 1961 appears like *Rugospora* but shows comparatively little or no cameration. See *Velamispories* for a further discussion of these two genera.

Rugospora lactucosa Higgs *et al.* 1988

Plate 4 Figure f

1984 *Convolutispora* sp. Higgs & Streel, Pl. 2, Fig. 9.

1988 *Rugospora lactucosa* Higgs *et al.*, pp. 72-73, Pl. 12, Figs, 10, 13, 14.

1996 *Rugospora lactucosa* Higgs *et al.*; Higgs, Pl. 6, Fig. 1.

Description: Miospores, radial, trilete, camerate; amb subcircular; intexine laevigate; exoexine thin with laevigate, densely distributed, highly sinuous folds; suturae straight, simple.

Dimensions: Total length: 58 (93) 127 μm , width: 49 (79) 120 μm , inner body length: 47 (82) 122 μm , width: 40 (65) 103 μm (4 specimens).

NWMF borehole distribution: 431.07 to 39.11 m depths.

Remarks: Conforms closely to the description by Higgs *et al.* (1988) but the NWMF borehole spores are smaller than the sizes quoted by Higgs *et al.* (1988; 94 (124) 160 μm), but the latter specimens were oxidised and so may have expanded in size during processing.

Rugospora vieta Higgs *et al.* 1988

Plate 4 Figure g

1988 *Rugospora vieta* Higgs *et al.*, p. 73, Pl. 12, Figs. 9, 11, 12.

Description: Miospores, radial, trilete, camerate; amb subcircular to convexly triangular; intexine laevigate, conformable with the amb; exoexine thin, laevigate to minutely granulose with dense, fine folds; suturae straight, occasionally with narrow labra; rare taper point folds.

Dimensions: Total length: 45 (58) 69 μm , width: 38 (51) 60 μm , inner body length: 36 (49) 62 μm , width: 34 (43) 57 μm (8 specimens).

NWMF borehole distribution: 442.66 to 73.95 m depths.

Genus ***SCHOPFITES*** Kosanke 1950

Type species: *Schopfites dimorphus* Kosanke 1950

1950 *Schopfites* Kosanke, p. 52.

Generic description: Miospores, radial, trilete; exine on the proximal face laevigate, the distal face has densely distributed, blunt to round projections that range in length from 2 to 12 μm ; suturae with thin or broad labra; rare folds on the thinner proximal surface.

Schopfites claviger (Sullivan) Higgs *et al.* 1988

Plate 4 Figures h to l

- 1968 *Schopfites claviger* Sullivan, p. 121, Pl. 25, Figs. 9, 10.
- 1970 *Schopfites claviger* Sullivan; Clayton, Pl. 3, Figs. 3-5.
- 1972 *Schopfites claviger* Sullivan; Bertelsen, Pl. 4, Figs. 4, 6, 7.
- 1973 *Schopfites claviger* Sullivan; Neves *et al.*, Pl. 3, Fig. 7.
- 1974 *Schopfites claviger* Sullivan; Neves & Ioannides, Pl. 6, Fig. 1.
- 1977 *Schopfites claviger* Sullivan; Clayton *et al.*, p. 35, Pl. 7, Fig. 4, p. 37, Pl. 8, Figs. 3, 4.
- 1977 *Schopfites claviger* Sullivan; Owens *et al.*, Pl. 1, Fig. 14.
- 1979 *Schopfites claviger* Sullivan; Welsh, Pl. 1, Fig. 2.
- 1980 *Schopfites claviger* Sullivan; Phillips & Clayton, Figs. 8 M, N.
- 1984 *Schopfites claviger* Sullivan; Scot *et al.*, p. 313, Figs. 2 g, h.
- 1985 *Schopfites claviger* Sullivan; Clayton, p. 23, Fig. 2 d.
- 1987 *Schopfites claviger* Sullivan; Utting, Pl. 2, Fig. 4.
- 1988 *Schopfites claviger* (Sullivan) Higgs *et al.*, pp. 59-60, Pl. 5, Figs. 1-10.
- 1994 *Schopfites claviger* (Sullivan) Higgs *et al.*; Avchimovitch & Turnau, p. 258, Pl. 1, Figs. 1-4.
- 1994 *Schopfites claviger* (Sullivan) Higgs *et al.*; Mahdi & Butterworth, p. 164, Fig. 7, number 6.
- 1997 *Schopfites claviger* (Sullivan) Higgs *et al.*; Carson & Clayton, Pl. 1, Figs. 1, 2.
- 2002 *Schopfites claviger* (Sullivan) Higgs *et al.*; Stephenson *et al.*, p. 106, Fig. 10, number 13.
- 2003 *Schopfites claviger* (Sullivan) Higgs *et al.*; Melo & Loboziak, p. 197, Pl. 6, Fig. 5.

- 2005 *Schopfites claviger* (Sullivan) Higgs *et al.*; Dueñas & Césari, p. 143, Fig. 2 H.
- 2005 *Schopfites claviger* (Sullivan) Higgs *et al.*; Turnau *et al.*, p. 96, Fig. 3 e.
- 2007 *Schopfites claviger* (Sullivan) Higgs *et al.*; Higgs & Forsythe, p. 189, Pl. 1, Figs. R-S.
- 2016 *Schopfites claviger* (Sullivan) Higgs *et al.*; Lopes *et al.*, p. 65, Pl. 1, Fig. 2.

Description: Miospores, radial, trilete; amb subcircular to convexly triangular; exine thin, laevigate to minutely granulose with clava, total height: 1.5 (3) 5.5 μm , caput width: 1 (2) 3 μm , columella height: 0.5 (1) 3.5 μm , columella width: 0.5 (1) 2 μm (100 clava); suturae indistinct, simple; compression folds common.



Figure 86. Diagram to define the dimensions of the clava of *Schopfites claviger*.

Dimensions: Length: 37 (52) 75 μm , width: 26 (38) 61 μm (50 specimens).

NWMF borehole distribution: 501.18 to 42.46 m depths.

Schopfites claytonii Mahdi & Butterworth 1994

Plate 4 Figure m

- 1970 *Schopfites cf. claviger* (Sullivan) Clayton, p. 588, Pl. 3, Fig. 6.
- 1994 *Schopfites claytonii* Mahdi & Butterworth, p. 168, Fig. 7, numbers 1-5.

Description: Miospores, radial, trilete; amb subcircular; exine thin; minutely granulose on both faces with a mixture of discrete, densely distributed pila and clava, height: 1.5 (2) 3 μm (16 elements) on the distal face; suturae slightly sinuous with narrow labra.

Dimensions: Length: 30 (37) 47 μm , width: 24 (31) 40 μm (10 specimens).

NWMF borehole distribution: 468.42 to 331.15 m depths.

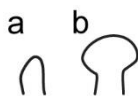


Figure 87. (a) Pila and (b) clava of *Schopfites claytonii*.

***Schopfites delicatus* (Higgs) Higgs *et al.* 1988**

Plate 4 Figure n

- 1975 *Schopfites delicatus* Higgs pp. 396-397, Pl. 2, Figs. 6, 7.
- 1979 *Schopfites delicatus* Higgs; Welsh, Pl. 1, Fig. 2.
- 1980 *Ceratosporites delicatus* (Higgs) Van der Zwan, p. 220, Pl. 18, Fig. 6.
- 1983 *Schopfites delicatus* Higgs; Welsh & Owens, Pl. 1, Figs. 8, 9.
- 1984 *Schopfites delicatus* Higgs; Higgs & Clayton, p. 23, Pl. 1, Fig. 8.
- 1988 *Schopfites delicatus* (Higgs) Higgs *et al.*, p. 60, Pl. 5, Figs. 10, 15.
- 1988 *Schopfites delicatus* Higgs *et al.*; Turner & Spinner, Pl. 3, Figs. 6, 9.
- 1990 *Schopfites delicatus* (Higgs) Higgs *et al.*; Clayton & Turnau, p. 51, Pl. 1, Fig. 5.
- 1994 *Schopfites delicatus* (Higgs) Higgs *et al.*; Mahdi & Butterworth, p. 164, Fig. 7, number 7.
- 2019 *Schopfites delicatus* (Higgs) Higgs *et al.*; Marshall *et al.*, p. 271, Fig. 6, number 9.

Description: Miospores, radial, trilete; amb subcircular; exine thin; proximal surface laevigate, distal face laevigate to minutely granulose with discrete pila, height: 1 (2) 4 µm (100 pila); suturae, simple, straight; compression folds common.

Dimensions: Length: 30 (46) 52 µm, width: 24 (34) 44 µm (30 specimens).

NWMF borehole distribution: 499.18 to 39.11 m depths.

Comparisons: *Schopfites claviger* resembles *S. delicatus* but it has a greater size range (37 to 75 μm) than *S. delicatus* (30 to 52 μm) and its sculpture is more robust and of greater height (figures 88 and 89). However, it could be argued that *S. delicatus* is simply a juvenile form of *S. claviger*. Until these spores are found *in situ*, this debate cannot be resolved.

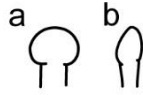


Figure 88. Comparison of the morphology of (a) the clava of *Schopfites claviger* and (b) the pila of *Schopfites delicatus*.

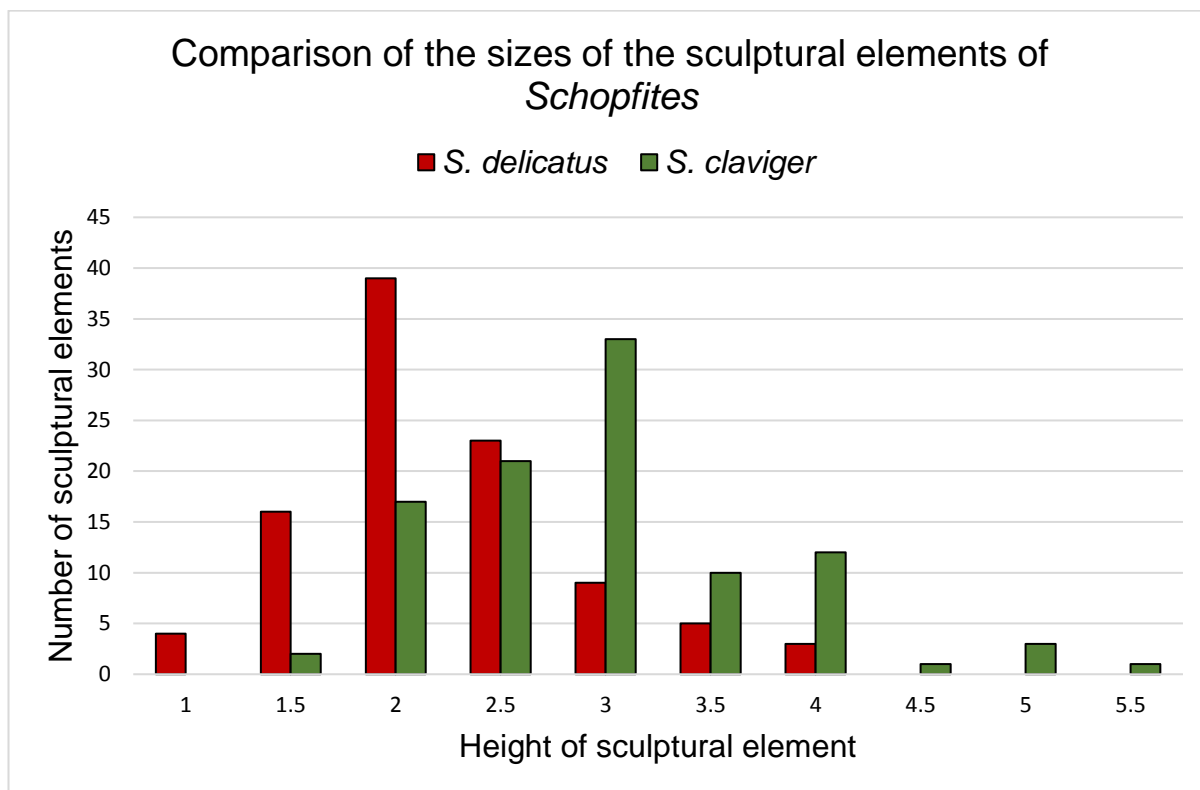


Figure 89. Comparisons of the sizes of the pila of *Schopfites delicatus* and the clava of *S. claviger* (in μm).

Genus **SPELAEOTRILETES** Neves & Owens 1966

Type species: *Spelaeotriletes triangulus* Neves & Owens 1966

1966 *Spelaeotriletes* Neves & Owens, pp. 342-344.

Generic description: Miospores, radial, trilete, camerate; amb oval to convexly triangular; intexine thin, circular in outline; exoexine laevigate to minutely granulose, with a mix of small coni, grana and verrucae, which vary in density and show variable fusion to form short irregular ridges, the sculpture is mainly located on the distal surface, encroaching on to the proximal surface mainly in the radial positions; contact faces large and laevigate, taper point folds common.

Spelaeotriletes crustatus Higgs 1975

Plate 4 Figure o

1975 *Spelaeotriletes crustatus* Higgs, p. 399, Pl. 6, Figs. 7-9; *non* Pl. 6, Figs. 4-6.

1977 *Spelaeotriletes exiguus* Keegan, p. 556, Pl. 4, Figs. 7-10.

1978 *Spelaeotriletes resolutus* Higgs *In*: Van der Zwan & Van Veen, Pl. 2, Fig. 1.

1980 *Spelaeotriletes resolutus* Higgs *In*: Van der Zwan, Pl. 18, Fig. 5.

1984 *Spelaeotriletes crustatus* Higgs; Byvsheva *et al.*, p. 39.

1988 *Spelaeotriletes crustatus* Higgs; Avchimovitch *et al.*, Pl. 4, Fig. 10.

1988 *Spelaeotriletes crustatus* Higgs; Higgs *et al.*, pp. 73-74, Pl. 13, Figs. 8, 9.

1992 *Spelaeotriletes crustatus* Higgs; Avchimovitch, Pl. 8, Fig. 14.

1993 *Spelaeotriletes crustatus* Higgs; Playford & McGregor, Pl. 15, Figs. 7-9.

Description: Miospores, radial, trilete, camerate; amb subcircular to convexly triangular; intexine thin, laevigate, conformable with the amb; exoexine thin, minutely granulose, occasionally with discrete spinae, length: up to 1 µm; suturae distinct, straight to sinuous, bordered by labra, height: up to 4 µm, terminating in curvaturae; occasional taper point folds.

Dimensions: Total length: 39 (60) 87 µm; inner body length: 27 (43) 58 µm (30 specimens).

NWMF borehole distribution: 501.18 m to 39.11 m depths.

Remarks: Conforms closely to the description by Higgs (1975), although the NWMF borehole spores are smaller than those recorded by Higgs (1975; 55 (70) 110 µm), which were oxidised and so may have expanded in size during processing.

Comparison: *Cristatisporites echinatus* Playford 1963 appears like *S. crustatus* but has a thicker exoexine with pila and longer spinae, the suturae do not terminate in curvaturae and the spores are generally larger.

***Spelaeotriletes microspinosus* Neves & Ioannides 1974**

Plate 4 Figure p

1973 *Spelaeotriletes microspinosus* Neves & Ioannides; Neves *et al.*, Pl. 3, Fig. 14.

1974 *Spelaeotriletes microspinosus* Neves & Ioannides, p. 81, Pl. 8, Figs. 1, 3.

1988 *Spelaeotriletes microspinosus* Neves & Ioannides; Higgs *et al.*, p. 74, Pl. 13, Figs. 5, 7.

1994 *Spelaeotriletes microspinosus* Neves & Ioannides; Mahdi & Butterworth, p. 165, Fig. 8, number 1.

2002 *Spelaeotriletes microspinosus* Neves & Ioannides; Stephenson *et al.*, p. 106, Fig. 10, number 14.

Description: Miospores, radial, trilete, camerate; amb subcircular to convexly triangular; intexine thin: 1 µm, laevigate; exoexine thin: 1 µm with densely distributed, discrete spinae, tapering to a sharp point, length: 0.5 to 1.5 µm; suturae distinct, straight to sinuous, bordered with narrow labra, terminating in curvaturae.

Dimensions: Total length: 30 (41) 52 μm , width: 28 (37) 44 μm ; inner body length: 23 (30) 43 μm , width: 20 (26) 29 μm (10 specimens).

NWMF borehole distribution: 399.52 to 49.88 m depths.

***Spelaeotriletes resolutus* Higgs 1975**

Plate 4 Figure q

1975 *Spelaeotriletes resolutus* Higgs, p. 400, Pl. 6, Figs. 7-9.

1980 *Spelaeotriletes crustatus* Higgs; Van der Zwan, Pl. 18, Fig. 3.

1988 *Spelaeotriletes resolutus* Higgs; Higgs *et al.*, pp. 74-76, Pl. 13, Figs. 10, 11, 15.

Description: Miospores, radial, trilete, camerate; amb subcircular to convexly triangular; intexine thin, laevigate, conformable with the amb; exoexine thin: 1 μm , minutely granulose with discrete, evenly distributed, verrucae, height: 1 to 2 μm , base width: 1 to 3 μm , blunt-topped spinae, height: 1 to 3 μm , and pila, height: 0.5 to 2 μm ; suturae distinct, straight to sinuous, bordered with narrow labra, height: 1 μm , terminating in curvaturae; folds common.

Dimensions: Total length: 37 (54) 73 μm , width: 29 (44) 57 μm ; inner body length: 28 (43) 63 μm , width: 24 (37) 49 μm (9 specimens).

NWMF borehole distribution: 496.62 to 54.56 m depths.

Genus **VELAMISPORITES** Bharadwaj & Venkatachala 1961

Type species: *Velamisporites rugosus* Bharadwaj & Venkatachala 1961

1961 *Velamisporites* Bharadwaj & Venkatachala, p. 25.

1966 *Rugospora* Neves & Owens, pp. 350, 352, Fig. 2.

- 1978 *Rugospora* (Neves & Owens) Turnau, p. 11.
 1991 *Velamispores* Bharadwaj & Venkatachala 1961; Ravn, pp. 95-96.
 2003 *Velamispores* Bharadwaj & Venkatachala 1961; Di Pasquo *et al.*, pp. 289-290 ["amplified diagnosis"].

Generic description: Miospores, radial, trilete; amb circular, oval to convexly triangular; exine thick, laevigate to minutely granulose, with a series of plications that present a pseudoreticulate appearance; prominent suturae.

Comparison: The genus *Rugospora* (Neves & Owens) Turnau 1978 appears like *Velamispores* but is camerate.

Discussion: The genera *Velamispores* and *Rugospora* have been discussed by various authors (Turnau 1978, Ravn 1991, Di Pasquo *et al.* 2003, Azcuy & di Pasquo 2006, Melo & Playford 2012) who have given arguments on whether both genera should be regarded as separate, or if *Velamispores* is a senior synonym of *Rugospora*. A summary of those opinions and the outcome regarding this thesis are given below:

Initially, to accommodate the difference in age, Bharadwaj & Venkatachala (1961) erected the genus *Velamispores* to classify Lower Carboniferous spores that they had compared to Mesozoic *Perotrilites* Couper (1953, 1958). Their original description was of a more or less laevigate intexine with a wrinkled and granulose exoexine.

Neves & Owens (1966) erected *Rugospora* to encompass spores with a laevigate intexine and microverrucose exoexine with plications. This description was very similar to that of *Velamispores*, but Neves & Owens (1966) described *Rugospora* as being 'camerate'.

Turnau (1978) emended *Rugospora* to include spores with an unsculptured exoexine, but Ravn (1991) considered that Turnau's (1978) emendation rendered *Rugospora* functionally synonymous with *Velamispores*.

Accepting that sculpture of the exoexine was not regarded as a defining character, Ravn (1991) also added that using the relative degree of cameration cited by Neves & Owens (1966) to maintain separate genera, was inappropriate. Ravn (1991) argued that as the taxonomy of those types of camerate spores was so poorly defined, that not all species previously assigned to *Rugospora* could be assigned to *Velamispорites*.

Di Pasquo *et al.* (2003) considered that Turnau's (1978) emendment showed that *Rugospora* should be considered a junior synonym of *Velamispорites* and used Ravn's (1991) argument to validate this assertion. Additionally, regarding the degree of cameration of each genus, di Pasquo *et al.* (2003) concluded that the separation of the exinal layers in *Velamispорites* was variable.

Azcuy & di Pasquo (2006) concluded that *Rugospora* is a junior synonym of *Velamispорites* based on their agreement with Ravn (1991) and di Pasquo *et al.* (2003). However, Melo & Playford (2012), who provisionally accepted Ravn's (1991) contention that *Velamispорites* should be regarded as a senior synonym of *Rugospora*, reiterated Ravn's (1991) remark that some species included in *Rugospora* may not be attributable to *Velamispорites*.

Therefore, as only *Velamispорites corporatus* (*Rugospora corporata*), *V. minutus* (*R. minuta*) and *V. polyptychus* (*R. polyptycha*) were discussed by the aforementioned authors, the genera *Velamispорites* and *Rugospora* are retained separately in this thesis, with the species *lactucosa* and *vieta* being maintained under the genus *Rugospora* as they are described as being 'camerate' rather than 'variably camerate'.

Velamispорites corporatus (Neves & Owens) Ravn 1991

Plate 4 Figure r

1966 *Rugospora corporata* Neves & Owens, p. 353, Pl. 2, Figs. 4, 5.

1968 *Rugospora corporata* Neves & Owens var. *laevigata* Neville, p. 450.

- 1971 *Rugospora corporata* Neves & Owens; Marshall & Williams, Pl. 1, Fig. 24.
- 1977 *Rugospora corporata* Neves & Owens; Clayton *et al.*, p. 51, Pl. 15, Fig. 21.
- 1991 *Velamispories corporatus* (Neves & Owens) Ravn, p. 96, Pl. 29, Fig. 1.
- 1993 *Rugospora corporata* Neves & Owens; Turner & Spinner, Pl. 3, Fig. 6.
- 1994 *Rugospora corporata* Neves & Owens; Mahdi & Butterworth, p. 165, Fig. 8, number 15.

Description: Miospores, radial, trilete; amb subcircular to oval; exine thin: 2 µm, minutely granulose with irregular folds; suturae straight with narrow labra.

Dimensions: Total length: 62 (100) 143 µm, width: 38 (75) 92 µm, inner body length: 62 (86) 115 µm, width: 37 (63) 77 µm (5 specimens).

NWMF borehole distribution: 316.72 to 54.56 m depths.

Velamispories minutus (Neves & Ioannides) Ravn 1991

Plate 4 Figure s

- 1972 *Rugospora minuta* Neves & Ioannides; Bertelsen, p. 63, Pl. 12, Figs. 1-4.
- 1974 *Rugospora minuta* Neves & Ioannides, pp. 79-80, Pl. 8, Figs. 7, 8.
- 1977 *Rugospora minuta* Neves & Ioannides; Clayton *et al.*, p. 35, Pl. 7, Fig. 9, p. 37, Pl. 8, Fig. 23.
- 1978 *Rugospora minuta* Neves & Ioannides; Turnau, p. 11, Pl. 4, Figs. 5, 19, 24.
- 1980 *Rugospora minuta* Neves & Ioannides; Phillips & Clayton, Fig. 9 D.
- 1987 *Rugospora minuta* Neves & Ioannides; Utting, Pl. 3, Figs. 19-21.
- 1988 *Rugospora minuta* Neves & Ioannides; Higgs *et al.*, p. 73, Pl. 12, Fig. 6.
- 1989 *Rugospora minuta* Neves & Ioannides; Brindley & Spinner, p. 220, Fig. 5, numbers 12-14.
- 1991 *Velamispories* sp. cf. *V. minutus* (Neves & Ioannides) Ravn, p. 97.
- 1992 *Rugospora minuta* Neves & Ioannides; Avchimovitch, Pl. 11, Fig. 15.
- 1994 *Rugospora minuta* Neves & Ioannides; Mahdi & Butterworth, p. 165, Fig. 8, number 8.

- 1997 *Rugospora minuta* Neves & Ioannides; Carson & Clayton, Pl. 2, Fig. 14.
 2007 *Rugospora minuta* Neves & Ioannides; Higgs & Forsythe, p. 191, Pl. 2, Fig. E.
 2012 *Velamispurites minutus* (Neves & Ioannides) Ravn; Melo & Playford, p. 126, Pl. 11, Figs. 4, 5.

Description: Miospores, radial, trilete; amb subcircular to convexly triangular; exine thin, minutely granulose with closely spaced, sinuous folds; suturae straight.

Dimensions: Length: 31 (36) 44 µm, width: 27 (34) 50 µm (30 specimens).

NWMF borehole distribution: 500.98 to 39.11 m depths.

Velamispurites polyptychus (Neves & Ioannides) Ravn 1991

Plate 4 Figure t

- 1974 *Rugospora polyptycha* Neves & Ioannides; p. 80, Pl. 8, Figs. 2, 5.
 1975 *Rugospora polyptycha* Neves & Ioannides; Higgs, Pl. 4, Fig. 10.
 1977 *Rugospora polyptycha* Neves & Ioannides; Clayton *et al.*, p. 33, Pl. 6, Fig. 9, p. 35, Pl. 7, Fig. 14.
 1977 *Rugospora polyptycha* Neves & Ioannides; Owens *et al.*, Pl. 2, Fig. 9.
 1978 *Rugospora polyptycha* Neves & Ioannides; Turnau, Pl. 4, Fig. 14.
 1980 *Rugospora polyptycha* Neves & Ioannides; Phillips & Clayton, Fig. 9 F.
 1984 *Rugospora polyptycha* Neves & Ioannides; Higgs & Clayton, p. 25, Pl. 2, Fig. 6.
 1984 *Rugospora polyptycha* Neves & Ioannides; Scot *et al.*, p. 313, Fig. 2 y.
 1985 *Rugospora polyptycha* Neves & Ioannides; Clayton. p. 23, Fig. 2 m.
 1988 *Rugospora polyptycha* Neves & Ioannides; Higgs *et al.*, p. 73, Pl. 12, Fig. 8.
 1988 *Rugospora polyptycha* Neves & Ioannides; McNestry, Pl. 3, Fig. 2.
 1988 *Rugospora polyptycha* Neves & Ioannides; Turner & Spinner, Pl. 2, Fig. 5.
 1991 *Velamispurites polyptychus* (Neves & Ioannides) Ravn, p. 98.

- 1994 *Rugospora polyptycha* Neves & Ioannides; Mahdi & Butterworth, p. 165, Fig. 8, number 12.
- 1996 *Rugospora polyptycha* Neves & Ioannides; Higgs, Pl. 6, Fig. 6.
- 2012 *Velamispories polyptychus* (Neves & Ioannides) Ravn; Melo & Playford, pp. 126-127, Pl. 11, Fig. 6.

Description: Miospores, radial, trilete; amb subcircular to convexly triangular; exine thin, laevigate to minutely granulose with closely spaced, irregularly distributed, convoluted ridges bisected by longitudinal grooves; suturae sinuous; occasional folds.

Dimensions: Total length: 48 (69) 101 μm , width 35 (54) 71 μm (13 specimens).

NWMF borehole distribution: 496.62 to 43.99 m depths.

Remarks: The bisected longitudinal grooves distinguish *V. polyptychus* from other species of *Velamispories*.

Genus **VERRUCOSISPORITES** (Ibrahim) Smith 1971

Type species: *Verrucosisporites verrucosus* (Ibrahim) Ibrahim 1933

- 1933 *Verrucosisporites* Ibrahim.
- 1967 *Verrucosisporites* (Ibrahim) Smith & Butterworth, p. 147.
- 1971 *Verrucosisporites* (Ibrahim) Smith, pp. 43-49.

Generic description: Miospores, radial, trilete; amb circular, subtriangular or roundly triangular, margin generally crenulate but may be undulate to irregularly lobate; exine predominantly verrucate but may include small rugulae, coni or bacula, sculptural elements generally densely distributed but may be variable, verrucae are circular, polygonal, reniform or irregular in plan view, and in profile may be domed or the sides may taper to varying degrees and the apices may be flat, angled or well rounded, with the height equal to or less than the breadth;

suturæ generally simple, if labra are present, they do not exceed the height of the sculpture; contact areas may have smaller sculptural elements.

***Verrucosisporites baccatus* Staplin 1960**

Plate 4 Figure u

- 1960 *Verrucosisporites baccatus* Staplin, p. 12, Pl. 2, Figs. 4, 10.
 1967 *Verrucosisporites baccatus* Staplin; Smith & Butterworth, pp. 147-148, Pl. 4, Figs. 17, 18.
 1971 *Verrucosisporites baccatus* Staplin; Marshall & Williams, Pl. 1, Fig. 3.
 1973 *Verrucosisporites baccatus* Staplin; Neves *et al.*, Pl. 4, Fig. 5.
 1974 *Verrucosisporites baccatus* Staplin; Neves & Ioannides, Pl. 5, Fig. 18.
 1977 *Verrucosisporites baccatus* Staplin; Clayton *et al.*, p. 43, Pl. 11, Fig. 3.
 1991 *Verrucosisporites baccatus* Staplin; Ravn, Pl. 4, Fig. 8.
 2010 *Verrucosisporites baccatus* Staplin; Owens *et al.*, p. 31, Pl. 1, Fig. 6.
 2010 *Verrucosisporites baccatus* Staplin; Pérez Loinaze, p. 107, Pl. 1, Fig. 9.
 2016 *Verrucosisporites baccatus* Staplin; Lopes *et al.*, p. 65, Pl. 1, Fig. 12.

Description: Miospores, radial, trilete; amb subcircular; exine thin; minutely granulose with discrete, unevenly distributed, verrucae, height: < 1 µm; suturæ distinct, straight, simple; contact areas often exhibit fewer verrucae; occasional compression folds.

Dimensions: Length: 42 (59) 85 µm, width: 30 (44) 76 µm (30 specimens).

NWMF borehole distribution: 500.98 to 43.99 m depths.

Remarks: Conforms closely to the description by Staplin (1960), although the NWMF borehole spores are smaller than those recorded by Staplin (1960; 70–104 µm), which were oxidised and so may have expanded in size during processing.

Verrucosisporites congestus Playford 1963

Plate 4 Figure v

- 1963 *Verrucosisporites congestus* Playford, p. 13, Pl. 2, Figs. 11–13.
- 1969 *Verrucosisporites* cf. *congestus* Playford; n° 2887 of Lanzoni & Magloire, Pl. I, Figs. 11, 12.
- 1969 *Verrucosisporites congestus* Playford; Varma, Pl. 1, Figs. 13, 14, 18.
- 1980 *Verrucosisporites congestus* Playford; Van der Zwan, pp. 215-216, Pl. 25, Figs. 1-5.
- 1988 *Verrucosisporites nitidus* (Naumova) Playford; Higgs *et al.*, p. 62, Pl. 6, Fig. 1.
- 1994 *Verrucosisporites congestus* Playford; Turnau *et al.*, p. 293, Pl. 1, Fig. 1.
- 2000 *Verrucosisporites congestus* Playford; Melo & Loboziak, p. 156, Pl. 1, Fig. 6.
- 2010 *Verrucosisporites congestus* Playford; Pérez Loinaze, p. 107, Pl. 1, Fig. 10.
- 2012 *Verrucosisporites congestus* Playford; Playford & Melo, pp. 21-22, Pl. 3, Figs. 10-12.
- 2015 *Verrucosisporites congestus* Playford; Ariana-Sab *et al.*, Pl. 4, Figs. 4, 7.

Description: Miospores, radial, trilete; amb subcircular to irregular; exine: 2 to 4 μm , laevigate with discrete, regularly distributed, verrucae, height: 1 (5) 9.5 μm (105 verrucae) with polygonal bases, width: 2 (8) 25 μm (95 bases) and rounded, smooth tops; suturae straight, simple.

Dimensions: Length: 30 (57) 82 μm , width: 23 (42) 60 μm (10 specimens).

NWMF borehole distribution: 491.43 to 90.33 m depths.



Figure 90. Verrucae of *Verrucosisporites congestus*.

Verrucosisporites depressus Winslow 1962

Plate 4 Figure w

- 1962 *Verrucosisporites depressus* Winslow, p. 63, Pl. 19, Fig. 7.
- 1978 *Verrucosisporites tuberculatus* (Kedo) Turnau, p. 7, Pl. 1, Fig. 13.
- 1980 *Verrucosisporites depressus* Winslow; Van der Zwan, pp. 216–217, Pl. 23, Figs. 2-7.
- 1994 *Verrucosisporites depressus* Winslow; Turnau *et al.*, p. 293, Pl. 1, Figs. 2 a, b.
- 2000 *Verrucosisporites depressus* Winslow; Melo & Loboziak, p. 156, Pl. 1, Fig. 8.
- 2012 *Verrucosisporites depressus* Winslow; Playford & Melo, p. 22, Pl. 3, Figs. 13-15.

Description: Miospores, radial, trilete; amb subcircular; exine thin, laevigate with discrete, densely distributed, dome topped verrucae, height: <1 µm; suturae straight, simple.

Dimensions: Length: 31 (37) 45 µm, width: 24 (32) 39 µm (30 specimens).

NWMF borehole distribution: 501.18 to 56.84 m depths.

Remarks: Conforms closely to the description by Winslow (1962), although the NWMF borehole spores are smaller than those recorded by Winslow (1962; 52.5 to 72 µm), which were oxidised and so may have expanded in size during processing.

Verrucosisporites gibberosus (Hacquebard) Higgs *et al.* 1988

Plate 4 Figure x

- 1957 *Raistrickia? gibberosa* Hacquebard, p. 310, Pl. 2, Fig. 10.

- 1963 *Pustulatisporites gibberosus* (Hacquebard) Playford, Pl. 3, Figs. 18-20.
 1968 *Verrucosisporites scoticus* Sullivan, p. 121, Pl. 25, Figs. 11, 12.
 1971 *Pustulatisporites gibberosus* (Hacquebard) Playford; Johnson & Marshall, Pl. 23, Fig. 6.
 1978 *Pustulatisporites gibberosus* (Hacquebard) Playford; Turnau, Pl. 1, Figs. 26, 27.
 1988 *Verrucosisporites gibberosus* (Hacquebard) Higgs *et al.*, p. 62, Pl. 6, Fig. 5.
 2012 *Verrucosisporites gibberosus* (Hacquebard) Higgs *et al.*; Playford & Melo, pp. 22-23, Pl. 3, Figs. 16-18.

Description: Miospores, radial, trilete; amb subcircular to convexly triangular; exine: 1 to 3 μm , laevigate with straight- to slightly tapering-sided, round-topped, discrete, evenly spaced verrucae, height: 1 (3.5) 9 μm , base width: 1.5 (5) 11.5 μm (107 elements); suturae simple, straight.

Dimensions: Length: 31 (43) 64 μm , width: 25 (36) 51 μm (19 specimens).

NWMF borehole distribution: 501.11 to 253.41 m depths.

Comparisons: *Pustulatisporites dolbii* Higgs *et al.* 1988 appears like *V. gibberosus* but the verrucae are shorter with narrower bases, they are of variable density, occasionally their bases may touch and they have round or flat tops.



Figure 91. Various shaped verrucae of *Verrucosisporites gibberosus*.

Verrucosisporites irregularis Phillips & Clayton 1980

Plate 5 Figure a

- 1980 *Verrucosisporites irregularis* Phillips & Clayton, p. 126, Figs. 8 O, P, T.

- 1988 *Verrucosisporites irregularis* Phillips & Clayton; Higgs *et al.*, p. 62, Pl. 5, Figs. 18, 19.
- 2005 *Verrucosisporites irregularis* Phillips & Clayton; Dueñas & Césari, p. 144, Fig. 2 c.
- 2012 *Verrucosisporites irregularis* Phillips & Clayton; Playford & Melo, pp. 23-24, Pl. 4, Figs. 1, 2.

Description: Miospores, radial, trilete; amb subcircular to convexly triangular; exine thin: < 1 to 3 μm , laevigate with densely distributed, irregular verrucae, height: 1 (2) 3 μm (27 verrucae), base width: 2 to 3 μm (10 bases), with pointed, rounded, flattened or bulbous tops, and tapering or parallel sides, mostly discrete although some fuse to form short ridges; suturae straight, simple; occasional compression folds.

Dimensions: Length: 36 (58) 85 μm , width: 26 (48) 62 μm (9 specimens).

NWMF borehole distribution: 465.04 to 54.56 m depths.



Figure 92. Irregular verrucae of *Verrucosisporites irregularis*.

***Verrucosisporites nitidus* Playford 1963**

Plate 5 Figure b

- non 1953 *Lophotriletes grumosus* Naumova, p. 57, Pl. 7, Figs. 14, 15.
- 1956 *Lophotriletes* aff. *grumosus* Naumova; Ishchenko, p. 40, Pl. 7, Fig. 74.
- 1963 *Converrucosisporites parvinodosus* Playford, p. 15, Pl. 3, Figs. 7-9.
- 1963 *Verrucosisporites nitidus* (Naumova) Playford, pp. 13–14, Pl. 3, Figs. 3-6.
- 1963 *Verrucosisporites congestus* Playford, p. 13, Pl. 2, Figs. 11-13.
- 1964 *Verrucosisporites grumosus* (Naumova) Sullivan, pp. 1252-1253, Pl. 1, Figs. 9-15.
- 1969 *Verrucosisporites nitidus* (Naumova) Playford; Varma, p. 306, Pl. 1, Fig. 15.

- 1970 *Verrucosisporites nitidus* (Naumova) Playford; Clayton, p. 592, Pl. 4, Fig. 7.
- 1970 *Verrucosisporites nitidus* (Naumova) Playford; Dolby & Neves, p. 637, Pl. 1, Fig. 8.
- 1971 *Verrucosisporites nitidus* Playford; Playford, pp. 15-16, Pl. 3, Figs. 1-6.
- 1972 *Verrucosisporites nitidus* (Naumova) Playford; Bertelsen, p. 30, Pl. 3, Figs. 9, 10.
- 1973 *Verrucosisporites nitidus* (Naumova) Playford; Neves *et al.*, Pl. 3, Fig. 9.
- 1974 *Verrucosisporites nitidus* Playford; Neves & Ioannides, Pl. 6, Fig. 2.
- 1975 *Verrucosisporites nitidus* (Naumova) Playford; Higgs, Pl. 3, Figs. 7-9.
- 1975 *Verrucosisporites nitidus* (Naumova) Playford; Turnau, Pl. 2, Fig. 5.
- 1977 *Verrucosisporites nitidus* (Naumova) Playford; Clayton *et al.*, p. 29, Pl. 4, Figs. 19-20, p. 29, Pl. 5, Fig. 6, p. 33, Pl. 6, Fig. 15.
- 1977 *Verrucosisporites nitidus* (Naumova) Playford; Keegan, p. 553, Pl. 3, Figs. 1, 2, 4, 7, 10, 13.
- 1977 *Verrucosisporites nitidus* (Naumova) Playford; Owens *et al.*, Pl. 1, Fig. 13.
- 1978 *Verrucosisporites nitidus* (Naumova) Playford; Playford, p. 116, Pl. 3, Figs. 20-22.
- 1978 *Verrucosisporites nitidus* (Naumova) Playford; Turnau, Pl. 1, Fig. 12.
- 1980 *Verrucosisporites nitidus* Playford; Phillips & Clayton, Figs. 8 R-S.
- 1980 *Verrucosisporites nitidus* Playford; Van der Zwan, p. 126, Pl. 24, Figs. 1-5.
- 1984 *Verrucosisporites nitidus* Playford; Byvscheva *et al.*, p. 39, Pl. 1, Figs. 1, 2.
- 1984 *Verrucosisporites nitidus* (Naumova) Playford; Higgs & Clayton, p. 23, Pl. 1, Figs. 15, 16.
- 1984 *Verrucosisporites nitidus* (Naumova) Playford; Scot *et al.*, p. 313, Fig. 2 f.
- 1985 *Verrucosisporites nitidus* (Naumova) Playford; Clayton, p. 23, Fig. 2 e.
- 1987 *Verrucosisporites nitidus* Playford; Utting, Pl. 2, Fig. 2.
- 1988 *Verrucosisporites nitidus* (Naumova) Playford; Avchimovitch *et al.*, p. 175, Pl. 2, Figs. 5, 6.
- 1988 *Verrucosisporites nitidus* (Naumova) Playford; Higgs *et al.*, p. 62, Pl. 6, Figs. 2-4, non Fig. 1.
- 1988 *Verrucosisporites nitidus* (Naumova) Playford; McNestry, Pl. 1, Fig. 3.
- 1988 *Verrucosisporites nitidus* (Naumova) Playford; Turner & Spinner, Pl. 3, Fig. 5.

- 1990 *Verrucosisporites mesogrumosus* (Kedo) Byvscheva; Clayton & Turnau, Pl. 2, Figs. 4, 6.
- 1990 *Verrucosisporites nitidus* Playford; Playford, Pl. 2, Figs. 5, 6.
- 1992 *Verrucosisporites nitidus* (Naumova) Playford; Avchimovitch, Pl. 11, Fig. 11.
- 1992 *Verrucosisporites nitidus* (Naumova) Playford; Higgs *et al.*, Pl. 1, Fig. 1.
- 1993 *Verrucosisporites nitidus* Playford; Playford & McGregor, p. 22, Pl. 9, Figs. 1, 2.
- 1994 *Verrucosisporites nitidus* Playford; Turnau *et al.*, pp. 290-291, Pl. 1, Figs. 13-16.
- 1996 *Verrucosisporites nitidus* Playford; Higgs, pp. 279-280, Pl. 1, Figs. 13-15.
- 1997 *Verrucosisporites nitidus* (Naumova) Playford; Carson & Clayton, Pl. 1, Fig. 4.
- 2000 *Verrucosisporites nitidus* Playford; Melo & Loboziak, p. 156.
- 2002 *Verrucosisporites nitidus* (Naumova) Playford; Higgs *et al.*, p. 150, Pl. 2, Fig. 11.
- 2002 *Verrucosisporites nitidus* (Naumova) Playford; Stephenson *et al.*, p. 106, Fig. 10, number 2.
- 2005 *Verrucosisporites nitidus* Playford; Dueñas & Césari, pp. 143-144, Fig. 2 M.
- 2005 *Verrucosisporites nitidus*; Turnau *et al.*, p. 96, Fig. 3 g.
- 2007 *Verrucosisporites nitidus* (Naumova) Playford; Higgs & Forsythe, p. 189, Pl. 1, Fig. D.
- 2008 *Verrucosisporites nitidus* (Naumova) Playford; Heal & Clayton, p. 35, Pl. 1, Fig. 4.
- 2010 *Verrucosisporites nitidus* (Naumova) Playford; Owens *et al.*, p. 31, Pl. 1, Fig. 9.
- 2012 *Verrucosisporites nitidus* Playford; Playford & Melo, p. 25, Pl. 5, Figs. 2, 3; Pl. 7, Fig. 13.

Description: Miospores, radial, trilete; amb subcircular to convexly triangular; exine: 1 to 3 µm, laevigate with discrete, evenly distributed verrucae, height: 1 (2) 4 µm (100 verrucae) with rounded tops and polygonal bases, width: 2 (4) 16 µm (95 bases); suturae straight to sinuous, simple; occasional taper point folds.

Dimensions: Length: 28 (40) 61 μm , width: 21 (33) 58 μm (16 specimens).

NWMF borehole distribution: 501.18 to 133.11 m depths.



Figure 93. (a) and (b) verrucae of *Verrucosisporites nitidus*.

***Verrucosisporites scoticus* Sullivan 1968**

Plate 5 Figure c

1968 *Verrucosisporites scoticus* Sullivan, p. 21, Pl. 25, Figs. 11, 12.

1972 *Verrucosisporites scoticus* Sullivan; Bertelsen, Pl. 4, Fig. 5.

1984 *Verrucosisporites scoticus* Sullivan; Scot *et al.*, p. 313, Fig. 2 e.

1985 *Verrucosisporites scoticus* Sullivan; Clayton, p. 23, Fig. 2 c.

Description: Miospores, radial, trilete; amb subcircular; exine thin: 1 μm , laevigate with discrete, evenly distributed verrucae, height: 1 (3) 5.5 μm (48 verrucae), base width: 1.5 (4) 7 μm (46 bases), with tapering sides and rounded to flattened tops and occasionally surmounted by a small spine; suturae straight with narrow labra.

Dimensions: Length: 29 (35) 47 μm , width: 23 (30) 40 μm (8 specimens).

NWMF borehole distribution: 501.18 to 133.11 m depths.



Figure 94. Verrucae of *Verrucosisporites scoticus*.

3.2. MEGASPORES

Genus ***DIDYMOSPORITES*** Chaloner 1958

Type species: *Didymosporites scottii* Chaloner 1958

1958 *Didymosporites* Chaloner, pp. 198-200.

Generic description: Megaspores occurring as a tetrad composed of two large thin-walled fertile spores and two minute abortive ones, all enclosed within a loose cuticular network.

Didymosporites scottii Chaloner 1958

Plate 5 Figures d and e

1952 "Two well-developed megaspores" Surange p. 84, Pl. 4, Figs. 29, 30.

1958 *Didymosporites scottii* Chaloner, p. 198, Pl. 1, Fig. 1.

1960 *Didymosporites* sp. Staplin p. 35, Pl. 1, Fig. 12.

1966 *Didymosporites scottii* Chaloner; Sullivan & Marshall, Pl. 4, Fig. 8.

1967 *Didymosporites scottii* Chaloner; Butterworth & Spinner, p. 13, Pl. 2, Figs. 15, 20.

1984a *Didymosporites scottii* Chaloner; Spinner, p. 41, Pl. 1, Figs. 10, 11.

1984b *Didymosporites scottii* Chaloner; Spinner, Pl. 4, Fig. 6.

1990 *Didymosporites scottii* Chaloner; Hemsley, pp. 143-151, Pl. 3, Figs. 1-5, Pl. 4, Figs. 1-7, Pl. 5, Figs. 1-6.

1991 *Didymosporites scottii* Chaloner; Ravn, Pl. 2, Fig. 27.

Description: Megaspores consisting of two large spores, separated by two small abortive spores, enveloped in a membrane. Large spores: radial, trilete; amb subcircular to oval; exine thin, minutely granulose; suturae short, simple; compression folds common. Small abortive spores: radial, trilete; amb circular; laevigate; suturae simple. Enclosing cuticular membrane: thin to fibrous.

Dimensions: Total length (longest axis of tetrad): 200 (359) 470 μm (18 specimens); width of large spores: 94 (165) 225 μm (17 specimens), width of small spores: 14 (30) 60 μm (12 specimens).

NWMF borehole distribution: 501.18 m to 93.38 m depths.

Remarks: The largest spores are most commonly found as individuals, separated from the rest of the tetrad and its encompassing membrane. They could, therefore, be assigned erroneously to a species of *Calamospora* as they are morphologically similar.

Dimensions: Length: 92 (259) 680 μm , width: 87 (214) 530 μm (60 specimens).

Remarks: The age range for this species has been stated as Viséan and Namurian (Chaloner 1958) and Upper Viséan (Sullivan 1964) and it has not been recorded previously from the Tournaisian.

Affinity: *Stauropteris burntislandica* P. Bertrand 1909. The affinity was identified by Chaloner (1958) from *in situ* tetrads of *D. scottii* from *Bensonites fusiformis* Scott 1908, which had been identified as megasporangia by Surange (1952) and found in association with *S. burntislandica*.

Genus **LAEVIGATISPORITES** (Ibrahim) Potonié & Kremp 1954

Type species: *Laevigatisporites primus* (Wicher) Potonié & Kremp 1954

1933 *Laevigatisporites* Ibrahim.

1954 *Laevigatisporites* (Ibrahim) Potonié & Kremp, p. 125.

Generic description: Megaspores, radial, trilete; amb subcircular; exine thick, laevigate; suturae indistinct, terminating in curvaturae; compression folds common.

Laevigatisporites cf. cheveriensis (Bell) Glasspool & Scott 2005

Plate 5 Figure f

1960 *Triletes cheveriensis* Bell, p. 29, Pl. 3, Figs. 5-7; Pl. 5, Fig. 3.

2005 *Laevigatisporites cf. cheveriensis* (Bell) Glasspool & Scott, p. 224, Pl. 2, Figs. a, b.

Description: Megaspores, radial, trilete; amb circular to convexly triangular; exine thick, laevigate; sutures distinct, straight, approximately 20 µm in height, converging to form a small apical prominence, the signagula of Glasspool *et al.* (2000); a low arcuate ridge envelops the trilete.

Dimensions: Length: 485 to 520 µm (2 specimens).

NWMF borehole distribution: 470.45 to 290.75 m depths.

Remarks: Although smaller than the specimens described by Glasspool *et al.* (2000) at 900 to 1200 µm in diameter, these megaspores conform closely to the description by Glasspool & Scott (2005).

Genus ***LAGENICULA*** (Bennie & Kidston) Spinner 1969

Type species: *Lagenicula horrida* Zerndt 1934

1886 *Triletes* Bennie & Kidston.

1954 *Lagenoisporites* Potonié & Kremp, p. 152.

1962 *Dijkstraea* Pant & Srivastava, p. 98.

1961 *Rostratispora* Bharadwaj & Venkatachala, p. 25.

1969 *Lagenicula* (Bennie & Kidston) Spinner, pp. 442-443.

Generic description: Megaspores, radial, trilete, camerate; amb subcircular; intexine thin, often folded; exoexine laevigate or with verrucae, coni, spinae, pila,

bacula or more complex forms; suturae with laesurae that increase in height gradually to an apical prominence at the proximal pole, terminating in curvaturae; thickening of the exine of the contact areas, which are laevigate or with smaller elements than those on the distal surface.

Lagenicula mixta (Winslow) Wellman *et al.* 2009

Plate 5 Figure g

1962 *Triletes catenulatus* var. *mixtus* Winslow, p. 33.

2009 *Lagenicula (Triletes) mixta* (Winslow) Wellman *et al.*, pp. 52-56.

Description: The single completely opaque specimen's details were obscured; amb convexly triangular; spinae, height: 11 (12) 13 μm (5 spinae), base width: 9 (10) 11 μm (5 bases).

Dimensions: Length: 760 μm , width: 650 μm (1 specimen).

NWMF borehole distribution: 418.85 m depth only.

Remarks: The outline of the NWMF borehole specimen appears similar to spores of *Lagenicula mixta*. The dimensions given by Wellman *et al.*, (2009; length 561 (808) 1001 μm and width 451 (648) 858 μm) incorporate the dimensions of the NWMF borehole spore.

Genus ***SETISPORA*** (Butterworth & Spinner) Spinner 1982

Type species: *Setispora pseudoreticulata* Butterworth & Spinner 1967

1967 *Setispora* Butterworth & Spinner, pp. 15-16.

1982 *Setispora* (Butterworth & Spinner) Spinner, pp. 304-306.

Generic description: Megaspores, radial, trilete; amb subspherical; exine thick, folded or irregularly thickened, laevigate or sculptured; suturae distinct, straight or slightly wavy with characteristic raised laesurae formed by densely distributed or fused fimbriae; contact areas distinct, laevigate.

***Setispora pannosa* (Alvin) Spinner 1982**

Plate 5 Figures h and i

- 1933 *Lagenicula subpilosa* Ibrahim.
- 1933 *Setosi-sporites subpilosus* Ibrahim, p. 27, Pl. 5, Fig. 40.
- 1944 *Triletes subpilosus* (Ibrahim) Schopf *et al.*, p. 26.
- 1946 *Triletes subpilosus* (Ibrahim) Dijkstra, pp. 46-47, Pl. 11, Figs. 116-128.
- 1955 *Lagenicula subpilosa* (Ibrahim) Potonié & Kremp, p. 120, Pl. 4, Fig. 21.
- 1966 *Triletes pannosus* Alvin, pp. 488-490, Pl. 76, Figs. 1-6.
- 1982 *Setispora pannosus* (Alvin) Spinner, pp. 308-310, Pl. 2, Figs. 1, 2; Pl. 3, Figs. 1-3.
- 1987 *Lagenicula subpilosa* (Ibrahim) Potonié & Kremp; Bartram, p. 192, Fig. 3 a.
- 1990 *Setispora pannosa* Spinner; Bateman & Rothwell, p. 147, Fig. 9 a.
- 1992 *Setispora pannosa* Spinner; Bateman, p. 42, Pl. 5, Figs. 50-53.
- 1996 *Lagenicula subpilosa* (Ibrahim) Potonié & Kremp; Turner & Spinner, Pl. 6, Figs. 1-3, 5, 6, 8.

Description: Megaspores, radial, trilete; amb circular; exine thick with spinae, discrete, recurved, tapering, often to an oval termination, height: 120 (170) 275 μm (17 spinae), with swollen bases exhibiting 'buttressing'; suturae form a gula with a basal constriction, surrounded by a laevigate portion leading to several narrow rows of densely distributed spinae that become less densely spaced across the rest of the proximal and distal faces.

Dimensions: Length: 370 (1288) 2000 μm (17 specimens).

NWMF borehole distribution: 501.11 to 49.88 m depths.

Affinity: *Oxroadia conferta* Bateman 1992. The affinity was identified from *in situ* spores that had been macerated from an intact cone borne by *O. conferta* from Oxroad Bay, Scotland (Bateman 1992, pp. 41 to 42).

Setispora pseudoreticulata (Butterworth & Spinner) Spinner 1982

Plate 5 Figure j

1967 *Setispora pseudoreticulata* Butterworth & Spinner, p. 16, Pl. 4, Figs. 1, 3, 4, 6.

1982 *Setispora pseudoreticulata* (Butterworth & Spinner) Spinner, pp. 306-308, Pl. 1, Figs. 1-4.

Description: As the NWMF borehole yielded no complete specimens, the characteristic reticulate nature of the exine forms the basis for this identification.

Spine length: 115 (144) 160 µm (5 spines from 2 specimens).

Dimensions: N/A.

NWMF borehole distribution: 477.71 to 100.59 m depths.

Genus **SETOSISPORITES** (Ibrahim) Dybová-Jachowicz *et al.* 1979

Type species: *Setosisporites hirsutus* (Loose) Ibrahim 1933

1933 *Setosi-sporites* Ibrahim.

1954 *Setosisporites* Potonié & Kremp, p. 152.

1979 *Setosisporites* Dybová-Jachowicz *et al.* p. 420.

Generic description: Megaspores, radial, trilete; amb circular to oval; exine thick, laevigate or with bacula, verrucae or coni that may be so densely distributed that

their bases touch; suturae distinct, terminating in curvaturae and with a distinctive basally constricted subgula at the central apex; contact areas laevigate or with small verrucae.

***Setosisporites* sp. A**

Plate 5 Figure k

Description: Megaspores, radial, trilete; amb convexly triangular; minutely granulose with discrete, irregularly spaced verrucae that diminish in height: 9 to 3 μm , and base width: 7 to 3 μm from the amb to the centre of proximal face; sutures distinct, straight, converging to form a small apical prominence (signagula) and terminating in curvaturae.

Dimensions: Length: 250 to 320 μm , width: 190 to 235 μm (2 specimens).

NWMF borehole distribution: 472.81 m to 430.37 m depths.

Comparisons: These spores are not identified as those listed below for the reasons outlined:

- *S. aries* (Winslow) Dybová-Jachowicz *et al.* 1979 has capilli and spinae of height: 35 to 125 μm on the distal face, has a signangula that is significantly larger (200 to 460 μm) and is too large with a diameter of 920 to 1200 μm .
- *S. brevispinosus* (Zerndt) Brzozowska 1968 has a sculpture of short spines and not verrucae.
- *S. clavatus* (Brzozowska) Spinner 1969 has a sculpture of pila and not verrucae.
- *S. dybovae* Karczewska 1967 has a laevigate distal face and is too large with a diameter of 500 to 937 μm .
- *S. hirsutus* (Loose) Ibrahim 1933 has evenly distributed, branched and unbranched sculptural elements length: 35 to 50 μm , width: 8 to 20 μm and is too large with a diameter of 500 to 800 μm .

- *S. indianensis* (Chaloner) Spinner 1969 has a sculpture of grana and coni, height: 20 µm, base width: 10 to 15 µm and is too large with a diameter of 875 to 1615 µm.
- *S. pilatus* Spinner 1965 has club-shaped pili and bacula of height: 10 to 15 µm and base width: 2 to 6 µm and is too large with a diameter of 450 to 700 µm.
- *S. praetextus* (Zerndt) Potonié & Kremp 1955 is too large with a diameter of 800 to 1800 µm.
- *S. pseudotenuispinosus* Piérart 1958 has a larger gula (height: 80 to 150 µm, width: 80 to 200 µm) and grana to 5 µm in diameter on the distal face.
- *S. reticulatus* Karczewska 1967 has a reticulum with round and ovate lumina and is too large with a diameter of 350 to 587 µm.
- *S. splendidus* (Zerndt) Spinner 1969 has mammillate coni, height: 12 to 35 µm and base width: 30 to 75 µm and is too large with a diameter of 935 to 1625 µm.

Genus ***TRIANGULATISPORITES*** (Potonié & Kremp) Karczewska 1976

Type species: *Triangulatisporites triangulatus* (Zerndt) Potonié & Kremp 1954

1954 *Triangulatisporites* Potonié & Kremp, p. 163.

1976 *Triangulatisporites* (Potonié & Kremp) Karczewska, pp. 342-343.

Generic description: Megaspores, radial, trilete, camerate; amb circular, subtriangular or triangular; intexine subcircular, proximally laevigate to minutely granulose, distally usually reticulate, but may be microreticulate, vermiculate or almost laevigate; exoexine laevigate or minutely granulose, proximal face reticulate, granulate, vermiculate, tuberculate, verrucate-conate or minutely granulose, distal face is variably reticulate; equatorial zona, finely granular, reticulate, or mostly radially striate, usually folded; suturae straight or sinuous, thickened contact areas.

Triangulatisporites membranatus Butterworth & Spinner 1967

Plate 5 Figure I

1967 *Triangulatisporites membranatus* Butterworth & Spinner, pp. 17-18, Pl. 3, Figs. 8-10; Pl. 4, Figs. 2, 5, 10.

1988 *Triangulatisporites membranatus* Butterworth & Spinner; Turner & Spinner, Pl. 8, Figs. 1, 3.

Description: Megaspore, radial, trilete, camerate; amb circular to convexly triangular; laevigate with discrete, densely distributed bacula and verrucae, height: 2 µm on the proximal face, and discrete, densely distributed bacula, height to 12 µm on the distal face, sculpture continuous from the central body across to the equatorial zona; suturae slightly sinuous with raised laesurae, bordered by an arcuate ridge forming the curvaturae; taper-point folds.

Dimensions: Total length: 335 µm, width: 255 µm, inner body length: 250 µm, width: 205 µm (1 specimen).

NWMF borehole distribution: 290.75 m depth only.

Remarks: Conforms to the description by Butterworth & Spinner (1967) although the NWMF borehole spore is smaller than those recorded by Butterworth & Spinner (1967; 450 (539) 650 µm), which were oxidised and so may have expanded in size during processing.

Genus ***TUBERCULATISPORITES*** (Ibrahim) Potonié & Kremp 1954

Type species: *Tuberculatisporites tuberosus* (Ibrahim) Ibrahim 1933

1933 *Tuberculatisporites* Ibrahim.

1954 *Tuberculatisporites* (Ibrahim) Potonié & Kremp, p. 138.

Generic description: Megaspores, radial, trilete; amb circular to rounded triangular; size: 400-3000 μm in diameter; exine with sparsely distributed coni, spinae or verrucae; suturae simple; contact faces laevigate or with smaller elements.

Tuberculatisporites mamillarius (Bartlett) Potonié & Kremp 1955

Plate 5 Figure m

1928 *Tuberculatisporites mamillarius* Bartlett.

1955 *Tuberculatisporites mamillarius* (Bartlett) Potonié & Kremp.

1985 *Tuberculatisporites mamillarius* (Bartlett) Potonié & Kremp; Collinson *et al.*, p. 379, Figs. 1 c, g.

1987 *Tuberculatisporites mamillarius* (Bartlett) Potonié & Kremp; Bartram, p. 192, Fig. 3 f.

Description: As no complete specimens were found in the NWMF borehole sediments, the outline shape and sutures cannot be described. The identification is based on the distinctive sculpture. This consists of discrete, circular, broad-based verrucae, each with a centrally-placed spinose projection, verrucae width: 36 (49) 73 μm (12 verrucae), total height: 35 (47) 66 μm (12 spines).

Dimensions: N/A

NWMF borehole distribution: 115.33 m to 49.88 m depths.

Remarks: Spinner (1968) gave the maximum diameter of the spore as between 500 and 3000 μm . The long edge of one of the NWMF borehole spores measured 550 μm , which falls within this size range. Horst (1955) described the sculpture of *T. mamillarius* (at 40 to 65 μm) as being larger than that of *T. brevispiculus* (at 16 to 18 μm ; Pendleton & Wellman 2012) and forms the basis of this species identification.

Genus **UNIDENTIFIED****Spore Type D** Spinner 1983

Plate 5 Figure n

1983 Spore Type D Spinner, p. 128, Pl. 4, Figs. 1, 2.

Description: Megaspores, radial, trilete; amb subcircular; intexine thin, laevigate, conformable with the amb; exoexine thin, minutely granulose with discrete, densely distributed verrucae, height: < 1 µm; suturae simple; compression folds common.

Dimensions: Total length: 50 (194) 510 µm, width: 35 (165) 435 µm, inner body length: 45 (151) 335 µm, width: 40 (125) 320 µm (49 specimens).

NWMF borehole distribution: 496.62 to 54.56 m depths.

3.3. POLLENGenus **REMYSPORITES** Butterworth & Williams 1958

Type species: *Remysporites magnificus* (Horst) Butterworth & Williams 1958

1958 *Remysporites* Butterworth & Williams, p. 386-387.

Generic description: Monosaccate pollen, radial, trilete, camerate; amb circular to oval; intexine thin, circular; exoexine laevigate; compression folds common.

Remysporites magnificus (Horst) Butterworth & Williams 1958

Plate 5 Figure o

- 1943 *Triletes (Zonales) magnificus* Horst (thesis), Text-Fig. 37.
- 1955 *Endosporites magnificus* (Horst) Potonié & Kremp *In*: Horst, p. 194, Pl. 21, Fig. 37.
- 1956 *Endosporites magnificus* (Horst) Potonié & Kremp, p. 161.
- 1958 *Remysporites magnificus* (Horst) Butterworth & Williams, pp. 387-388, Pl. 4, Figs. 7-9.
- 1960 *Remysporites albertensis* Staplin, p. 35, Pl. 8, Figs. 8, 10.
- 1961 *Remysporites magnificus* (Horst) Butterworth & Williams; Bharadwaj & Venkatachala, p. 40, Pl. 10, Fig. 149.
- 1961 *Remysporites magnificus* (Horst) Butterworth & Williams; Neves, p. 272, Pl. 34, Fig. 1.
- 1967 *Remysporites magnificus* (Horst) Butterworth & Williams; Smith & Butterworth, p. 278, Pl. 23, Fig. 8.
- 1968 *Remysporites magnificus* (Horst) Butterworth & Williams; Neville, Pl. 2, Fig. 3.
- 1973 *Remysporites magnificus* (Horst) Butterworth & Williams; Neves *et al.*, Pl. 5, Fig. 18.
- 1977 *Remysporites magnificus* (Horst) Butterworth & Williams; Clayton *et al.*, p. 49, Pl. 14, Fig. 17.
- 1989 *Remysporites magnificus* (Horst) Butterworth & Williams; Brindley & Spinner, p. 220, Fig. 5, number 21, p. 224, Fig. 7, number 12.
- 1991 *Remysporites magnificus* (Horst) Butterworth & Williams; Ravn, Pl. 29, Fig. 5.
- 1993 *Remysporites magnificus* (Horst) Butterworth & Williams; Turner & Owens, p. 194, Fig. 3, number 10.
- 2010 *Remysporites magnificus* (Horst) Butterworth & Williams; Owens *et al.*, p. 37, Pl. 3, Fig. 5.

Description: Monosaccate pollen, radial, trilete, camerate; amb subcircular; intexine thin, laevigate, conformable with the amb; exoexine thin with densely distributed verrucae and coni; suturae simple, straight; taper point folds common.

Dimensions: Total length: 68 (129) 200 μm , width: 50 (103) 160 μm ; inner body length: 43 (100) 175 μm , width: 35 (77) 133 μm (18 specimens).

NWMF borehole distribution: 500.98 m to 54.56 m depths.

Remarks: The intexine, if found separated from its exoexine, resembles spores of *Punctatisporites* (see the 'Discussion' section following the *Punctatisporites* generic description).

Affinity: *Protopitys scotica* Walton 1957. Smith (1962) reported *in situ* spores from sporangia on a fertile shoot from Loch Humphrey Burn, Dumbartonshire, and figured them in Plate 35 Figs. 1 to 3 of slide FSC 1371. For further details refer to Section 5.5.3 and Figure 113.

3.4. ACRITARCHS

Genus **ACANTHOTRILETES** (Naumova) Potonié & Kremp 1954

Type species: *Acanthotriletes ciliatus* (Knox) Potonié & Kremp 1954

1939 *Acanthotriletes* Naumova, p. 355.

1949 *Acanthotriletes* Naumova; Naumova, p. 54.

1954 *Acanthotriletes* (Naumova) Potonié & Kremp, p. 133.

1976 *Acanthotriletes* Naumova 1939 ex. 1949; Jansonius & Hills, p. 25.

2006 *Acanthotriletes* Naumova 1939 ex. 1949; Jansonius *et al.*, p. 5538.

Generic description: Algal palynomorphs, radial, trilete with densely distributed, tapering, round-tipped spinae that measure longer than twice the diameter.

Remarks: Jansonius & Hills (1976) assigned the genus *Acanthotriletes* to (Lower Palaeozoic) acritarchs rather than to the spores of higher plants on the basis of the original type specimen *Acanthotriletes primigenus* Naumova 1949 being an acritarch. Later, Potonié & Kremp (1954) designated *Acanthotriletes ciliatus* (*Spinospores ciliatus* Knox 1950) as the (neotype) type species.

***Acanthotriletes socraticus* Neves & Ioannides 1974**

Plate 5 Figure p

1974 *Acanthotriletes socraticus* Neves & Ioannides, p. 75, Pl. 5, Figs. 14, 16.

1978 *Acanthotriletes socraticus* Neves & Ioannides; Turnau, Pl. 1, Figs. 18, 19.

1994 *Acanthotriletes socraticus* Neves & Ioannides; Mahdi & Butterworth, p. 163, Fig. 6, number 17.

Description: Algal palynomorphs, radial, trilete; amb subcircular, oval or convexly triangular; exine thin: 1 to 2 μm , laevigate with robust, discrete, sparsely (rare) to densely spaced (common), tapered spinae and coni with pointed, blunt, or recurved tips, spinae length: 1 (3) 7 μm (212 spinae), longer spinae frequently exhibit expanded bases, base width: 0.5 (2) 5 μm (91 bases), base height: 1 (3) 4 μm (10 bases); suturae simple; taper point folds frequent.



Figure 95. Diagram to define the dimensions of the spinae with expanded bases of *Acanthotriletes socraticus*.

Dimensions: Length: 27 (37) 52 μm , width: 15 (30) 50 μm (53 specimens).

NWMF NWMF borehole distribution: 500.98 to 73.95 m depths.

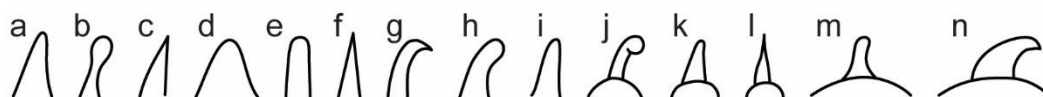


Figure 96. (a) Most common (b) few (c) some and (d) sparse spinae (e) to (i) examples of the variability of the spinae and (j) to (n) spinae with expanded bases of *Acanthotriletes socraticus*.

Genus **CARBANEULETES** Spinner 1983

Type species: *Carbaneuletes circularis* Spinner 1983

1983 *Carbaneuletes* Spinner, pp. 118-120.

Generic description: Algal palynomorphs; amb circular to elliptical; size: 300 to 600 μm in diameter; two-layered wall, the outer layer is characterised by muri and lumina of variable dimensions forming a reticulate pattern, the inner layer is finely granulose.

Carbaneuletes* cf. *micromuratus

Plate 5 Figure q

Description: Algal palynomorphs, alete; amb spherical to reniform; exine thin; outer layer has a fine reticulum of narrow muri and lumina with circular to polygonal outlines, the inner layer is minutely granulose; folds are common.

Dimensions: Length: 60 (74) 88 μm (13 specimens), width: 32 (54) 73 μm (12 specimens).

NWMF borehole distribution: 465.04 m to 39.11 m depths.

Remarks: The small size of the muri and lumina distinguish *C. micromuratus* from other species of *Carbaneuletes*. *C. cf. micromuratus* conforms closely to the

description of *C. micromuratus* by Spinner (1983) but the size range quoted (350 to 420 μm) is far larger than that for the NWMF borehole specimens.

3.5. EUGLENOIDS

Genus **CHOMOTRILETES** Naumova 1937

Type species: *Chomotriletes vedugensis* Naumova 1953

1937 *Chomotriletes* Naumova, p. 355.

Generic description: Algal palynomorphs; amb circular or ellipsoidal; size 30 to 70 μm in diameter; sculpture of comparatively regularly distributed concentric or spiral ridges that may bifurcate.

Chomotriletes multivittatus Playford 1978

Plate 5 Figure r

1978 *Chomotriletes multivittatus* Playford, p. 144, Pl. 13, Figs. 1-10.

1987 *Chomotriletes multivittatus* Playford; Utting, Pl. 5, Fig. 18.

Description: Algal palynomorphs, alete; amb subcircular to irregular; exine thin, laevigate with multiple (difficult to count owing to their small size) concentrically arranged costae, muri height: 0.5 to 1 μm (10 muri) < 0.5 to 1 μm apart.

Dimensions: Length: 33 (41) 49 μm , width: 27 (36) 43 (8 specimens).

NWMF borehole distribution: 472.81 to 90.33 m depths.

Chomotriletes vedugensis Naumova 1953

Plate 1 Figure s

1953 *Chomotriletes vedugensis* Naumova, p. 58, Pl. 7, Figs. 21, 22.

1996 *Chomotriletes vedugensis* Naumova; Marshall *et al.*, p. 455, Fig. 3, number 18.

Description: Algal palynomorphs, alete; amb subcircular to convexly triangular; exine thin with multiple (between 5 and 7) concentrically arranged costae, muri height: 0.5 (1) 2 μm (27 muri) < 0.5 to 1 μm apart.

Dimensions: Length: 37 (48) 64 μm , width: 32 (40) 55 μm (7 specimens).

NWMF borehole distribution: 501.18 to 77.99 m depths.

Comparison: *C. vedugensis* differs from *C. multivittatus* by its broader costae.

3.6. SCOLECODONTS

Morphotype A

Broadly triangular outline with posterior bulbous plate. Slightly to strongly concave ventral margin, concave dorsal margin, edentulate to denticulate, possessing up to 3 denticles, terminating in a hook.

Morphotype B

Like Morphotype A but anterior hooks more strongly recurved.

Morphotype C

Elongate piece with straight or slightly sinuous dentary. Many (minimum 4) denticles, ranging from low points with flattened tops or steeply posteriorly-directed tips to phylliform, rounded and irregular.

Morphotype D

Like Morphotype C but with fewer denticles (3-5 only). Denticles posteriorly-directed, anterior-most denticle is largest and often more upright.

Morphotype E

Like Morphotype D but 2 denticles only (although secondary denticles may be present). Anterior denticle largest, denticle terminations commonly sharp.

Morphotype F

Square-circular compound jaw of multiple sharp denticles arranged in a circular pattern of varying sizes.

EXPLANATION OF PLATES 1 TO 5

Scale bar = 10 μm , except where indicated. BGS sample number in brackets e.g. (SSK38112), followed by light microscope (Olympus BH-2 No. 205255) and England Finder co-ordinates.

PLATE 1

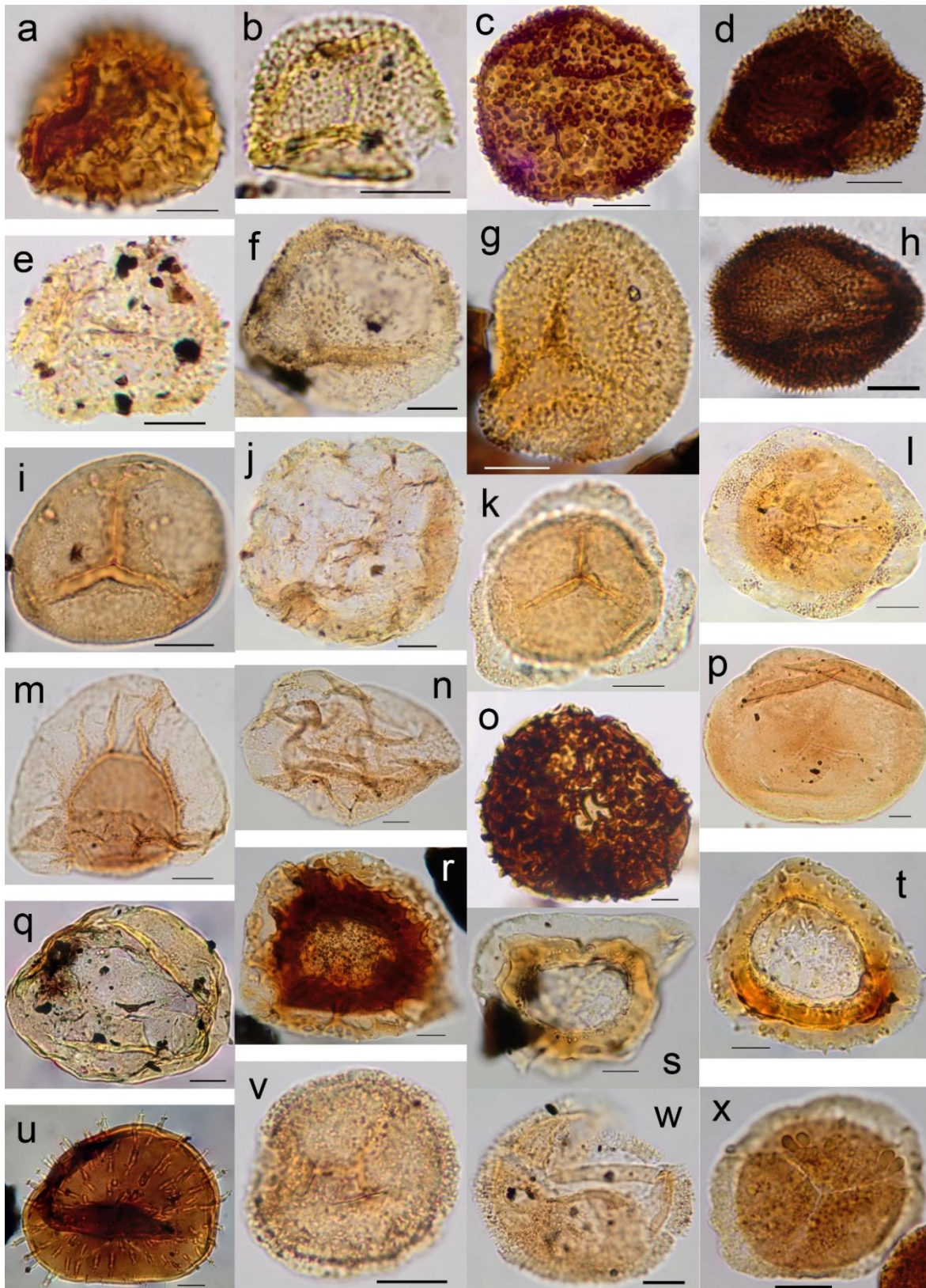


PLATE 1

- a. *Acinosporites* cf. *acanthomammillatus* (SSK39200), 126.9, 06.0, V27/0
- b. *Anaplanisporites baccatus* (SSK38002), 135.7, 11.5, Q36/2
- c. *Anaplanisporites centrosus* (SSK38112), 125.0, 09.7, R25/4
- d. *Anaplanisporites* sp. A (SSK38742), 118.0, 20.1, G18/1 (tetrad)
- e. *Anaplanisporites* sp. B (SSK38717), 129.6, 18.2, J30/2
- f. *Apiculatisporis* sp. A (SSK38394), 131.2, 10.0, R31/0
- g. *Apiculiretusispora fructicosa* (SSK37853), 118.2, 14.2, N18/2
- h. *Apiculiretusispora multisetata* (SSK38052), 115.9, 10.9, Q16/0
- i. *Apiculiretusispora nitida* (SSK39149), 106.2, 17.2, J5/4
- j. *Apiculiretusispora* sp. A (SSK38443), 127.3, 19.9, G27/2
- k. *Auroraspora asperella* (SSK37853), 124.6, 13.8, N25/0
- l. *Auroraspora macra* (SSK37853), 119.1, 05.8, V18/4
- m. *Auroraspora solisorta* (SSK39214), 132.3, 116.4, K33/3
- n. *Baculatisporites fusticulus* (SSK39149), 104.1, 18.9, H4/0
- o. *Bascaudaspora submarginata* (SSK38010), 124.9, 07.7, T25/0
- p. *Calamospora nigrata* (SSK37853), 122.1, 06.9, U22/0
- q. *Calamospora perrugosa* (SSK38017), 122.3, 08.7, S20/4
- r. *Cingulizonates bialatus* (distal face) (SSK38010), 134.0, 11.1, Q34/2
- s. *Cingulizonates bialatus* (proximal face) (SSK38114), 110.9, 13.7, N11/3
- t. *Cingulizonates* sp. A (SSK38434), 122.4, 17.9, J23/1
- u. *Claytonispora distincta* (SSK37853), 117.9, 15.6, L17/4
- v. *Colatisporites decorus* (SSK39149), 103.7, 20.8, F3/2
- w. *Colatisporites denticulatus* (SSK39149), 105.6, 10.3, R5/2
- x. *Colatisporites?* *papillatus* (SSK37863), 137.4, 12.2, P38/1

PLATE 2

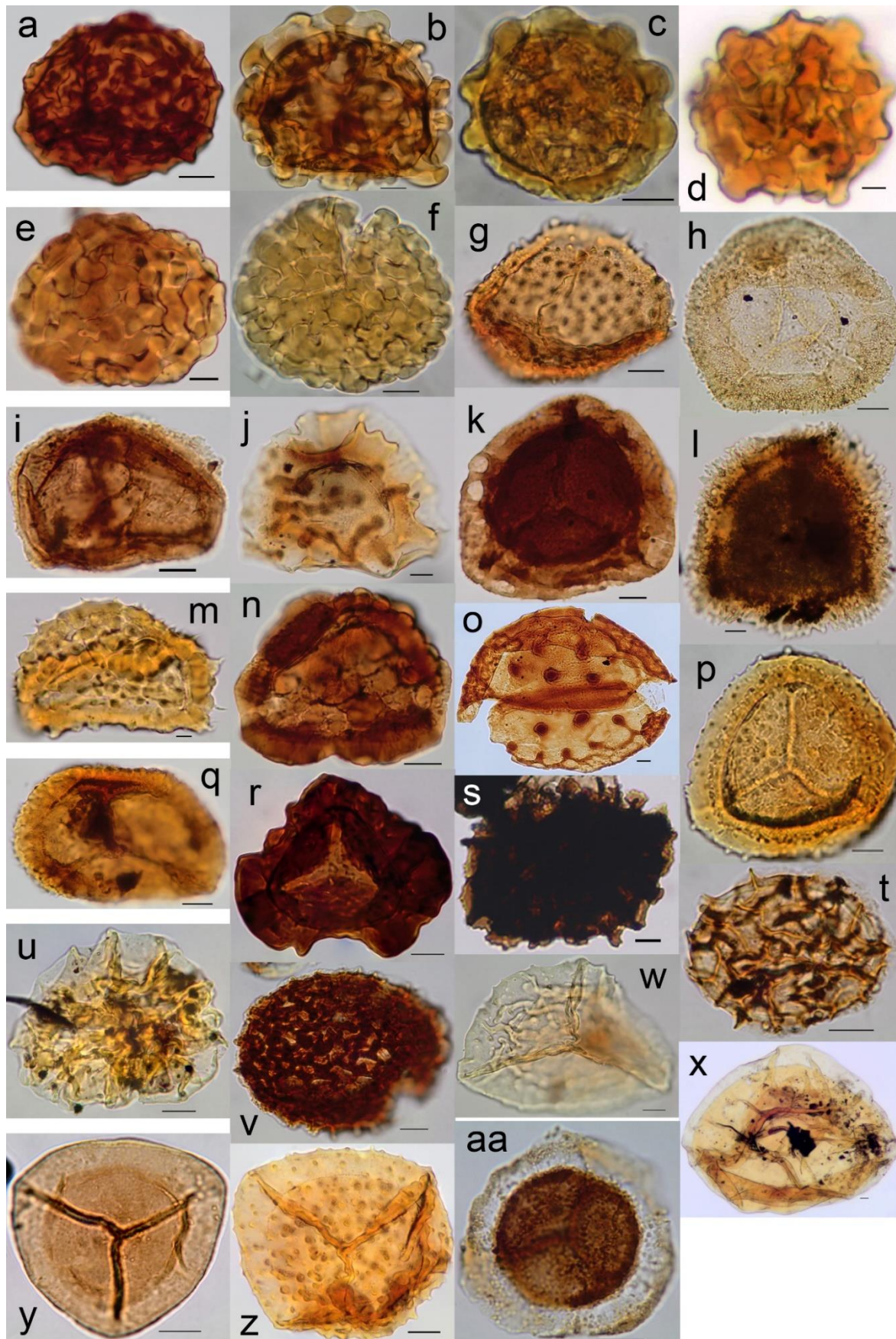


PLATE 2

- a. *Convolutispora caliginosa* (SSK37883), 136.8, 16.7, L37/2
- b. *Convolutispora circumvallata* (SSK39149), 105.2, 22.7, D5/0
- c. *Convolutispora florida* (SSK38248), 117.6, 15.1, M18/1
- d. *Convolutispora harlandii* (SSK38714), 122.2, 10.7, Q22/4
- e. *Convolutispora major* (SSK38002), 127.1, 18.2, J28/1
- f. *Convolutispora mellita* (SSK38424), 108.6, 22.3, D8/4
- g. *Crassispora aculeata* (SSK39226), 128.9, 08.9, S29/0
- h. *Crassispora trychera* (SSK38394), 130.3, 19.7, G31/0
- i. *Crassispora* cf. *trychera* (SSK39010) 135.26 m, 132.2, 16.9
- j. *Cristatisporites bellus* (SSK38723), 104.1, 17.0, K4/1
- k. *Cristatisporites echinatus* (SSK38236), 108.2, 20.6, F8/0
- l. *Cristatisporites indignabundus* (SSK38114), 130.7, 10.5, Q31/4
- m. *Cristatisporites matthewsii* (SSK38723), 100.0, 09.1, S8/0
- n. *Cristatisporites menendezii* (SSK37919), 133.2, 19.6, G34/0
- o. *Curriculumonoletes orbis* (SSK38489) 119.1, 12.5, O17.0
- p. *Cymbosporites cyathus* (SSK38774), 128.7, 07.3, U29/0
- q. *Cymbosporites magnificus* (SSK39155), 117.3, 12.0, P17/2
- r. *Densosporites variomarginatus* (SSK38239), 110.0, 07.3, U10/0
- s. *Dictyotriletes fimbriatus* (SSK38010), 112.7, 14.2, N12/2
- t. *Dictyotriletes fragmentimurus* (SSK38436), 100.8, 13.7, N1/3
- u. *Dictyotriletes pactilis* (SSK38061), 126.0, 13.8, N26/0
- v. *Dictyotriletes trivialis* (SSK37932), 130.4, 12.0, P31/0
- w. *Discernisporites irregularis* (SSK38229), 125.0, 18.2, J25/2
- x. *Discernisporites macromanifestus* (SSK38434), 106.1, 20.6, F6/0
- y. *Discernisporites micromanifestus* (SSK38495), 127.5, 09.3, S28/0
- z. *Discernisporites sullivanii* (SSK37932), 109.9, 09.7, R10/0
- aa. *Endoculeospora gradzinskii* (SSK39149), 122.8, 04.7, W23/3

PLATE 3

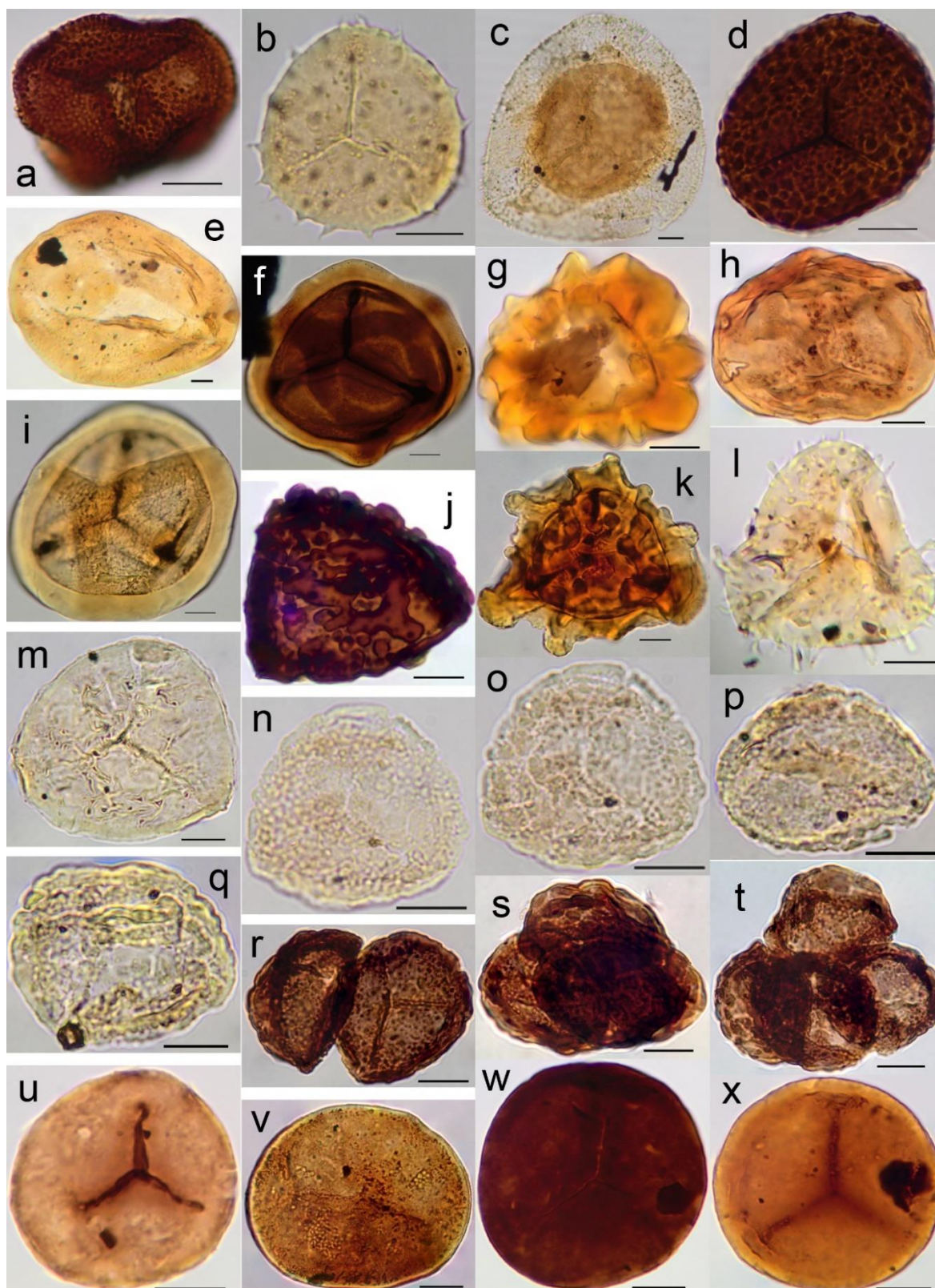


PLATE 3

- a. *Geminospora lemurata* (SSK38119), 131.8, 19.1, G32/3
- b. *Grandispora echinata* (SSK38061), 124.0, 05.5, W24/2
- c. *Grandispora microdecora* (SSK37871), 135.0, 07.6, U35/2
- d. *Granulatisporites pustulatus* (SSK38382), 132.1, 01.5, Z31/4
- e. *Insculptospora incrustata* (SSK38010), 140.9, 06.9, U42/3
- f. *Knoxisporites literatus* (SSK38662), 129.8, 06.9, U30/3
- g. *Knoxisporites polymorphus* (SSK38792), 126.1, 20.0, G26/2
- h. *Knoxisporites pristinus* (SSK39193), 111.6, 19.7, G11/0
- i. *Knoxisporites triangularis* (SSK38191), 113.2, 15.0, M13/0
- j. *Lophozonotriletes tuberosus* (SSK38408), 107.9, 14.9, M7/1
- k. *Monilospora mutabilis* (SSK38714), 111.2, 13.5, N11/3
- l. *Pilosisporites verutus* (SSK38438), 129.7, 18.8, H29/1
- m. *Plicatispora scolecophora* (SSK38424), 113.6, 07.9, T13/0
- n. *Prolycospora claytonii* (SSK38175), 119.1, 02.4, Z19/0 (proximal face)
- o. *Prolycospora claytonii* (SSK38175), 119.1, 02.4, Z19/0 (distal face)
- p. *Prolycospora claytonii* (SSK38175), 103.2, 16.3, L2/2
- q. *Prolycospora claytonii* (SSK38175), 111.3, 09.8, R11/0
- r. *Prolycospora claytonii* (SSK38190), 129.5, 17.9, J30/1 (dyad)
- s. *Prolycospora claytonii* (SSK38190), 130.6, 17.7, J31/3 (tetrad)
- t. *Prolycospora claytonii* (SSK38190), 127.8, 12.0, P28/1 (tetrad)
- u. *Punctatisporites irrasus* (SSK38479), 113.6, 13.4, N13/4
- v. *Punctatisporites? limbatus* (SSK38075), 130.6, 11.0, Q30/1
- w. *Punctatisporites planus* (SSK38479), 116.6, 13.4, N16/4
- x. *Punctatisporites solidus* (SSK38479), 110.7, 17.6, J10/0

PLATE 4

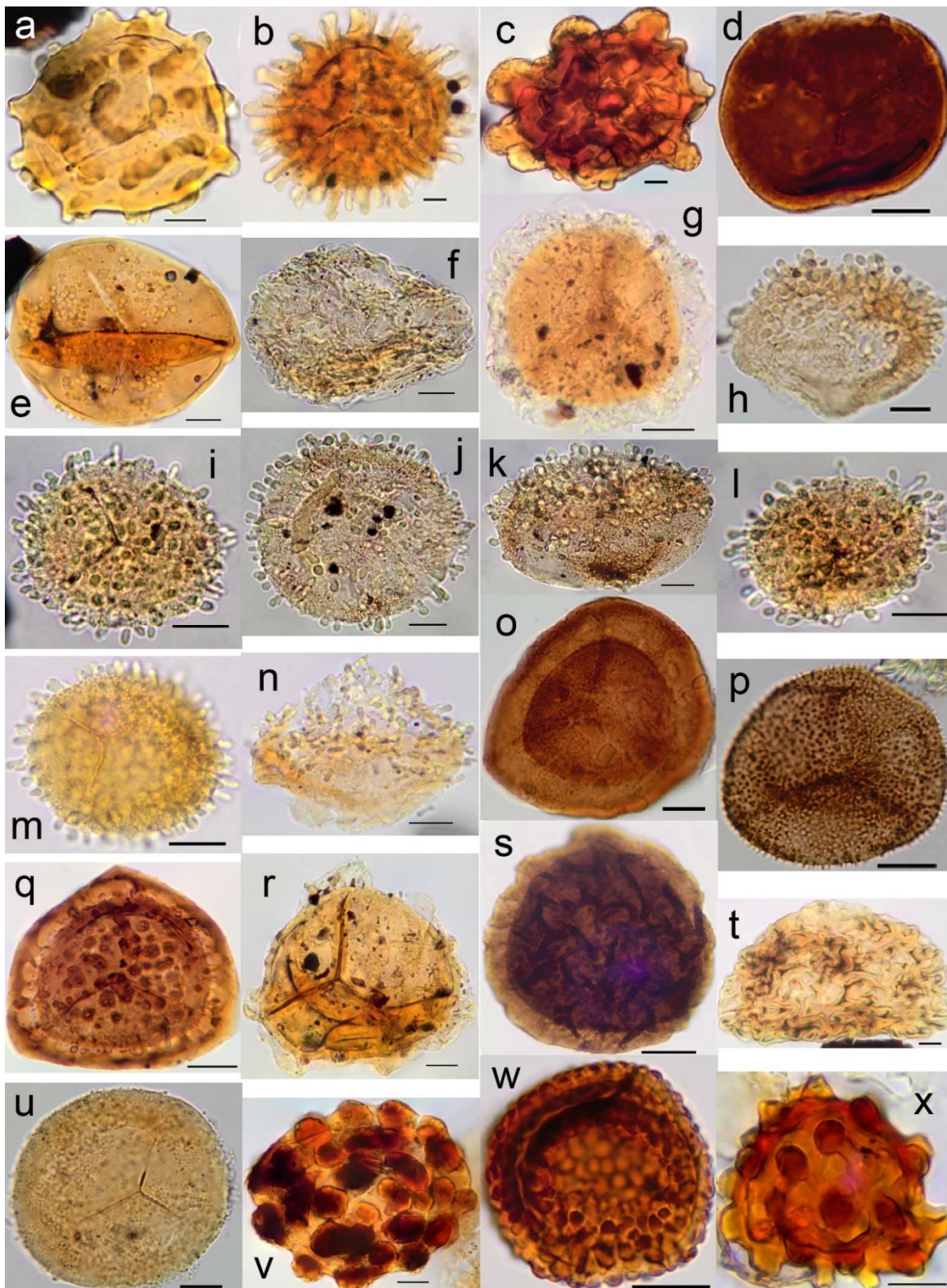


PLATE 4

- a. *Pustulatisporites dolbii* (SSK37996), 110.8, 09.5, S10/2
- b. *Raistrickia corynoges* (SSK37996), 115.8, 02.8, Z15/2
- c. *Raistrickia* cf. *ponderosa* (SSK39226), 106.1, 15.3, M6/1
- d. *Retusotriletes incohatus* (SSK37853), 115.9, 04.7, W15/4
- e. *Retusotriletes rotundus* (SSK37853), 125.0, 06.8, U25/0
- f. *Rugospora lactucosa* (SSK38774), 127.5, 08.1, X27/2
- g. *Rugospora vieta* (SSK38438), 127.3, 16.1, L28/1
- h. *Schopfites claviger* (SSK37895), 120.3, 21.2, E20/0
- i. *Schopfites claviger* (SSK38190), 127.8, 08.3, T28/1 (distal face)
- j. *Schopfites claviger* (SSK38424), 128.1, 20.2, F28/4 (distal face)
- k. *Schopfites claviger* (SSK37853), 131.4, 09.1, S31/2
- l. *Schopfites claviger* (SSK37853), 128.2, 05.5, L28/0
- m. *Schopfites claytonii* (SSK38236), 130.6, 15.0, M31/0
- n. *Schopfites delicatus* (SSK37895), 121.0, 12.1, Z21/0
- o. *Spelaeotriletes crustatus* (SSK38742), 102.2, 15.8, L1/2
- p. *Spelaeotriletes microspinosus* (SSK39233), 129.0, 05.1, W29/0
- q. *Spelaeotriletes resolutus* (SSK38479), 125.6, 19.9, G26/1
- r. *Velamisorites corporatus* (SSK38714), 130.2, 09.0, S31/3
- s. *Velamisorites minutus* (SSK38735), 110.4, 08.8, S10/0
- t. *Velamisorites polyptychus* (SSK37883), 140.3, 06.4, V41/0
- u. *Verrucosisporites baccatus* (SSK38424), 129.2, 08.2, T29/0
- v. *Verrucosisporites congestus* (SSK38002), 113.7, 16.4, L13/2
- w. *Verrucosisporites depressus* (SSK37853), 141.8, 09.3, S42/2
- x. *Verrucosisporites gibberosus* (SSK37854), 129.9, 19.6, G30/0

PLATE 5

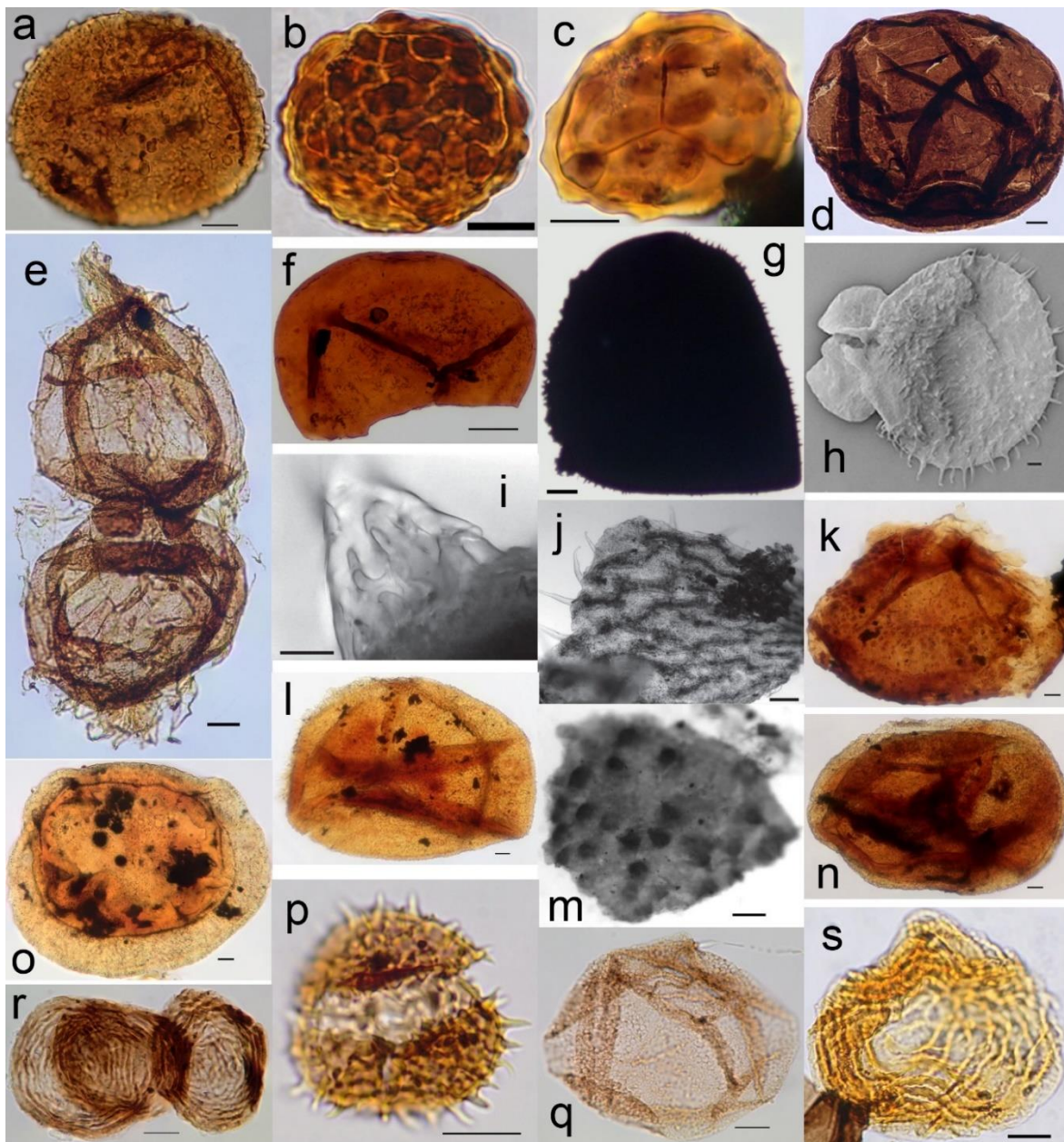


PLATE 5

- a. *Verrucosisporites irregularis* (SSK38438), 126.7, 04.0, M31/1
- b. *Verrucosisporites nitidus* (SSK37947), 117.7, 09.4, S18/1
- c. *Verrucosisporites scoticus* (SSK37947), 115.3, 07.7, T15/3

MEGASPORES

- d. *Didymosporites scottii* (large spore) (SSK38489) (megaspores strew slide), 114.3, 22.4, E13/2
- e. *Didymosporites scottii* (tetrad) (SSK38492) (picked megaspores slide), 120.0, 20.4, F20/0,
- f. *Laevigatisporites* cf. *cheveriensis* (SSK38434) (picked megaspores slide), 109.0, 12.3, O8/3
- g. *Lagenicula mixta* (SSK38103) (picked megaspores slide), 122.9, 08.6, S22/0
- h. *Setispora pannosa* SEM image of an entire megaspore from Pease Bay (sample: 17/05/1, SEM stub 1), scale bar = 100 µm
- i. *Setispora pannosa* infrared image of a spine base (SSK38046) (picked megaspores slide), 121.7, 19.8, G20/4
- j. *Setispora pseudoreticulata*, infrared image to highlight reticulate exine, (SSK38046) (picked megaspores slide), 122.0, 17.9, J20/0, scale bar = 100 µm
- k. *Setosisporites* sp. A (SSK37969) (megaspores strew slide), 122.3, 03.6, X21/4
- l. *Triangulatisporites membranatus* (SSK38434) (picked megaspores slide), 113.7, 15.7, L13/1
- m. *Tuberculatisporites mamillarius*, infrared image of exine piece showing spines, (SSK39233) (megaspores strew slide), 107.9, 20.1, F8/3, scale bar = 100 µm
- n. Spore Type D (SSK38434) (picked megaspores slide), 106.7, 16.8, K5/2

POLLEN

- o. *Remysporites magnificus* (SSK38042), 107.0, 19.4, G6/4

ACRITARCHS

- p. *Acanthotriletes socraticus* (SSK39200), 126.0, 13.3, O26/2
- q. *Carbaneuletes* cf. *micromuratus* (SSK39247), 130.9, 10.0, R31/0

EUGLENOIDS

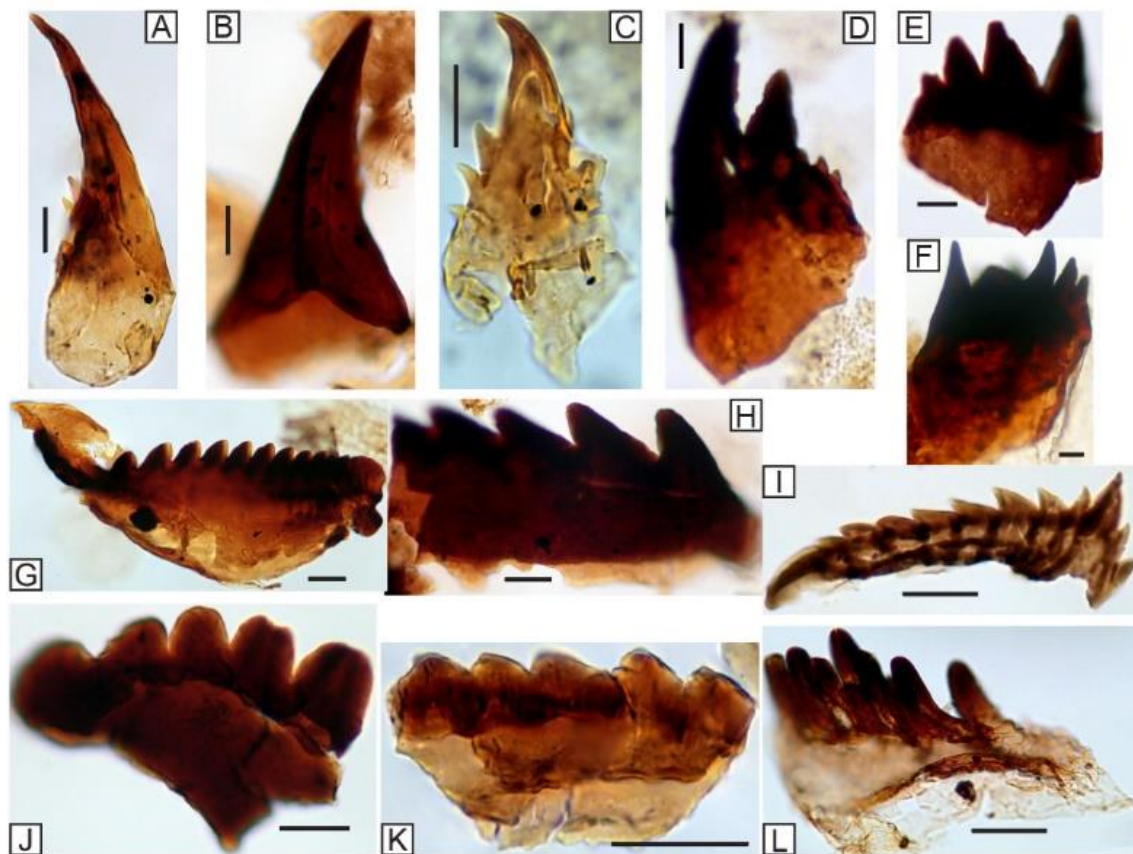
- r. *Chomotriletes multivittatus* (SSK38229), 118.0, 03.4, Y18/0
- s. *Chomotriletes vedugensis* (SSK38730), 113.9, 14.4, M13/4

SCOLECODONTS

EXPLANATION OF PLATE 6

Scale bar = 20 µm. Plate photograph reference, scolecodont morphotype (as defined in Section 3.6), depth of core sample, light microscope co-ordinates (Olympus BH-2 No. 205255), BGS sample reference number, England Finder co-ordinates, type of slide that contained the scolecodont specimen (i.e. Miospore = miospore strew slide, Ultrasonic = ultrasonic treated miospore strew slide, Megaspore = megaspore strew slide).

PLATE 6



- A. B, 93.38 m, 122.8, 12.3, SSK39170, O22/3, Miospore.
 B. A, 148.71 m, 124.1, 17.2, SSK38986, J23/3, Ultrasonic.
 C. A, 231.57 m, 125.3, 03.0, SSK38681, Y25/1, Miospore.
 D. E, 231.57 m, 101.5, 03.8, SSK38681, X1/3, Miospore.
 E. D, 148.71 m, 121.0, 17.4, SSK38986, J20/0, Ultrasonic.
 F. F, 368.83 m, 115.7, 11.3, SSK38191, P14/4, Megaspore.
 G. C, 253.41 m, 132.0, 13.8, SSK38489, N31/2, Miospore.
 H. C, 148.71 m, 130.0, 19.3, SSK38986, G29/0, Ultrasonic.
 I. C, 148.71 m, 126.0, 17.5, SSK38986, J25/0, Ultrasonic.
 J. C, 367.64 m, 127.8, 20.0, SSK38195, F27/0, Ultrasonic.
 K. C, 367.64 m, 111.9, 07.2, SSK38195, U11/1, Ultrasonic.
 L. C, 501.18 m, 125.8, 10.0, SSK37853, S25/0, Miospore.

CHAPTER 4

TOURNAISIAN BIOZONATION

This section interprets the palynomorph data for a biozonation scheme. For the TW:eed project, assigning an accurate biozonation to the NWMF borehole core was one of the main objectives. This would enable the scattered tetrapod sites to be interconnected and the fossils they contained to be relatively dated. Their anatomical developments towards increasing terrestriality could then be incorporated into cladistical analyses including the time dimension.

4.1. Challenges

Unfortunately, two substantial challenges had to be overcome to achieve this aim.

4.1.1. The NWMF borehole did not encompass the entire Ballagan Formation

As the junction with the Devonian Kinnesswood Formation, which underlies the Tournaisian Ballagan Formation, was not reached in the NWMF borehole, two key spore taxa were used to produce a composite section between the Burnmouth outcrop at the base and the borehole above. This was achieved by matching the first large peak of abundance of the microspore *Anaplanisporites baccatus* and the first occurrence of the miospore *Prolycospora claytonii* in both sections (Figure 97).

Most of the data presented herein comes from the NWMF borehole core, owing to its higher recovery and better preservation, with the outcrop section being used for the remainder at the base.

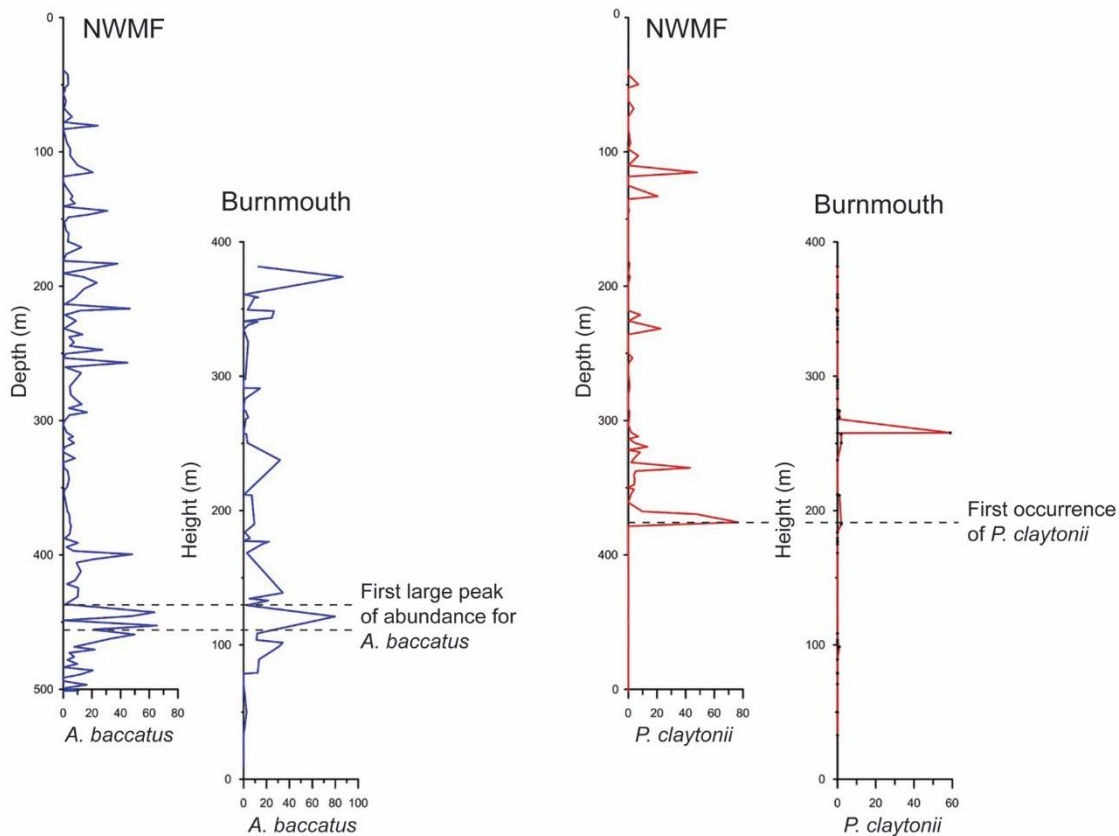
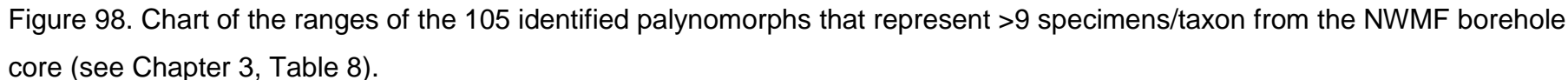


Figure 97. Two key spore taxa, *Anaplanisporites baccatus* (in blue) and *Prolycospora claytonii* (in red), were used to splice together the NWMF borehole and the Burnmouth outcrop to obtain a complete record of the Ballagan Formation (produced by John Marshall 2017).

4.1.2. The new data did not fit published Tournaisian biozonation schemes

Unfortunately, the results of plotting the ranges for the NWMF borehole spores (Figure 98) did not easily lend themselves to an existing biozonation. The majority of the top 10 most commonly occurring spores (defined as the number of spores per sample, which accounted for 60% of all spores), showed different ranges to the published schemes (Table 9).



Spore taxon	Total No.	Total as %	Mean No. spores/sample
<i>A. baccatus</i>	4,932	12.5	30.4
<i>C. trychera</i>	3,764	9.6	20.9
<i>C. decorus</i>	3,237	8.2	17.8
<i>C. denticulatus</i>	2,426	6.2	16.0
<i>A. asperella</i>	2,252	5.7	13.7
<i>A. macra</i>	1,760	4.5	10.7
<i>S. claviger</i>	1,599	4.1	12.3
<i>P. claytonii</i>	1,271	3.2	22.3
<i>A. fruticosa</i>	1,241	3.2	9.3
<i>P. scolecophora</i>	1,040	2.6	6.5
TOTAL	23,522		

Table 9. The top 10 most abundant spores that were extracted from the NWMF borehole core. Total number of all spores = 39,389. Total number of top 10 spores = 23,522 (= 59.7% of all spores).

4.2. Correlation to published biozonation schemes

To understand this information, the borehole data was applied to the published miospore zonation schemes of Higgs *et al.* (1988) and Turnau (1978).

4.2.1. The zonation scheme of Higgs *et al.* (1988)

Higgs *et al.* (1988) amalgamated palynological investigations on the Tournaisian rocks of Ireland from previously published, unpublished and freshly acquired sources. They erected a zonal scheme based on the ranges of selected taxa, which was tested on many Tournaisian successions in Ireland (Figure 99). The recognition of these zones has allowed the age dating and correlation of different Tournaisian successions in Britain and Western Europe.

STRATIGRAPHY		SPORE BIOZONES	SELECTED SPECIES APPEARING IN THE BIOZONE	SELECTED SPECIES DISAPPEARING IN THE BIOZONE	
CARBONIFEROUS	CHADIAN	VISEAN V1a	Pu		
	COURCEYAN	Tn3c TOURNAISIAN Tn3	CM	← <i>Lycospora pusilla</i>	
		Tn3a	PC	← <i>Convolutispora circumvallata</i> <i>Schopfites claviger</i>	← <i>H. explanatus</i> <i>C. cristifer</i> <i>L. malevkensis</i> <i>L. triangulatus</i>
		Tn2 b/c	BP	← <i>Crassispora trychera</i> <i>Anaplanisporites baccatus</i> <i>Prolycospora rugulosa</i>	
		Tn2 TOURNAISIAN Tn2	HD	← <i>Colatisporites decorus</i>	
		Tn2a	VI	← <i>Spelaettriletes pretiosus</i> <i>Raistrickia clavata</i> <i>R. condylosa</i> <i>Kraeuselisporites mitratus</i> <i>Granulatisporites microgranifer</i>	← <i>S. obtusus</i> <i>S. resolutus</i>
		Tn1b	LN	← <i>Vallatisporites vallatus</i> <i>Spelaettriletes balteatus</i>	
		Tn1 TOURNAISIAN Tn1	LE	← <i>Neoraistrickia cymosa</i>	
		Tn1b	LL	← <i>Umbonatisporites distinctus</i> <i>Kraeuselisporites hibernicus</i>	
	'STRUNIAN'	Tn1a-b		← <i>Crassispora maculosa</i> <i>Spelaettriletes obtusus</i> <i>Cyrtospora cristifer</i>	← <i>R. lepidophyta</i> <i>V. pusillites</i> <i>Rugospora flexuosa</i> <i>Diducites versabilis</i> <i>Crassispora catenata</i> <i>Ancyrospora</i> spp.
DEVONIAN			← <i>Umbonatisporites abstrusus</i>	← <i>Retispora cassicula</i> <i>Auroraspora torquata</i>	
			← <i>Verrucosporites nitidus</i> <i>Vallatisporites verrucosus</i> <i>Lophozonotrilites malevkensis</i>		
			← <i>Hymenozonotrilites explanatus</i>		
			← <i>Retispora lepidophyta</i> <i>Vallatisporites pusillites</i>		

Figure 99. The miospore biozones and their characteristic taxa of Higgs *et al.* (1988) with the Tournaisian biozones coloured. From Higgs *et al.* (1988).

Using the data from the NWMF borehole core, the ranges of the taxa used to define each of the five Tournaisian biozones of Higgs *et al.* (1988) were plotted into a condensed range chart (Figure 100). Of the 66 taxa used to define the Tournaisian biozonal assemblages, 47 (71%) were present in the NWMF borehole core. Unfortunately, those indicator taxa appeared in a different sequence and were often of low abundance and, so, were of little value for stratigraphic dating purposes.

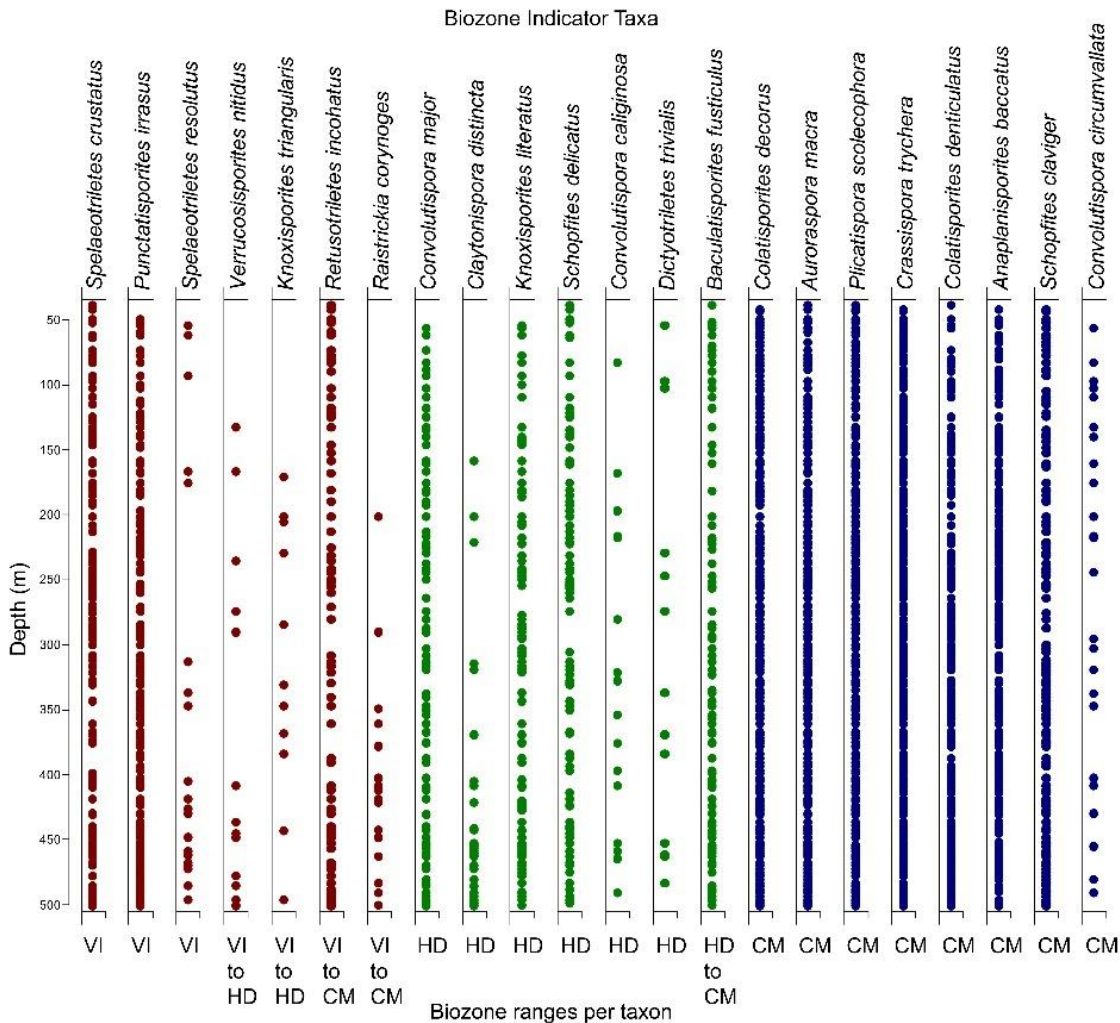


Figure 100. Range chart (presence-absence) of the distribution of the diagnostic taxa used to define the palynozones of Higgs *et al.* (1988) that were present in the NWMF borehole core. The colour changes denote the start of each biozone.

This outcome challenged the Higgs *et al.* (1988) miospore zonation scheme and suggested that there were complex contributing factors. These included that

despite a large number of productive samples (473) from multiple outcrop localities and borehole cores (83) having been recorded across a wide area of Ireland, and that many of the sample sites were hundreds of metres in depth/height, the number of samples taken was often low and the sampling intervals were irregular and widely spaced.

In contrast, the systematic 1 m sampling (where possible) of the NWMF borehole core, yielded a significantly higher palynomorph recovery (82%) at a regular and fine sampling scale. However, as the NWMF borehole did not encompass the entire Tournaisian, data had to be incorporated from the Burnmouth outcrop site (see Section 4.1).

At the base of the Tournaisian sequence at Burnmouth, the palynological assemblage was dominated by *Retusotriletes incohatus* and *Plicatispora scolecophora*, which indicated the VI biozone (Marshall *et al.* 2019). The CM biozonal spores appeared at a height of 70 m, suggesting that the VI interval had been short. Additionally, the HD biozonal indicator species *Claytonispora distincta* and *Neoraistrickia cymosa* were present at Burnmouth.

The next significant inception at Burnmouth was *Prolycospora claytonii* at 189.9 m (Marshall *et al.* 2019). As *P. claytonii* has few records in Western Europe, it had not been regarded as important for British biozonation (Clayton & Turnau 1990). However, it was a major component in Eastern European palynological assemblages and formed the basis for an alternative biozonation (Turnau 1978, Avchimovitch & Turnau 1994).

4.2.2. The zonation scheme of Turnau (1978)

Turnau (1978) identified four spore zones from 33 borehole cores from a continuous succession of marine sediments from the DCB to the Lower Viséan of western Pomerania (Poland; Figure 101).

AGE		S P O R E ZONES/SUBZONES	SPECIES, FIRST APPEARING IN ZONE/SUBZONE	SPECIES LAST OCCURRING IN ZONE/SUBZONE	TYPICAL ASSOCIATION OF SPECIES	
CARBONIFEROUS	LOWER VISEAN	1	<i>Rugospora minuta</i>		<i>Prolycospora claytonii</i> <i>Anaplanisporites cf. delicatus</i> <i>Apiculiretusispora multiseta</i> <i>Gorgonispora multiplicabilis</i> <i>Auroraspora cf. solisortus</i>	<i>Auroraspora panda</i> <i>Auroraspora macra</i> <i>Crassispora trychera</i> <i>Rugospora minuta</i> <i>Schopfites claviger</i>
		<i>Prolycospora claytonii</i> Cl _u	<i>Auroraspora cf. solisortus</i> <i>Auroraspora panda</i> <i>Gorgonispora multiplicabilis</i> <i>Apiculiretusispora dominans</i>	<i>Convolutispora major</i>	<i>Prolycospora claytonii</i> <i>Anaplanisporites cf. delicatus</i> <i>Apiculiretusispora multiseta</i> <i>Auroraspora cf. solisortus</i>	<i>Auroraspora panda</i> <i>Schopfites claviger</i> <i>Raistrickia corynages</i> <i>Crassispora trychera</i>
	TOURNAISIAN	3	<i>Prolycospora claytonii</i> <i>Anaplanisporites cf. delicatus</i> <i>Apiculiretusispora multiseta</i> <i>Dictyotriletes membranireticulatus</i> <i>Dictyotriletes margodentatus</i>	<i>Tumulispora rarituberculata</i> <i>Tumulispora dentata</i> <i>Tumulispora obscura</i>	<i>Prolycospora claytonii</i> <i>Anaplanisporites cf. delicatus</i> <i>Apiculiretusispora multiseta</i> <i>Verrucosporites nitidus</i> <i>Punctatisporites ciniae</i>	<i>Dictyotriletes margodentatus</i> <i>Crassispora trychera</i> <i>Umbonatisporites distinctus</i>
		<i>Convolutispora major</i> Ma	<i>Tumulispora dentata</i> <i>Convolutispora major</i> <i>Umbonatisporites distinctus</i> <i>Pustulatisporites gibberosus</i>	<i>Perotriletes ordinarius</i> <i>Dictyotriletes submarginatus</i> <i>Punctatisporites ciniae</i> <i>Raistrickia corynages</i>	<i>Grandispora explanata</i> II <i>Archaeozonotriletes incrassatus</i>	<i>Auroraspora macra</i> <i>Verrucosporites nitidus</i> <i>Punctatisporites glaber</i> <i>Convolutispora major</i>
	DEVONIAN	1	<i>Tumulispora rarituberculata</i> <i>Knoxisporites literatus</i> <i>Corbulispora subalveolaris</i> <i>Raistrickia variabilis</i>	<i>Spelaeotriletes lepidophytus</i> s.l. <i>Rugospora versabilis</i>	<i>Spelaeotriletes lepidophytus</i> s.l. <i>Tumulispora rarituberculata</i> <i>Grandispora lupata</i> <i>Grandispora conspicua</i>	<i>Knoxisporites literatus</i> <i>Rugospora versabilis</i>
		<i>Grandispora lupata</i> Lu	<i>Spelaeotriletes lepidophytus</i> var. <i>tener</i> <i>Grandispora lupata</i>		<i>Spelaeotriletes lepidophytus</i> s.l. <i>Grandispora lupata</i> <i>Grandispora conspicua</i> <i>Rugospora versabilis</i>	

Figure 101. The miospore biozones and their characteristic taxa of Turnau (1978) with the Carboniferous Tournaisian biozones coloured. After Turnau (1978).

Higgs *et al.* (1988, p. 48) discussed Turnau's (1978) miospore zonation scheme, noting how the assemblages of the CI Zone (defined by the presence of *Prolycospora claytonii*) show many compositional similarities with the CM Biozone of Britain and Ireland. The palynomorph data from the NWMF borehole core also agrees with this statement.

Note: Turnau (1978) used *Anaplanisporites cf. delicatus* for *Anaplanisporites baccatus*.

Therefore, following the biozonation scheme of Turnau (1978), the diagnostic taxa used to define the four biozones were plotted from the NWMF borehole core data (Figure 102). Of the 78 taxa used to define the biozonal assemblages, 33 (42%) were present in the NWMF borehole core. Unfortunately, as with the Higgs *et al.* (1988) biozonation, the indicator taxa for the Turnau (1978) scheme appeared in a different sequence and were often in low abundance, again rendering them of little value for relative dating purposes.

However, in the original scheme, the Tournaisian CI biozone was divided into two subzones – lower and middle, with the difference between them being based on the percentage abundance of each taxon (Turnau 1978; Table 10). Turnau (1978) acknowledged that “index species occur in small quantities”, which made it difficult to divide the zone. Therefore, using the NWMF borehole core data, the CI biozone is not subdivided here.

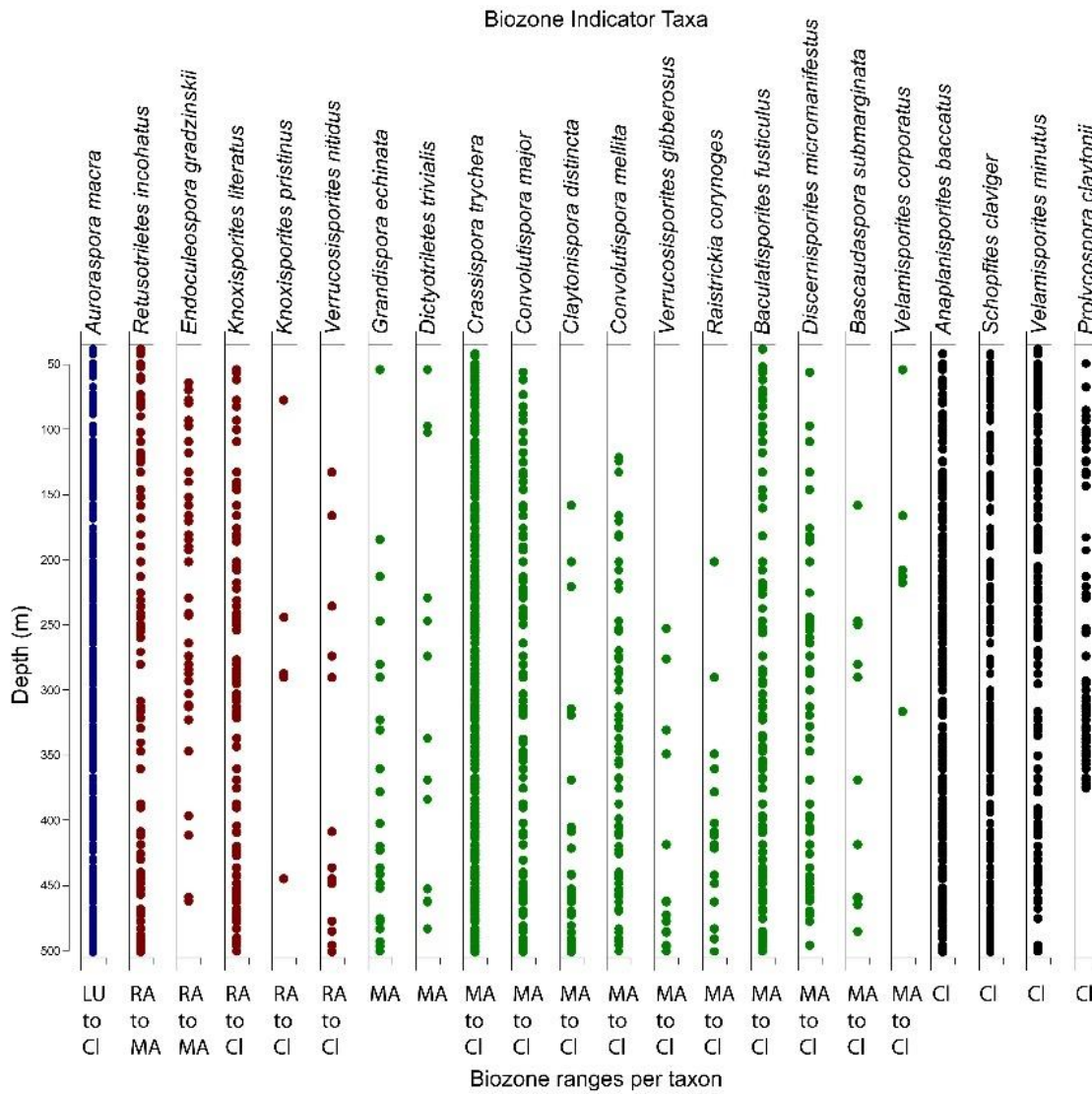


Figure 102. Range chart (presence-absence) of the distribution of the spores used to define the palynozones of Turnau (1978) that were present in the NWMF borehole core. The colour changes denote the start of each biozone.

Spore taxon	CI biozone	
	lower	middle
<i>A. multiseta</i>	2-9%	1-5.5%
<i>C. trychera</i>	2.5-17%	---
<i>A. macra</i>	2.5%	---
<i>A. baccatus</i>	5%	35-78%
<i>P. claytonii</i>	to 12%	14-55%
<i>V. nitidus</i>	2%	---
<i>C. cf. commodus</i>	---	to 3.5%

Table 10. The spores used to define the two subzones of the Tournaisian CI biozone of Turnau (1978) and their varying abundances.

Turnau (1978) also noted how the middle and upper subzones were strongly influenced by a “not distant flora” and “some monotonous local flora”, which she used to explain the impoverished taxa. The mutually exclusive relationship of the plants represented by *Anaplanisporites baccatus* (*Oxroadia conferta*) and *Prolycospora claytonii* (*Genomosperma kidstoni*) had not been recognised at the time and explain the fluctuating relative abundances of the CI indicator taxa (Figure 103).

In the NWMF borehole, *A. baccatus* was the most commonly occurring spore (12.5% of all spores; mean 30.4 spores per sample). Its parent plant, *O. conferta*, represented an r-selected habit and thrived in disturbed conditions (Bateman 1992). However, *G. kidstoni*, the parent plant of *P. claytonii*, exhibited a K-selected habit and indicated more stable conditions on the Ballagan floodplain.

The high relative abundance of *A. baccatus* diminished noticeably with the inception of *P. claytonii* at 376.05 m (Figure 103). But when *P. claytonii* declined, *A. baccatus* returned. This pattern was repeated when the relative abundance of *P. claytonii* declined for a second time. Therefore, unless regular, fine-scale sampling was employed, the subtleties of the mutually exclusive relationship of these two plants would be missed.

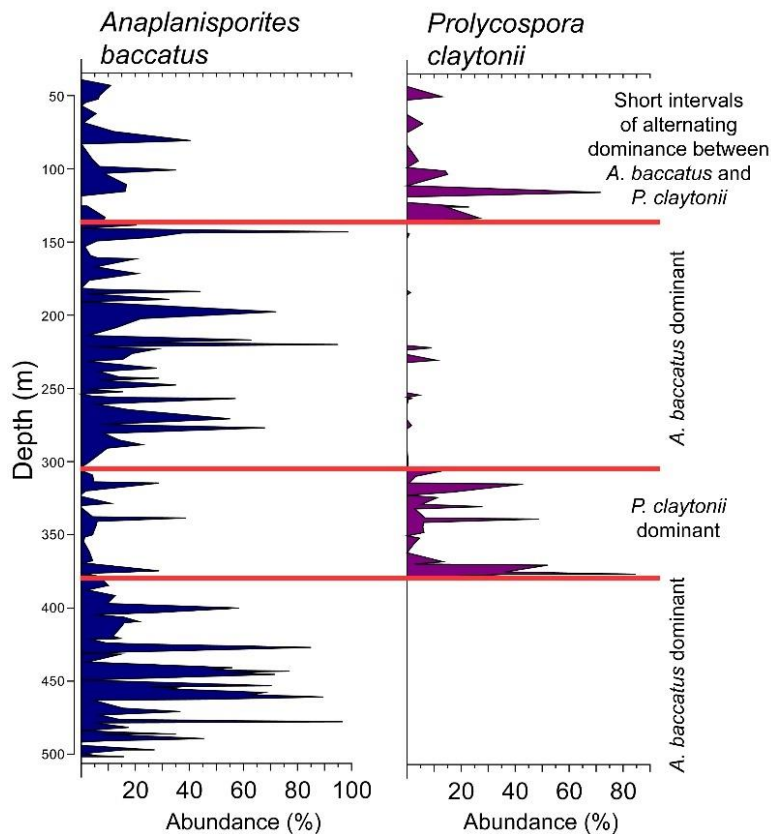


Figure 103. Chart to show the varying relative abundances of *A. baccatus* (= *Oxroadia conferta* plant) and *P. claytonii* (= *Genomosperma kidstoni* plant) and how their peaks never overlap indicating a mutually exclusive relationship (see Sections 5.4.1 and 5.4.2 for details of the plant affinities).

4.3. The newly proposed biozonation scheme for the Tournaisian

Adding together the data from the NWMF borehole core and the Burnmouth outcrop and applying the zonal indicator taxa from Higgs *et al.* (1988) and Turnau (1978), potentially results in five palynozones for the entire Tournaisian: VI → HD (from Burnmouth) → PC → CM → Cl.

However, the distinction between the PC and the CM zones is the appearance of *Schopfites claviger* to define the start of the CM zone. Considering the nature of *S. claviger* as an indicator of drier climate conditions (Van der Zwan *et al.* 1985 – see Section 5.8), and that its presence and relative abundance was, therefore, driven by the climate (see Figure 117 in Section 5.8), meant that it was considered inappropriate as a biozonal indicator taxon and was discounted here.

Therefore, the palynozones for the Tournaisian Ballagan Formation start with the brief survival phase of the VI (*Vallatisporites verrucosus*–*Retusotriletes incohatus*) zone, then the recovery period starts with the HD (*Kraeuselisporites hibernicus*–*Claytonispora distincta*) zone and moved into the PC (*Spelaeotriletes pretiosus*–*Raistrickia clavata*) and CI (*Prolycospora claytonii*) zones (Figure 104).

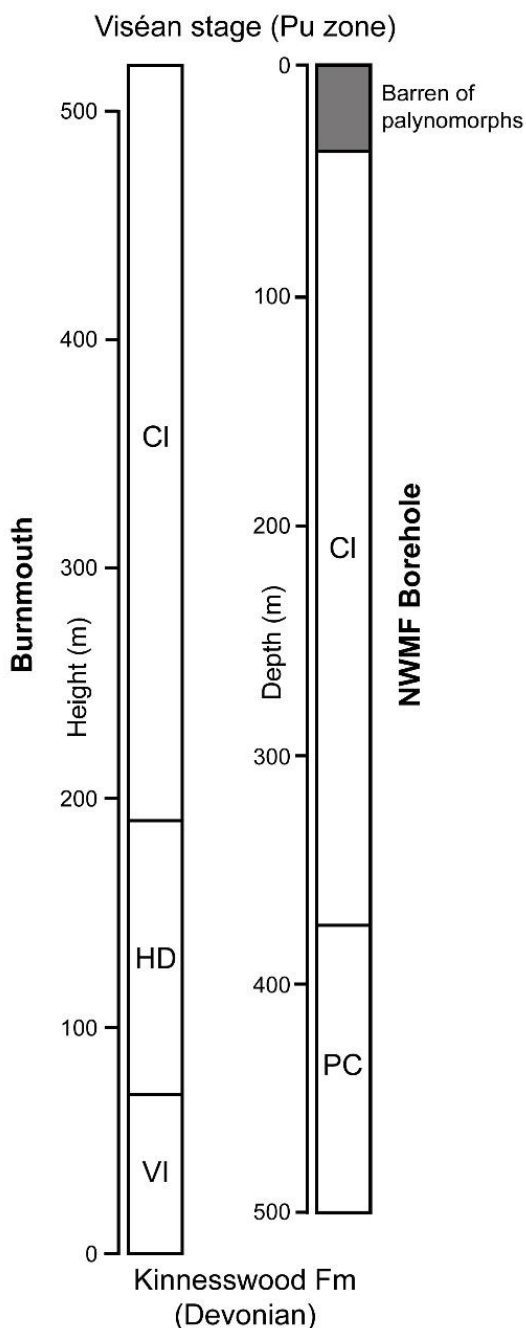


Figure 104. Comparing the biozones for the Burnmouth outcrop (left) and the NWMF borehole core (right) to encompass the entire 12 million years of the Tournaisian Ballagan Formation.

CHAPTER 5

PLANT RECOVERY

In addition to applying a biozonation scheme to the palynological data from the NWMF borehole core, the recovery of the plant life following the EDME was one of the main outcomes of the TW:eed project (see Section 1.8). To achieve this, a range of statistical analyses was performed on the semi-quantitative counts of the identified palynomorphs.

5.1. Principal Component Analysis (PCA)

Firstly, to establish the dominant flora of the Ballagan environment, a PCA was performed to define any outgroups of spore taxa. Outgroups indicate the taxa that are different to all other palynomorphs and, so, could represent the dominant plants that were responding to changes in the Ballagan environment.

Using PAST software, a 95% similarity grouping was added which represents the 95% of taxa that are most like each other, in terms of the group's average value, and forms the 'in-group'. Therefore, all palynomorphs positioned outside of it must be 'outgroup' taxa (Figure 105). This process defined 8 outgroup taxa (see Section 2.11.3).

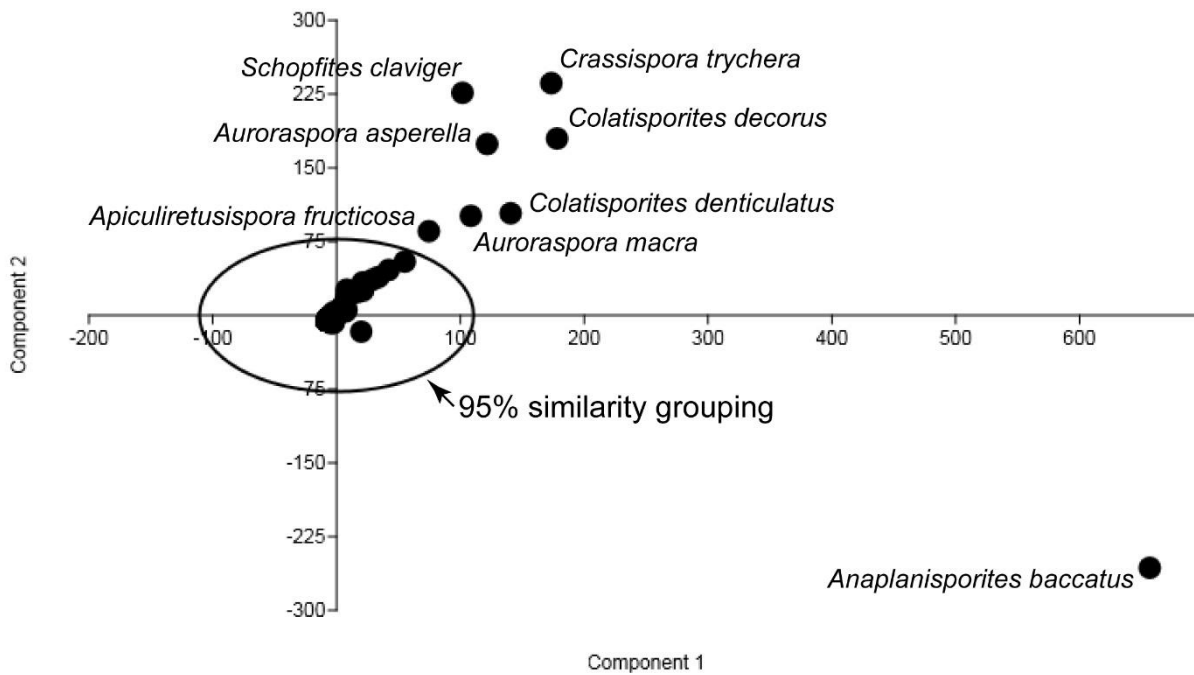


Figure 105. The results of the PCA of palynomorphs from the NWMF borehole core identified 8 outgroup taxa which are labelled.

5.2. Relative abundances

To interpret the plant recovery, Tilia software was used to illustrate the fluctuating relative abundances through time of 12 significant palynomorphs (see Section 2.11.2). The 12 taxa comprised the 8 outgroup taxa identified from the PCA, with 4 additional taxa with recognised botanical affinities, believed to be important to understanding the post-EDME recovery (Figure 106).

The changes in the relative abundance data demonstrated that the outgroup taxa were continuously present throughout the core, but that the remaining 4 taxa had more variable distributions. The distribution of the palynomorphs was then used to map the changes in their parent plants' relative abundances.

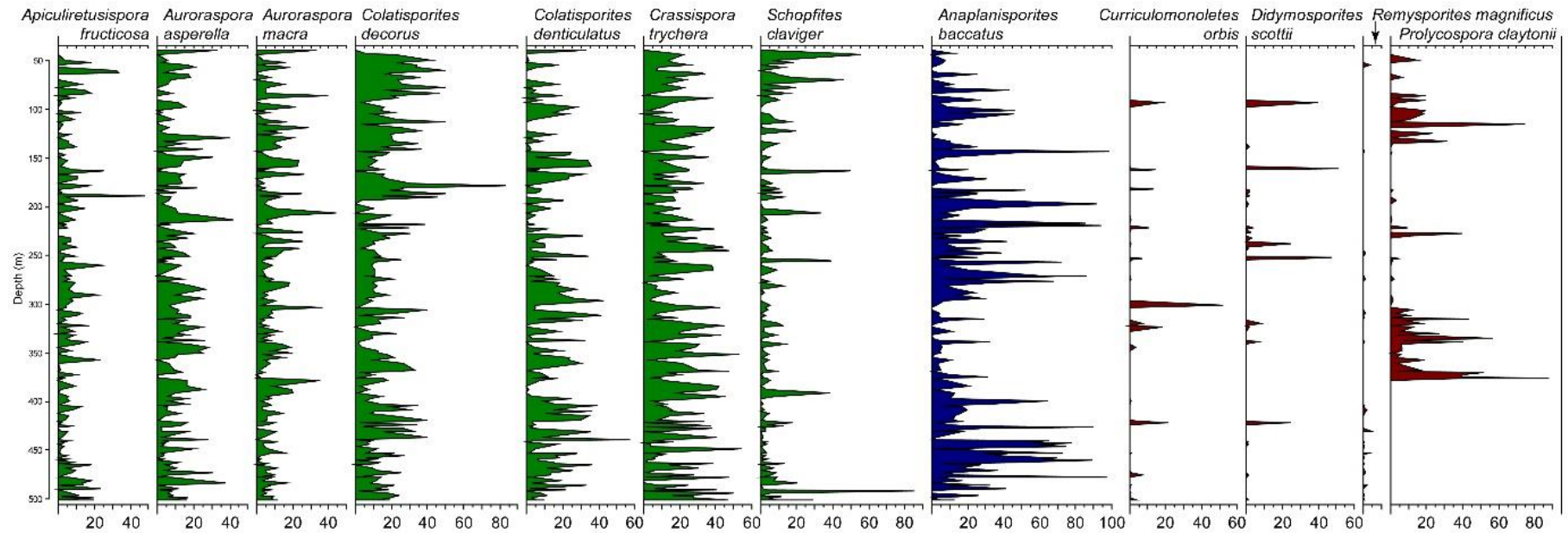


Figure 106. The fluctuating relative abundances (by percentage of sample) of 12 significant palynomorph taxa from the NWMF borehole core used to illustrate the plant recovery in the Ballagan environment. Eight taxa represent the PCA outgroup (in green and blue) and four taxa with recognised botanical affinities (in red). Greater peaks indicate higher abundance and the depth is stratigraphically constrained.

Note: One of the main limitations of determining the nature of the plant recovery has been the lack of published plant affinities. There seems to be a historical reticence for palaeobotanists to involve palaeopalynologists in identifying spores/pollen found *in situ* in fossil plants (e.g. Long 1960a, Plate I, Figures 2-3). Fortunately, where palynomorphs have at least been mentioned, the original microscope slides can potentially be investigated by palaeopalynologists (see Section 5.4.2.).

5.3. Plant affinities

At the base of the Tournaisian, the simple survival flora of the VI palynozone was recognised in the lowest beds at Burnmouth (Smithson *et al.* 2012, Marshall *et al.* 2019). The arrival of *Claytonispora distincta* and *Neoraistrickia cymosa* then signified the start of the HD-biozone and the beginning of the recovery flora at the base of the borehole. A clear increase in spore diversity followed, with the vegetation becoming dominated by a series of plants in sequence (Figure 110).

5.4. The dominant plants of the Ballagan environment

This section focusses on the limited number of known plant associations to infer the activity of the parent plants from their palynomorphs.

5.4.1. *Oxroadia conferta* Bateman 1992

The most common spore from the NWMF borehole core was *Anaplanisporites baccatus* which, with its megaspore *Setispora pannosa* (see Plate 1 figure b and Plate 5 figures h and i respectively) has been identified within the sporangia of *Oxroadia conferta* (Bateman 1992). An early rhizomorphic lycopsid, *O. conferta* was described in detail from permineralised and fusainised plants found *in situ* within volcanic ashes from Oxroad Bay, Scotland (Bateman 1992, Bateman & Rothwell 1990). Semi-prostrate and pseudoherbaceous, *Oxroadia* was well adapted to form high-density populations of mono-specific communities, resembling extant briar patches (Bateman 1992). Its small size and simple anatomy were consistent with r-selection and its repeated occurrence within a

sequence of volcanic ash from the nearby Tantallon Vent indicated that it was able to thrive in unstable conditions (Bateman 1988, 1992).

The relative abundance of *A. baccatus* changed throughout the core with two main episodes (501 to 368 m and 367 to 42 m; Figure 118). Its noticeable relative decline around 370 m borehole depth marks the start of the stepwise progression in the dominance of 3 new taxa (Figure 113).

5.4.2. *Genomosperma kidstoni* (Calder) Long 1960

The first of the inception taxa was *Prolycospora claytonii* (see Plate 3 figures n to t) which indicated the arrival of a new pteridosperm *Genomosperma kidstoni* (Figure 110). Subsequent to an extensive literature research of Albert Long's work carried out by John Marshall, study of the slides of the Albert Long Collection at the Hunterian Museum, Glasgow in 2018 revealed multiple specimens of *Prolycospora claytonii* in the ovules of *G. kidstoni* (figures 107 and 108). Based on this finding, *G. kidstoni* is presumed to be the parent plant of *P. claytonii*. But as *G. kidstoni* has only been identified from specimens of petrified seeds (Long 1960a), a full reconstruction of the plant has yet to be published, so its growth habit is currently unknown. However, *G. kidstoni* was not a lycopod as no lycopod megaspores occurred with the spore samples that contained *P. claytonii*.

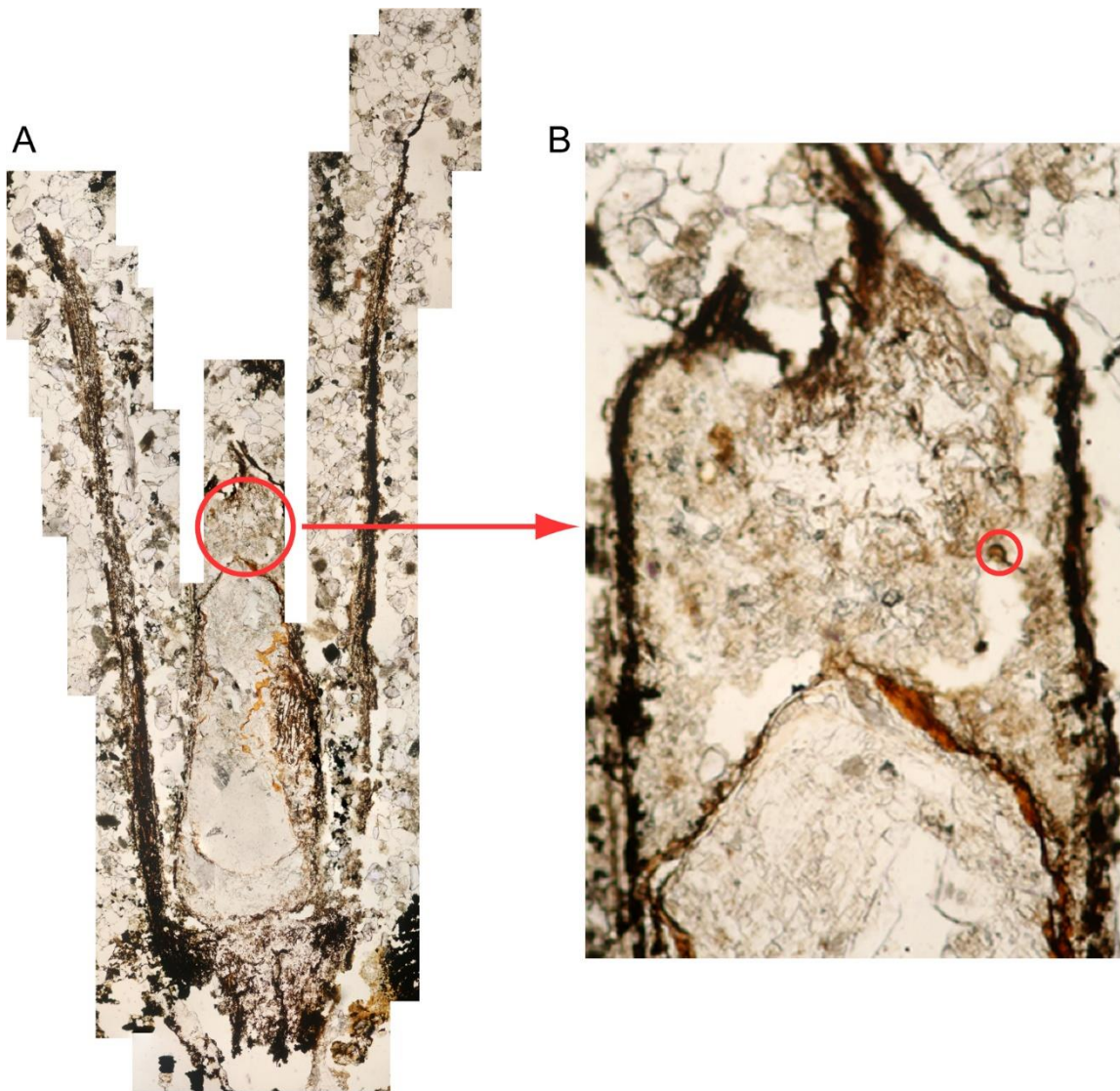


Figure 107. A. Microphotogrammetry of a *Genomosperma kidstoni* nucellus (central part of ovule) x4, slide FSC1116 K5 housed in the Albert Long Collection at the Hunterian Museum, Glasgow with the pollen chamber circled in red. B. Close up of the pollen chamber of A with spore C of Figure 108 circled in red.

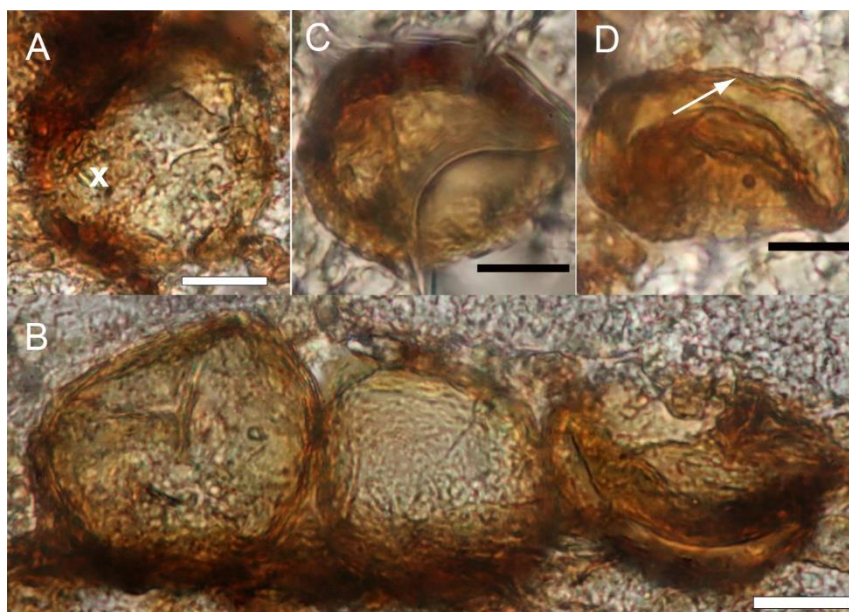


Figure 108. Photomicrograph of *Prolycospora claytonii* spores inside an ovule of *Genomosperma kidstoni* housed in the Albert Long Collection at the Hunterian Museum, Glasgow. The x inside A highlights the infragranular sculpture of the proximal face. The arrow in D indicates the outline of the verrucae on the distal face. A and B slide FSC1100, C and D slide FSC1116 K5. Scale bars = 10 μ m.

5.4.3. Putative Medullosan pteridosperm

As the relative abundance of *Prolycospora claytonii* declined, the spore *Curculomonoletes orbis*, first identified from a borehole in Errol, Scotland, then became dominant (McLean & Neves 2003; see Plate 2 figure o). Morphologically resembling *Schopfipollenites* i.e. being large (100-500 μ m in length) and monolete (Figure 109), it has characteristics typical of Medullosan pollen and may be ascribed to Medullosan pteridosperms (Taylor 1976, Taylor & Millay 1979, McLean & Neves 2003). Additionally, *Schopfipollenites* has been found in Medullosan organs (Taylor 1976). *C. orbis*, therefore, indicated the arrival of a second, new, seed plant to the Ballagan environment (Figure 110).

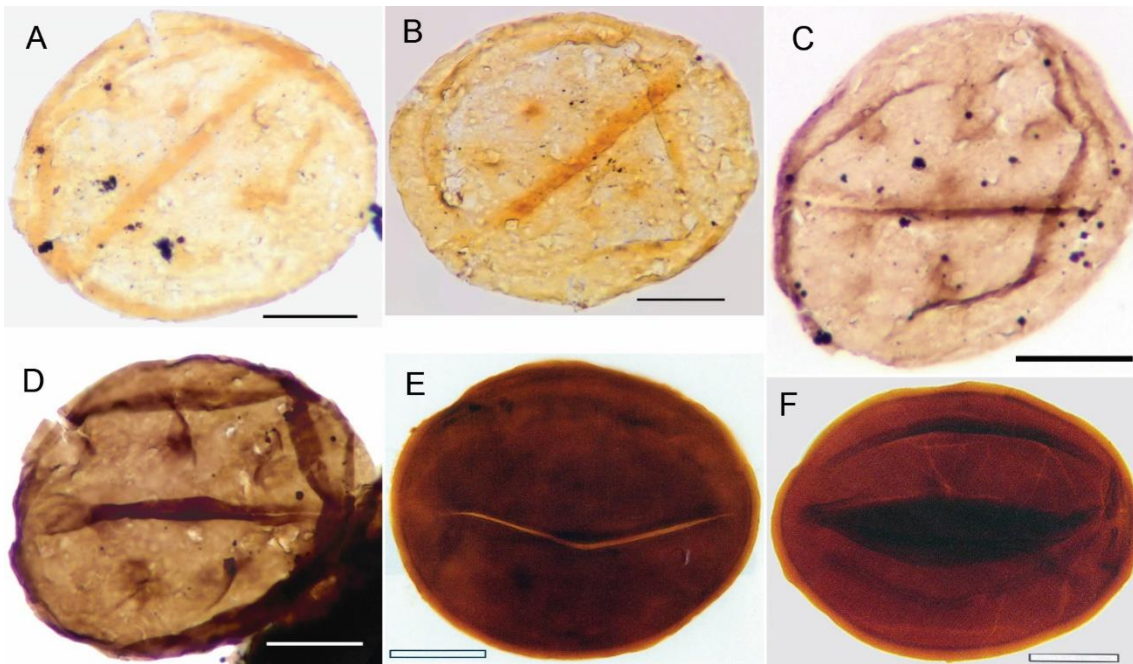


Figure 109. A to D photomicrographs of *Curriculomonoletes orbis* from the NWMF borehole core and E to F *Monoletes* (=Schopfipollenites) pollen grains to compare their morphological similarities. A to D slide details and England Finder coordinates given: A and B = 421.68 m depth (picked megaspores slide), 123.7, 09.3, S23/2 and 106.8, 19.8, F5/4 respectively. C and D = 475.82 m depth (megaspores strew slide), 118.7, 23.2, C18/0 and 110.7, 22.0, E10/0 respectively. Scale bars = 50 μm . E Proximal surface of *Monoletes* pollen grain showing median deflection of suturae. F Distal surface of *Monoletes* pollen. Scale bars = 100 μm . From Taylor *et al.* (2009 p. 592, figures 14.153 and 14.154 respectively).

5.4.4. *Stauropteris burntislandica* Bertrand 1909

The acme of *C. orbis* was then replaced by *Didymosporites scottii*. This distinctive tetrad (see Plate 5 figures d and e) has been found in sporangia of the coenopterid fern *Stauropteris burntislandica* (Figure 110), based on petrifications of the rachis and its branches and megasporangia *Bensonites fusiformis* Scott 1908 (Chaloner 1958). It had highly branched fronds up to 15 cm long and formed an important part of the understorey vegetation (Surange 1952).

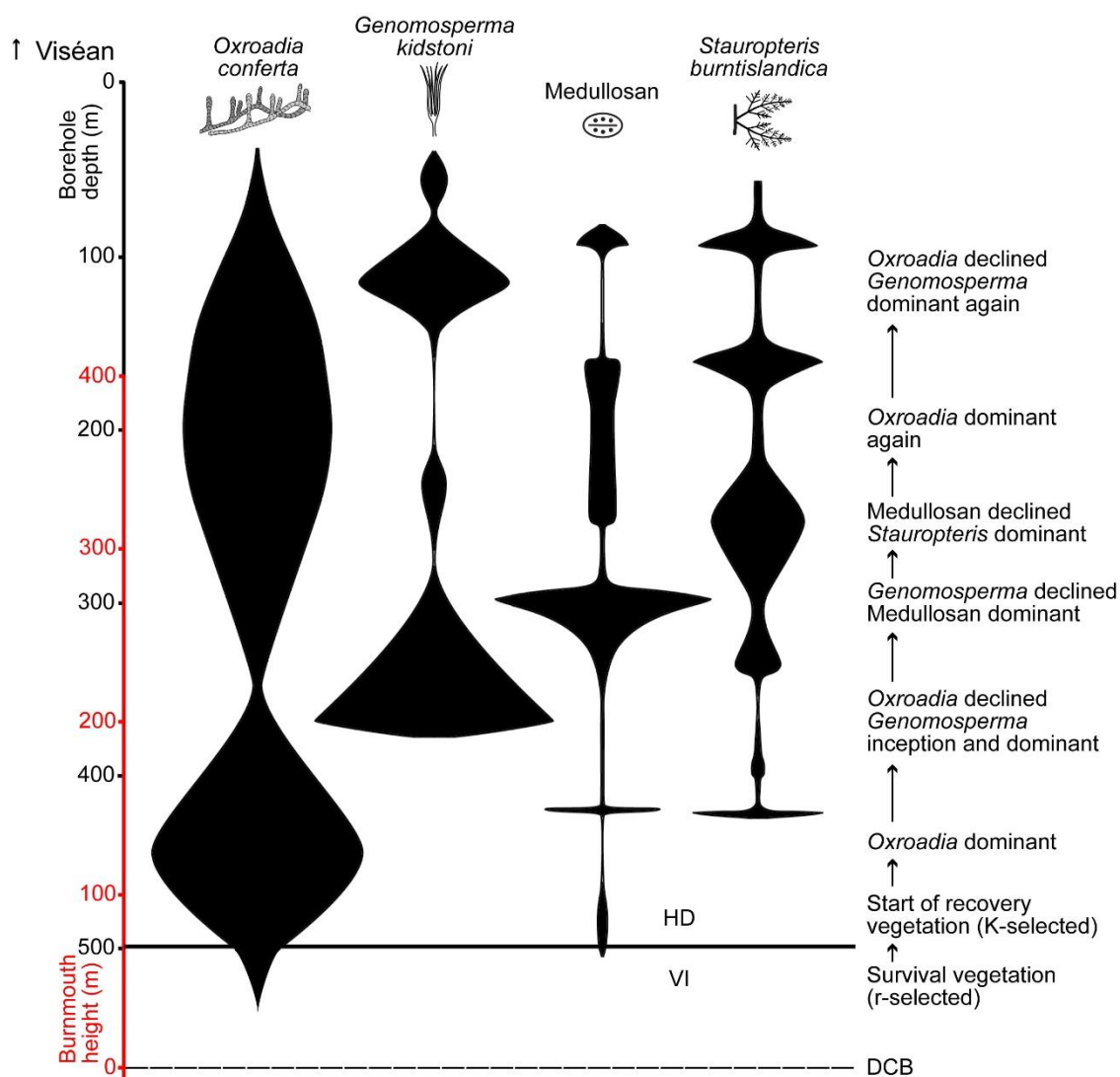


Figure 110. A summary diagram of the plant recovery interpreted from relative palynomorph abundance of the Tournaisian Ballagan environment. The DCB is shown at the base with the VI-HD biozones boundary above. On the left-hand axis are the Burnmouth outcrop heights (red) and NWMF borehole depths (black). The spindle plots (centre) show the relative abundances of the dominant plants (wider shape = higher abundance). A summary description of the changing dominant plants is listed on the right-hand side.

5.5. Other plants of the Ballagan environment

In addition to the dominant plants, the continuous presence of two species of *Colatisporites* revealed a background relative abundance of two further seed plants (Figure 106). Also, the intermittent occurrence of *Remysporites magnificus* pollen (and the relative abundance of *Punctatisporites* spores – see Section 5.5.3), indicated that a progymnosperm was present.

5.5.1. *Lyrasperma scotica* (Calder) Long 1960b

Multiple specimens of *Colatisporites denticulatus* spores (see Plate 1 figure w), have been found within the ovule of *Lyrasperma scotica* (Figure 111). Found as petrified seeds from Langton Burn and the River Whitadder near Edrom in Berwickshire, *L. scotica*, has been interpreted as a small, shrubby pteridosperm with an unbranched, erect trunk that formed part of the understorey vegetation (Long 1960b, Retallack & Dilcher 1988).

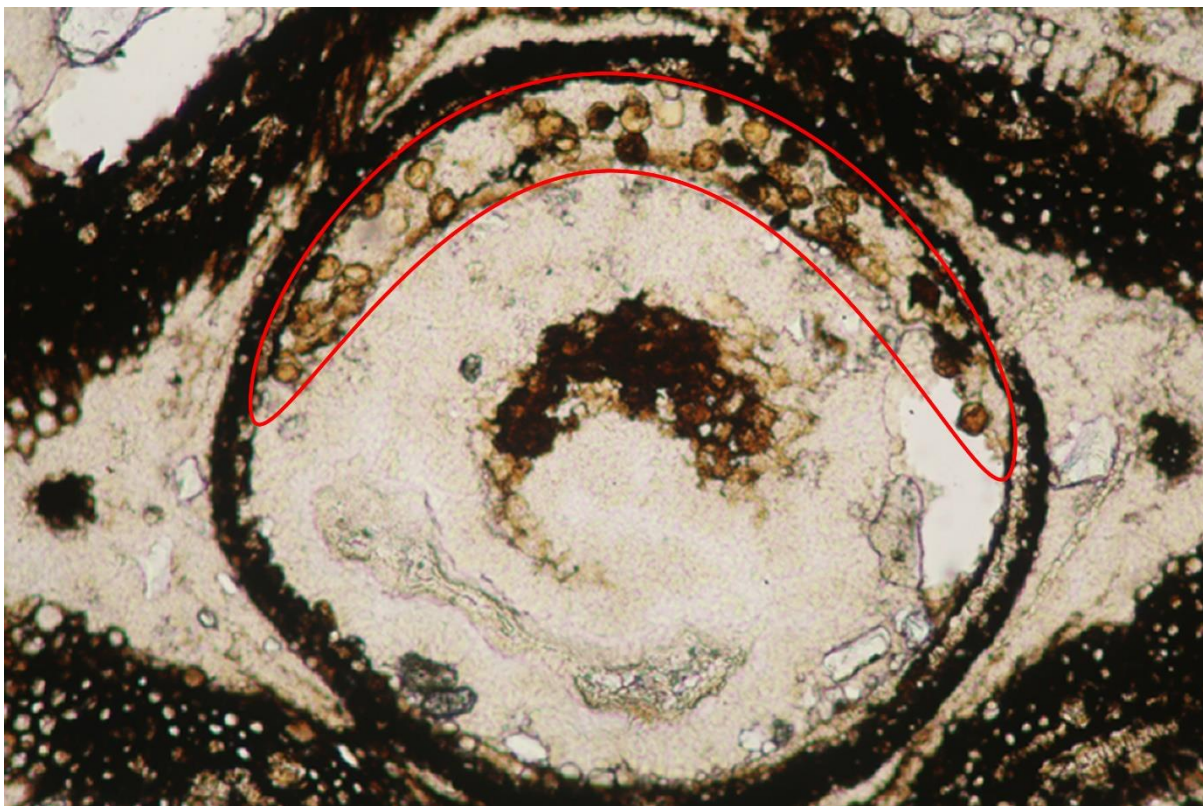


Figure 111. Photomicrograph of part of the ovule of *Lyrasperma scotica* (slide FSC1411 Albert Long Collection, Glasgow) containing multiple specimens of *Colatisporites denticulatus* highlighted in red. Magnification x4.

5.5.2. *Stamnostoma huttonense* Long 1960c

Multiple specimens of *Colatisporites decorus* spores (see Plate 1 figure v), have been found within the ovule of *Stamnostoma huttonense* (Figure 112). Described from petrified seeds from the River Whitadder near Hutton Bridge, *S. huttonense* has been interpreted as a tree-sized pteridosperm with conifer-like wood and trunks up to 25 m in length and 1.4 m in diameter (Long 1960c, Retallack & Dilcher 1988).

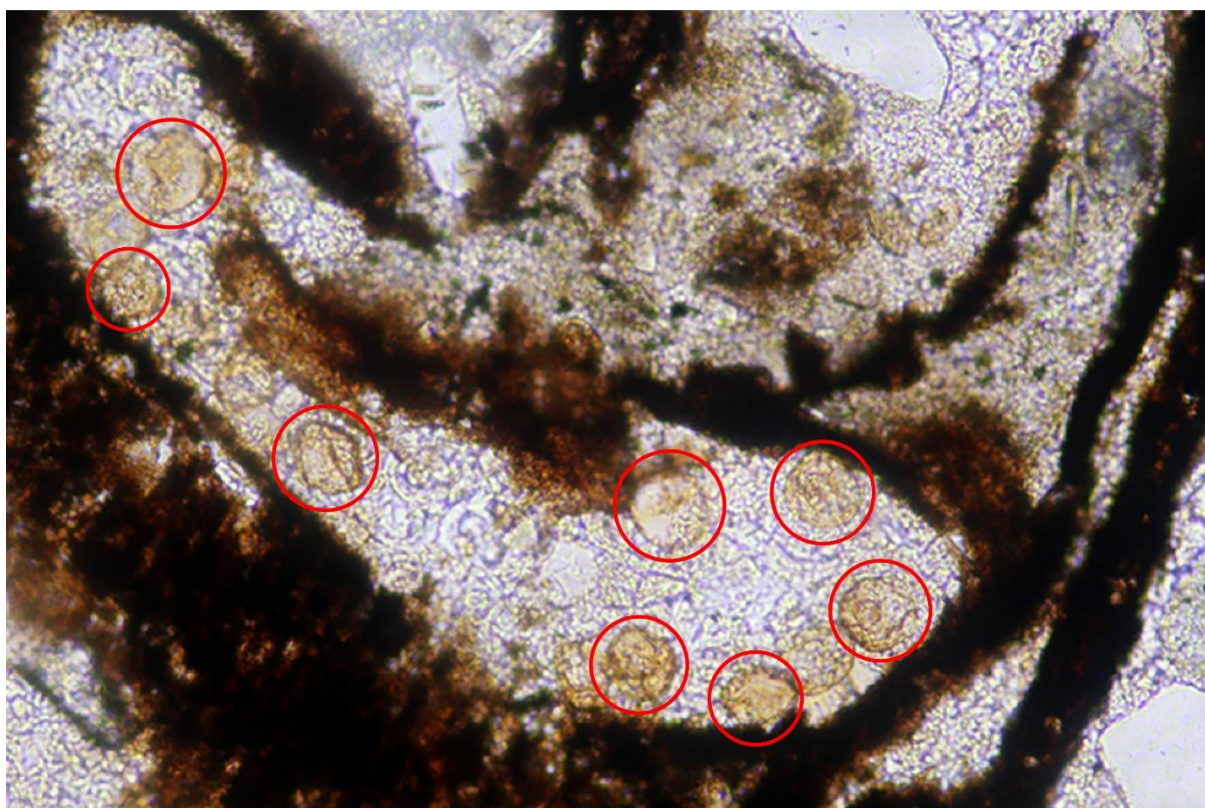


Figure 112. Photomicrograph of part of an ovule of *Stamnostoma huttonense* (slide FSC1148 Albert Long Collection, Glasgow) containing multiple specimens of *Colatisporites decorus* highlighted in red circles. Magnification x10.

5.5.3. *Protopitys scotica* Walton 1957

Although *Remysporites magnificus*, the monosaccate progymnosperm pollen of *Protopitys scotica* (Plate 5 figure o), appeared throughout most of the NWMF borehole core (Figure 106), it only occurred in low numbers (1 to 6) in any one sample (Smith 1962, Walton 1969). The majority of specimens, 28 of 36 (78%), appeared in the lower 100 m (500.98 to 404.50 m), and became increasingly intermittent to the last specimen at 54.56 m depth.

Protopitys scotica (stem with branches and sporangia) was found partly petrified from Loch Humphrey Burn, Dunbartonshire (Walton 1957). However, the whole plant has not yet been reconstructed, so its dimensions are not currently available (Taylor *et al.* 2009).

A review of the type specimen (Smith 1962) in the Hunterian Museum, Glasgow in 2018 revealed complete and partial specimens of *R. magnificus*. These showed how the inner body, which strongly resembles *Punctatisporites* spores, often separates from its exoexinal layer (Figure 113). This means that some specimens of *Punctatisporites* may represent the inner bodies that have become separated from their exoexines.

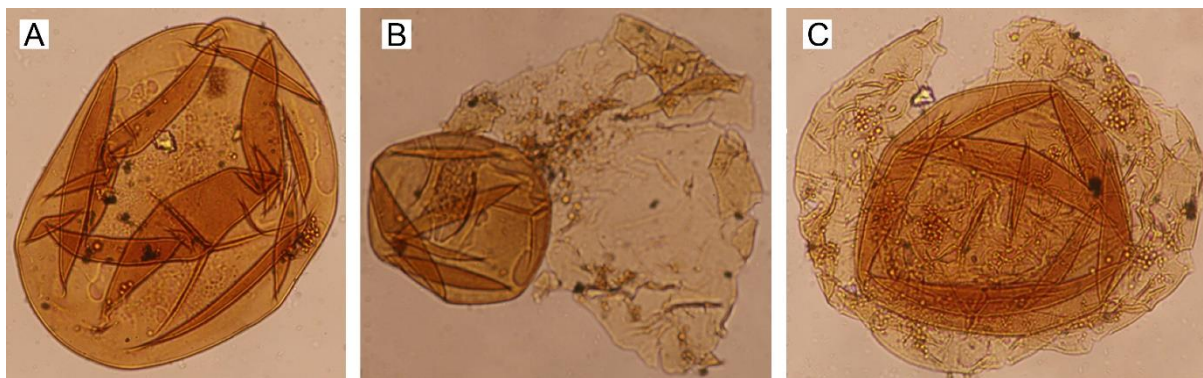


Figure 113. Three grains of *Remysporites magnificus* from the *Protopitys scotica* type slide FSC1372 at the Hunterian Museum, Glasgow. A. Laevigate *Punctatisporites*-type inner body. B. Laevigate *Punctatisporites*-type inner body (left-hand side) with laevigate to finely sculptured exine partially surrounding the

inner body (right-hand side). C. Complete specimen of *R. magnificus* with the laevigate inner body (centre) inside the laevigate to finely sculptured exoexine.

5.6. Summary

Despite the paucity of published records determining the plant affinities for Tournaisian palynomorphs, evidence from the NWMF borehole core has shown how the plant life of the Ballagan environment recovered from the EDME. After a brief survival phase of simple, r-selected vegetation, more complex, K-selected recovery vegetation became dominant. This was formed by an array plant types (i.e. a lycopsid, pteridosperms and a rare progymnosperm) that exhibited a variety of forms from shrubs to trees and produced a structured ecosystem. The driving forces behind the recovery of the Ballagan environment will now be addressed.

5.7. Palaeoenvironment – Introduction

When completing the spore counts (see Section 2.10), it became apparent that some samples contained few taxa (minimum 5) and some had many (maximum 35) and that this phenomenon was happening in a repeated pattern. A simple chart was produced to visualise this (Figure 114).

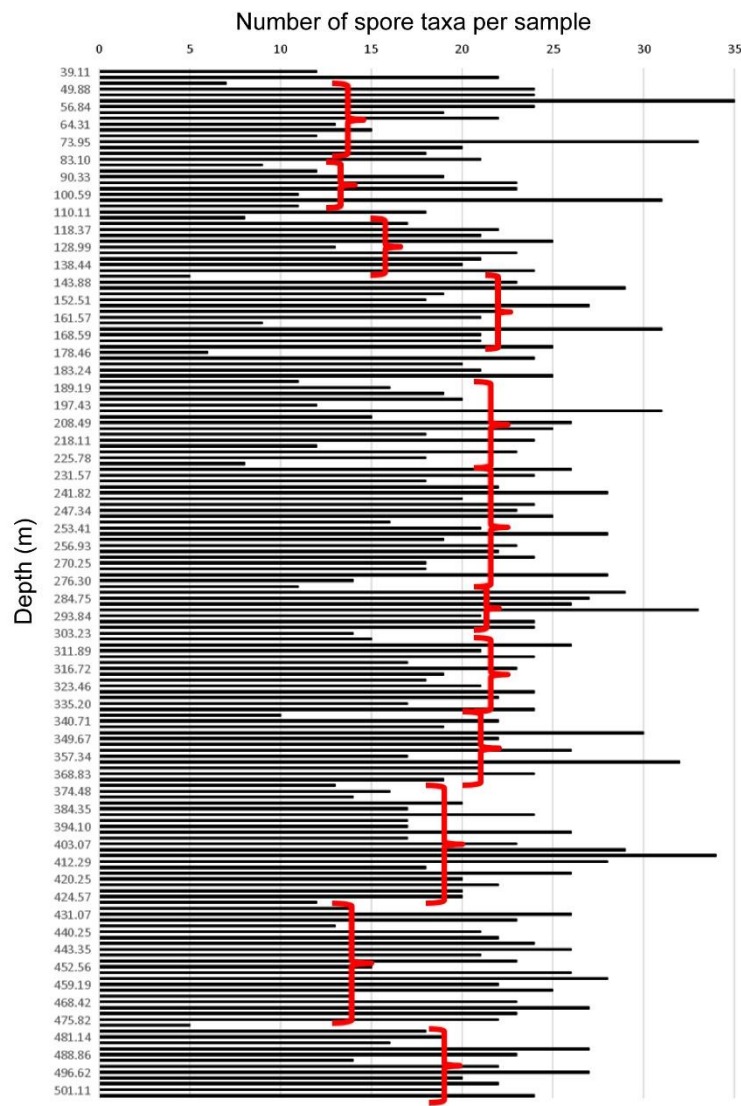


Figure 114. Simple non-depth constrained chart of the total number of spore taxa per NWMF borehole core sample with possible groupings indicated by the red brackets.

This finding warranted further investigation to clarify any trends.

5.7.1. Constrained Incremental Sum of Squares (CONISS)

Using Tilia software, a CONISS analysis was performed on the 8 outgroup taxa (identified in the PCA) and the 4 taxa with recognised botanical affinities (see Sections 5.1 and 5.2) to divide the palynomorph sequences into distinctive natural assemblages of taxa (Figure 115; see Section 2.11.4).

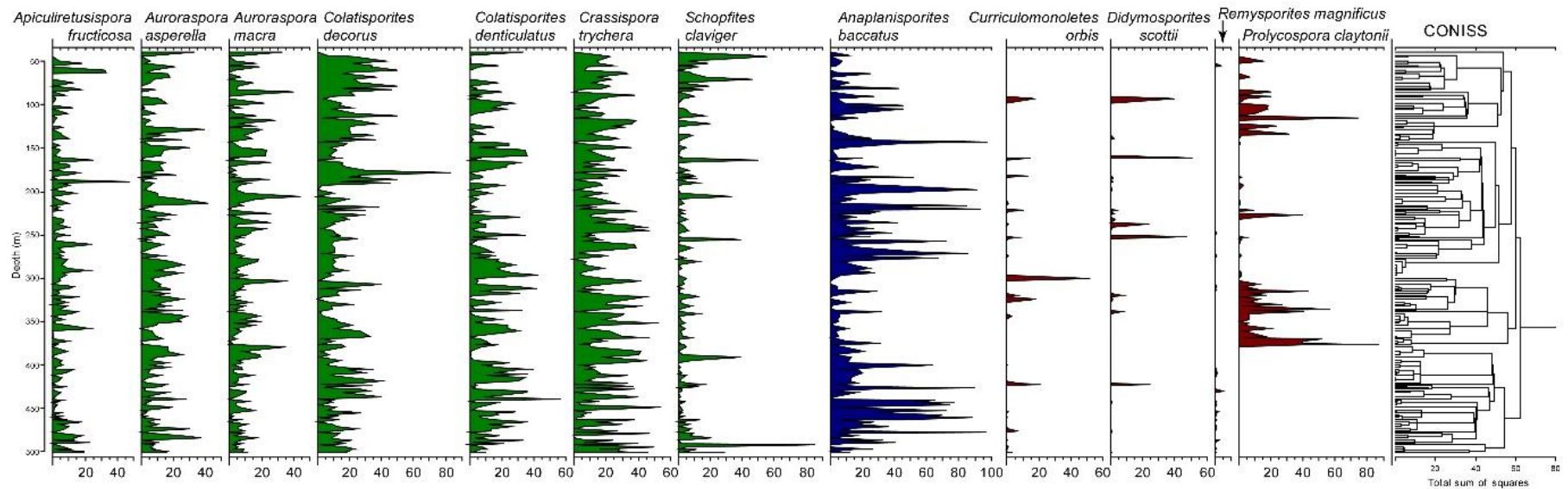


Figure 115. Chart of the fluctuating relative abundances of 12 significant spore taxa by depth (m) used to illustrate the plant recovery in the Ballagan environment. A CONISS dendrogram (on the right-hand side) identifies distinctive natural assemblages of spores.

However, the relative abundance data did not reveal any obvious patterns until the broad scale CONISS dendrogram's clusters were grouped together and highlighted (Figure 116).

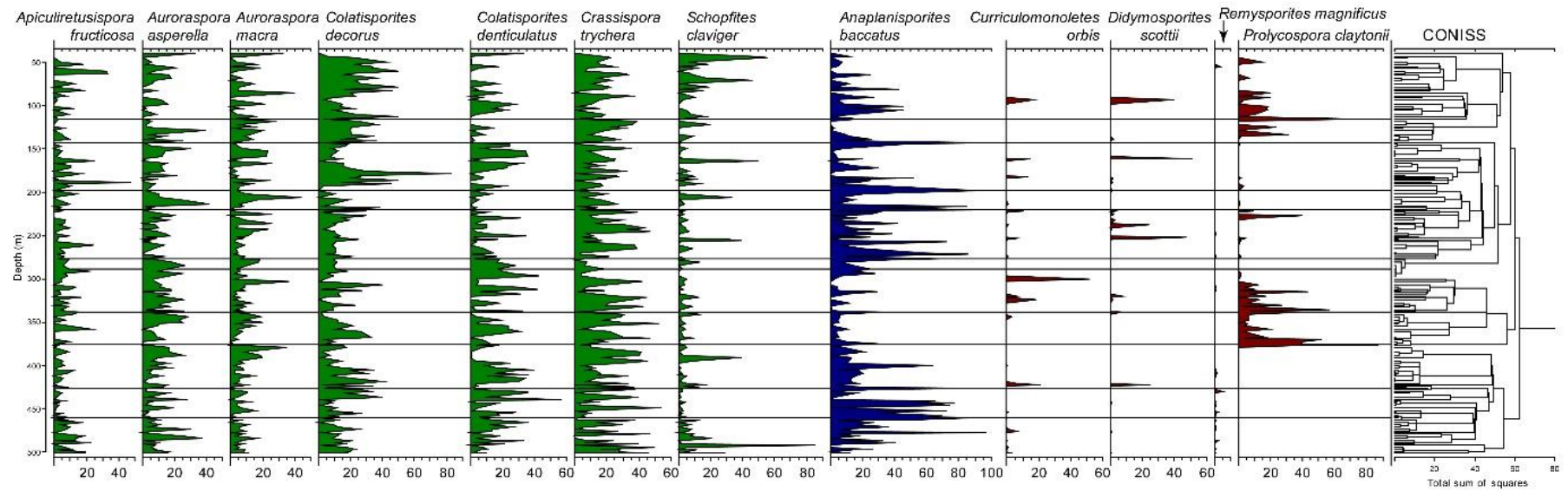


Figure 116. Figure 115 with horizontal lines added to signify that the spore clusters produced by the CONISS analysis could be further grouped.

These grouped clusters were further analysed to track palaeoclimatic changes through the Tournaisian.

5.8. *Schopfites claviger*

To evaluate the pronounced differences in Lower Carboniferous palynological assemblages of North and South Euramerica, Van der Zwan *et al.* (1985) plotted palynomorphs against climate-sensitive rocks to construct humidity curves and climate zones. Starting with the spore taxa that Van der Zwan *et al.* (1985) used to classify each climatic zone, data from the NWMF borehole core were applied to investigate the Ballagan environment.

Using *Schopfites claviger* to define drier climatic conditions (Van der Zwan *et al.* 1985), the grouped clusters were applied to its fluctuating relative abundance and found to be a good match with higher abundance (generally) indicating drier conditions and lower abundance or absence of *S. claviger* representing wetter times (Figure 117). Therefore, using the fluctuating relative abundance of *Schopfites claviger* defined drier and wetter climatic intervals and, as these intervals were repeated, they suggested periodicity.

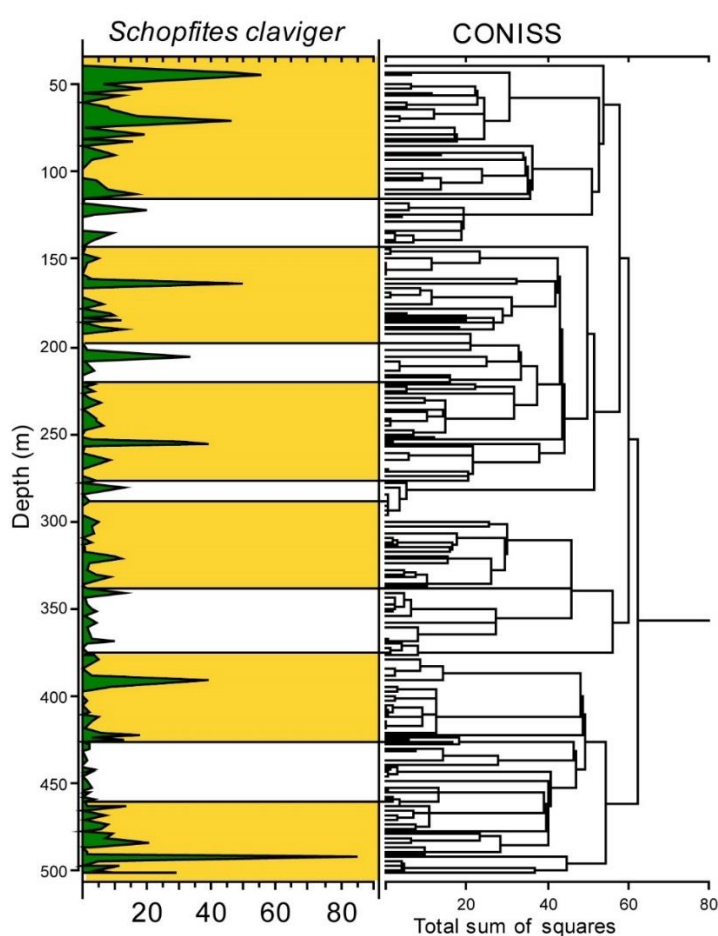


Figure 117. Extract from Figure 116 showing the fluctuating relative abundance of *Schopfites claviger* from the NWMF borehole core. The grouped clusters produced a good match with greater relative abundance indicating drier conditions (shaded in yellow).

5.9. Palaeosols

To understand the range of palaeoclimates available to the earliest terrestrial tetrapods, the 216 palaeosols identified in the NWMF borehole core were described and interpreted by Kearsley *et al.* (2016). Four pedotypes were identified:

1. Inceptisols were the most common (42%). They develop over relatively short time periods, from hundreds to thousands of years and may have formed close to fluvial channels (Retallack 1998, Kraus 1999).
2. Gleyed Inceptisols were the next most common (27%). Their gleyed character, brecciation and carbon preservation of vertical roots with sporadic lateral branches, suggest that these soils formed on a mineral (non-peat) substrate in wetlands that were dominated by herbaceous or shrubby vegetation (Greb *et al.* 2006).
3. Vertisols represented 9% of the palaeosols, but were only present in the uppermost 300 m. They likely developed above the water table on relatively small isolated areas on the floodplain and indicated increasing aridity later in the Tournaisian.
4. The final pedotype was Entisol (22%). These develop on the more active areas of the floodplain of many modern fluvial systems, for example on sand bars that have been stable for long enough for plants to become established.

Additionally, using the palaeosol compositions to estimate the mean annual rainfall, a range of 1000-1500 mm per year was calculated (Kearsley *et al.* 2016).

The presence of deep vertic cracks and gypsum and anhydrite deposits suggested a strongly seasonal climate with repeated cycles of wetting and drying (Kearsey *et al.* 2016).

5.9.1. Palaeosols and palynomorphs

As palaeosols indicate subaerial conditions, they provide a direct record of changes in the climate and landscape architecture (Retallack 1993, Sheldon & Tabor 2009). To investigate the distinctive natural assemblages of the palaeosols, the variable occurrences and thicknesses of the 4 pedotypes were plotted by depth and another CONISS analysis was performed (Figure 118).

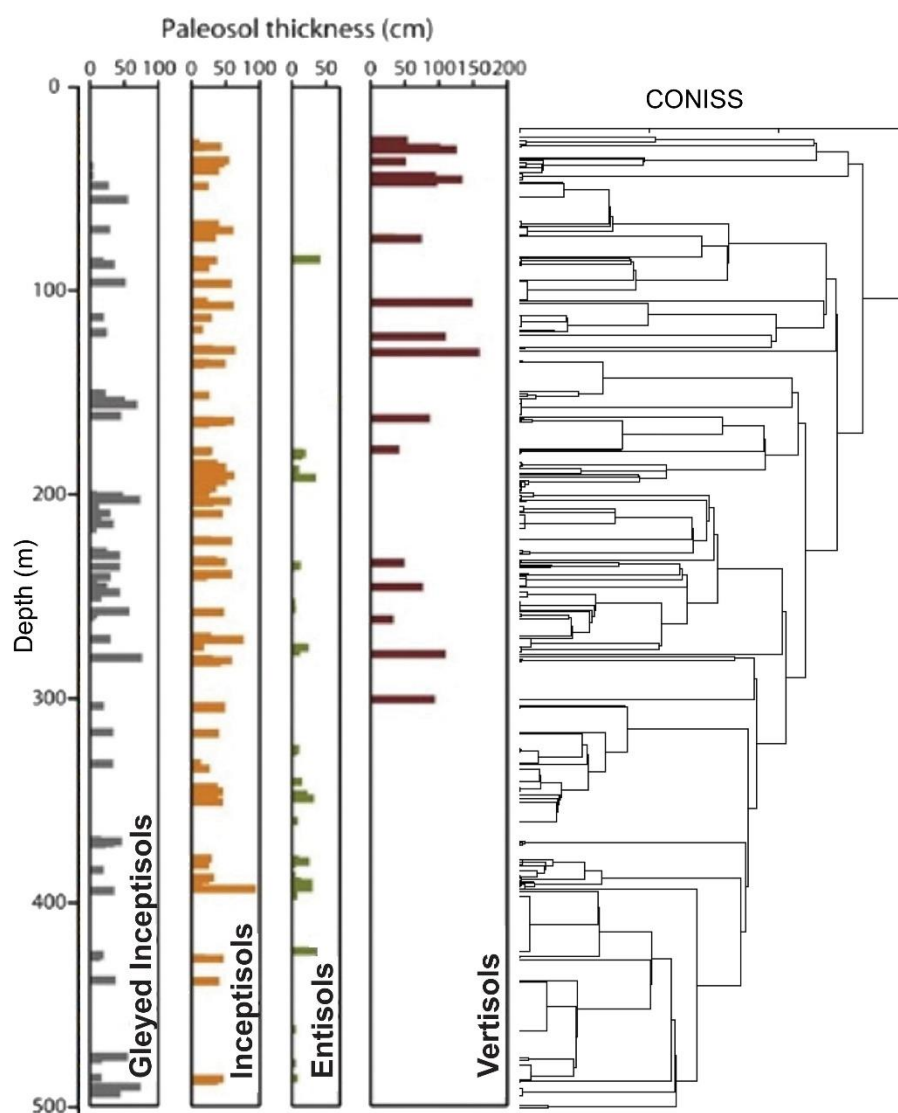


Figure 118. The occurrences (by depth) and thicknesses (horizontal length) of the palaeosols from the NWMF borehole core (left-hand side; after Kearsey *et al.* 2016) with CONISS dendrogram (right-hand side) to show the clusters of distinctive natural assemblages.

When the independently-produced CONISS dendrograms for the palaeosols and the palynomorphs were compared, they revealed close matches between the clusters. This interconnection indicated, for the first time, that soils and palynomorphs could be related directly to each other (Figure 119). Therefore, combining the results of the palynological and palaeosol CONISS analyses increased the robusticity of the palaeoenvironmental analyses from each proxy.

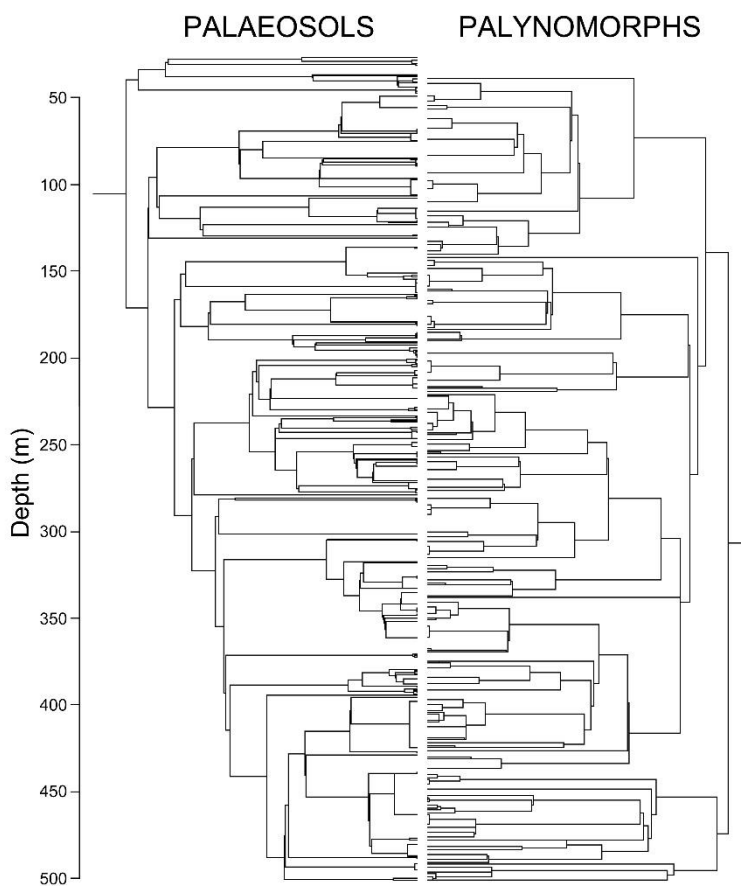


Figure 119. A comparison of the CONISS dendrograms for the palaeosols and the palynomorphs from the NWMF borehole.

5.10. Roots

Root structures were abundant through all of the palaeosols, from shallow mats and thin hair-like traces to large axes of *Stigmaria ficoides* (Sternberg) Brongniart 1839 (Figure 120; Kearsley *et al.* 2016).



Figure 120. Photograph of a large *in situ* axis of *Stigmaria ficoides* from the Burnmouth outcrop section, British National Grid reference: NT 95797 60944. Note the spiral rootlet bases highlighted inside the red rectangle.

Although no direct correlation has been established between the length of plant roots and the size of their corresponding aerial portions, rooting depths of 80 to 100 cm, recorded in the palaeosols at Burnmouth, could have been associated with arborescent plants (Raven & Edwards 2001, Algeo & Scheckler 1998, Kearsley *et al.* 2016).

At other sections near Foulden (6 km away from Burnmouth), gleyed inceptisols were dominated by small shrubby pteridosperms such as *Lyrasperma scotica* (Retallack & Dilcher 1988). Tall forest trees, such as *Stamnostoma huttonense*, have also been found, which are considered to have favoured well drained soils (Retallack & Dilcher 1988). This suggests that forested areas were restricted to the deeper, better drained palaeosols (Kearsley *et al.* 2016).

The presence of *Stigmaria ficoides* indicated the intermittent presence of large arborescent lycopsids growing on a stable substrate. However, these roots did not belong to the Lepidodendroid lycopods as their miospore *Lycospora pusilla* has a

Viséan inception and predates all of the Ballagan Formation. The Tournaisian big lycopod trees must, therefore, have been producing a (currently) unknown spore.

5.11. Anastomosing river channels

Members of the TW:eed project team found evidence of 3 to 36 m thick fluvial sandstone bodies at the Burnmouth outcrop (Figure 121). Some of these bodies (at 174 to 181 m heights; Figure 122) have been interpreted as anastomosing river channels and are included here as they demonstrate the stabilising effect of vegetation on river systems.



Figure 121. Fluvial sandstones (outlined in black) at Burnmouth. Scale bar = 100 m. Courtesy of Sarah Davies 2016.

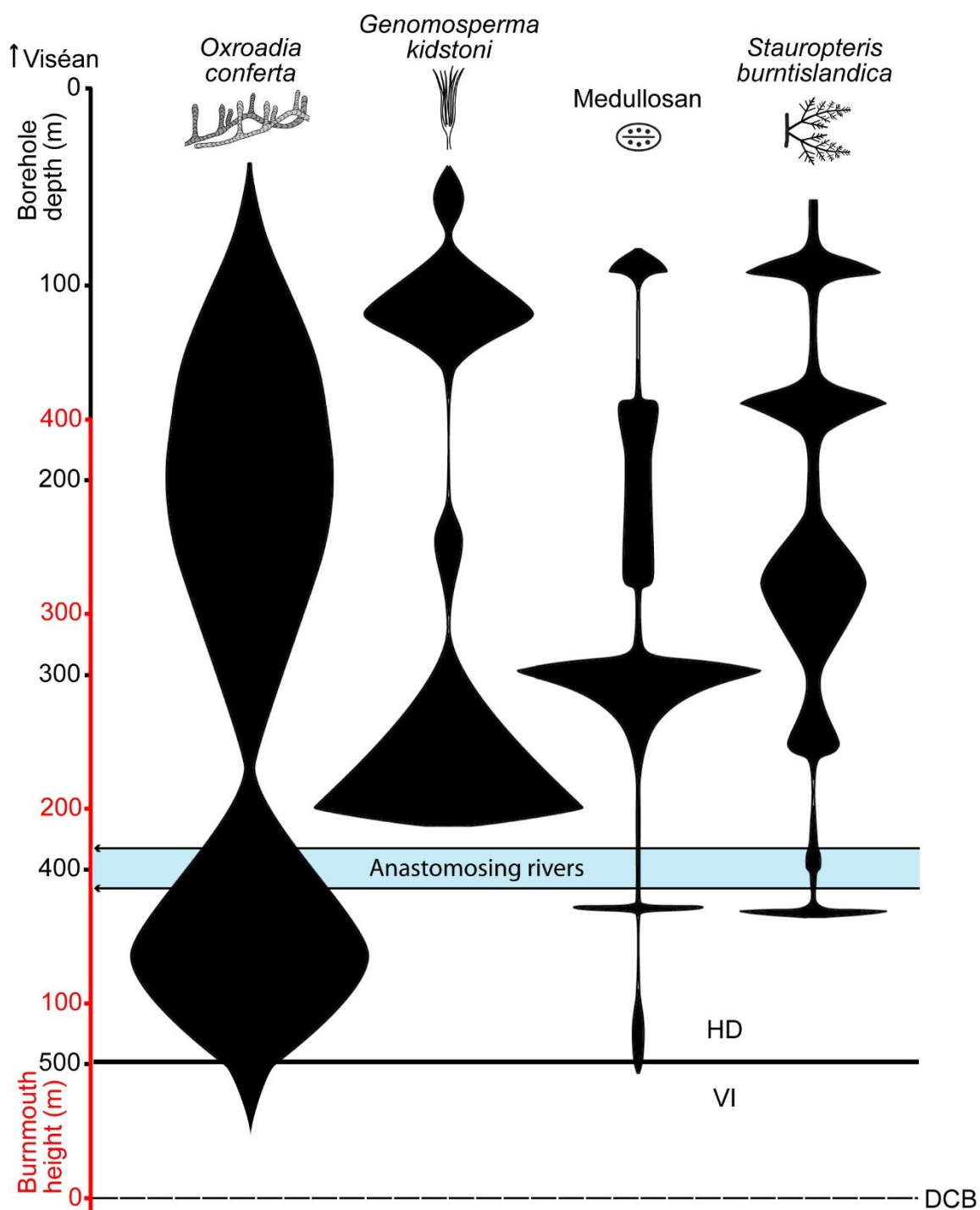


Figure 122. Summary diagram of the plant recovery of the Tournaisian Ballagan environment (Figure 110) with the location of the fluvial sandstone bodies at the Burnmouth outcrop that are interpreted as anastomosing river channels highlighted in blue.

5.11.1. The evolution of anastomosing river channels

Before the evolution of terrestrial plant life, fluvial systems experienced high rates of sedimentation and erosion with the lateral migration of channels for many tens of kilometres (Schumm 1968, Rainbird 1992, MacNaughton *et al.* 1997). The expansion of vegetation caused profound effects on the development of fluvial systems through time.

The increased rhizoid and root activity of the earliest vegetation began to stabilise substrates by promoting the storage of fines and acted as a buffer between rainfall, runoff and evaporation (Algeo & Scheckler 1998, Allen & Gastaldo 2006, Davies & Gibling 2010, Knighton 1998). Although initially the effects on sediment binding, yield and discharge and bank stability were limited, the increase in the size and diversity of arborescent plants promoted the density of their root networks to attach and bind themselves to the depositional surface (Davies & Gibling 2010, 2011). This greatly boosted the stability of entire floodplains and provided more habitats for plants to exploit (Davies & Gibling 2011).

Anabranching rivers are systems of multiple channels with stable (vegetated) alluvial islands that divide flows at channel capacity and anastomosing rivers are a low-energy, organic-rich subset of this group (Nanson & Knighton 1996). The stratigraphic correlation between the first appearance of anastomosing rivers and the continuing development of arborescent land plants is strong (Davies & Gibling 2011).

That avulsion was the primary means of channel movement is inferred by the lack of lateral continuity between the channels (Davies & Gibling 2011). Avulsions are commonly linked to vegetation and include blockage by *in situ* plants, log jams and the growth of levees (Jones & Schumm 1999, Abbe & Montgomery 2003).

The mechanisms for triggering avulsions became common, for the first time, during the Carboniferous (Davies & Gibling 2011). Arborescent plants produce more mechanically complex wood, which resists comminution during transport (Rowe & Speck 2004, Davies & Gibling 2011). This contributed to the increased

supply of large woody debris (LWD) to river systems, which affected channel dynamics (Davies & Gibling 2011, Abbe & Montgomery 2003). Carboniferous rivers were, therefore, not only more likely to receive large volumes of LWD than previously, but also to retain it, which contributed to channel blockage (Davies & Gibling 2011).

Incidentally, the oldest example of anastomosing river channels published, so far, was recorded from the Viséan Kekiktuk Formation of Alaska (Melvin 1993). However, the evidence for anastomosing sand bodies found at the Burnmouth outcrop indicates that they developed earlier – in the Tournaisian stage.

5.12. Megaspores analysis

Further to the miospore data, Tilia software was used to plot the distribution and relative abundances of the megaspore taxa for the NWMF borehole core (see Section 2.15). Figure 123 shows that none of the megaspore taxa appeared continuously throughout the core, instead, their distribution was more intermittent.

A CONISS analysis was performed to cluster together distinctive natural assemblages of the megaspores, which showed broadly two phases of distribution interrupted by a 36 m megaspore-free gap (Figure 123). Phase 1 (501 to 374 m) exhibited the greatest relative abundance and diversity (82% of all inceptions and 60% of all megaspore-containing samples). Phase 2 (338 to 49 m) showed their sporadic return with lower relative abundance and diversity.

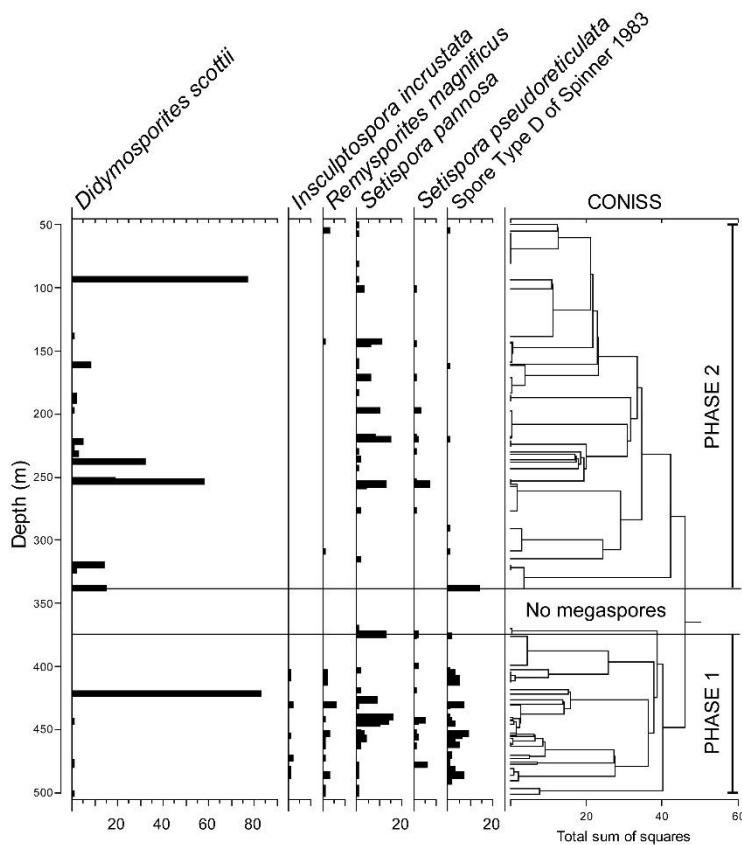


Figure 123. The distribution and relative abundances of the megaspores from the NWMF borehole core with a CONISS dendrogram. The two megaspore phases and the megaspore-free interlude are annotated.

When the miospore cluster groupings were added to the megaspore data to add the climate information, this showed that the majority of the megaspores were distributed in the drier phases, inferring their plants' preference for a drier climate (Figure 124). Indeed, the megaspore-free interlude coincided with the second of the wetter phases of the Ballagan environment.

Conversely, most of the *Setispora pannosa* megaspores were present in wetter phases, which implies that its parent plant, *Oxroadia conferta*, had a wide climatic tolerance, in addition to being able to withstand unstable substrates. This finding provides further evidence for *O. conferta* being a hardy, coloniser plant.

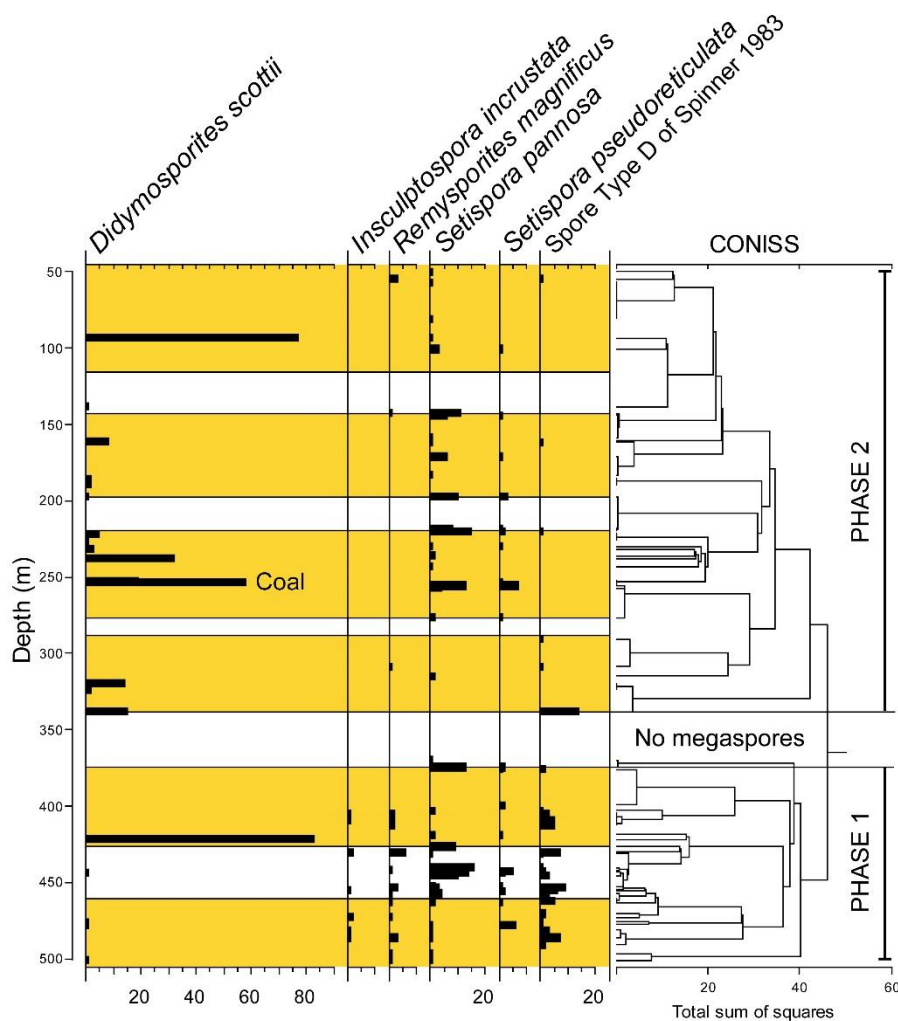


Figure 124. Figure 123 with the drier climatic phases from the *Schopfites claviger* miospore data shaded in yellow (see Section 5.8). The location of a thin coal horizon representing *in situ* peat is also shown (see Section 5.13).

5.13. Coal analysis

During the core sampling, a thin (2 cm) coal seam was discovered at 256.10 m depth (Figures 124 and 125). To determine its plant composition, the megaspore content was investigated. Also, chemical analyses of the coal were made to determine its rank and type (see Section 2.16).

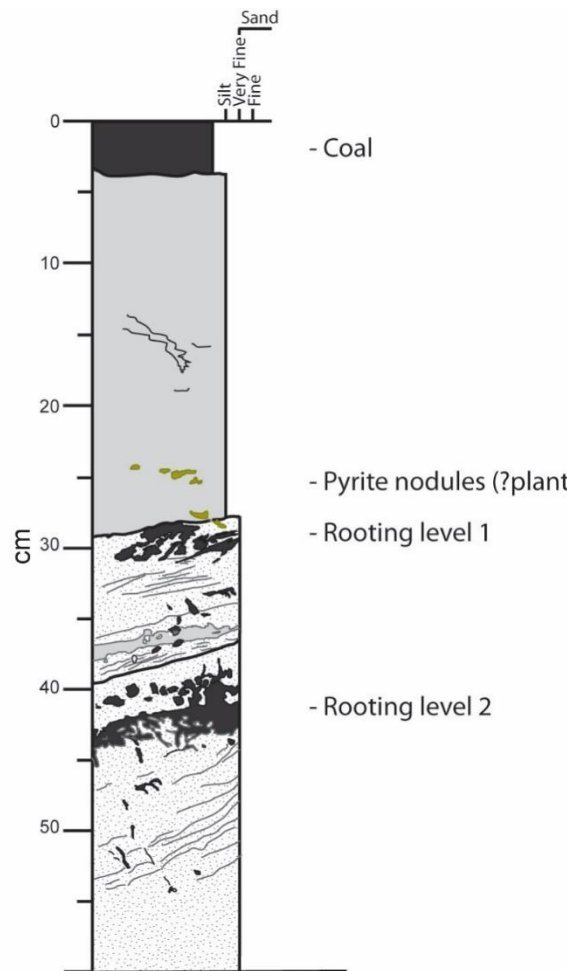


Figure 125. Log of a coal horizon at 256.10 m depth in the NWMF borehole core. From Kearsey *et al.* (2016).

5.13.1. Megaspore content

After processing (see Section 2.16), most of the coal was found to contain abundant megaspores of only two species: *Didymosporites scottii* (58%) and *Setispora pannosa* (41%; Figure 126). This showed that it was mostly vitrinite and did not contain *Botryococcus* (algae).

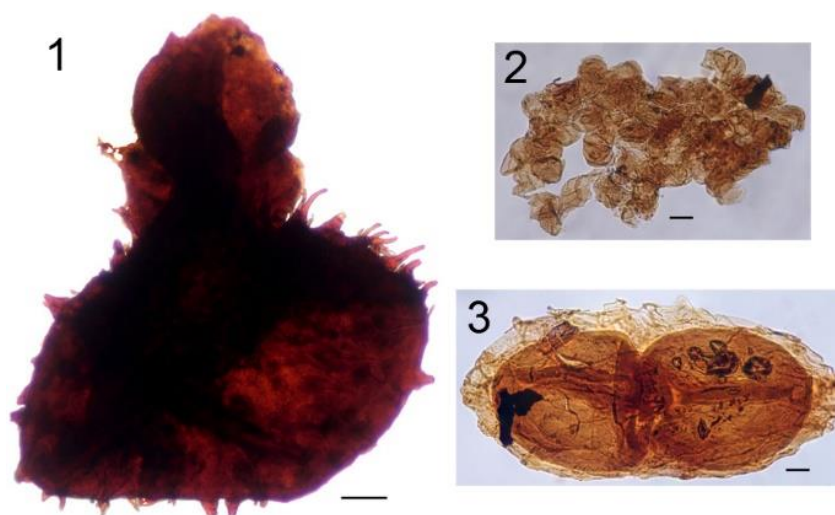


Figure 126. Megaspores isolated from the coal seam of the NWMF borehole core. 1. *Setispora pannosa*. Scale bar = 50 µm. 2. A mass of *Anaplanisporites baccatus* (the microspore of *S. pannosa*). 3. *Didymosporites scottii* tetrad. Scale bars = 20 µm.

A PCA of the coal megaspores allocated *Setispora pannosa* and *Didymosporites scottii* as outgroup taxa (Figure 127). This highlighted that both parent plants (*Oxroadia conferta* and *Stauropteris burntislandica* respectively) represented dominant plants in the Ballagan environment.

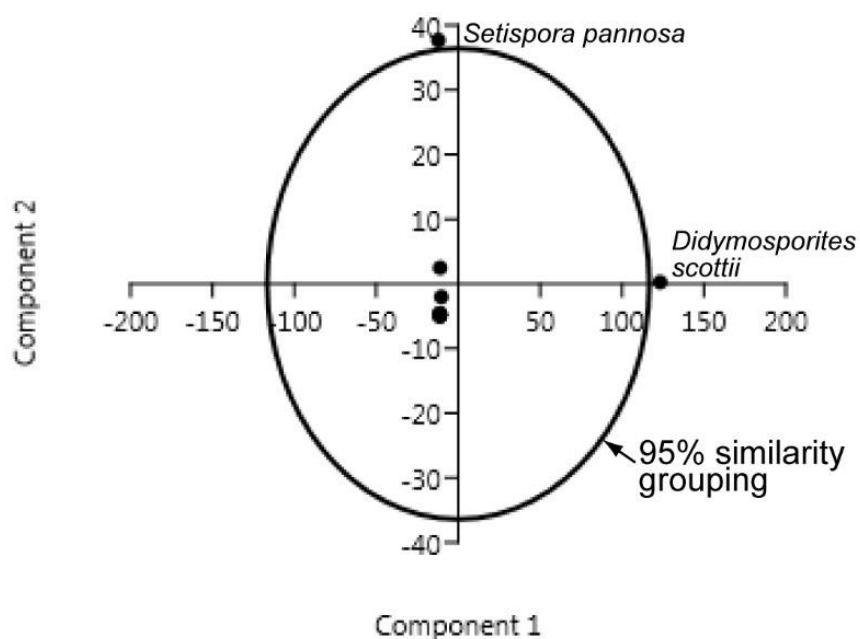


Figure 127. A PCA of the megaspores from the coal horizon of the NWMF borehole core revealed two outgroup taxa (*Setispora pannosa* and *Didymosporites scottii*).

5.13.2. Further analyses

Elemental analysis was performed by OEA Laboratories Limited (see Section 2.16.1.1; tables 11 and 12) and the total ash content was 23.9% (see Section 2.16.1.2).

Sample ID	% Nitrogen	% Carbon	% Hydrogen	% Sulphur	% Oxygen
SSK42061	0.71	53.25	3.86	7.63	12.15
SSK42061	0.71	53.26	3.73	7.67	12.07
Mean	0.71	53.25	3.80	7.65	12.11

Table 11. Results of the elemental analysis of two samples of the same coal from the NWMF borehole core.

	Organic components (recalculated)
C	70.0%
H	5.0%
O	15.9%
N	0.9%
S	10.1%

Table 12. Recalculated elemental analysis results from Table 11.

To identify the type of coal, the atomic ratios of O/C and H/C were plotted on a Van Krevelen diagram (Figure 128; see Appendix 16 for the calculations used).

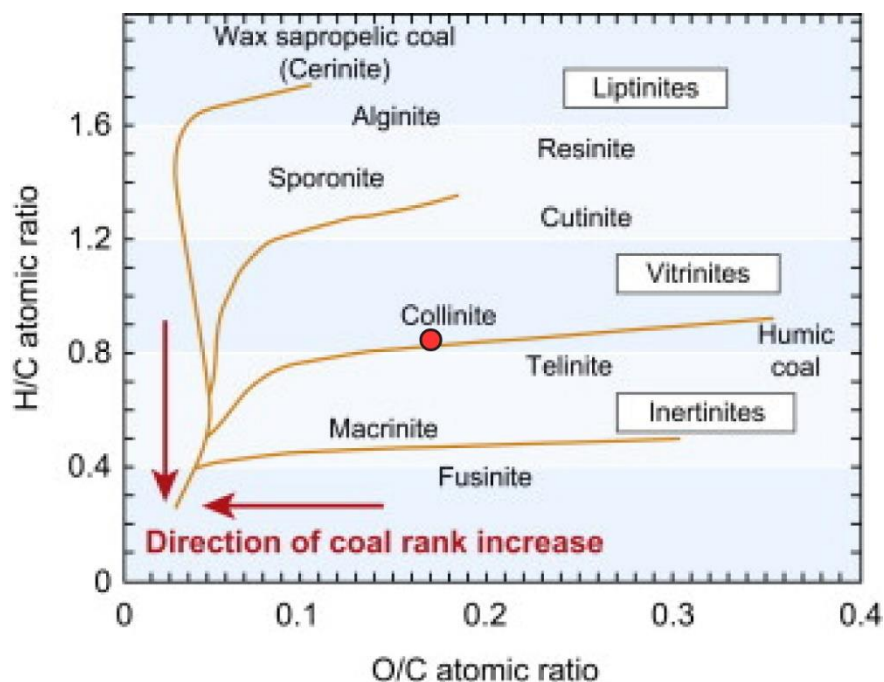


Figure 128. Van Krevelen diagram with the H/C and O/C atomic ratios of the coal sample from the NWMF borehole core (256.10 m) marked as a red circle. After Flores (2014).

The Van Krevelen diagram shows that the coal was of low rank. This was confirmed by its low vitrinite reflectance value (0.54%; D. K. Carpenter 2016 pers. comm.).

Using a peat compression rate of about 10:1, the 2 cm coal layer gave an original peat layer of approximately 20 cm in depth (Stach *et al.* 1982). With a peat accumulation rate of 3–4 mm/year (tropical forests; Stach *et al.* 1982), this equated to about 50-70 years for the peat layer to form.

5.13.3. Conclusions

The results of these analyses indicated that the coal sample from the NWMF borehole core was a carbonaceous mudstone consisting of predominantly well-preserved spores of terrestrial plants rather than algae, it was of low thermal maturity and contained a high amount of ash.

The coal was produced in an enclosed pool surrounded by lycopods and ferns in a very stable, wetland community. However, as no roots were found at the base of the coal layer (Figure 125), the plants that formed it had not been growing *in situ* and had been transported into the pool.

5.14. Scolecodonts

A total of 80 scolecodont specimens were found in 23 of the NWMF borehole core's palynological samples (see Section 2.17). Tilia software was used to plot the distribution and abundances of the scolecodonts (Figure 129).

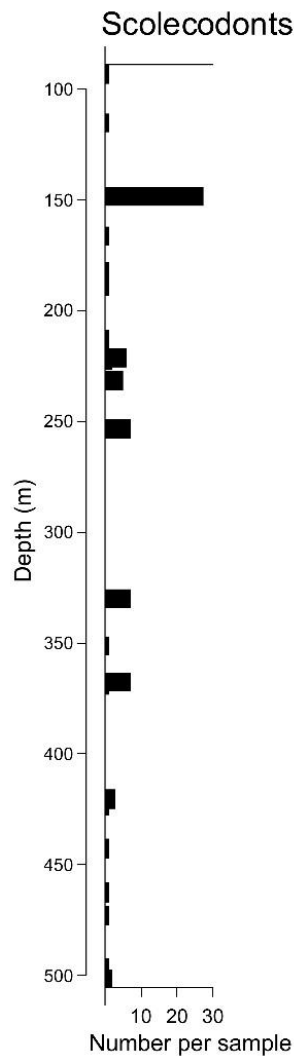


Figure 129. The distribution and numbers of scolecodonts identified in palynological samples from the NWMF borehole core.

As Palaeozoic scolecodonts are considered to have inhabited various, often marginal, marine environments, the samples containing them represent a coastal locality with rare marine transgressions onto the Ballagan floodplain (Szaniawski 1996; Bennett *et al.* 2016).

5.15. Summary

To investigate the potential palaeoenvironmental controls on the plant recovery of the Ballagan area following the EDME, a variety of proxies was used.

The diversity of palaeosols indicated a dynamic floodplain with a strongly seasonal climate, which became increasingly dry towards the end of the Tournaisian. On a broader palaeoclimate scale, the varying relative abundances of *Schopfites claviger* signified a repeating pattern of drier and wetter climate intervals, suggesting periodicity.

Analysis of the megaspores showed that while the majority of their parent plants preferred a drier climate, *Oxroadia conferta* (represented by *Setispora pannosa*) exhibited a broad climate tolerance. Furthermore, the copious megaspores that formed a coal horizon indicated that *Oxroadia conferta* (lycopsid), which produced thickets and *Stauropteris burntislandica* (fern), an important understorey plant, were highly significant to the Ballagan area during the Tournaisian. Also, evidence from roots indicated that there were forested areas and that these were restricted to deeper, better drained soils.

The presence of fluvial sandstone bodies, interpreted as signifying anastomosing river channels, highlighted the stabilising effect of plants on river systems. However, the intermittent presence of palynomorph samples that contained scolecodonts revealed occasional marine transgressions onto the floodplain.

CHAPTER 6

CONCLUSIONS

This research focusses on the recovery of the early Carboniferous vegetation after the End Devonian Mass Extinction (EDME) – an interval associated with the evolution of terrestrial vertebrate animals (tetrapods).

Of crucial importance was the gap in the fossil record in the Tournaisian and Viséan stages that coincided with the transition of fully aquatic animals to those occupying fully terrestrial habitats. Known as ‘Romer’s Gap’, this time span contained the transitional forms of fossil tetrapods that showed the developmental stages that were necessary to adapt fully to terrestrial conditions and the order in which those characters arose.

To address this conundrum, the *Tetrapod World: early evolution and diversification* (TW:eed) project investigated the fossils and environments of the Tournaisian stage of the early Carboniferous. The work presented here forms one component of this much larger project.

The expansion of the terrestrial habitats of plants produced a significant rise in atmospheric oxygen levels that enabled arthropod herbivores to colonise terrestrial habitats. Shortly after the initial arthropod clades became terrestrialised, the first semi-terrestrial tetrapods appeared and both groups quickly showed major originations and radiations.

Invertebrates form a major food source for extant animals and so the expansion of the invertebrates’ habitats onto land would have been a strong driver for the tetrapods to follow suit. Once the transition onto land had been made, tetrapods continued to evolve in tandem with new forms of plant life to exploit the newly emerging habitats and food webs.

The tetrapods under investigation by the TW:eed project were found in the Tournaisian Ballagan Formation of the Midland Valley of Scotland and the

Northumberland Trough in England. Studying cores from a borehole provided a relative timeframe for the biotic and environmental recovery following the EDME. The Norham West Mains Farm (NWMF) borehole was, therefore, commissioned to produce a high resolution, continuous record of the Ballagan Formation sediments. Importantly, this was the first time that the Ballagan Formation had been cored specifically for an integrated palaeontological and palaeoclimatic project.

To investigate the plant recovery following the EDME, palynomorph-containing material from the NWMF borehole core was examined. Palynomorphs were present in 82% of the samples which ranged from 501.18 m to 39.11 m. Systematic descriptions were made for the 40,558 most abundant miospores/microspores, all megaspores, pollen, acritarchs and euglenoids, which represent 50 genera and 103 species. These data form the basis for the palynological analysis of the biozonation and plant recovery discussions.

Obtaining a continuous record at the base of the Ballagan Formation was the most important objective to enable the recovery phase immediately after the EDME to be studied. However, the Ballagan Formation was thicker than anticipated at the drill site for the drill rig capacity which was 500 m depth. Therefore, to complete the palynological study, the base of the nearby outcrop locality at Burnmouth was integrated with the borehole data.

Using the NWMF borehole core to produce an accurate biozonation was one of the main objectives of the TW:eed project to interconnect the scattered tetrapod sites and to date the fossils they contained. Unfortunately, the NWMF borehole palynomorphs did not easily lend themselves to the published miospore zonation schemes of either Higgs *et al.* (1988) or Turnau (1978). Of the taxa used to define the published biozones, not all of them were present in the NWMF borehole core, the ones that were appeared in different sequences and were often of low abundance.

The main reason for these discrepancies was that the number of samples taken by Higgs *et al.* (1988) and Turnau (1978) was often low and the sampling intervals were irregular and widely spaced. By contrast, the NWMF borehole core was

sampled systematically at 1 m intervals and, therefore, gave better quality datasets.

Nevertheless, compiling the data from the NWMF borehole core and the Burnmouth outcrop and applying the zonal indicator taxa from Higgs *et al.* (1988) and Turnau (1978), resulted in recognising four palynozones for the Tournaisian Ballagan Formation: starting with the brief survival phase of the VI (*Vallatisporites verrucosus*–*Retusotriletes incohatus*) zone, the recovery period began with the HD (*Kraeuselisporites hibernicus*–*Claytonispora distincta*) zone and moved into the PC (*Spelaetriletes pretiosus*–*Raistrickia clavata*) and CI (*Prolycospora claytonii*) zones.

Revealing the recovery of the plant life following the EDME was another main outcome of the TW:eed project. Despite a paucity of published records determining the plant affinities for Tournaisian palynomorphs, evidence from the NWMF borehole core has shown that after a brief survival phase of simple, r-selected vegetation, more complex K-selected recovery vegetation became dominant. This was formed by an array of plant types that exhibited a variety of forms from shrubs to trees and produced a structured ecosystem (Figure 130).

To investigate the driving forces behind the recovery of the Ballagan environment after the EDME, a CONISS analysis of the 8 outgroup taxa and the 4 inception taxa produced distinctive natural assemblages which were grouped together to track palaeoclimatic changes through the Tournaisian. Applying the grouped clusters to the fluctuating relative abundance of the miospore *Schopfites claviger*, which represented drier climatic conditions, displayed a repeating pattern of drier and wetter climate intervals.

As palaeosols provide a direct record of changes in the climate and landscape architecture, comparing the CONISS dendrograms for the palaeosols identified in the NWMF borehole core and the palynomorphs revealed a correlation. This showed, for the first time, that fossil soils and palynomorphs can be related directly. The diversity of palaeosols indicated a dynamic floodplain with a strongly

seasonal climate which became increasingly dry towards the end of the Tournaisian. This finding agreed with the palynomorph data.

Root structures were abundant through all of the palaeosols and could be associated with arborescent plants. The presence of *Stigmaria ficoides* indicated intermittent large arborescent lycopods growing on a stable substrate. However, these roots did not belong to the Lepidodendroid lycopods as their miospore *Lycospora pusilla* has a Viséan inception and predates all of the Ballagan Formation. The Tournaisian big lycopod trees must, therefore, have been producing a presently unidentified spore.

Evidence of fluvial sandstone bodies interpreted as anastomosing river channels found at the Burnmouth outcrop demonstrates the stabilising effect of vegetation on river systems. However, the oldest published example of anastomosing river channels is from the Viséan of Alaska (Melvin 1993), but the evidence for anastomosing sand bodies found at the Burnmouth outcrop indicates that they developed earlier – in the Tournaisian stage.

Further to the miospore data, the megaspores from the NWMF borehole core showed a sporadic distribution and a CONISS analysis showed two distinct phases interrupted by a megaspore-free gap. When the climate information from the miospore data was added to the distribution of the megaspores, this showed that they were mostly present in the drier phases, inferring their plants' preference for a drier climate. The megaspore-free interlude also matched a wetter phase of the Ballagan environment. Conversely, most of the *Setispora pannosa* megaspores were present in wetter phases, which implies that its parent plant, *Oxroadia conferta*, had a wide climatic tolerance, in addition to being able to withstand unstable substrates. This provides further evidence for *O. conferta* being a hardy, coloniser plant.

During the core sampling, a thin coal seam was discovered. Analyses showed that it was a carbonaceous mudstone consisting of predominantly well-preserved spores of terrestrial plants rather than algae. It was of low thermal maturity, contained a high amount of ash and took about 50–70 years to form. The

abundant megaspores *Setispora pannosa* and *Didymosporites scottii* indicated that their respective parent plants, the thicket producing *Oxroadia conferta* (lycopsid), and *Stauropteris burntislandica* (fern), an important understorey plant, formed the coal. It, therefore, represented an enclosed pool surrounded by lycopods and ferns in a stable, wetland community.

A total of 80 scolecodont specimens were found in 23 of the NWMF borehole core's palynological samples. Their intermittent presence revealed a coastal locality with rare marine transgressions onto the Ballagan floodplain.

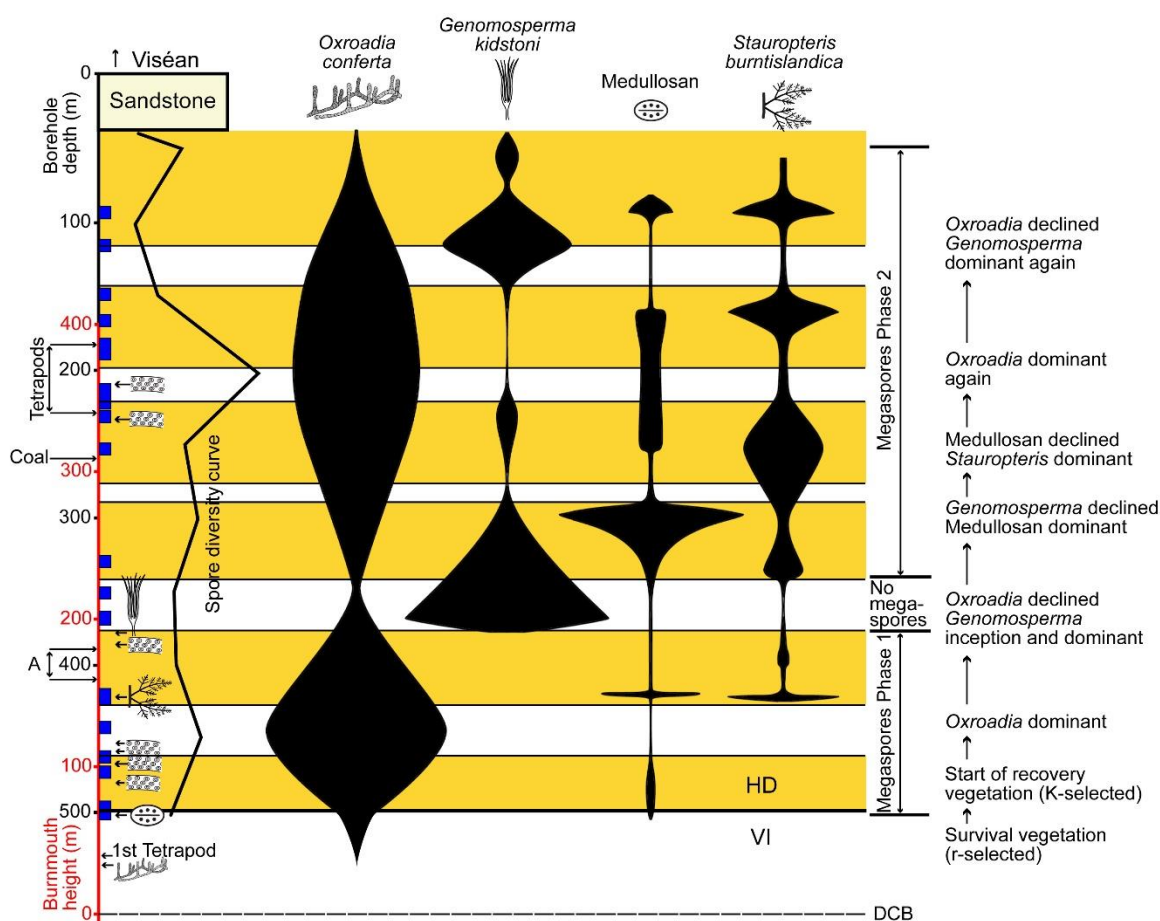



Figure 130. Summary of the floral recovery of the Tournaisian Ballagan environment. The DCB is shown at the base. The VI-HD biozones boundary is shown above. On the left-hand side are the Burnmouth outcrop heights (red) and the NWMF borehole depths (black) shown in metres. The spindle diagrams represent the relative abundances (wider shape = higher abundance) of the dominant plants. On the left-hand side are the inceptions of *O. conferta*, a putative

medullosan pteridosperm, *S. burntislandica* and *G. kidstoni* (the key to the plant icons is at the top of the diagram), the heights of the Lepidodendroid roots () , tetrapods and anastomosing river channels (A) found at outcrop and the depth of the coal horizon from the NWMF borehole core. The blue squares denote the borehole samples that contained scolecodonts. The spore diversity curve is shown beneath the sandstone body. The two phases of the megaspores' distribution are shown on the right-hand side. A summary description of the changing dominant plants is listed to the far right. The drier climatic intervals are shaded yellow.

APPENDIX 1

TW:eed project team staff profiles

This is a brief summary of the responsibilities of the main staff involved in the TW:eed project, with their qualifications and research interests by institution.

THE UNIVERSITY OF CAMBRIDGE



Professor Jennifer A. Clack FRS

Emeritus Professor of Vertebrate Palaeontology

Department of Zoology

University of Cambridge

Jenny has made major contributions to early tetrapod palaeontology, especially discovering, describing and analysing new and recently prepared material from the late Devonian and early Carboniferous periods. This work has changed perceptions about the evolution of tetrapod limbs, breathing and hearing and is now included in standard biology textbooks.

Her research interests encompass: the origin, phylogeny and radiation of early tetrapods and their relatives among the lobe-finned fish. The "fish-tetrapod" transition and the evolution of terrestriality. The timing and sequence of skeletal and other changes that occurred during the transition and the origin and relationships of the diverse tetrapods of the Late Palaeozoic. The origins of the modern radiations of tetrapods.

Accolades

- 2008 Daniel Giraud Elliott medal – The National Academy of Sciences, USA
- 2009 Fellow of the Royal Society
Foreign Honorary Member of the American Academy of Arts and Sciences
- 2013 Honorary Doctorate – University of Chicago
T. Neville George Medal – The Geological Society of Glasgow
- 2014 Foreign Honorary Member of the Royal Swedish Academy of Sciences
Honorary doctorate – The University of Leicester
- 2015 The Lapworth Medal – The Palaeontological Association



Dr Timothy R. Smithson

Post-Doctoral Research Associate
Department of Zoology
University of Cambridge

With over 20 years of prospecting, Tim was the main source of new tetrapod localities in the Borders Region of Scotland. Specifically targeting Tournaisian deposits, he combined his extensive knowledge of the geology and palaeontology of the region with a previous academic record of the description and analysis of early Carboniferous tetrapods.



Keturah Z. Smithson

Post-Graduate Research Assistant
Department of Zoology
University of Cambridge

Ket studied Zoology at the University of Leicester, where she won the Henry Walter Bates Award for being the top graduate in her class. She worked alongside the palaeontologists on the TW:eed Project, specifically focussing on micro-CT scanning many of the specimens and reconstructing their 3D images.

THE UNIVERSITY OF LEICESTER



Professor Sarah J. Davies

Professor of Sedimentology

Head of School

Course Director: Geology

School of Geography, Geology and the Environment

University of Leicester

Sarah has over 20 years' experience and numerous publications in clastic sedimentology and sequence stratigraphy.

As a clastic sedimentologist, her research seeks to understand the processes that controlled deposition and erosion in non-marine and shallow-marine settings preserved in the geological record. Her most recent research focused on fine-grained sedimentary successions from these settings and examined how these depositional environments evolve spatially and temporally.

Her research awards include the TW:eed Project's NERC Consortium Grant (2012-2016): research at Leicester provided insights into the environmental conditions that existed during the rebuilding of an early Carboniferous ecosystem and contributed to the preferential preservation of early tetrapods. This work built on earlier research evaluating the global Carboniferous sedimentary record to elucidate the climate response to glacial events.

Sarah also leads the European Petrophysics Consortium for the International Ocean Discovery Program (IODP). Research Associates within the consortium provide expertise in the fields of downhole logging, core petrophysics and core-log integration IODP expeditions for the global research community. Sarah is involved in a number of industry- and NERC-funded projects combining sedimentology and petrophysics for stratigraphic and resource (conventional and unconventional) analysis: ongoing projects at Leicester are funded by NERC's Oil and Gas Innovation Fund.

Accolades

- 2007 The British Sedimentological Research Group Roland Goldring Award for noteworthy published research in any field of sedimentology
- 2015 The Geological Society's Coke Medal for her exceptional contribution to geology



Dr Carys E. Bennett

Post-doctoral Research Associate

School of Geography, Geology and the Environment

University of Leicester

Carys is interested in palaeoclimate and fossils and is an ostracod specialist, with experience of Carboniferous sedimentology, macro- and micro-faunas, palynology and geochemistry.

For the TW:eed project, Carys performed extensive logging and sampling of the rocks of the Ballagan Formation, particularly at Burnmouth, but also at numerous other sites in the region and for the NWMF borehole. To investigate the palaeoenvironmental and palaeoclimatic context of tetrapod evolution Carys has analysed the sedimentology, stratigraphy and isotope geochemistry of the Ballagan Formation. One of the main findings of her study of non-marine ostracods, was the potential use of ostracod shell geochemistry as a palaeoclimatic indicator.

Carys's research interests include early Carboniferous palaeoclimates and palaeoenvironments as the setting for tetrapod evolution, the Devonian/Carboniferous ecological radiation of ostracods into non-marine environments and the micro-scale assessment of the fidelity of fossil preservation and ultrastructure to use fossils as palaeoenvironmental proxies; using primarily ostracods (Devonian to Recent) and trilobite eyes (Ordovician).



Janet E. Sherwin

Post-Graduate Research Assistant

School of Geography, Geology and the Environment

University of Leicester

Janet used optical and electron microscopy and petrographic analysis to understand the processes of deposition and depositional environments, particularly of fine-grained sediments. Janet was primarily interested in the sediments exposed at Coquetdale.

THE UNIVERSITY OF SOUTHAMPTON



Professor John E. A. Marshall

Professor of Earth Science

Ocean and Earth Science

National Oceanography Centre Southampton

University of Southampton

John's work focusses on understanding Mid-Palaeozoic biotic events, palaeoclimates and marine to terrestrial teleconnections. The international dimension of his Devonian research is emphasised by projects in East Greenland, sub-polar Urals, Bolivia, Falkland Islands and China. Other Devonian research highlights include marine Devonian sediments in Scotland, progymnosperm heterospory, seed origins and the age relationships of the early tetrapods. He is Secretary of the Sub-Commission on Devonian Stratigraphy, Past-President of the Commission Internationale de la Microflore du Paléozoïc (CIMP) and a subject editor of the Journal of the Geological Society, London.

John specialises in palynology, petroleum geology and Earth system history and his research interests incorporate: Mid Palaeozoic Mass Extinction Events, the spread of the Devonian forests, sedimentary organic matter in landfill sites, early seed plants, petroleum source rocks and Devonian oil and gas reservoirs in South America, North Africa and the Moray Firth.



Emma J. Reeves

Post-Graduate Research Assistant

Ocean and Earth Science

National Oceanography Centre Southampton

University of Southampton

For the TW:eed project, I sampled, processed and analysed plant spores from the NWMF borehole core to assist with the development of a new quantitative palynostratigraphy for the earliest Carboniferous and to develop an integrated environmental model and a refined spore/ostracod zonation scheme. I studied BSc (Hons) Geology with Biology at Royal Holloway College, University of London and completed MRes in Vertebrate Palaeontology at the University of Southampton in 2013.



David K. Carpenter

PhD student

Ocean and Earth Science

National Oceanography Centre Southampton

University of Southampton

For the TW:eed project, Dave examined the distribution and physical characteristics of charcoal within the Burnmouth section, to reconstruct wildfire activity during Romer's Gap. This provided insights into the atmospheric oxygen content during the Tournaisian, and formed part of a NERC-funded PhD project entitled "Charcoal, forests and Earth's Palaeozoic geochemical oxygen cycle". Dave studied Geological Sciences at the University of Leeds, and completed his MSc in Palaeobiology at the University of Bristol.

THE BRITISH GEOLOGICAL SURVEY



Dr David Millward

Senior Geologist

BGS Scotland

The Lyell Centre

Edinburgh

Dave was a geological surveyor for 35 years and led the BGS mapping and stratigraphical interpretation programme on the Carboniferous of northern England for the last 10 years. He collaborated with Professor Melanie Leng on the interpretation of carbon and oxygen isotope records in the Carboniferous of the UK and has extensive experience of deep drilling programmes, including the Newcastle deep geothermal drilling project. He is a Chartered Geologist and a John Phillips medallist (2009) of the Yorkshire Geological Society, awarded for his stratigraphical work in northern England.



Dr Timothy I. Kearsey

Geologist

BGS Scotland

The Lyell Centre

Edinburgh

Tim is a survey geologist with specific expertise in palaeosols and their use as climate indicators, and in stable isotopes in carbonates, gained through his PhD at Plymouth University and on a research project on the Permo-Triassic extinction event in the southern Ural Mountains of Russia.

NERC ISOTOPE GEOSCIENCES LABORATORY



Professor Melanie J. Leng

Head of the Stable Isotope Group

NERC Isotope Geosciences Laboratory

BGS Keyworth and University of Leicester

Nottingham

Melanie holds a Visiting Chair in Isotope Geoscience at the University of Nottingham and is Visiting Professor at the University of Leicester. She is a recognised expert in stable isotope geochemistry and has published widely on carbon and oxygen isotope records and climate change.

NATIONAL MUSEUM OF SCOTLAND



Dr Nicholas C. Fraser

Head of the Department of Natural Sciences

National Museum of Scotland

Edinburgh

Nick has over 25 years' experience of vertebrate palaeontology research, with a significant publications record. He has led many field operations in a variety of strata worldwide, including large-scale excavations in China, the east North American Coastal Plain and 10 successive field seasons in the dinosaur-rich Jurassic Badlands of Wyoming, USA.

Nick's interdisciplinary research focuses on the Triassic period and he has published extensively on Triassic faunas and floras. Nick is particularly interested in tanystropheids, marine reptiles with enormously elongate necks. He works closely with colleagues at the Institute of Vertebrate Palaeontology and Palaeoanthropology (IVPP) in Beijing, Peking University and the Chicago Field Museum of Natural History to investigate these strange animals from the Middle Triassic of southern China.

Nick is an Adjunct Professor in the Department of Geosciences, Virginia Tech and Honorary Fellow in Geosciences, Edinburgh University.



Dr Stig A. Walsh

Senior Curator of Vertebrate Palaeobiology
Department of Natural Sciences
National Museum of Scotland
Edinburgh

Stig's has worked and published on a wide variety of marine and terrestrial vertebrates, including early tetrapods and uses X-ray micro computed-tomographic (μ CT) techniques to investigate the evolution of the vertebrate brain and senses (palaeoneurology).

Nerve and sensory structures rarely fossilise, so palaeoneurology must rely on information recorded by the bone that were associated with the structures in life. This evidence, such as the relative size of parts of the brain cavity, the diameter of nerve canals and the form of other bony anatomical structures such as the inner ear, can provide insight into the behaviour and sensory abilities of extinct animals. Current approaches in palaeoneurology apply numerical modelling to the neurosensory structures of living species to interpret the same structures preserved in fossils.

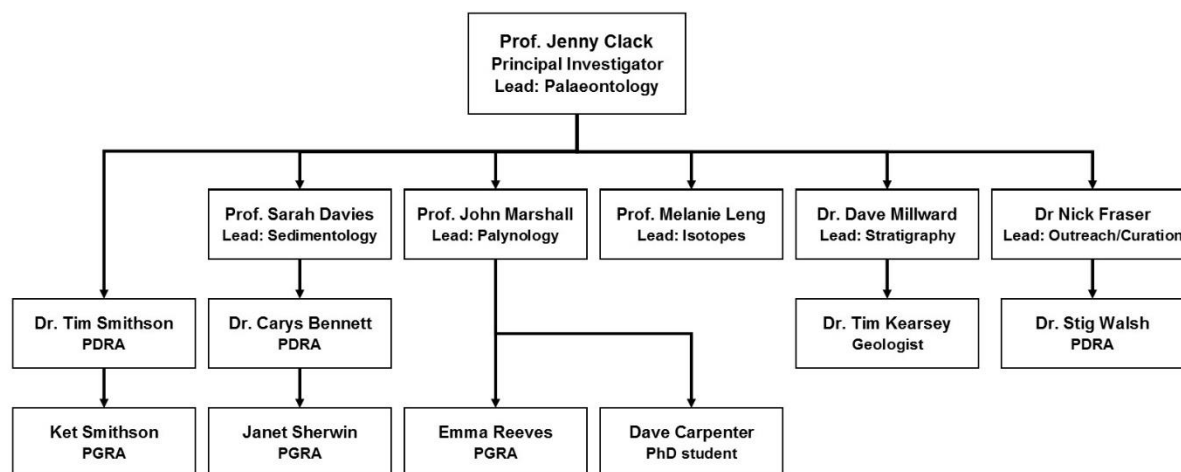


Figure 131. Organisational diagram to show the relationships between the core TW:eed team members and the project frameworks.

Additionally, the core TW:eed teams were ably assisted by many other people, including Masters and PhD students, volunteers and professional scientists.

APPENDIX 2

Work Instruction: Sampling procedure

This work instruction details the steps that were taken to sample the NWMF borehole core for palynological specimens (see Section 2.6.1).

1. The BGS 'Record of samples taken during inspection' worksheet was prepared by annotating the box and core run (CR) numbers for the next box of core to be sampled.
2. The field notebook was prepared by annotating the box's starter depth (Figure 29).
3. The box of core was visually inspected for suitable horizons to sample:
 - For palynology: the samples were dark coloured (not red (oxidised) or green (reduced)) and not coarse grained.
 - For isotopes: samples were taken with every palynology sample, where there were significant changes in the lithology and where requested.
4. Using a metal rule, the centre of each horizon was measured from the base of the box and the measurement was annotated in a field notebook (Figure 132).

BGS reference	Measurement from base of core box m/cm	Depth of sample	Any other information
SSK38168	1.23	378.60	
SSK38169	6	378.27	378.33
SSK38170	73	377.40	TS only
SSK38171	1.27	377.06	
SSK38172	15	376.68	376.83 TS only
SSK38173	54	376.29	
SSK38174	1.15	375.68	Plants
SSK38174	78	376.05	
SSK38176	85	374.48	Plants 375.33 Fossil
SSK38177	1.39	373.94	
SSK38178	1.40	373.93	TS only
SSK38179	1.51	373.82	
SSK38180	10	373.73	373.83 TS only
SSK38181	13	373.70	
SSK38182	47	373.36	TS only
SSK38183	70	373.18	
SSK38184	1.50	372.33	
SSK38185	16	372.17	372.33
SSK38186	76	371.57	TS only

Figure 132. Photograph of the field notebook being completed during sampling with the BGS reference number (e.g. SSK38186), the measurement of the base of the sample from the base of the core box, the depth that measurement represented in the borehole, any further information e.g. TS only = sample taken for thin section only.

5. The paperwork was completed:

- Ensuring the IS(M) number has been written/stamped on each 'Borehole Subsample' label.
- Writing the sample depth measurement in the 'Depth' section of each of the three copies of the 'Borehole Subsample' label.
- Where no thin sections were taken, writing this information in the 'Sample Type' column.
- Where additional thin sections were requested, writing this information in the 'Sample Type' column.

6. One copy of the label was adhered to the 'Record of samples taken during inspection' worksheet in the 'Sample Number (Barcode Label)' column.
7. One copy of the label was adhered to a white card.
8. The final copy of the label was adhered to the palynology sample bag which was also annotated with a 'P' to demarcate it as a palynology sample (Figure 133).

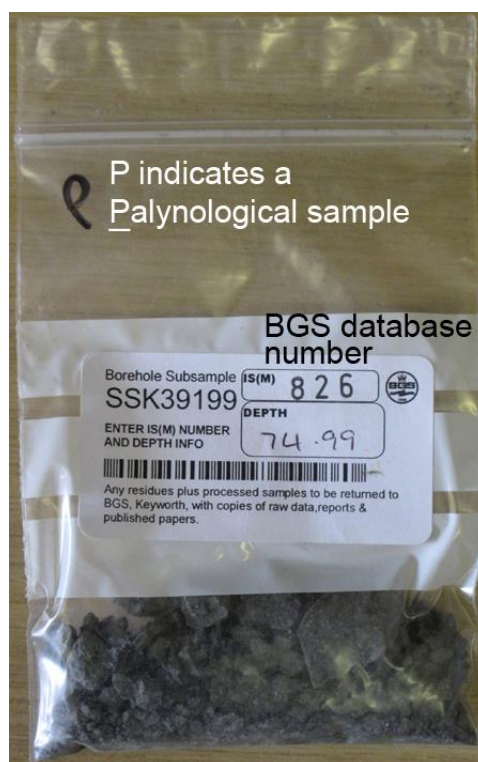


Figure 133. A bag containing a sedimentary sample taken from the core where: P indicated it was a palynological sample, SSK39199 was the BGS borehole sample number, 826 was the BGS database number (i.e. the NWMF borehole was number 826), 74.99 was the depth of the sample in metres.

9. Additional sample bags were annotated with the unique sample reference number and the sample depth. They were marked with 'TS' for the thin sections and with 'I' for isotopes.
10. The section of sediment to be sampled was removed carefully, ensuring that the direction up core was noted.
11. The thin section samples were prepared first (if appropriate) by carefully removing as much of the sediment in a continuous column and marking the

way 'up' with an arrow drawn on the sample. It was then wrapped in tin foil and 'Top' was written on the uppermost surface with arrows drawn on to mark the up core direction. They were then placed in a sample bag that had been annotated with 'TS'.

12. For the palynology and isotope samples (where appropriate) equal amounts of approximately 15 g were placed into each bag.
13. The white card with the 'Borehole Subsample' label was placed in the space left where the samples had been removed.
14. Any extraneous sediment was brushed from the work surface to reduce contamination between samples.
15. An Excel spreadsheet of each sample number, depth and type was maintained. Where additional samples for thin sections had been requested, they were highlighted in yellow.

APPENDIX 3

Work Instruction: Processing palynological samples

This work instruction details the steps that were taken to process the palynological samples that were taken from the NWMF borehole core (see Section 2.7).

Before any processing could begin, basic laboratory attire was worn (Figure 134):

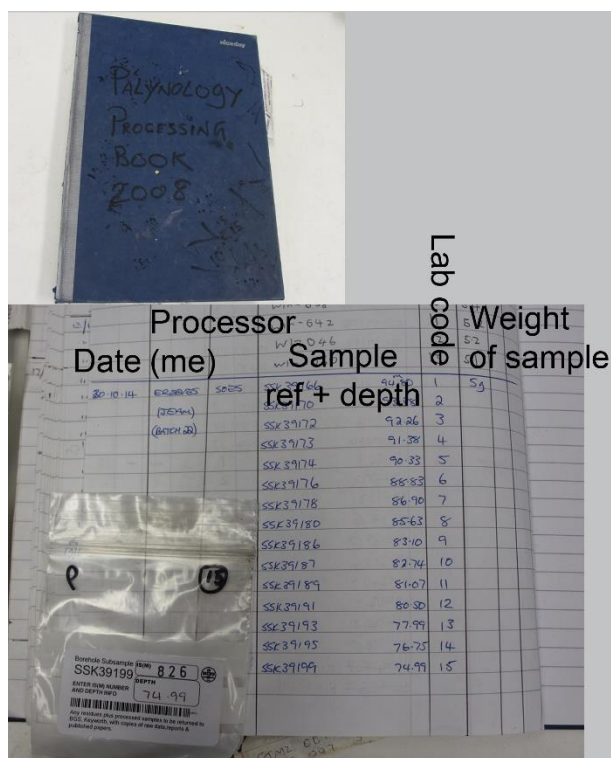
- long hair tied back.
- long sleeve top to cover arms.
- long trousers to cover legs.
- lab coat to protect clothes.
- safety glasses to protect eyes.
- purple nitrile gloves to protect hands.



Figure 134. Me wearing basic laboratory attire.

Preparation

1. Sample containers were labelled 1 to 15 (15 containers were used for each batch as they fitted most safely into the fume cupboard's working space).
2. 15 bags of samples to be processed and 15 empty bags were labelled 1 to 15.
3. The logbook was completed (Figure 135):
 - Date
 - Who did the processing (me (JEAM))
 - From (SOES)
 - Sample details i.e. SSK number, depth and NWMF borehole
 - Code (lab code on beakers)
 - Weight of sample i.e. 5 g or 5.0
 - Ox (number of minutes oxidised in Nitric acid – not applicable)
 - Lyco (number of *Lycopodium* tablets used – not applicable)
 - Sieve mesh size



Processor	Date (me)	Sample ref. + depth	Lab code	Weight of sample
JEAM	2010-10-14	SSK39170	94.30	1
JEAM	(BATCH 22)	SSK39172	92.86	3
		SSK39173	91.38	4
		SSK39174	90.33	5
		SSK39176	88.83	6
		SSK39178	86.90	7
		SSK39180	85.63	8
		SSK39186	83.10	9
		SSK39187	82.74	10
		SSK39189	81.07	11
		SSK39191	80.50	12
		SSK39193	77.99	13
		SSK39195	76.25	14
		SSK39199	74.99	15

Figure 135. Photograph of the 'Palynology Processing Book' that was completed before processing palynological rock samples (top) and the details that were entered (bottom).

4. Each sample was parcelled in scrap paper with the ends folded over to prevent loss and crushed into pea-sized chips by hitting with the hammer on a metal block (Figure 136).



Figure 136. Hammer (Draper 1 lb on left-hand side) and metal block (right-hand side) used to crush rock samples to pea-sized chips before processing.

5. 5 g of the crushed sample was weighed using the balance (Ohaus Model No. C305-5 Serial No. 47832 Capacity 300 x .1g) (Figure 137) and added to the empty sample bag of the appropriate number.



Figure 137. Ohaus balance used to weigh rock samples before processing.

6. Any remaining sample was returned to the original sample bag.
7. The sample to be processed was separated from the rest to avoid mix up.
8. Each container was rinsed with clean water.
9. The crushed sample was added to the appropriately numbered container, ensuring sample bag was emptied completely (figures 138 to 140).



Figure 138. Numbered bags of crushed rock samples (at the bottom) to be placed into the correspondingly numbered containers (at the top) before processing.



Figure 139. Adding the numbered rock sample to the correspondingly numbered container before processing.



Figure 140. Containers with rock samples to be processed.

Stage 1: Hydrochloric acid (HCl)

This stage takes 2 days to complete and removed fluorides from the samples.

In conjunction with the basic laboratory attire, HCl PPE was worn: green boots, white apron, black HCl gloves and full-face visor.

1. The numbered containers with the samples were placed into the fume cupboard (Figure 141).

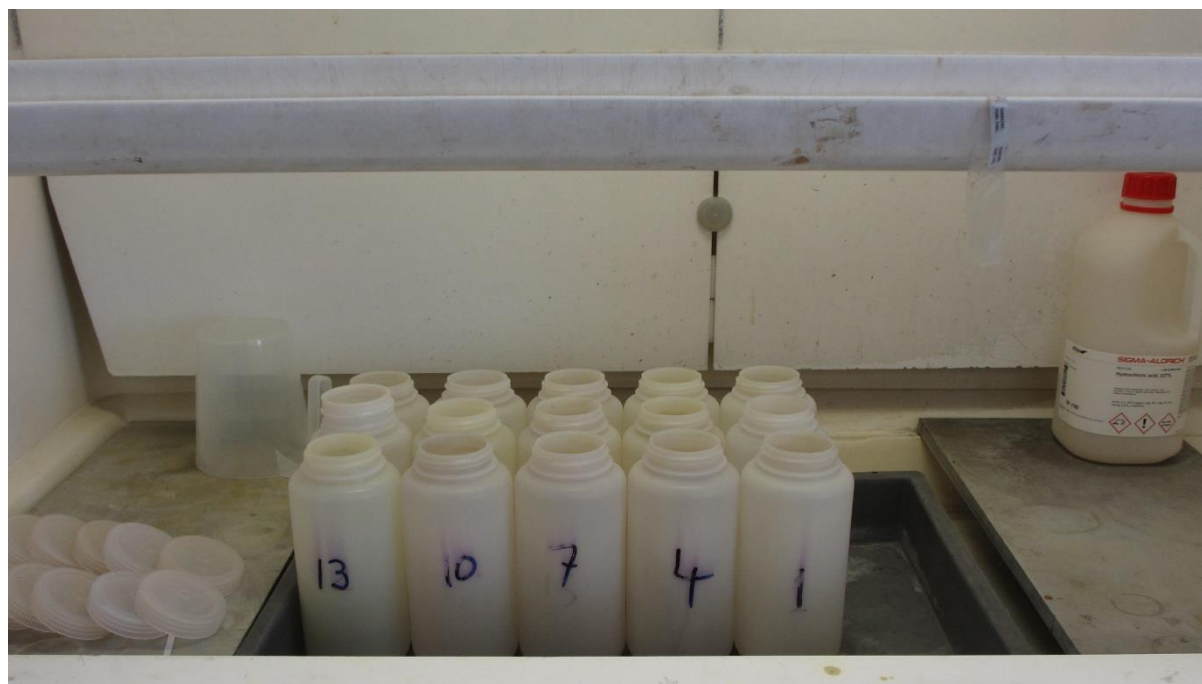


Figure 141. Photograph of numbered containers with rock samples in the fume cupboard prior to processing.

2. The water tap was turned on and the water was kept running.
3. The scrubbers were also turned on.
4. Some $\geq 37\%$ HCl was poured into a measuring jug.
5. The lid of the HCl container was replaced after each use to prevent spillage in case it was knocked over.
6. About 1 cm depth of HCl was poured into each container which was arranged safely each time.
7. When complete, any remaining HCl was poured back into its container, which was closed securely and placed out of the way on the right-hand side of the fume cupboard.

8. The measuring jug was washed and left upside down on the left-hand side to dry.
9. The hands were washed thoroughly.
10. The water was turned off and the fume cupboard was closed (Figure 142).

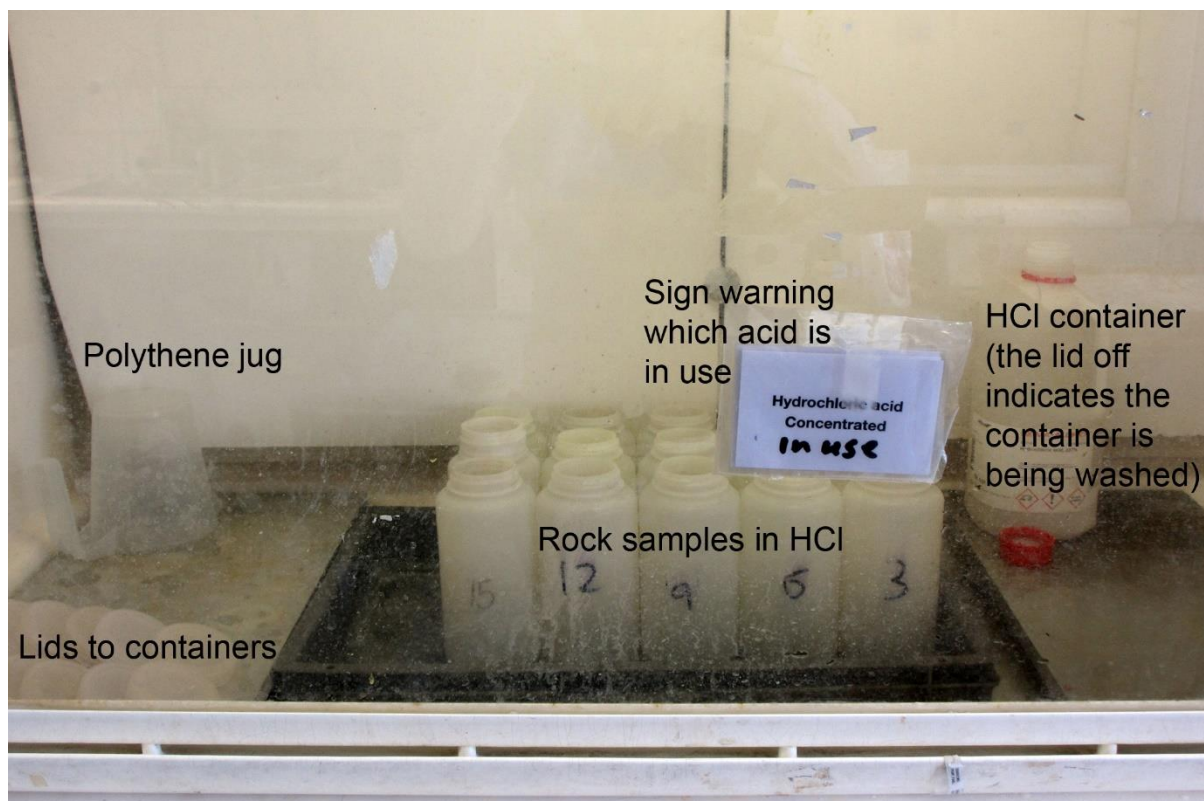


Figure 142. Photograph of numbered containers with rock samples in the fume cupboard during processing using hydrochloric acid.

The next day:

In conjunction with the basic laboratory attire, HCl PPE was worn (as above).

1. The fume cupboard was opened and checked that it was working correctly by observing that the strip on the edge of the opener was drawn into the fume cupboard.
2. The water tap was switched on and the measuring jug was placed at the front of the cupboard.

3. As much of the HCl as possible was poured slowly and carefully from each container into the measuring jug, trying not to disturb the residue.
4. When complete, the hands were rinsed and the hatch to the side of the fume cupboard was opened.
5. The measuring jug containing the spent HCl was carried carefully from inside the fume cupboard to the side hatch and the HCl was poured inside, rinsing the jug with the water in the receptacle. (The spent HCl is used to remove fluoride from the sink system.)
6. The measuring jug was placed back inside the fume cupboard, the hands were washed and the hatch door was closed.
7. The measuring jug was washed and left upside down on left hand side to dry.
8. Any acid was rinsed from the outside of each container.
9. Gripping a section of the water hose tightly to increase the pressure, each container was filled with tap water, swirling it to rinse the acid from the residue and arranged safely inside the fume cupboard.
10. The hands were washed thoroughly, the fume cupboard was closed and the scrubbers and the water were turned off.
11. 2 hours later, the water from each container was poured into the fume cupboard's sink and replaced with fresh water.
12. This was repeated until each container was pH neutral, which was tested by using an acid test strip.

Stage 2: Hydrofluoric acid (HF)

This stage takes 3 days to complete and removes silicates from the samples.

Safety note: Everyone had to be observed when using concentrated HF in case of exposure, as even small splashes to naked skin can be fatal. In case of exposure, the observer must immediately guide the operator under the emergency shower (Figure 143), activate the water flow, gather the Calgonate® emergency first aid kit (to treat HF burns) (Figure 144) and contact the emergency ambulance service.

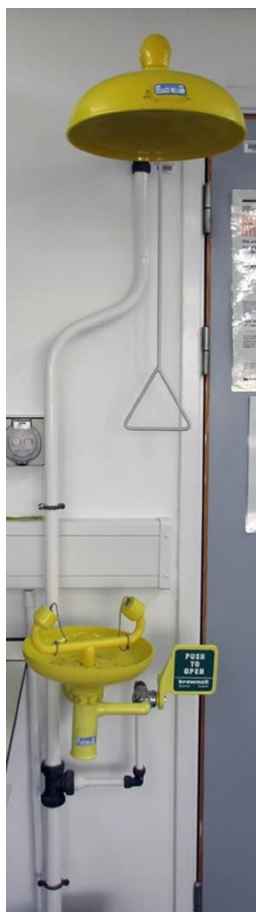


Figure 143. Photograph of the emergency shower and eye wash station in the Palynology Processing Laboratories at NOCS for use in case of extensive exposure of naked skin or the eyes to hydrofluoric acid.



Figure 144. Photograph of the Calgonate® emergency first aid kit that contains a 2.5% topical calcium gluconate gel to treat HF burns.

In conjunction with the basic laboratory attire, HF PPE was worn: black boots, over-trousers, apron, black HF gloves and full-face visor.

1. The fume cupboard was opened and checked that it was working correctly by observing that the strip on the edge of the opener was drawn into the fume cupboard.
2. The water tap and the scrubbers were turned on.
3. The neutral water from all of the samples was poured off, trying not to disturb the residue.
4. The first sample container was placed to the front of the fume cupboard.
5. The HF bottle was opened and the lid was put to one side.
6. A 2 cm depth of 60% HF was poured into the sample's container.
7. The HF bottle was put down on the right-hand side of the fume cupboard, its plastic lid was screwed on firmly and it was placed out of the way.
8. The lid of the sample's container was put on and tightened, then the acid was swirled around the container to pick up any residue that was adhering to its sides.
9. The lid was loosened to prevent explosion and the container was placed safely away from the operator.
10. This step was continued until all sample containers contained HF.
11. Unused HF bottles were placed safely to the back of the fume cupboard.
12. Any empty HF bottles were washed by filling with water and emptying 3 times before being placed upside down at the back of the fume cupboard on the left-hand side to dry.
13. The hands and cuffs were washed thoroughly, the fume cupboard was closed and the water was turned off.

The next day:

In conjunction with the basic laboratory attire, HF PPE was worn: black boots, over-trousers, apron, black HF gloves and full-face visor.

Safety note: Everyone had to be observed when using concentrated HF (see above).

1. The fume cupboard was opened and checked that it was working correctly by observing that the strip on the edge of the opener was drawn into the fume cupboard and the water tap was turned on.
2. The lid of each container was tightened and the container was shaken vigorously, keeping the base of the container about 1 cm above the base of the crate, with the lid being held down.
3. Each lid was re-loosened.
4. The hands and cuffs were washed thoroughly, the fume cupboard was closed and the water was turned off.

The following day:

In conjunction with the basic laboratory attire, HF PPE was worn: black boots, over-trousers, apron, black HF gloves and full-face visor.

Safety note: Everyone had to be observed when using concentrated HF and during the first diluted pouring off (see above).

1. The fume cupboard was opened and checked that it was working correctly by observing that the strip on the edge of the opener was drawn into the fume cupboard and the water tap was turned on.
2. At arm's length, each container was filled with tap water, while gripping a section of the water hose to increase the pressure and swirling the water around the container to rinse the acid from the residue (Figure 145).



Figure 145. Photograph of me gripping a section of the water hose to increase the pressure to rinse the HF acid from the rock sample.

3. Each container was arranged safely in the fume cupboard (Figure 146).
4. The lids were washed and left upside down on left hand side to dry.
5. The hands were washed thoroughly and the fume cupboard was closed.

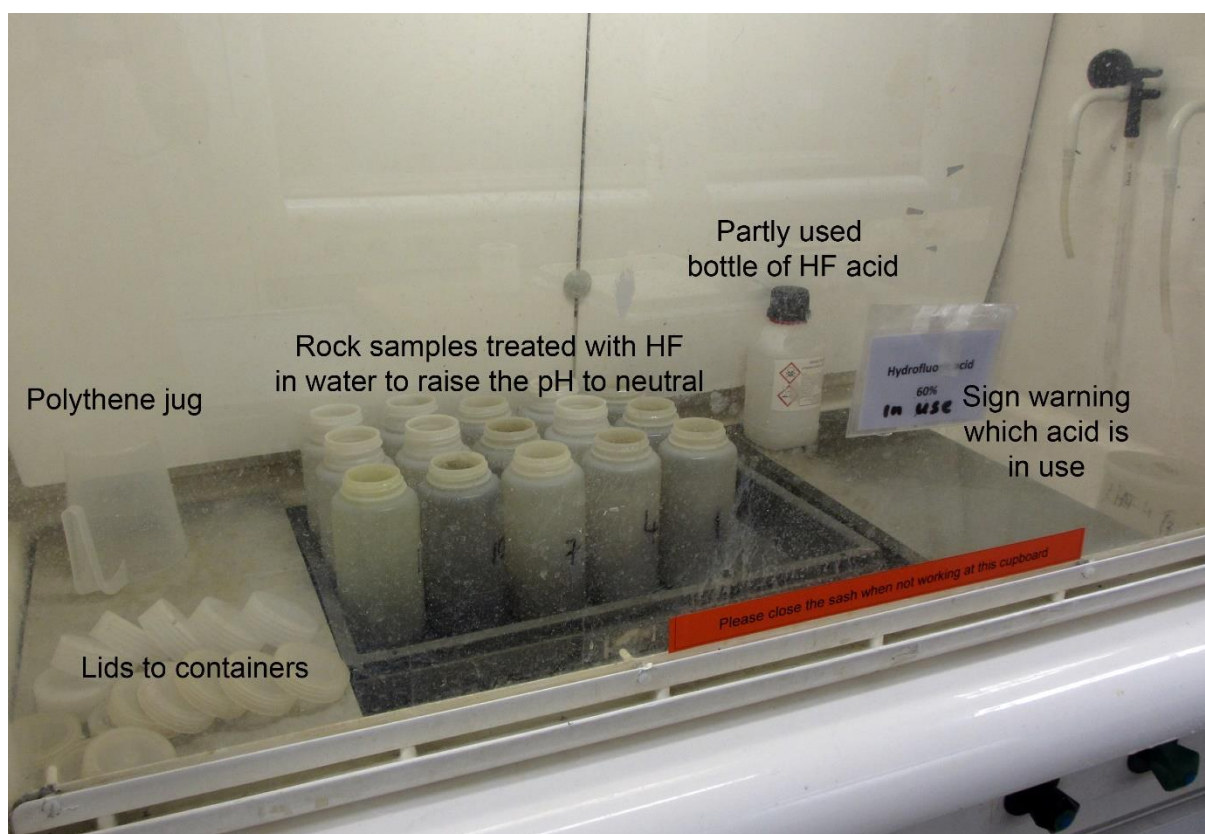


Figure 146. Photograph of numbered containers with rock samples in the fume cupboard during processing using hydrofluoric acid.

6. 2 hours later, the water from each container was poured off carefully to avoid disturbing the residue and replaced with fresh water (Figure 147).
7. The scrubbers were switched off the water was not turned off as it is used to dilute the HF acidified water from the sink.



Figure 147. Me carefully pouring off the HF acidified water, taking care not to disturb the residue.

8. This step was repeated until each container was pH neutral, which was tested by using an acid test strip.
9. Any empty, dry HF containers were placed outside the fume cupboard for disposal.

Stage 3: Sieving

This stage takes about 2 hours and places the residue into glass beakers to be boiled in HCl.

In conjunction with the basic laboratory attire, HF PPE was worn: black boots, over-trousers, apron, black HF gloves and full-face visor.

1. 15 glass beakers labelled 1 to 15 were collected and placed onto a tray next to the operator.
2. The large sieve with a 15 μm mesh (Figure 148) was gathered with lots of squeeze water bottles filled with deionised water and placed inside the fume cupboard.

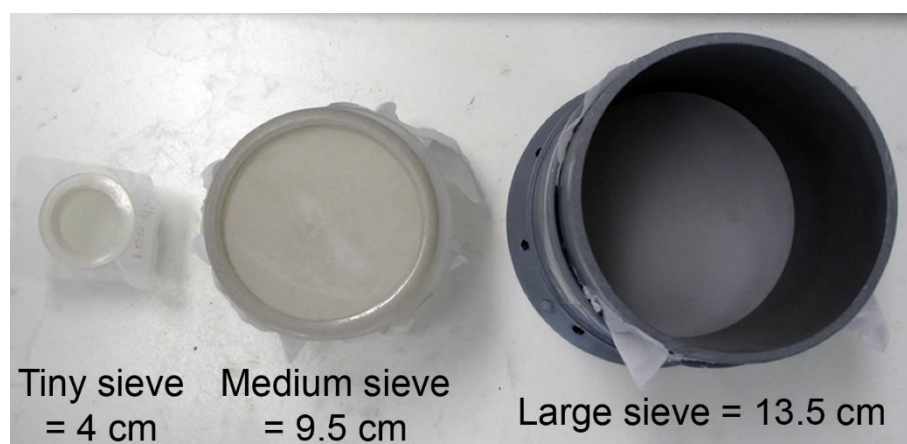


Figure 148. Photograph of the 3 sizes of sieves (with their diameter in cm) used to concentrate the residue from palynomorph processing before storage in vials.

3. The water was turned on and some of the residue from the first container was poured into the sieve.
4. Squeezing the end of the water how to produce a powerful jet, the residue was dispersed and particles that were $<15\ \mu\text{m}$ in size were forced through the mesh and not retained.
5. This was repeated until there were no visible particles left in the container.
6. When empty, the container was rinsed with fresh water which was also poured into the sieve and subjected to the water jet.
7. Using a squeeze bottle, deionised water was squirted carefully around the sieve to rinse all of the residue into one area which was washed into a beaker of the same number as the container.
8. The sieve was separated carefully to wash any remaining residue off the sieve and the mesh into the glass beaker (Figure 149).

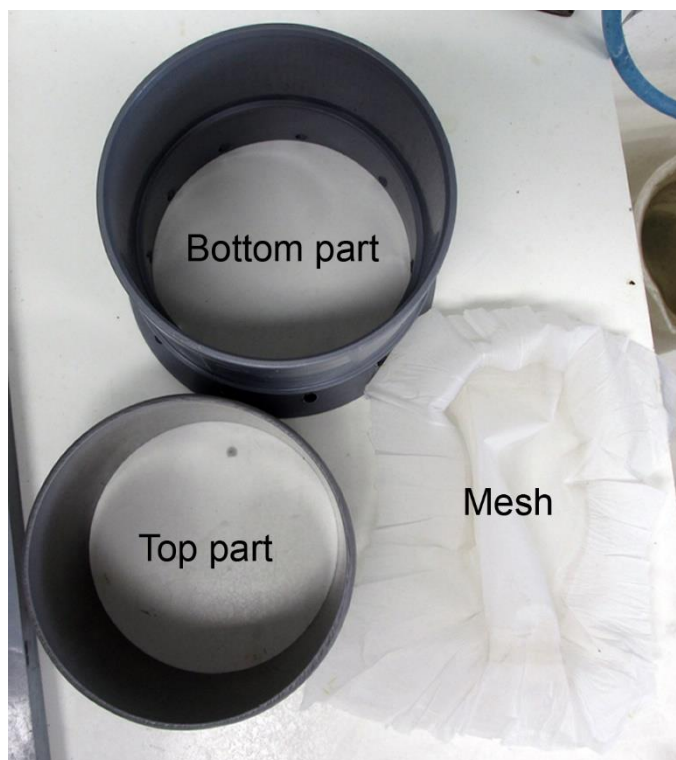


Figure 149. Photograph of the large sieve after it had been taken apart.

9. The mesh and sieve were washed with flowing water and the glass beaker was then put back onto the tray out of the way.
10. The sieve was reassembled by putting its base onto the shelf with part of it overhanging to prevent a vacuum forming.
11. The mesh was placed upside down on the base of the sieve ensuring that it was centred and taut.
12. The upper part of the sieve was placed on top of the mesh and pressed down sharply in one movement with the heels of both hands.
13. The mesh had to be centred within the sieve and taut otherwise the next sample would be lost!
14. This process was repeated for all of the samples.

Stage 4: Boiling in hydrochloric acid (HCl)

This stage removes fluorides that formed during processing in HF.

In conjunction with the basic laboratory attire, HCl PPE was worn: green boots, white apron, black HCl gloves and full-face visor.

1. The medium sieve (Figure 148) with a 15 μm mesh, the elasticated grey stand (Figure 150) and lots of squeeze water bottles filled with deionised water were placed inside the fume cupboard.



Figure 150. Photograph of the elasticated grey stand used to house the medium sieve to enable it to drain while setting the next sample to boil.

2. The lab water pump was attached to the rear water tap inside the fume cupboard (Figure 151).

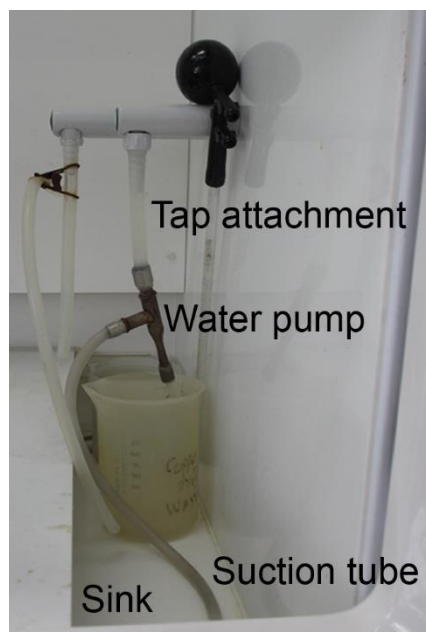


Figure 151. Photograph of the laboratory water pump attached to the water tap inside a fume cupboard.

3. The Bunsen burner, stand and mat were placed inside the fume cupboard on the left-hand side and the Bunsen burner's tube was attached to the gas nozzle.
4. Using the lab water pump all but 25 ml of water was removed from each of the beakers and 25 ml of HCl was added.
5. Half closing the Bunsen burner's oxygen intake, the gas flow was turned on and ignited using the gas lighter.
6. The Bunsen burner's air intake was opened fully to get a hotter, blue flame and the scrubbers were switched on.
7. Using the tongs, a glass beaker was placed carefully onto the burner stand to boil.
8. When it started to boil, a quick count to 60 was made (Figure 152).

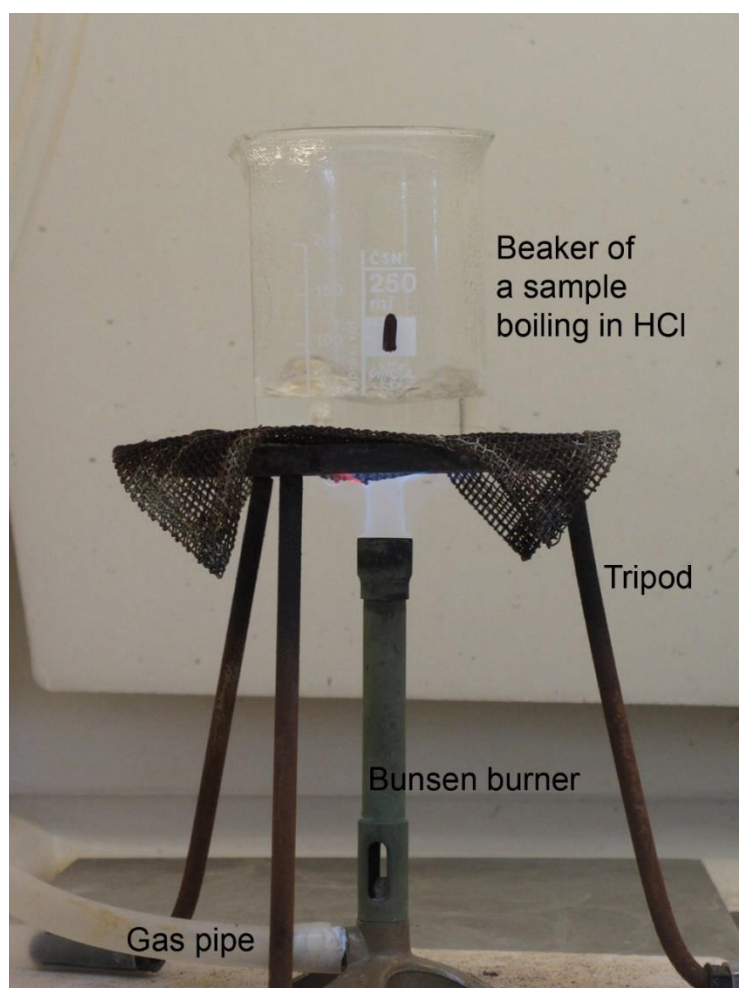


Figure 152. Boiling residue in hydrochloric acid to remove fluorides formed during processing with hydrofluoric acid.

9. Using the tongs, the beaker was removed carefully and water was added to the top of the beaker to neutralise the acid.
10. The contents were sieved back into the same glass beaker.
11. Using the tongs, the next glass beaker was placed carefully onto the burner stand to start to boil while the sieve was prepared for the next sample.
12. The sieve's rim, base and mesh were washed and the sieve was reassembled.
13. This process was repeated for all of the samples.

Cleaning

At this point, the processing of the rock samples to produce a palynomorph residue had been completed. The containers and fume cupboard that had been

used had to be cleaned thoroughly to prevent contamination of other samples that would be processed subsequently.

Wearing basic laboratory attire:

1. A dish- and bottle-brush and some detergent in a glass beaker were placed into the fume cupboard.
2. Dipping the dish brush into the detergent, the inside of the neck of each container was cleaned.
3. Dipping the bottle brush into the detergent, the inside of each container was washed, paying particular attention to the base and shoulder areas.
4. The containers were then rinsed with flowing water and placed into the dishwasher (with the lids) (Figure 153).



Figure 153. Photographs of the dishwasher used to clean the containers, lids and beakers used in palynological processing – door closed (left hand side) and door open (right hand side).

5. The lids were placed upside down in the cutlery tray and the containers were arranged upside down in the bottom tray.

6. A dishwasher tablet was put into the slot on the door.
7. The 'On' button was pressed, 'Econo' mode was selected and the 'Start button' was activated.
8. To clean the fume cupboard, the fume cupboard shower was used.
9. The front lip was removed and placed it inside the empty cupboard.
10. The shower was switched on using the black tap on full and switched off after 5 minutes.

Labelling the vials

For ease of storage, the palynomorph residues were placed into polythene vials, which were labelled with the sample details.

Wearing basic laboratory attire:

1. The PC in the Palynology Processing Laboratories, NOCS, was switched on and the 'Palynology' username was selected.
2. The label printer (Figure 154) was switched on and the correct size label cartridge (DK 11204 17 x 54 mm Multipurpose label) was loaded before opening the software or the labels would not print.



Figure 154. Photograph of the Brother QL-570 label printer used to label vials and slides containing palynological specimens.

3. The desktop icon for the 'P-touch Editor' labelling programme was activated (Figure 155) and the 'OK' button in the 'which printer' window was clicked.

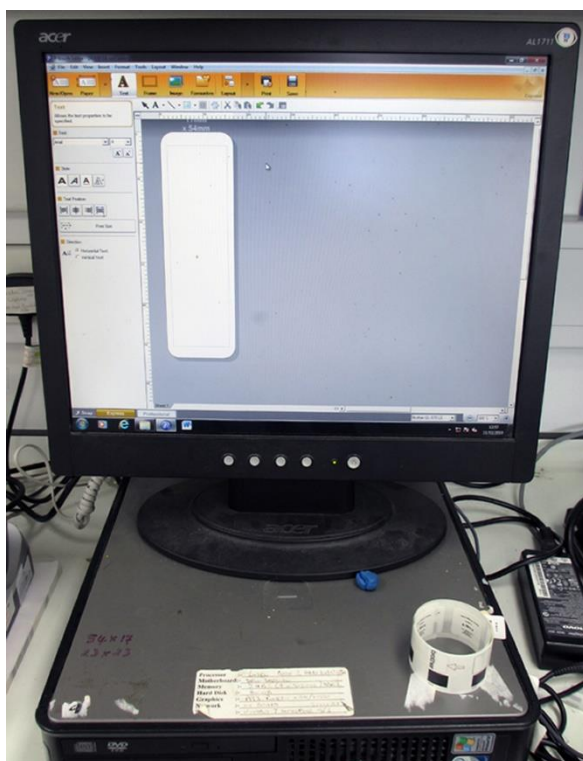


Figure 155. Photograph of the PC in the Palynology Processing Laboratories with P-touch Editor software showing a blank vial label on the screen.

4. The 'File' drop down menu, then the 'Open' option were selected and the file in 'Emma R's' folder in 'My Documents' was opened.
5. The SSK number, underscore number (which corresponded to the lab sample number) and the depth were amended for each sample.
6. The 'File' drop down menu, then the 'Print' option and the 'Print' button were selected.
7. The label was adhered by wrapping it around the vial with the left hand side down first so that the other end stuck to itself).

Putting the samples into vials

Once the vials had been labelled, the corresponding palynomorph residues were added for safe storage and later analysis.

Wearing basic laboratory attire:

1. A metal vial rack, clamp (Figure 156), tiny sieve (Figure 148) with 15 μm mesh and a squeeze bottle with an extra narrow spout attachment containing deionised water were used at the draining board and sink.

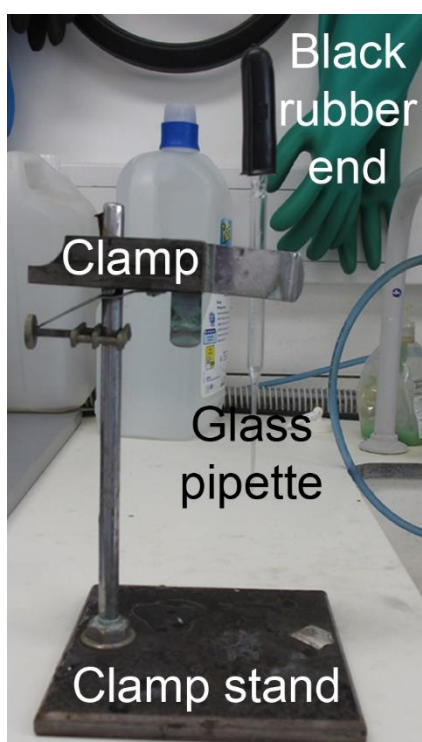


Figure 156. Photograph of the clamp and pipette used to transfer palynological residues into vials.

2. The contents of the first beaker were poured into the sieve, allowing the water to go down the drain.
3. The sieve's contents were rinsed into the appropriately labelled vial using the squeeze bottle.
4. The sieve was taken apart carefully and the mesh was washed.

5. The sieve was remade and all of the samples were placed into labelled vials in this manner (Figure 157).



Figure 157. Photograph of processed palynological samples from the NWMF borehole core that have been transferred to labelled vials.

Producing stew slides

To ascertain the general spore composition of the processed samples, temporary stew slides were made.

Wearing basic laboratory attire:

1. A clean, empty beaker, a clean pipette with a black rubber bulb, a clean microscope slide, a piece of white roll, a squeeze bottle with a narrow nozzle filled with deionised water (Figure 158) and a permanent marker pen were used.

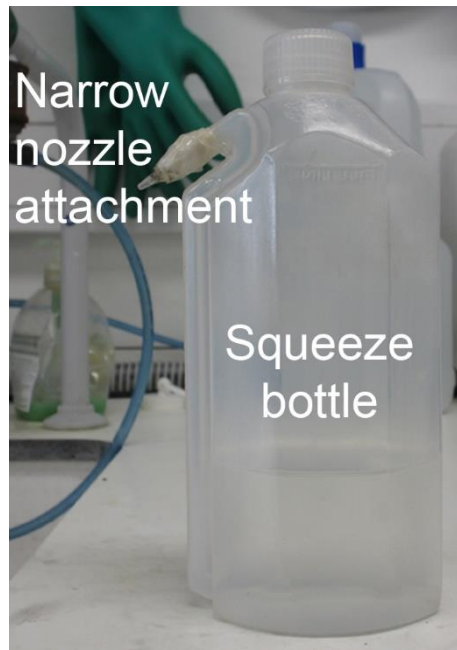


Figure 158. Photograph of a squeeze bottle containing deionised water with a narrow nozzle attachment.

2. The Nikon Eclipse E800 10x magnification light microscope was switched on.
3. Most of the water was carefully emptied out of the sample's vial using the pipette without disturbing the residue.
4. The residue and a little bit of the water were mixed together using the pipette and a drop was put onto the microscope slide.
5. The slide was inspected using the microscope and its contents were noted down very basically e.g. charcoal, minerals, wood, spores etc. and this information was added to the NWF_Paly sampling_MASTER.xls database (Figure 159).

The screenshot displays an Excel spreadsheet with two main sections: 'Sample details' and 'Processing diary'.

Sample details:

Sample Number	Lab sample No.	Sample depth	Processing information
SSK37851	1	501.29	Stuffed with mostly charcoal, some wood, few spores.
SSK37852	2	501.25	Charcoal, wood, minerals, few spores. 150 = wood, no
SSK37853	3	501.18	Charcoal, wood, lots of spores and species of spores. 1
SSK37854	4	501.11	Packed with charcoal and wood, lots of spores and spe
SSK37855	5	501.05	Lots of small pieces of charcoal and wood, lots of spore
SSK37856	6	500.98	Lots of small pieces of charcoal and wood, few spores.
SSK37857	7	500.91	Charcoal, wood, minerals, few spores. 150 = not much
SSK37859	8	500.02	Large pieces of charcoal, minerals, no spores. 15
SSK37860	9	499.98	Large pieces of charcoal, wood, no spores. 150 = lots of
SSK37861	10	499.53	Few small pieces of charcoal, quite a lot of minerals, rar
SSK37862	11	499.34	Lots of small pieces of charcoal, some small pieces of w
SSK37863	12	499.18	Charcoal, wood, minerals, lots of species of spores. 15
SSK37864	13	498.98	Small pieces of charcoal, minerals, few small pieces of v
SSK37866	14	498.48	Small pieces of charcoal, minerals, few small pieces of v
SSK37867	15	498.38	Small pieces of charcoal and wood, minerals, no spores
SSK37871	1	497.13	Crammed with small pieces of charcoal and wood, few
SSK37875	2	496.62	Crammed with small pieces of charcoal and wood, spor
SSK37879	3	495.55	Crammed with tiny charcoal pieces, few small pieces of
SSK37881	4	494.99	Small pieces of charcoal and wood, minerals, poorly pr
SSK37883	5	493.86	Small pieces of charcoal and wood, lots of species of sp
SSK37891	6	492.41	Lots of small pieces of charcoal, minerals, rare small pie
SSK37895	7	491.43	Lots of small and large pieces of charcoal, wood, lots of
SSK37900	8	490.79	Charcoal, wood, lots of spores and species of spores, n
SSK37908	9	488.86	Crammed with tiny pieces of charcoal, minerals, few sp
SSK37913	10	487.35	Not much: charcoal, minerals, no spores. 150 = few wo
SSK37919	11	486.25	Crammed with tiny pieces of charcoal, tiny pieces of wo
SSK37921	12	485.93	Crammed with tiny pieces of charcoal and wood, spore
SSK37926	13	484.52	Not much: charcoal, wood, spores, minerals. 150 = few
SSK37932	14	483.53	Not much: charcoal, wood, lots of spores and species o

Processing diary:

Date	Processing information
05/11/13	crushed and weighed samples ready
06/11/13	1 cm HCl and left overnight
06/11/13	11/13 poured off HCl and filled with water to neutralise. Completed lab book.
07/11/13	11/13 poured off water and replaced with fresh water
08/11/13	11/13 tested for pH - neutral. All samples neutral pH.
11/11/13	11/13 poured off water and added 2 cm HCl
12/11/13	11/13 poured off HCl and topped up with water x 2
13/11/13	11/13 poured off HCl and topped up with water. Removed lid and topped up with water
14/11/13	11/13 tested pH - first 2 vials still acidic. Poured off and replaced with water
15/11/13	11/13 poured off water and sieved into beakers. Left beakers on fume cupboard to be processed on Monday
18/11/13	11/13 used tucky thing to remove all but 25 ml of water, then added 25 ml of HCl. Boiled HCl for 60 seconds and topped up with cold water. Sieved the beaker contents and washed back into the beaker with deionised water. Sieved the beaker contents into vials via tiny sieve. Note the depths of each sample on the lid

Figure 159. Screen shot of part of the NWF_Paly sampling_MASTER.xls database that included details of which samples had been processed for palynomorphs, a very basic list of what each sample contained e.g. wood, spores, minerals (samples that had been top-sieved for megaspores were additionally annotated with '150 =' and then the contents e.g. wood, spores) and diary-style entries of which processing steps each batch had received.

- The slide's contents were rinsed carefully back into its vial by tipping one corner of the slide over the mouth of the vial and spraying a little deionised water onto the slide.
- The slide was wiped dry with the white roll and used for the next sample.
- The vial's lid was annotated with 'None', 'Few' or 'Lots' (of spores) using the permanent marker pen (Figure 160). This information was also added to the NWF_Paly sampling_MASTER.xls database (Figure 159).

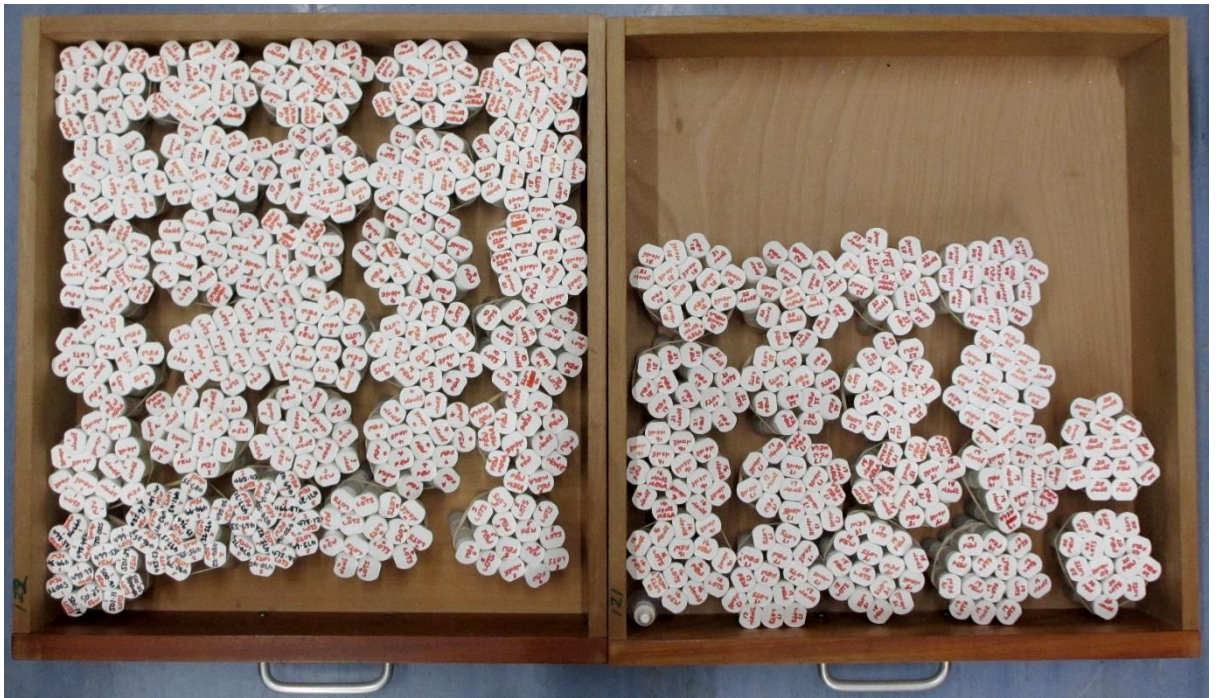


Figure 160. Photograph of vials containing palynomorph residues from NWMF borehole core samples, grouped into processing batches of 15. The lids were marked with the batch number and the relative quantity of palynomorphs contained within (None/Few/Lots). Vials that contained megaspores were annotated with 'MEGA' and had also been top-sieved.

Top sieving

'Top sieving' collects palynomorphs in the $> 150 \mu\text{m}$ size fraction, with the aim of isolating megaspores from the miospores that form the $> 15 \mu\text{m}$ and $< 150 \mu\text{m}$ size fraction.

Wearing basic laboratory attire:

1. A metal vial rack (Figure 161), clamp, tiny sieve with $150 \mu\text{m}$ mesh, a clean beaker and a squeeze bottle with an extra narrow spout attachment, full of deionised water were used with the draining board and sink.

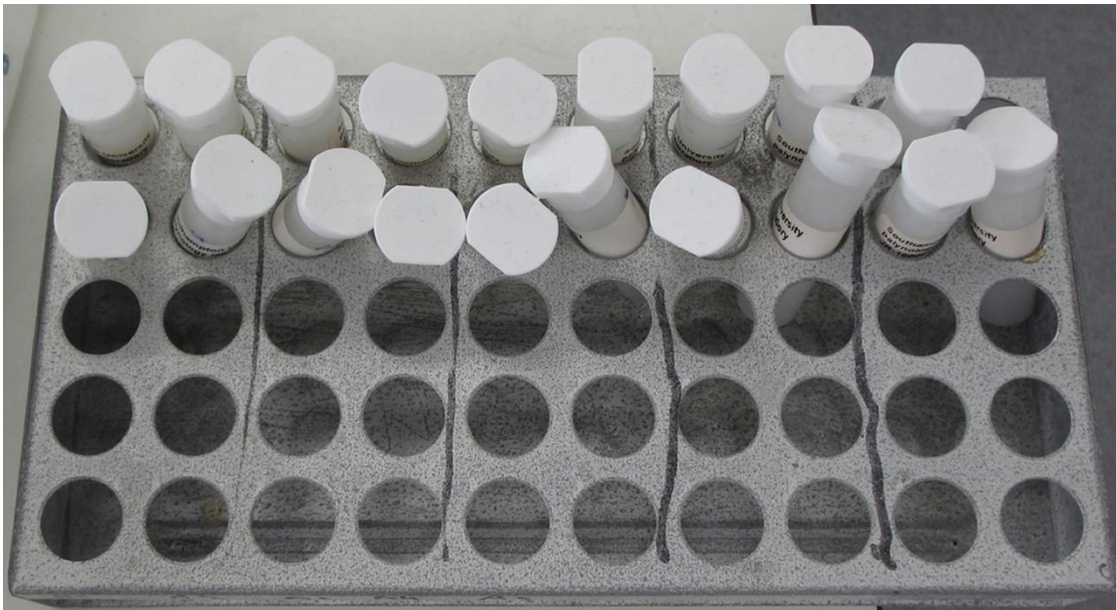


Figure 161. Photograph of a metal vials rack with palynological samples in vials.

2. Each vial's contents were poured through the tiny sieve with the 150 μm mesh, with the clean beaker beneath to recapture the smaller size fraction.
3. The sieve's contents were rinsed into the appropriately labelled megaspores vial (denoted by the addition of '(150 μm)' after the depth on the label and 'MEGA' on the lid) with deionised water from the squeeze bottle.
4. The beaker contents were rinsed back into the appropriately labelled (miospores) vial with deionised water.
5. The sieve was taken apart and washed before being reassembled for the next sample.
6. The NWF_Paly sampling_MASTER.xls database was amended with the megaspores information (by editing the 'Processing information' column with '150 =' and a brief description of the contents i.e. megaspores, minerals).

Making permanent slides

Permanent slides were made to facilitate the identification of the palynomorphs contained in each sample of the NWMF borehole core and to preserve them for the future.

Wearing basic laboratory attire:

1. A clean plastic vial, squeeze bottles filled with deionised water, a clean pipette with a black rubber bulb, a slide tray and a box of coverslips (Menzel-Gläser cover glass 22x32 mm #1 Part No. 12322118) were used.
2. 15 coverslips (one batch = 15 samples) were placed into numbered segments of the slide tray (Figure 162).



Figure 162. Photograph of a slide tray with numbered segments to place coverslips containing palynological samples during drying before being made into permanent slides.

3. Extraneous water was removed from the first sample vial using the pipette.
4. Approximately 6 drops of the sample were added to a clean vial with 2 drops of dispersant (dilute detergent) and diluted with deionised water.
5. The first coverslip was coated with the dilute residue by pipetting a drop onto each of the four corners and then a larger drop in the centre to coalesce them all.
6. Any remaining residue was rinsed back into the correspondingly labelled vial.
7. The unlabelled vial was washed thoroughly with deionised water.
8. The rest of the coverslips were coated with diluted residues, keeping them in order and left to dry overnight.
9. Using a plastic pipette, a 'I' shape was drawn with some Elvacite® 2044 onto a slide (Clarity 1.0 to 1.2 mm thick) (leaving space for the label) and

immediately placed upside down onto a coverslip, then lifted and turned over, to ensure that the coverslip had adhered to the Elvacite (the coverslip could be manipulated carefully into a central position).

10. The slides were left to dry completely for at least 3 days.

Note: Copious amounts of Elvacite were used to mount megaspores as they are so large that pockets of air could become trapped which degrades the specimens.

Labelling the slides

After the slides had been made, but while they were drying, they were labelled with the sample's details.

Wearing basic laboratory attire:

1. The PC in the Palynology Processing Laboratories, NOCS, was switched on and the 'Palynology' username was selected.
2. The label printer was switched on, ensuring that the correct size label cartridge (DK-11221 23 x 23 mm Square Paper Label) was loaded before opening the software or the labels would not print.
3. The desktop icon for the 'P-touch Editor' labelling programme was activated and the 'OK' button in the 'which printer' window was clicked.
4. The 'File' drop down menu and then the 'Open' option were selected and the file in 'Emma R's' folder in 'My Documents' was opened.
5. The SSK number, underscore number (which corresponded to the lab sample number) and the depth were amended for each sample. (an asterisk was also added after the 'm' of the depth for slides that contained 150 μ m material i.e. m*).
6. The 'File' drop down menu was selected, then the 'Print' option and the 'Print' button.
7. The label was adhered to the opposite end of the slide to the coverslip (Figure 163).

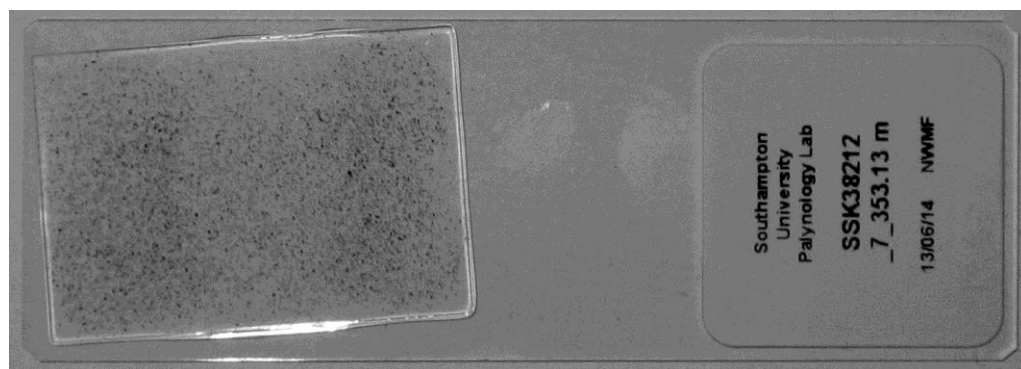


Figure 163. Photograph of a slide containing palynomorphs from the NWMF borehole core.

APPENDIX 4

Work Instruction: Canon EOS 70D operating instructions

This work instruction details the steps that were taken to operate the Canon EOS 70D DSLR camera that was used to produce photomicrographs to record and identify the palynology specimens (see Section 2.9.1).

1. The camera was activated using the on/off switch on the right hand side (ensuring that the dial was set to 'C' and the video function was off).
2. The 'EOS Utility – EOS 70D' window opened automatically on the desktop.
3. The 'Camera settings/Remote shooting' option was selected with the 'Live View shoot' option towards the bottom of the 'EOS 70D' window.
4. The eye dropper button on the 'Remote Live View window' was used to set the white balance by clicking on the photograph's background.
5. Clicking the big black button towards the top right hand side of the 'EOS 70D' window took the photograph.
6. To save the photograph, it was selected in the 'Digital Photo Professional' window, then the 'File' drop down menu and the 'Save As' option were selected.
7. The appropriate folder was chosen, or a new one was created, then the file was named according to the convention: Depth in metres, allocated spore name, microscope co-ordinates in JPEG format e.g. 408.98 m *Auroraspora corporiga* qry 113.1 09.6.

APPENDIX 5

Work Instruction: Olympus Stream (Basic) operating instructions

This work instruction details the steps that were taken to operate the Olympus Stream (Basic) software that was used with an Olympus BH-313 light microscope with an Olympus SC30 3 Megapixel camera to produce high quality, publishable light photomicrographs (see Section 2.9.1).

1. The microscope was switched on and the Olympus Stream software was opened.
2. The left screen was used to operate the software and the right screen was used to view the specimens.
3. The 'Live' button on the right-hand side was selected, ensuring that the correct magnification, corresponding to that used on the microscope, was selected on the top bar.
4. To correct the white balance, the 'White Balance On ROI' button (dropper icon) above the 'Live' button was selected and a square was drawn in the background of the image.
5. To take the photograph the 'Snap' button on the right-hand side was clicked.
6. The 'Image' drop down menu, the 'Burn In Info' option and the 'Yes' button were selected to add the scale bar.
7. The 'File' drop down menu, then the 'Save as' option were selected and a name for the file was entered, changing the format to JPEG (JFIF) (*.jpg).

Notes: As the camera used low light, the light level had to be kept low on the microscope. When the software crashed, clicking the 'Live' button on the right-hand side reopened it.

The Olympus Stream software was also used to measure palynomorphs and their features much more quickly and accurately than by doing so manually:

1. Ensuring that the correct magnification was selected, the 'Measure' drop down menu, then the 'Arbitrary line' option were selected.
2. To measure a palynomorph or a feature (e.g. a sculptural element), one end of the object was selected to produce a measurement line, which was dragged to the other end and the length was noted.
3. To remove the line, the 'Esc' or 'Delete' key on the keyboard was selected.
4. To keep the line in place (i.e. to photograph it), the second end was clicked.
5. To remove the line, it was selected by clicking on it and then the 'Delete' key on the keyboard was pressed.

APPENDIX 6

Work Instruction: Infrared microscope set up

This work instruction details the settings that were used with the infrared microscope and the steps to take infrared photomicrographs (see Section 2.9.2).

Initially, an approximately 5 second delay between adjusting the microscope and viewing those changes on the laptop made focusing very haphazard. To rectify this problem, in the 'Setting' window, the 'Buffer Size (minutes)' option in the 'Capture' tab was set to zero, which disabled the disk buffering when watching the TV. However, as this did not seem to make a discernible difference, the 'Use Game Mode for analog' option was selected again in the 'Advanced Options' tab and the computer was restarted. According to the software's 'Help' files: "In normal mode the TV/video displayed in WinTV is delayed for a few seconds, because it is buffered on hard drive or in memory. In Game Mode the analog TV/Video is displayed without delay. You should enable Game Mode if you intend to connect a game console to the video input of WinTV." In this instance the CCD video camera was acting as a games console and, so, selecting this option eliminated the output delay.

The details for the software and the settings used were: Hauppauge WinTV v7.0.31347 (CD 3.2) ©2012 Hauppauge Computer Works Inc.

- General settings:
 - Languages: English
 - Video Renderer: EVR
 - Monitor Shape: 16:9
- Capture settings:
 - Default Analog Recording Quality: Best
 - Analog Aspect Ratio: 4:3
 - Buffer Size (minutes): 0
 - Snapshot File Type: .JPG
 - Vertical Resolution: Native
- Devices settings:

- Device: WinTV-USB-Live2
- MAC Address: 000DFEAE5143
- All Channels settings:
 - Preset: 1
 - Channel Name: S-Video
 - Channel Source: S-Video
- Favorites settings:
 - Preset: 0
 - Channel Name: Composite
 - Channel Source: Composite
 - Preset: 1
 - Channel Name: S-Video
 - Channel Source: S-Video
- Parental Control settings:
 - None were set up as there was no video content unsuitable for under 18s
- Advanced Options settings:
 - TV: Automatically Start Live TV
 - TV: Block Windows Screen Saver
 - TV: Use Game Mode for analog (slip disabled, requires reboot)
 - TV: Enable Picture-In-Picture

To save the files, the correct folder had to be created/selected before the snapshots were taken. As the Microphotometry room at NOCS does not have a network connection, to save the IR images, a new folder was created using Windows Explorer, named 'WinTV IR snapshots' and located on the Desktop. Within this master folder, one folder was created per picked megaspore slide and named using the standard format e.g. SSK38434 290.75 m, where SSK38434 = the BGS allocated number standard on all documentation and the master database and 290.75 m = the depth.

These slide folders were subdivided into one subfolder per specimen because the WinTV software named the files automatically, which could not be amended at the

time: e.g. capture_20140923 _111916, where 20140923 = the date of image capture and 111916 = the time of image capture.

To take the photomicrographs:

1. The 'Settings' button, then the 'Capture' tab were selected.
2. In the 'Snapshots' section opposite the 'Snapshot Directory' the 'Browse' button was selected and then the folder to collate the snapshots was opened.
3. The master folder into which the new folder would be placed was selected and then the 'Make New Folder' button.
4. The name of the new folder was entered and the 'Return' button was selected.
5. The 'OK' button to close the 'Browse for Folder' window and the 'OK' button to close the 'WinTV Settings' window were selected.

Although there was no indication that the photograph had been taken, it was automatically saved in the folder designated in the 'Snapshot Directory'.

The main limitation with this approach was the lack of scale bar generation in the Hauppauge WinTV software. To overcome this problem, the specimen was also photographed using the light microscope. Then it was composited and resized using Photoshop to match the infrared version exactly. The scale bar was then simply dragged from the light microscope version to the infrared image.

APPENDIX 7

Work Instruction: Using Tilia software to produce range charts

This work instruction details the steps that were taken to produce range charts (see Section 2.11.1).

Tilia software was written by Dr. Eric C. Grim of the University of Minnesota and was designed specifically for managing and graphing palaeontological data such as pollen. It is free to students or costs \$250 for a lifetime professional license.

1. A new document was created in Tilia.
2. The names of the taxa were copied from Excel and pasted into the 'Name' column of Tilia.
3. The depths of the samples were copied from Excel and pasted into Tilia beginning in cell H1 (they had to be in ascending order for the software to run).
4. The word 'spore' was typed into the 'Group' column, and then copied and pasted next to all of the taxa.
5. The palynology data was copied from Excel and pasted into Tilia beginning in cell H3 ensuring that:
 - There were no blank cells (if the cells had no values, they had to contain a zero).
 - The totals of the data columns were greater than zero or Tilia would not run.
 - Columns that equalled zero were deleted.
6. To put the data into inception order, it was quicker to reorder it in Excel:
 - The data was selected.
 - The 'Conditional Formatting' drop down menu, the 'Highlight cell rules', and the 'Greater than' option were selected.
 - In the 'Format cells that are GREATER THAN:' window '0' (zero) was typed, then the 'OK' button was selected.
 - Starting at 501.18 m, the coloured cells were reordered by the first appearance of the taxon.

7. The 'Make diagram' button was selected, then the 'Yes' button to save the spreadsheet.
8. The file was named and the appropriate folder was opened or created and the 'Save' button was selected.
9. The 'Graph style' button, then the 'Select Variables' button were selected.
10. The 'Select All' button and the 'OK' button were selected.
11. The 'Presence' tab, the 'Apply' button (as a quick visual check) and then the 'OK' button were selected.
12. To re-orientate the taxa names, the 'Graph style' window was dragged out of the way and the 'X-axes' button was clicked.
13. The 'Name' tab was selected and the 'Text' 'Angle' was change to 90.
14. The 'Apply' button was selected to check the results.
15. To move the taxa names, the 'Center' tick box was selected and the 'Apply' button to check the results.
16. The 'OK' button was selected when finished.
17. To add colour to the data, clicking the 'Select Variables' button enabled the taxa to be selected to change the colour and the 'OK' button was selected.
18. In the 'Color' drop down menu, the required colour was chosen and, then the 'Apply' button was selected.
19. These actions were repeated for the other taxa as required. When complete the 'OK' button was selected.
20. To save the chart, the 'File' drop down menu and then the 'Save As' option were selected.
21. The chart was named and the 'Save' button was clicked.

This saved the chart as a Tilia diagram which most software cannot open. To resolve this, the resulting file was saved as an Enhanced Windows Metafile (emf) format, which could be opened in Adobe Illustrator for editing:

- The 'File' drop down menu and then the 'Export' option were selected.
- The chart was named and the 'Save' button was selected.
- This saved the chart in Enhanced Windows Metafile (emf) format, which could be opened in Adobe Illustrator for editing.

APPENDIX 8

Work Instruction: Using Tilia software to relative abundance charts

This work instruction details the steps that were taken to produce relative abundance charts using Tilia software (see Section 2.11.2).

1. A new document was created in Tilia.
2. The names of the taxa were copied from Excel and pasted into the 'Name' column of Tilia.
3. The depths of the samples were copied from Excel and pasted into Tilia beginning in cell H1 (they had to be in ascending order for the software to run).
4. The word 'spore' was typed into the 'Group' column, and then copied and pasted next to all of the taxa.
5. The palynology data was copied from Excel and pasted into Tilia beginning in cell H3 ensuring that:
 - There were no blank cells (if the cells had no values, they had to contain a zero).
 - The totals of the data columns were greater than zero or Tilia would not run.
 - Columns that equalled zero were deleted.
6. The 'Make diagram' button was selected, then the 'Yes' button to save the spreadsheet.
7. The file was named and the appropriate folder was opened or created and the 'Save' button was selected.
8. To add colour to the data, clicking the 'Select Variables' button enabled the taxa to be selected to change the colour and the 'OK' button was selected.
9. In the 'Main Curve' drop down menu, the required colour and then the 'Apply' button were selected.
10. These actions were repeated for the other taxa as required. When complete the 'OK' button was selected.
11. To save the chart, the 'File' drop down menu and then the 'Save As' option were selected.
12. The chart was named and the 'Save' button was clicked.

This saved the chart as a Tilia diagram which most software cannot open. To resolve this:

- The 'File' drop down menu and then the 'Export' option were selected.
- The chart was named and the 'Save' button was selected.
- This saved the chart in Enhanced Windows Metafile (emf) format, which could be opened in Adobe Illustrator for editing.

APPENDIX 9

Work Instruction: Using PAST software to perform a Principal Component Analysis (PCA)

This work instruction details the steps that were taken to perform a Principal Component Analysis (PCA; see Section 2.11.3).

PAST (PAleontological STatistics v 3.19), a free comprehensive statistics package, designed specifically for palaeontological studies (Hammer, Harper & Ryan 2001), was used to perform a Principal Component Analysis (PCA). This was used to identify outgroup spore taxa which represented plants that were statistically different from all of the others and may, therefore, have represented a controlling factor in the plant recovery following the EDME.

1. The PAST3.exe file was run from the 'Downloads' folder.
2. The input data file (which is a matrix of multivariate data, with items in rows (i.e. spore taxa) and variates in columns (i.e. depths (m)) was generated:
 - In Excel, the data was edited to this format:

	Depth 501.18 →
Spore taxa ↓	

- In PAST, the 'Row attributes' tick box was selected in the 'Show' window, then the species names were copied and pasted from Excel to the 'Name' column in PAST.
- The 'Row attributes' tick box was selected (to close it) and the 'Column attributes' tick box was selected.
- The depths were copied and pasted from Excel to the 'Name' column in PAST.
- The 'Column attributes' tick box was selected to hide the extraneous data.
- The remaining data was copied from Excel and pasted into the top left-hand side cell in PAST.

3. All of the data was selected in PAST using the blank grey button above row 1 and to the left of column 1.
4. The 'Multivariate' drop down menu, then the 'Ordination' option and the 'Principal Components (PCA)' option were selected.
5. The 'Scatter plot' tab was clicked to select:
 - The '95% ellipses' tick box.
 - The 'Row labels' tick box.
6. Click the 'Graph settings' button.
7. In the 'Graph preferences' window, 3 windows were edited:
 - In the 'Appearance' window:
 - The tick was removed from the 'Colors' tick box.
 - The 'Thick lines' tick box was selected.
 - The 'Font' was changed to Arial size 12.
 - The 'Symbol size' was increased to 7.
 - In the 'Size (pixels)' window:
 - The Width setting was changed to 800 and the Height setting to 500.
 - In the 'Export' window:
 - The format was changed from SVG to TIF.
 - The 'Save as...' button was clicked, the appropriate folder was selected and a file name was entered.
8. The 'Save' button, then the 'Close' button and the next 'Close' button were selected.

APPENDIX 10

Work Instruction: Using Tilia software to perform a Constrained Incremental Sum of Squares (CONISS) analysis

This work instruction details the steps that were taken to perform a CONISS analysis using Tilia software (see Section 2.11.4).

Having identified the outgroup taxa using Principal Component Analysis (Section 3.6.2) a CONISS analysis was performed to divide them into distinctive natural assemblages. The assemblages could be further grouped and the spores' fluctuating abundances were then used to track palaeoclimatic changes through the Tournaisian.

1. A new document was created in Tilia.
2. The names of the taxa were copied from Excel and pasted into the 'Name' column of Tilia.
3. The depths of the samples were copied from Excel and pasted into Tilia beginning in cell H1 (they had to be in ascending order for the software to run).
4. The word 'spore' was typed into the 'Group' column, and then copied and pasted next to all of the taxa.
5. The palynology data was copied from Excel and pasted into Tilia beginning in cell H3 ensuring that:
 - There were no blank cells (if the cells had no values, they had to contain a zero).
 - The totals of the data columns were greater than zero or Tilia would not run.
 - Columns that equalled zero were deleted.
6. The 'Make sums' button (Σ) was selected to open the 'Sums' window.
7. In the 'Name' column 'Sum spore' was typed.
8. In the middle window, the Code 's' was typed and the Name 'sum pollen', then in the 'Include Groups' drop-down menu, 'spore' was selected.
9. Click the 'green tick' button was selected to add this information to the list.
10. The Code 't' was typed and the Name 'sum total', then in the 'Include Groups' drop down menu, 'spore' was selected.

11. The 'green tick' button was selected to add this information to the list.
12. In the upper window, in the 'Base' column, the code 's' was selected to base the sum onto the sum of all palynomorphs and the 'OK' button was selected.
13. The 'Make percents' button (%) was selected, which generated a 'Percents' spreadsheet, as shown by the 'Percents' tab at the bottom left hand side of the screen.
14. The 'Insert' drop down menu, then the 'Worksheet' option and the 'CONISS' option were selected.
15. In the 'Transfer Data From' window, the 'Percents Sheet' radio button was selected.
16. In the 'Groups included in analysis' window, the tick box next to the 'spore' option and the 'OK' button were selected.
17. This produced a 'CONISS' tab at the bottom left hand side of the screen (next to the 'Percents' tab).
18. The 'CONISS' tab was selected and then the 'Tools' drop down menu and the 'Cluster Analysis' option were selected to open the 'Constrained Incremental Sums of Squares' window.
19. Clicking in the 'Output file for diagram (*.dgx)' window, the CONISS file name was given the suffix '_CONISS' just before the '.dgx' file extension.
20. In the 'Type of Data' window, the 'Percentages' radio button was selected.
21. In the 'Type of Analysis' window the 'Stratigraphically constrained' radio button was selected.
22. In the 'Data Transformation/Dissimilarity Coefficient' window, the default 'Square root transformation (Edwards & Cavalli-Sforza's chord distance)' was chosen.
23. Clicking the 'Run Analysis' button produced the 'CONISS Results' window.
24. Closing the window, a 'Confirm to convert values in CONISS worksheet to percentages?' window appeared and the 'Yes' button was selected.
25. To add the CONISS dendrogram, the 'Percents' worksheet tab was selected.
26. The 'Make diagram' button was selected.
27. A 'Confirm spreadsheet must be saved first. Save now?' window appeared and the 'Yes' button was selected.
28. The 'Cluster Analysis' button was selected.

29. In the 'Cluster Analysis' window, the 'Open .dgc File' button was selected and the CONISS file (produced above) was opened.
30. In the 'Dendrogram scale' window, the 'Total sum of squares' option and the 'OK' button were selected.
31. To remove the 'sum spore', 'sum pollen' and 'sum total' columns, the 'Variables' button was selected.
32. The 'sum spore', 'sum pollen' and 'sum total' tick boxes in the 'skip' column and then the 'OK' button were selected.
33. To change the colour scheme of the chart, the 'Graph Style' button was selected.
34. The 'Select Variable' button and then the tick boxes for the taxa to change their colour and the 'OK' button were selected.
35. The 'Main Curve:' drop down menu was selected and the required colour was chosen.
36. The 'Apply' button was clicked to see the outcome.
37. Steps 34 (deselecting the taxa that had already been coloured) to 36 were repeated as necessary, then the 'OK' button was selected.
38. To highlight grouped clusters, the 'Zones' button was selected.
39. The 'Level' of the line to denote the grouping was entered e.g. 100 (for 100 m depth), then the 'green tick' button was selected to add the zone.
40. Any further zones were added as necessary, then the 'OK' button was selected.
41. To save the chart, the 'File' drop down menu and then the 'Save As' option were selected.
42. The chart was named and the 'Save' button was clicked.

This saved the chart as a Tilia diagram which most software cannot open. To resolve this:

- The 'File' drop down menu and then the 'Export' option were selected.
- The chart was named and the 'Save' button was selected.
- This saved the chart in Enhanced Windows Metafile (emf) format, which could be opened in Adobe Illustrator for editing.

Note: In the 'Data Transformation/Dissimilarity Coefficient' window, there were 4 options:

- Square root transformation (Edwards & Cavalli-Sforza's chord distance)
- Sample vectors normalized to unit length (Orloci's chord distance)
- Variables standardized to mean 0, SD 1 (Standard Euclidean distance)
- No data transformation (Euclidean distance)

The palynomorph data was run using each of the 4 options and a visual inspection of the resultant CONISS charts was performed. As they all gave similar results the default 'Square root transformation' was chosen.

APPENDIX 11

Work Instruction: Using Photoshop software to manipulate microphotographs

This work instruction details the steps that were taken to manipulate microphotographs using Photoshop software (see Section 2.12).

1. The Photoshop software was activated and all of the images to be merged were opened. (Note: all files had to be formatted to RGB or greyscale).
2. A new document was created using the 'International paper' A4 size.
3. The 'Windows' drop down menu, then the 'Arrange' option and the 'Float All in Windows' option were selected to stack the windows to enable easy access to each image.
4. The new document was brought to the side away from the image files.
5. Each of the image files were dragged onto the new document in order to produce a series of layers.
6. The images were aligned semi-automatically using the 'Snap' function in the 'View' drop down menu, by placing each image in the top left hand corner of the new document.
7. Each of the layers in the window on the right hand side were selected (excluding the background layer).
8. The 'Edit' drop down menu, the 'Auto-Blend Layers...' option, the 'Stack Images' option and the 'Seamless Tones and Colors' radial button were selected and then the button.
9. The resultant image was cropped to remove empty space and the file was saved.

Notes: To reduce the size, the files were saved in JPEG format. The JPEG Image option Quality of 12 was chosen to conserve the image quality in case further photographic manipulation would be required later. Any extraneous empty space was removed using the 'Crop' tool. To improve the image quality, the tonal intensity levels were also adjusted using the 'Autolevels' option.

APPENDIX 12

Work Instruction: Fossil sampling

This work instruction details the steps that were taken to sample the NWMF borehole core for fossils (see Section 2.14).

Equipment:

- Safety glasses to protect eyes.
- Sturdy 'impact resistant' glove to protect hand.
- Sturdy 'impact resistant' footwear to protect feet.
- Lab coat or overalls to keep clean!
- Fossil hammer to extract samples.
- Hand lens to inspect fossils.
- Cardboard trays of various sizes to store fossils.
- Logbook to record the fossil finds.
- Tape measure or rule to measure the sample depths.

Working on each box in order from the base upwards:

1. The log for that box was checked for any fossil horizons that had already been noted during the logging.
2. Some of the logs had highlighted areas where samples needed to be taken for further analysis. These samples were taken first before searching for further specimens.
3. A section of core to be inspected was removed from the box.
4. Using the square face of a fossil hammer which was held at an angle of approximately 45°, the recurved side of the core was hit.
5. If this was insufficient to cleave it, the recurved side was continually struck in a straight line around its circumference.
6. If the rock cleaved easily, the flat face of the core was gently tapped with the tapered face of the fossil hammer in a straight line.
7. Because the fossils helped the bedding planes to split apart, the rocks were split across their width rather than in pieces.

8. Both the part and counterpart were kept and placed into an appropriately sized tray.
9. The depth of the sample (or depth range for large facies) were measured and noted on the side of the tray.
10. In the logbook, the depth (or depth range) was entered with a very brief description of the fossil e.g. ostracods, shell, plant fragment (if unsure of its identification, 'indet.' was written).
11. Any significant sedimentary features were also taken as rock samples that were placed into a large sample bag, which was annotated with the depth range and what the feature was. This data was entered into a separate log with a BGS 'SSK' numbered sticker.

APPENDIX 13

Work Instruction: Megaspore picking

This work instruction details the steps that were taken to pick megaspores by hand from a wet residue (see Section 2.15).

A low power Wild Heerbrugg M3C stereoscopic binocular microscope with power supply unit 463 6V A.C. 20W was used with assorted pipettes, a watch glass, coverslips (Menzel-Gläser cover glass 22x32 mm #1 Part No. 12322118), plastic tubing, a glass beaker, a squeeze bottle filled with deionised water and some white roll.

1. Excess water was removed from the sample using a pipette.
2. The sample was poured onto a watch glass.
3. The watch glass was placed onto the microscope's light platform.
4. The power supply unit was switched on and the light power was increased as required.
5. Using a narrowed pipette* with a piece of plastic tubing fitted inside, the other end of the tubing was placed into the operator's mouth.
6. Using the capillary action of the pipette combined with gentle chewing action of the teeth on the tubing, megaspores and pieces of megaspore were isolated for picking.
7. When the specimen was inside the end of the pipette, the pipette was moved to the cover slip and a very gentle blowing action was employed to release the megaspore onto the cover slip and the sample number was annotated
8. This process was repeated until all of the megaspores had been picked.
9. The remaining sample was returned to its vial by gently swirling it on the watch glass to consolidate the sample as much as possible, then the edge of the watch glass was tipped over the mouth of the vial to pour in the contents.
10. Keeping the watch glass on the edge of the vial, the squeeze bottle was used to rinse the remaining residue into the vial.
11. The watch glass was dried thoroughly with the white roll and each pipette was rinsed with deionised water into a beaker.

12. The Counts of MEGAspores.xls database was annotated with brief details of what had been picked.
13. To switch off the power supply, the luminescence of the bulb was lowered first, then the button was switched to the off position (this helped to prevent the bulb from blowing).

*To produce a narrowed pipette, a regular glass pipette was placed over a Bunsen burner flame to heat it. Using narrow metal tongs, the end of the pipette was pulled gently until it lengthened. The elongated pipette was then broken at the required position.

APPENDIX 14

Work Instruction: Using the ultrasonic probe to remove AOM from palynology samples that contained scolecodonts

This work instruction details the steps that were taken to remove AOM from palynology samples that contained scolecodonts using the ultrasonic probe (see Section 2.17).

Wearing basic laboratory attire, palynological samples that contained scolecodonts and a high quantity of AOM were additionally subjected to the ultrasonic processor (Jencons (Scientific) Limited).

A polythene tube, squeeze bottles containing deionised water, and the tiny and medium sieves with 15 µm meshes were collected.

1. The ultrasonic probe was rinsed with deionised water and activated inside a clean polythene tube for 2 pulses of 10 seconds to ensure that it was clean.
2. A sample was transferred to the polythene tube and placed onto the end of the probe.
3. The probe was secured in the blue box housing.
4. The water was topped up if necessary (but not overfilled as spillage could have resulted in the loss of the sample).
5. The door was closed to reduce the noise.
6. The 'Start' button was pressed and the probe was activated for 10 seconds.
7. The 'Reset' button was pressed to stop it and the probe was activated for another 10 seconds.
8. The probe and tube were lifted carefully out of the housing.
9. The sample tube was removed.
10. The sample was decanted into the medium sieve to capture the residue, which was rinsed into the tiny sieve to return the residue to the sample's vial.
11. The probe, polythene tube and both sieves were washed thoroughly between the samples to prevent contamination.

APPENDIX 15

Work Instruction: Using Tilia to plot scolecodonts data

This work instruction details the steps that were taken to use Tilia software to plot the distribution and abundances of scolecodonts that had been found in the borehole samples (see Sections 2.17 and 5.14).

1. A new document was created in Tilia.
2. 'Scolecodont' was typed into the 'Name' and 'Group' columns.
3. The depths of the samples were copied from Excel and pasted into Tilia beginning in cell H1 (they had to be in ascending order for the software to run).
4. The scolecodont data was copied from Excel and pasted into Tilia beginning in cell H3 ensuring that:
 - There were no blank cells (if the cells had no values, they had to contain a zero).
 - The totals of the data columns were greater than zero or Tilia would not run.
 - Columns that equalled zero were deleted.
5. The 'Make diagram' button was selected.
6. The 'Graph style' button and then select the 'Select Variables' button were selected.
7. 'Scolecodont' was selected and the 'OK' button was clicked.
8. The 'Histogram' tab was selected.
9. In the 'Style' option, the 'Bars' radio button was selected.
10. In the 'Bars' option, the 'Use Thickness Variable' tick box was selected (to remove the tick).
11. The 'Bar Thickness' was changed to 0.2 and the 'Apply' button was selected for a visual check and then the 'OK' button was clicked.
12. To save the chart, the 'File' drop down menu and then the 'Save As' option were selected.
13. The chart was named and the 'Save' button was clicked.

This saved the chart as a Tilia diagram which most software cannot open. To resolve this:

- The 'File' drop down menu and then the 'Export' option were selected.
- The chart was named and the 'Save' button was selected.
- This saved the chart in Enhanced Windows Metafile (emf) format, which could be opened in Adobe Illustrator for editing.

APPENDIX 16

Work Instruction: Calculating Van Krevelen values

This work instruction details the steps that were taken to calculate the atomic weights of O/C and H/C to be plotted onto a Van Krevelen diagram to identify the type of coal that was found in the NWMF borehole core (see Section 5.13.2).

1. Subtract the inorganic (ash) content from 100% to calculate the total organic quantity:

Total %	Inorganic (ash) %	Organic %
100	- 23.9	= 76.1

2. Divide the mean values for each element in Table 11 by the total organic amount and multiply by 100 to convert to percentages:

	Mean values from Table 11	Calculation	Organic components (recalculated)
C	53.25	$53.25/76.1 \times 100$	70.0%
H	3.80	$3.80/76.1 \times 100$	5.0%
O	12.11	$12.11/76.1 \times 100$	15.9%
N	0.71	$0.71/76.1 \times 100$	0.9%
S	7.65	$7.65/76.1 \times 100$	10.1%

3. Divide the recalculated value for the organic components (above) by the atomic weight for each element:

	Atomic weight	Calculation	Result
C	12.011	$70.0/12.011$	5.83
H	1.008	$5.0/1.008$	4.96
O	15.999	$15.9/15.999$	0.99

4. Divide the atomic weights of H by C and O by C:

Elements	Calculation	Van Krevelen value
H/C	4.96/5.83	0.85
O/C	0.99/5.83	0.17

5. Plot on a Van Krevelen diagram (Figure 128).

APPENDIX 17



INTERNATIONAL CHRONOSTRATIGRAPHIC CHART

www.stratigraphy.org

International Commission on Stratigraphy

v 2018/07



Eonothem / Eon		Erathem / Era		System / Period		Series / Epoch	Stage / Age	GSSP	numerical age (Ma)
Phanerozoic	Cenozoic	Quaternary	Holocene	U/L	Meghalayan	present	0.0042		
				M	Northgrippian	0.0082			
			Pleistocene	L/E	Greenlandian	0.0117			
					Upper	0.126			
				Middle			0.781		
							1.80		
		Pliocene				2.58			
						3.600			
		Neogene	Miocene			5.333			
						7.246			
						11.63			
						13.82			
						15.97			
						20.44			
	Paleogene	Oligocene			23.03				
					27.82				
		Eocene			33.9				
					37.8				
					41.2				
					47.8				
		Paleocene			56.0				
					59.2				
				61.6					
				66.0					
	Mesozoic	Cretaceous	Upper			72.1 ± 0.2			
						83.6 ± 0.2			
						86.3 ± 0.5			
					89.8 ± 0.3				
					93.9				
					100.5				
		Lower			~ 113.0				
					~ 125.0				
					~ 129.4				
					~ 132.9				
					~ 139.8				
					~ 145.0				
Mesozoic	Jurassic	Upper			152.1 ± 0.9				
					157.3 ± 1.0				
					163.5 ± 1.0				
		Middle			166.1 ± 1.2				
					168.3 ± 1.3				
					170.3 ± 1.4				
					174.1 ± 1.0				
	Lower			182.7 ± 0.7					
				190.8 ± 1.0					
				199.3 ± 0.3					
				201.3 ± 0.2					
	Triassic	Upper			~ 208.5				
					~ 227				
					~ 237				
Middle				~ 242					
				247.2					
				251.2					
				251.902 ± 0.024					
Permian	Lopingian			254.14 ± 0.07					
				259.1 ± 0.5					
	Guadalupian			265.1 ± 0.4					
				268.8 ± 0.5					
				272.95 ± 0.11					
	Cisuralian			283.5 ± 0.6					
				290.1 ± 0.26					
Carboniferous	Pennsylvanian			295.0 ± 0.18					
				298.9 ± 0.15					
				303.7 ± 0.1					
	Mississippian	Upper			307.0 ± 0.1				
					315.2 ± 0.2				
		Lower			323.2 ± 0.4				
					330.9 ± 0.2				
Carboniferous	Middle			346.7 ± 0.4					
				358.9 ± 0.4					
	Lower								



INTERNATIONAL CHRONOSTRATIGRAPHIC CHART

www.stratigraphy.org

International Commission on Stratigraphy

v 2018/07

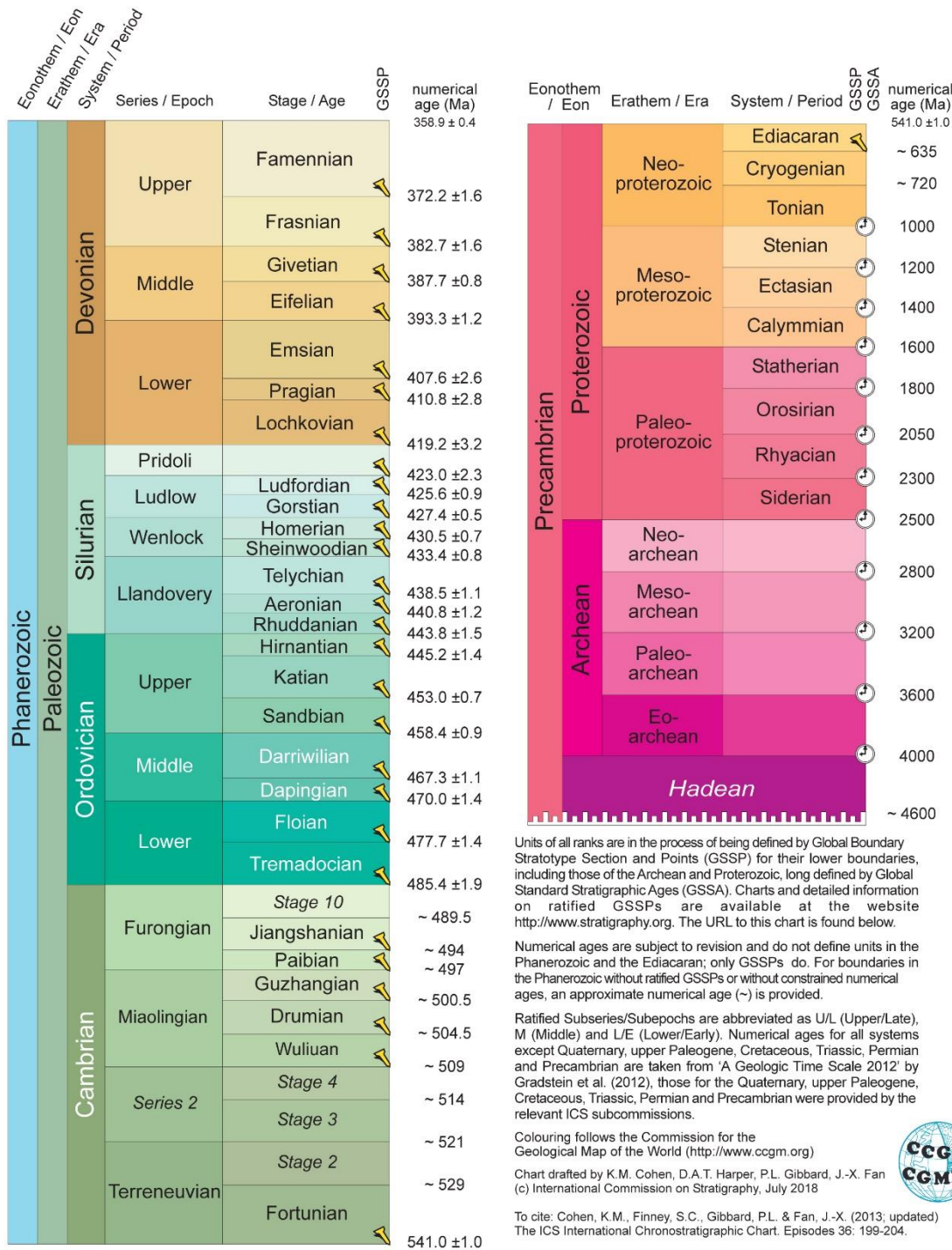


Figure 164. International Chronostratigraphic Chart (2018) indicating the Ages, Epochs, Periods, Eras and Eons of all geological time. From stratigraphy.org.

APPENDIX 18

Suprageneric classification of the NWMF borehole palynomorphs

Anteturma PROXIMEGERMINANTES Potonié 1970

Turma TRILETES (Reinsch) Dettmann 1963

Suprasubturma ACAMERATITRILETES Neves & Owens 1966

Subturma AZONOTRILETES (Luber) Dettmann 1963

Infraturma LAEVIGATI (Bennie & Kidston) Potonié 1956

Genus *CALAMOSPORA* Schopf *et al.* 1944

Calamospora nigrata (Naumova) Allen 1965

Calamospora perrugosa (Loose) Schopf *et al.* 1944

Calamospora spp.

Genus *PLICATISPORA* Higgs *et al.* 1988

Plicatispora scolecophora (Neves & Ioannides) Higgs *et al.* 1988

Genus *PUNCTATISPORITES* (Ibrahim) Potonié & Kremp 1954

Punctatisporites irrasus Hacquebard 1957

Punctatisporites? limbatus Hacquebard 1957

Punctatisporites planus Hacquebard 1957

Punctatisporites solidus Hacquebard 1957

Infraturma RETUSOTRILETI Streel *In: Becker et al.* 1974

Genus *RETUSOTRILETES* (Naumova) Richardson 1965

Retusotriletes incohatus Sullivan 1964

Retusotriletes rotundus (Streel) Streel 1967

Genus *APICULIRETUSISPORA* (Streel) Streel 1967

Apiculiretusispora fructicosa Higgs 1975

Apiculiretusispora multiseta (Luber) Butterworth & Spinner 1967

Apiculiretusispora nitida Owens 1971

Apiculiretusispora sp. A Higgs *et al.* 1988

Infraturma APICULATI (Bennie & Kidston) R. Potonié 1954

Genus *ANAPLANISPORITES* Jansonius 1962

Anaplanisporites baccatus (Hoffmeister *et al.*) Smith & Butterworth 1967

Anaplanisporites centrosus Higgs *et al.* 1988

Anaplanisporites sp. A

Anaplanisporites sp. B
Genus *APICULATISPORIS* (Ibrahim) Oschurkova 2003
Apiculatisporis sp. A
Genus *BACULATISPORITES* Thomson & Pflug 1953
Baculatisporites fusticulus Sullivan 1968
Genus *GRANULATISPORITES* (Ibrahim) Schopf *et al.* 1944
Granulatisporites pustulatus Hacquebard & Barss 1957
Genus *PILOSISPORITES* (Delcourt & Sprumont) Döring 1965
Pilosisporites verutus Sullivan & Marshall 1966
Genus *PUSTULATISPORITES* Potonié & Kremp 1954
Pustulatisporites dolbii Higgs *et al.* 1988
Genus *SCHOPFITES* Kosanke 1950
Schopfites claviger (Sullivan) Higgs *et al.* 1988
Schopfites claytonii Mahdi & Butterworth 1994
Schopfites delicatus (Higgs) Higgs *et al.* 1988
Subinfraturma *VERRUCATI* Dybová & Jachowicz 1957
Genus *LOPHOZONOTRILETES* (Naumova) Van der Zwan 1980
Lophozonotriletes tuberosus Sullivan 1964
Genus *PROLYCOSPORA* Turnau 1978
Prolycospora claytonii Turnau 1978
Genus *VERRUCOSISPORITES* (Ibrahim) Smith 1971
Verrucosisporites baccatus Staplin 1960
Verrucosisporites congestus Playford 1963
Verrucosisporites depressus Winslow 1962
Verrucosisporites gibberosus (Hacquebard) Higgs *et al.* 1988
Verrucosisporites irregularis Philips & Clayton 1980
Verrucosisporites nitidus Playford 1963
Verrucosisporites scoticus Sullivan 1968
Subinfraturma *NODATI* Dybová & Jachowicz 1957
Genus *CLAYTONISPOORA* Playford & Melo 2012
Claytonispora distincta (Clayton) Playford & Melo 2012
Infraturma *BACULATI* Dybová & Jachowicz 1957
Genus *RAISTRICKIA* (Schopf *et al.*) Potonié & Kremp 1954
Raistrickia corynoges Sullivan 1968

- Raistrickia* cf. *ponderosa*
- Infraturma MURORNATI Potonié & Kremp 1954
- Genus *ACINOSPORITES* Richardson 1965
- Acinosporites* cf. *acanthomammillatus*
- Genus *CONVOLUTISPORA* Hoffmeister *et al.* 1955
- Convolutispora caliginosa* Clayton & Keegan *In: Clayton et al.* 1982
- Convolutispora circumvallata* Clayton 1970
- Convolutispora florida* Hoffmeister *et al.* 1955
- Convolutispora harlandii* Playford 1962
- Convolutispora major* (Kedo) Turnau 1978
- Convolutispora mellita* Hoffmeister *et al.* 1955
- Genus *DICTYOTRILETES* (Naumova) Smith & Butterworth 1967
- Dictyotriletes fimbriatus* (Winslow) Kaiser 1970
- Dictyotriletes fragmentimurus* Neville *In: Neves et al.* 1973
- Dictyotriletes pactilis* Sullivan & Marshall 1966
- Dictyotriletes trivialis* Naumova *In: Kedo* 1963
- Infraturma CINGULATI (Potonié & Klaus) Dettmann 1963
- Genus *BASCAUDASPORA* Owens 1983
- Bascaudaspora submarginata* (Playford) Higgs *et al.* 1988
- Genus *KNOXISPORITES* (Potonié & Kremp) Neves & Playford 1961
- Knoxisporites literatus* (Waltz) Playford 1963
- Knoxisporites polymorphus* (Naumova) Braman & Hills 1992
- Knoxisporites pristinus* Sullivan 1968
- Knoxisporites triangularis* Higgs *et al.* 1988
- Genus *MONILOSPORA* (Hacquebard & Barss) Staplin 1960
- Monilospora mutabilis* (Staplin) Clayton *In: Neves et al.* 1973
- Infraturma PATINATI Butterworth & Williams 1958
- Genus *CYMBOSPORITES* Allen 1965
- Cymbosporites cyathus* Allen 1965
- Cymbosporites magnificus* (McGregor) McGregor & Camfield 1982
- Suprasubturma CAMERATITRILETES Neves & Owens 1966
- Infraturma MONOPSEUDOSACCITI Smith & Butterworth 1967
- Genus *AURORASPORA* Hoffmeister *et al.* 1955
- Auroraspora asperella* (Kedo) Van der Zwan 1980

Auroraspora macra Sullivan 1968

Auroraspora solisorta Hoffmeister *et al.* 1955

Genus *COLATISPORITES* Williams *In: Neves et al.* 1973

Colatisporites decorus (Bharadwaj & Venkatachala) Williams *In: Neves et al.* 1973

Colatisporites denticulatus Neville *In: Neves et al.* 1973

Colatisporites? papillatus Ravn 1991

Genus *DISCERNISPORITES* (Neves) Neves & Owens 1966

Discernisporites irregularis Neves 1958

Discernisporites macromanifestus (Hacquebard) Higgs *et al.* 1988

Discernisporites micromanifestus (Hacquebard) Sabry & Neves 1971

Discernisporites sullivanii Higgs & Clayton 1984

Genus *GRANDISPORA* (Hoffmeister *et al.*) McGregor 1973

Grandispora echinata Hacquebard 1957

Grandispora microdecora Phillips & Clayton 1980

Genus *INSCULPTOSPORA* Marshall 1985

Insculptospora incrustata (Arkhangelskaya) Marshall 1985

Genus *RUGOSPORA* (Neves & Owens) Turnau 1978

Rugospora lactucosa Higgs *et al.* 1988

Rugospora vieta Higgs *et al.* 1988

Genus *SPELAEOTRILETES* Neves & Owens 1966

Spelaeotrilites crustatus Higgs 1975

Spelaeotrilites microspinosus Neves & Ioannides 1974

Spelaeotrilites resolutus Higgs 1975

Genus *VELAMISPORITES* Bharadwaj & Venkatachala 1961

Velamisporites corporatus (Neves & Owens) Ravn 1991

Velamisporites minutus (Neves & Ioannides) Ravn 1991

Velamisporites polyptychus (Neves & Ioannides) Ravn 1991

Subturma MEMBRANATITRILETES Neves & Owens 1966

Infraturma CONTINUATI Neves & Owens 1966

Genus *GEMINOSPORA* (Balme) Owens 1971

Geminospora lemurata (Balme) Playford 1983

Subturma SOLUTITRILETES Neves & Owens 1966

Infraturma DECORATI Neves & Owens 1966

Genus *ENDOCULEOSPORA* (Staplin) Turnau 1975
Endoculeospora gradzinskii Turnau 1975

Subturma ZONOLAMINATITRILETES Smith & Butterworth 1967

Infraturma CRASSITI (Bharadwaj & Venkatachala) Smith & Butterworth 1967

Genus *CRASSISPORA* (Bharadwaj) Sullivan 1964
Crassispora aculeata Neville 1968
Crassispora trychera Neves & Ioannides 1974
Crassispora cf. *trychera*

Infraturma CINGULICAVATI Smith & Butterworth 1967

Genus *CINGULIZONATES* (Dybová & Jachowicz) Butterworth *et al.* In: Staplin & Jansonius 1964
Cingulizonates bialatus (Waltz) Smith & Butterworth 1967
Cingulizonates sp. A

Genus *CRISTATISPORITES* (Potonié & Kremp) Butterworth *et al.* 1964
Cristatisporites bellus Bharadwaj & Venkatachala 1961
Cristatisporites echinatus Playford 1963
Cristatisporites indignabundus (Loose) Staplin & Jansonius 1964
Cristatisporites matthewsii Higgs *et al.* 1988
Cristatisporites menendezii (Menéndez & Azcuy) Playford 1978

Genus *DENSOSPORITES* (Berry) Butterworth *et al.* 1964
Densosporites variomarginatus Playford 1963

Turma MONOLETES Ibrahim 1933

Suprasubturma PERINOMONOLITI Erdtman 1947

Genus *CURRICULOMONOLETES* McLean & Neves 2003
Curculomonoletes orbis McLean & Neves 2003

Anteturma MEGASPORITES Pant 1962

Turma TRILETES (Reinsch) Potonié & Kremp 1954

Suprasubturma AZONOTRILETES Lubert 1935

Subturma LAEVIGATI (Bennie & Kidston) Potonié & Kremp 1954

Genus *LAEVIGATISPORITES* (Ibrahim) Potonié & Kremp 1954
Laevigatisporites cf. *cheveriensis* (Bell) Glasspool & Scott 2005

Subturma APICULATI (Bennie & Kidston) Potonié & Kremp 1954

Suprainfraturma GRANULATI-VERRUCOSI Bharadwaj & Tiwari 1970

Genus *TUBERCULATISPORITES* (Ibrahim) Potonié & Kremp 1954
Tuberculatisporites mamillarius (Bartlett) Potonié & Kremp 1955

Suprainfraturma PILOSI Bharadwaj & Tiwari 1970

Genus *SETISPORA* (Butterworth & Spinner) Spinner 1982
Setispora pannosa (Alvin) Spinner 1982
Setispora pseudoreticulata (Butterworth & Spinner) Spinner 1982

Suprasubturma LAGENOTRILETES Potonié & Kremp 1954

Subturma GULATI Bharadwaj 1957

Genus *LAGENICULA* (Bennie & Kidston) Spinner 1969
Lagenicula mixta (Winslow) Wellman *et al.* 2009

Genus *SETOSISPORITES* (Ibrahim) Dybová-Jachowicz *et al.* 1979
Setosisporites sp. A

Suprasubturma ZONALES Bennie & Kidston 1886

Subturma ZONOTRILETI Waltz 1938

Suprainfraturma ZONATI Potonié & Kremp 1954

Infraturma HYMENOZONATI Piérart 1975

Genus *TRIANGULATISPORITES* (Potonié & Kremp) Karczewska 1976
Triangulatisporites membranatus Butterworth & Spinner 1967

Genus UNIDENTIFIED
 Spore Type D Spinner 1983

Turma ALETES

Subturma AZONALETES

Infraturma PSILONAPITI

Genus *DIDYMOSPORITES* Chaloner 1958
Didymosporites scottii Chaloner 1958

Anteturma POLLENITES R. Potonié 1931

Turma SACCITES Erdtman 1947

Subturma MONOSACCITES (Chitaley) Potonié & Kremp 1954

Infraturma EXTRORNATI Butterworth & Williams 1958

Genus *REMYSPORITES* Butterworth & Williams 1958
Remysporites magnificus (Horst) Butterworth & Williams 1958

Group ACRITARCHA Evitt 1963

Genus *ACANTHOTRILETES* (Naumova) Potonié & Kremp 1954

Acanthotriletes socraticus Neves & Ioannides 1974

Genus *CARBANEULETES* Spinner 1983

Carbaneuletes cf. *micromuratus*

Group EUGLENIDA (Bütschli 1884) Simpson 1997

Genus *CHOMOTRILETES* Naumova 1937

Chomotriletes multivittatus Playford 1978

Chomotriletes vedugensis Naumova 1953

APPENDIX 19

List of additional identified palynomorphs not included in Chapter 3

- Acanthotriletes acritarchus* Neville *In: Neves et al.* 1973
Acanthotriletes macrogaleatus Phillips & Clayton 1980
Acanthotriletes persibus Higgs 1975
Anapiculatisporites hispidus Butterworth & Williams 1958
Anapiculatisporites hystricosus Playford 1963
Anaplanisporites atheticus Neves & Ioannides 1974
Auroraspora corporiga Higgs *et al.* 1988
Bascaudaspora canipa Owens 1983
Bascaudaspora collicula (Playford) Higgs *et al.* 1988
Bascaudaspora mischkinensis (Byvscheva) Byvscheva *In: Byvscheva et al.* 1988
Calamospora microrugosa (Ibrahim) Schopf *et al.* 1944
Camptotriletes cristatus Sullivan & Marshall 1966
Camptotriletes paprothii Higgs & Streeel 1984
Carbaneuletes reticulata (Butterworth & Spinner) Spinner 1983
Chelinospora ligurata Allen 1965
Cirratiradites elegans (Waltz) Potonié & Kremp 1956
Convolutispora ampla Hoffmeister *et al.* 1955
Convolutispora crassa Playford 1962
Convolutispora jugosa Smith & Butterworth 1967
Convolutispora labiata Playford 1962
Convolutispora laminosa Neves 1961
Convolutispora usitata Playford 1962
Convolutispora vermiformis Hughes & Playford 1961
Corbulispora cancellata (Waltz) Bharadwaj & Venkatachala 1961
Corbulispora equigranulata (Neville) Ravn 1991
Corbulispora sagenoformis (Sullivan) Ravn 1991
Corbulispora vitilis (Sullivan & Marshall) Ravn 1991
Crassispora maculosa (Knox) Sullivan 1964
Cristatisporites aculeatus (Hacquebard) Potonié 1960
Cyclogranisporites palaeophytus Neves & Ioannides 1974

Cyrtospora cristifer (Luber) Van der Zwan 1979
Densosporites anulatus (Loose) Smith & Butterworth 1967
Densosporites dentatus (Waltz) Potonié & Kremp 1956
Densosporites rarispinosus Playford 1963
Densosporites spitsbergensis Playford 1963
Densosporites tenuis Hoffmeister *et al.* 1955
Dibolisporites uncatatus (Naumova) McGregor & Camfield 1982
Dictyotriletes clatriformis (Artüz) Sullivan 1964
Dictyotriletes flavus Keegan 1977
Dictyotriletes micromurornatus Hemsley *et al.* 1994
Dictyotriletes minor Naumova 1953
Dictyotriletes tessellatus Hibbert & Lacey 1969
Discernisporites sp. A Higgs *et al.* 1988
Endoculeospora setacea (Kedo) Avchimovitch & Higgs *In: Avchimovitch et al.* 1988
Geminospora spongiata Higgs *et al.* 1988
Geminospora sp. A Higgs *et al.* 1988
Gorgonispora crassa (Winslow) Higgs *et al.* 1988
Gorgonispora multiplicabilis (Kedo) Turnau 1978
Grandispora cornuta Higgs 1975
Grandispora gracilis (Kedo) Higgs *et al.* 2000
Grandispora saurota (Higgs *et al.*) Playford & McGregor 1993
Grandispora senticosa (Ishchenko) Byvscheva 1985
Grandispora spinosa Hoffmeister *et al.* 1955
Grandispora tamarae Loboziak *In: Higgs et al.* 2000
Grandispora uncata (Hacquebard) Playford 1971
Knoxisporites cinctus (Luber & Waltz) Butterworth & Williams 1958
Knoxisporites concentricus (Byvscheva) Playford & McGregor 1993
Knoxisporites dissidius Neves 1961
Knoxisporites hederatus (Ishchenko) Playford 1963
Knoxisporites margarethae Hughes & Playford 1961
Kraeuselisporites hibernicus Higgs 1975
Lophozonotriletes dentatus Hughes & Playford 1961
Lophozonotriletes malevkensis Naumova *In: Kedo* 1963

Monilospora dignata Playford 1963
Murospora aurita (Waltz) Playford 1962
Murospora dubitata Higgs 1975
Neoraistrickia cymosa Higgs *et al.* 1988
Neoraistrickia variabilis Mahdi & Butterworth 1994
Plicatispora quasilabrata (Higgs) Higgs *et al.* 1988
Prolycospora rugulosa (Butterworth & Spinner) Melo & Playford 2012
Radiizonates mirabilis Phillips & Clayton 1980
Raistrickia boleta Staplin 1960
Raistrickia condylosa Higgs 1975
Raistrickia minor (Kedo) Neves & Dolby 1967
Raistrickia nigra Love 1960
Raistrickia pistillata Hacquebard 1957
Raistrickia saetosa (Loose) Schopf *et al.* 1944
Raistrickia spathulata (Winslow) Higgs 1975
Raistrickia sp. A Higgs *et al.* 1988
Raistrickia variabilis Dolby & Neves 1970
Reticulatisporites cancellatus (Waltz) Playford 1962
Reticulatisporites carnosus (Knox) Neves 1964
Reticulatisporites reticulatus (Ibrahim) Ibrahim 1933
Savitrisporites nux (Butterworth & Williams) Sullivan 1964
Secarisporites remotus Neves 1961
Spelaeotriletes asperatus Ravn 1991
Spelaeotriletes balteatus (Playford) Higgs 1975
Spinozonotriletes impensus Higgs *et al.* 1988
Tholisporites scoticus Butterworth & Williams 1958
Tricidarisorites arcuatus Neville *In: Neves et al.* 1973
Tricidarisorites balteolus Sullivan & Marshall 1966
Umbonatisporites abstrusus (Playford) Clayton 1970
Umbonatisporites variabilis Hibbert & Lacey 1969
Vallatisporites vallatus Hacquebard 1957
Vallatisporites verrucosus Hacquebard 1957
Verrucosisporites gobbettii Playford 1962
Verrucosisporites scurrus (Naumova) McGregor & Camfield 1982

APPENDIX 20

List of accompanying material

- Clack, J. A., Bennett, C. E., Carpenter, D. K., Davies, S. J., Fraser, N. C., Kearsey, T. I., Marshall, J. E. A., Millward, D., Otoo, B. K. A., **Reeves, E. J.**, Ross, A. J., Ruta, M., Smithson, K. Z., Smithson, T. R. and Walsh, S. A., 2016, Phylogenetic and environmental context of a Tournaisian tetrapod fauna, *Nature Ecology & Evolution*, 1, 1-11, DOI: 10.1038/s41559-016-0002
- Bennett, C. E., Howard, A. S., Davies, S. J., Kearsey, T. I., Millward, D., Brand, P. J., Browne, M. A. E., **Reeves, E. J.** & Marshall, J. E. A., 2017, Ichnofauna record cryptic marine incursions onto a coastal floodplain at a key Lower Mississippian tetrapod site. *Palaeogeography, Palaeoclimatology, Palaeoecology*, 468, 287-300
- Marshall, J. E. A., **Reeves, E. J.**, Bennett, C. E., Davies, S. J., Kearsey, T. I., Millward, D., Smithson, T. R. & Brown, M. A. E., 2019, Reinterpreting the age of the uppermost 'Old Red Sandstone' and Early Carboniferous in Scotland. *Earth and Environmental Science Transactions of the Royal Society of Edinburgh*, 1-14

I contributed to the NWMF borehole palynological studies in Clack *et al.* 2016 and Marshall *et al.* 2019 and I provided information on the borehole scolecodonts and produced Figure 4 on page 292 in Bennett *et al.* 2017.

LIST OF REFERENCES

- Abbe, T. B. & Montgomery, D. R., 2003, Patterns and processes of wood debris accumulation in the Queets river basin, Washington. *Geomorphology*, 51, 81–107.
- Algeo, T. J. & Scheckler, S. E., 1998, Terrestrial marine teleconnections in the Devonian: links between the evolution of land plants, weathering processes and marine anoxic events, *Phil. Trans. R. Soc. Lond. B*, 353, 113-130.
- Allen, J. P. & Gastaldo, R. A., 2006, Sedimentology and taphonomy of the Early to Middle Devonian plant-bearing beds of the Trout Valley Formation, Maine. *Geological Society of America*, Special Paper 309, 57-333.
- Allen, K. C., 1965, Lower and middle Devonian spores of North and Central Vestspitsbergen. *Palaeontology*, 8, 687-748.
- Allen, P. A. & Marshall, J. E. A., 1981, Depositional environments and palynology of the Devonian south east Shetland Basin – a summary. *Scott. J. Geol.*, 17, 257-273.
- Alvin, K. L., 1965, A new fertile lycopod from the Lower Carboniferous of Scotland. *Palaeontology*, 8, 281-293.
- Alvin, K., 1966, Two cristate megaspores from the Lower Carboniferous of Scotland. *Palaeontology*, 488-491.
- Anderson, J. S., Smithson, T., Mansky, C. F., Meyer, T. & Clack, J., 2015, A diverse tetrapod fauna at the base of ‘Romer’s Gap’, *PLoS ONE*, 10, 1-27.
- Anderson, P. S. L., Friedman, M., Brazeau, M. D. & Rayfield, E. J., 2011, Initial radiation of jaws demonstrated stability despite faunal and environmental change. *Nature*, 476, 206–209.
- Andrews, J. E. & Nabi, G., 1998, Palaeoclimatic significance of calcretes in the Dinantian of the Cockburnspath Outlier (East Lothian-North Berwickshire). *Scottish Journal of Geology*, 34, 153-64.
- Ariana-Sab, M., Spina, A., Cirilli, S. & Daneshian, J., 2015, The palynostratigraphy of the Lower Carboniferous (middle Tournaisian-late Viséan) Shishtu Formation from the Howz-e-Dorah section, southeast Tabas, Central Iranian Basin. *Palynology*, 1-31.
- Arkhangelskaya, A. D., 1963, New species of spores from Devonian deposits of the Russian Platform, *Trudy VNIGRI*, No. 37, 18-30 [in Russian].

- Armstrong, H. A. & Purnell, M. A., 1987, Dinantian conodont biostratigraphy of the Northumberland Trough. *Journal of Micropalaeontology*, 6, 97-112.
- Artüz, S., 1957, Die Spora dispersae der Türkischen Steinkohle vom Zonguldak-Gebiet, Istanbul. Univ. Fen. Fak. Mecm, 22, 239-263.
- Avchimovitch, V. I. & Higgs, K. *In*: Avchimovitch, V. I., Byvscheva, T. V., Higgs, K., Streel, M. & Umnova, V. T., 1988, Miospore systematics and stratigraphic correlation of Devonian-Carboniferous boundary deposits in the European part of the USSR and Western Europe. *Cour. Forsch.-Inst. Senckenberg*, 100, 169-191.
- Avchimovitch, V. I. & Turnau, E., 1994, The Lower Carboniferous *Prolycospora claytonii* Zone of Western Pomerania and its equivalents in Belorussia and Northwestern Europe. *Annales Societatis Geologorum Poloniae*, 63, 249-63.
- Avchimovitch, V. I., 1992, Zonation and spore complexes of the Devonian and Carboniferous boundary deposits of the Pripyat Depression (Byelorussia). *Annales de la Société géologique de Belgique*, 15, 425-451.
- Avchimovitch, V. I., Byvscheva, T. V., Higgs, K., Streel, M. & Umnova, V. T., 1988, Miospore systematics and stratigraphic correlation of Devonian-Carboniferous boundary deposits in the European part of the USSR and Western Europe. *Cour. Forsch.-Inst. Senckenberg*, 100, 169-191.
- Azcuy, C. L. & di Pasquo, M., 2006, Additional systematic information on early Carboniferous palynoflora from the Ambo Formation, Pongo de Mainique, Peru. *Revista Brasileira de Paleontologia*, 9, 41-52.
- Balarino, M. L., Correa, G. A., Gutiérrez, P. R., Cariglino, B. & Carrevedo, M. L., 2015, The palynology of the La Deheza Formation (Carboniferous-Permian; Upper Palaeozoic), Paganzo Basin, San Juan Province, Argentina. *Palynology*, 1-21.
- Balme, B. E. & Hassell, C. W., 1962, Upper Devonian spores from the Canning Basin, Western Australia. *Micropalaeontology*, 8, 1-28.
- Balme, B. E., 1960, Notes on some Carboniferous microfloras from Western Australia. *Congr. Strat. Carb.*, 4th (Heerlen), C. R., 1, 25-31.
- Balme, B. E., 1962, Upper Devonian (Frasnian) spores from the Carnarvon Basin, Western Australia. *The Palaeobotanist*, 9, 1-10.
- Barnard, P. D. W., 1959, On *Eosperma oxroadense* gen. et sp. nov.: a new Lower Carboniferous seed from East Lothian. *Ann. Bot.*, 23, 284-296.

- Barnosky, A. D., Matzke, N., Tomiya, S., Wogan, G. O. U., Swartz, B., Quental, T. B., Marshall, C., McGuire, J. L., Lindsey, E. L., Maguire, K. C., Mersey, B. & Ferrer, E. A., 2011. Has the Earth's sixth mass extinction already arrived? *Nature*, 471, 51-57.
- Bartlett, H. H., 1928, Fossils of the Carboniferous coal pebbles of the glacial drift of Ann Arbor. *Pap. Mich. Acad. Sci.*, 9, 11-28.
- Bartram, K. M., 1987, Lycopod succession coals: an example from the Low Barnsely Seam (Westphalian B), Yorkshire, England. *In*: Scott, A. C. (Ed.), Coal and Coal-bearing Strata: Recent Advances, *Geological Society Special Publication No. 32*, pp. 187-199.
- Bateman, R. M. & Rothwell, G. W., 1990, A reappraisal of the Dinantian floras at Oxroad Bay, East Lothian, Scotland. 1. Floristics and the development of whole plant concepts. *Transactions of the Royal Society of Edinburgh: Earth Sciences*, 81, 127-159.
- Bateman, R. M. & Scott, A. C., 1990, A reappraisal of the Dinantian floras at Oxroad Bay. 2. Volcanicity, palaeoenvironments and palaeoecology. *Trans. Roy. Soc. Edin: Earth Sciences*, 81: 161-194.
- Bateman, R. M., 1988, Palaeobotany and palaeoenvironments of Lower Carboniferous floras from two volcanigenic terrains in the Scottish Midland Valley – Doctoral thesis, London University. 452. pp.
- Bateman, R. M., 1992, Morphometric reconstruction, palaeobiology and phylogeny of *Oxroadia gracilis* Alvin emend. and *O. conferta* sp. nov. Anatomically preserved rhizomorphic Lycopside from the Dinantian of Oxroad Bay, SE Scotland. *Palaeontographica, Abt. B: Palaeophytology*, 228, 29-103.
- Beck, C. B. & Wight, D. C., 1988, Progymnosperms. *In*: Beck, C.B. (Ed.) Origin and Evolution of Gymnosperms. Columbia University Press, New York, 57–61.
- Becker, G., Bless, M. J. M., Streel, M. & Thorez, J., 1974, Palynology and ostracod distribution in the Upper Devonian and basal Dinantian of Belgium and their dependence on sedimentary facies. *Meded. Rijks. Geol. Dienst.*, 25, 9-99.
- Becker, R. T., 1992, Zur Kenntnis von Hemberg-Stufe und *Allulata*-Schiefer im Nordsauerland (Oberdevon, Rheinisches Schiefergebirge, GK 4611 Hohenlimburg). *Berl. geowiss. Abh.*, E3, 3-43.

- Becker, R. T., 1993, Anoxia, eustatic changes, and Upper Devonian to lowermost Carboniferous global ammonoid diversity. *In: House, M. R. (Ed.) The Ammonoidea: environment, ecology and evolutionary change. The Systematics Association Special Volume 47*, Clarendon Press: Oxford, pp. 115-164.
- Becker, R. T., 1996, New faunal records and holostratigraphic correlation of the Hasselbachtal D/C boundary Auxiliary Stratotype (Germany). *Ann. Soc. Geol. Belg.*, 117, 19-45.
- Bell, W. A., 1960, Mississippian Horton Group of Type Windsor-Horton District Nova Scotia. *Geological Survey of Canada Memoir* 314, 1-58.
- Bengtson, P., 1988, Open nomenclature. *Palaeontology*, 31, 223-227.
- Bennett, C. E., Howard, A. S., Davies, S. J., Kearsey, T. I., Millward, D., Brand, P. J., Browne, M. A. E., Reeves, E. J. & Marshall, J. E. A., 2017, Ichnofauna record cryptic marine incursions onto a coastal floodplain at a key Lower Mississippian tetrapod site. *Palaeogeography, Palaeoclimatology, Palaeoecology*, 468, 287-300 (see Appendix 19).
- Bennett, C. E., Kearsey, T. I., Davies, S. J., Millward, D., Clack, J. A., Smithson, T. R. & Marshall, J. E. A., 2016, Early Mississippian sandy siltstones preserve rare vertebrate fossils in seasonal flooding episodes. *Sedimentology*, 63, 1677–700.
- Bennie, J. & Kidston, R., 1886, On the occurrence of spores in the Carboniferous formation of Scotland: (read 21st April 1886). *Royal Physical Society*.
- Benton, M. J. & Harper, D. A. T., 2009, Introduction to palaeobiology and the fossil record, Wiley-Blackwell, 591 pp.
- Benton, M. J., 1993, The Fossil Record II, Chapman & Hall, London.
- Benton, M. J., 1995, Diversification and extinction in the history of life. *Science*, 268, 52-58.
- Benton, M. J., 2015, Vertebrate Palaeontology, Wiley Blackwell, 468 pp.
- Berner, R. A., 1991, A model for atmospheric CO₂ over Phanerozoic time. *American Journal of Science*, 291, 339–376.
- Berry, C. M. & Fairon-Demaret, M., 2001, The Middle Devonian Flora revisited. *In: Gensel, P. G., Edwards, D. (Eds.), Plants Invade the Land: Evolutionary and Environmental Perspectives*. Columbia University Press, pp. 120–139.

- Berry, C. M., & Marshall, J. E. A., 2015, Lycopsid forests in the early Late Devonian paleoequatorial zone of Svalbard. *Geology*, 43, 1043-1046.
- Berry, W., 1937, Spores from the Pennington coal, Rhea County, Tennessee. *Amer. Mid. Natl.*, 18, 155-160.
- Bertelsen, F., 1972, A Lower Carboniferous Microflora from the Ørslev No. 1 Borehole, Island of Falster, Denmark, Danm. *Geol. Unders.*, 2, series 99, 1-78.
- Bertrand, P., 1909, Étude de la fronde des Zygoptéridées. Lille: Danel
- Bharadwaj, D. C. & Venkatachala, B. S., 1961, Spore assemblage out of a Lower Carboniferous shale from Spitsbergen. *The Palaeobotanist*, 10, 18-47.
- Bharadwaj, D. C., 1957, The spore flora of the Velener Schichten (Lower Westphalian D) in the Ruhr Coal Measures. *Palaeontographica B*, 102, 110-138.
- Boisvert, C. A., Joss, J. M. P. & Ahlberg, P. E., 2013, Comparative pelvic development of the axolotl (*Ambystoma mexicanum*) and the Australian lungfish (*Neoceratodus forsteri*): Conservation and innovation across the fish-tetrapod transition. *Evodevo*, 4, 3.
- Braman, D. R. & Hills, L. V., 1992, Upper Devonian and Lower Carboniferous miospores, western District of Mackenzie and Yukon Territory, Canada. *Canadian Soc. of Petroleum Geologists*.
- Brand, U., 1993, Global perspective of Famennian–Tournaisian oceanography: geochemical analysis of brachiopods. *Ann. Soc. Géol. Belg.*, 115, 491–496.
- Brazeau, M. D., 2009, The braincase and jaws of a Devonian ‘acanthodian’ and modern gnathostome origins. *Nature*, 457, 305–308.
- Brenchley, P. J., Marshall, J. D. & Underwood, C. J., 2001, Do all mass extinctions represent an ecological crisis? Evidence from the Late Ordovician. *Geol. J.*, 36, 329–340.
- Brindley, S. & Spinner, E., 1989, Palynological assemblages from Lower Carboniferous deposits, Burntisland district, Fife, Scotland. *Proc. Yorks. Geol. Soc.*, 47, 215-231.
- Brongniart, A., 1839, *Observations sur la structure intérieure du Sigillaria elegans comparée à celle des Lepidodendron et des Stigmaria et à celle des végétaux vivants*.

- Brown, M. A. E. & Monro, S. K., 1989, Evolution of the coal basins of central Scotland, Xle Congr s International de Stratigraphie et de G ologie du Carbonif re, Beijing. *Compte Rendu*, 5, 1-9.
- Browne, M. A. E., Dean, M. T., Hall, I. H., McAdams, A. D., Monro, S. K. & Chisholm, J. I., 1999, A lithostratigraphical framework for the Carboniferous rocks of the Midland Valley of Scotland. *British Geol. Surv. Res. Rep. RP/99/07*.
- Brzozowska, M., 1968, Rodzaj *Setosporites* (Ibrahim 1933) Potoni  & Kremp 1954 w karbonie Zag bia Lubelskiego. *Prace Instytutu Geologicznego*, 55, 5-57.
- Butterworth, M. A. & Spinner, E. In: Turnau, E., 1978, Spore Zonation of Uppermost Devonian and Lower Carboniferous Deposits of Western Pomerania. *Mededlingen Rijks Geologische Dienst*, 30, 1-35.
- Butterworth, M. A. & Spinner, E. In: Turnau, E., 1979, Correlation of Upper Devonian and Carboniferous deposits of Western Pomerania, based on spore study [in Polish, English summary]. *Ann. Soc. Geol. Polon.*, 49, 231-269.
- Butterworth, M. A. & Spinner, E., 1967, Lower Carboniferous spores from North-west England. *Paleontology*, 10, 1-24.
- Butterworth, M. A. & Williams, R. W., 1958, The small spore floras of coals in the Limestone Coal Group and Upper Limestone Group of the Lower Carboniferous of Scotland. *Trans. Roy. Soc. Edin, LXIII*, Part II, 353-390.
- Butterworth, M. A., Jansonius, J., Smith, A. H. V. & Staplin, F. L., 1964, *Densosporites* (Berry) Potoni  & Kremp and related genera. In: *Compte Rendu du 5me Congr s Internationale de Stratigraphie et de G ologie du Carbonif re*, Paris 1963. Pp. 1049-1057.
- Byvscheva, T. V. In: Byvscheva, T. V., Tchirokova, E. V. & Avchimovitch, V. I., 1988, Etapy razvitya flory (po sporam) na rubezhe devona i karbona. Granitsa devona i karbona na territorii SSSR. Nauka Tekhn., Minsk, 326-335.
- Byvscheva, T. V., 1985, Spores from deposits from the Tournaisian and Vis an stages of the Russian Plate. *Trudy Vsesoiuznogo Nauchno-Issledovatel'sogo Geologoraz-vedochnogo Neftianogo Instituta (VNIGNI)* 253, 80-158 [in Russian].

- Byvscheva, T. V., Higgs, K. & Streel, M., 1984, Spore correlations between the Rhenish slate mountains and the Russian platform near the Devonian-Carboniferous boundary. *Cour. Forsch.-Inst. Senckenberg*, 67, 37-45.
- Byvscheva, T., 1957, A spore-pollen description of the terrigenous rock complex of the Lower Carboniferous of the Melekess and Busuluk deep wells. *Doklady Akademii Nauk SSSR*, 116, pp. 1009-1011.
- Calder, M. G., 1938, On some undescribed Species from the Lower Carboniferous Flora of Berwickshire; together with a note on the genus *Stenomyelon* Kidson, *Trans. Roy. Soc. Edin.*, 59, 309-331.
- Cao, C., Love, G. D., Hays, L. E., Wang, W., Shen, S. & Summons, R. E., 2009, Biogeochemical evidence for euxinic oceans and ecological disturbance presaging the end-Permian mass extinction event. *Earth and Planetary Science Letter*, 281, 188-201.
- Caplan, M. L. & Bustin, R. M., 1999, Devonian–Carboniferous Hangenberg mass extinction event, widespread organic-rich mudrock and anoxia: causes and consequences. *Palaeogeography, Palaeoclimatology, Palaeoecology*, 148, 187-207.
- Caputo, M. V., 1985, Late Devonian glaciation in South America. *Palaeogeography, Palaeoclimatology, Palaeoecology*, 51, 291–317.
- Caputo, M. V., Crowell, J. C., 1985, Migration of glacial centers across Gondwana during Paleozoic Era. *Geol. Soc. Amer. Bull.* 96, 1020–1036.
- Caputo, M. V., Melo, J. H. G., Streel, M. & Isbell, J. L., 2008, Late Devonian and Early Carboniferous glacial records of South America. *In*: Fielding, C. R., Frank, T. D. & Isbell, J. L. (Eds.), *Resolving the Late Paleozoic Ice Age in Time and Space: Geological Society of America Special Paper 441*.
- Caro-Moniez, M., 1962, Sur un niveau à spores du Dévonien supérieur du Sondage de Tournai (Belgique). *Soc. Géol. Nord, Ann*, 82, 111-115.
- Carson, B. & Clayton, G., 1997, The Dinantian (lower Carboniferous) Palynostratigraphy of Rügen, Northern Germany. *Prace Państwowego Instytutu Geologicznego CLVII, 1997, Proceedings of the XIII International Congress on the Carboniferous and Permian*, 219-227.
- Cascales-Miñana, B. & Cleal, C. J., 2013, The plant fossil record reflects just two great extinction events. *Terra Nova*, 26, 195-200.

- Cascales-Miñana, B. & Meyer-Berthaud, B., 2014, Diversity dynamics of Zosterophyllopsida. *Lethaia*, 47, 205–215.
- Cavalli-Sforza, L. L. & Edwards, A. W. F., 1967, Phylogenetic Analysis: Models and estimation procedures. *Evolution*, 21, 550-570.
- Chadwick, R. A, Holliday, D. W., Holloway, S. & Hulbert, A. G., 1995, The structure and evolution of the Northumberland-Solway Basin and adjacent areas. *British Geological Survey Technical Report WA/89/26*.
- Chaloner, W. G., 1954, Mississippian megaspores from Michigan and adjacent states. *Contr. Mus. Palaeont. Univ. Mich.*, 12, 23-35.
- Chaloner, W. G., 1958, Isolated Megaspore Tetrads of *Stauropteris burntislandica*, *Annals of Botany*, N. S. Vol. 22, No. 86, 197-204.
- Chen, D. & Ahlberg, P. E., 2009, A partial tetrapod lower jaw from “Romer’s Gap.” *Journal of Vertebrate Paleontology*, 29, 76A.
- Clack, J. A. & Finney, S. M., 2005, *Pederpes finneyae*, an articulated tetrapod from the Tournaisian of western Scotland. *Journal of Systematic Palaeontology*, 2, 311–346.
- Clack, J. A., 1997, Devonian tetrapod trackways and trackmakers; a review of the fossils and footprints. *Palaeogeography, Palaeoclimatology, Palaeoecology*, 130, 227-250.
- Clack, J. A., 1998, The Scottish Carboniferous tetrapod *Crassigyrinus scoticus* (Lydekker)—Cranial anatomy and relationships. *Trans. R. Soc. Edinb. Earth Sci.*, 88, 127–142.
- Clack, J. A., 2002, An early tetrapod from ‘Romer’s Gap.’ *Nature*, 418, 72–76.
- Clack, J. A., 2002a, Gaining ground, the origin and early evolution of tetrapods. *Life of the Past*, Indiana University Press, Bloomington, 369 pp.
- Clack, J. A., 2006, The emergence of early tetrapods. *Palaeogeography Palaeoclimatology Palaeoecology*, 232, 167–89.
- Clack, J. A., 2007, Devonian climate change, breathing, and the origin of the tetrapod stem group. *Integr. Comp. Biol.*, 47, 510–23.
- Clack, J. A., 2009, The Fish-Tetrapod Transition: New fossils and interpretations. *Evo Edu Outreach*, 2, 213-223.
- Clayton, G. & Keegan, J. B. *In*: Clayton, G., Keegan, J. B. & Sevastopulo, G. D., 1982, Palynology and stratigraphy of late Devonian and early Carboniferous rocks, Ardmore, County Waterford, Ireland. *Pollen et Spores*, 24, 511-521.

- Clayton, G. & Turnau, E., 1990, Correlation of the Tournaisian miospore zonations of Poland and the British Isles. *Annales Societatis Geologorum Poloniae*, 60, 45–58.
- Clayton, G. *In*: Neves, R., Gueinn, K. J., Clayton, G., Ioannides, N. & Neville R. S. W., 1973, Palynological correlations within the Lower Carboniferous of Scotland and northern England. *Trans. R. Soc. Edinburgh*, 69, 23-70.
- Clayton, G., 1970, A Lower Carboniferous Miospore Assemblage from the Calcareous Sandstone Measures of the Cockburnspath Region of Eastern Scotland. *Pollen et Spores*, 12, 577-600.
- Clayton, G., 1985, Plant miospores from the Dinantian of Foulden, Berwickshire, Scotland. *Trans. Roy. Soc. Edin: Earth Sciences*, 76, 21-24.
- Clayton, G., 1995, Carboniferous miospore and pollen assemblages from the Kingdom of Saudi Arabia. *Review of Palaeobotany and Palynology*, 89, 115-123.
- Clayton, G., Coquel, R., Doubinger, J., Gueinn, K. J., Loboziak, S., Owens, B. & Streel, M., 1977, Carboniferous miospores of western Europe: Illustration and zonation. *Mededelingen rijks geologische dienst*, 29, 1-71.
- Clayton, G., Johnston, I. S., Sevastopulo, G. D. & Smith, D. G., 1980, Micropalaeontology of a Courceyan (Carboniferous) borehole section from Ballyvergin, County Clare, Ireland. *J. Earth Sci. R. Dubl. Soc.*, 3, 81-100.
- Clement, G., Ahlberg, P. E., Blieck, A., Blom, H., Clack, J. A., Poty, E., Thorez, J. & Janvier, P., 2004, Devonian tetrapod from western Europe. *Nature*, 427, 412– 413.
- Coates, M. I., 1996, The Devonian tetrapod *Acanthostega gunnari* Jarvik: Postcranial anatomy, basal tetrapod relationships and patterns of skeletal evolution. *Trans. Roy. Soc. Edinb.*, 87, 363–421.
- Coates, M. I., Jeffery, J. E. & Ruta, M., 2002, Fins to limbs: what the fossils say. *Evol. Dev.*, 4, 390–401.
- Coates, M. I., Ruta, M. & Friedman, M., 2008, Ever since Owen: Changing perspectives on the early evolution of tetrapods. *Annu. Rev. Ecol. Evol. Syst.*, 39, 571–592.
- Cohen, K. M., Finney, S. C., Gibbard, P. L. & Fan, J.-X. (2013; updated) The ICS International Chronostratigraphical Chart, *Episodes*, 36, 199-204.
<http://www.stratigraphy.org/ICSchart/ChronostratChart2018-07.pdf>

- Collinson, M. E., Batten, D. J., Scott, A. C. & Ayonghe, S. N., 1985, Palaeozoic, Mesozoic and contemporaneous megaspores from the Tertiary of southern England: indicators of sedimentary provenance and ancient vegetation. *J. geol. Soc. London*, 142, 375-395.
- Combaz, A. & Streel, M., 1970, Microfossiles végétaux du Tournaisien inférieur dans le 'core drill' de Brévillers (Pas-de-Calais, France). *In: 'Colloques sur la stratigraphie du Carbonifère. Congrès et Colloques Univ. Liège*, 55, 227-240.
- Copper, P., 1986, Frasnian/Famennian mass extinction and cold water oceans. *Geology*, 14, 835–839.
- Couper, R. A., 1953, Upper Mesozoic and Cainozoic spores and Pollen grains from New Zealand. *New Zealand Geol. Surv. Paleont. Bult.*, 22, 1-77.
- Couper, R. A., 1958, British Mesozoic microspores and pollen grains. A systematic and stratigraphic study. *Palaeontographica B*, 103, 75-179.
- Daeschler, E. B., Shubin, N. H. & Jenkins, F. A. Jr., 2006, A Devonian tetrapod-like fish and the evolution of the tetrapod body plan. *Nature*, 440, 757-763.
- Danzé, J., Levet-Carette, J. & Loboziak, S., 1964, Révision des spores du genre *Tuberculatisporites* Ibrahim du Bassin Houiller du Nord de la France. *Rev. Micropaléont.*, 7, 14-30.
- Davies, N. S. & Gibling, M. R., 2010, Cambrian to Devonian evolution of alluvial systems: The sedimentological impact of the earliest land plants. *Earth-Science Reviews*, 98, 171-200.
- Davies, N. S. & Gibling, M. R., 2011, Evolution of fixed-channel alluvial plains in response to Carboniferous vegetation. *Nature Geoscience*, 4, 629-633.
- de Jersey, N. J., 1966, Devonian spores from the Adavale Basin. SG Reid, Government Printer.
- De Vleeschouwer, D., Rakocinski, M., Racki, G., Bond, D. P. G., Sobien, K. & Clarys, P., 2013, The astronomical rhythm of Late Devonian climate change (Kowala section, Holy Cross Mountains, Poland). *Earth and Planetary Science Letters*, 365, 25–37.
- Decombeix, A-L., Meyer-Berthaud, B. & Galtier, J., 2011, Transitional changes in arborescent lignophytes at the Devonian-Carboniferous boundary. *J. Geol. Soc. Lond.*, 168, 547-557.

- Decombeix, A.-L., Meyer-Berthaud, B., Galtier, J., Talent, J. A. & Mawson, R., 2011, Arborescent lignophytes in the Tournaisian vegetation of Queensland (Australia): paleoecological and paleogeographical significance. *Palaeogeography, Palaeoclimatology, Palaeoecology*, 301, 39-55.
- Deegan, C. E., 1973, Tectonic control of sedimentation at the margin of a Carboniferous depositional basin in Kirkcudbrightshire. *Scottish Journal of Geology*, 9, 1-28.
- Delcourt, A. F. & Sprumont, G., 1955, Les spores et grains de pollen du Wealdien du Hainaut. *Mem. Soc. Belg. Géol.*, 4, 1-73.
- Di Pasquo, M., Azcuy, C. L. & Souza, P. A., 2003, Palinología del Carbonífero Superior del Subgrupo Itararé en Itaporanga, Cuenca Paraná, Estado de São Paulo, Brazil. Parte 1: sistemática de esporas y paleofitoplancton. *Ameghiniana*, 40, 277-296.
- Dijkstra, S. J., 1946, Eine monographische Bearbeitung der karbonischen Megasporen mit besonderer Berücksichtigung von Südlimburg (Niederlande). *Meded. geol. Sticht., Maastricht (C)*, 3, 1-101.
- DiMichele, W. A. & Bateman, R. M., 1996, Plant paleoecology and evolutionary inference: two examples from the Paleozoic. *Review of Palaeobotany and Palynology*, 160, 154-162.
- DiMichele, W. A. & Hook, R. W., 1992, Paleozoic terrestrial ecosystems. In: Behrensmeyer, A. K., Damuth, J. D., DiMichelle, W. A., Potts, R., Sues, H. D. & Wing, S. L. (Eds.), *Terrestrial Ecosystems through Time*, University of Chicago Press, Chicago, IL, pp. 205–325.
- Dolby, G. & Neves, R., 1970, Palynological evidence concerning the Devonian-Carboniferous boundary in the Mendips, England. *Compte Rendu 6e Congres Intern. Strat. Geol. Carbonif.*, Sheffield 1967, Volume 2, pp. 631-646.
- Döring, H., 1965, Die Sporenpaläontologische Gliederung des Wealden in Westmecklenburg (Struktur Werle). *Geologie*, 14, 1-118.
- Dueñas, H. & Césari, S. N., 2005, Systematic study of early Carboniferous palynological assemblages from the Llanos Orientales Basin, Colombia. *Revista del Museo Argentino de Ciencias Naturales, n. s.*, 7, 139-152.
- Dybová, S. & Jachowicz, A., 1957, Microspores of the Upper Silesian coal measures. *Ins. Geol. Warsaw*, 328 pp.

- Dybová-Jachowicz, S., Jachowicz, A., Karczewska, J., Lachkar, G., Loboziak, S., Pierart, P., Turnau, E. & Zoldani, Z., 1979, Preliminary note on revision of Carboniferous megaspores with Gula. Principles of Classification, *Acta Palaeontologica Polonica*, 24, 411-422.
- Eder, W. & Franke, W., 1982, "Death of Devonian reefs." *Neues Jahrbuch für Geologie und Paläontologie, Abhandlungen*, 163, 241-243.
- Edwards, D. & Wellman, C. H., 2001, Embryophytes on land: the Ordovician to Lochkovian (Lower Devonian) record. *In*: Gensel, P. G., Edwards, D. (Eds.), *Plants Invade the Land: Evolutionary and Environmental Perspectives*. Columbia University Press, pp. 3–28.
- Eisenack, A., 1944, Über einige pflanzliche Funde in Geschieben, nebst Bemerkungen zum Hystrichosphaerideen–Problem. *Zeitschrift für Geschiebeforschung und Flachlandsgeologie*, 19, 103-124.
- Erwin, D. H., 1998, The end and the beginning: recoveries from mass extinctions. *Trends Ecol. Evol.*, 13, 344–349.
- Fairon-Demaret M., 1986, Some uppermost Devonian megafloras: a stratigraphical review. *Annales de la Société géologique de Belgique*, 109, 43–48.
- Fairon-Demaret, M., 1996, The plant remains from the Late Famennian of Belgium: a review. *The Palaeobotanist*, 45, 201–208.
- Falcon-Lang, H. J., 1999, The early Carboniferous (Courceyan–Arundian) monsoonal climate of the British Isles: evidence from growth rings in fossil woods. *Geological Magazine*, 136, 177-87.
- Feng, L., Huaicheng, Z. & Shu, O., 2008, Late Carboniferous–Early Permian palynology of Baode (Pao-te-chou) in Shanxi Province, North China. *Geol. J.*, 43, 487-510.
- Fielding, C. R., Frank, T. D., Birgenheier, L. P., Rygel, M. C., Jones, A. T., & Roberts, J., 2008, Stratigraphic record and facies associations of the late Paleozoic ice age in eastern Australia (New South Wales and Queensland). *In*: Fielding, C. R., Frank, T. D. & Isbell, J. L. (Eds.), *Resolving the Late Paleozoic Ice Age in Time and Space*, *Geological Society of America Special Paper* 441.

- Finnegan, S., Heim, N. A., Peters, S. E. & Fischer, W. W., 2012, Climate change and the selective signature of the Late Ordovician mass extinction. *PNAS*, 109, 6829-6834.
- Flores, R. M., 2014, Coal and coalbed gas: Fueling the future. Elsevier Science, pp. 720.
- Friedman, M. & Sallan, L. C., 2012, Five hundred million years of extinction and recovery: A Phanerozoic survey of large-scale diversity patterns in fishes. *Palaeontology*, 55, 707-742.
- Friend, P. F., Alexander-Marrak, P. D., Nicholson, J. & Yeats, A. K., 1976, Devonian sediments of East Greenland II: sedimentary structures and fossils. *Medd. GrønL.*, 206, 91.
- Gensel, P. G., 2008, The earliest land plants. *Annual Review of Ecology, Evolution and Systematics*, 39, 459–477.
- Gensel, P. G., Kotyk, M. E. & Basinger, J. F., 2001, Morphology of Above-and Below-Ground Structures in Early Devonian (Pragian–Emsian) Plants. *In: Plants invade the land: evolutionary and environmental perspectives*, Columbia University Press, p. 83.
- Glasspool, I. J. & Scott, A. C., 2005, An early Carboniferous (Mississippian), Tournaisian, megaspore assemblage from Three Mile Plains, Nova Scotia, Canada. *Review of Palaeobiology and Palynology*, 134, 219-236.
- Glasspool, I. J., Edwards, D. & Axe, L., 2004, Charcoal in the Silurian as evidence for the earliest wildfire. *Geology*, 33, 589–592.
- Glasspool, I. J., Hemsley, A. R., Scott, A. C. & Golitsyn, A., 2000, Ultrastructure and affinity of Lower Carboniferous megaspores from the Moscow Basin, Russia. *Review of Palaeobotany and Palynology*, 109, 1-31.
- Godfrey, S. J., 1989, The postcranial skeleton of the Carboniferous tetrapod *Greererpeton burkemorani* Romer 1969. *Philos. Trans. R. Soc. Lond B Biol. Sci.*, 323, 75–133.
- Göppert, H. R., 1845, In Wimmer's Flora von Schlesien. 2nd Ed. Breslau.
- Greb, S. F., DiMichele, W. A., Gastaldo, R. A., 2006, Evolution and importance of wetlands in earth history. In: Greb, S. F., DiMichele, W. A. (Eds.), *Wetlands through time*. Geological Society of America, Special Paper 399, 1-40.
- Greig, D. C., 1988, Geology of the Eyemouth District. *Memoirs of the British Geological Survey*, Sheet 34 (British Geological Survey, Keyworth, UK).

- Groppo, J., 2017, An introduction to the nature of coal. *In*: Coal Combustion Products (CCPs): Characteristics, utilization and beneficiation, pp. 3-20.
- Hacquebard, P. A. & Barss, M. S., 1957, A Carboniferous spore assemblage in coal from the South Nahanni River area, Northwest Territories. *Geological Survey of Canada Bulletin* 40, 1-63.
- Hacquebard, P. A., 1957, Plant spores in coal from the Horton Group (Mississippian) of Nova Scotia. *Micropaleontology*, 3, 301-324.
- Hammer, Ø., Harper, D. A. T. & Ryan, P. D., 2001, PAST: Palaeontological Statistics software package for education and data analysis. *Palaeontologia Electronica*, 4, 9 pp.
- Hao, S., Xue, J., Guo, D. & Wang, D., 2010, Earliest rooting system and root:shoot ratio from a new Zosterophyllum plant. *New Phytol.*, 185, 217-225.
- Heal, S. & Clayton, G., 2008, The palynology of the Hannibal Shale (Mississippian) of Northeastern Missouri, USA and correlation with Western Europe. *Palynology*, 32, 27-37.
- Hemsley, A. R., 1990, The ultrastructure of the exine of the megaspores in two Palaeozoic seed-like structures. *Review of Palaeobotany and Palynology*, 63, 137-152.
- Hemsley, A. R., Clayton, G. & Galtier, J., 1994, Further studies on a late Tournaisian (Lower Carboniferous) flora from Loch Humphrey Burn, Scotland: spore taxonomy and ultrastructure. *Review of Palaeobiology and Palynology*, 81, 213-231.
- Hesselbo, S. P., Robinson, S. A., Surlyk, F. & Piasecki, S., 2002, Terrestrial and marine extinction at the Triassic-Jurassic boundary synchronized with major carbon-cycle perturbation: A link to initiation of massive volcanism? *Geological Society of America*, 30, 251-254.
- Hibbert, F. A. & Lacey, W. S., 1969, Miospores from the Lower Carboniferous basement beds in the Menai Straits region of Caernarvonshire, north Wales. *Palaeontology*, 12, 420-440.
- Higgs, K. & Clayton, G., 1984, Tournaisian miospore assemblages from Maesbury in the eastern Mendips, England. *J. Micropalaeontol.*, 3, 17-28.
- Higgs, K. & Russell, K. J., 1981, Upper Devonian microfloras from southeast Iveragh, County Kerry, Ireland, *Geol. Surv. Ire. Bull.*, 3, 17-50.

- Higgs, K. & Streel, M., 1984, Spore stratigraphy at the Devonian-Carboniferous boundary in the northern "Rheinisches Schiefergebirge", Germany. *Cour. Foursch.-Inst. Senckenberg*, 67, 157-179.
- Higgs, K. *In*: Van der Zwan, C. J. & Van Veen, P. M., 1978, The Devonian-Carboniferous Transition sequence in Southern Ireland: Integration of Palaeogeography and palynology. *Palinologia*, 1, 469-479.
- Higgs, K. *In*: Van der Zwan, C. J., 1980, Aspects of late Devonian and early Carboniferous palynology of southern Ireland. III. Palynology of Devonian-Carboniferous transition sequences with special reference to the Bantry Bay area, Co. Cork. *Review of Palaeobotany and Palynology*, 30, 165-286.
- Higgs, K. T. & Forsythe, E., 2007, Mississippian microfloras from the South Munster Basin, Ireland. *Comunicações Geológicas*, 94, 175-194.
- Higgs, K. T., 1996, Taxonomy and systematic study of some Tournaisian (Hastarian) spores from Belgium. *Review of Palaeobotany and Palynology*, 93, 269-297.
- Higgs, K. T., Dreesen, R., Duser, M. & Streel, M., 1992, Palynostratigraphy of the Tournaisian (Hastarian) rocks in the Namur Synclinorium, West Flanders, Belgium. *Review of Palaeobotany and Palynology*, 72, 149-158.
- Higgs, K. T., Finucane, D. & Tunbridge, I. P., 2002, Late Devonian and early Carboniferous microfloras from the Hakkari Province of southeastern Turkey. *Review of Palaeobotany and Palynology*, 118, 141-156.
- Higgs, K. T., Prestianni, C., Streel, M. & Thorez, J., 2013, High resolution miospore stratigraphy of the Upper Famennian of eastern Belgium and correlation with the conodont zonation. *Geologica Belgica*, 16, 84-94.
- Higgs, K., 1975, Upper Devonian and Lower Carboniferous miospore assemblages from Hook Head, County Wexford, Ireland. *Micropalaeontology*, 21, 393-419.
- Higgs, K., Avkhimovitch, V. I., Loboziak, S., Maziane-Serraj, N., Stempien-Salek, M & Streel, M., 2000, Systematic study and stratigraphic correlation of the *Grandispora* complex in the Famennian of northwest and eastern Europe. *Review of Palaeobotany and Palynology*, 112, 207-228.
- Higgs, K., Clayton, G. & Keegan, J. B., 1988, Stratigraphic and Systematic Palynology of the Tournaisian Rocks of Ireland. *The Geological Survey of Ireland*, Special Paper Number 7, 1-93.

- Hillier, R. D., Edwards, D. & Morrissey, L. B., 2008, Sedimentological evidence for rooting structures in the Early Devonian Anglo-Welsh Basin (UK), with speculation on their producers. *Palaeogeography, Palaeoclimatology, Palaeoecology*, 270, 366–388.
- Hiltmann, W., 1967, Über die Sporenführung des Kernprofils der Bohrung Contern FG11 (Unterer Lias, Luxemburg). *Service géologique de Luxembourg publication*, 17, pp. 137-206.
- Hoffmeister, W. S., Staplin, F. L. & Malloy, R. E., 1955, Mississippian plant spores from the Hardinsburg Formation of Illinois and Kentucky. *Journal of Palaeontology*, 29, 372-399.
- Holland, T., 2010, Upper Devonian osteichthyan remains from the Genoa River, Victoria, Australia. *Memoirs of Museum Victoria*, 67, 35-44.
- Holmen, K., 2000, The global carbon cycle. In: Jacobson, M. C., Charlson, R. J., Rodhe, H. & Orians, G. (Eds.) *Earth System Science: Biogeochemical Cycles to Global Change*. Elsevier, New York.
- Holmes, R., 1980, The Carboniferous amphibian *Proterogyrinus scheeli* Romer and the early evolution of tetrapods. *Philos. Trans. R. Soc. Lond. B Biol. Sci.*, 306, 431–524.
- Horst, U., 1943, Mikrostratigraphischer Beitrag zum Vergleich des Namurs von West-Oberschleisen und Mährisch-Ostrau. Thesis, Tech. Hochsch., Berlin
- Horst, U., 1955, "Die Sporae dispersae des Namurs von Westoberschlesien und Mährisch-Ostrau". *Palaeontographica, Abt. B*, 98, 137-236.
- House, M., 1985, Correlation of mid-Paleozoic ammonoid evolutionary events with global sedimentary perturbations. *Nature*, 313, 17-22.
- Hughes, N. F. & Playford, G., 1961, Palynological reconnaissance of the Lower Carboniferous of Spitsbergen. *Micropalaeontology*, 7, 27-44
- Ibrahim, A. G., 1932, Beschreibung von Sporenformen aus Flöz Ägir. In: Potonié, R. Sporenformen aus den Flözen Ägir und Bismarck des Ruhrgebietes, *Neues Jahrb.*, Beilage-Band 67, Abt. B, 447-449.
- Ibrahim, A. G., 1933, Sporenformen des Ägirhorizontes des Ruhrreviers, Dissertation TH Berlin 1932, 1-46.
- Isaacson, P. E., Díaz-Martínez, E., Grader, G. W., Kalvoda, J., Babek, O. & Devuyst, F. X., 2008, Late Devonian-earliest Mississippian glaciation in

- Gondwanaland and its biogeographic consequences. *Palaeogeography, Palaeoclimatology, Palaeoecology*, 268, 126-142.
- Ishchenko, A. M., 1952, Atlas of the microspores and pollen of the Middle Carboniferous of the western part of the Donetz Basin. *Izd. Akad. Nauk. Ukrainian SSR, Inst. Geol. Nauk.*, 1-83 [in Russian].
- Ishchenko, A. M., 1956, Spores and pollen of the Lower Carboniferous sediments of the western extension of the Donetz Basin and their stratigraphic importance, Trudy Instituta Geologicheskikh Nauk, Kiev. *Stratigraphic and Palaeontologic Series*, Contribution 11, 1-185.
- Ishchenko, A. M., 1958, Spore-pollen analysis of the Lower Carboniferous sediments of the Dnieper-Donets Basin, *Ibid.*, 17, 1-188 [in Russian].
- Jablonski, D., 2005, Mass extinctions and macroevolution. *Paleobiology*, 31, 192–210.
- Janis, C. M. & Keller, J., 2001, Modes of ventilation in early tetrapods: Costal aspiration as a key feature of amniotes. *Acta Palaeontol. Pol.*, 46, 137–170.
- Jansonius, J. & Hills, I. V., 1976, Genera file of fossil spores, Special Publication – Dept. Geology, University of Calgary, Canada.
- Jansonius, J., 1962, Palynology of Permian and Triassic sediments, Peace River area, Western Canada. *Palaeontographica B*, 110, 35-98.
- Jansonius, J., Hills, I. V. & Hartkopf-Fröder, 2006, Genera file of fossil spores - Supplement 14, Special Publication – Dept. of Geology and Geophysics, University of Calgary, Canada.
- Janvier, P., 1996, Early Vertebrates, Clarendon Press, Oxford, 393 pp.
- Janvier, P., 2003, Early Vertebrates, Clarendon Press, 408 pp.
- Jarvik, E., 1996, The Devonian tetrapod *Ichthyostega*. *Fossils and Strata*, 40, 1–206.
- Jarvis, E., 1990, New palynological data on the age of the Kiltorcan Flora of Co. Kilkenny, Ireland. *Journal of Micropaleontology*, 9, 87–94.
- Johnson, G. A. L. & Marshall, A. E., 1971, Tournaisian beds in Ravenstonedale, Westmorland. *Proceedings of the Yorkshire Geological Society*, 38, 261-280.
- Johnson, J. G., Klapper, G. & Sandberg, C. A., 1985, Devonian eustatic fluctuations in Euramerica. *Bull. Geol. Soc. Amer.*, 96, 567-587.
- Jones, L. S. & Schumm, S. A., 1999. In: Fluvial Sedimentology VI, Smith, N. D. & Rogers, J., (Eds.), Blackwell, pp. 171-178.

- Kaiser, H., 1970, Die Oberdevon-Flora der Bäreninsel. 3. Mikroflora des höheren Oberdevons und des Unterkarbons. *Palaeontographica B*, 129, 71-124.
- Kaiser, S. I., 2005, Mass extinctions, climatic and oceanographic changes at the Devonian/Carboniferous boundary, PhD Thesis, Bochum, Germany, 160 pp.
- Kaiser, S. I., Aretz, M. & Becker, R. T., 2015, The global Hangenberg Crisis (Devonian-Carboniferous transition): review of a first-order mass extinction. *In*: Becker, R. T., Königshof, P. & Brett, C. E. (Eds.) Devonian Climate, Sea Level and Evolutionary Events. *Geological Society London*, Special Publications, 423, 51 pp.
- Karczewska, J., 1967, Carboniferous spores from the Chelm 1 Boring (Eastern Poland). *Acta Palaeontologica Polonica*, 12, 267-345.
- Karczewska, J., 1976, Megaspores of the Turma zonales from the Carboniferous of Poland. Part II – Reconsideration of the genus *Triangulatisporites*. *Acta Palaeontologica Polonica*, 21, 333-363.
- Kearsey, T. I., Bennett, C. E., Millward, D., Davies, S. J., Gowing, C. J. B., Kemp, S. J., Leng, M. J., Marshall, J. E. A. & Browne, M. A. E., 2016, The terrestrial landscapes of tetrapod evolution in earliest Carboniferous seasonal wetlands of SE Scotland. *Palaeogeography, Palaeoclimatology, Palaeoecology*, 457, 52–69.
- Kedo, G. I., 1957, Spores from the supra-salt Devonian deposits of the Pripyat Basin and their stratigraphic significance. *Rep. Palaeont. Strat. Byelorussian SSR*, 2, 3-43 [in Russian]
- Kedo, G. I., 1963, Spores of the Tournaisian stage of the Pripyat Basin and their stratigraphic significance. *Rep. Palaeont. Strat. Byelorussian*, 4, 3-121 [in Russian]
- Kedo, G. I., 1966, Spores of Tournaisian Stage of Pripyat Depression and their stratigraphical value [in Russian], *Paleontologiya i Stratigrafiya BSSR*, 4, 3-121.
- Kedo, G. I., 1974, New spore forms from the Upper Devonian of the Pripyat Depression. *In*: Golubtsov, W. K. & Manjkin, S. S. (Eds.), Paleozoic spores of Byelorussia (Pripyat Valley), 3-72 [in Russian].
- Keegan, J. B. & Penney, S. R., 1978, Lower Carboniferous miospore assemblages from the Portlaw area, County Wexford, Ireland. *Pollen et Spores*, 20, 569-581.

- Keegan, J. B., 1977, Late Devonian and Early Carboniferous miospores from the Galley Head – Leap Harbour region of southwest Ireland. *Pollen et Spores*, 19, 545-573.
- Kemp, E. M. & Playford, G. *In*: Playford, G., 1971, Lower Carboniferous spores from the Bonaparte Gulf Basin, Western Australia and Northern Territory, Commonwealth of Australia, Department of National Development, Bureau of Mineral Resources. *Geology and Geophysics*, Bulletin 115, 1-70.
- Klaus, W., 1960, Sporen der Karnischen Stufe der ostalpinen Trias. *Jb. Geol.*, 5, 107-183.
- Knighton, D., 1998, Fluvial forms and processes: a new perspective. Arnold, London. 383 pp.
- Knox, E. M., 1948, The microspores in coals of the Limestone Coal Group in Scotland. *Trans. Instn. Miner. Engrs., Lond.*, 101, 98-112.
- Knox, E. M., 1950, The Spores of *Lycopodium*, *Phylloglossum*, *Selaginella* and *Isoetes* and their value in the study of microfossils of Palaeozoic age. *Transactions and Proceedings of the Botanical Society of Edinburgh*, 35, 209-357.
- Kosanke, R. M., 1950, Pennsylvanian spores of Illinois and their use in correlation, State of Illinois, *State Geological Survey Bulletin* No. 74, 1-128.
- Kraus, M. J., 1999, Paleosols in clastic sedimentary rocks: their geologic applications. *Earth Science Reviews*, 47, 41-70.
- Labandeira, C. C., 2005, Invasion of the continents: cyanobacterial crusts to tree-inhabiting arthropods. *Trends Ecol. Evol.*, 20, 253–62.
- Lakin, J. A., Marshall, J. E. A., Troth, I. & Harding, I. C., 2016, Greenhouse to icehouse: A biogeostratigraphic review of latest Devonian-Mississippian glaciations and their global effects. *Geological Society, London, Special Publications*, 423, 439-464.
- Lang, W. H., 1925, Contributions to the Study of the Old Red Sandstone Flora of Scotland: I. On Plant-remains from the Fish-beds of Cromarty: II. On a Sporangium-bearing Branch-system from the Stromness Beds. Robert Grant & Son.
- Lanzoni, E. & Magloire, L., 1969, Associations palynologiques et leurs applications stratigraphiques dans le Dévonien supérieur et Carbonifère inférieur duk

- Grand Erg Occidentale (Sahara algérien). *Revue de l'Institut Français du Pétrole*, 24, 441-469.
- Laveine, J-P., 1965, Contribution à l'étude des microspores de différents niveaux du Westphalien C inférieur. Correlations palynologiques entre les groupes d'Auchel-Bruay et de Bethune-Noeux. *Ann. Soc. Géol. Nord*, 85, 129-153.
- Lebedev, O. A. & Coates, M. I., 1995, The postcranial skeleton of the Devonian tetrapod *Tulerpeton curtum* Lebedev. *Zool. J. Linn. Soc.*, 114, 307-48.
- Leeder, M. R., 1974, Lower Border Group (Tournaisian) fluviodeltaic sedimentation at the palaeogeography of the Northumberland Basin. *Proceedings of the Yorkshire Geological Society*, 40, 129-180.
- Leeder, M. R., 1982, Upper Palaeozoic basins of the British Isles: Caledonide inheritance versus Hercynian plate margin processes. *Journal of the Geological Society of London*, 139, 481-494.
- Leeder, M. R., 1988, Recent developments in Carboniferous geology: a critical review with implications for the British Isles and north-west Europe. *Proceedings of the Geologists' Association*, 99, 70-100.
- Leeder, M. R., 1992, Dinantian. In: *Geology of England and Wales*, Duff, P. M. D. & Smith, A. J. (Eds.), London: The Geological Society, 207-238.
- Lele, K. M. & Streel, M., 1969, Middle Devonian (Givetian) plant microfossils from Goé (Belgium). *Annales de la Société géologique de Belgique*, 92, 89-121.
- Leschik, G., 1956, Sporen aus dem Salzton des Zechsteins von Neuhoof (bei Fulda). *Palaeontographica*, 100, 122-142.
- Lindström, S., 2003, Carboniferous palynology of the Loppa High, Barents Sea, Norway. *Norwegian Journal of Geology*, 83, 333-349.
- Loboziak, S. In: Higgs, K., Avkhimovitch, V. I., Loboziak, S., Maziane-Serraj, N., Stempien-Salek, M. & Streel, M., 2000, Systematic study and stratigraphic correlation of the *Grandispora* complex in the Famennian of northwest and eastern Europe. *Review of Palaeobotany and Palynology*, 112, 207-228.
- Long, A. G., 1960a, On the structure of *Calymmatotheca kidstonii* Calder (emended) and *Genomosperma latens* gen. et sp. nov. from the Calciferous Sandstone Series of Berwickshire. *Trans R. Soc. Edinburgh*, 64, 29-44.
- Long, A. G., 1960b, On the Structure of *Samaropsis scotica* Calder (emended) and *Eurystoma angulare* gen. et sp. nov., Petrified Seeds from the

- Calciferous Sandstone Series of Berwickshire. *Trans. R. Soc. Edinburgh*, 64, 262-280.
- Long, A. G., 1960c, *Stamnostoma huttonense* gen. et sp. nov. – A Pteridosperm seed and cupule from the Calciferous Sandstone Series of Berwickshire. *Trans. R. Soc. Edinburgh*, 64, 201-215.
- Loose, F. In: Potonié, R. O., Ibrahim, A. & Loose, F., 1932, Sporenformen aus den Flözen Ägir und Bismarck des Ruhrgebietes. *Neues Jahrbuch Mineralogie Geologie und Paläontologie*, 67, 438-54 [in German].
- Loose, F., 1934, Sporenformen aus dem Flöz Bismarck des Ruhrgebietes. *Inst. Paläobot. u. Petrog. d. Brennsteine Arb.*, 4, 127-164.
- Lopes, G. & Mangerud, G., 2017, Palaeobiology collection: Palynological study. Department of Earth Science, University of Bergen report, 44 pp.
- Lopes, G., Mangerud, G., Clayton, G. & Mørk, A., 2016, New insights on East Finnmark Platform palynostratigraphy and palaeogeography – A study of three shallow cores from a Mississippian succession in the Barents Sea, Norway. *Palaeogeog., Palaeoclimat., Palaeoecol.*, 450, 60-76.
- Love, L. G., 1960, Assemblages of small spores from the Lower Oil-Shale group of Scotland. *Proc. Roy. Soc. Edinb.*, 67, 99-126.
- Luber, A. A. & Waltz, I. E., 1938, Classification and stratigraphical value of spores of some Carboniferous coal deposits in the USSR. *Trav. Inst. Géol, URSS*, 105, 1-45 [in Russian].
- Luber, A. A. In: Luber, A. A. & Waltz, I. E., 1938, Classification and stratigraphical value of spores of some Carboniferous coal deposits in the USSR. *Trav. Inst. Géol, URSS*, 105, 1-45 [in Russian].
- Luber, A. A. In: Pokrovskaya, I. M., 1966, Methods of paleopollen studies. *Paleopollinology*, pp. 29-60. Nedra Leningrad.
- Luber, A. A., 1955, Atlas of the spore and pollen grains of the Palaeozoic deposits of Kazakhstan. *Akademiya Nauk Kazakhskoi SSR*, Alma-Ata, 1-125.
- Lumsden, G. I., Tulloch, W., Howells, M. F. & Davies, A., 1967, The geology of the neighbourhood of Langholm. *Memoir of the Geological Survey of Great Britain*, Sheet 11 (Scotland), London HMSO.
- MacNaughton, R. B., Dalrymple, R. W. & Narbonne, G. M., 1997, Early Cambrian braid-delta deposits, MacKenzie Mountains, north-western Canada. *Sedimentology*, 44, 587–609.

- Mahdi, S. A. & Butterworth, M. A., 1994, Palynology of the Dinantian Lower Border Group of the Solway Basin. *Proceedings of the Yorkshire Geological Society*, 50, 157-171.
- Mahdi, S. A. & Butterworth, M. A., 1994, Palynology of the Dinantian Lower Border Group of the Solway Basin. *Proceedings of the Yorkshire Geological Society*, 50, 157-171.
- Marshall, A. E. & Williams, J. E., 1971, Palynology of the Yoredale 'Series' in the Roman Wall District of Western Northumberland, Northern England. *Compte rendu 6e congres intern. Strat. Geol. Carbonif.*, Sheffield 1967, 3, 1147-1158.
- Marshall, J. E. A. & Allen, K. C., 1982, Devonian miospore assemblages from Fair Isle, Shetland. *Palaeontology*, 25, 277-312.
- Marshall, J. E. A. & Fletcher, 2002, Middle Devonian (Eifelian) spores from a fluvial dominated lake margin in the Orcadian Basin, Scotland. *Rev. Palaeobot. and Palynol.*, 118, 195-209.
- Marshall, J. E. A., 1985, *Insculptospora*, a new genus of Devonian camerate spore with a sculptured intexine. *Pollen et Spores*, 27, 453-470.
- Marshall, J. E. A., 1995, A simple cost-effective infra-red microscope for palynology. *Journal of Micropalaeontology*, 14, 106.
- Marshall, J. E. A., 1996, *Rhabdosporites langii*, *Geminospora lemurata* and *Contagisporites optivus*: an origin for heterospory within the Progymnosperms. *Rev. Palaeobot. and Palynol.*, 93, 159-189.
- Marshall, J. E. A., Reeves, E. J., Bennett, C. E., Davies, S. J., Kearsey, T. I., Millward, D., Smithson, T. R. & Brown, M. A. E., 2019, Reinterpreting the age of the uppermost 'Old Red Sandstone' and Early Carboniferous in Scotland. *Earth and Environmental Science Transactions of the Royal Society of Edinburgh*, 1-14 (refer to Appendix 19).
- Marshall, J. E. A., Rogers, D. A. & Whiteley, M. J., 1996, Devonian marine incursions into the Orcadian Basin, Scotland. *J. Geol. Soc., London*, 153, 451-466.
- Maziane, N., Higgs, K. T. & Streel, M., 1999, Revision of the late Famennian miospore zonation scheme in eastern Belgium. *J. Micropalaeo.*, 18, 17-25.
- McAllister, J. A., 1989, Dakota Formation tracks from Kansas: implications for the recognition of tetrapod subaqueous traces. *In*: Gillette, D. D. & Lockley, M. G.

- (Eds.), *Dinosaur Tracks and Traces*. Cambridge University Press, pp. 343-348.
- McElwain, J. C. & Punyasena, S. W., 2007, Mass extinction events and the plant fossil record. *Trends in Ecology and Evolution*, 22, 548-557.
- McGregor, D. C. & Camfield, M., 1982, Middle Devonian miospores from the Cape de Bray, Weatherall, and Hecla Bay Formations of Northeastern Melville Island, Canadian Arctic. *Geological Survey of Canada, Bulletin*, 348, 1-105.
- McGregor, D. C. & Owens, B., 1966, Illustrations of Canadian fossils: Devonian spores of eastern and northern Canada. *Geological Survey of Canada, Paper* 66-30, 1-66.
- McGregor, D. C., 1960, Devonian spores from Melville Island Canadian Arctic Archipelago. *Palaeontology*, 3, 26-44.
- McGregor, D. C., 1973, Lower and Middle Devonian spores of Eastern Gaspé, Canada. I. Systematics. *Palaeontographica B*, 142, 1-77.
- McLean, D. & Neves, R., 2003, A new genus of monolete land plant spores from the Ballagan Formation (Tournaisian, Early Carboniferous) of Scotland. *Review of Palaeobotany and Palynology*, 126, 153-162.
- McNestry, A., 1988, The Palynostratigraphy of two uppermost Devonian-Lower Carboniferous borehole sections in South Wales. *Review of Palaeobotany and Palynology*, 56, 69-87.
- Melo, J. H. G. & Loboziak, S., 2000, Viséan miospore biostratigraphy and correlation of the Poti Formation (Parnaba Basin, northern Brazil). *Rev. Palaeobot. and Palynol.*, 112, 147-165.
- Melo, J. H. G. & Loboziak, S., 2003, Devonian-Early Carboniferous miospore biostratigraphy of the Amazon Basin, northern Brazil. *Review of Palaeobotany and Palynology*, 124, 131-202.
- Melo, J. H. G. & Playford, G., 2012, Miospore palynology and biostratigraphy of Mississippian strata of the Amazonas Basin, Northern Brazil (Part Two), *AASP Contributions Series No. 47*, 93-201.
- Melvin, J., 1993, Evolving fluvial style in the Kekiktuk Formation (Mississippian), Endicott Field Area, Alaska: Base level response to contemporaneous tectonism. *AAPG Bull.* 77, 1723-1744.

- Menéndez, C. A. & C. L. Azcuy, 1972, *Ancistrospora* A new genus of miospore from the Carboniferous of Argentina. *Revista Española de Micropalaeontologia*, 4, 157-168.
- Meyer-Berthaud, B. & Decombeix, A.-L., 2009, L'évolution des premiers arbres: les strategies dévoniennes. *Comptes Rendus Palevol*, 8, 155–165.
- Meyer-Berthaud, B., Soria, A. & Decombeix, A-L., 2010, The land plant cover in the Devonian: a reassessment of the evolution of the tree habit, *Geological Society Special Publications*, 339, 59-70.
- Millward, D., Davies, S. J., Brand, P. J., Browne, M. A. E., Bennett, C. E., Kearsey, T. I., Sherwin, J. E. & Marshall, J. E. A., 2018, Palaeogeography of tropical seasonal coastal wetlands in northern Britain during the early Mississippian Romer's Gap. *Earth and Environmental Science Trans. Roy. Soc. Edin.*, 1-22.
- Millward, D., Kearsey, T. & Browne, M. A. E., 2013, Norham West Mains Farm Borehole: operations report. British Geological Survey, Geology and Regional Geophysics Programme Internal Report IR/13/033.
- Mortimer, M. G. & Chaloner, W. G., 1972, The palynology of concealed Devonian rocks of Southern England. *Bull. Geol. Surv. G. B.*, 39, 1-56.
- Mortimer, M. G., Chaloner, W. G. & Llewellyn, P. G., 1978, Lower Carboniferous (Tournaisian) Miospores and Megaspores from Breedon Cloud Quarry, Leicestershire. *The Mercian Geologist*, 3, 375-385.
- Myrow, P. M., Ramezani, J., Hanson, A. E., Bowring, S. A., Racki, G. & Rakocinski, M., 2014, High precision U-Pb age and duration of the latest Devonian (Famennian) Hangenberg event and its implications. *Terra Nova*, 26, 222-229.
- Nanson, G. C. & Knighton, A. D., 1996, Anabranching rivers: Their cause, character and classification. *Earth Surf. Process. Landforms*, 21, 217-239.
- Naumova, S. N. In: Kedo, G. I., 1963, Spores of the Tournaisian stage of the Pripyat Basin and their stratigraphic significance. *Rep. Palaeont. Strat. Byelorussian*, 4, 3-121 [in Russian].
- Naumova, S. N., 1937, Spores and pollen of USSR coals, Tr. 17 Session Intern. geol. Congress, Goskomizdat. [in Russian].
- Naumova, S. N., 1939, Spores and pollen of the coals of the USSR. *Transactions of the 17th International Geological Congress Moscow (1937)*, 1, 353-364.

- Naumova, S. N., 1941, Coal of 'Second Baku', *Sov. Geol.*, 11, 82-89 [in Russian].
- Naumova, S. N., 1949, *Izv. Akad. Nauk SSSR, ser. Geol.*, 4.
- Naumova, S. N., 1953, Spore-pollen complexes of the Upper Devonian of the Russian Platform and their stratigraphic significance. *Transactions of the Institute of Geological Sciences, Academy of Science, SSSR*, 143, (Geol. Ser. 60), 1-204 [in Russian].
- Naumova, S. N., 1966. *In: McGregor, D. C. & Owens, B., Illustrations of Canadian fossils: Devonian spores of eastern and northern Canada. Geological Survey of Canada, Paper 66-30*, 1-66.
- Nelson, J. S., 2006, *Fishes of the World*, Wiley, Hoboken, N. J., 4th Ed.
- Neves, R. & Dolby, G., 1967, An assemblage of miospores from the Portishead beds (Upper Old Red Sandstone) of the Mendip Hills, England. *Pollen et Spores*, 9, 607-614.
- Neves, R. & Ioannides N., 1974, Palynology of the Lower Carboniferous (Dinantian) of the Spilmersford Borehole East Lothian Scotland. *Bulletin of the Geological Survey of Great Britain*, No. 45, pp. 73-97.
- Neves, R. & Owens, B., 1966, Some Namurian camerate miospores from the English Pennines. *Pollen et Spores*, 8, 337-360.
- Neves, R. & Playford, G., 1961, 'The dispersed spore' genus *Knoxisporites* Potonié and Kremp, 1954. *C. r. Commission Internationale de Microflore du Paléozoïque*, Krefeld, pp. 9.
- Neves, R., 1958, Upper Carboniferous plant spores assemblages from the *Gastrioceras subcrenatus* Horizon. North Staffordshire. *Geol. Mag.*, 95, 1-19.
- Neves, R., 1961, Namurian plant spores from the southern Pennines, England. *Palaeontology*, 4, 247-279.
- Neves, R., Gueinn, K. J., Clayton, G., Ioannides, N. & Neville R. S. W., 1973, Palynological correlations within the Lower Carboniferous of Scotland and northern England. *Trans. R. Soc. Edinburgh*, 69, 23-70.
- Neville, R. S. W. *In: Clayton, G. & Turnau, E., 1990, Correlation of the Tournaisian miospore zonations of Poland and the British Isles. Ann. Soc. Geol. Polon.*, 60: 45-58.
- Neville, R. S. W. *In: Neves, R., Gueinn, K. J., Clayton, G., Ioannides, N. S., Neville, R. S. W. & Kruszkowska, K., 1973, Palynological correlations within the Lower Carboniferous of Scotland and Northern England. The Royal*

Society of Edinburgh Transactions, 69, 23-70.

Neville, R. S. W. In: Neves, R., Gueinn, K. J., Clayton, G., Ioannides, N. S.,
Neville, R. S. W. & Kruszkowska, K., 1973, Palynological correlations within
the Lower Carboniferous of Scotland and Northern England. *The Royal
Society of Edinburgh Transactions*, 69, 23-70.

Neville, R. S. W., 1968, Ranges of selected spores in the upper Viséan of the East
Fife Coast section between St. Monance and Pittenweem. *Pollen et Spores*,
10, 431-462.

Oschurkova, M. V., 2003, Morphology, classification and description of form
genera of Late Paleozoic miospores. *Ministry of Natural Resources of the
Russian Federation*. VSEGEI Press, 378 pp. [in Russian].

Owens, B., 1971, Miospores from the Middle and early Upper Devonian rocks of
the Western Queen Elizabeth Island, Arctic Archipelago. *Pap. Geol. Surv.
Can.*, 70-38, 1-157.

Owens, B., 1983, *Bascaudaspora* gen. nov., a new reticulate miospore genus from
the Namurian of northern England. *Rep. inst. Geol. Sci.*, No. 83/10, 45-49.

Owens, B., Gueinn, K. J. & Cameron, I. B., 1977, A Tournaisian miospore
assemblage from the Altagoan Formation (Upper Calciferous Sandstone),
Draperstown, Northern Ireland. *Pollen et Spores*, 19, 313-324.

Owens, B., McLean, D., Simpson, K. R. M., Shell, P. M. J. & Robinson, R., 2010,
Reappraisal of the Mississippian palynostratigraphy of the East Fife coast,
Scotland, United Kingdom. *Palynology*, 29, 23-47.

Pacton, M., Gorin, G. E. & Vasconcelos, C., 2011, Amorphous organic matter –
Experimental data on formation and the role of microbes. *Review of
Palaeobotany and Palynology*, 166, 253-267.

Pant, D. D. & Srivastava, G. K., 1962, Structural studies on Lower Gondwana
megaspores part 2. Specimens from Brazil and Mhukuni coalfield,
Tanganyika. *Palaeontographica B*, 111, 96-111.

Paproth, E. & Streel, M., 1984, The Devonian-Carboniferous boundary. *Cour.
Forsch. Inst. Senckenberg*, 67, 231-239.

Paproth, E., Feist, R. & Flajs, G., 1991, Decision on the Devonian-Carboniferous
boundary stratotype. *Episodes*, 14, 331-335.

- Paterson, I. B. & Hall, I. H. S., 1986, Lithostratigraphy of the late Devonian and early Carboniferous rocks in the Midland Valley of Scotland. *Report of the British Geological Survey*.
- Peel, M. C., Finlayson, B. L. & McMahon, T. A., 2007, Updated world map of the Köppen-Geiger climate classification. *Hydrology and Earth System Sciences Discussions, European Geosciences Union*, 11, 1633-1644.
- Pendleton, J. L. & Wellman, C. H., 2012, Pennsylvanian (mid-Bolsovian to Asturian) megaspores and large pollen of the Bristol Coalfield, UK. *Journal of Micropalaeontology*, 32, 87-106.
- Pérez Loinaze, V., 2008, Systematic palynological study of the Cortaderas Formation, (Mississippian) Río Blanco Basin, Argentina. Part 2. *Ameghiniana (Rev. Asoc. Paleontol. Argent.)*, 45, 421-441.
- Pérez Loinaze, V., 2010, A Mississippian miospore biozone for Southern Gondwana. *Palynology*, 31, 101-117.
- Petrou, A. & Zapitis, C., 2016, Fishes. *In: An introduction to the wildlife of Cyprus*, Sparrow, D. J. & John, E. (Eds.).
- Phillips, W. E. A. & Clayton, G., 1980, The Dinantian clastic succession of Clare Island, County Mayo. *Journal of Earth Science Royal Dublin Society*, 2, 115-135.
- Piérart, P., 1958, L'utilisation des mégaspores en stratigraphie houillère. *Bull. Soc. Belge Géol. Paléont. Hydrol.*, 67, 50-78.
- Playford, G. & McGregor, D. C., 1993, Miospores and organic-walled microphytoplankton of Devonian-Carboniferous boundary beds (Bakken Formation), Southern Saskatchewan: A systematic and stratigraphic appraisal. *Geological survey of Canada, Bulletin 445*
- Playford, G. & Melo, J. H. G., 2012, Miospore palynology and biostratigraphy of Mississippian strata of the Amazonas Basin, Northern Brazil, Part One. *AASP Contributions Series*, 47, 3-89.
- Playford, G. & Satterthwait, D. F., 1985, Lower Carboniferous (Viséan) spores of the Bonaparte Gulf Basin, Northwestern Australia: Part One. *Palaeontographica B*, 195, 129-152.
- Playford, G., 1962, Lower Carboniferous microfloras of Spitsbergen. *Palaeontology*, 5, 550-618.

- Playford, G., 1963, Lower Carboniferous microfloras of Spitsbergen – Part Two. *Palaeontology*, 5, 619-678.
- Playford, G., 1963, Miospores from the Mississippian Horton Group, Eastern Canada. *Geol. Surv. Canada, Bull.* 107, 1-47.
- Playford, G., 1971, Lower Carboniferous spores from the Bonaparte Gulf Basin, Western Australia and Northern Territory, Commonwealth of Australia, Department of National Development, Bureau of Mineral Resources. *Geology and Geophysics*, Bulletin 115, 1-70.
- Playford, G., 1972, Trilete spores of *Umbonatisporites* in the Lower Carboniferous of northwestern Australia. *Geol. Palaontol. Abh.*, 141, 301-315.
- Playford, G., 1976, Plant microfossils from the Upper Devonian and Lower Carboniferous of the Canning Basin, Western Australia. *Palaeontographica B*, 158, 1-71.
- Playford, G., 1978, Lower Carboniferous spores from the Ducabrook Formation, Drummond Basin, Queensland. *Palaeontographica B*, 167, 105-160.
- Playford, G., 1983, The Devonian miospore genus *Geminospora* Balme 1962: a reappraisal based upon topotypic *G. lemurata* (type species). *Mem. Ass. Australis. Palaeontols*, 1, 311-325.
- Playford, G., 1990, Proterozoic and Paleozoic Palynology of Antarctica: A review. *In*: Taylor, T. N. & Taylor, E. L. (Eds.), *Antarctic Paleobiology*, Springer, New York, pp. 51-70.
- Potonié, R. & Kremp, G. *In*: Horst, U., 1955, "Die Sporae dispersae des Namurs von Westoberschlesien und Mährisch-Ostrau". *Palaeontographica, Abt. B*, 98, 137-236.
- Potonié, R. & Kremp, G., 1954, Die Gattungen der paläozoischen Sporae dispersae und ihre Stratigraphie. *Geol. Jb.*, 69, 111-194.
- Potonié, R. & Kremp, G., 1955, Die Sporae dispersae des Ruhrkarbons, ihre Morphographie und Stratigraphie mit Ausblicken auf Arten anderer Gebiete und Zeitabschnitte, Teil I. *Palaeontographica B*, 98, 1-136.
- Potonié, R. & Kremp, G., 1956, Die Sporae dispersae des Ruhrkarbons, ihre Morphographie und Stratigraphie mit Ausblicken auf Arten anderer Gebiete und Zeitabschnitte, Teil II. *Palaeontographica B*, 99.

- Potonié, R., 1958, Synopsis der Gattungen der Sporae dispersae. Teil II. Sporites (Nachträge), *Saccites*, *Aletes*, *Praecolpates*, *Polyplicates*, *Monocolpates*. *Beih. Geol. Jb.*, 31, 1-114.
- Powell, C. McA., & Veevers, J. J., 1987, Namurian uplift in Australia and South America triggered the main Gondwanan glaciation. *Nature*, 326, 177–179.
- Prestianni, C., Sautois, M. & Denayer, J., 2016, Disrupted continental environments around the Devonian-Carboniferous Boundary: introduction of the *tener* event. *Geologica Belgica*, 19, 135-145.
- Rainbird, R. H., 1992, Anatomy of a large-scale braid-plain quartzarenite from the Neoproterozoic Shaler Group, Victoria Island, Northwest Territories, Canada. *Canadian Journal of Earth Sciences*, 29, 2537–2550.
- Raup, D. M. & Sepkoski, J. J., 1982, Mass extinctions in the marine fossil record. *Science*, 215, 1501-1503.
- Raup, D. M., 1994, The role of extinction in evolution. *Proc. Natl. Acad. Sci. USA*, 91, 6758-6763.
- Raven, J. A. & Edwards, D., 2001, Roots: evolutionary origins and biogeochemical significance. *Journal of Experimental Botany*, 52, 381–401.
- Ravn, R. L., 1986, Palynostratigraphy of the Lower and Middle Pennsylvanian coals of Iowa, *Iowa Geological Survey Technical Paper No. 7*, 1-245
- Ravn, R. L., 1991, Miospores of the Kekiktuk Formation (Lower Carboniferous) Endicott Field Area, Alaska North Slope, *AASP Contribution Series Number 27*, 1-115.
- Read, W. A. & Johnson, S. R. H., 1967, The sedimentology of sandstone formations within the Upper Old Red Sandstone and lowest Calcareous Sandstone measures west of Stirling, Scotland. *Scottish Journal of Geology*, 3, 242-267.
- Read, W. A., 1988, Controls on Silesian sedimentation in the Midland Valley of Scotland, 22-241. *In: Sedimentation in a synorogenic basin complex: the Upper Carboniferous of northwest Europe*, Besly, B. M. & Kelling, G. (Eds.), Blackie: Glasgow & London.
- Reichow, M. K., Pringle, M. S., Al'Mukhamedov, A. I., Allen, M. B., Andreichev, V. L., Buslov, M. M., Davies, C. E., Fedoseev, G. S., Fitton, J. G., Inger, S., Medvedev, A. Ya., Mitchell, C., Puchkov, V. N., Safonova, I. Yu., Scott, R. A. & Saunders, A. D., 2009, The timing and extent of the eruption of the

- Siberian Traps large igneous province: Implications for the end-Permian environmental crisis. *Earth & Planetary Science Letters*, 277, 9-20.
- Retallack, G. J. & Dilcher, D. L., 1988, Reconstruction of selected seed ferns. *Ann. Missouri Bot. Gard.*, 75, 1010-1057.
- Retallack, G. J., 1993, Classification of palaeosols: discussion. *Geological Society of America, Bulletin*, 105, 383-400.
- Retallack, G. J., 1998, Fossil soils and completeness of the rock and fossil record. *In: Donovan, S. K., Paul, C. R. R. (Eds.), The adequacy of the fossil record*, Wiley & Sons Ltd.
- Richardson, J. B., 1960, Spores from the Middle Old Red Sandstone of Cromarty, Scotland. *Palaeontology*, 3, 45-63.
- Richardson, J. B., 1962, Spores with bifurcate processes from the Middle Old Red Sandstone of Scotland. *Palaeontology*, 5, 171-194.
- Richardson, J. B., 1965, Middle Old Red Sandstone spore assemblages from the Orcadian Basin North-East Scotland. *Palaeontology*, 7, 559-605.
- Robinson, J. M. & Berner, R. A., 1991, Land plants and weathering. *Science*, 252, 860.
- Rogers, D. A., 1990, Probable tetrapod tracks rediscovered in the Devonian of Scotland. *J. Geol. Soc. London*, 147, 746-748.
- Romer, A. S., 1956, The early evolution of land vertebrates. *Proceedings of the American Philosophical Society*, 100, 151-167.
- Rowe, N. & Speck, T., 2004. *In: The Evolution of Plant Physiology*, Helmsley, A. R. & Poole, I. (Eds.), Elsevier, pp. 297-326.
- Ruta, M. & Clack, J. A., 2006, A review of *Silvanerpeton miripedes*, a stem amniote from the Lower Carboniferous of East Kirkton, West Lothian, Scotland. *Trans. Roy. Soc. Edinb.: Earth Sci.*, 97, 31-63.
- Sabry, H. & Neves, R. *In: Turnau, E., 1978, Spore Zonation of Uppermost Devonian and Lower Carboniferous Deposits of Western Pomerania. Mededlingen Rijks Geologische Dienst*, 30, 1-35.
- Sabry, H. & Neves, R., 1971, Palynological evidence concerning the unconformable Carboniferous basal measures in the Sanquhar Coalfield, Dumfriesshire, Scotland. *C. R. 6th Cong. Avanc. Edut. Stratigr. Geol. Carb.* (Sheffield 1967), 4, 1441-1458.

- Sahney, S. & Benton, M. J., 2008, Recovery from the most profound mass extinction of all time. *Proc. Biol. Sci.*, 275, 759–765.
- Sallan, L. & Galimberti, A. K., 2015, Body-size reduction in vertebrates following the end-Devonian mass extinction. *Science*, 350, 812-815.
- Sallan, L. C. & Coates, M. I., 2010, End-Devonian extinction and a bottleneck in the early evolution of modern jawed vertebrates, *PNAS*, 107, 10131-10135.
- Sallan, L. C. & Friedman, M., 2012, Five hundred million years of extinction and recovery: A Phanerozoic survey of large-scale diversity patterns in fishes. *Palaeontology*, 55, 707-742.
- Sallan, L. C., Kammer, T. W., Ausich, W. I. & Cook, L. A., 2011, Persistent predator-prey dynamics revealed by mass extinction. *PNAS*, 108, 8335-8338.
- Sandberg, C. A. & Ziegler, W., 1996, Devonian conodont biochronology in geologic time calibration. *Senckenbergiana lethaea*, 76, 259-265.
- Sarjeant, W. A. S., 1974, A history and bibliography of the study of fossil vertebrate footprints in the British Isles. *Palaeogeography, Palaeoclimatology, Palaeoecology*, 16, 265-378.
- Schopf, J. M. *In*: Schopf, J. M., Wilson, L. R. & Bentall, R., 1944, An annotated synopsis of Paleozoic fossil spores and the definition of generic groups. *Report on Investigation of Illinois State Geological Survey*, 91, 1-66.
- Schopf, J. M., 1938, Spores from the Herrin (No. 6) coal bed in Illinois, State of Illinois, Department of Registration and Education, Division of the State Geological Survey, Urbana, Illinois, pp. 5-73.
- Schopf, J. M., Wilson, L. R. & Bentall, R., 1944, An annotated synopsis of Paleozoic fossil spores and the definition of generic groups. *Report on Investigation of Illinois State Geological Survey*, 91, 1-66.
- Schulte, P., Laia Alegret, L., Arenillas, I., Arz, J. A., Barton, P. J., Bown, P. R., Bralower, T. J., Christeson, G. L., Claeys, P., Cockell, C. S., Collins, G. S., Deutsch, A., Goldin, T. J., Goto, K., Grajales-Nishimura, J. M., Grieve, R. A. F., Gulick, S. P. S., Johnson, K. R., Kiessling, W., Koeberl, C., Kring, D. A., MacLeod, K. G., Matsui, T., Melosh, J., Montanari, A., Morgan, J. V., Neal, C. R., Nichols, D. J., Norris, R. D., Pierazzo, E., Ravizza, G., Rebolledo-Vieyra, M., Reimold, W. U., Robin, E., Salge, T., Speijer, R. P., Sweet, A. R., Urrutia-Fucugauchi, J., Vajda, V., Whalen, M. T. and Willumsen, P. S., 2010, The

- Chicxulub asteroid impact and mass extinction at the Cretaceous-Paleogene Boundary. *Science*, 327, 1214-1218.
- Schumm, S. A., 1968, Speculations concerning paleohydraulic controls of terrestrial sedimentation. *Geological Society of America Bulletin*, 79, 1573–1588.
- Scotese, C. R. & McKerrow, W. S., 1990, Revised world maps and introduction. *In*: McKerrow, W. S. & Scotese, C. R. (Eds.), *Palaeozoic palaeogeography and biogeography. Geol. Soc. Mem.*, 12, 1-21.
- Scott, A. C. & Galtier, J. G., 1985, Distribution and ecology of early ferns. *Proc. Roy. Soc. Edin.*, 868, 141-149.
- Scott, A. C., Galtier, J. & Clayton, G., 1984, Distribution of anatomically preserved floras in the Lower Carboniferous in Western Europe. *Transactions of the Royal Society of Edinburgh*, 75, 311–340.
- Scott, R., 1908, On *Bensonites fusiformis* sp. nov. a fossil associated with *Stauropteris burntislandica* and on the sporangia of the latter. *Ann. Bot., Lond.*, 22, 683-687.
- Scott, W. B., 1986, Nodular carbonates in the Lower Carboniferous, Cementstone Group of the Tweed embayment, Berwickshire: evidence for a former sulphate evaporate. *Scottish Journal of Geology*, 22, 325-345.
- Sepkoski, J. J., 2002, A compendium of fossil marine animal genera. *Bull. Am. Paleontol.*, 363, 1–560.
- Sheldon, N. D. & Tabor, N. J., 2009, Quantitative paleoenvironmental and paleoclimatic reconstruction using palaeosols. *Earth Science Reviews*, 95, 1-52.
- Shu, D., Vannier, J., Luo, H., Chen, L., Zhang, X. & Hu, S., 1999, Anatomy and lifestyle of Kunmingella (Arthropoda, Bradoriida) from the Chengjiang fossil Lagerstätte (lower Cambrian; southwest China). *Lethaia*, 32, 279-298.
- Shu, D-G., Conway Morris, S., Han, J., Zhang, Z.-F., Yasui, K., Janvier, P., Chen, L., Zhang, X.-L., Liu, J.-N., Li, Y. & Liu, H.-Q., 2003, Head and backbone of the early Cambrian vertebrate *Haikouichthys*. *Nature*, 421, 526–529.
- Shubin, N. H., Daeschler, E. B. & Coates, M. I., 2004, The early evolution of the tetrapod humerus. *Science*, 304, 90–93.

- Shubin, N. H., Daeschler, E. B. & Jenkins, F. A. Jr., 2006, The pectoral fin of *Tiktaalik roseae* and the origin of the tetrapod limb. *Nature Articles*, 440, 764-771.
- Shubin, N. H., Daeschler, E. B. & Jenkins, F. A. Jr., 2014, Pelvic girdle and fin of *Tiktaalik roseae*. *PNAS*, 111, 893-899.
- Silvestro, D., Cascales-Miñana, B., Bacon, C. D. & Antonelli, A., 2015, Revisiting the origin and diversification of vascular plants through a comprehensive Bayesian analysis of the fossil record. *New Phytologist*, 207, 425-436.
- Simakov, K. V., 1993, The dynamics and biochronological structure of the Hangenbergian bioevent. *Palaeogeography, Palaeoclimatology, Palaeoecology*, 104, 127-137.
- Sleeman, A. G., Reilly, T. A. & Higgs, K., 1978, Preliminary stratigraphy and palynology of five sections through the Old Head Sandstone and Kinsale Formations (Upper Devonian to Lower Carboniferous), on the west side of Cork Harbour. *Bull. geol. Surv. Ireland*, 2, 167-186.
- Smith, A. H. V. & Butterworth, M. A., 1967, Miospores in the coal seams of the Carboniferous of Great Britain, *Special papers in Palaeontology* No. 1., The Palaeontological Association, London, 309-311.
- Smith, A. H. V., 1971, Microfossiles organiques du Paleozoique. 4. Les spores. 2. Le genre *Verrucosisporites* par A. H. V. Smith. *Commission Internationale de Microflore du Paleozoique, Centre National de la Recherche Scientifique*, 35-87.
- Smith, D. L., 1962, Three fructifications from the Scottish Lower Carboniferous. *Palaeontology*, 5, 225-237.
- Smithson, T. R. & Panchen, A. L., 1990, The pelvic girdle and hind limb of *Crassigyrinus scoticus* (Lydekker) from the Scottish Carboniferous and the origin of the tetrapod pelvic skeleton. *Trans. R. Soc. Edinb. Earth Sci.*, 81, 31-44.
- Smithson, T. R. & Wood, S. P., 2009a, Bridging Romer's Gap: New tetrapods from the basal Carboniferous of the Scottish Borders. *Journal of Vertebrate Paleontology*, 29, 183A.
- Smithson, T. R. & Wood, S. P., 2009b, Closing Romer's Gap: New tetrapods and arthropods from the basal Carboniferous of the Scottish Borders. *Palaeontological Association Newsletter*, 72, 32-33.

- Smithson, T. R., Wood, S. P., Marshall, J. E. A. & Clack, J. A., 2012, Earliest Carboniferous tetrapod and arthropod faunas from Scotland populate Romer's Gap. *PNAS*, 109, 4532–37.
- Spinner, E., 1965, Westphalian D megaspores from the Forest of Dean Coalfield, England. *Palaeontology*, 8, 82-106.
- Spinner, E., 1969, Megaspore assemblages from Viséan deposits at Dunbar, East Lothian, Scotland. *Palaeontology*, 12, 441-458.
- Spinner, E., 1982, Further studies on the megaspore *Setispora* Butterworth & Spinner 1967. *Pollen et Spores*, 24, 301-313.
- Spinner, E., 1983, Some new sporomorphs from the Lower Carboniferous of NW England. *Pollen et Spores*, 15, 117-139.
- Spinner, E., 1984a, The occurrence and distribution of megaspores in the Drybrook Sandstone and associated measures in the Forest of Dean basin, Gloucestershire, England. *J. micropalaeontol.*, 3, 37-41.
- Spinner, E., 1984b, New evidence on the sporomorph genus *Carbaneuletes* Spinner 1983, from the Lower Carboniferous deposits of the Forest of Dean basin, Gloucestershire, England. *Pollen et Spores*, 26, 117-126.
- Stach, E., Mackowsky, M-Th., Teichmüller, Taylor, G. H., Chandra, D. & Teichmüller, R., 1982, Stach's Textbook of Coal Petrology, 3rd Ed., Gebrüder Borntraeger Berlin-Stuttgart, 535 pp.
- Staplin, F. L. & Jansonius, J., 1964, Elucidation of some Palaeozoic Densospores. *Palaeontographica B*, 114, 95-117.
- Staplin, F. L., 1960, Upper Mississippian Plant Spores from the Golata Formation, Alberta, Canada. *Palaeontographica B*, 1-40.
- Steemans, P., 2000, Miospore evolution from the Ordovician to the Silurian. *Review of Palaeobotany and Palynology*, 113, 189–196.
- Steemans, P., Le Hérisse, A., Melvin, J., Miller, M. A., Paris, F., Verniers, J. & Wellman, C. H., 2009, Origin and Radiation of the Earliest Vascular Land Plants. *Science*, 324, 353.
- Stein, W. E., Mannolini, F., Hernick, L. V., Landing, E. & Berry, C. M., 2007, Giant cladoxylopsid trees resolve the enigma of the Earth's earliest fossil stumps at Gilboa. *Nature*, 446, 904–907.

- Stephenson, M., Williams, M., Monaghan, A., Arkley, S. & Smith, R., 2002, Biostratigraphy and Palaeoenvironments of the Ballagan Formation (Lower Carboniferous) in Ayrshire. *Scottish Journal of Geology*, 38, 93-111.
- Sternberg, K. M. von, 1820, Versuch einer geognostischbotanischen Darstellung der Flora der Vorwelt 1, Fleischer, Leipzig.
- Stevens, L. G., Hilton, J., Rees, A. R., Rothwell, G. W. & Bateman, R. M., 2010, Systematics, phylogenetics and reproductive biology of *Flemingites arcuatus* sp. nov., an exceptionally preserved and partially reconstructed Carboniferous arborescent lycopsid. *Int. J. Plant Sci.*, 171, 783-808.
- Stössel, I., 1995, The discovery of a new Devonian tetrapod trackway in SW Ireland. *J. Geol. Soc. London*, 152, 407-413.
- Streel, M. In: Becker, G., Bless, M. J. M., Streel, M. & Thorez, J., 1974, Palynology and ostracod distribution in the Upper Devonian and basal Dinantian of Belgium and their dependence on sedimentary facies. *Meded. Rijks. Geol. Dienst.*, 25, 9-99.
- Streel, M., 1964, Une association due spores du Givétien Inférieur de la Vesdre, a Goé (Belgique). *Ann. Soc. Géologique de Belgique*, 87, 236-261.
- Streel, M., 1967, Association de spores du Dévonien inférieur belge et leur signification stratigraphique. *Ann. Soc. Géol. De Belgique*, 90, 11-54.
- Streel, M., 1986, Miospore contribution to the upper Famennian–Strunian event stratigraphy. *Ann. Soc. Géol. Belg.*, 109, 75–92.
- Streel, M., 2000, Global Famennian climates based on palynomorph quantitative analysis. In: Rodrigues, M. A. C. & Pereira, E. (Eds.), Ordovician – Devonian palynostratigraphy in western Gondwana: Update, Problems and Perspectives, pp. 77-103.
- Streel, M., Caputo, M. V., Loboziak, S. & Melo, J. H. G., 2000, Late Frasnian-Famennian climates based on palynomorph analyses and the question of the late Devonian glaciations. *Earth Science Reviews*, 52, 121-173.
- Sullivan, H. J. & Marshall, A. E., 1966, Viséan spores from Scotland. *Micropalaeontology*, 12, 265-285.
- Sullivan, H. J., 1964, Miospores from the Drybrook Sandstone and associated measures in the Forest of Dean basin, Gloucestershire. *Palaeontology*, 7, 351-392.

- Sullivan, H. J., 1964, Miospores from the Lower Limestone Shales (Tournaisian) of the Forest of Dean basin, Gloucestershire, Cinquième Congrès International de Stratigraphie et de Géologie due Carbonifère, Paris, 1963. *Compte rendu*, 3, 1249-1260.
- Sullivan, H. J., 1968, A Tournaisian spore flora from the Cementstone Group of Ayrshire, Scotland. *Palaeontology*, 11, 351-392.
- Sundberg, F. A., Bennington, J. B., Wizevich, M. C. & Bambach, R. K., 1990, Upper Carboniferous (Namurian) amphibian trackways from the Bluefield Formation, West Virginia, USA. *Ichnos*, 1, 111-124.
- Surange, K. R., 1952, The Morphology of *Stauropteris burntislandica* P. Bertrand and its Megasporangium *Bensonites fusiformis* R. Scott. *Philosophical Transactions of the Royal Society of London Series B Biological Sciences*, 237, 73-91.
- Szaniawski, H., 1996, Scolecodonts. In: Jansonius & McGregor, Palynology: Principles and applications I, pp. 337-354.
- Taugourdeau-Lantz, J., 1967, Spores nouvelles du Frasnien du Bas-Boulonnais (France). *Rev. Micropaléont.*, 10, 48-60.
- Taylor, T. N. & Millay, M. A., 1979, Pollination Biology and Reproduction in Early Seed Plants. *Review of Palaeobotany and Palynology*, 27, 329-355.
- Taylor, T. N., 1976, The Ultrastructure of *Schopfipollenites*: Orbicules and tapetal membranes. *American Journal of Botany*, 63, 857-862.
- Thiergart, F., 1938, Die Pollenflora der Niederlausitzer Braunkohle, besonders. In: Profil der Grube Marga bei Senftenberg. *Preuss. Geol. Landesanst., Jahrb*, Berlin, vol. 58.
- Thomson, P. W. & Pflug, H. D., 1953, Pollen und Sporen des Mitteleuropäischen Tertiärs. *Palaeontographica B*, 94, 1-138.
- Trapp, E., Kaufmann, B., Mezger, K., Korn, D. & Weyer, D., 2004, Numerical calibration of the Devonian-Carboniferous boundary: Two new U-Pb ID-TIMS single-zircon ages from Hasselbachtal (Sauerland, Germany). *Geology*, 32, 857-860.
- Turnau, E., 1975, Microflora of the Famennian and Tournaisian deposits from boreholes of northern Plant. *Acta Geologica Polonica*, 25, 505-528.

- Turnau, E., 1978, Spore Zonation of Uppermost Devonian and Lower Carboniferous Deposits of Western Pomerania. *Mededlingen Rijks Geologische Dienst*, 30, 1-35.
- Turnau, E., Avchimovitch, V. I., Byvcheva, T. V., Clayton, G., Higgs, K. T. & Owens, B., 1994, Taxonomy and stratigraphical distribution of *Verrucosisporites nitidus* Playford 1964 and related species. *Rev. Palaeobot. and Palynol.*, 81, 289-295.
- Turnau, E., Trzepierczyńska, A. & Protas, A., 2005, Palynostratigraphy of the Mississippian Łobżonka Formation of Western Pomerania (NW Poland). *Geological Quarterly*, 49, 93-98.
- Turner, N. & Owens, B., 1993, Palynological evidence for an early Namurian age of the Cornbrook Sandstone Formation, Clee Hill, Shropshire. *Proc. Yorks. Geol. Soc.*, 49, 189-196.
- Turner, N. & Spinner, E., 1988, A palynological study of the Lower Carboniferous strata (Dinantian), from Titterstone Clee, Shropshire, England. *Pollen et Spores*, 30, 429-459.
- Turner, N. & Spinner, E., 1990, Palynological evidence for the age of the Coal Measures of the Titterstone Clee Coalfield, Shropshire, England. *Proc. Yorks. Geol. Soc.*, 48, 81-98.
- Turner, N. & Spinner, E., 1993, A palynostratigraphic study of Namurian-Westphalian deltaic sequences of the southern central Pennine Basin, Derbyshire, England. *Rev. Palaeobot. and Palynol.*, 77, 23-43.
- Turner, N. & Spinner, E., 1996, Namurian (Arnsbergian/Chokierian) megaspore assemblages from northeast England. *Rev. Palaeobot. and Palynol.*, 94, 211-230.
- Utting, J. & Neves, R., 1970, Miospores from the Devonian-Carboniferous transition beds of the Avon gorge, Bristol, England. *Congr. Coll. Univ. Liege*, 55, 411-422.
- Utting, J., 1987, Palynology of the Lower Carboniferous Windsor Group and Windsor-Canso boundary beds of Nova Scotia and their equivalents in Quebec, New Brunswick and Newfoundland. *Geological Survey of Canada, Bulletin* 374, 1-93.

- Van der Zwan, C. J., 1979, Aspects of late Devonian and early Carboniferous palynology of Southern Ireland. I. The *Cyrtospora cristifer* morphon. *Review of Palaeobotany and Palynology*, 28, 1-20.
- Van der Zwan, C. J., 1980, Aspects of late Devonian and early Carboniferous palynology of southern Ireland. III. Palynology of Devonian-Carboniferous transition sequences with special reference to the Bantry Bay area, Co. Cork. *Review of Palaeobotany and Palynology*, 30, 165-286.
- Van der Zwan, C. J., Boulter, M. C. & Hubbard, R. N. L. B., 1985, Climatic change during the Lower Carboniferous in Euramerica, based on multivariate statistical analysis of palynological data. *Palaeogeography, Palaeoclimatology, Palaeoecology*, 52, 1-20.
- Varma, C. P., 1969, Lower Carboniferous miospores from the Albert Oil Shales (Horton Group) of New Brunswick, Canada. *Micropalaeontology*, 15, 301-324.
- Veevers, J. J., & Powell, C. McA., 1987, Late Paleozoic glacial episodes in Gondwanaland reflected in transgressive-regressive depositional sequences in Euramerica, *Geological Society of America Bulletin*, 98, 475-487.
- Visscher, H., 1966, Palaeobotany of the Mesophytic III: Plant microfossils from the Upper Bunter of Hengelo, the Netherlands. *Acta Botanica Neerlandica*, 15, 316-375.
- Walliser, O. H., 1984, Pleading for a natural D/C boundary. *Courier Forschungsinstitut Senckenberg*, 67, 241-246.
- Walton, J., 1957, On *Protopitys* (Göppert): with a description of a fertile specimen *Protopitys scotica* sp. nov. from the Calciferous Sandstone Series of Dunbartonshire. *Trans. Roy. Soc. Edin.*, 63, 333-340.
- Walton, J., 1969, On the structure of a silicified stem of *Protopitys* and associated roots with it from the Carboniferous limestone, Lower Carboniferous (Mississippian) of Yorkshire, England. *Am. J. Bot.*, 56, 808-813.
- Waltz, I. E. In: Lubert A. A. & Waltz, I. E., 1941, Atlas of microspores and pollen from the Paleozoic USSR, Soviet Union Geol. Inst. Trans. (Vsegei), A. N. Kryshtofovich (Ed.), 139, 1-107 [in Russian]
- Waltz, I. E. In: Lubert, A. A. & Waltz, I. E., 1938, Classification and stratigraphical value of spores of some Carboniferous coal deposits in the USSR. *Trav. Inst. Géol, URSS*, 105, 1-45 [in Russian].

- Wang, K., Attrep, M. Jr. & Orth, C. J., 1993, Global iridium anomaly, mass extinction and redox change at the Devonian-Carboniferous boundary. *Geology*, 21, 1071-1074.
- Wang, Q., Geng, B. Y. & Dilcher, D. L., 2005, New perspectives on the architecture of the late Devonian arborescent lycopsid *Leptophloeum rhombicum* (Leptophloeaceae). *American Journal of Botany*, 92, 83-91.
- Ward, P., Labandeira, C., Laurin, M. & Berner, R. A., 2006, Confirmation of Romer's Gap as a low oxygen interval constraining the timing of initial arthropod and vertebrate terrestrialisation. *Proc. Nat. Acad. Sci.*, 103, 16818–16822.
- Warren, A. A., Jupp, R. & Bolton, B., 1986, Earliest tetrapod trackway. *Alcheringa*, 10, 183-186.
- Warren, J. W. & Wakefield, N. A., 1972, Trackways of tetrapod vertebrates from the Upper Devonian of Victoria, Australia. *Nature*, 238, 469-470.
- Waters, C. N., Browne, M. A. E., Dean, M. T. & Powell, J. H., 2007, Lithostratigraphical Framework for Carboniferous Successions of Great Britain (Onshore). British Geological Survey Research Report RR/07/001.
- Waters, C. N., Somerville, I. D., Jones, N. S., Cleal, C. J., Collinson, J. D., Waters, R. A., Besly, B. M., Dean, M. T., Stephenson, M. H., Davies, J. R., Freshney, E. C., Jackson, D. I., Mitchell, W. I., Powell, J. H., Barclay, W. J., Browne, M. A. E., Leveridge, B. E., Long, S. L. & McLean, D. (Eds.), 2011, A revised correlation of Carboniferous rocks in the British Isles. Special Report 26. London: Geological Society of London.
- Wellman, C. H. & Gray, J., 2000, The microfossil record of early land plants. *Philosophical Transactions of the Royal Society of London, Series B (Biological Sciences)*, 355, 717–731.
- Wellman, C. H., Arioli, C., Spinner, E. G. & Vecoli, M., 2009, Morphology and wall ultrastructure of the megaspore *Lagenicula (Triletes) mixta* (Winslow 1962) comb. nov. from the Carboniferous (Early Mississippian: mid Tournaisian) of Ohio, USA. *Review of Palaeobotany and Palynology*, 156, 51-61.
- Welsh, A. & Owens, B., 1983, Early Dinantian miospore assemblages from the Caldon Low Borehole, Staffordshire, England. *Pollen et Spores*, 25, 253-264.

- Welsh, A., 1979, Stratigraphic palynology of Early Dinantian Strata in Shallow boreholes at Ravenstonedale, Cumbria. *J. Univ. Sheffield Geol. Soc.*, Vol. 7.4.
- Wicher, C. A., 1934, Sporenformen der Flammkohle des Ruhrgebietes. *Arb. Inst. Paläobot.*, 4, 165-212.
- Williams, H. S., Nowlan, G. S., Barnes, C. R. & Batten, R. S. R., 1999, The Ledge section at Cow Head, western Newfoundland as a GSSP candidate for the lower boundary of the second stage of the Ordovician System: new data and discussion of the graptolite, conodont and chitinozoan assemblages. A Report to the IUGS/ICS Subcommittee on Ordovician Stratigraphy. June 1999, pp. 1–30.
- Williams, J. E. *In*: Neves, R., Gueinn, K. J., Clayton, G., Ioannides, N. S., Neville, R. S. W. & Kruszewska, K., 1973, Palynological correlations within the Lower Carboniferous of Scotland and Northern England. *The Royal Society of Edinburgh Transactions*, 69, 23-70.
- Wilson, G. V., Edwards, W. N., Knox, J., Jones, R. C. B., Flett, S. J. S., Stephens, J. V. & Watson, D. M. S., 1935, The Geology of the Orkneys. *Mere. Geol. Surv. Scotland*, 117-122.
- Wing, S. L., 2004, Mass extinctions in plant evolution. *In*: Extinctions in the History of Life, Taylor, P. D. (Ed.), pp. 61–97, Cambridge University Press.
- Winslow, M. R., 1962, Plant spores and other microfossils from Upper Devonian and Lower Mississippian rocks of Ohio. *USGS Professional Paper 364*, pp. 1-93.
- Wolff, H., 1934, Mikrofossilien des Pliozäna Humodils der Grube Freigericht bei Dettingen a. M. und Vergleich mit älteren Schichten des Tertiärs so wie Posttertiären Ablagerungen. *Cat. of Foss. Spores and Pollen*, 4, 36-50.
- Wright, V. P., 1990, Equatorial aridity and climatic oscillations during the early Carboniferous, southern Britain. *J. Geol. Soc. London*, 147, 359-363.
- Wright, V., Vanstone, S. & Robinson, D., 1991, Ferrolysis in Arundian alluvial palaeosols: evidence of a shift in the early Carboniferous monsoonal system. *J. Geol. Soc.*, 148, 9-12.
- Young, G. C., 1993, Middle Palaeozoic macrovertebrate biostratigraphy of eastern Gondwana. *In*: Long, J. A. (Ed.), Palaeozoic Vertebrate Biostratigraphy and Biogeography. Belhaven Press, London, pp. 277-292.

Zerndt, J., 1934, Mégaspores due Bassin Houiller Pol., I. *Trav. Géol. De l'Ac. Pol.*